Analysis of Kinetic Models and Macroscopic Continuum Equations for Rarefied Gas Dynamics

by
Yingsong Zheng
B. Eng., University of Science and Technology of China, 1996
M. Eng., University of Science and Technology of China, 1999

A Dissertation Submitted in Partial Fulfillment of the Requirements for the Degree of
DOCTOR OF PHILOSOPHY
in the
Department of Mechanical Engineering

We accept this dissertation as conforming
to the required standard

Supervisor: Dr. Henning Struchtrup

Abstract

The Boltzmann equation is the basic equation to describe rarefied gas flows. Some kinetic models with simple expressions for the collision term have been proposed to reduce the mathematical complexity of the Boltzmann equation. All macroscopic continuum equations can be derived from the Boltzmann equation or kinetic models through the Chapman-Enskog method, Grad's moment method, etc.

This thesis is divided into three parts. In the first part, existing kinetic models (BGK model, ES-BGK model, $\nu(C)$-BGK model, S model, and Liu model), and two newly proposed $\nu(C)$-ES-BGK type kinetic models are described and compared, based on properties that need to be satisfied for a kinetic model. In the new models a meaningful expression for the collision frequency is used, while the important properties for a kinetic model are retained at the same time.

In the second part of this work, the kinetic models (BGK, ES-BGK, $\nu(C)$-BGK, and two new kinetic models) are tested numerically for one-dimensional shock waves and one-dimensional Couette flow. The numerical scheme used here is based on Mieussens's discrete velocity model (DVM). Computational results from the kinetic models are compared to results obtained from the Direct Simulation Monte Carlo method (DSMC). It is found that for hard sphere molecules the results obtained from the two new kinetic models are very similar, and located in between the results from the ES-BGK and the $\nu(C)$-BGK models, while for Maxwell molecules the two new kinetic models are identical to the ES-BGK model. For one-dimensional shock waves, results from the new kinetic model II fit best with results from DSMC; while for one-dimensional Couette flow, the ES-BGK model is suggested.

Also in the second part of the work, a modified numerical scheme is developed from Mieussens's original DVM. The basic idea is to use a linearized expression of the

reference distribution function, instead of its exact expression, in the numerical scheme. Results from the modified scheme are very similar to the results from the original scheme for almost all done tests, while 20-40 percent of the computational time can be saved.

In the third part, several sets of macroscopic continuum equations are examined for one-dimensional steady state Couette flow. For not too large Knudsen numbers (Kn<=0.1) in the transition regime, it is found that the original and slightly linearized regularized 13 moment equations give better results than Grad's original 13 moment equations, which, however, give better results than the Burnett equations, while the Navier-Stokes-Fourier equations give the worst results, which is in agreement with the expectation. For large Knudsen number situations (Kn>0.1), it turns out that all macroscopic continuum equations tested fail in the accurate description of flows, while the Grad's 13 moment equations can still give better results than the Burnett equations.

Examiners:

Table of contents

Nomenclature

Symbols

a	Coefficient in reference distribution function
A	A function used in new kinetic models in Sections 2.3.1 and 3.2.2
b	A number used in the ES-BGK model and new kinetic models to adjust the Prandtl number
B	A function used in new kinetic models in Sections 2.3.1 and 3.2.2
BB1, BB2...	Some function used in Appendix B and C
c	Microscopic particle velocity
C	Peculiar velocity
f	Mass distribution function
F	Numerical flux (only in Sections 3.2.1 and 4.2.1), or dimensionless reference distribution
g	Relative speed of the colliding particles
I	Number of total position nodes
$\mathbf{I}$	Unit matrix
J	Number of discrete velocities
$\mathbf{J}$	Jacobian
k	Boltzmann constant, or positive real wave number (only in Section 5.2.2)
Kn	Knudsen number
l	Mean free path
L	Domain width or Characteristic geometry length
m	Mass of one microscopic particle, or a parameter defined as $m_{ijk} = \rho_{<ijk>}$
n	Order of potential
N	Avogadro's number
p	Pressure
Pr	Prandtl number
q	Heat flux
r	Distance between two particles

R Gas constant, or a parameter defined as $R_{ij} = \rho_{rr<ij>} - 7RT\sigma_{ij}$

S Collision term

$\widehat{S}_m$, $\widetilde{S}_m$ intermediate expression for collision term in Section 2.2

t Time

T Temperature

u Macroscopic flow velocity

x-y-z Cartesian coordinates

X1-X2-X3 Cartesian coordinates

Greek

γ Coefficient in reference distribution function

Γ Coefficient in reference distribution function

δ Delta function

Δ Parameter used in moment equations, defined as $\Delta = \rho_{rrss} - 15\frac{p^2}{\rho}$

Δa Difference of a parameter a

Δt time step

Λ Parameter used to determine Prandtl number in new kinetic models

ε Angle of collision (only in Eq. (1.2)), or a scaling parameter (in Section 5.3.1)

$\boldsymbol{\varepsilon}$ Inverse matrix of λ in the ES-BGK model and the new kinetic model I

η Dimensionless peculiar velocity

θ Angle of collision

κ Thermal conductivity

λ A complex number in the expression of plane wave in Section 5.2.2 ($\lambda = \lambda_R + \lambda_i$)

$\boldsymbol{\lambda}$ A matrix used in the ES-BGK model and the new kinetic models

μ Viscosity

ν Collision frequency

$\hat{\nu}_0(n)$ A constant used in the expression of collision frequency

ρ Mass density, or with some subscript to mean high degree moment

ρe Density of internal energy

σ Scattering factor (only in Eq. (1.2)), or trace-free pressure

τ Collision time

ϕ Power interaction potentials between particles

ψ Flux limiter function

φ Some macroscopic parameter

Φ A function used in the Burnett equations

χ Production of entropy

Ψ Polynomial of peculiar velocity

ω Power index in the power law of viscosity as a function of temperature

$\Omega_1^{(2)}(2)$ A coefficient in the Liu model

Ω A function defined in Eq. (5.29)

ζ A coefficient in Eq. (5.31)

$\mathbf{Y}$ A vector used in Appendix E

$\mathbf{M}$ Inverse matrix of $\mathbf{\Pi}$ (used in Appendix E)

$\mathbf{E}$ Spectral matrix of $\boldsymbol{\varepsilon}$ (used in Appendix E)

$\mathbf{\Pi}$ Modal matrix of matrix $\boldsymbol{\varepsilon}$ (used in Appendix E)

Subscript

BGK BGK model

D Downstream side of shock wave

E Equilibrium

ES ES-BGK model

i Index of position node, or index of coordinates (only used in u_i, p_{ij} σ_{ij}, ρ_{ijk}, ρ_{rrij}, R_{ij} and m_{ijk})

ini Initial state

j Index of discrete velocity, or index of coordinates (only used in p_{ij} σ_{ij}, ρ_{ijk}, ρ_{rrij}, R_{ij} and m_{ijk})

j_1, j_2, j_3 Index of discrete velocity at x, y, or z direction

k	Iteration number (only in the N-R algorithm in the Appendix B), or index of coordinates
L	Liu model
m	Kinetic model
M	Maxwellian
Min	Minimum value
Max	Maximum value
NI	New kinetic model I
NII	New kinetic model II
p	Plates in Couette flow
$p1$	Plate one in Couette flow
ref	Reference
S	S model
U	Upstream side of shock wave
x,y,z	One set index of coordinates
γ	$\nu(C)$-BGK model
0	Values at some reference state
< >	Trace-free

Superscript

B	Burnett equations
$G13$	Grad 13
K	Kinetic model
M	Moment method
n	Index of time step
(n)	nth order term in the C-E expansion
NSF	Navier-Stokes-Fourier equations
$R13I$	original R13
$R13II$	slightly linearized R13
1	Particle 1
$'$	State after collision

$\bar{}$	Coefficient small compared to 1.0
$\wedge$	Dimensionless value
$\sim$	Functions computed in the N-R algorithm, or amplitude of the plane wave (only in Section 5.2.2)

Acronyms

C-E	Chapman – Enskog
DSMC	Direct simulation Monte Carlo method
DVM	Discrete velocity method
G13	Grad 13 moment equations
MM	Maxwellian molecules
N-R	Newton – Raphson algorithm
NSF	Navier-Stokes-Fourier equations
1DSW	One-dimensional shock wave problem
1DCF	One-dimensional Couette flow problem
R13	Regularized 13 moment equations
R13s	Two types (original and slightly linearized) regularized 13 moment equations
HS	Hard sphere molecules

List of Tables

List of Figures

Acknowledgements

First of all, I would like to thank my advisor, Dr. Henning Struchtrup, for his support, which comes in many ways. His enthusiasm and real excitement with all aspects of applied science is infectious, which made me imagine trying things that previously I thought myself incapable of doing. The research study has been fascinating.

I would also like to thank everyone who provided valuable assistance by sharing his or her own expertise. In particular, I wish to thank: Dr. Luc Mieussens for lots of helpful discussion about his discrete velocity model; Dr. Yongcai Liu for many helpful discussions, especially about numerical calculations; Toby Thatcher for discussion about Mathematica; Dr. Sadik Dost for helping during the topic change of my Ph.D study; Adam Schuetze for providing the DSMC computations. Other people I would like to thank include, but absolutely not only, Ozan Peksoy, Maurice Bond, Mehmet Yildiz, MacMurray Whale (previous advisor), Ray Brougham, Rong Zheng.

Finally, I am grateful to my family and friends, especially my wife Yingzi Zhang, for their support and encouragements.

Chapter 1 Introduction

1.1 Background

The subject of rarefied gas dynamics can be conveniently defined as the study of gas flows in which the average value of the distance between two subsequent collisions of a molecule (the so-called mean free path) is not negligible in comparison with a typical length of the flow structure being considered. This situation is encountered in the areas of aerodynamics, environmental problems, aerosol reactors, micromachines, vacuum industry, etc [1].

In the microscopic theory[1] of rarefied gas dynamics, the state variable is the distribution function. In this thesis the term "distribution function" always refers to the mass distribution function, which is the mass of one microscopic particle m times the number distribution function (or phase density) that is often used in kinetic theory. The distribution function $f(\mathbf{x},\mathbf{c},t)$ specifies the density of microscopic particles with velocity $\mathbf{c}$ at time t and position $\mathbf{x}$. The particles, which can be thought of as idealized atoms, move freely in space unless they undergo collisions. The corresponding evolution of f is described by the Boltzmann equation [1, 3-5], which, when external forces are omitted, is written as

$$\frac{\partial f}{\partial t} + c_i \frac{\partial f}{\partial x_i} = S(f) . \tag{1.1}$$

Here, the first term on the left hand side describes the local change of f with time, the second term on the left hand side is the convective change of f, and the term on the right hand side describes the change of f due to collisions among particles.

For the Boltzmann equation, the expression of the collision term $S(f)$ is written as [6]

$$S(f) = \int (f' f'^1 - f f^1) \sigma g \sin\theta d\theta d\varepsilon d\mathbf{c}^1 , \tag{1.2}$$

---

[1] In some references (e.g. [2]), it is said that the Boltzmann equation describes the gas on a *mesoscopic* level, instead of a *microscopic* level.

where the superscript 1 denotes parameters for particle 1, which is the collision partner of the particle considered, the superscript $'$ denotes parameters for the state after collision, $g = |\mathbf{c} - \mathbf{c}^1|$ is the relative speed of the colliding particles, σ is the scattering factor, and ε and θ are the angles of collision.

The Boltzmann equation is a nonlinear integro-differential equation, and difficult to handle. Therefore, some alternative, simpler expressions have been proposed to replace the Boltzmann collision term. These are known as collision models, and any Boltzmann-like equation where the Boltzmann collision integral is replaced by a collision model is called a model equation or a kinetic model [3, 4]. Kinetic models are discussed in detail in Chapter 2.

In macroscopic continuum theory of rarefied gas dynamics, the state of gas is described by macroscopic parameters (or say moments), such as mass density ρ, macroscopic flow velocity **u**, temperature T, and so on, which depend on position **x** and time t. These quantities can be recovered from the distribution f by taking velocity averages of the corresponding microscopic parameters such as

$$\rho = \int f d\mathbf{c}, \qquad \rho u_i = \int c_i f d\mathbf{c}, \qquad \rho e = \frac{3}{2} p = \frac{3}{2} \rho RT = \int \frac{C^2}{2} f d\mathbf{c},$$

$$p_{ij} = \int f C_i C_j d\mathbf{c} = p\delta_{ij} + \sigma_{ij}, \ \sigma_{ij} = \int f C_{<i} C_{j>} d\mathbf{c}, \ q_i = \frac{1}{2} \int C^2 C_i f d\mathbf{c}, \tag{1.3}$$

$$\rho_{ijk} = \int f C_i C_j C_k d\mathbf{c}, \ \ \rho_{rrij} = \int f C^2 C_i C_j d\mathbf{c},$$

where ρe is the density of internal energy, $R = k/m$ is the gas constant, k is Boltzmann's constant, $\mathbf{C} = \mathbf{c} - \mathbf{u}$ is the peculiar velocity (therefore, $g = |\mathbf{c} - \mathbf{c}^1| = |\mathbf{C} - \mathbf{C}^1|$, $d\mathbf{c} = d\mathbf{C}$), p is the hydrostatic pressure, p_{ij} is the pressure tensor, σ_{ij} is the trace-free part of pressure tensor (bracket in subscript denotes the symmetric and trace-free part of a tensor, such as, $C_{<i} C_{j>} = C_i C_j - \frac{1}{3} C^2 \delta_{ij}$), q_i is the heat flux, ρ_{ijk} is a third-degree moment, and ρ_{rrij} is a

fourth-degree moment. Eq. (1.3.c) gives the definition of temperature from the ideal gas law.

A key non-dimensional parameter to describe rarefaction effects in rarefied gas dynamics is the local Knudsen number $\mathrm{Kn} = l/L$, which is defined as the ratio of the local mean free path of particles l over a characteristic geometric length L or a length over which a large variation of a macroscopic quantity may take place [7, 8]. The usual continuum equations (such as the Navier-Stokes-Fourier equations) are only applicable for Kn<<1.

Multiplying the Boltzmann equation (Eqs. (1.1-1.2)) successively by 1, c_i, and $\frac{c^2}{2}$, then integrating over **c**, and utilizing the conservation laws of mass, momentum and energy

$$\int S d\mathbf{c} = 0, \qquad \int c_i S d\mathbf{c} = 0, \quad \frac{1}{2}\int c^2 S d\mathbf{c} = 0, \tag{1.4}$$

yields the conservation laws for mass, momentum and energy at the macroscopic level,

$$\begin{aligned} &\frac{\partial \rho}{\partial t} + \frac{\partial(\rho u_i)}{\partial x_i} = 0, \\ &\frac{\partial \rho u_i}{\partial t} + \frac{\partial(\rho u_i u_j + p_{ij})}{\partial x_j} = 0, \\ &\frac{\partial\left(\rho e + \frac{1}{2}\rho u_i^2\right)}{\partial t} + \frac{\partial\left[\rho e u_j + \frac{1}{2}\rho u^2 u_j + u_i p_{ij} + q_j\right]}{\partial x_j} = 0. \end{aligned} \tag{1.5}$$

Note that this set of equations, which should be satisfied by any set of macroscopic continuum equations, is not closed, unless additional equations for σ_{ij}, and q_i are given.

The traditional way to obtain expressions of σ_{ij} and q_i from kinetic theory is the Chapman-Enskog (C-E) method [3, 5, 9], which is a perturbation method that seeks the

distribution function f in the form of an expression in powers of the small parameter Kn, i.e.

$$f = \sum_{n=0}^{\infty} \mathrm{Kn}^n f^{(n)} . \tag{1.6}$$

In this method, a factor $1/\mathrm{Kn}$ is inserted in front of the collision term, that is to say, the Boltzmann equation (or a kinetic model equation) to be considered is

$$\frac{\partial f}{\partial t} + c_i \frac{\partial f}{\partial x_i} = \frac{1}{\mathrm{Kn}} S(f) \tag{1.7}$$

(which is the same as the Boltzmann equation (or a kinetic model equation) in dimensionless form). Substituting the expression of f in Eq. (1.6) into Eqs. (1.7, 1.2), and equating the coefficients of the same power of Kn yields a set of equations for $f^{(n)}$. By solving this set of equations, an asymptotic solution of the distribution function f is obtained (note that Kn=1 is set in the ultimate expression).

The distribution obtained from the zeroth order expansion is the Maxwellian distribution f_M,

$$f = f^{(0)} = f_M = \rho \sqrt{\left(\frac{1}{2\pi RT}\right)^3} \cdot \exp\left(-\frac{C^2}{2RT}\right). \tag{1.8}$$

The corresponding set of macroscopic equations are the Euler equations where $\sigma_{ij} = q_i = 0$.

The first order expansion yields the Navier-Stokes-Fourier (NSF) equations with

$$\sigma_{ij} = -2\mu \frac{\partial u_{<i}}{\partial x_{j>}}, \quad q_i = -\kappa \frac{\partial T}{\partial x_i}, \tag{1.9}$$

where μ is the viscosity, and κ is the thermal conductivity.

Burnett and super-Burnett equations are obtained from the second and third order expansion respectively [10-13]. Both sets of equations suffer from instabilities and

sometimes give unphysical behavior in steady state processes. Attempts to improve these equations mostly are non-satisfactory [10, 14, 15].

The moment method is another traditional way to obtain macroscopic continuum theory from kinetic theory [5, 6, 9, 16, 17]. In this method, the state of gas is described by a set of moments, which include but will not be limited to ρ, u_i (or ρu_i), T, p_{ij} and q_i. Multiplication of the Boltzmann equation (or a kinetic model equation) by a set of N polynomials of the peculiar velocity Ψ_A (A=1,..., N) and subsequent integration over velocity space yields the N moment equations to determine the N moments $\rho_A = \int \Psi_A f dc$. These equations do not form a closed system for the N moments being considered, since some higher degree moments and production terms (moments of the collision term) are contained in the equations. A closure assumption is required that allows to relate the additional moments and the production terms to the variables, which can be achieved if the distribution function f defined in the closure assumption only depends on those N moments. There are two basic ways to find the distribution function for the closure, Grad's method [9, 16], and Levermore's method [17-19].

There are two major points of criticism against Grad's method. One is that Grad's systems fail to describe smooth shock structures for Mach numbers above a critical value (such as 1.65 for the 13 moment set) [20]. Another one is that it is very difficult to develop criteria for the choice of moments that must be considered, for the equations are not related a priori to the Kn number as a smallness parameter [15].

For the Levermore moment method, the advantage is that every system derived is always hyperbolic (not like Grad's systems, which might loss their hyperbolic property depending on the values of the fields, such as heat flux, stress, etc. [21]) and possess a locally dissipated entropy [22]. The disadvantage is that the systems derived generally have non-convex domains of definition, and the equilibrium stated is typically located on the boundary of the defined domain with singular fluxes [23].

The C-E method and the moment method are completely independent of each other, since they were derived from different premises. However, from a method of Maxwellian iteration, which is essentially equivalent to a C-E expansion of the moment equations, the NSF equations and the Burnett equations can be derived from certain sets of Grad's moment equations [14, 24, 25].

Recently, a new set of moment equations, the Regularized 13 moment (R13) equations, has been developed in [26], based on a regularization of Grad's 13 moment equations. It has been shown that the equations are linearly stable for all wavelengths and frequencies, lead to smooth shock structures for all Mach numbers [26, 27], and the description of Knudsen boundary layers from these equations are better than the description from the Burnett equations [10].

A similar set of equations, which is called the slightly linearized R13 equations, has been developed from a new method [15]. This new method is based on accounting orders in the Kn number, and provides a direct link between Grad type equations and the Kn number. All sets of equations derived from this method, the Euler equations and the NSF equations in zeroth and first order, the slightly linearized Grad 13 equations in second order, the slightly linearized R13 equations in third order, and so on, are stable for disturbances of all wavelengths and frequencies. Therefore, we can say that this new method provides a common umbrella for sets of equations that up to now were thought to stem from very different arguments [15].

The main aim of the Direct Simulation of Monte Carlo (DSMC) method is to calculate practical flows through the use of the collision mechanics (considered on a probabilistic rather than a deterministic basis, which cause the noise phenomenon in results of DSMC) of model molecules, which number is some hundred of thousand or million, but still is extremely small in comparison with the number of molecules that would be present in the real gas flow in most applications. For each of simulated molecules, the space coordinates and velocity components are stored in memory and are modified with time as the molecules are simultaneously followed through representative collisions and

boundary interactions in the simulated region of space. The calculation is unsteady and the steady solutions are obtained as asymptotic limits of unsteady solutions. At or near continuum gas flow (low Knudsen number) situations, the DSMC calculation is very complicated and time consuming [1].

1.2 Motivation and objective

Some kinetic models with simple expressions for the collision term (such as BGK model [3, 28], ES-BGK model [11, 29-33], $\nu(C)$-BGK model [34, 35], S model [31, 36, 37], and Liu model [38-40]) have been proposed to reduce the mathematical complexity of the Boltzmann equation. Up to now, physical meaningful expressions for the collision frequency as function of microscopic velocity have not been applied in any existing kinetic model. One aim of this work is to propose and examine some new kinetic models, in which a meaningful expression for collision frequency is used, while retaining the important properties for a kinetic model, such as transport coefficients and Prandtl number, at the same time.

In order to compare kinetic models and to see which one can be suggested to use for future work, numerical tests need be done, and these form the second part of this work. Numerical tests are performed for one-dimensional shock waves (1DSW) and one-dimensional Couette flow (1DCF). The numerical scheme used is Mieussens's Discrete Velocity Model (DVM) [34, 41-44] with some necessary modifications. The main advantage of Mieussens's DVM is that the distribution function remains always positive, and that conservation laws and dissipation of entropy are ensured in the discrete equations. Another advantage is that computational time is saved, since the number of discrete velocities does not need to be too large. These features are achieved since the reference distribution function f_{ref} is not discretized directly, but determined by the minimum entropy principle (therefore, the values of coefficients in the discrete reference distribution are not identical to those in the continuous reference distribution). Further, in order to save computational time and reduce the complexity of the program, a modified numerical scheme is developed. The basic idea is to use a linearized expression of the reference distribution, instead of its exact expression, in the numerical scheme. For

comparison, results from the Direct Simulation Monte Carlo (DSMC) calculations are used, since the DSMC method is equivalent to solving the Boltzmann equation for a monatomic gas undergoing binary collisions. Indeed, both can be derived from the Liouville equation [3, 6, 45, 46], and the classical Bird's DSMC software is available in the public domain [47, 48].

In the scope of macroscopic continuum theory of rarefied gas dynamics, there are the NSF equations and the Burnett equations from the C-E expansion method, as well as the Grad13 equations, the original R13 equations, and the slightly linearized R13 equations, which are obtained by the moment method or related methods. In the third part of this work, the above sets of macroscopic equations derived from kinetic models (BGK and ES-BGK) will be compared with the kinetic models themselves. The idea is that a set of macroscopic equations can be considered to be better than another one, when its results are closer to the results from kinetic models. Numerical tests are performed for one dimensional Couette flow at steady state, and the Maxwell molecules.

Since boundary conditions for the extended sets of macroscopic equations (Burnett, G13, R13s) are still in development, and non-mature [15, 26, 49], a testing method has been developed that does not require knowledge of the boundary conditions. In the test, trace-free pressure and heat flux are computed from the NSF, the Burnett, the Grad13 and the R13s equations, where values of the moments in the respective expressions are chosen to be the values obtained from results of the kinetic models. The computed trace-free pressure and heat flux are then compared to the values from the kinetic models directly to check the quality of the computed results. Third-degree and fourth-degree moments will be tested similarly (for Grad13 and R13s only).

Chapter 2 Kinetic models

2.1 Introduction

The Boltzmann equation is a nonlinear integro-differential equation, and is very difficult to handle. Therefore, some alternative, simpler expressions have been proposed for the collision term, which are known as collision models, and any transport equation where the Boltzmann collision integral $S(f)$ (Eq. (1.2)) is replaced by a collision model $S_m(f)$ is called a model equation or a kinetic model [3, 4].

A collision model $S_m(f)$ needs to retain the main properties satisfied by the Boltzmann collision integral [3, 4, 17, 34, 50]. These are:

(1) It guarantees the conservation of mass, momentum and energy, which is Eq. (1.4).

(2) The production of entropy χ is always positive (H-theorem)

$$\chi = -k\int \ln f \cdot S_m d\mathbf{c} \geq 0 . \tag{2.1}$$

(3) In equilibrium, $S_m(f_E) = 0$, and therefore, the equilibrium distribution f_E is equal to the Maxwellian distribution f_M (Eq. 1.8).

(4) Yield the right transport coefficients viscosity μ, thermal conductivity κ, and Prandtl number $\Pr = \frac{5R}{2}\frac{\mu}{\kappa}$ at the hydrodynamic limit. The Prandtl number Pr is close to 2/3 for all physically meaningful collision factors σ, calculated by means of the C-E method from the Boltzmann equation [9]. $\Pr \cong \frac{2}{3}$ for ideal monatomic gas is also found in experiments [51].

(5) The collision term $S_m(f)$ depends on the peculiar velocity $\mathbf{C} = \mathbf{c} - \mathbf{u}$, and not the microscopic velocity **c**, since the Boltzmann equation is invariant under Galilean transformation.

(6) Predict positive distribution f at any situation for the kinetic model.

It is difficult to prove the last issue strictly (*The author has not seen any literature related to the proof*). What can be done is to apply the model to some real situations, such

as shock waves, Couette flow, etc. If the distribution f is not positive for some range of velocity **c** in the problem, then we can say that the model does not satisfy this property, at least in that specific situation.

2.2 Motivation of kinetic equation and expression of collision frequency

For motivation of a kinetic equation, we simplify the Boltzmann collision term Eq. (1.2) in three steps [35, 52].

Step 1: Because of the collisions, the distribution will tend to a distribution f_m for which the Boltzmann collision term vanishes (means equilibrium). Thus $\ln f_m$ must be a linear combination of the collisional invariants 1, c_i and $c^2/2$. The distribution $f'f'^1$ in the collision term Eq. (1.2) refer to the velocities after the collision, which means they may be replaced by $f_m' f_m'^1$,

$$S(f) \to \hat{S}_m = \int (f_m' f_m'^1 - f f^1) \sigma g \sin\theta d\theta d\varepsilon d\mathbf{c}^1 . \tag{2.2}$$

Step 2: Since $\ln f_m$ must be a linear combination of the collisional invariants, we may replace $f_m' f_m'^1$ by $f_m f_m^1$,

$$\hat{S}_m \to \tilde{S}_m = f_m \int f_m^1 \sigma g \sin\theta d\theta d\varepsilon d\mathbf{c}^1 - f \int f^1 \sigma g \sin\theta d\theta d\varepsilon d\mathbf{c}^1 . \tag{2.3}$$

Step 3: The difference between the two integrals may be neglected. This last step leads to the collision term of a kinetic model

$$\tilde{S}_m \to S_m = \nu(f_m - f), \tag{2.4}$$

where the collision frequency is identified as

$$\nu(x_i, t, C_i) = \int f_m^1 \sigma g \sin\theta d\theta d\varepsilon d\mathbf{c}^1 . \tag{2.5}$$

One should not rely on the above equation as the exact value for collision frequency ν because all the assumptions in steps 1-3 will lead to errors. However, it is possible to

choose the function ν so as to fit the transport coefficients (viscosity and thermal conductivity) to measurements.

When power interaction potentials between particles are applied, to simulate the real situation, [5, 6, 34] $\phi \sim r^{-(n-1)}$ ($n>3$, where ϕ is the interaction potential, r is the distance between particles, and n gives the order of the potential, n=5 represents Maxwell molecules, and $n \to \infty$ describes hard sphere molecules), one can show [6] that

$$\sigma g \sin\theta d\theta = g^{(n-5)/(n-1)} s_0 ds_0 \tag{2.6}$$

where $s_0 = s_0(\theta)$.

Combining Eqs. (2.5-2.6), considering f_m as the Maxwellian f_M, and after some manipulation, the expression of collision frequency in spherical coordinates can be reduced to

$$\nu_n(\eta) = 2\pi \hat{v}_0(n) \cdot \frac{\rho}{\pi^{3/2}} \cdot (2RT)^{\frac{n-5}{2(n-1)}} \cdot \frac{n-1}{3n-7} \cdot \int_0^\infty \frac{\xi e^{-\xi^2}}{\eta} \left[(\xi+\eta)^{\frac{3n-7}{n-1}} - |\xi-\eta|^{\frac{3n-7}{n-1}} \right] d\xi, \tag{2.7}$$

where $\hat{v}_0(n) = \int s_0 ds_0 d\varepsilon$ is a constant which depends on the interaction potential, but is independent on the macroscopic gas properties. $\xi = \frac{C^1}{\sqrt{2RT}}$ and $\eta = \frac{C}{\sqrt{2RT}}$ are dimensionless peculiar velocities.

2.3 Existing kinetic models

Several kinetic models have been proposed and developed in the past. Among them, BGK model [3, 28], ES-BGK model [11, 29-33], $\nu(C)$-BGK model [34, 35][2], S model [31, 36, 37], and Liu model [38-40] are commonly used. These models will be described briefly, and compared in this section. Table 2.1 shows their basic properties, such as whether the models fulfill the requirements 1-6 in the above section.

[2] This model was also discussed in [3, 53], but explicit form of the collision frequency was not discussed there. In [54-56], this model is discussed only for the hard sphere molecules (denoted as rigid-sphere molecular model).

The collision term $S_m(f)$ in all above kinetic models can be written as

$$S_m(f) = -\nu\left(f - f_{ref}\right), \tag{2.8}$$

where ν is the collision frequency, which is a constant with respect to velocity **C** in the above models except for the $\nu(C)$-BGK model, and f_{ref} is a specific reference distribution function, which depends on the model.

The BGK model is the simplest kinetic model, in which $f_{ref} = f_M$. This model is widely used for theoretical considerations, but it gives Pr=1. All models described below were introduced to correct this failure.

The ES-BGK model (ellipsoidal statistical BGK) is also known as Gaussian-BGK model, in which $f_{ref} = f_{ES}$, and

$$f_{ES} = \rho \cdot \left(\det\left(2\pi\lambda_{ij}\right)\right)^{-1/2} \cdot \exp\left(-\frac{1}{2} C_i \varepsilon_{ij} C_j\right). \tag{2.9}$$

Here, the matrix $\boldsymbol{\lambda}$ is defined as

$$\lambda_{ij} = RT\delta_{ij} + b\,\sigma_{ij}/\rho = (1-b)RT\delta_{ij} + b\,p_{ij}/\rho, \tag{2.10}$$

where b is a parameter that serves to adjust the Prandtl number, δ_{ij} is the unit matrix, and $\boldsymbol{\varepsilon}$ is the inverse of the tensor $\boldsymbol{\lambda}$. b must be in the interval $[-1/2,1]$ to ensure that λ_{ij} is positive definite. This expression for the reference distribution f_{ES} is defined by the following ten conditions (the first five conditions are the conservation laws),

$$\int (f_{ES} - f)\,d\mathbf{c} = 0,\ \int C_i (f_{ES} - f)\,d\mathbf{c} = 0,\ \int C^2 (f_{ES} - f)\,d\mathbf{c} = 0,$$
$$\int C_{<i} C_{j>} (f_{ES} - f)\,d\mathbf{c} = \nu(b-1)\sigma_{ij} \quad . \tag{2.11}$$

From Eqs. (2.9-2.11, 1.3), one can get

$$\int f_{ES}\,d\mathbf{c} = \rho,\quad \int C_i f_{ES}\,d\mathbf{c} = 0,\ \int C_i C_j f_{ES}\,d\mathbf{c} = \rho\lambda_{ij} = (1-b)p\delta_{ij} + bp_{ij}, \tag{2.12}$$

which will be used in the numerical work in Chapters 3 and 4.

Only recently, Andries et al. succeeded in proving the validity of the H-theorem for the ES-BGK model [32, 33], which revived the interest in this model.

The Burnett equations for the ES-BGK model with power interaction potentials have been proposed and examined by Zheng and Struchtrup in [11]. The ES-BGK Burnett equations are found to be identical to the Burnett equations for the Boltzmann equation only in the case of Maxwell molecules, while the Burnett coefficients exhibit some differences for other interaction types (e.g. hard sphere molecules). The linear stability of the ES-BGK Burnett equations is also discussed in [11] and the main results are given in Section 5.2.

The $\nu(C)$-BGK model is also called as BGK model with velocity-dependent collision frequency, in which $f_{ref} = f_\gamma$, and

$$f_\gamma = a \cdot \exp\left(-\Gamma C^2 + \gamma_i C_i\right). \tag{2.13}$$

Here, the coefficients a, $\Gamma > 0$, γ are chosen so as to guarantee the conservation of mass, momentum and energy. In general situations, the explicit theoretical expressions of a, Γ, γ cannot be given, and only numerical values are obtained from these five constraints.

At the small Kn number situations, the distribution f and the reference distribution f_γ should be close to Maxwellian f_M, then approximate explicit expressions of a, Γ, γ can be obtained through the first order C-E method. In these situations, one finds [34, 35]

$$a = \rho\left(\frac{1}{2RT}\right)^{3/2}, \qquad \Gamma = \frac{1}{2RT}, \qquad \gamma_i = \frac{1}{3pT}\frac{\partial T}{\partial x_i}\int \frac{f_M}{\nu}\left(\frac{C^2}{2RT} - \frac{5}{2}\right)C^2 d\mathbf{c},$$

$$f_\gamma \approx f_M\left(1 + \frac{8}{3\sqrt{\pi}}\frac{C_i}{T}\frac{\partial T}{\partial x_i}\int_0^\infty \frac{\eta^4\left(\eta^2 - 5/2\right)^2}{\nu(\eta)} e^{-\eta^2} d\eta\right), \tag{2.14}$$

where $\eta = \frac{C}{\sqrt{2RT}}$ is a dimensionless velocity[3]. The transport coefficients and the Prandtl number can be obtained from this model as

$$\mu = \frac{16p}{15\sqrt{\pi}} \int_0^\infty \frac{\eta^6}{\nu(\eta)} e^{-\eta^2} d\eta, \qquad \kappa = \frac{8pR}{3\sqrt{\pi}} \int_0^\infty \frac{\eta^4 \left(\eta^2 - 5/2\right)^2}{\nu(\eta)} e^{-\eta^2} d\eta,$$

$$\Pr = \frac{5R}{2}\frac{\mu}{\kappa} = \frac{\int_0^\infty \frac{\eta^6}{\nu(\eta)} e^{-\eta^2} d\eta}{\int_0^\infty \frac{\eta^4 \left(\eta^2 - 5/2\right)^2}{\nu(\eta)} e^{-\eta^2} d\eta}. \tag{2.15}$$

In principle, the collision frequency $\nu(\eta)$ can be assumed to be any function with two unknown coefficients, which are determined by experimental values of viscosity μ and thermal conductivity κ (or one experimental parameter and the condition Pr=2/3). Some expressions of $\nu(\eta)$ can be found in [34]. Here, only one expression, which will be used in the numerical test in Chapters 3 and 4, is listed.

$$\hat{\nu} = a\left(1.0 + \gamma\eta^2\right), \tag{2.16}$$

with two coefficients $a = 0.0268351$ and $\gamma = 14.2724$, where $\hat{\nu}$ is the dimensionless collision frequency, which is defined as

$$\hat{\nu} = \frac{\mu}{p}\nu. \tag{2.17}$$

However, expressions of $\nu(C)$ based on the Boltzmann collision term (Eq. (2.7)) do not give the proper Pr number [34].

The S model was proposed by E. M. Shakhov [31, 36, 37], in which $f_{ref} = f_S$, and

$$f_S = f_M\left(1 + \frac{2q_i C_i}{15pRT}\left(\frac{C^2}{2RT} - \frac{5}{2}\right)\right). \tag{2.18}$$

---

[3] $\int \Psi d\mathbf{c} = 4\pi(2RT)^{3/2} \int_0^\infty \Psi \eta^2 d\eta$ for any scalar function $\Psi(\eta)$.

The Liu model was proposed by G. Liu [38-40], in which $f_{ref} = f_L$, and

$$f_L = f_M\left(1+\frac{p_{ij}C_{<i}C_{j>}}{2pRT}+\frac{2q_iC_i}{5pRT}\left(\frac{C^2}{2RT}-\frac{5}{2}\right)\right) - \frac{f_M}{\nu}\frac{4\rho}{5pRTm}\Omega_1^{(2)}(2)\left(p_{ij}C_{<i}C_{j>}+\frac{8q_iC_i}{15}\left(\frac{C^2}{2RT}-\frac{5}{2}\right)\right) \tag{2.19}$$

Here $\Omega_1^{(2)}(2)$ is a coefficient, which is found in [12, 38].

Since heat flux is a vector, and the range of the peculiar velocity is $(-\infty,\infty)$, f_S and f_L will become negative for large values of the peculiar velocity. The further result is that the distribution function f from these two kinetic models would be negative for some range of peculiar velocity.

Table 2.1: Comparison of kinetic models

Kinetic models	BGK model	ES-BGK model	$\nu(C)$-BGK model	S model	Liu model	New model I	New model II
f_{ref} in collision term $S_m(f)$	f_M (Eq. (1.8))	f_{ES} (Eq. (2.9))	f_γ (Eqs. (2.13-2.14))	f_S (Eq. (2.18))	f_L (Eq. (2.19))	f_{NI} (Eqs. (2.20, 2.23))	f_{NII} (Eqs. (2.38, 2.43))
Collision frequency ν	Velocity independent	Velocity independent	Velocity dependent	Velocity independent	Velocity independent	Velocity dependent	Velocity dependent
Related references	[3, 28]	[11, 29-33]	[34, 35]	[31, 36, 37]	[38-40]	This work	This work
1. Conservation of mass, momentum and energy	Satisfied	Satisfied	Satisfied	Satisfied	Satisfied	Satisfied	Satisfied
2. H-theorem	Proved	Proved	Proved	Only proved in the near local equilibrium situations	Only proved in the near local equilibrium situations	Only proved in small Kn number situations	Only proved in small Kn number situations
3. In equilibrium, $f = f_M$	Yes	Yes	Yes	Yes	Yes	Yes	Yes
4. Viscosity μ, Thermal conductivity κ, and Prandtl number Pr	$\mu = \frac{p}{\nu}$ $\kappa = \frac{5}{2}\frac{pR}{\nu}$ Pr=1.0	$\mu = \frac{p}{\nu}\frac{1}{1-b}$ $\kappa = \frac{5}{2}\frac{pR}{\nu}$ $\mathrm{Pr} = 1/(1-b)$	Eq. (2.15)	$\mu = \frac{p}{\nu}$ $\kappa = \frac{15pR}{4\nu}$ Pr=2/3	$\mu = \frac{5kT}{8\Omega_1^{(2)}(2)}$ $\kappa = \frac{75k^2T}{32m\Omega_1^{(2)}(2)}$ Pr=2/3	Eq. (2.26)	Eq. (2.44)
5. Galilean invariance	Satisfied	Satisfied	Satisfied	Satisfied	Satisfied	Satisfied	Satisfied
6. Positiveness of f (To the author's best knowledge)	Satisfied	Satisfied	Satisfied	Possibly not	Not true in some situations	Satisfied	Satisfied
Remark	Simplest model; f_{ref} is a local isotropic Gaussian	f_{ref} is a local anisotropic Gaussian; Can simplify to the BGK model when $b=0$.	In order to obtain Pr=2/3, the expression of velocity-dependent frequency does not met with the physics.			1. Satisfy the requirements of realistic collision frequency and correct transport coefficients 2. Can simplify to the ES-BGK model and the $\nu(C)$-BGK model at certain conditions	

2.4 Two new $\nu(C)$-ES-BGK type kinetic models

In the existing kinetic models, the collision frequency ν is assumed to be an average value, which is not dependent on the velocity **C**, except for the $\nu(C)$-BGK model. For real gases, however, the collision frequency is a function of the velocity **C**. The **C**-dependence of ν has an important influence on the results at large Kn situations (e.g. $\mathrm{Kn} \geq 0.1$), and thus $\nu(C)$ in kinetic models should be close to the value predicted from the Boltzmann equation. However, when the realistic collision frequency is used in the $\nu(C)$-BGK model, the Prandtl number is not 2/3, but very close to unity [34].

Therefore, we propose a new type kinetic model, in which the realistic collision frequency can be used, while the transport coefficients are predicted correctly (including $\mathrm{Pr} = 2/3$). The idea is to combine the anisotropic Gaussian of the ES-BGK model and the velocity-dependent collision frequency of the $\nu(C)$-BGK model to develop a new kinetic model, named as ES-BGK model with velocity-dependent collision frequency, or $\nu(C)$-ES-BGK model. There are two ways to create the reference distribution f_{ref} following this idea, which will be referred to as new kinetic model I and II.

2.4.1 New kinetic model I

In this new kinetic model, the collision term $S_m(f)$ is

$$S_m(f) = -\nu(C)(f - f_{NI}),$$

$$f_{NI} = a \cdot \exp\left(-\frac{1}{2}\Gamma\varepsilon_{ij}C_iC_j + \gamma_iC_i\right). \tag{2.20}$$

Here, the matrix ε_{ij} is the same expression as in the ES-BGK model. The coefficients a, Γ (>0), γ are chosen so as to guarantee the conservation of mass, momentum and energy.

In general situations, explicit expressions of a, Γ (>0), γ cannot be given, and only numerical values can be obtained from the five conservation laws Eq. (1.4). At small

Knudsen number situations, approximate explicit expressions of a, Γ, γ can be given through the first order C-E method, and this is described in the following.

At small Kn number situations, any distribution is close to a Maxwellian distribution, so that (when we only keep the zero and first order terms)

$$a=\rho\left(\frac{1}{2RT}\right)^{3/2}(1-\hat{a}),\qquad \Gamma=1-\hat{\Gamma},\qquad \varepsilon_{ij}=\frac{\delta_{ij}}{RT}-\frac{b\sigma_{ij}}{pRT},$$

$$\Gamma\varepsilon_{ij}=\frac{\delta_{ij}}{RT}-\hat{\Gamma}\frac{\delta_{ij}}{RT}-\frac{b\sigma_{ij}}{pRT},\quad \gamma_i=\hat{\gamma}_i, \tag{2.21}$$

$$f_{NI}\approx f_M\left(1-\hat{a}+\frac{\hat{\Gamma}C^2}{2RT}+\frac{b\sigma_{ij}C_iC_j}{2pRT}+\hat{\gamma}_iC_i\right).$$

Here, the values of the undetermined coefficients $\hat{a}$, $\hat{\Gamma}$ and $\hat{\gamma}_i$ are small compared to 1. The value of parameter b must lie in the interval [-0.5, 1], which is the same range as b in the ES-BGK model, to ensure the matrix ε_{ij} is positive definite.

After performing the first order C-E expansion, one finds

$$f=f_{NI}-\frac{f_M}{\nu}\left[\frac{C_iC_j}{RT}\frac{\partial u_{<i}}{\partial x_{j>}}+\frac{C_i}{T}\frac{\partial T}{\partial x_i}\left(\frac{C^2}{2RT}-\frac{5}{2}\right)\right]. \tag{2.22}$$

This approximate solution fulfills the five conservation laws for any distribution f_{NI}, thus, the coefficients $\hat{a}$, $\hat{\Gamma}$ and $\hat{\gamma}_i$ cannot be determined from these conditions. However, the distribution f must reproduce the first five moments, which are density, velocity and pressure (Eq.(1.3)). It follows

$$\hat{a}=\hat{\Gamma}=0,$$

$$\hat{\gamma}_i=\frac{1}{3pT}\frac{\partial T}{\partial x_i}\int\frac{f_M}{\nu}\left(\frac{C^2}{2RT}-\frac{5}{2}\right)C^2d\mathbf{c}, \tag{2.23}$$

$$f_{NI}=f_M\left[1+\frac{bC_iC_j}{2pRT}\sigma_{ij}+\frac{C_i}{3pT}\frac{\partial T}{\partial x_i}\int\frac{f_M}{\nu}\left(\frac{C^2}{2RT}-\frac{5}{2}\right)C^2d\mathbf{c}\right].$$

At last, for small Kn numbers, one finds

$$f = f_M\left[1+\frac{bC_iC_j}{2pRT}\sigma_{ij}+\frac{C_i}{3pT}\frac{\partial T}{\partial x_i}\int\frac{f_M}{\nu}\left(\frac{C^2}{2RT}-\frac{5}{2}\right)C^2 d\mathbf{c}\right] - \frac{f_M}{\nu}\left[\frac{C_iC_j}{RT}\frac{\partial u_{<i}}{\partial x_{j>}}+\frac{C_i}{T}\frac{\partial T}{\partial x_i}\left(\frac{C^2}{2RT}-\frac{5}{2}\right)\right] \quad (2.24)$$

After computing pressure tensor and heat flux vector from the above first order C-E expansion, one finds

$$\sigma_{ij} = -\frac{1}{1-b}\frac{32p}{15\sqrt{\pi}}\int_0^\infty \frac{\eta^6}{\nu(\eta)}e^{-\eta^2}d\eta\cdot\frac{\partial u_{<i}}{\partial x_{j>}}, \quad (2.25)$$

$$q_i = -\frac{8pR}{3\sqrt{\pi}}\int_0^\infty \frac{\eta^4\left(\eta^2-5/2\right)^2}{\nu(\eta)}e^{-\eta^2}d\eta\cdot\frac{\partial T}{\partial x_i}.$$

Therefore, the transport coefficients and the Prandtl number obtained from this kinetic model are

$$\mu = \frac{1}{1-b}\frac{16p}{15\sqrt{\pi}}\int_0^\infty \frac{\eta^6}{\nu(\eta)}e^{-\eta^2}d\eta,$$

$$\kappa = \frac{8pR}{3\sqrt{\pi}}\int_0^\infty \frac{\eta^4\left(\eta^2-5/2\right)^2}{\nu(\eta)}e^{-\eta^2}d\eta, \quad (2.26)$$

$$\mathrm{Pr} = \frac{5R}{2}\frac{\mu}{\kappa} = \frac{1}{1-b}\frac{\int_0^\infty \frac{\eta^6}{\nu(\eta)}e^{-\eta^2}d\eta}{\int_0^\infty \frac{\eta^4\left(\eta^2-5/2\right)^2}{\nu(\eta)}e^{-\eta^2}d\eta} = \frac{\Lambda}{1-b},$$

where Λ is defined as

$$\Lambda = \frac{\int_0^\infty \frac{\eta^6}{\nu(\eta)}e^{-\eta^2}d\eta}{\int_0^\infty \frac{\eta^4\left(\eta^2-5/2\right)^2}{\nu(\eta)}e^{-\eta^2}d\eta}. \quad (2.27)$$

Combining Eqs. (2.7, 2.17, 2.26.a), one finds, after some manipulation, the following expressions for the new kinetic model I,

$$\hat{v}_0(n)=\frac{1}{1-b}\frac{8}{15}\frac{p}{\mu}\frac{A(n)}{\rho(2RT)^{\frac{n-5}{2(n-1)}}\frac{n-1}{3n-7}},$$

$$\nu(n,\eta)=\frac{1}{1-b}\frac{16}{15\sqrt{\pi}}\frac{p}{\mu}\cdot A(n)\cdot B(n,\eta), \tag{2.28}$$

$$\hat{\nu}(n,\eta)=\frac{1}{1-b}\frac{16}{15\sqrt{\pi}}\cdot A(n)\cdot B(n,\eta),$$

where

$$A(n)=\int_{\eta=0}^{\infty}\frac{\eta^6 e^{-\eta^2}}{B(n,\eta)}d\eta, \tag{2.29}$$

$$B(n,\eta)=\int_{\xi=0}^{\infty}\frac{\xi e^{-\xi^2}}{\eta}\left[(\xi+\eta)^{\frac{3n-7}{n-1}}-|\xi-\eta|^{\frac{3n-7}{n-1}}\right]d\xi.$$

For Maxwell molecules where $n=5$, A and B are constants[4],

$$A(n=5)=0.9375, \quad B(n=5,\eta)=1.77245. \tag{2.30}$$

$$\hat{\nu}(n=5,\eta)=\frac{1}{1-b}\frac{16}{15\sqrt{\pi}}\cdot A(n=5)\cdot B(n=5,\eta)=\frac{1}{1-b}$$

For hard sphere molecules where $n=\infty$, one finds [12, 34]

$$B(n=\infty,\eta)=\int_{\xi=0}^{\infty}\frac{\xi e^{-\xi^2}}{\eta}\left[(\xi+\eta)^3-|\xi-\eta|^3\right]d\xi=\frac{B(n=\infty,\eta=0)}{2}\left\{e^{-\eta^2}+\frac{\sqrt{\pi}}{2}\left(\frac{1}{\eta}+2\eta\right)erf(\eta)\right\},$$

$$\hat{\nu}(n=\infty,\eta)=\frac{1}{2}\frac{1}{1-b}\frac{16}{15\sqrt{\pi}}\cdot A(n=\infty)\cdot B(n=\infty,\eta=0.0)\left\{e^{-\eta^2}+\frac{\sqrt{\pi}}{2}\left(\frac{1}{\eta}+2\eta\right)erf(\eta)\right\}, \tag{2.31}$$

where $A(n=\infty)=0.308855$, $B(n=\infty,\eta=0.0)=3.0$, and $erf(\eta)$ is the error function, which is defined as

$$erf(\eta)=\frac{2}{\sqrt{\pi}}\int_0^{\eta}e^{-t^2}dt.$$

For other values of n, the integration in Eq. (2.7) needs to be done numerically.

For ideal gases, it is well known that the viscosity μ is a function of temperature, which can be described as [9]

[4] The computation uses a Mathematica program [57].

$$\mu(T) = \mu_0 \left(\frac{T}{T_0} \right)^{\omega}, \qquad (2.32)^5$$

where μ_0, the viscosity at the reference temperature T_0, will be used to determine $\hat{v}_0(n)$, and ω is a positive number of order 1. From Eqs. (2.7, 2.26.a, 2.32), we can see that

$$\omega = \frac{n+3}{2(n-1)}. \qquad (2.33)$$

For real monatomic gas, the n value locates in between five and infinity, and the ω value locates in between 0.5 and 1.0. That is to say, Maxwell molecules and hard sphere molecules are the two limiting situations of molecular models for real monatomic gas.

Table 2.2 several n and corresponding b and Pr values for the new kinetic models

N	ω	Λ	b for Pr=2/3	b=-0.5	
				Pr	$\frlvert Pr-2/3 \frrvert / 2/3$
5	1	1.0	-0.50	2/3=0.6667	0.000
6	0.9	1.00839	-0.5126	0.6723	0.008
231.0/31.0	0.81	1.01327	-0.5199	0.6755	0.013
10	0.72	1.01572	-0.5236	0.6771	0.016
13	0.67	1.01615	-0.5242	0.6774	0.016
20	0.61	1.01566	-0.5235	0.6771	0.016
∞	0.50	1.0126	-0.5189	0.6751	0.013

Notes: The computation of Λ (Eq. 2.27) uses a Mathematica program.

Table 2.2 gives numerical results of the Prandtl number, Eq. (2.26.c), for several n values. It is seen that in order to obtain Pr=2/3, the b value should be a little smaller than –0.5, which is the low limit of this new kinetic model to ensure the matrix ε_{ij} is positive definite. Therefore in the application of this new kinetic model, b is chosen as –0.5, and Pr will be a number which very near to 2/3. For Maxwell molecules, b = –0.5 will obtain Pr=2/3. Therefore, our requirement, which is that realistic collision frequencies are used and the transport coefficients are predicted correctly in one kinetic model, is met.

[5] Besides this, some other expression can be found in the literature, such as the Sutherland's law [58].

When $\nu(C)$ is not constant, and b=0 (which implies that $\varepsilon_{ij} = \varepsilon\delta_{ij}$), the new kinetic model I is identical to the $\nu(C)$-BGK model. When $\nu(C)$ is constant (therefore $\gamma_i = \hat{\gamma}_i = 0.0$ from Eq. (2.23)), this new kinetic model is identical to the ES-BGK model.

At last, let us consider the H-theorem for this new kinetic model. Since the explicit theoretical expression of a, Γ (>0), γ cannot be given in the general situations, the H-theorem is hard to prove in general[6]. When small Kn number situations are considered, it is found that the H-theorem is indeed satisfied. In these specific situations, from Eqs. (2.22, 2.24), one gets

$$\begin{aligned} \ln f \cong \ln f_M &+ \frac{b\sigma_{ij}}{2pRT}C_iC_j + \frac{8}{3\sqrt{\pi}}\frac{C_i}{T}\frac{\partial T}{\partial x_i}\int\frac{e^{-\eta^2}\eta^4\left(\eta^2-5/2\right)}{\nu}d\eta \\ &-\frac{1}{\nu}\frac{C_iC_j}{RT}\frac{\partial u_{<i}}{\partial x_{j>}} - \frac{1}{\nu}\frac{C_i}{T}\frac{\partial T}{\partial x_i}\left(\frac{C^2}{2RT}-\frac{5}{2}\right) \end{aligned}, \qquad (2.34)$$

$$S_m = \nu\left(f_{NI}-f\right) = f_M\left[\frac{C_iC_j}{RT}\frac{\partial u_{<i}}{\partial x_{j>}} + \frac{C_i}{T}\frac{\partial T}{\partial x_i}\left(\frac{C^2}{2RT}-\frac{5}{2}\right)\right].$$

Utilizing the conservation law Eq. (1.4), and after some manipulation, the production of entropy to the first order is

$$\begin{aligned} \chi &= -k\int\ln f\cdot S_m d\mathbf{c} \\ &= k\int f_M\left(A_1C_iC_j + \frac{1}{\nu}A_2C_iC_j + A_3C_iC_jC^2 + \frac{1}{\nu}A_4C_iC_jC^2\right)d\mathbf{c}, \\ &\quad + k\int f_M\left(\frac{1}{\nu}A_5C_iC_jC^4 + A_6C_iC_jC_kC_l + \frac{1}{\nu}A_7C_iC_jC_kC_l\right)d\mathbf{c} \end{aligned} \qquad (2.35)$$

where

$$A_1 = \frac{20}{3\sqrt{\pi}}\frac{1}{T^2}\frac{\partial T}{\partial x_i}\frac{\partial T}{\partial x_j}\int\frac{e^{-\eta^2}\eta^4\left(\eta^2-5/2\right)}{\nu}d\eta, \qquad A_2 = \frac{25}{4}\frac{1}{T^2}\frac{\partial T}{\partial x_i}\frac{\partial T}{\partial x_j},$$

$$A_3 = -\frac{4}{3\sqrt{\pi}}\frac{1}{RT^3}\frac{\partial T}{\partial x_i}\frac{\partial T}{\partial x_j}\int\frac{e^{-\eta^2}\eta^4\left(\eta^2-5/2\right)}{\nu}d\eta, \qquad A_4 = -\frac{5}{2}\frac{1}{RT^3}\frac{\partial T}{\partial x_i}\frac{\partial T}{\partial x_j},$$

$$A_5 = \frac{1}{4}\frac{1}{R^2T^4}\frac{\partial T}{\partial x_i}\frac{\partial T}{\partial x_j}, \qquad A_6 = \frac{b\mu}{pR^2T^2}\frac{\partial u_{<i}}{\partial x_{j>}}\frac{\partial u_{<k}}{\partial x_{l>}}, \qquad A_7 = \frac{1}{R^2T^2}\frac{\partial u_{<i}}{\partial x_{j>}}\frac{\partial u_{<k}}{\partial x_{l>}}.$$

[6] Several ways have been attempted, such as to utilize the method used to prove the H-theorem of the ES-BGK model, or the method for the $\nu(C)$-BGK model, or even the combination of these two methods, but, so far, all attempts failed.

Since

$$\int f_M A_1 C_i C_j d\mathbf{c} = \frac{20}{3\sqrt{\pi}} \frac{p}{T^2} \left(\frac{\partial T}{\partial x_i} \right)^2 \int \frac{e^{-\eta^2} \eta^4 \left(\eta^2 - 5/2 \right)}{\nu} d\eta ,$$

$$\int f_M \frac{A_2}{\nu} C_i C_j d\mathbf{c} = \frac{50}{3\sqrt{\pi}} \frac{p}{T^2} \left(\frac{\partial T}{\partial x_i} \right)^2 \int \frac{e^{-\eta^2} \eta^4}{\nu} d\eta ,$$

$$\int f_M A_3 C_i C_j C^2 d\mathbf{c} = -\frac{20}{3\sqrt{\pi}} \frac{p}{T^2} \left(\frac{\partial T}{\partial x_i} \right)^2 \int \frac{e^{-\eta^2} \eta^4 \left(\eta^2 - 5/2 \right)}{\nu} d\eta ,$$

$$\int f_M \frac{A_4}{\nu} C_i C_j C^2 d\mathbf{c} = -\frac{40}{3\sqrt{\pi}} \frac{p}{T^2} \left(\frac{\partial T}{\partial x_i} \right)^2 \int \frac{e^{-\eta^2} \eta^6}{\nu} d\eta ,$$

$$\int f_M \frac{A_5}{\nu} C_i C_j C^4 d\mathbf{c} = \frac{8}{3\sqrt{\pi}} \frac{p}{T^2} \left(\frac{\partial T}{\partial x_i} \right)^2 \int \frac{e^{-\eta^2} \eta^8}{\nu} d\eta ,$$

$$\int f_M A_6 C_i C_j C_k C_l d\mathbf{c} = \frac{2b\rho\mu}{p} \left(\frac{\partial u_{<i}}{\partial x_{j>}} \right)^2 ,$$

$$\int f_M \frac{A_7}{\nu} C_i C_j C_k C_l d\mathbf{c} = \frac{32\rho}{15\sqrt{\pi}} \left(\frac{\partial u_{<i}}{\partial x_{j>}} \right)^2 \int \frac{e^{-\eta^2} \eta^6}{\nu} d\eta ,$$

therefore,

$$\begin{aligned} \frac{\chi}{k} = & \frac{8p}{3\sqrt{\pi} T^2} \left(\frac{\partial T}{\partial x_i} \right)^2 \int \frac{e^{-\eta^2} \eta^4 \left(\eta^2 - 5/2 \right)^2}{\nu} d\eta \\ & + \rho \left(\frac{\partial u_{<i}}{\partial x_{j>}} \right)^2 \left(\frac{2b\mu}{p} + \frac{32}{15\sqrt{\pi}} \int \frac{e^{-\eta^2} \eta^6}{\nu} d\eta \right) \end{aligned} \tag{2.36}$$

Utilizing Eq. (2.26), one finally gets

$$\chi = k \cdot \left[\frac{\kappa}{RT^2} \left(\frac{\partial T}{\partial x_i} \right)^2 + \frac{2\mu\rho}{p} \left(\frac{\partial u_{<i}}{\partial x_{j>}} \right)^2 \right] \geq 0 . \tag{2.37}$$

2.3.2 New kinetic model II

This time, the collision term $S_m(f)$ is chosen as

$$\begin{aligned} S_m(f) &= -\nu \left(f - f_{NII} \right) , \\ f_{NII} &= a \cdot \exp\left(-\Gamma_{ij} C_i C_j + \gamma_i C_i \right) . \end{aligned} \tag{2.38}$$

Here, $\nu(C)$ is the collision frequency, and the coefficients a, Γ_{ij} ($\Gamma_{ij}=\Gamma_{ji}\geq 0$), γ_i are chosen so as to satisfy the following 10 equations, which are given by analogy with the ES-BGK model (Eq. (2.11) and $\nu=\frac{p}{(b-1)\mu}$ for the ES-BGK model)

$$\int(f_{NII}-f)\nu d\mathbf{c}=0,\ \int C_i(f_{NII}-f)\nu d\mathbf{c}=0,\ \int C^2(f_{NII}-f)\nu d\mathbf{c}=0,$$

$$\int C_{<i}C_{j>}(f_{NII}-f)\nu d\mathbf{c}=-\frac{p}{\mu}\sigma_{ij}. \tag{2.39}$$

In general situations, explicit expressions for a, Γ_{ij}, γ_i cannot be given, and only numerical values can be obtained. For small Kn number situations, approximate explicit expressions of a, Γ_{ij}, γ_i can be obtained through the first order C-E method, and further the H-theorem can be proved in these situations.

At small Kn number situations, any distribution is close to a Maxwellian distribution, so that

$$a=\rho\left(\frac{1}{2RT}\right)^{3/2}(1-\hat{a}),\qquad \Gamma_{ij}=\frac{\delta_{ij}}{2RT}-\hat{\Gamma}_{ij},\qquad \gamma_i=\hat{\gamma}_i,$$

$$f_{NII}\approx f_M\left(1-\hat{a}+\hat{\Gamma}_{ij}C_iC_j+\hat{\gamma}_iC_i\right). \tag{2.40}$$

Here, the values of undetermined coefficients $\hat{a}$, $\hat{\Gamma}_{ij}$ and $\hat{\gamma}_i$ are small, compared to 1.

After performing the first order C-E expansion, one finds

$$f=f_{NII}-\frac{f_M}{\nu}\left[\frac{C_iC_j}{RT}\frac{\partial u_{<i}}{\partial x_{j>}}+\frac{C_i}{T}\frac{\partial T}{\partial x_i}\left(\frac{C^2}{2RT}-\frac{5}{2}\right)\right]. \tag{2.41}$$

This approximate solution fulfills the 10 constraint equations (Eq. (2.39)) for any distribution f_{NII}, since $\sigma_{ij}=-2\mu\frac{\partial u_{<i}}{\partial x_{j>}}$ for small Kn number situations. Thus, the coefficients $\hat{a}$, $\hat{\Gamma}_{ij}$ and $\hat{\gamma}_i$ cannot be determined from these conditions. However, the

distribution f must reproduce the first 5 moments, which are density, velocity and pressure (Eq.(1.3)). It follows

$$a = \hat{\Gamma}_{ii} = 0.0, \quad \hat{\gamma}_i = \frac{1}{3pT}\frac{\partial T}{\partial x_i}\int \frac{f_M}{\nu}\left(\frac{C^2}{2RT} - \frac{5}{2}\right)C^2 d\mathbf{c}. \tag{2.42}$$

If we use the first 10 moments, which are density, velocity, and whole pressure tensor, to determine the expression of coefficients, we get

$$\sigma_{ij} = 2pRT\hat{\Gamma}_{ij} - \frac{32p}{15\sqrt{\pi}}\int_0^\infty \frac{\eta^6}{\nu(\eta)} e^{-\eta^2} d\eta \cdot \frac{\partial u_{<i}}{\partial x_{j>}}.$$

Then we cannot express trace-free pressure tensor and viscosity as a function of collision frequency, which will give trouble to relate Pr and $\nu(\eta)$.

Since $\hat{\Gamma}_{ij}$ is only requested to be a trace free tensor from the above equation (2.42), the choice of $\hat{\Gamma}_{ij}$ is not unique. For an easy treatment, the expression of $\hat{\Gamma}_{ij}$ would be chosen to be as simple as possible. However, choosing $\hat{\Gamma}_{ij} = 0$ reproduces the $\nu(C)$-BGK model. Therefore, here we choose the second simplest choice of $\hat{\Gamma}_{ij}$, which is a linear function of the trace free tensor σ_{ij}. Since the unit of $\hat{\Gamma}_{ij}$ should be the same as the unit of $\frac{1}{RT}$, the expression of $\hat{\Gamma}_{ij}$ would be $\hat{\Gamma}_{ij} = \frac{b}{2pRT}\sigma_{ij}$. The parameter b is introduced to adjust the Prandtl number. The range of b is $-1 \le b \le 0.5$, which is proved in the following paragraph, in order to make matrix Γ_{ij} positive definite, which is a little different from the range of b value in the ES-BGK model.

Since the tensor Γ_{ij} must be positive definite, there is some limitation for the value of b. Based on the idea given in [33], one can find the range of b. To simplify the description, here we only show the derivation for the matrices in a diagonal basis (matrices in a non-diagonal basis can be transformed into matrices in a diagonal basis).

$$\Gamma_{ij}=\frac{\delta_{ij}}{2RT}-\frac{b\sigma_{ij}}{2pRT}=\frac{(1+b)\delta_{ij}}{2RT}-\frac{bp_{ij}}{2pRT}$$

$$=\frac{1}{2pRT}\begin{bmatrix}(1+b)p-bp_{11} & 0 & 0\\ 0 & (1+b)p-bp_{22} & 0\\ 0 & 0 & (1+b)p-bp_{33}\end{bmatrix}$$

$$=\frac{1}{6pRT}\begin{bmatrix}(1+b)(p_{11}+p_{22}+p_{33})-3bp_{11} & 0 & 0\\ 0 & (1+b)(p_{11}+p_{22}+p_{33})-3bp_{22} & 0\\ 0 & 0 & (1+b)(p_{11}+p_{22}+p_{33})-3bp_{33}\end{bmatrix}$$

$$=\frac{(1-2b)}{6pRT}\begin{bmatrix}p_{11} & 0 & 0\\ 0 & p_{22} & 0\\ 0 & 0 & p_{33}\end{bmatrix}+\frac{(1+b)}{6pRT}\begin{bmatrix}p_{22} & 0 & 0\\ 0 & p_{33} & 0\\ 0 & 0 & p_{11}\end{bmatrix}+\frac{(1+b)}{6pRT}\begin{bmatrix}p_{33} & 0 & 0\\ 0 & p_{11} & 0\\ 0 & 0 & p_{22}\end{bmatrix}$$

In order to make Γ_{ij} positive definite for any situation, and since p_{11}, p_{22} and p_{33} are positive, $1-2b\geq 0$ and $1+b\geq 0$ need be satisfied. That is to say, $-1\leq b\leq 0.5$.

At last, for small Kn numbers, one finds

$$f_{NII}=f_M\left[1+\frac{bC_iC_j}{2pRT}\sigma_{ij}+\frac{C_i}{3pT}\frac{\partial T}{\partial x_i}\int\frac{f_M}{\nu}\left(\frac{C^2}{2RT}-\frac{5}{2}\right)C^2d\mathbf{c}\right],$$

$$f=f_M\left[1+\frac{bC_iC_j}{2pRT}\sigma_{ij}+\frac{C_i}{3pT}\frac{\partial T}{\partial x_i}\int\frac{f_M}{\nu}\left(\frac{C^2}{2RT}-\frac{5}{2}\right)C^2d\mathbf{c}\right]$$
$$-\frac{f_M}{\nu}\left[\frac{C_iC_j}{RT}\frac{\partial u_{<i}}{\partial x_{j>}}+\frac{C_i}{T}\frac{\partial T}{\partial x_i}\left(\frac{C^2}{2RT}-\frac{5}{2}\right)\right], \qquad (2.43)$$

which is the same expression as f in the new kinetic model I (Eq. (2.24)). Therefore, the transport coefficients can be obtained from this model as

$$\mu=\frac{1}{1-b}\frac{16p}{15\sqrt{\pi}}\int_0^\infty\frac{\eta^6}{\nu(\eta)}e^{-\eta^2}d\eta,$$

$$\kappa=\frac{8pR}{3\sqrt{\pi}}\int_0^\infty\frac{\eta^4\left(\eta^2-5/2\right)^2}{\nu(\eta)}e^{-\eta^2}d\eta, \qquad (2.44)$$

$$\mathrm{Pr}=\frac{1}{1-b}\frac{\int_0^\infty\frac{\eta^6}{\nu(\eta)}e^{-\eta^2}d\eta}{\int_0^\infty\frac{\eta^4\left(\eta^2-5/2\right)^2}{\nu(\eta)}e^{-\eta^2}d\eta}=\frac{\Lambda}{1-b},$$

where Λ is defined as Eq. (2.27).

It can be seen from Eq. (2.44) and Table 2.2 that Pr=2/3 can be satisfied for any power index n in this new kinetic model, for $-1 \le b \le 0.5$ this time in order to make the matrix Γ_{ij} positive definite. Therefore, our requirement, which is that realistic collision frequencies are used and the transport coefficients are predicted correctly in one kinetic model, is met.

It is easy to find that the new kinetic model II can be simplified into the ES-BGK model when $\nu(C)$ is set constant, while the $\nu(C)$-BGK model is recovered for $\Gamma_{ij} = \Gamma \delta_{ij}$.

Let us consider the H-theorem for this new kinetic model II. Since the explicit theoretical expression of a, Γ_{ij} (>0), γ cannot be given in general situations, the H-theorem is hard to prove in general situations[7]. When small Kn number situations are considered, we find that the H-theorem is indeed satisfied, which proof is the same as the proof for the new kinetic model I.

2.4 Conclusion

Several existing kinetic models (BGK model, ES-BGK model, $\nu(C)$-BGK model, S model, and Liu model) have been compared, based on properties that need to be satisfied for a kinetic model. The main disadvantage of these existing kinetic models is that a meaningful expression for collision frequency (Eq. (2.7)) and $\Pr \cong 2/3$ can not be reached at the same time. In order to overcome this shortcoming, two new $\nu(C)$-ES-BGK type kinetic models have been proposed here, which both can be simplified to the ES-BGK model and the $\nu(C)$-BGK model. The next step will be to apply these kinetic models in numerical computations, to see which new kinetic model is better, and whether the new kinetic models can give better results than existing kinetic models or not. This will be the task of Chapters 3 and 4.

---

[7] Several ways have been attempted, such as the method used to prove the H-theorem of the ES-BGK model, or the method for the $\nu(C)$-BGK model, or even the combination of these two methods, but, so far, all attempts failed.

Chapter 3 Numerical work on one-dimensional shock waves

3.1 Introduction of shock wave

A shock wave is a thin transitive area propagating with supersonic speed in which there is a sharp change of moments, in particular a speed change from supersonic to subsonic and increases in density and temperature. Shock waves arise at explosions, detonations, supersonic movements of bodies, and so on [59].

The problem we consider in this chapter is the one-dimensional shock wave problem (1DSW) at steady state, in which the changes of moments are along the x direction in an x-y-z Cartesian frame (or the X1 direction in an X1-X2-X3 Cartesian frame), and the boundary conditions are the equilibrium states at upstream and downstream sides.

In the 1DSW, the macroscopic flow velocity $u_1 \neq 0$, and $u_2 = u_3 = 0$, therefore for trace-free pressure tensor elements, we have

$$\sigma_{11} = -2\sigma_{22} = -2\sigma_{33}. \tag{3.1}$$

From the conservation law Eq (1.5) it is realized that the fluxes of mass, momentum, and energy, which are ρu_1, $\rho u_1^2 + p_{11}$, and $1.5pu_1 + 0.5\rho u_1^3 + p_{11}u_1 + q_1$, must be constant in the whole domain at the steady state of 1DSW. Since $p_{11} = p$ and $q_1 = 0$ for equilibrium state, these conditions, known as the Rankine – Hugoniot relations [9, 60], at this situation can be written as

$$\begin{aligned} \rho_U u_U &= \rho_D u_D, \\ \rho_U u_U^2 + p_U &= \rho_D u_D^2 + p_D, \\ 2.5p_U u_U + 0.5\rho_U u_U^3 &= 2.5p_D u_D + 0.5\rho_D u_D^3, \end{aligned} \tag{3.2}$$

where the subscript U denotes the equilibrium state at upstream side, and the subscript D denotes the equilibrium state at downstream side.

The Mach number is defined as

$$\mathrm{Ma} = \frac{u_U}{a}, \tag{3.3}$$

where $a = \frac{5}{3}\sqrt{RT_U}$ is the sound speed at the upstream equilibrium state..

3.2 Numerical scheme

The numerical scheme we use is based on Mieussens's Discrete Velocity Model (DVM). We will briefly recall the main ideas of this method and give some remarks in this section and Section 4.2, and some flow diagrams of computational programs are shown in appendix A. For a complete description, please refer to [34, 41-44].

3.2.1 Introduction of explicit scheme

Any kinetic model equation for 1DSW can be written as

$$\frac{\partial f}{\partial t} + c_x \frac{\partial f}{\partial x} = \nu\left(f_{ref} - f\right), \tag{3.4}$$

where the collision frequency ν and the reference distribution function f_{ref} are different for different kinetic models.

The finite volume method is used to discretize the above equation. The space variable x is discretized on a uniform grid defined by nodes (centers of finite volumes) $x_i = (i-1)\Delta x + x_1$, $i = 1, \cdots I$, $\Delta x = \frac{L}{I}$, L is the domain width, I is the total number of position points. The microscopic velocities are discretized as (for any position point and time step t_n, they are the same)

$$c_x^{j_1} = c_{x,\min} + (j_1 - 1)\Delta c_x,\ c_x^1 = c_{x,\min},\ c_x^{J_1} = c_{x,\max},\ j_1 = 1, \cdots J_1,\ \Delta c_x = \frac{c_{x,\max} - c_{x,\min}}{J_1 - 1},$$

$$c_y^{j_2} = c_{y,\min} + (j_2 - 1)\Delta c_y,\ c_y^1 = c_{y,\min},\ c_y^{J_1} = c_{y,\max},\ j_2 = 1, \cdots J_2,\ \Delta c_y = \frac{c_{y,\max} - c_{y,\min}}{J_2 - 1},$$

$$c_z^{j_3} = c_{z,\min} + (j_3 - 1)\Delta c_z,\ c_z^1 = c_{z,\min},\ c_z^{J_3} = c_{z,\max},\ j_3 = 1, \cdots J_3,\ \Delta c_z = \frac{c_{z,\max} - c_{z,\min}}{J_3 - 1}.$$

Here for 1DSW, since the macroscopic velocity has a non-zero value only in x direction, $c_y^{j_2}$ and $c_z^{j_3}$ are chosen symmetrically, and are the same set (that is $c_{y,\min} = -c_{y,\max}$, $c_{y,(J_2+1)/2} = 0$, $c_{y,\min} = -c_{z,\min}$, $c_{z,\min} = -c_{z,\max}$), while $c_x^{j_1}$ and $c_x^{j_1} - u_{x,i}$ are not symmetric, because the macroscopic flow velocity $u_{x,i}$ varies with position. The total number of discrete velocities at one position is $J_1 J_2 J_3$. In the following description a dense notation is used where

$$f\left(x_i, t_n, c_x^{j_1}, c_y^{j_2}, c_z^{j_3}\right) = f\left(x_i, t_n, c_j\right) = f_{i,j_1,j_2,j_3}^n = f_{i,j}^n.$$

Since the microscopic velocities are discrete, not continuous, then macroscopic quantities (i.e. the moments), which are continuous integrals of f, now must be replaced by discrete sums on the velocity grid. For instance the density must be computed according to

$$\rho_i^n = \sum_{j_1=1}^{J_1}\sum_{j_2=1}^{J_2}\sum_{j_3=1}^{J_3} f_{i,j_1,j_2,j_3}^n \Delta c_x \Delta c_y \Delta c_z = \sum_{j=1}^{J} f_{i,j}^n \Delta \mathbf{c}.$$

The discretized kinetic model equation based on the above finite volume scheme is

$$f_{i,j}^{n+1} = f_{i,j}^n - \frac{\Delta t_n}{\Delta x}\left(F_{i+\frac{1}{2},j}^n - F_{i-\frac{1}{2},j}^n\right) - \Delta t_n \nu_{i,j}^n \left(f_{i,j}^n - f_{ref,i,j}^n\right), \tag{3.5}$$

where Δt_n is the time step, and the numerical fluxes are defined as

$$F_{i+\frac{1}{2},j}^n = \frac{1}{2}\left[c_x^{j_1}\left(f_{i+1,j}^n + f_{i,j}^n\right) - \left|c_x^{j_1}\right|\left(f_{i+1,j}^n - f_{i,j}^n - \psi_{i+\frac{1}{2},j}^n\right)\right], \tag{3.6}$$

which is a Helen Yee's second-order flux expression [41, 61, 62] with the flux limiter function

$$\psi_{i+\frac{1}{2},j}^n = \text{minmod}\left(f_{i,j}^n - f_{i-1,j}^n, f_{i+1,j}^n - f_{i,j}^n, f_{i+2,j}^n - f_{i+1,j}^n\right). \tag{3.7}$$

The definition of the minmod function is

$$\text{minmod}(a,b) = \begin{cases} a & ab > 0 \text{ and } |a| < |b| \\ b & ab > 0 \text{ and } |a| > |b| \\ 0 & ab < 0 \end{cases}, \text{ and } \text{minmod}(a,b,c) = \text{minmod}(\text{minmod}(a,b),c).$$

When distributions at near boundary positions, such as $f_{1,j}^{n+1}$, $f_{2,j}^{n+1}$, $f_{I-1,j}^{n+1}$ and $f_{I,j}^{n+1}$, are wanted, information about boundary conditions (such as $f_{-1,j}^n$, $f_{0,j}^n$, $f_{I+1,j}^n$, $f_{I+2,j}^n$, where

nodes $i=-1$, 0, I+1, I+2 are ghost cells beyond boundaries) are needed from the above discretized equations (Eqs. (3.5-3.7)). Since the upstream and downstream flows are at equilibrium states which do not change with time, $f^n_{-1,j}=f^n_{0,j}=f_{0,j}$ and $f^n_{I+1,j}=f^n_{I+2,j}=f_{I+1,j}$. How to obtain $f_{0,j}$ and $f_{I+1,j}$ will be discussed in section 3.2.5. An iterative technique is applied to obtain the solution at steady state, which results are what we are interested in.

3.2.2 Collision frequency

The discrete dimensionless collision frequency, corresponding to Eq. (2.17) for the continuous situation, is defined as

$$\hat{\nu}^n_{i,j}=\frac{\mu^n_i}{p^n_i}\nu^n_{i,j}, \tag{3.8}$$

The expression of $\hat{\nu}^n_{i,j}$ is different for various kinetic models. In particular,

$$\hat{\nu}^n_{BGK,i,j}=1.0 \tag{3.9}$$

for the BGK model, and

$$\hat{\nu}^n_{ES,i,j}=\frac{1}{1-b}=\mathrm{Pr}, \tag{3.10}$$

for the ES-BGK model. Recall that $-\frac{1}{2}\le b\le 1$ and that $b=-0.5$ to get Pr=2/3. For the $\nu(C)$-BGK model, and the new kinetic models I and II, $\hat{\nu}^n_{i,j}$ are not constant.

For the $\nu(C)$-BGK model, $\hat{\nu}^n_{\gamma,i,j}$ is a function with two unknown coefficients (such as Eq. (2.16) for the continuous situation), which are obtained from experimental viscosity and thermal conductivity, or one experimental transport coefficient and condition $\mathrm{Pr}=\frac{2}{3}$. There are several expressions for $\hat{\nu}(\eta)$ in [34], while in this work we only focus on

$$\hat{\nu}^n_{i,j}=a^n_i\left(1.0+\gamma^n_i\left(\eta^n_{i,j}\right)^2\right). \tag{3.11}$$

We have

$$\int_0^\infty \Psi(\eta) 4\pi\eta^2 d\eta = \iiint \Psi(\eta) d\eta_x d\eta_y d\eta_z \tag{3.12}$$

for any scalar function $\Psi(\eta)$. The left hand side in the above equation is an integral in spherical coordinates, while the right hand side in the above equation is an integral in Cartesian coordinates. Using this, it follows from Eq. (2.15) that

$$\frac{16}{15\sqrt{\pi}} \int \frac{\eta^6}{\hat{\nu}} e^{-\eta^2} d\eta = \frac{16}{15\sqrt{\pi}} \int \frac{\eta^6}{\hat{\nu}} e^{-\eta^2} \frac{1}{4\pi\eta^2} d\boldsymbol{\eta} = \frac{4}{15\pi^{3/2}} \int \frac{\eta^4}{\hat{\nu}} e^{-\eta^2} d\boldsymbol{\eta} = 1,$$

$$\frac{32}{45\sqrt{\pi}} \int \frac{\eta^4 \left(\eta^2 - 5/2\right)^2}{\hat{\nu}} e^{-\eta^2} d\eta = \frac{8}{45\pi^{3/2}} \int \frac{\eta^2 \left(\eta^2 - 5/2\right)^2}{\hat{\nu}} e^{-\eta^2} d\boldsymbol{\eta} = 1.$$

Therefore the two conditions used for the discretized $\nu(C)$-BGK model to get the two coefficients are

$$\frac{4}{15\pi^{3/2}} \sum_{j=1}^{J} \frac{\left(\eta_{i,j}^n\right)^4}{\hat{\nu}_{i,j}^n} \cdot \exp\left(-\left(\eta_{i,j}^n\right)^2\right) \Delta\boldsymbol{\eta}_{i,j}^n = 1, \tag{3.13}$$

$$\frac{8}{45\pi^{3/2}} \sum_{j=1}^{J} \frac{\left(\eta_{i,j}^n\right)^2 \left(\left(\eta_{i,j}^n\right)^2 - 5/2\right)^2}{\hat{\nu}_{i,j}^n} \cdot \exp\left(-\left(\eta_{i,j}^n\right)^2\right) \Delta\boldsymbol{\eta}_{i,j}^n = 1,$$

where $\Delta\boldsymbol{\eta}_{i,j}^n = \Delta\eta_{i,j_1}^n \Delta\eta_{i,j_2}^n \Delta\eta_{i,j_3}^n = \dfrac{\Delta \mathbf{c}}{\left(2RT_i^n\right)^{3/2}}$. These two conditions are solved by the Newton–Raphson (N-R) algorithm [63] (also known as the steepest descent technique [64], or as Newton method with a backtracking linesearch [65]) in this work, the flow chart for this method to obtain two coefficients is similar to Figure A.1 in Appendix A.

For the new kinetic models I and II, from Eq. (2.28-2.31), we have the following expression for discrete situation,

$$\hat{\nu}\left(n, \eta_{i,j}^n\right) = \frac{1}{1-b} \frac{16}{15\sqrt{\pi}} \cdot A(n) \cdot B\left(n, \eta_{i,j}^n\right), \tag{3.14}$$

with

$$A(n) = \sum_{j=1}^{J} \frac{\left(\eta_{i,j}^n\right)^4 \exp\left(-\left(\eta_{i,j}^n\right)^2\right)}{4\pi B\left(n, \eta_{i,j}^n\right)} \Delta\boldsymbol{\eta}_{i,j}^n,$$[8]

[8] In the derivation, Eq. (3.12) need be used.

$$B(n,\eta_{i,j}^n)=\int_{\xi=0}^{\infty}\frac{\xi e^{-\xi^2}}{\eta_{i,j}^n}\left[\left(\xi+\eta_{i,j}^n\right)^{\frac{3n-7}{n-1}}-\left|\xi-\eta_{i,j}^n\right|^{\frac{3n-7}{n-1}}\right]d\xi.$$

For Maxwell molecules where $n=5$,

$$\hat{\nu}\left(n=5,\eta_{i,j}^n\right)=\frac{1}{1-b}$$

and for hard sphere molecules where $n=\infty$,

$$\hat{\nu}\left(n=\infty,\eta_{i,j}^n\right)=\frac{1}{1-b}\frac{8}{15\sqrt{\pi}}\cdot A(n=\infty)\cdot B(n=\infty,\eta_{i,j}^n=0.0)\left\{\exp\left(-\left(\eta_{i,j}^n\right)^2\right)+\frac{\sqrt{\pi}}{2}\left(\frac{1}{\eta_{i,j}^n}+2\eta_{i,j}^n\right)erf\left(\eta_{i,j}^n\right)\right\},$$

with $A(n=\infty)=0.308855$, $B(n=\infty,\eta_{i,j}^n=0.0)=3.0$, and $erf\left(\eta_{i,j}^n\right)$ is the error function. After some numerical calculation, it is found that $\Pr\cong 2/3$ is indeed satisfied in the discrete situation as well as the continuous situation for the new kinetic models and all test cases we did.

3.2.3 Reference distribution $f_{ref,i,j}^n$ (original)

The main feature of Mieussens's DVM is that the reference distribution function f_{ref} is not discretized directly, but determined by the minimum entropy principle (Therefore, the values of coefficients in the discrete reference distribution are not identical to them in continuous situation, such as $\gamma_{BGK,i}^n\neq 0.0$ in the following Eq. (3.16) for the BGK model, while it is zero in the continuous situation). Coefficients in the reference distribution $f_{ref,i,j}^n$ of all kinetic models (e.g. Γ in Eq. (2.13)) are obtained through the N–R algorithm in this work. A nonlinear system is easier and more robust to be solved when magnitudes of the equations are the same, therefore dimensionless quantities are used in the program. Expressions of Jacobians used in the N-R algorithm are given in Appendix B. The dimensionless reference distribution $F_{ref,i,j}^n$ is defined such that

$$f_{ref,i,j}^n=F_{ref,i,j}^n\frac{\rho_i^n}{\Delta \mathbf{c}}. \tag{3.15}$$

For the BGK model, the dimensionless reference distribution is

$$F^n_{BGK,i,j} = \frac{f^n_{BGK,i,j}\Delta\mathbf{c}}{\rho^n_i} = a^n_{BGK,i} \cdot \exp\left(-\Gamma^n_{BGK,i}\left(\eta^n_{i,j}\right)^2 + \gamma^n_{BGK,i}\eta^n_{i,j_1}\right), \tag{3.16}$$

and the conditions to determine the three coefficients ($a^n_{BGK,i}$, $\Gamma^n_{BGK,i}$ and $\gamma^n_{BGK,i}$) are the conservation laws Eq. (1.4), which is given in the discrete case as

$$\sum_{j=1}^{J} F^n_{BGK,i,j} = 1,\ \sum_{j=1}^{J} \eta^n_{i,j_1} F^n_{BGK,i,j} = 0,\ \sum_{j=1}^{J} \frac{\left(\eta^n_{i,j}\right)^2}{1.5} F^n_{BGK,i,j} = 1. \tag{3.17}$$

For the ES-BGK model, the dimensionless reference distribution is

$$F^n_{ES,i,j} = a^n_{ES,i} \cdot \exp\left(-\Gamma^n_{ES,xx,i}\left(\eta^n_{i,j_1}\right)^2 - \Gamma^n_{ES,yy,i}\left(\left(\eta^n_{i,j_2}\right)^2 + \left(\eta^n_{i,j_3}\right)^2\right) + \gamma^n_{ES,i}\eta^n_{i,j_1}\right), \tag{3.18}$$

and the conditions to determine the four coefficients are the discrete form of Eq. (2.12),

$$\sum_{j=1}^{J} F^n_{ES,i,j} = 1, \quad \sum_{j=1}^{J} \eta^n_{i,j_1} F^n_{ES,i,j} = 0,$$

$$\sum_{j=1}^{J} \left(\eta^n_{i,j_1}\right)^2 F^n_{ES,i,j} = \frac{\lambda^n_{xx,i}}{2RT^n_i} = \frac{1}{2p^n_i}\left(\frac{p^n_{BGK,xx,i}}{\mathrm{Pr}} + \left(1 - \frac{1}{\mathrm{Pr}}\right)p^n_{xx,i}\right),$$

$$\sum_{j=1}^{J} \left(\eta^n_{i,j_1}\right)^2 F^n_{ES,i,j} = \frac{\lambda^n_{yy,i}}{2RT^n_i} = \frac{1}{2p^n_i}\left(\frac{p^n_{BGK,yy,i}}{\mathrm{Pr}} + \left(1 - \frac{1}{\mathrm{Pr}}\right)p^n_{yy,i}\right). \tag{3.19}$$

Here we have used the abbreviations $p^n_{BGK,xx,i} = \sum_{j=1}^{J}\left(C^n_{x,i}\right)^2 f^n_{BGK,i,j}\Delta\mathbf{c}$ and $p^n_{BGK,yy,i} = \sum_{j=1}^{J}\left(C^n_{y,i}\right)^2 f^n_{BGK,i,j}\Delta\mathbf{c}$, which are pressure tensor components computed with the reference distribution function of the BGK model. Since the macroscopic flow velocity $u^n_{x,i}$ varies with position and time step, the discrete velocity set ($c_{x,i}$ and $C^n_{x,i}$) has a lack of symmetry, so that $p^n_{BGK,xx,i}$ is not exactly the same as $p^n_{BGK,yy,i}$ or p^n_i (Note: computational results show that their values are very close to each other). Using Eq. (3.19) as conditions to determine coefficients can ensure the discrete collision operator is zero (means at equilibrium state) if and only if $f^n_{i,j} = f^n_{BGK,i,j}$ [42].

For the $\nu(C)$-BGK model, the dimensionless reference distribution is

$$F^n_{\gamma,i,j} = a^n_{\gamma,i} \cdot \exp\left(-\Gamma^n_{\gamma,i}\left(\eta^n_{i,j}\right)^2 + \gamma^n_{\gamma,i}\eta^n_{i,j_1}\right), \tag{3.20}$$

and the conditions to determine the three coefficients are the discrete form of Eq. (1.4),

$$\sum_{j=1}^{J} \hat{v}^n_{i,j} \frac{\left(f^n_{\gamma,i,j} - f^n_{i,j}\right)}{\rho^n_i} \Delta\mathbf{c} = 0, \ \sum_{j=1}^{J} \hat{v}^n_{i,j}\eta^n_{i,j_1} \frac{\left(f^n_{\gamma,i,j} - f^n_{i,j}\right)}{\rho^n_i} \Delta\mathbf{c} = 0,$$

$$\sum_{j=1}^{J} \hat{v}^n_{i,j}\left(\eta^n_{i,j}\right)^2 \frac{\left(f^n_{\gamma,i,j} - f^n_{i,j}\right)}{\rho^n_i} \Delta\mathbf{c} = 0. \tag{3.21}$$

For the new kinetic model I, the dimensionless reference distribution is

$$F^n_{NI,i,j} = a^n_{NI,i} \cdot \exp\left(-\Gamma^n_{NI,i}\left(\Gamma^n_{ES,xx,i}\left(\eta^n_{i,j_1}\right)^2 + \Gamma^n_{ES,yy,i}\left(\left(\eta^n_{i,j_2}\right)^2 + \left(\eta^n_{i,j_3}\right)^2\right)\right) + \gamma^n_{NI,i}\eta^n_{i,j_1}\right), \tag{3.22}$$

and the conditions to determine the three coefficients are the discrete form of Eq. (1.4)

$$\sum_{j=1}^{J} \hat{v}^n_{i,j} \frac{\left(f^n_{NI,i,j} - f^n_{i,j}\right)}{\rho^n_i} \Delta\mathbf{c} = 0, \ \sum_{j=1}^{J} \hat{v}^n_{i,j}\eta^n_{i,j_1} \frac{\left(f^n_{NI,i,j} - f^n_{i,j}\right)}{\rho^n_i} \Delta\mathbf{c} = 0,$$

$$\sum_{j=1}^{J} \hat{v}^n_{i,j}\left(\eta^n_{i,j}\right)^2 \frac{\left(f^n_{NI,i,j} - f^n_{i,j}\right)}{\rho^n_i} \Delta\mathbf{c} = 0. \tag{3.23}$$

For the new kinetic model II, the dimensionless reference distribution is

$$F^n_{NII,i,j} = a^n_{NII,i} \cdot \exp\left(-\Gamma^n_{NII,xx,i}\left(\eta^n_{i,j_1}\right)^2 - \Gamma^n_{NII,yy,i}\left(\left(\eta^n_{i,j_2}\right)^2 + \left(\eta^n_{i,j_3}\right)^2\right) + \gamma^n_{NII,i}\eta^n_{i,j_1}\right), \tag{3.24}$$

and the conditions to determine the four coefficients are the discrete form of Eq. (2.39),

$$\sum_{j=1}^{J} \hat{v}^n_{i,j} \frac{\left(f^n_{NII,i,j} - f^n_{i,j}\right)}{\rho^n_i} \Delta\mathbf{c} = 0, \ \sum_{j=1}^{J} \hat{v}^n_{i,j}\eta^n_{i,j_1} \frac{\left(f^n_{NII,i,j} - f^n_{i,j}\right)}{\rho^n_i} \Delta\mathbf{c} = 0,$$

$$\sum_{j=1}^{J} \hat{v}^n_{i,j}\left(\eta^n_{i,j_1}\right)^2 \frac{\left(f^n_{NII,i,j} - f^n_{i,j}\right)}{\rho^n_i} \Delta\mathbf{c} = \frac{\left(p^n_{BGK,xx,i} - p^n_{xx,i}\right)}{2p^n_i}, \tag{3.25}$$

$$\sum_{j=1}^{J} \hat{v}^n_{i,j}\left(\eta^n_{i,j_2}\right)^2 \frac{\left(f^n_{NII,i,j} - f^n_{i,j}\right)}{\rho^n_i} \Delta\mathbf{c} = \frac{\left(p^n_{BGK,yy,i} - p^n_{yy,i}\right)}{2p^n_i}.$$

3.2.4 Reference distribution $f^n_{ref,i,j}$ (linearized)

As we see from the above section, equations to determine coefficients in the reference distribution $f^n_{ref,i,j}$ form a nonlinear system, and the N-R algorithm (or some other non-linear solver) is needed to solve the equations. This makes computation program complex and requires a considerable amount of computational time.

In order to simplify the program and save computational time, and simultaneously get almost the same results, the author proposes to use linearized reference distributions $f^n_{ref,i,j}$, instead of the original non-linear functions $f^n_{ref,i,j}$ in the program. If this is done, the unknown coefficients follow from a linear system of equations, which can be solved much faster. The reference distributions are expanded around the Maxwellian distribution, and the expressions of linearized dimensionless reference distributions are given in the following, while the corresponding linear equations can be found in Appendix C.

For the BGK model, the linearized dimensionless reference distribution is

$$F^n_{BGK,i,j} = \exp\left(-\left(\eta^n_{i,j}\right)^2\right)\left(a1^n_{BGk,i} + a2^n_{BGK,i}\eta^n_{i,j_1} + a3^n_{BGK,i}\left(\eta^n_{i,j}\right)^2\right). \tag{3.26}$$

For the ES-BGK model, the linearized dimensionless reference distribution is

$$F^n_{ES,i,j} = \exp\left(-\left(\eta^n_{i,j}\right)^2\right)\cdot\left(a1^n_{ES,i} + a2^n_{ES,i}\eta^n_{i,j_1} + a3^n_{ES,i}\left(\eta^n_{i,j_1}\right)^2 + a4^n_{ES,i}\left(\left(\eta^n_{i,j_2}\right)^2 + \left(\eta^n_{i,j_3}\right)^2\right)\right), \tag{3.27}$$

and this choice makes results of the ES-BGK model with linearized $f^n_{ref,i,j}$ and $b=0$ identical to results of the BGK model with linearized $f^n_{ref,i,j}$.

For the $\nu(C)$-BGK model, the linearized dimensionless reference distribution is

$$F^n_{\gamma,i,j} = \exp\left(-\left(\eta^n_{i,j}\right)^2\right)\cdot\left(a1^n_{\gamma,i} + a2^n_{\gamma,i}\eta^n_{i,j_1} + a3^n_{\gamma,i}\left(\eta^n_{i,j}\right)^2\right). \tag{3.28}$$

For the new kinetic model I, the linearized dimensionless reference distribution is

$$F^n_{NI,i,j} = \exp\left(-\left(\eta^n_{i,j}\right)^2\right)\cdot\left(a1^n_{NI,i} + a2^n_{NI,i}\eta^n_{i,j_1} + a3^n_{NI,i}\left(a3^n_{ES,i}\left(\eta^n_{i,j_1}\right)^2 + a4^n_{ES,i}\left(\left(\eta^n_{i,j_2}\right)^2 + \left(\eta^n_{i,j_3}\right)^2\right)\right)\right). \tag{3.29}$$

For the new kinetic model II, the linearized dimensionless reference distribution is

$$F^n_{NII,i,j} = \exp\left(-\left(\eta^n_{i,j}\right)^2\right)\cdot\left(a1^n_{NII,i} + a2^n_{NII,i}\eta^n_{i,j_1} + a3^n_{NII,i}\left(\eta^n_{i,j_1}\right)^2 + a4^n_{NII,i}\left(\left(\eta^n_{i,j_2}\right)^2 + \left(\eta^n_{i,j_3}\right)^2\right)\right). \quad (3.30)$$

In the above, the reference distributions are expanded around the Maxwellian distribution, which is an isotropic Gaussian distribution. For the ES-BGK model, and the new kinetic models, in which an anisotropic Gaussian distribution is used in the original reference distribution, there is another way to build their linearized reference distribution, which is expanding their original reference distribution around an anisotropic Gaussian distribution. This choice is supposed to give better results than the first one, for the isotropic Gaussian distribution in the expression of first choice (Eq. (3.27)) is in fact a linear approximate expression of the anisotropic Gaussian distribution in Eq. (3.31). If we consider the discrete reference distribution at limiting situation (bounds of velocity grid approach to infinite and step of velocity grid approaches to zero), then we can recover the continuous reference distribution Eq. (2.9) from discrete reference distribution Eq. (3.18) or Eq. (3.31), but can not from Eq. (3.27). This is another reason why the second type linearized reference distribution is supposed to be better than the first type.

Following this idea, the second type linearized reference distribution for the ES-BGK model is

$$\begin{aligned} F^n_{ES,i,j} = \exp&\left(-\varepsilon^n_{ES,xx,i}\left(\eta^n_{i,j_1}\right)^2 - \varepsilon^n_{ES,yy,i}\left(\left(\eta^n_{i,j_2}\right)^2 + \left(\eta^n_{i,j_3}\right)^2\right)\right)\cdot \\ &\left(a1^n_{ES,i} + a2^n_{ES,i}\eta^n_{i,j_1} + a3^n_{ES,i}\left(\eta^n_{i,j_1}\right)^2 + a4^n_{ES,i}\left(\left(\eta^n_{i,j_2}\right)^2 + \left(\eta^n_{i,j_3}\right)^2\right)\right), \end{aligned} \quad (3.31)$$

where

$$\varepsilon^n_{ES,xx,i} = \frac{p^n_i}{\frac{p^n_{BGK,xx,i}}{\mathrm{Pr}} + \left(1-\frac{1}{\mathrm{Pr}}\right)p^n_{xx,i}} \text{ and } \varepsilon^n_{ES,yy,i} = \frac{p^n_i}{\frac{p^n_{BGK,yy,i}}{\mathrm{Pr}} + \left(1-\frac{1}{\mathrm{Pr}}\right)p^n_{yy,i}},$$

which are obtained from Eq. (3.19), are the discrete values of the dimensionless coefficient $\varepsilon_{ij}RT$ in the ES-BGK model. Because of the lack of symmetry of the discrete velocity set ($c_{x,i}$ and $C^n_{x,i}$), $p^n_{BGK,xx,i}$ is not exactly the same as $p^n_{BGK,yy,i}$ or p^n_i [42],

results from this for $b=0$ are not exactly the same as (but very close to) results from the BGK model with linearized reference distribution.

The second type linearized reference distribution for the new kinetic model I from the above idea is

$$F^n_{NI,i,j} = \exp\left(-\varepsilon^n_{ES,xx,i}\left(\eta^n_{i,j_1}\right)^2 - \varepsilon^n_{ES,yy,i}\left(\left(\eta^n_{i,j_2}\right)^2 + \left(\eta^n_{i,j_3}\right)^2\right)\right)\cdot \left(a1^n_{NI,i} + a2^n_{NI,i}\eta^n_{i,j_1} + a3^n_{NI,i}\left(a3^n_{ES,i}\left(\eta^n_{i,j_1}\right)^2 + a4^n_{ES,i}\left(\left(\eta^n_{i,j_2}\right)^2 + \left(\eta^n_{i,j_3}\right)^2\right)\right)\right)\cdot \tag{3.32}$$

The second type linearized reference distribution for the new kinetic model II from the above idea is

$$F^n_{NII,i,j} = \exp\left(-\varepsilon^n_{ES,xx,i}\left(\eta^n_{i,j_1}\right)^2 - \varepsilon^n_{ES,yy,i}\left(\left(\eta^n_{i,j_2}\right)^2 + \left(\eta^n_{i,j_3}\right)^2\right)\right)\cdot \left(a1^n_{NII,i} + a2^n_{NII,i}\eta^n_{i,j_1} + a3^n_{NII,i}\left(\eta^n_{i,j_1}\right)^2 + a4^n_{NII,i}\left(\left(\eta^n_{i,j_2}\right)^2 + \left(\eta^n_{i,j_3}\right)^2\right)\right)\cdot \tag{3.33}$$

3.2.5 Boundary conditions and initial guess

As described in the last paragraph of Section 3.2.1, the boundary conditions used for 1DSW are $f_{0,j}$ and $f_{I+1,j}$, which are the discrete equilibrium distribution (same expression as the reference distribution in the BGK model, which is Eqs. (3.15-3.16)) at the upstream and downstream sides. First, $f_{0,j}$ is obtained from the upstream values of density, velocity and temperature, which are given parameters, through the same idea as how to obtain the $f^n_{BGK,i,j}$. Then the three constant fluxes of mass, momentum, and energy, which are $M_0 = \sum_{j=1}^{J} c_x^{j_1} f_{0,j}\Delta\mathbf{c}$, $MF_0 = \sum_{j=1}^{J}\left(c_x^{j_1}\right)^2 f_{0,j}\Delta\mathbf{c}$, and $EF_0 = \frac{1}{2}\sum_{j=1}^{J} c_x^{j_1} c^2 f_{0,j}\Delta\mathbf{c}$, at the upstream side are computed from $f_{0,j}$. Then we compute the downstream mass flux (or say momentum) $M_{I+1} = M_0$, momentum flux $MF_{I+1} = MF_0$, and energy flux $EF_{I+1} = EF_0$, which correspond to the Rankine-Hugoniot relations Eq. (3.2). Last step is to compute the discrete equilibrium distribution at the

downstream side $f_{I+1,j}$ from the above three moments. In the program, the dimensionless distribution $F_{I+1,j}$ (which is not the same as Eq. (3.16)) is introduced,

$$F_{I+1,j} = f_{I+1,j}\Delta \mathbf{c} = a_{I+1} \cdot \exp\left(-\Gamma_{I+1}\left(\eta_{I+1,j}\right)^2 + \gamma_{I+1}\eta_{I+1,j}\right), \tag{3.34}$$

and the conditions to determine the three coefficients are

$$\frac{\sum_{j=1}^{J} c_x^{j_1} F_{I+1,j}}{M_{I+1}} = 1, \quad \frac{\sum_{j=1}^{J} \left(c_x^{j_1}\right)^2 F_{I+1,j}}{MF_{I+1}} = 1, \quad \frac{\sum_{j=1}^{J} c_x^{j_1} c^2 F_{I+1,j}}{2EF_{I+1}} = 1. \tag{3.35}$$

The same procedure was also used by Mieussens in his work [66]. Note that this approach to get $f_{I+1,j}$ guarantees conservation of fluxes at the discrete level, while downstream density ρ_{I+1}, velocity u_{I+1} and temperature T_{I+1} obtained from this way would be a little different from their values from the Rankine- Hugoniot relations at the continuous situation directly.

The shock wave is computed through time-stepping into steady state, and in the program, the initial guess $f_{i,j}^1$ is a step function, which is built by $f_{0,j}$ and $f_{I+1,j}$ with the jump occurring in the middle of the computational domain.

3.2.6 Time step, space grid and velocity grid

Since an explicit scheme is used, the time step Δt_n is limited by the CFL condition [41, 43]

$$\Delta t_n = \frac{a}{\max_{i,j}\left(\nu_{i,j}^n\right) + \max_{i,j_1}\left(\frac{\left|c_x^{j_1}\right|}{\Delta x}\right)}, \tag{3.36}$$

where $0 < a < 1.0$. In the program of this work, $a = 0.99$ is used. This restriction does not need to be applied if the implicit scheme of Mieussens's DVM [34, 41-44][9] is adopted. From Eq. (3.36), we know when the step of space grid Δx decreases, or bounds of velocity grid increases, the time step will decrease. If the time to reach steady state for

[9] The implicit scheme used by L. Mieussens in fact is not a fully implicit scheme, for the collision frequency used is still the value computed from previous time step.

certain kinetic model at certain flow situation is thought as a fixed number, then decrease Δx or increase bounds of velocity grid means more iteration steps are needed to reach steady state, and at the same time more computational time is needed for each iteration. Therefore, in the computation, large Δx and small bounds of velocity grid are preferred. For different kinetic models at the same flow situation, $\max_{i,j}\left(\nu_{i,j}^{n}\right)$, and further the time step Δt_n, would be different.

Since we wish to resolve the flow structure at the microscopic level, the step of space grid Δx should be much smaller than the mean free path (compute estimated value from boundary or initial conditions), which is the standard for choosing the number of position nodes in this work.

We follow Mieussens choice[10] for bounds and step of velocity grid, by choosing

$$\begin{aligned}
&c_{x,\min} \le \mathrm{Min}\left(u_{x,i} - 4\sqrt{RT_i}\right), \quad c_{x,\max} \ge \mathrm{Max}\left(u_{x,i} + 4\sqrt{RT_i}\right), \quad \Delta c_x \le \mathrm{Min}\left(\sqrt{RT_i}\right), \\
&c_{y,\min} \le \mathrm{Min}\left(u_{y,i} - 4\sqrt{RT_i}\right), \quad c_{x,\max} \ge \mathrm{Max}\left(u_{y,i} + 4\sqrt{RT_i}\right), \quad \Delta c_y \le \mathrm{Min}\left(\sqrt{RT_i}\right), \\
&c_{z,\min} \le \mathrm{Min}\left(u_{z,i} - 4\sqrt{RT_i}\right), \; c_{z,\max} \ge \mathrm{Max}\left(u_{z,i} + 4\sqrt{RT_i}\right), \; \Delta c_z \le \mathrm{Min}\left(\sqrt{RT_i}\right).
\end{aligned} \tag{3.37}$$

If the values at the boundaries of velocity and temperature are only known before the computation, then $i = 0, I+1$ in Eq. (3.37). If there were some results for the same problem from another computation (such as the NSF equations) before your computation, then $i = 0,1,...,I,I+1$ in Eq. (3.37) is suggested.

The above rules for time step, step of space grid, bounds and step of velocity grid are applied in the numerical tests in this chapter and Chapter 4. In order to study the influence of step of space grid, bounds and step of velocity grid on computational results, some tests with smaller step of space grid, larger bounds of velocity grid and smaller step of velocity grid have been done for comparison.

---

[10] In fact, Mieussens did not follow this choice strictly in his work (e.g. test case 1 in [42]), and explains this by saying "I tried a coarser velocity grid, an since the results where good as compared to DSMC, I stopped there." [66].

3.3 Test examples

One situation for weak shock wave (Ma=1.5), one for medium shock wave (Ma=3.0), and one for strong shock wave (Ma=6.0) have been tested, which are shown in Table 3.1. Table 3.2 shows the parameters used in the numerical tests of kinetic models. Cases 3.1-3.3 in Table 3.2 corresponds to the three situations in Table 3.1, and cases 3.4-3.7 are tested in order to see the effect of step of space grid, and cases 3.8-3.9 are tested in order to see the effect of bounds and step of velocity grid. In the tests, width of finite volume cell, bounds and number of discrete velocities are chosen following the description in Section 3.2.6. For each case in Table 3.2, the BGK model, the ES-BGK model with $b=-0.5$, the $\nu(C)$-BGK model with Eq. (3.11) as collision frequency, the new kinetic model I with $b=-0.5$, and the new kinetic model II with Pr=2/3 are tested. For each kinetic model, both original and linearized f_{ref} are applied in cases 3.1-3.7, while only original f_{ref} is applied in cases 3.8-3.9. Cases 3.8-3.9 are done much later than cases 3.1-3.7, and in order to save computational time, smaller number of iterations is used. The discussion in Section 3.4.2 shows the reason why we can choose smaller iteration number than the value in cases 3.1-3.6 in computation. Table 3.3 shows some common parameters used in the numerical tests of DSMC [67].

Table 3.1: Situations of numerical tests of kinetic models and DSMC for 1DSW

Situation	Mach Number	Upstream velocity (m)
Sa	1.5	1116.25
Sb	3.0	2232.5
Sc	6.0	4465.0

There are some common parameters in the numerical tests, which are: hard sphere molecules; material is Helium; upstream temperature is 160.0 K; upstream number density n is 2.889E21 1/m^3, viscosity at the reference temperature μ_0 is 1.86E-5 kg/m·s; reference temperature T_0 is 273.0 K [68]; Boltzmann's constant k is 1.381E-23 J/K; Avogadro's number N is 6.022E23 1/mol [60]; molecular mass of Helium m is 4.003

g/mol [69]. Mean free path at upstream side l is 1.287 mm, based on Cercignani's definition [1, 31, 67, 70][11]

$$l = \mu \frac{\sqrt{\frac{kT}{m}}}{nkT} \tag{3.38}$$

Table 3.2: Parameters in the numerical tests of kinetic models for 1DSW

Case	Situation	Domain width (m)	Running Iteration	Number of cells	$l/\Delta x$ [1]	Number of velocities	Bounds of velocities (m/s)	
							X1 direction	X2 (or X3)
3.1	Sa	0.04	80000	100	3.2	12*11*11	-2300, 3600	-2900, 2900
3.2	Sb	0.04	80000	100	3.2	18*17*17	-3800, 5500	-4500, 4500
3.3	Sc	0.04	40000 or 80000	100	3.2	32*30*30	-7000, 10100	-8100, 8100
3.4	Sa	0.04	80000	200	6.4	12*11*11	-2300, 3600	-2900, 2900
3.5	Sb	0.02	80000	100	6.4	18*17*17	-3800, 5500	-4500, 4500
3.6	Sc	0.02	40000 or 80000	100	6.4	32*30*30	-7000, 10100	-8100, 8100
3.7	Sb	0.02	80000	200	12.8	18*17*17	-3800, 5500	-4500, 4500
3.8	Sa	0.04	24000	100	3.2	22*21*21	-2300, 3600	-2900, 2900
3.9	Sa	0.04	24000	100	3.2	15*14*14	-3040, 4340	-3690, 3690

Note 1: mean free path use its value at upstream.

Table 3.3: Some common parameters in the numerical tests of DSMC for 1DSW

Parameter	Meaning	Value
FNUM	Number of real molecules represented by each simulated molecule	1.4445E15
MNM	Maximum number of simulator molecules	5E6
DTM (s)	Time step over which the movement and collision steps are uncoupled	1E-7
NIS	Number of time steps between samples	4
NSP	Number of samples between file updates	20
NPS	Number of updates to reach steady flow	100
NPT	Number of file updates to completion	20000
SP(1,1) (m)	Reference molecular diameter	2.19E-10
SP(3,1)	Viscosity-temperature index	0.5
SP(4,1)	The reciprocal of the VSS scattering parameter	1.0
SP(5,1) (kg)	Molecular mass	6.65E-27
MNC	Maximum number of cells	400
MNSC	Maximum number of sub cells	4000
SXB (m)	x-coordinates of the domain limit at upstream side	-0.02
DXB	x-coordinates of the domain limit at downstream side	0.02

3.4 Results and discussion

3.4.1 Some important notes on dealing with results

Since the explicit scheme is used, and the time step of each iteration is very small (its magnitude is 1.D-7 seconds from the computational results), the difference between two

[11] Here, we omit the coefficient $\sqrt{\pi}/2 \approx 1.25$.

adjacent iterations will be very small. Therefore, it is not too informative to show the convergence of results from the difference of macroscopic parameters between two adjacent iterations. Another issue is that it is the first time for us to run such kind of program, and we want to know the long running behavior of program, such as stability. Therefore, what we do is to let the program run a large number of iterations for each computation, and output the values of macroscopic parameters five times during each computation which are chosen as the iterations after 1/5, 2/5, 3/5, 4/5 and 5/5 of the whole iteration number, and then check the convergence from these outputs.

From the results, if one compares data based on an fixed position, the values of macroscopic parameters are found to change slowly, and there is some movement of the whole shock wave structure; but if one compares data after some shifting such that the point, where the density has the average value between its values at upstream and downstream, is fixed in the comparison, the values of macroscopic parameters are found to remain after some iteration, which means convergence is reached. That is to say, the whole shock wave structure is moving slowly along the x direction during the computation, while the shape remains unchanged after some time. For larger Mach numbers, this computational phenomenon becomes more apparent. As an example, Figure 3.1 shows density profiles at different iterations in case 3.3 computed with the BGK model, before and after the shifting.

Another issue found from the results is that even if the initial guess is the same for all kinetic models, the final location of the shock wave structure within the computational domain from computation using different kinetic models will not be the same. As an example, Figure 3.2 shows the final density profiles from the BGK model and the ES-BGK model in case 3.2 before and after the shifting.

The above two issues happen because there is no fixed coordinate label for the shock profile inherent to the problem [1, 34]. In order to make a fair comparison, all data will be analyzed only after the shifting, for the two reasons mentioned above. After shifting, the origin point $x=0$ in the new Cartesian frame is some special point, which would be the

point where the density takes on the arithmetic mean of the downstream and upstream values [1], or where the derivative of density takes on the maximum value [1], or where is defined by the following relation [34]

$$\int_{x_U}^{x^*}(\rho(x)-\rho_U)dx=\int_{x^*}^{x_D}(\rho_D-\rho(x))dx, \tag{3.39}$$

where subscript U means the upstream state, subscript D means downstream state, and the point x^* (which is called "equal area point" in [34]) is the new origin point. The above first and third ways for shifting has been applied by the author, and the results are found to be very similar.

Since the step of space grid Δx for same Mach number in different computation case would be different (such as for Ma=3.0, Δx in case 3.2 is not same value as it in case 3.5.), in order to do comparison, linear interpolation technology has been used to make Δx in each case for same Mach number is the same as the value used in the DSMC computation. Another reason using linear interpolation to add some nodes in results is to make the density at the new origin point meet the shifting condition in the above paragraph better.

In this chapter, all graphs and data are based on the first way of shifting, which means the new origin point is where the density is the mean value of its values at upstream and downstream, and the linear interpolation, which makes Δx in each case for same Mach number is the same as the value used in the DSMC computation.

In the discussion, the average relative error of some macroscopic parameters is often used, which is defined as

$$\overline{\Delta\varphi}=\frac{\sum_{i=1}^{I_{com}}\left|\frac{\varphi 1_i-\varphi 2_i}{\varphi 2_i}\right|}{I_{com}}, \tag{3.40}$$

where φ means the macroscopic parameter considered (in 1DSW, it would be density ρ, velocity u_1, temperature T, pressure p, trace-free pressure tensor element σ_{11} and σ_{22},

and heat flux q_1 [12]), $\varphi 1$ means the values of the macroscopic parameter considered at situation 1, $\varphi 2$ means the values of the macroscopic parameter considered at situation 2, subscript i denotes the position point, I_{com} means the total number of position points used in comparison (which might be not same as the number of cells in the DMSC, for the shifting makes the common domain part of two compared situations smaller than the original domain size), $\overline{\Delta\varphi}$ is the average relative error, which means the average value of the absolute value of relative errors of the macroscopic parameter considered at two situations for the position points considered.

Since relative error becomes meaningless when a quantity approaches zero, and the values of σ_{11}, σ_{22}, and q_1 near or at upstream and downstream states are near zero (e.g. see graphs (e-g) in Figures 3.7-3.9), then how to choose a domain to compute the average relative error of σ_{11}, σ_{22}, and q_1 is hard to decide. Therefore, the average relative error of σ_{11}, σ_{22}, and q_1 are not considered here, and when average relative error is mentioned in the description, we always mean the average relative error for ρ, u_1, T and p, not specific one parameter.

During the analysis of the computational results, two steps have been done for each kind of analysis (such as convergence and stability, effect of cell width, effect of linearized f_{ref}, effect of bounds and step of velocity grid, comparison among kinetic models and DSMC). The first step is to graph the output of one macroscopic parameter from different situations in one figure. The second step is to compute the average relative errors of macroscopic parameters. From these two steps, we can discuss how much difference the results obtained from two different situations[13].

---

[12] For 1DSW, other basic moments are equal to zero (such as u_2, u_3 q_2, q_3), or are related to these basic moments (such as $\sigma_{33} = \sigma_{22}$, $p_{33} = p_{22} = p + \sigma_{22}$, $p_{11} = p + \sigma_{11}$).

[13] Graphs and data from these two steps are too many to be shown in this thesis. If interested in graphs and data which are not shown, contact the author (or his supervisor) for them.

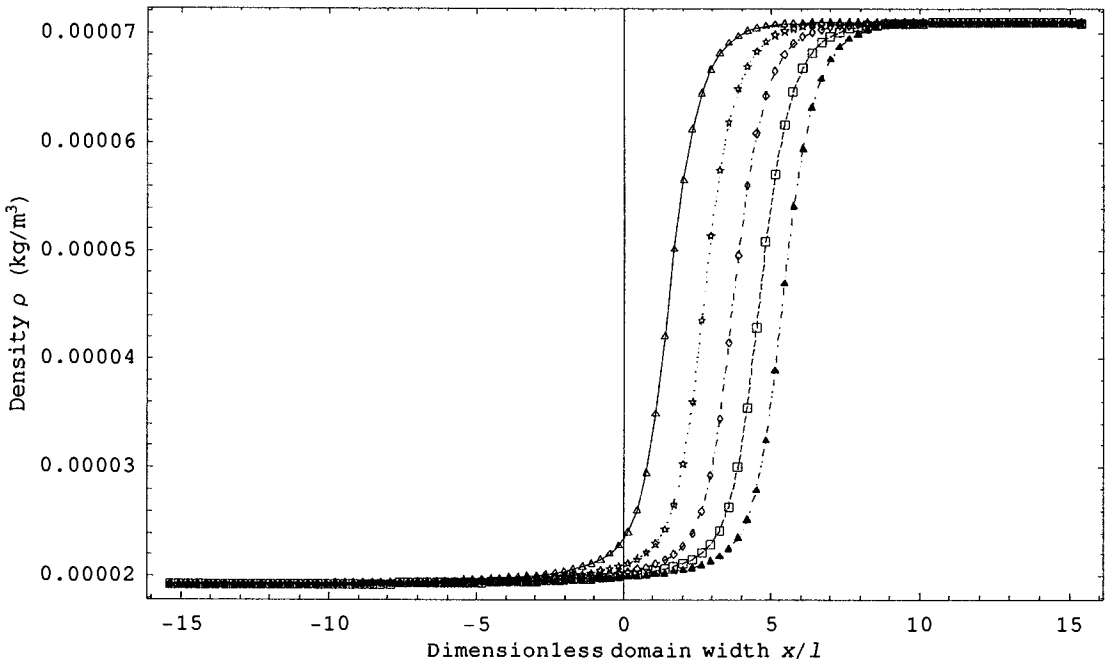

(a) Before shifting

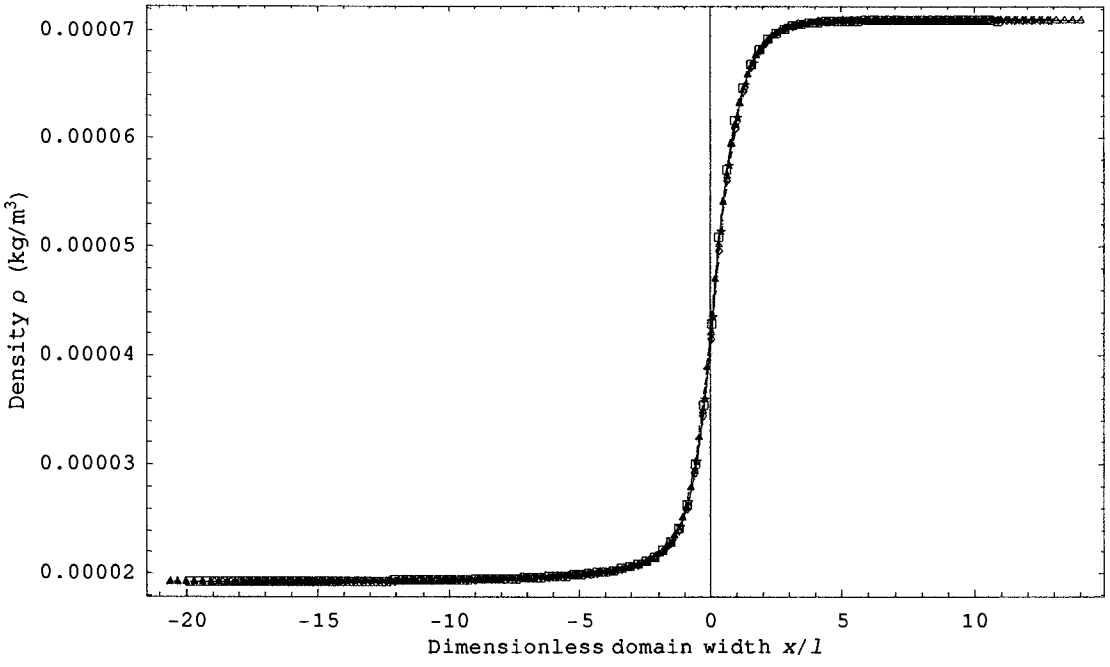

(b) After Shifting

Figure 3.1: Density profiles at five certain iterations (BGK model, case 3.3: Ma=6.0) (Triangle for Iteration=16000, Star for Iteration=32000, Diamond for Iteration=48000, Box for Iteration=64000, Triangle filled for Iteration=80000)

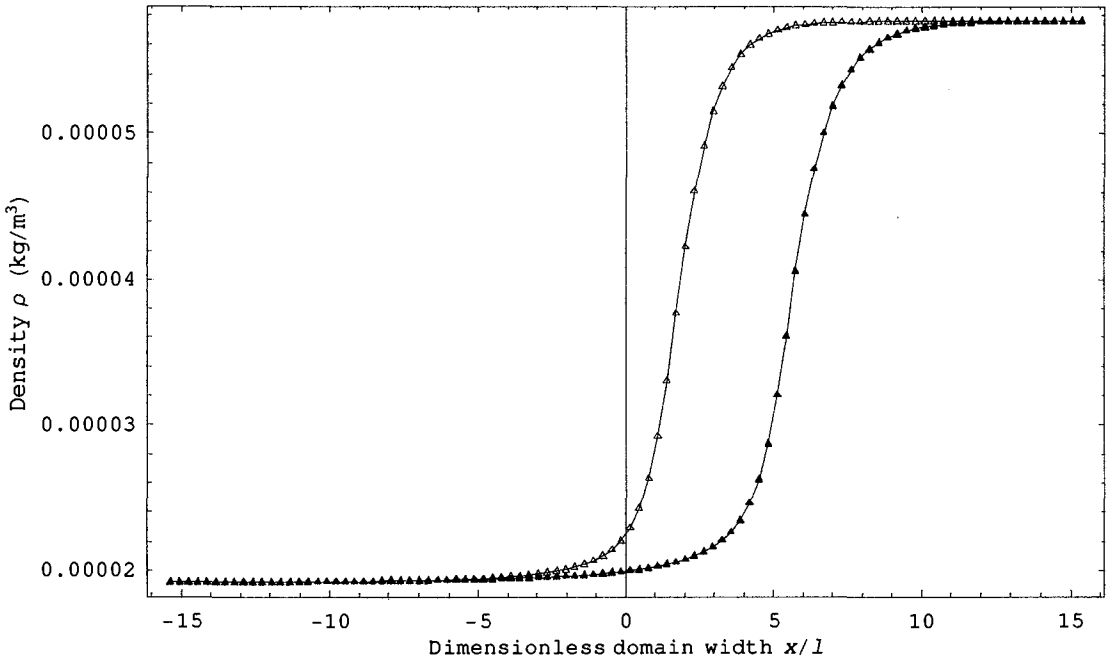

(a) Before shifting

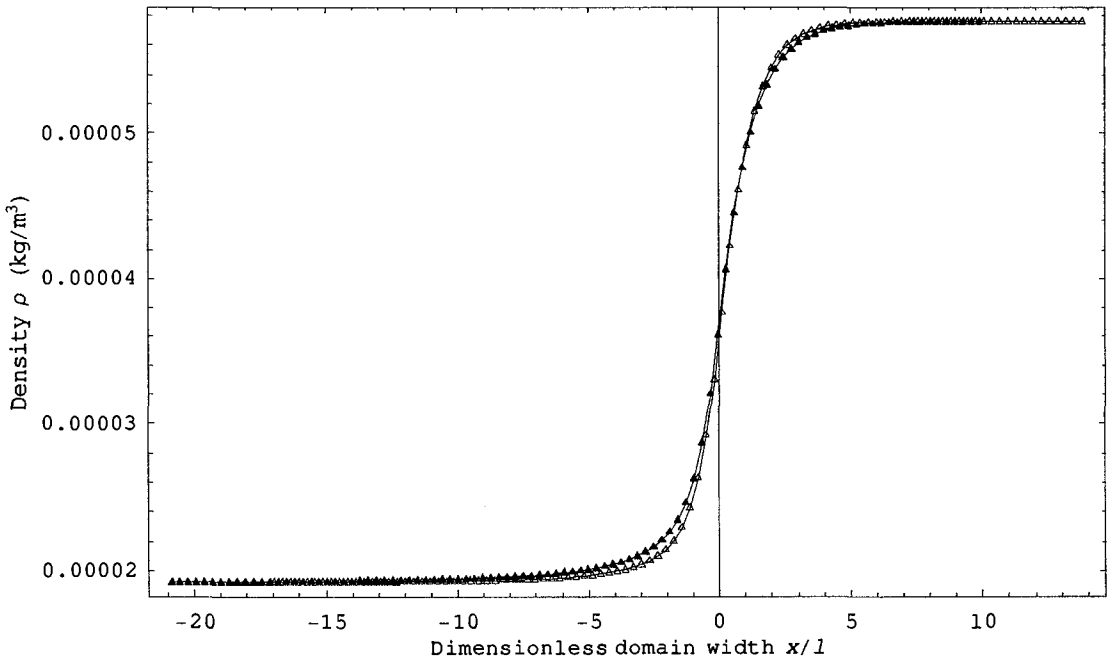

(b) After Shifting

Figure 3.2: Density profiles from BGK and ES-BGK models (case3.2: Ma=3.0) (Triangle for BGK, Triangle filled for ES-BGK)

3.4.2 Convergence of results

The two steps mentioned in the last paragraph of section 3.4.1 have been done to check convergence of results and stability of the program. In the first step, one macroscopic parameter after five certain numbers of iterations have been graphed in one figure to see whether the profiles are overlapped or not. This step has been done for all computations, and these graphs (e.g. graph (b) in Figure 3.1) show the results are converged. Then the average relative errors of macroscopic parameters among values after five certain iterations are computed, where the situation 1 in Eq. (3.39) now is the four intermediate iterations, while the situation 2 is the final iteration. The results show that those values of average relative errors are smaller than 0.01 for almost all cases. Note that this small difference of macroscopic parameters is obtained from two iterations, which distance is at least 4800 iterations. From the above two steps, it can be said that the computational results are converged, and the stability of the numerical scheme is good. Since computational results have been converged already at the iteration, which is 1/5 or 2/5 of final iteration, we do not need to compute so many iterations, when some proper criterion for convergence is developed and applied in the future. To find a proper criterion is a very useful task to save the computational time, meanwhile get the results converged.

Here the author would like to give a very simple estimation for time to reach the converged result. The BGK model for a homogeneous situation is used in the estimation, which can be written as

$$\frac{df}{dt}=\frac{\partial f}{\partial t}=-\nu(f-f_{BGK}), \tag{3.41}$$

where the collision frequency ν and the reference distribution function f_{BGK} are not function of time. Transform terms and do integration from initial situation ($t=0$ and $f=f_{ini}$) to the situation at time t, one gets

$$\int_{f=f_{ini}}^{f}\frac{1}{f-f_{BGK}}df=-\nu\int_{=0}dt,$$

$$\frac{f-f_{BGK}}{f_{ini}-f_{BGK}}=e^{-\nu t}, \tag{3.42}$$

where the mean free time $\tau = \frac{1}{\nu} = \frac{\mu}{p}$. If we say the converged result is reached when $\frac{f - f_{BGK}}{f_{ini} - f_{BGK}} = 10^{-4}$, then the estimated time to reach converged results is $t = 9.2\tau$.

For the 1DSW, let us compute the mean free time at upstream state, where the viscosity is computed from Eq. (2.32),

$$\tau = \frac{\mu}{p} = \frac{\mu_0 \left(\frac{T}{T_0}\right)^{\omega}}{nkT} = \frac{1.86\times10^{-5} \times \left(\frac{160.0}{273.0}\right)^{1}}{2.889\times10^{21} \times 1.381\times10^{-23} \times 160.0} = 1.7\times10^{-6}(\text{s}).$$

If we compute the mean free time at downstream state, the value is smaller than the above number. Therefore the magnitude of time to get converged result for the 1DSW from the above simple estimation is 10^{-5} s. The magnitude of total time step is $10^{-2} \sim 10^{-4}$ s (refer to Table 3.4, which shows the total time step (unit: seconds) for kinetic models in the computation of cases 3.1-3.3), which is much larger than the above estimated time, for all our computational results. Therefore, we can say that our computational results are the converged results from the above comparison.

Table 3.4: Total time step (seconds) for kinetic models in the computation of cases 3.1-3.3

Kinetic model / Case and situation	BGK	ES-BGK	$\nu(C)$-BGK	New I	New II
3.1 Sa	7.97D-3	8.23D-3	4.33D-3	7.47D-3	7.47D-3
3.2 Sb	4.85D-3	5.12D-3	2.01D-3	4.36D-3	4.36D-3
3.3 Sc	2.55D-3	1.36D-3	8.59D-4	1.13D-3	1.13D-3

Similar to the kinetic models, the DSMC program is run for a large number of iterations for each computation (parameter NPT in Table 3.2), in order to make sure the results are converged, and to study the long running behavior of program, and to eliminate the inherent stochastic noise of DSMC. Macroscopic parameters are output several times in the course of each computation. After similar analysis to kinetic models has been done, the results are realized to be converged, and the program is stable.

3.4.3 Discussion

Since the steady state is what we are interested in, we need to establish whether converged computational results are indeed results at steady state. In this part of the analysis, three fluxes (mass flux ρu_1, momentum flux $\rho u_1^2 + p_{11}$, and energy flux $1.5pu_1 + 0.5\rho u_1^3 + p_{11}u_1 + q_1$, which all should be constant in the whole domain at the steady state of 1DSW) can be used as a criterion. From the results, this criterion is indeed satisfied, see graphs (e, f, h-j) in Figures 3.7-3.9.

From the computational results in Table 3.4, it is shown that the $\nu(C)$-BGK model requires the smallest time step Δt_n (is only about 50% of Δt_n of other kinetic models) among the tested kinetic models, and Δt_n for other kinetic models are similar.

Results from the new kinetic model I and the new kinetic model II are similar (see Figures 3.7-3.9), and if the structure of program and computational time for one iteration is considered, the new kinetic model II is better than the new kinetic model I. The computational time for one iteration of the new kinetic model II is about 80% of the computational time needed for one iteration of the new kinetic model I. The reason is that when the reference distribution is solved (which occupy a large portion of computational time), the new kinetic model I needs results from the ES-BGK model, while the new kinetic model II does not, therefore the new kinetic model I need to perform the N-R algorithm to find coefficients of reference distributions three times, while the new kinetic model II only need to perform the N-R algorithm two times.

Let us consider the use of the linearized reference distribution f_{ref} discussed in Section 3.2.4. From Figures 3.3-3.5, which are examples to show temperature and heat flux profiles from kinetic models (the new kinetic model I is omitted, for its results are similar to results of the new kinetic model II) with original and linearized f_{ref} at Ma=1.5, 3.0 and 6.0 situations, and data obtained from the two steps mentioned in the last paragraph of section 3.4.1 (when the average relative error is computed, use the results

with original f_{ref} as the situation 2 in Eq. (3.39)), the following conclusions can be drawn (If it is not pointed out for which kinetic model, then it means the statement is applicable for all kinetic models).

- When the computational time for each time step is considered, using the linearized f_{ref} can save 20~35% time compared to using the original f_{ref} since coefficients in the linearized f_{ref} can be solved directly from a linear system, while the coefficients in the original f_{ref} need be solved through some iterative method, such as the N-R algorithm used in this work.

- When the Mach number increases, the difference between results obtained by using the linearized f_{ref} and results obtained by using the original f_{ref} also increases.

- For Ma=1.5 and 3.0, the average relative errors for all macroscopic parameters, all kinetic models and both types linearized f_{ref} are smaller than 0.01, except for the $\nu(C)$-BGK model in cases 3.5.

- For the BGK model, the average relative errors for all macroscopic parameters are smaller than 0.01 for all test situations.

- For the ES-BGK model, average relative errors for the second type linearized f_{ref} are much smaller than the values for the first type linearized f_{ref}, while both types are acceptable. Normally, the former values would be only one-tenth of the later ones, which are still smaller than 0.025 for Ma=6.0.

- For the $\nu(C)$-BGK model, the average relative errors would be 0.05 or higher, which are not acceptable, for Ma=3.0 and 6.0. (the reason for these large errors is still being investigated).

- For the new kinetic model I with hard sphere molecules, using the first type linearized f_{ref} in cases 3.1-3.6 gives divergent results (NaNQ appear in the output of the FORTRAN computation program), while using the second type linearized f_{ref} yields convergent results in cases 3.1-3.2, 3.4-3.5 (situation Sa and Sb) (average relative errors are smaller than 0.01) and some divergent results in cases 3.3 and 3.6 (situation Sc). Reasons why diverged results are obtained is still being investigated.

- For the new kinetic model II, the second type linearized f_{ref} does not give much better results than the first type linearized f_{ref}. The average relative errors are smaller than 0.030 for Ma=6.0.

Let us consider the effect of the step of space grid on computational results, based on the comparison of results from cases 3.4-3.6 with results from cases 3.1-3.3, and the comparison of results from case 3.7 with results from case 3.5 (situation Sb[14]). Average relative errors are smaller than 0.01 for weak shock waves (situation Sa), but would be large as 0.05 for medium and strong shock waves when results from cases 3.5-3.6 are compared with results from cases 3.2-3.3 (situation Sb and Sc). Average relative errors are smaller than 0.01 for medium shock waves when results from case 3.7 are compared to results from case 3.5. When the Mach number of 1DSW increases, the thickness of shock wave decreases first, and reach some minimum value at about Ma=3.0~5.0, then increases [1, 9, 26]. Based on our computation, choosing the step of space grid as one half or one third of mean free path at upstream side is not accurate enough for medium or strong shock waves, while one sixth of the mean free path would be enough. A smaller step of the space grid will increase the computational time for each time step and decrease the value of time step (which means more iterations need to be done to get converged results). It is not suggested, based on the author's experience (e.g. compute the new kinetic model I in case 3.6 with 40000 iterations need about one month, which is almost the limit running time for each computational job, on "Minerva", which is a

[14] For the $\nu(C)$-BGK model in case 3.7, only run Iteration=24802, the stop reason is the values of coefficients of collision frequency can not be gotten correctly from the N-R algorithm.

cluster of workstations provided by the University of Victoria, and is used for the computation), to do some further tests using smaller step of space grid than it used in case 3.6, before some ways are applied to decrease the computational time, such as an effective criterion to check the convergence, implicit numerical scheme, parallel computing, higher performance workstation, etc.

Let us consider the effect of bounds and step of velocity grid on computational results, based on the comparison of results from cases 3.8-3.9 with results from cases 3.1. Average relative errors are smaller than 0.005, which tell us that the use of Eq. (3.37) as standard for choice of bounds and step of velocity grid for 1DSW is acceptable.

As some example graphs to show the use of linearized f_{ref}, effect of step of space grid, effect of bounds and step velocity grid, Figure 3.3 shows the profiles of T and q_1 (heat flux along the shock wave direction) for Ma=1.5 (cases 3.1 and 3.4) with the ES-BGK model; Figure 3.4 shows the profiles of T and q_1 for Ma=3.0 (cases 3.2 and 3.5) with the $\nu(C)$-BGK model; Figure 3.5 shows the profiles of T and q_1 for Ma=6.0 (cases 3.3 and 3.6) with the new kinetic model II; Figure 3.6 shows the profiles of T and q_1 for Ma=1.5 (cases 3.1, 3.8 and 3.9) with the new kinetic model I.

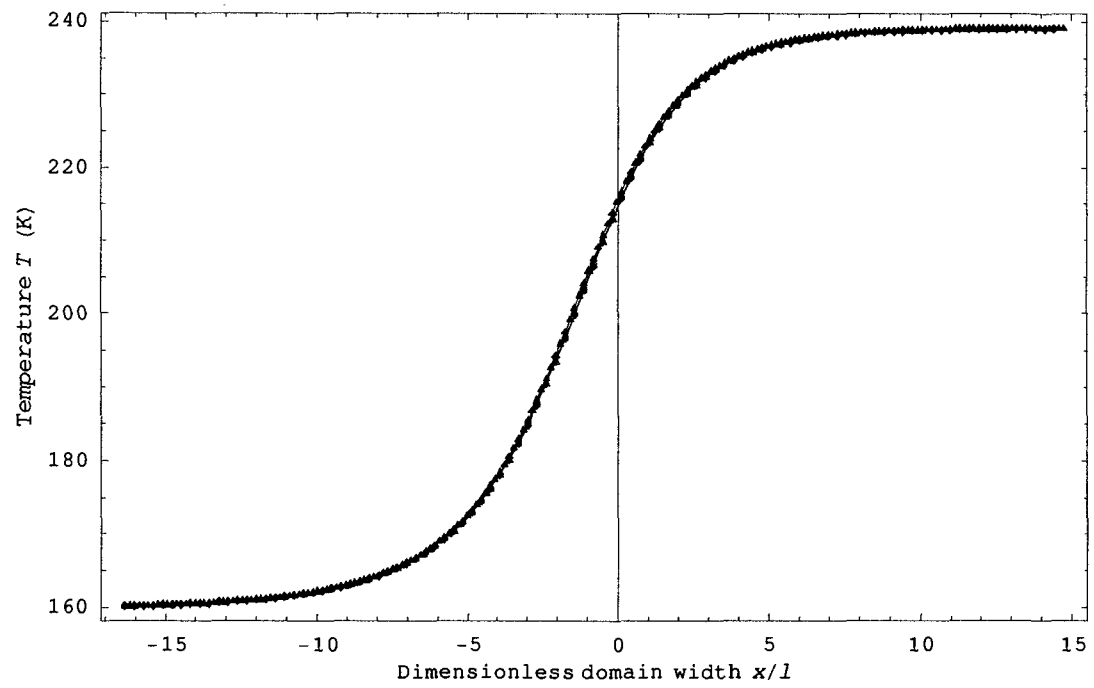

(a)

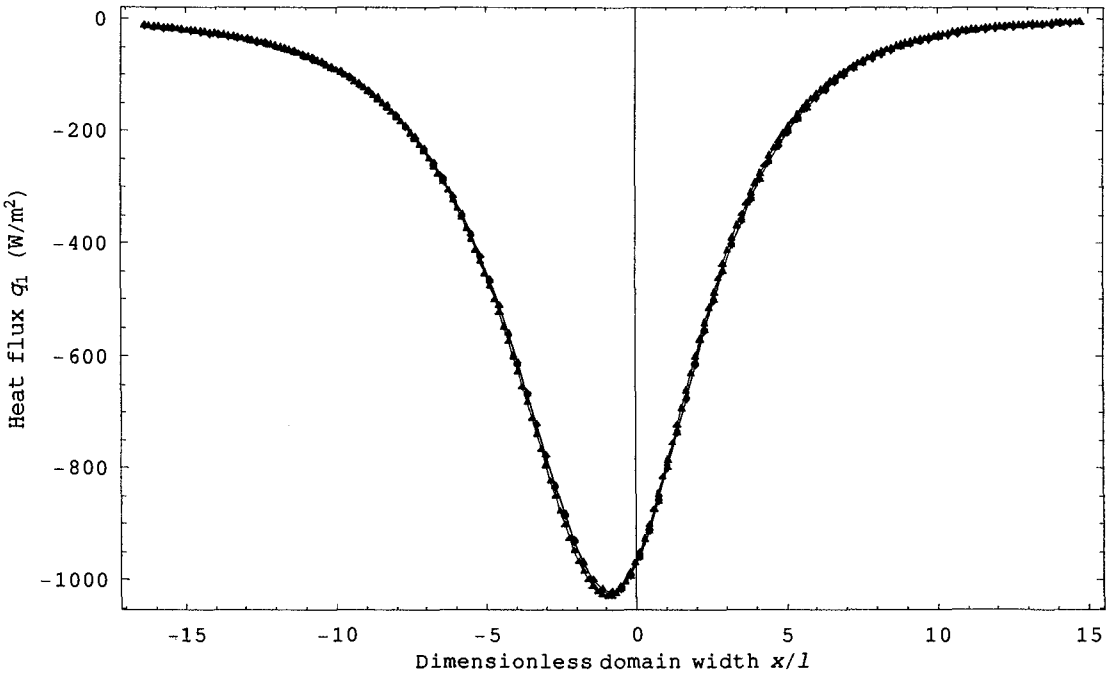

(b)

Figure 3.3: Results to show the use of linearized f_{ref} and the effect of step of space grid (Ma=1.5, ES-BGK model) (Triangle for the original f_{ref} in case 3.1, Triangle filled for the original f_{ref} in case 3.4, Diamond for the first type linearized f_{ref} in case 3.1, Diamond filled for the second type linearized f_{ref} in case 3.1)

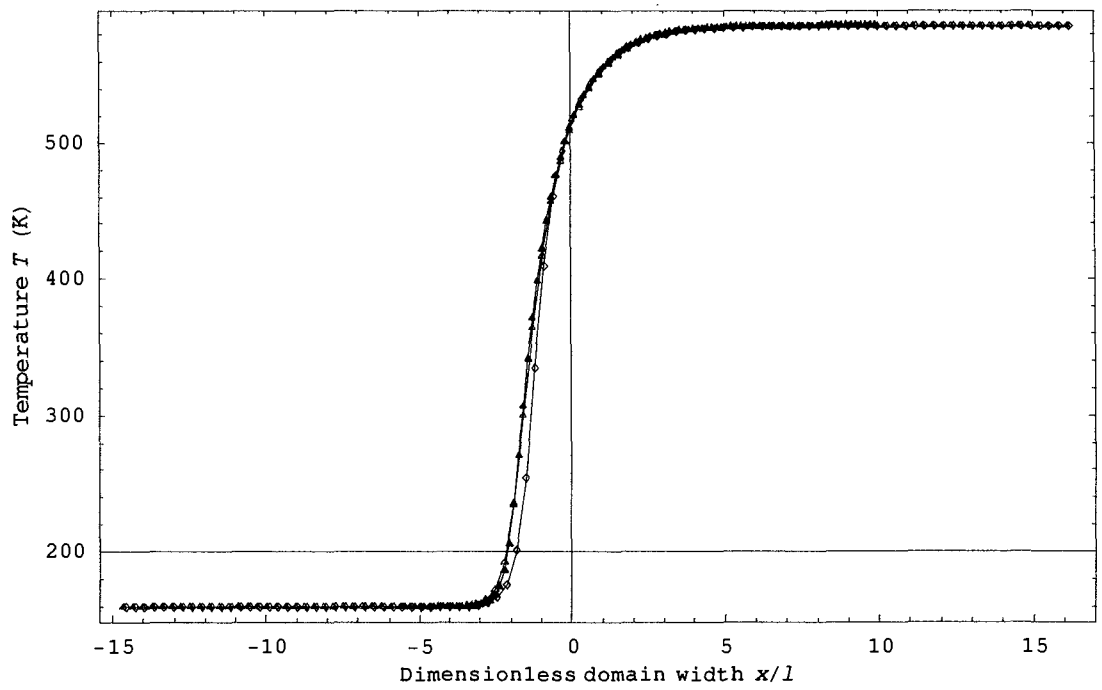

(a)

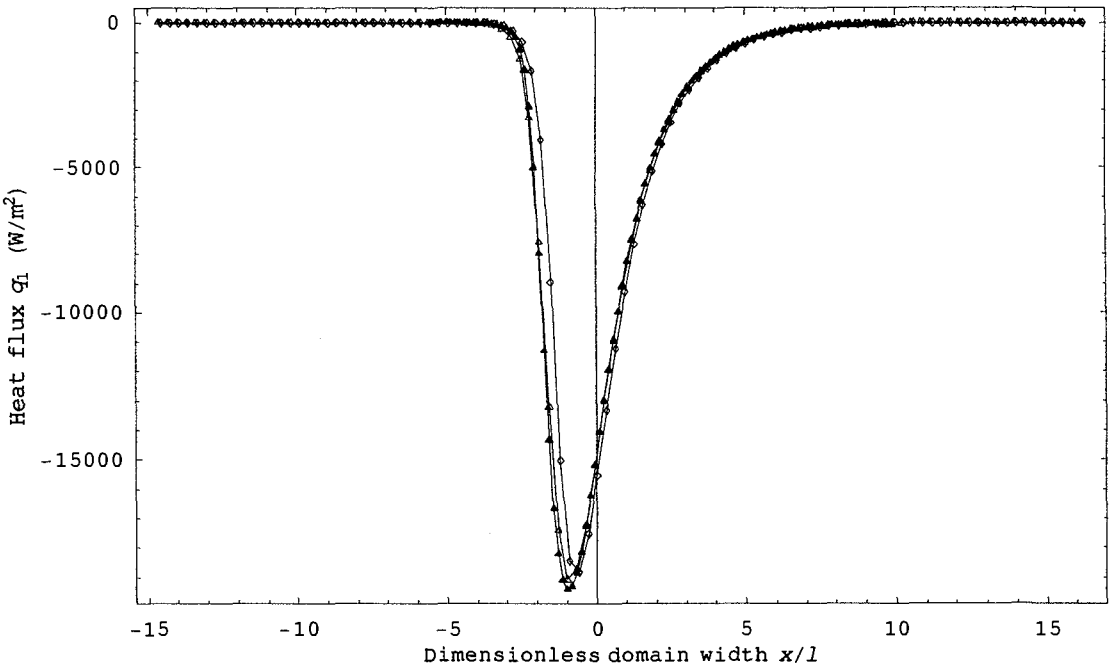

(b)

Figure 3.4: Results to show the use of linearized f_{ref} and the effect of step of space grid (Ma=3.0, $\nu(C)$-BGK model) (Triangle for the original f_{ref} in case 3.2, Triangle filled for the original f_{ref} in case 3.5, Diamond for the linearized f_{ref} in case 3.2)

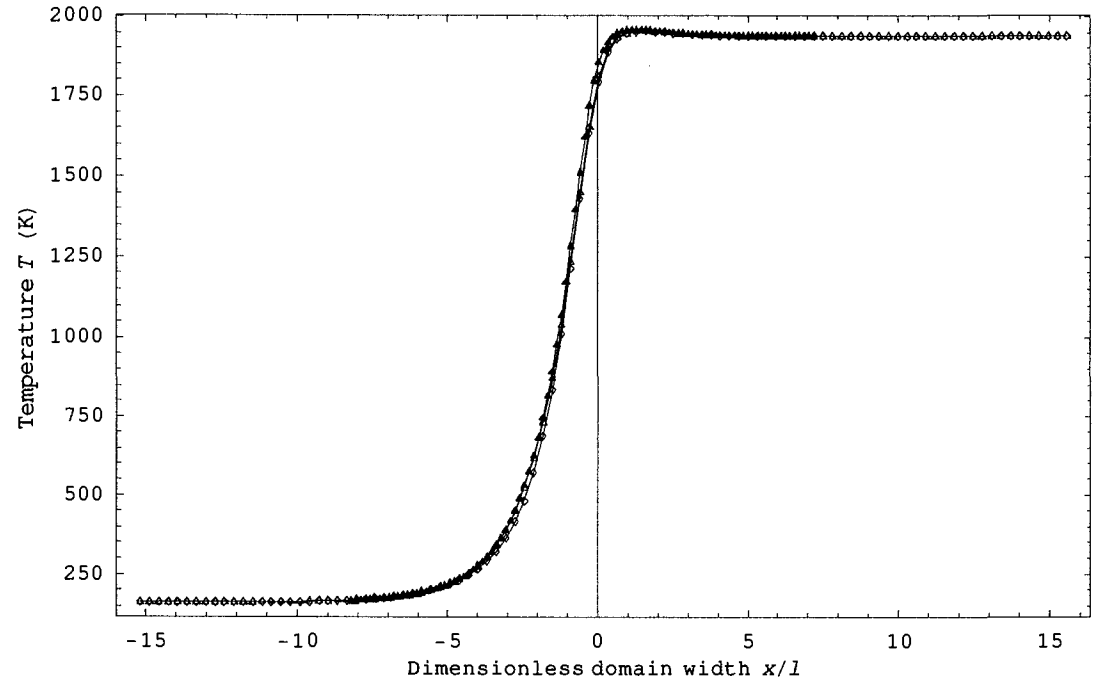

(a)

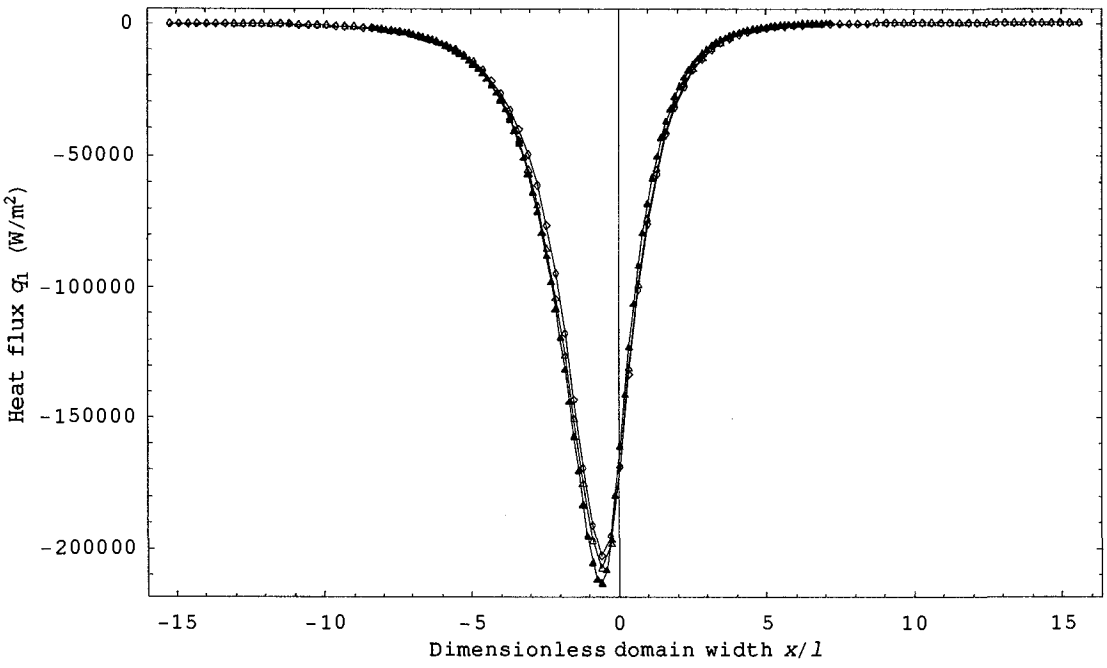

(b)

Figure 3.5: Results to show the use of linearized f_{ref} and the effect of step of space grid (Ma=6.0, new kinetic model II) (Triangle for the original f_{ref} in case 3.3, Triangle filled for the original f_{ref} in case 3.6, Diamond for the linearized f_{ref} in case 3.3)

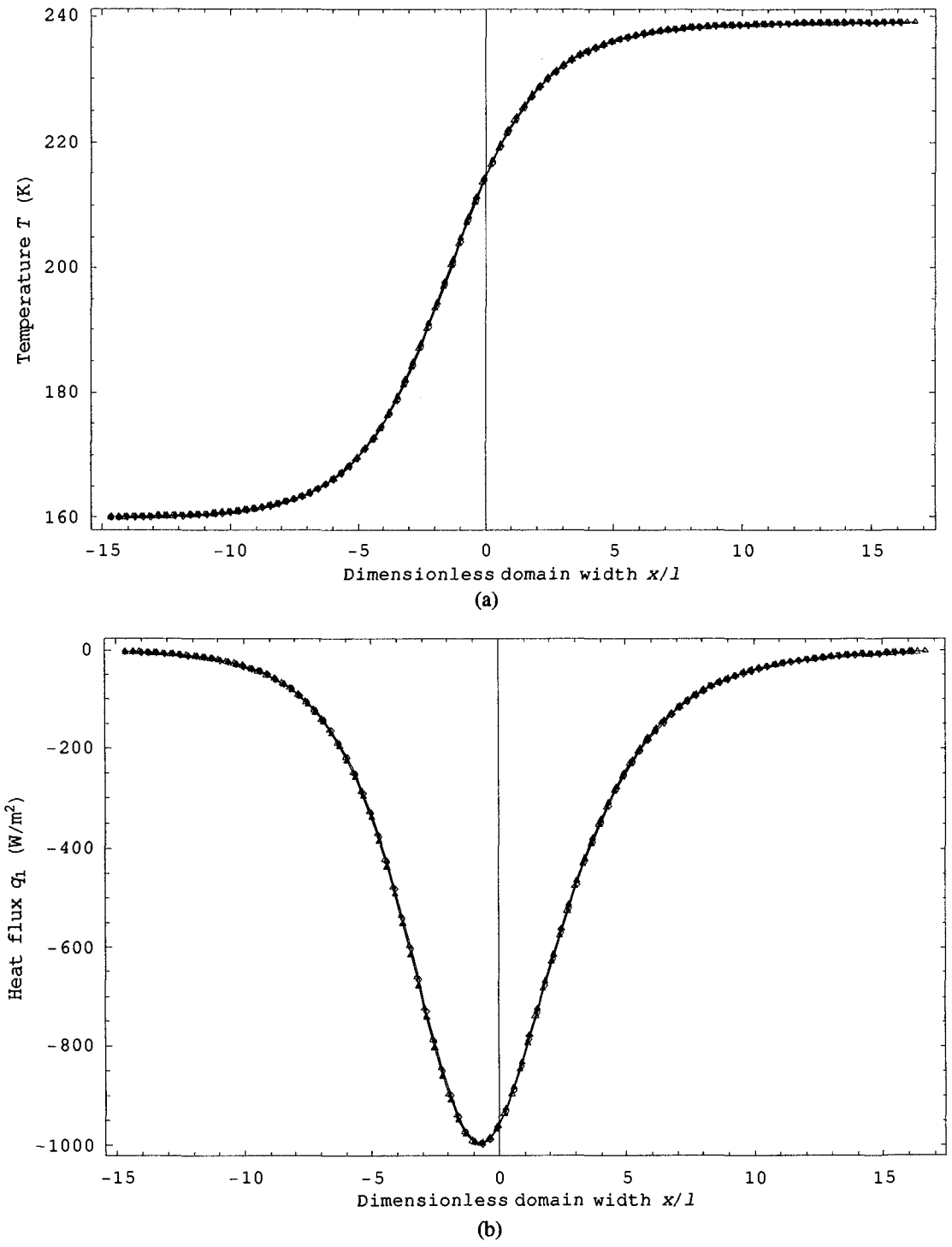

Figure 3.6: Results to show the effect of bounds and step of velocity grid (Ma=1.5, new kinetic model I) (Triangle for case 3.1, Triangle filled for case 3.8, Diamond for case 3.9)

3.4.4 Comparison with DSMC

Graphs and data to show the comparison of kinetic models and DSMC are obtained from the two steps mentioned in the last paragraph of Section 3.4.1. Table D.1 in Appendix D shows average relative errors of macroscopic parameters between kinetic models and DSMC in cases 3.4-3.6. Figures 3.7-3.9 show profiles of macroscopic parameters from kinetic models (cases 3.4-3.6) and DSMC at Ma=1.5, 3.0 and 6.0. The following points are realized from these graphs and data.

- For hard sphere molecules, results from the new kinetic models locate in between results from the ES-BGK model and results from the $\nu(C)$-BGK model. It is found that the shape of shock waves from the $\nu(C)$-BGK model is sharper than the shape of shock waves from the DSMC, while they are both sharper than results from the ES-BGK model. The above two points indicate that results from the new kinetic models are closer to results of DSMC than results from the BGK model, the ES-BGK model and the $\nu(C)$-BGK model.

- In the temperature profiles, graph (c) in Figure 3.9, for Ma=6.0 from the ES-BGK model, the new kinetic models and the DSMC exhibit the overshoot phenomenon, while results from the BGK model and the $\nu(C)$-BGK model do not have this phenomenon.

- The biggest difference between results from various kinetic models and results from DSMC always happens at the first half part of the shock wave structure.

- When the degree of moment becomes higher, the difference between moment obtained from kinetic models and moments from DSMC will be larger. For example, the difference of σ_{11}, σ_{22} and q_1 between kinetic models and DSMC from Figures 3.7-3.9 are larger than the difference of other parameters (ρ, u_1, T, and p).

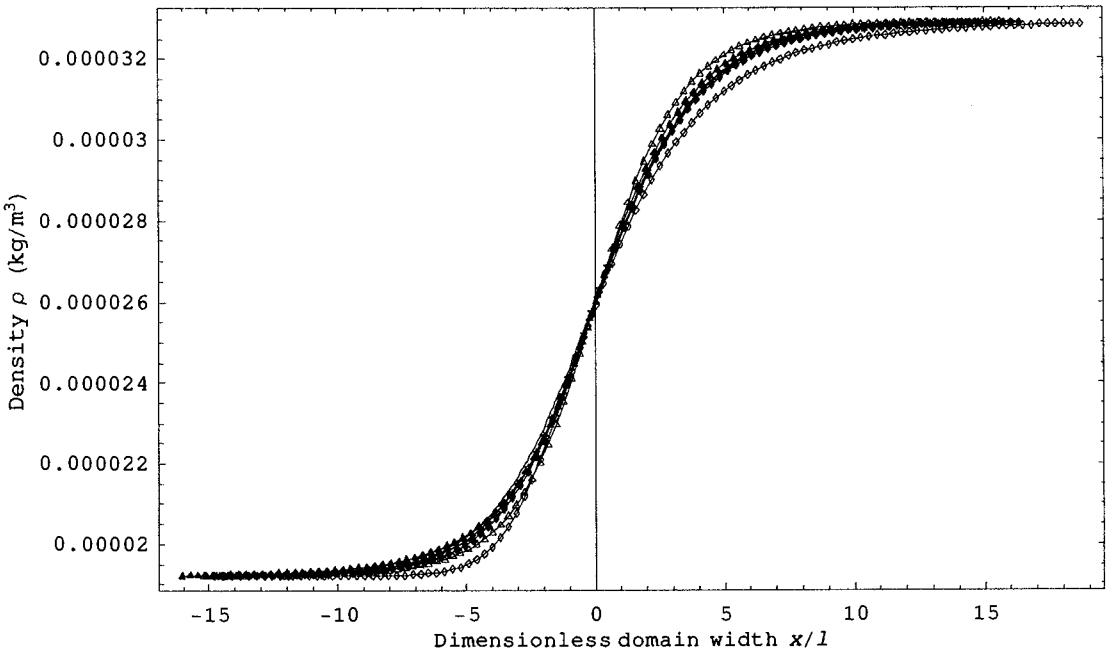

(a)

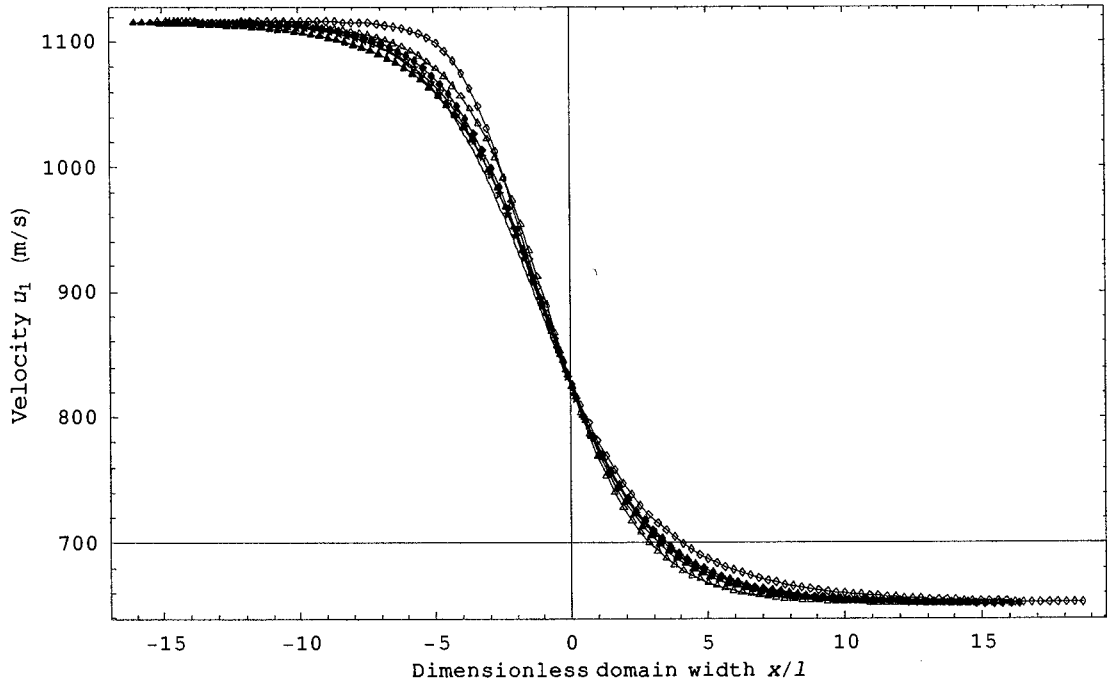

(b)

Figure 3.7: Comparison of kinetic models with DSMC (case 3.4: Ma=1.5) (Triangle for the BGK model, Triangle filled for the ES-BGK model, Diamond for the $\nu(C)$-BGK model, Diamond filled for the new kinetic model I, Star for the new kinetic model II, Line without symbols for the DSMC)

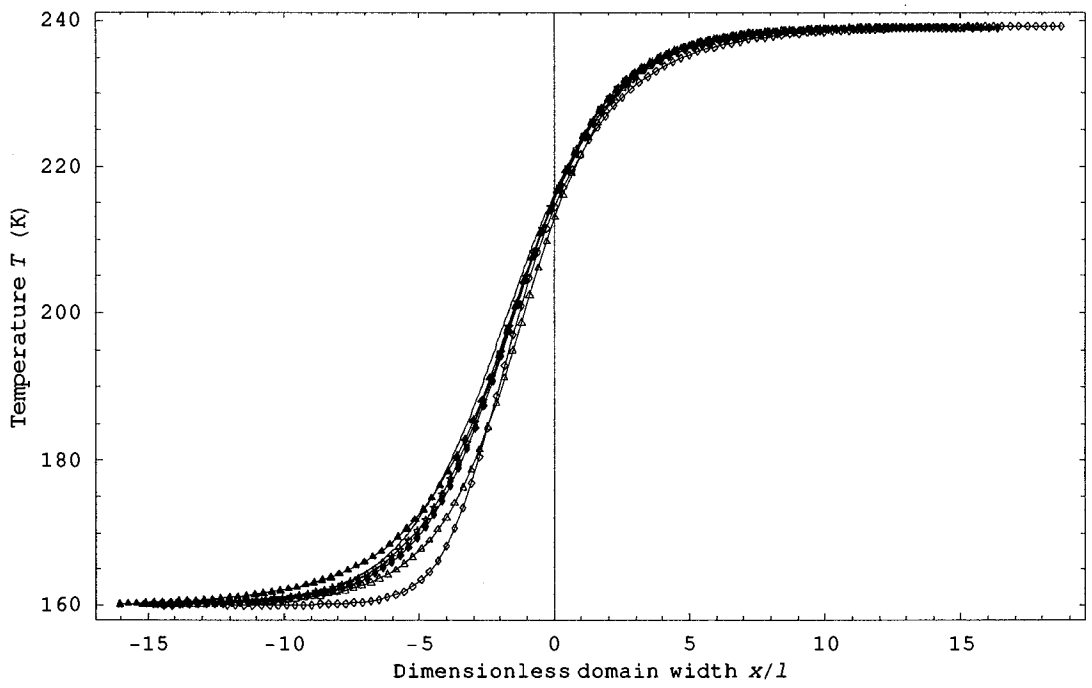

(c)

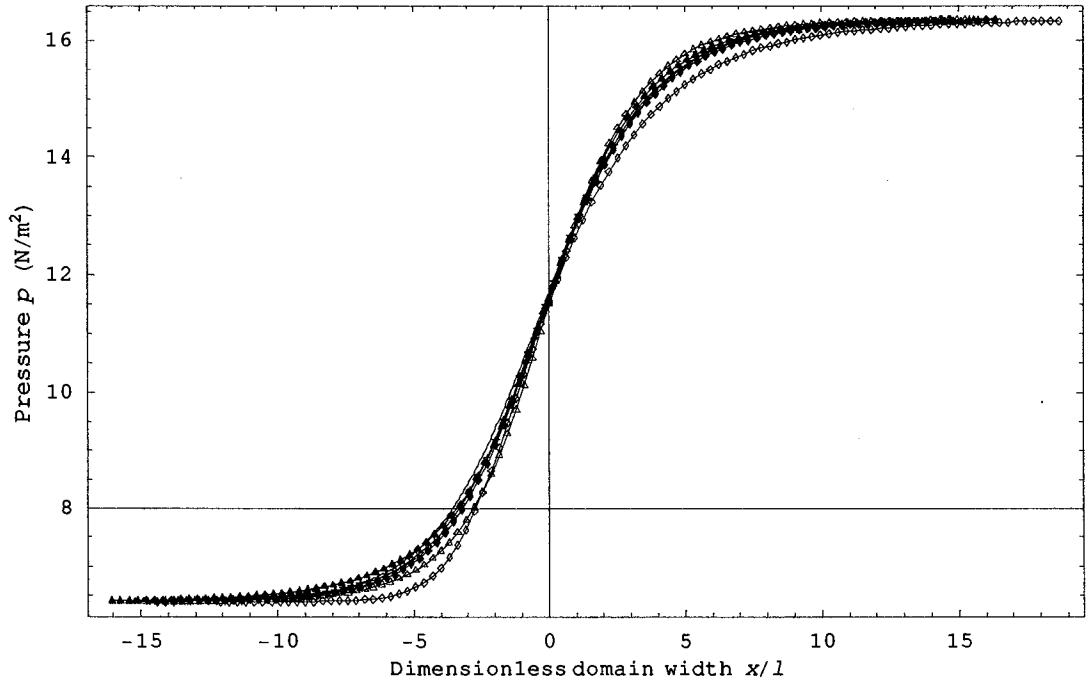

(d)

Figure 3.7: Comparison of kinetic models with DSMC (case 3.4: Ma=1.5) (Triangle for the BGK model, Triangle filled for the ES-BGK model, Diamond for the $\nu(C)$-BGK model, Diamond filled for the new kinetic model I, Star for the new kinetic model II, Line without symbols for the DSMC)

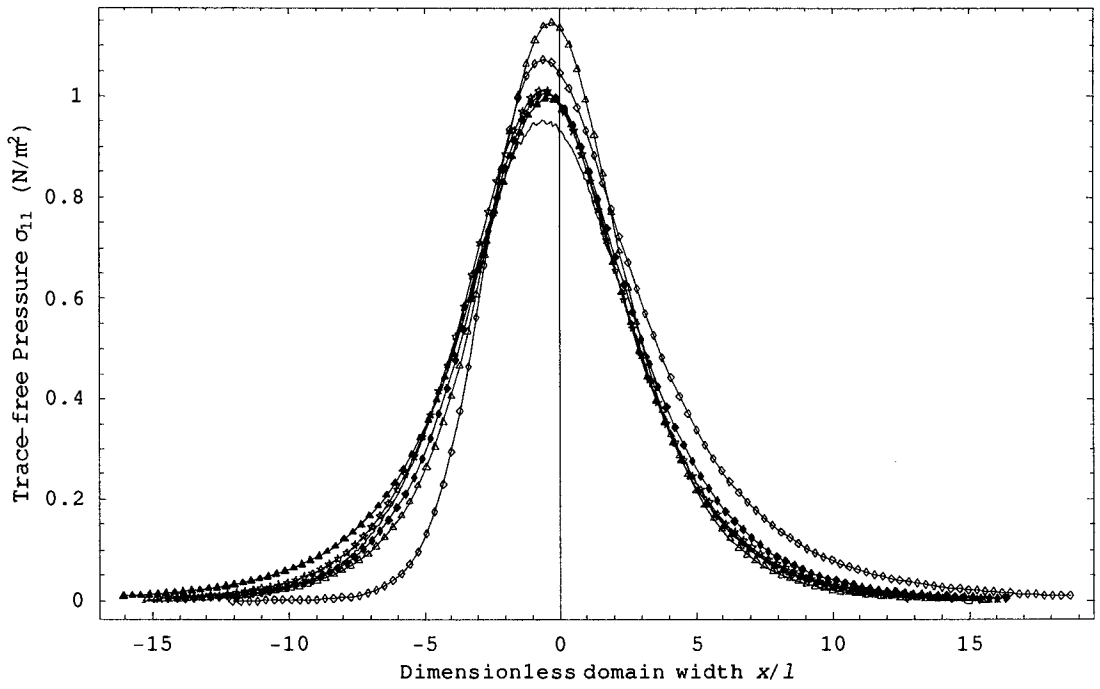

(e)

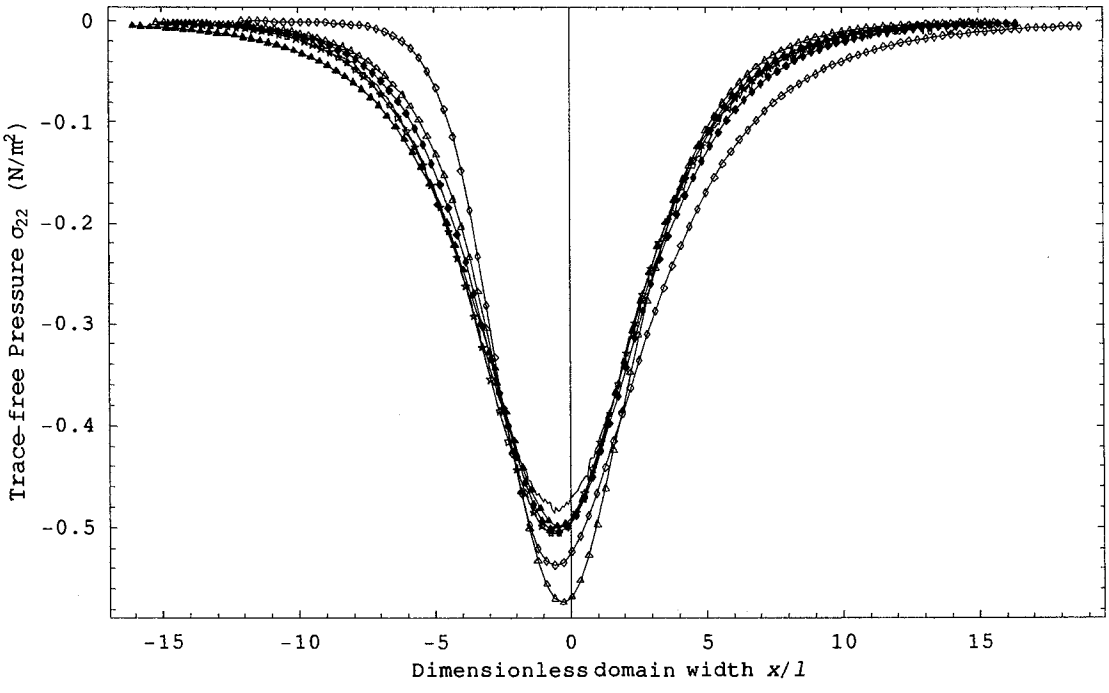

(f)

Figure 3.7: Comparison of kinetic models with DSMC (case 3.4: Ma=1.5) (Triangle for the BGK model, Triangle filled for the ES-BGK model, Diamond for the $\nu(C)$-BGK model, Diamond filled for the new kinetic model I, Star for the new kinetic model II, Line without symbols for the DSMC)

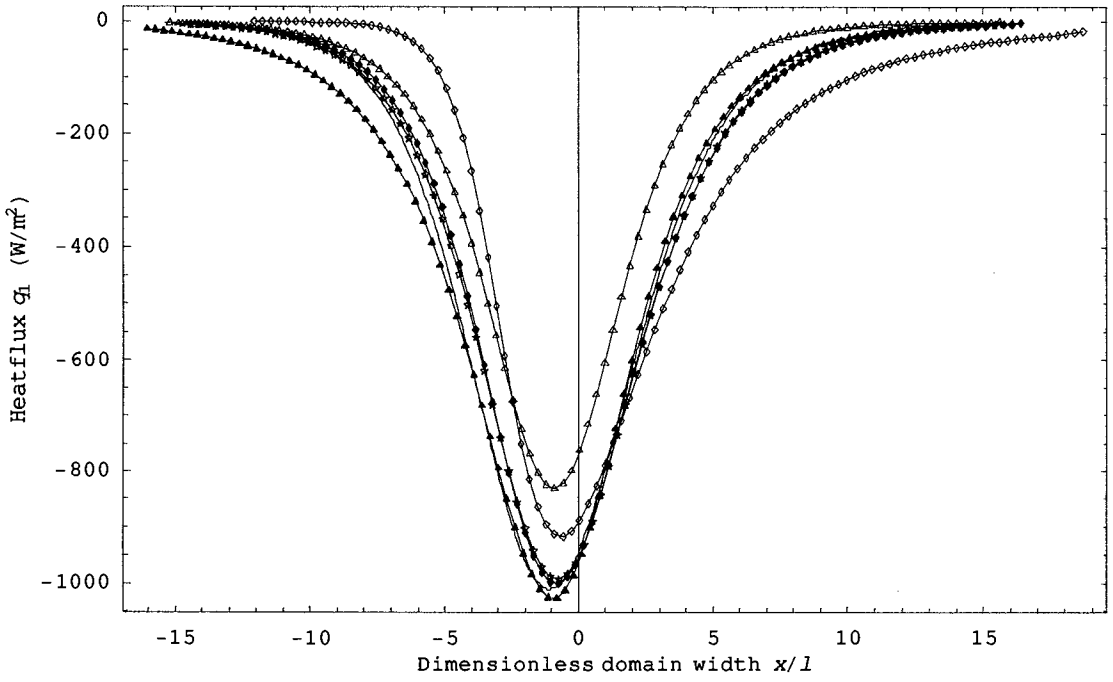

(g)

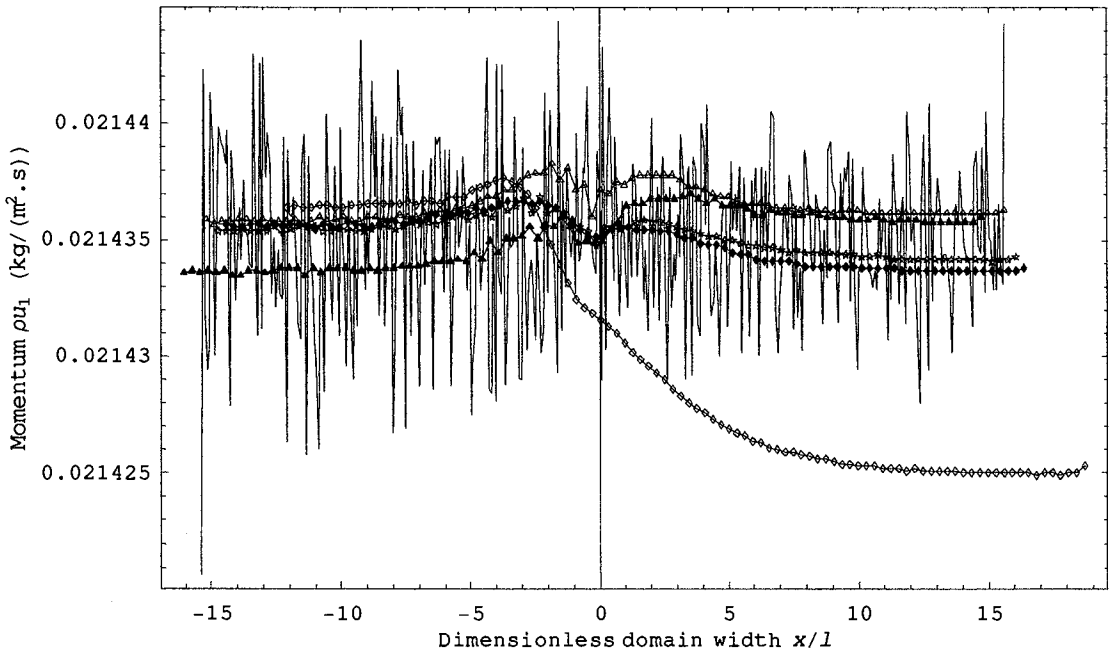

(h)

Figure 3.7: Comparison of kinetic models with DSMC (case 3.4: Ma=1.5) (Triangle for the BGK model, Triangle filled for the ES-BGK model, Diamond for the $\nu(C)$-BGK model, Diamond filled for the new kinetic model I, Star for the new kinetic model II, Line without symbols for the DSMC)

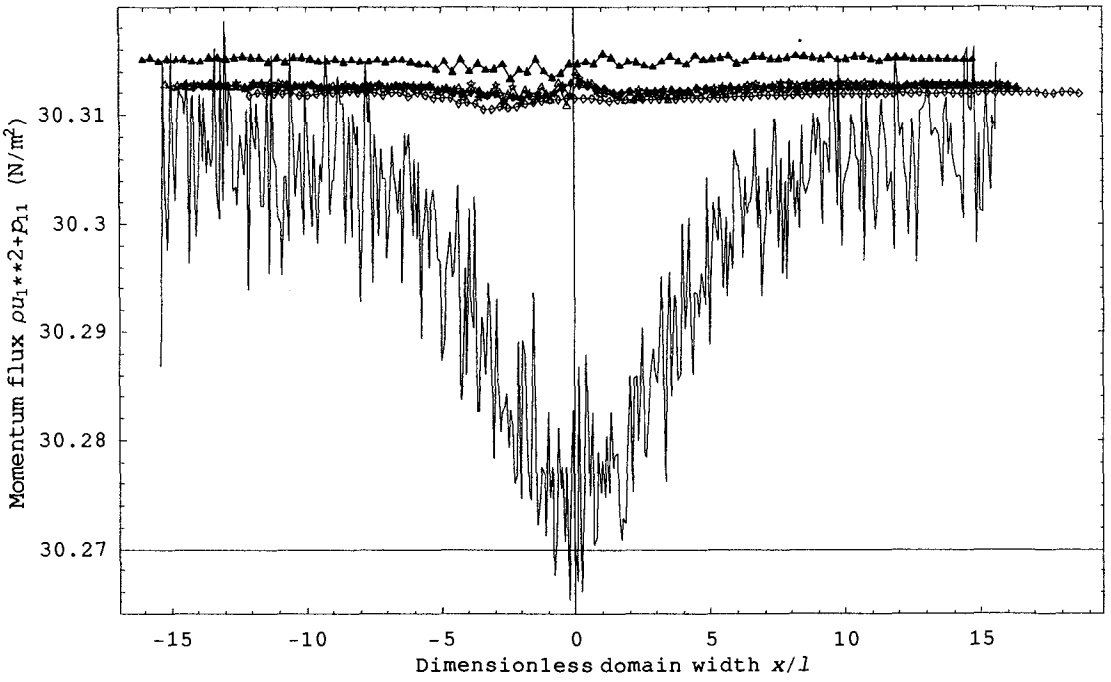

(i)

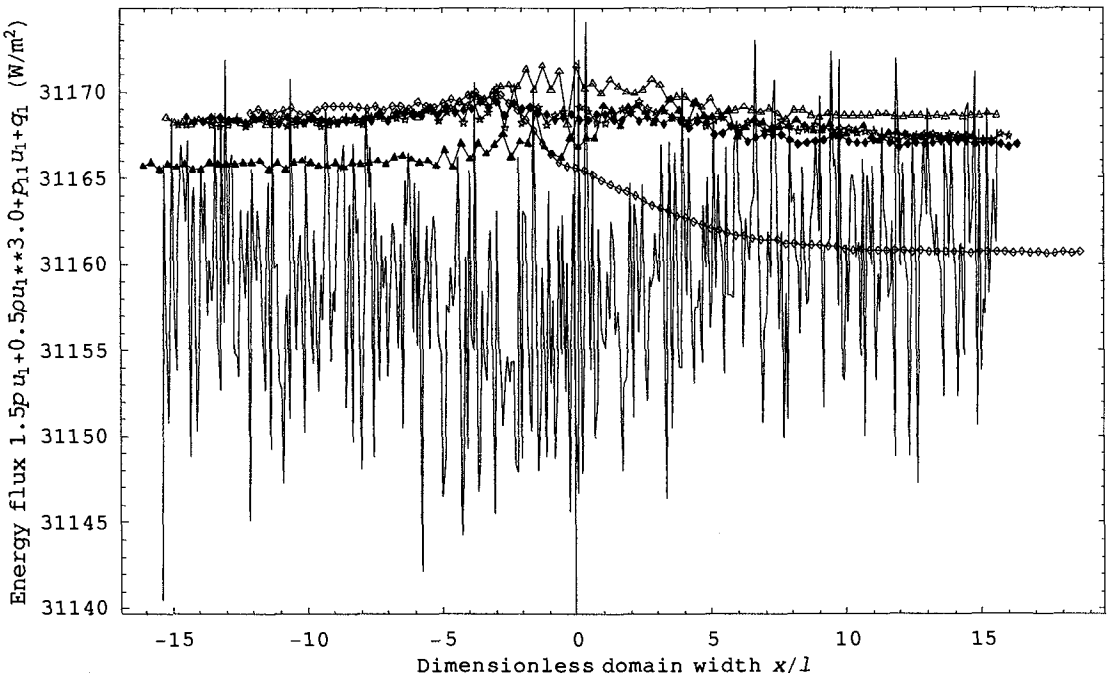

(j)

Figure 3.7: Comparison of kinetic models with DSMC (case 3.4: Ma=1.5) (Triangle for the BGK model, Triangle filled for the ES-BGK model, Diamond for the $\nu(C)$-BGK model, Diamond filled for the new kinetic model I, Star for the new kinetic model II, Line without symbols for the DSMC)

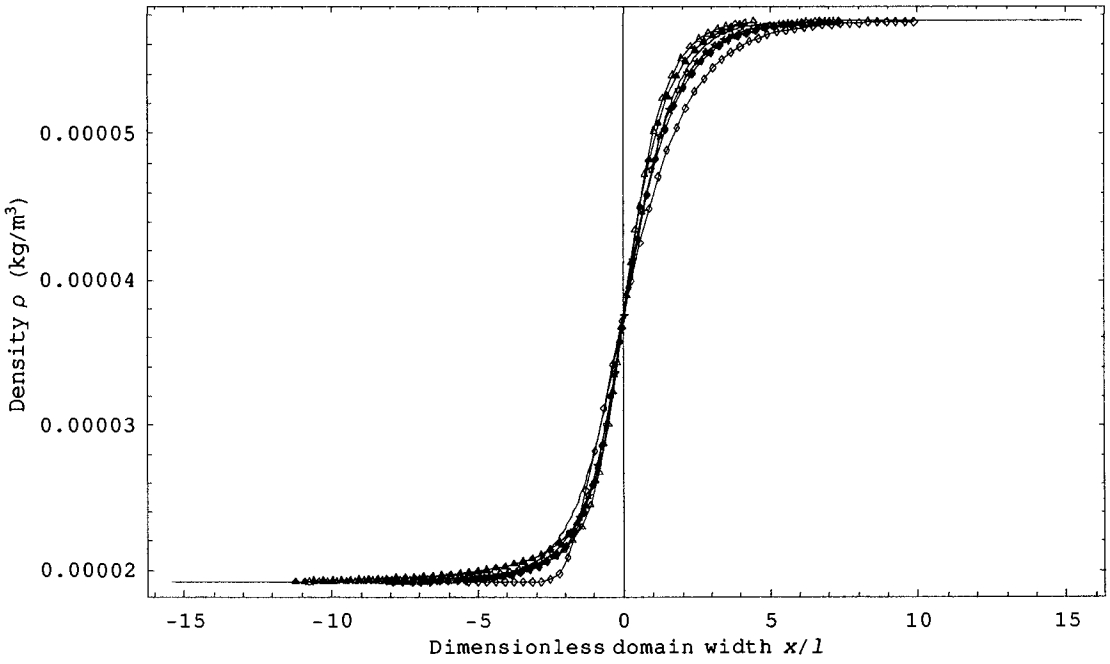

(a)

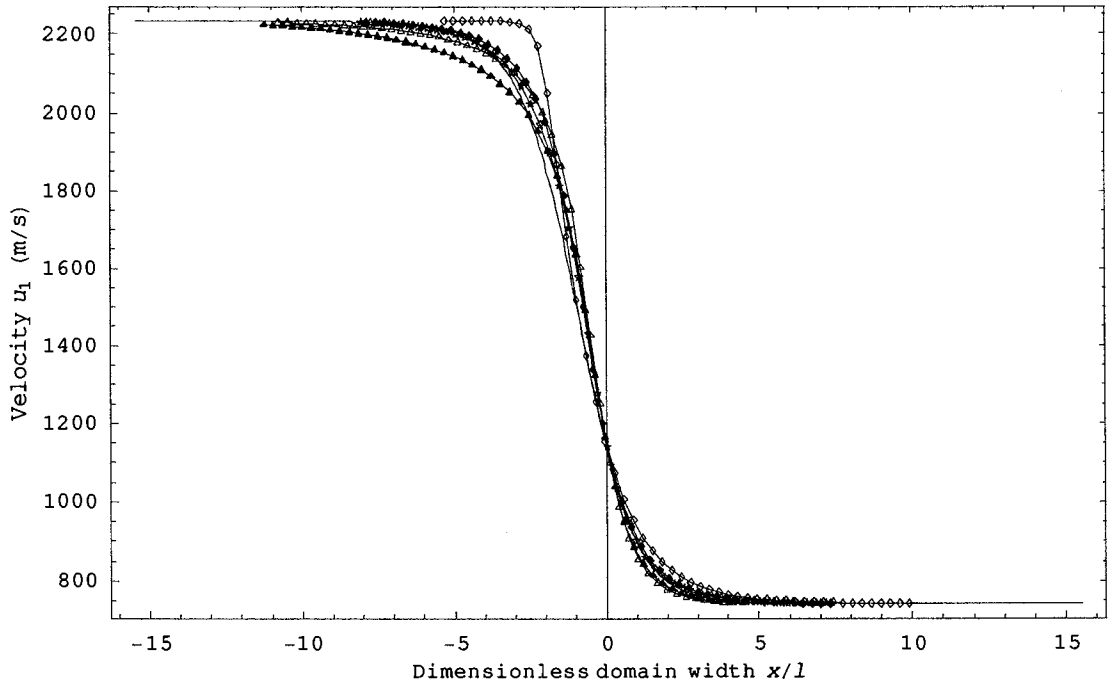

(b)

Figure 3.8: Comparison of kinetic models with DSMC (case 3.5: Ma=3.0) (Triangle for the BGK model, Triangle filled for the ES-BGK model, Diamond for the $\nu(C)$-BGK model, Diamond filled for the new kinetic model I, Star for the new kinetic model II, Line without symbols for the DSMC)

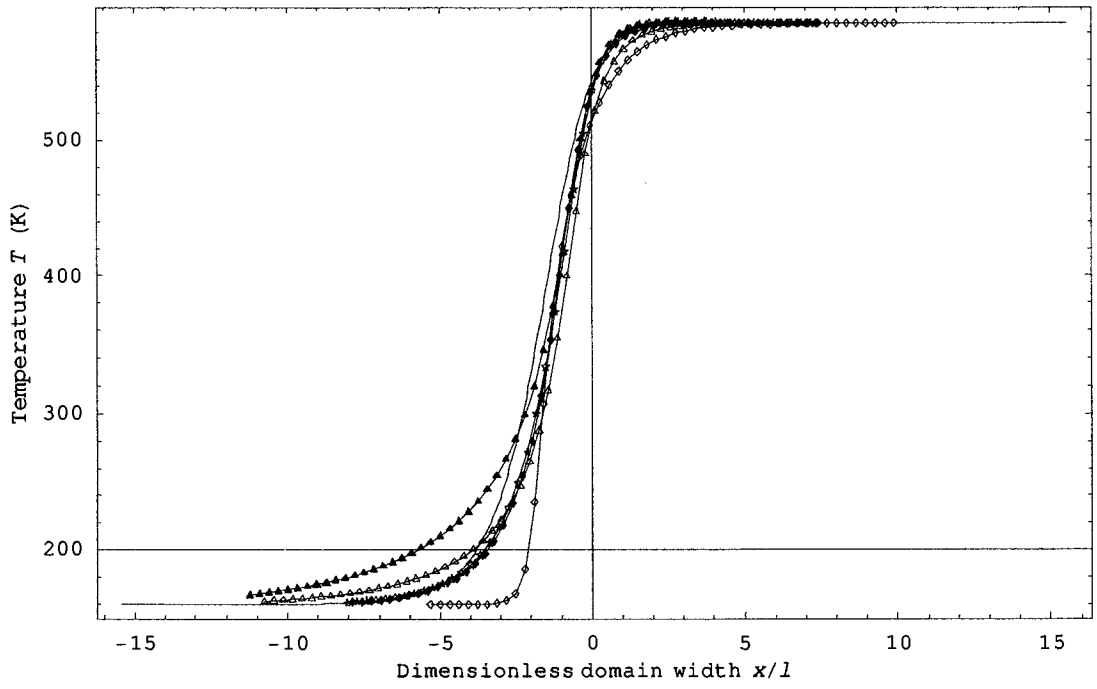

(c)

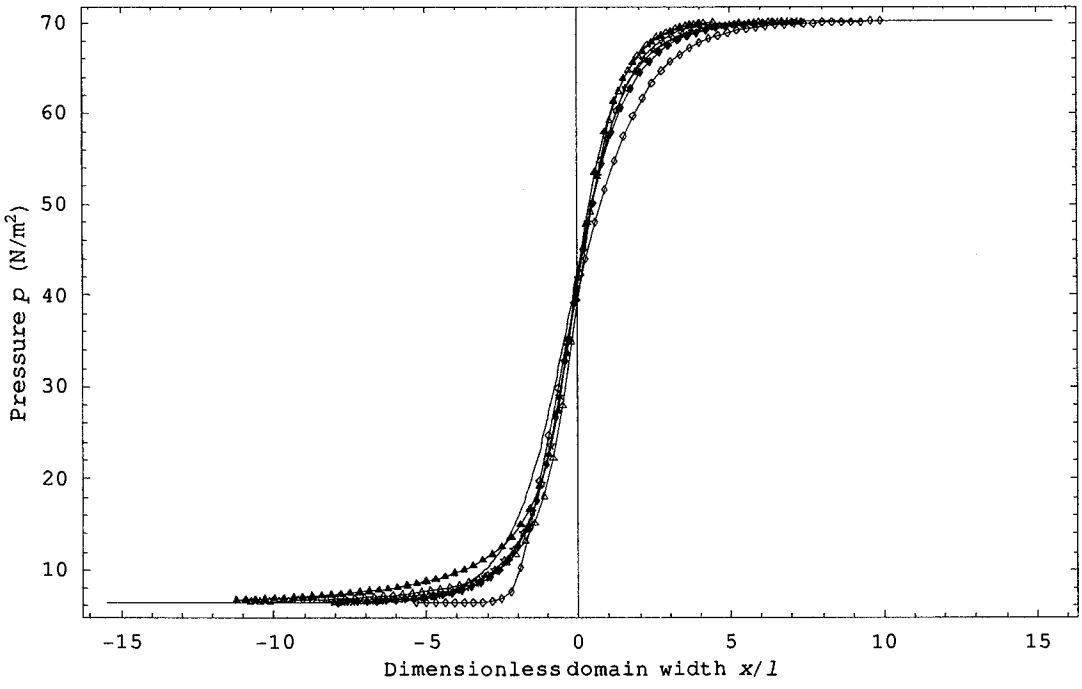

(d)

Figure 3.8: Comparison of kinetic models with DSMC (case 3.5: Ma=3.0) (Triangle for the BGK model, Triangle filled for the ES-BGK model, Diamond for the $\nu(C)$-BGK model, Diamond filled for the new kinetic model I, Star for the new kinetic model II, Line without symbols for the DSMC)

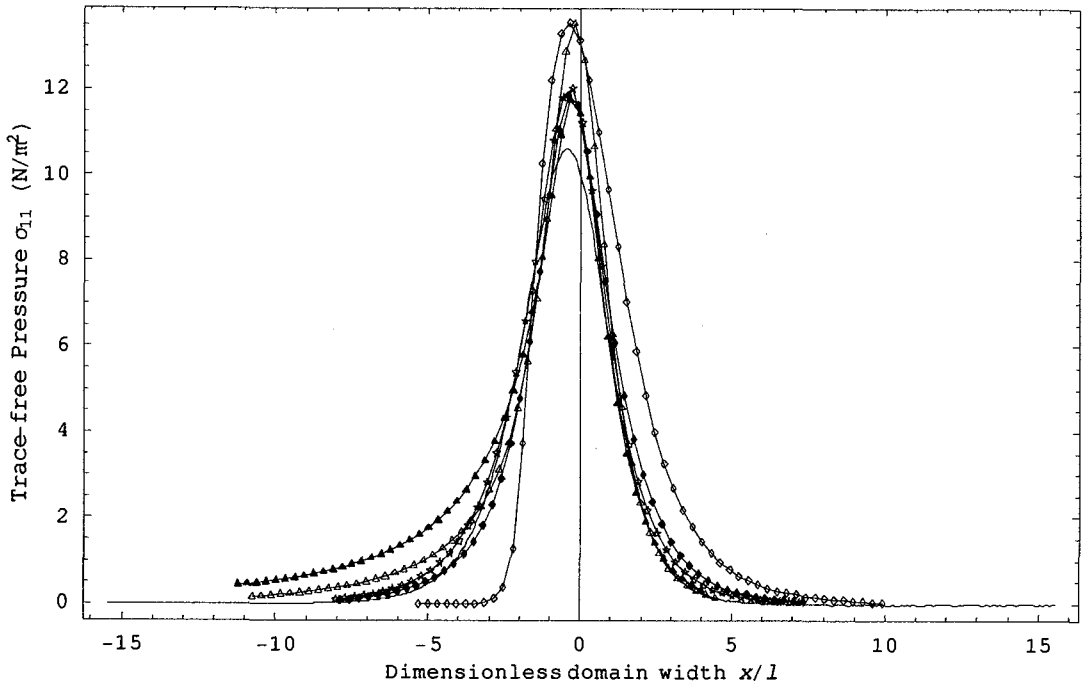

(e)

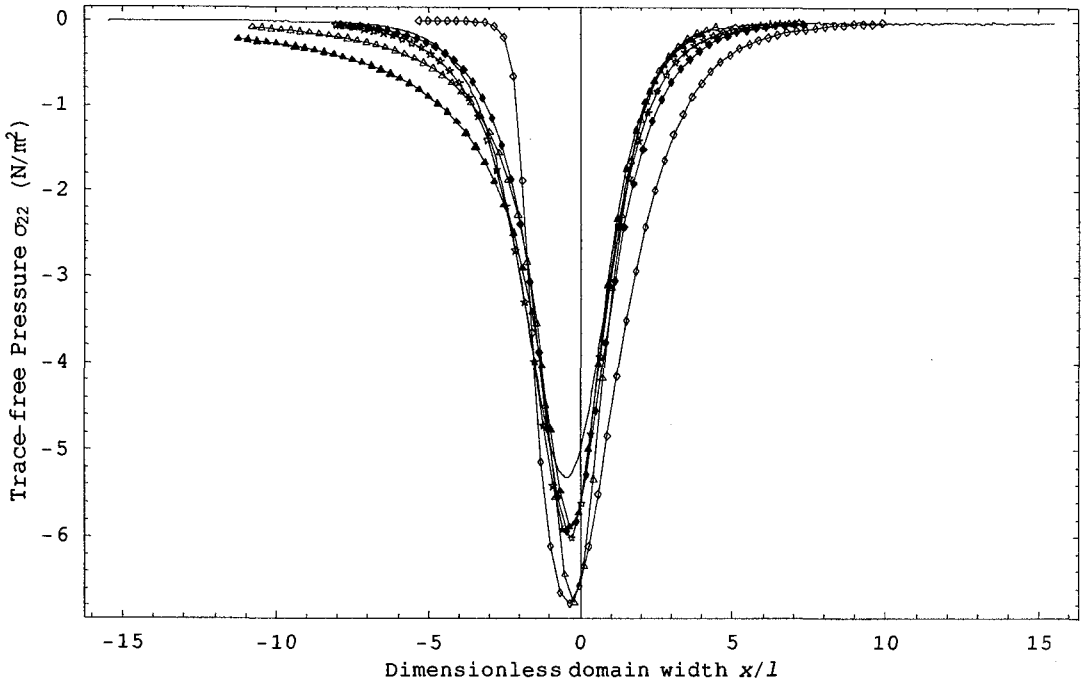

(f)

Figure 3.8: Comparison of kinetic models with DSMC (case 3.5: Ma=3.0) (Triangle for the BGK model, Triangle filled for the ES-BGK model, Diamond for the $\nu(C)$-BGK model, Diamond filled for the new kinetic model I, Star for the new kinetic model II, Line without symbols for the DSMC)

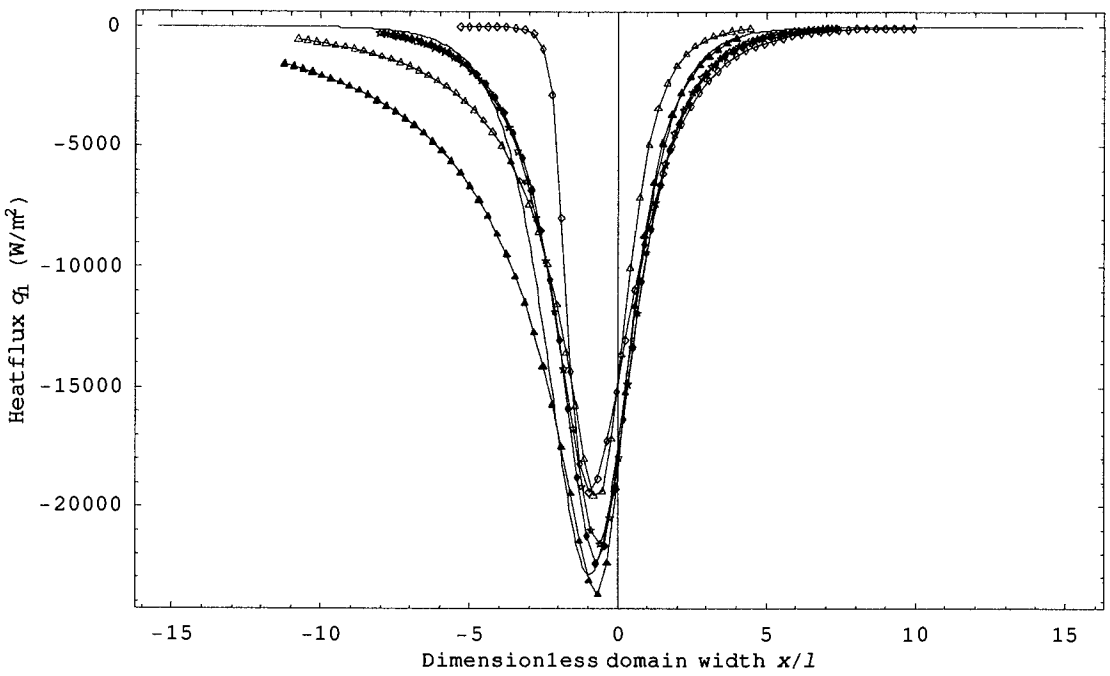

(g)

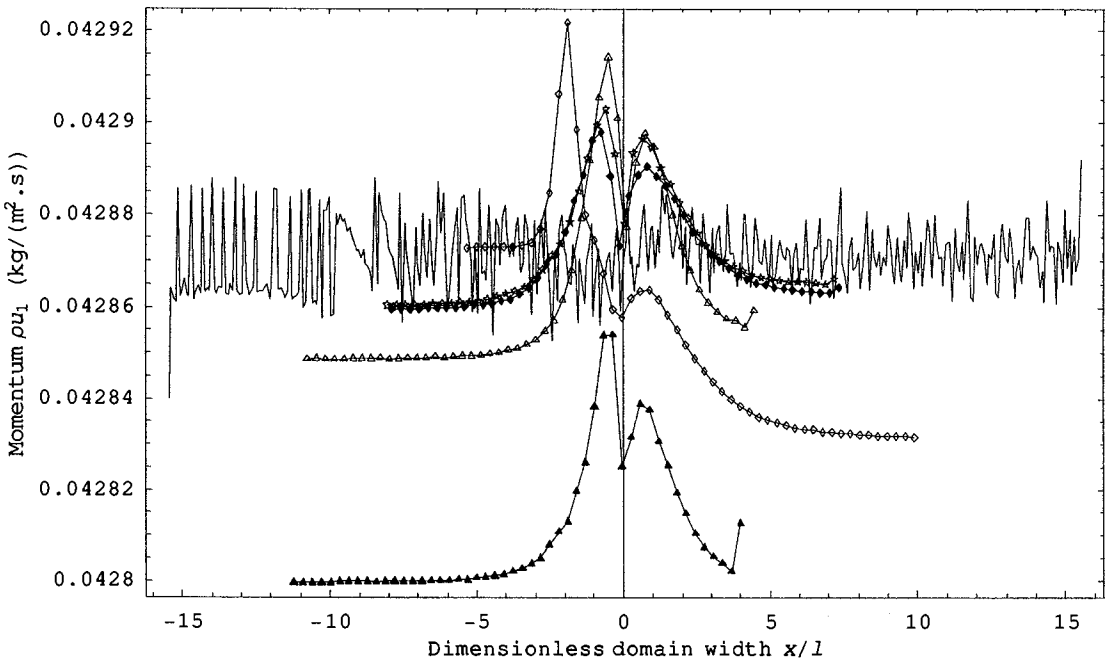

(h)

Figure 3.8: Comparison of kinetic models with DSMC (case 3.5: Ma=3.0) (Triangle for the BGK model, Triangle filled for the ES-BGK model, Diamond for the $\nu(C)$-BGK model, Diamond filled for the new kinetic model I, Star for the new kinetic model II, Line without symbols for the DSMC)

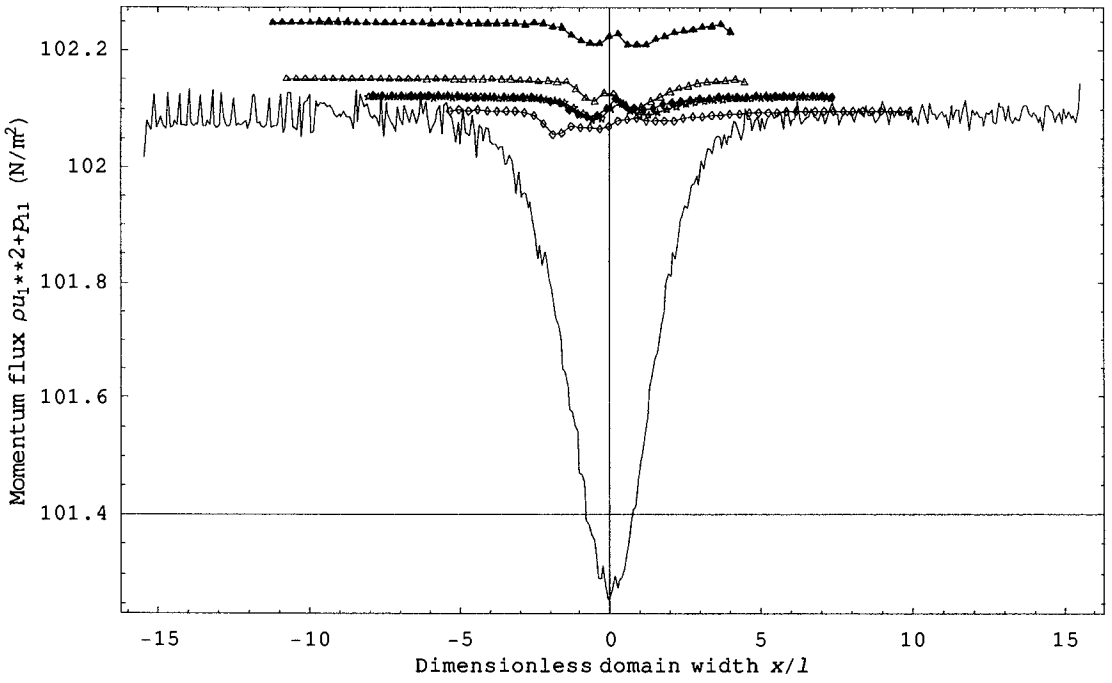

(i)

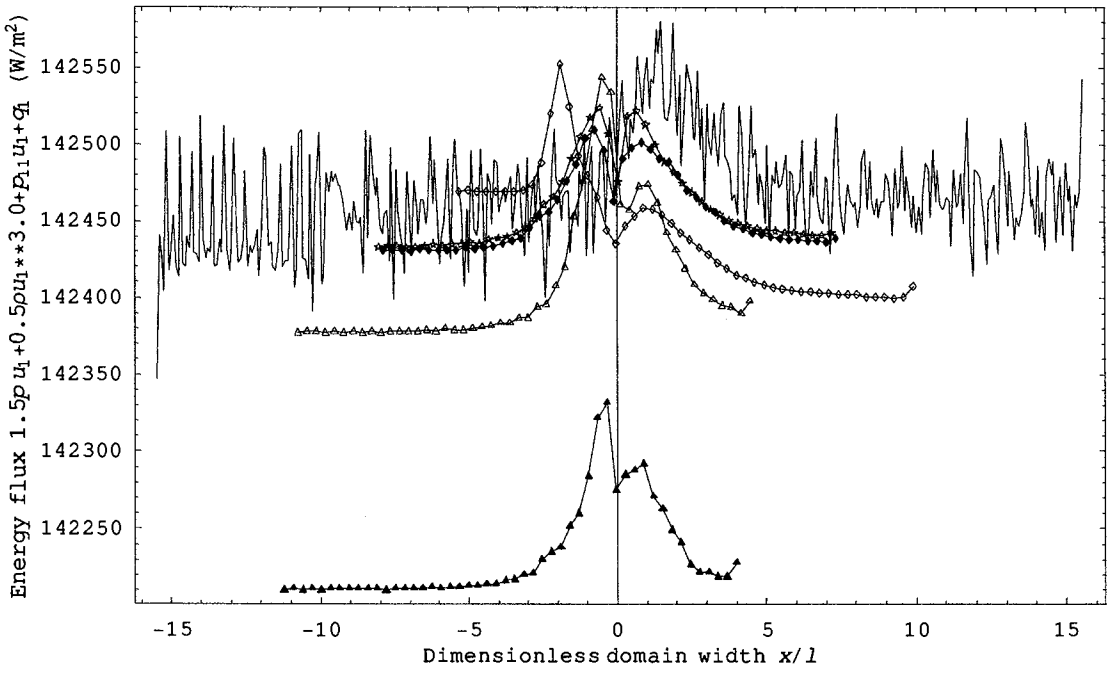

(j)

Figure 3.8: Comparison of kinetic models with DSMC (case 3.5: Ma=3.0) (Triangle for the BGK model, Triangle filled for the ES-BGK model, Diamond for the $\nu(C)$-BGK model, Diamond filled for the new kinetic model I, Star for the new kinetic model II, Line without symbols for the DSMC)

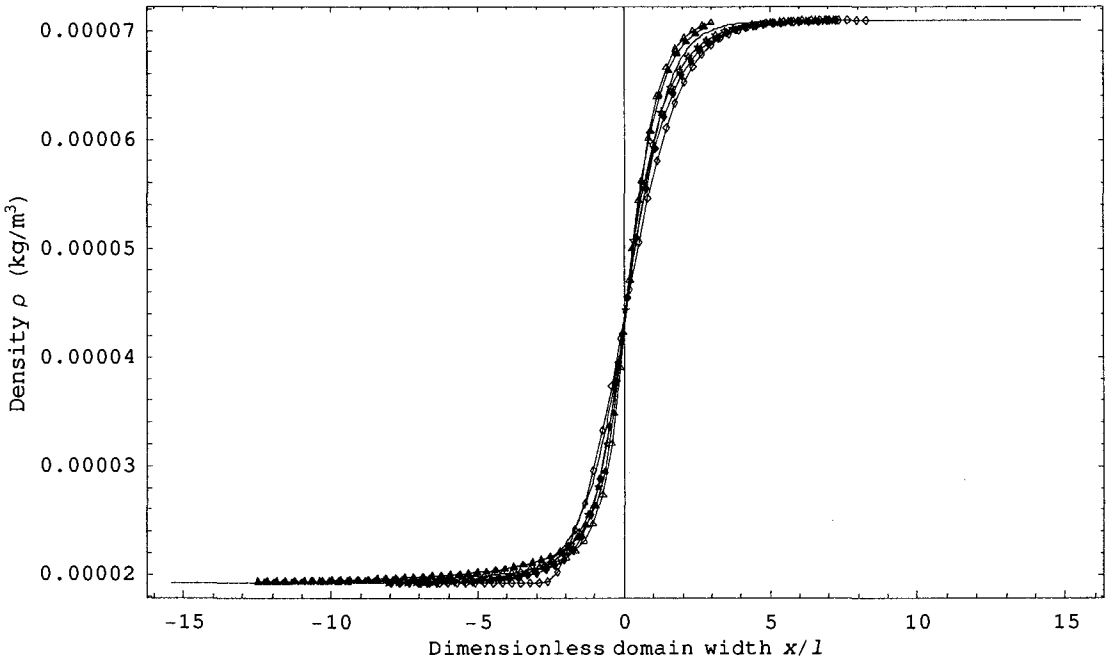

(a)

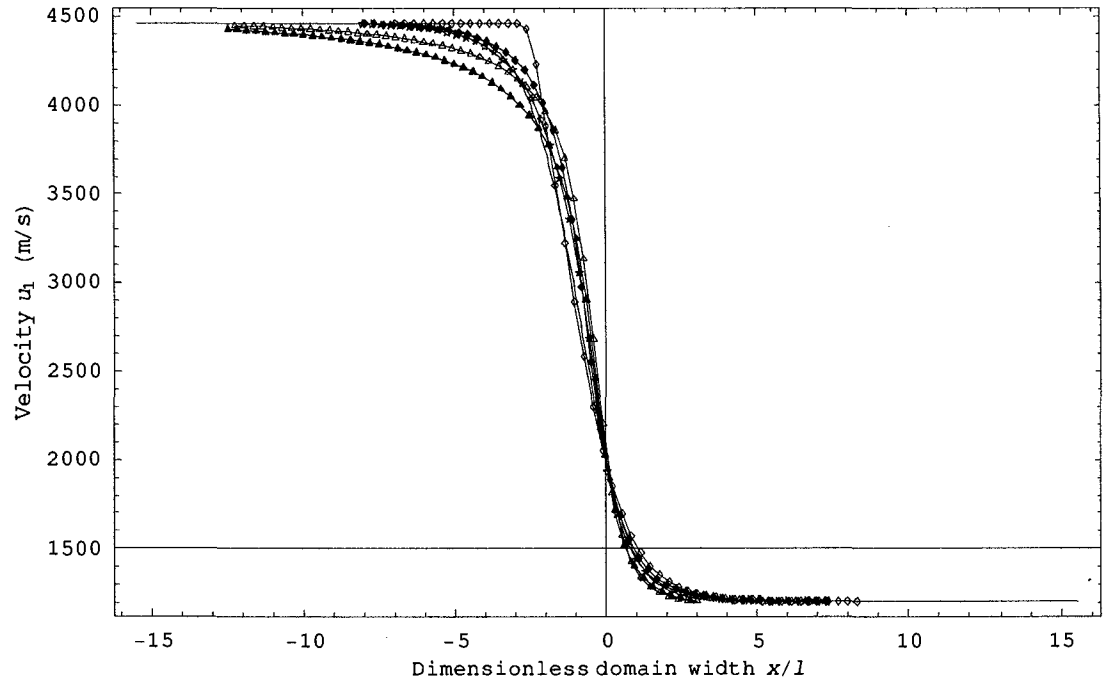

(b)

Figure 3.9: Comparison of kinetic models with DSMC (case 3.6: Ma=6.0) (Triangle for the BGK model, Triangle filled for the ES-BGK model, Diamond for the $\nu(C)$-BGK model, Diamond filled for the new kinetic model I, Star for the new kinetic model II, Line without symbols for the DSMC)

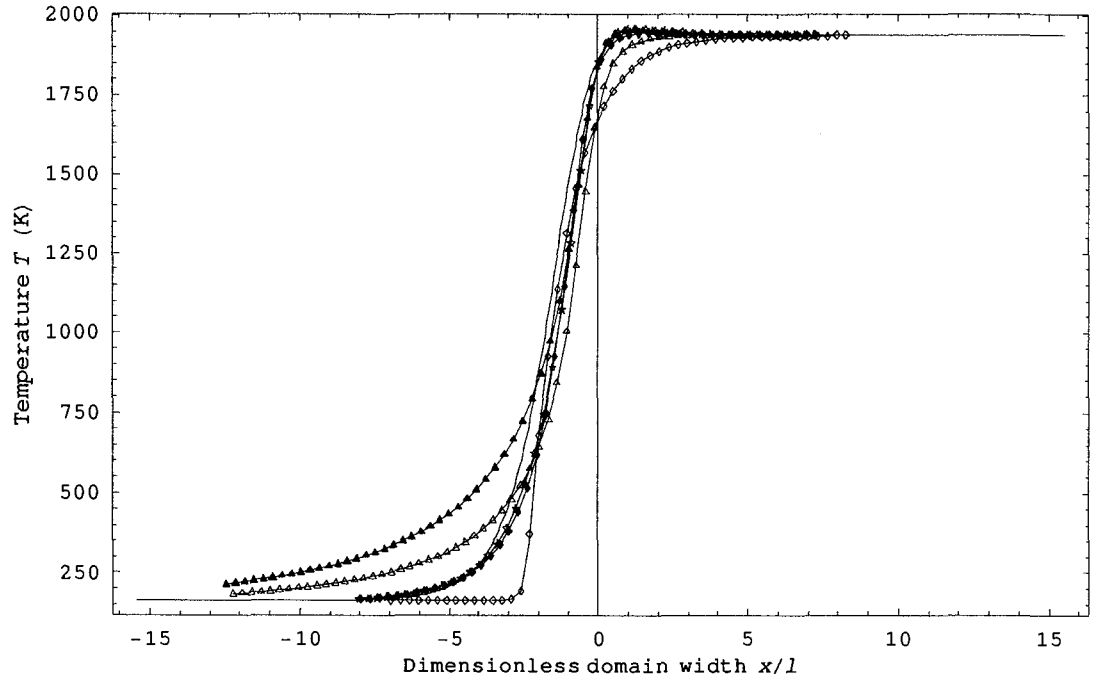

(c)

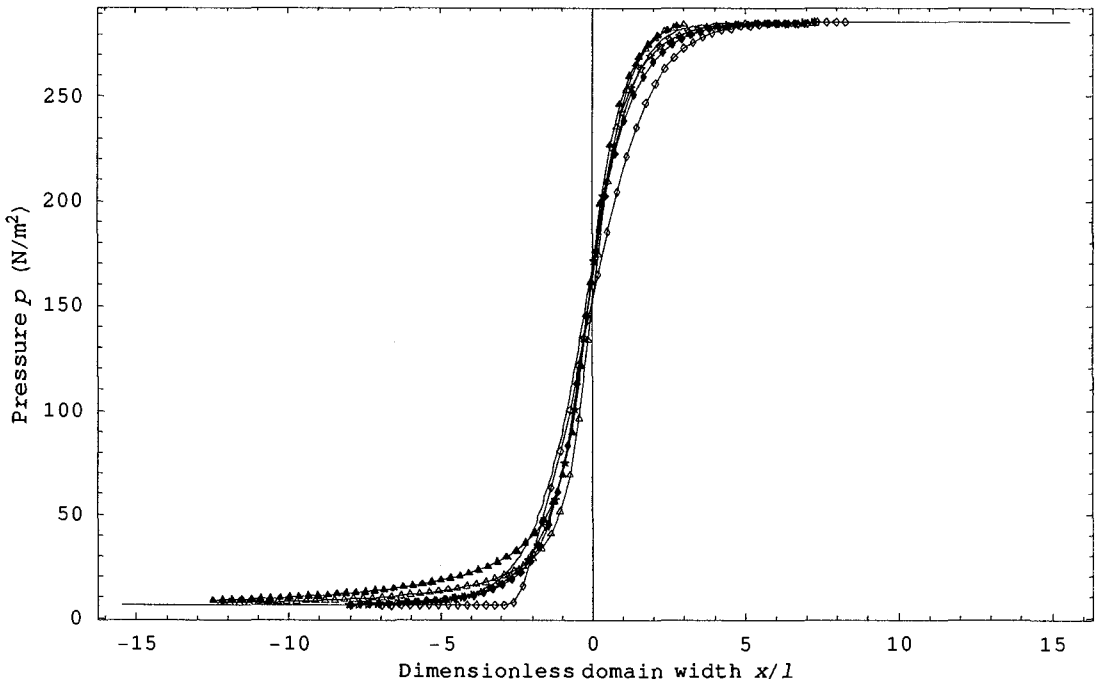

(d)

Figure 3.9: Comparison of kinetic models with DSMC (case 3.6: Ma=6.0) (Triangle for the BGK model, Triangle filled for the ES-BGK model, Diamond for the $\nu(C)$-BGK model, Diamond filled for the new kinetic model I, Star for the new kinetic model II, Line without symbols for the DSMC)

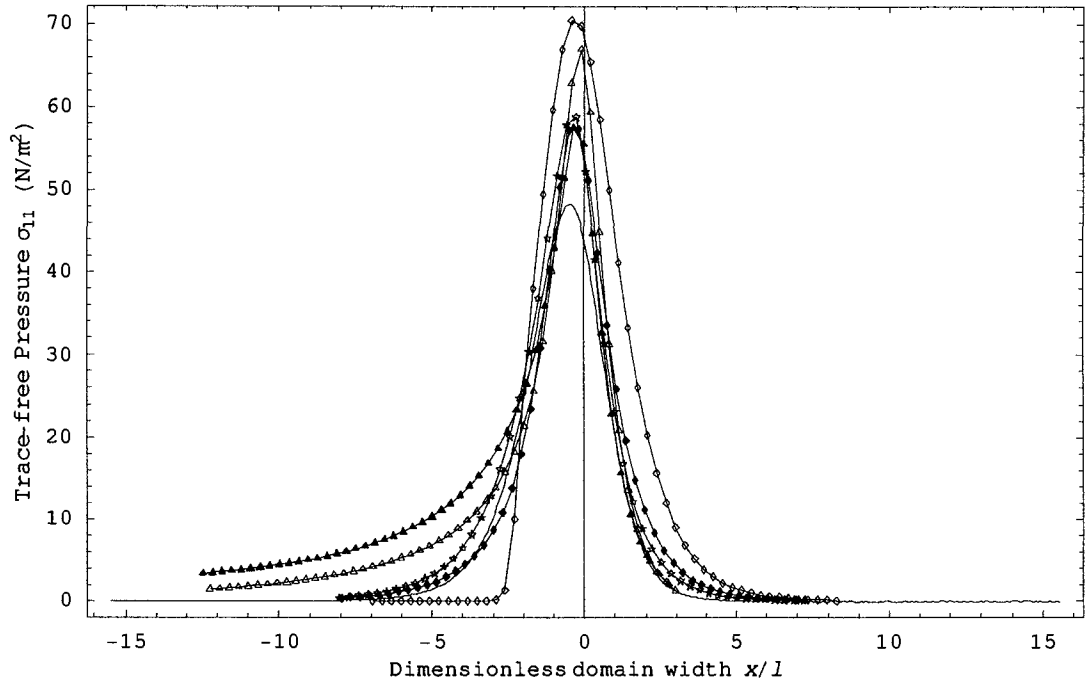

(e)

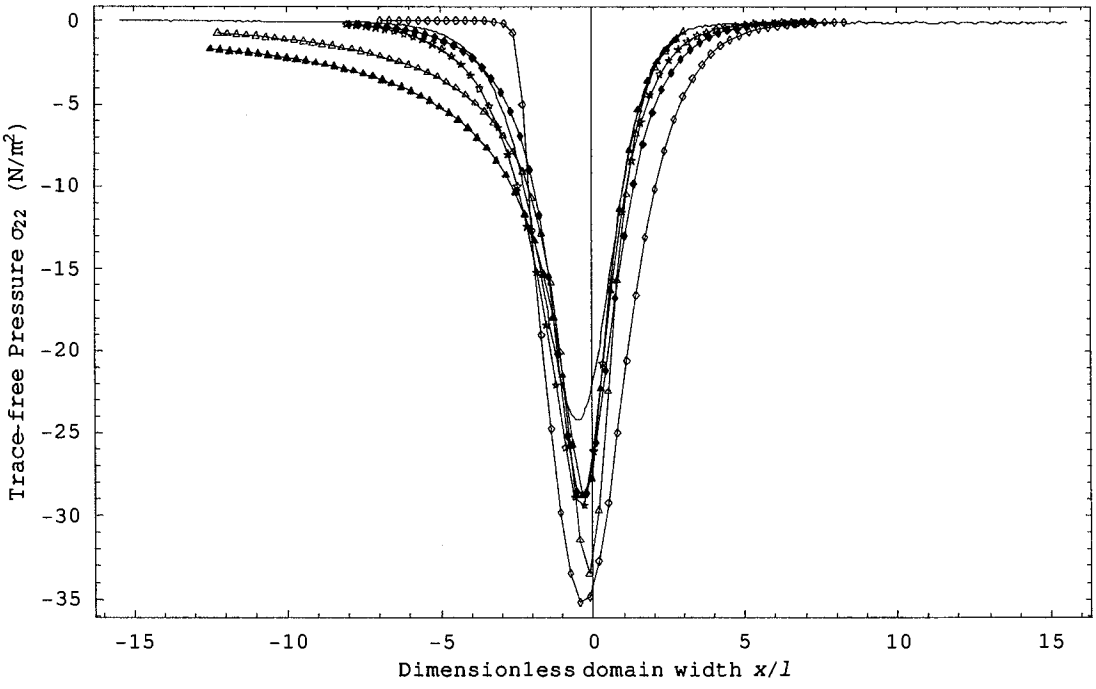

(f)

Figure 3.9: Comparison of kinetic models with DSMC (case 3.6: Ma=6.0) (Triangle for the BGK model, Triangle filled for the ES-BGK model, Diamond for the $\nu(C)$-BGK model, Diamond filled for the new kinetic model I, Star for the new kinetic model II, Line without symbols for the DSMC)

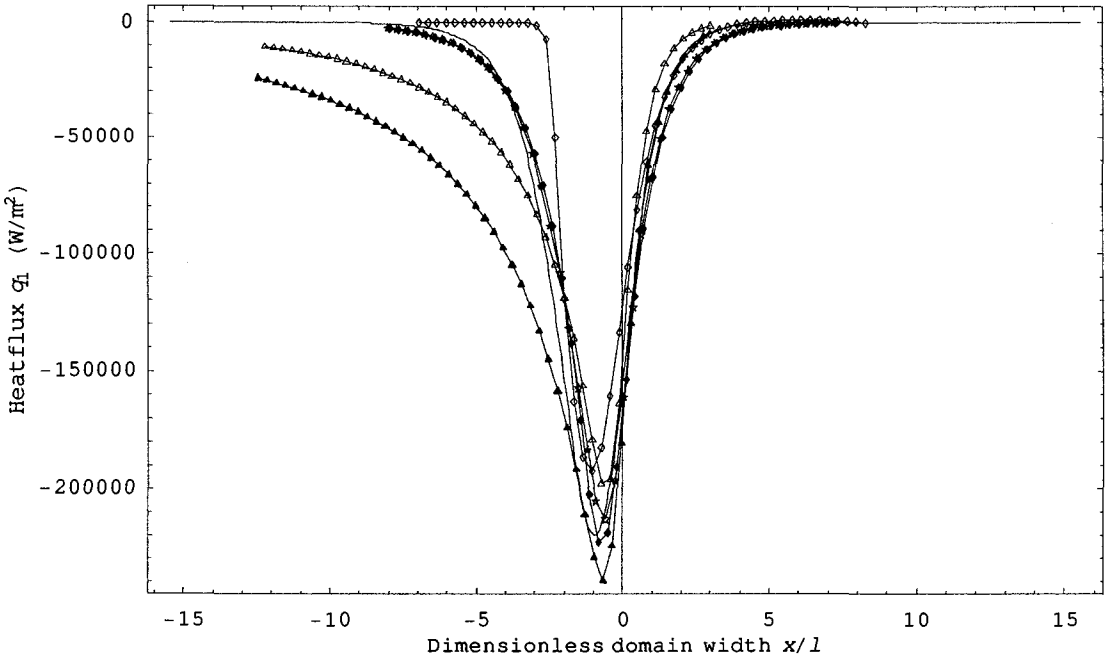

(g)

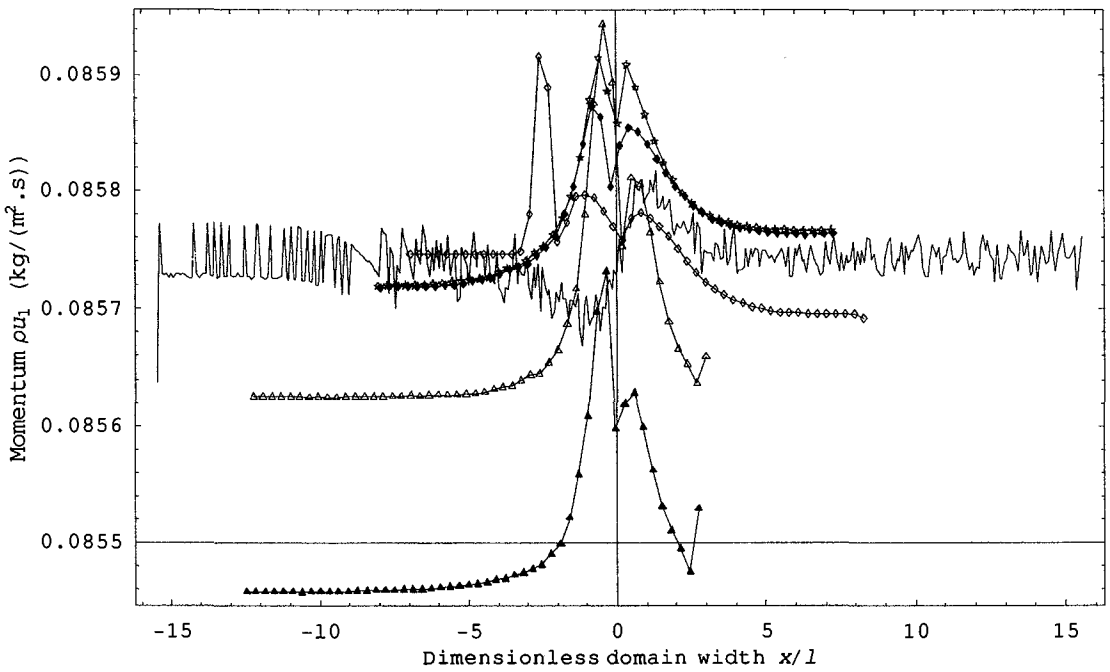

(h)

Figure 3.9: Comparison of kinetic models with DSMC (case 3.6: Ma=6.0) (Triangle for the BGK model, Triangle filled for the ES-BGK model, Diamond for the $\nu(C)$-BGK model, Diamond filled for the new kinetic model I, Star for the new kinetic model II, Line without symbols for the DSMC)

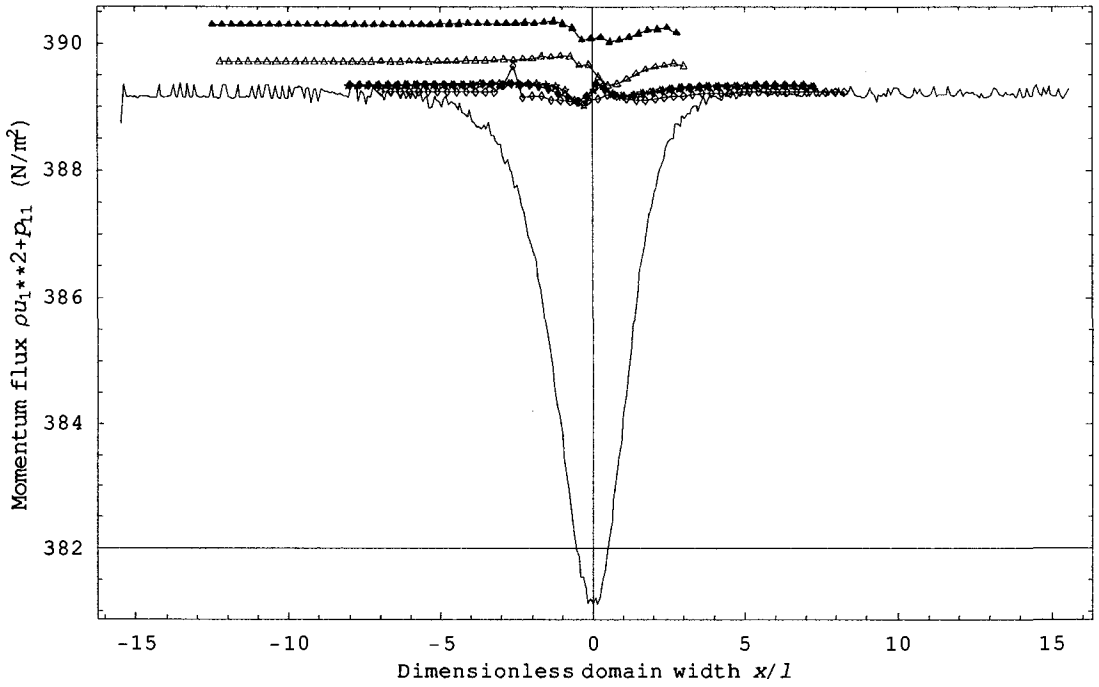

(i)

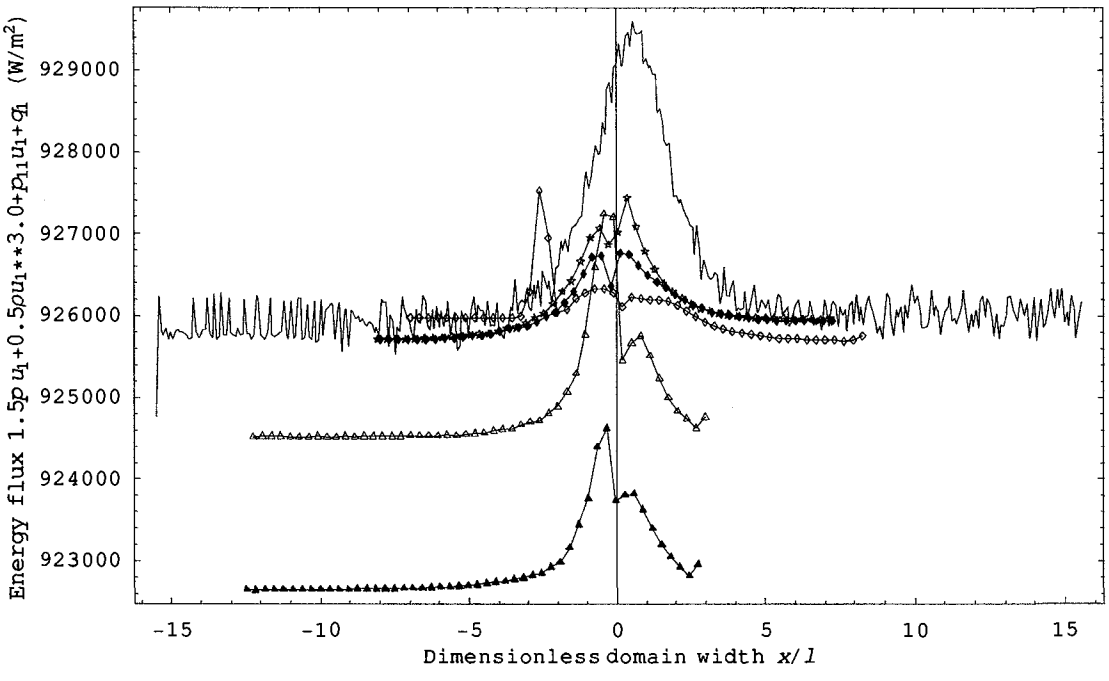

(j)

Figure 3.9: Comparison of kinetic models with DSMC (case 3.6: Ma=6.0) (Triangle for the BGK model, Triangle filled for the ES-BGK model, Diamond for the $\nu(C)$-BGK model, Diamond filled for the new kinetic model I, Star for the new kinetic model II, Line without symbols for the DSMC)

3.5 Conclusion

For the one-dimensional steady state shock wave problem, the following conclusions can be drawn from the results and discussion presented above.

(1) The explicit numerical scheme, based on Mieussens's DVM with necessary modification, works well and the program is stable for running.

(2) The second type linearized f_{ref} for the ES-BGK model and two new kinetic models is better than the first type linearized f_{ref} for them. The linearized f_{ref} can be used to replace the original f_{ref} to save computational time and get almost identical results at the same time. Exceptions are the following situations, in which no (or not good) results could be obtained: the $\nu(C)$-BGK model for medium and strong shock waves, the first type linearized f_{ref} of the new kinetic model I, and the second type linearized f_{ref} of the new kinetic model I for strong shock waves.

(3) The choice of bounds and step of velocity grid based on Eq. (3.37) is accurate enough, while the step of space grid need be smaller than about one sixth of the mean free path at upstream side for strong shock wave situations from our computation.

(4) Through the comparison of kinetic models with DSMC, it is seen that the new kinetic models give similar results, which are closer to DSMC than the other kinetic models. The new kinetic model II is suggested for the simulation of shock wave problems since its program structure is simpler than the program structure of the new kinetic model I, and the Prandtl number can be exactly equal to 2/3, instead of near to 2/3 in the new kinetic model I.

Chapter 4 Numerical work on one-dimensional Couette flow

4.1 Introduction of Couette flow

In the one-dimensional Couette flow (1DCF) problem considered in this chapter, there are two parallel infinite-size plates, one plate is fixed, while the other plate is moving with a certain velocity at x direction in a x-y-z Cartesian frame (or the X1 direction in a X1-X2-X3 Cartesian frame), and the direction perpendicular to the plates is the y direction (or the X2 direction). The temperatures of the two plates are the same, denoted as T_p. Initially the gas between the two plates is uniform, which temperature is same as T_p, the density is ρ_{ini}. What we are interested is the flow at steady state.

Some main characteristic dimensionless numbers of 1DCF are the Mach number, the Reynolds number and the Knudsen number, which are defined as

$$\begin{aligned} \mathrm{Ma} &= \frac{u_{p1}}{a_{p1}}, \\ \mathrm{Re} &= \frac{\rho_{ini} u_{p1} L}{\mu_{ini}}, \\ \mathrm{Kn} &= \frac{l}{L} \sim \frac{\mathrm{Ma}}{\mathrm{Re}}, \end{aligned} \tag{4.1}$$

where the mean free path l is defined as Eq. (3.38), u_{p1} is the speed of the moving plate, $a_{p1} = \sqrt{\frac{5}{3} R T_p}$ is the sound speed at plate temperature, L is the distance between the two plates, and μ_{ini} is the viscosity of gas at the initial state.

From the conservation law Eq. (1.5), one obtains for 1DCF at steady state after some manipulations,

$$\begin{aligned} u_2 &= 0, \qquad & \frac{\partial \sigma_{12}}{\partial y} &= 0, \\ \frac{\partial p_{22}}{\partial y} &= 0, \qquad & \frac{\partial (q_2 + \sigma_{12} u_1)}{\partial y} &= 0, \end{aligned} \tag{4.2}$$

which means that σ_{12}, $p_{22}(=p+\sigma_{22})$, and $q_2+\sigma_{12}u_1$ are constant in the whole domain at steady state, and this will be used to check whether the computed results are results at steady state or not , see Section 4.4.3.

One interesting observation is that from the NSF theory Eq. (1.9) follows that

$$\sigma_{11}^{NSF}=\sigma_{22}^{NSF}=q_1^{NSF}=0.$$

The computational results from the kinetic models and the DSMC shown below (graphs (g, h, j) in Figures 4.4-4.7) show that the above relations are not satisfied for larger Knudsen numbers, and only approximately satisfied for small Knudsen numbers. This shows that the NSF equations, which do not account for any rarefaction effects, are not sufficient to describe rarefied gas flow. The suitability for the NSF equations and other, higher order, macroscopic equations to describe Couette flow will be discussed in Chapter 5.

4.2 Numerical scheme

Since the idea and procedure of numerical scheme here is similar to the idea and procedure of numerical scheme in Chapter 3, we only describe the difference of the program owing to the different test situation. Therefore readers are suggested to go through Section 3.2 before reading this section.

4.2.1 Introduction of explicit scheme

Any kinetic model equation for 1DCF we consider can be expressed as

$$\frac{\partial f}{\partial t}+c_y\frac{\partial f}{\partial y}=\nu\left(f_{ref}-f\right). \tag{4.3}$$

The space variable y is discretized on a uniform grid defined by nodes (centers of finite volumes) $y_i=(i-0.5)\Delta y$, $i=1,\cdots I$, $\Delta y=\frac{L}{I}$, I is the number of total position points. In the following description a dense notation is used, where

$$f\left(y_i,t_n,c_x^{j_1},c_y^{j_2},c_z^{j_3}\right)=f_{i,j}^n.$$

The discretized kinetic model equation based on a finite volume scheme is

$$f_{i,j}^{n+1} = f_{i,j}^{n} - \frac{\Delta t_n}{\Delta y}\left(F^{n}_{i+\frac{1}{2},j} - F^{n}_{i-\frac{1}{2},j}\right) - \Delta t_n \nu^{n}_{i,j}\left(f^{n}_{i,j} - f^{n}_{ref,i,j}\right). \tag{4.4}$$

where the numerical fluxes are defined as

$$F^{n}_{i+\frac{1}{2},j} = \frac{1}{2}\left[c_y^{j_2}\left(f^{n}_{i+1,j} + f^{n}_{i,j}\right) - \left|c_y^{j_2}\right|\left(f^{n}_{i+1,j} - f^{n}_{i,j} - \psi^{n}_{i+\frac{1}{2},j}\right)\right], \tag{4.5}$$

and the CFL condition for the time step Δt_n becomes

$$\Delta t_n = \frac{a}{\max_{i,j}\left(\nu^{n}_{i,j}\right) + \max_{i,j}\left(\dfrac{\left|c_y^{j_2}\right|}{\Delta y}\right)}, \tag{4.6}$$

with $0.0 < a < 1.0$.

4.2.2 Reference distribution $f^{n}_{ref,i,j}$ (original)

The density profile at steady state is not the same as in the initial uniform flow state, therefore $u_{y,i} \neq 0.0$ need to be applied in the process of computation so that the flow can move along the y direction and reach steady state from the initial guess. $u_{y,i} = 0.0$ can be used as a criterion to see whether the final results are results at steady state or not. It is not a pure one-dimensional, but a two-dimensional, problem when reference distribution $f^{n}_{ref,i,j}$ is solved, which is an important difference between the programs for 1DCF and 1DSW. As before for 1DSW, a dimensionless reference distribution (defined as Eq. (3.15)) and the N-R algorithm are used. Expressions of Jacobians used in the N-R algorithm for 1DCF are given in Appendix B.

For the BGK model, the dimensionless reference distribution is

$$F^{n}_{BGK,i,j} = \frac{f^{n}_{BGK,i,j}\Delta \mathbf{c}}{\rho^{n}_{i}} = a^{n}_{BGK,i} \cdot \exp\left(-\Gamma^{n}_{BGK,i}\left(\eta^{n}_{i,j}\right)^2 + \gamma^{n}_{BGK,x,i}\eta^{n}_{i,j_1} + \gamma^{n}_{BGK,y,i}\eta^{n}_{i,j_1}\right), \tag{4.7}$$

and the conditions to determine the four coefficients ($a^{n}_{BGK,i}$, $\Gamma^{n}_{BGK,i}$, $\gamma^{n}_{BGK,x,i}$ and $\gamma^{n}_{BGK,y,i}$) are the conservation laws Eq. (1.4), which give in the discrete case

$$\sum_{j=1}^{J} F^{n}_{BGK,i,j} = 1, \qquad \sum_{j=1}^{J} \eta^{n}_{i,j_1} F^{n}_{BGK,i,j} = 0,$$

$$\sum_{j=1}^{J}\eta_{i,j_2}^{n}F_{BGK,i,j}^{n}=0,\qquad \sum_{j=1}^{J}\frac{(\eta_{i,j}^{n})^{2}}{1.5}F_{BGK,i,j}^{n}=1. \tag{4.8}$$

For the ES-BGK model, the dimensionless reference distribution is

$$F_{ES,i,j}^{n}=a_{ES,i}^{n}\cdot\exp\left(-\Gamma_{ES,xx,i}^{n}(\eta_{i,j_1}^{n})^{2}-\Gamma_{ES,yy,i}^{n}(\eta_{i,j_2}^{n})^{2}-\Gamma_{ES,zz,i}^{n}(\eta_{i,j_3}^{n})^{2}-\Gamma_{ES,xy,i}^{n}\eta_{i,j_1}^{n}\eta_{i,j_2}^{n}+\gamma_{ES,x,i}^{n}\eta_{i,j_1}^{n}+\gamma_{ES,y,i}^{n}\eta_{i,j_2}^{n}\right), \tag{4.9}$$

and the conditions to determine the seven coefficients are the discrete form of Eq. (2.12),

$$\begin{aligned}
&\sum_{j=1}^{J}F_{ES,i,j}^{n}=1,\ \sum_{j=1}^{J}\eta_{i,j_1}^{n}F_{ES,i,j}^{n}=0,\ \sum_{j=1}^{J}\eta_{i,j_2}^{n}F_{ES,i,j}^{n}=0,\\
&\sum_{j=1}^{J}(\eta_{i,j_1}^{n})^{2}F_{ES,i,j}^{n}=\frac{\lambda_{xx,i}^{n}}{2RT_i^{n}}=\frac{1}{2p_i^{n}}\left(\frac{p_{BGK,xx,i}^{n}}{\mathrm{Pr}}+\left(1-\frac{1}{\mathrm{Pr}}\right)p_{xx,i}^{n}\right),\\
&\sum_{j=1}^{J}(\eta_{i,j_2}^{n})^{2}F_{ES,i,j}^{n}=\frac{\lambda_{yy,i}^{n}}{2RT_i^{n}}=\frac{1}{2p_i^{n}}\left(\frac{p_{BGK,yy,i}^{n}}{\mathrm{Pr}}+\left(1-\frac{1}{\mathrm{Pr}}\right)p_{yy,i}^{n}\right),\\
&\sum_{j=1}^{J}(\eta_{i,j_3}^{n})^{2}F_{ES,i,j}^{n}=\frac{\lambda_{zz,i}^{n}}{2RT_i^{n}}=\frac{1}{2p_i^{n}}\left(\frac{p_{BGK,zz,i}^{n}}{\mathrm{Pr}}+\left(1-\frac{1}{\mathrm{Pr}}\right)p_{zz,i}^{n}\right),\\
&\sum_{j=1}^{J}\eta_{i,j_1}^{n}\eta_{i,j_2}^{n}F_{ES,i,j}^{n}=\frac{\lambda_{xy,i}^{n}}{2RT_i^{n}}=\frac{1}{2p_i^{n}}\left(\frac{p_{BGK,xy,i}^{n}}{\mathrm{Pr}}+\left(1-\frac{1}{\mathrm{Pr}}\right)p_{xy,i}^{n}\right).
\end{aligned} \tag{4.10}$$

For the $\nu(C)$-BGK model, the dimensionless reference distribution is

$$F_{\gamma,i,j}^{n}=a_{\gamma,i}^{n}\cdot\exp\left(-\Gamma_{\gamma,i}^{n}(\eta_{i,j}^{n})^{2}+\gamma_{\gamma,x,i}^{n}\eta_{i,j_1}^{n}+\gamma_{\gamma,y,i}^{n}\eta_{i,j_2}^{n}\right), \tag{4.11}$$

and the conditions to determine the four coefficients are the discrete form of Eq. (1.4),

$$\begin{aligned}
&\sum_{j=1}^{J}\hat{\nu}_{i,j}^{n}\frac{(f_{\gamma,i,j}^{n}-f_{i,j}^{n})}{\rho_i^{n}}\Delta\mathbf{c}=0,\ \sum_{j=1}^{J}\hat{\nu}_{i,j}^{n}\eta_{i,j_1}^{n}\frac{(f_{\gamma,i,j}^{n}-f_{i,j}^{n})}{\rho_i^{n}}\Delta\mathbf{c}=0,\\
&\sum_{j=1}^{J}\hat{\nu}_{i,j}^{n}\eta_{i,j_2}^{n}\frac{(f_{\gamma,i,j}^{n}-f_{i,j}^{n})}{\rho_i^{n}}\Delta\mathbf{c}=0,\ \sum_{j=1}^{J}\hat{\nu}_{i,j}^{n}(\eta_{i,j}^{n})^{2}\frac{(f_{\gamma,i,j}^{n}-f_{i,j}^{n})}{\rho_i^{n}}\Delta\mathbf{c}=0.
\end{aligned} \tag{4.12}$$

For the new kinetic model I, the dimensionless reference distribution is

$$F_{NI,i,j}^{n}=a_{NI,i}^{n}\cdot$$
$$\exp\left(-\Gamma_{NI,i}^{n}\left(\Gamma_{ES,xx,i}^{n}(\eta_{i,j_1}^{n})^{2}+\Gamma_{ES,yy,i}^{n}(\eta_{i,j_2}^{n})^{2}+\Gamma_{ES,zz,i}^{n}(\eta_{i,j_3}^{n})^{2}+\Gamma_{ES,xy,i}^{n}\eta_{i,j_1}^{n}\eta_{i,j_2}^{n}\right)+\gamma_{NI,x,i}^{n}\eta_{i,j_1}^{n}+\gamma_{NI,y,i}^{n}\eta_{i,j_2}^{n}\right), \tag{4.13}$$

and the conditions to determine the four coefficients are the discrete form of Eq. (1.4)

$$\sum_{j=1}^{J}\hat{v}_{i,j}^{n}\frac{\left(f_{NI,i,j}^{n}-f_{i,j}^{n}\right)}{\rho_i^n}\Delta\mathbf{c}=0,\ \sum_{j=1}^{J}\hat{v}_{i,j}^{n}\eta_{i,j_1}^{n}\frac{\left(f_{NI,i,j}^{n}-f_{i,j}^{n}\right)}{\rho_i^n}\Delta\mathbf{c}=0,$$
$$\sum_{j=1}^{J}\hat{v}_{i,j}^{n}\eta_{i,j_2}^{n}\frac{\left(f_{NI,i,j}^{n}-f_{i,j}^{n}\right)}{\rho_i^n}\Delta\mathbf{c}=0,\ \sum_{j=1}^{J}\hat{v}_{i,j}^{n}\left(\eta_{i,j}^{n}\right)^2\frac{\left(f_{NI,i,j}^{n}-f_{i,j}^{n}\right)}{\rho_i^n}\Delta\mathbf{c}=0. \tag{4.14}$$

For the new kinetic model II, the dimensionless reference distribution is

$$F_{NII,i,j}^{n}=a_{NII,i}^{n}\cdot$$
$$\exp\left(-\Gamma_{NII,xx,i}^{n}\left(\eta_{i,j_1}^{n}\right)^2-\Gamma_{NII,yy,i}^{n}\left(\eta_{i,j_2}^{n}\right)^2-\Gamma_{NII,zz,i}^{n}\left(\eta_{i,j_3}^{n}\right)^2-\Gamma_{NII,xy,i}^{n}\eta_{i,j_1}^{n}\eta_{i,j_2}^{n}+\gamma_{NII,x,i}^{n}\eta_{i,j_1}^{n}+\gamma_{NII,y,i}^{n}\eta_{i,j_2}^{n}\right), \tag{4.15}$$

and the conditions to determine the seven coefficients are the discrete form of Eq. (2.39),

$$\sum_{j=1}^{J}\hat{v}_{i,j}^{n}\frac{\left(f_{NII,i,j}^{n}-f_{i,j}^{n}\right)}{\rho_i^n}\Delta\mathbf{c}=0,\ \sum_{j=1}^{J}\hat{v}_{i,j}^{n}\eta_{i,j_1}^{n}\frac{\left(f_{NII,i,j}^{n}-f_{i,j}^{n}\right)}{\rho_i^n}\Delta\mathbf{c}=0,$$
$$\sum_{j=1}^{J}\hat{v}_{i,j}^{n}\eta_{i,j_2}^{n}\frac{\left(f_{NII,i,j}^{n}-f_{i,j}^{n}\right)}{\rho_i^n}\Delta\mathbf{c}=0,\ \sum_{j=1}^{J}\hat{v}_{i,j}^{n}\left(\eta_{i,j_1}^{n}\right)^2\frac{\left(f_{NII,i,j}^{n}-f_{i,j}^{n}\right)}{\rho_i^n}\Delta\mathbf{c}=\frac{\left(p_{BGK,xx,i}^{n}-p_{xx,i}^{n}\right)}{2p_i^n},$$
$$\sum_{j=1}^{J}\hat{v}_{i,j}^{n}\left(\eta_{i,j_2}^{n}\right)^2\frac{\left(f_{NII,i,j}^{n}-f_{i,j}^{n}\right)}{\rho_i^n}\Delta\mathbf{c}=\frac{\left(p_{BGK,yy,i}^{n}-p_{yy,i}^{n}\right)}{2p_i^n}, \tag{4.16}$$
$$\sum_{j=1}^{J}\hat{v}_{i,j}^{n}\left(\eta_{i,j_3}^{n}\right)^2\frac{\left(f_{NII,i,j}^{n}-f_{i,j}^{n}\right)}{\rho_i^n}\Delta\mathbf{c}=\frac{\left(p_{BGK,zz,i}^{n}-p_{zz,i}^{n}\right)}{2p_i^n},$$
$$\sum_{j=1}^{J}\hat{v}_{i,j}^{n}\left(\eta_{i,j_1}^{n}\eta_{i,j_2}^{n}\right)\frac{\left(f_{NII,i,j}^{n}-f_{i,j}^{n}\right)}{\rho_i^n}\Delta\mathbf{c}=\frac{\left(p_{BGK,xy,i}^{n}-p_{xy,i}^{n}\right)}{2p_i^n}.$$

4.2.3 Reference distribution $f_{ref,i,j}^{n}$ (linearized)

Only expressions of linearized dimensionless reference distribution functions are given here, while corresponding linear equations can be found in Appendix C.

For the BGK model, the linearized dimensionless reference distribution is

$$F_{BGK,i,j}^{n}=\exp\left(-\left(\eta_{i,j}^{n}\right)^2\right)\left(a1_{BGK,i}^{n}+a2_{BGK,i}^{n}\eta_{i,j_1}^{n}+a3_{BGK,i}^{n}\eta_{i,j_2}^{n}+a4_{BGK,i}^{n}\left(\eta_{i,j}^{n}\right)^2\right). \tag{4.17}$$

For the $\nu(C)$-BGK model, the linearized dimensionless reference distribution is

$$F^n_{\gamma,i,j} = \exp\left(-\left(\eta^n_{i,j}\right)^2\right)\left(a1^n_{\lambda,i} + a2^n_{\gamma,i}\eta^n_{i,j_1} + a3^n_{\gamma,i}\eta^n_{i,j_2} + a4^n_{\gamma,i}\left(\eta^n_{i,j}\right)^2\right). \tag{4.18}$$

For the ES-BGK model and two new kinetic models, as in 1DSW, there are two choices to build the linearized reference distribution. One is to expand the reference distribution around the Maxwellian distribution, and another one is to expand the reference distribution around an anisotropic Gaussian distribution. These two choices have been tested in this work to see which one gives the more similar results to the results with original reference distribution.

For the ES-BGK model, the linearized dimensionless reference distribution from the first choice is

$$F^n_{ES,i,j} = \exp\left(-\left(\eta^n_{i,j}\right)^2\right)\cdot$$
$$\left(a1^n_{ES,i} + a2^n_{ES,i}\eta^n_{i,j_1} + a3^n_{ES,i}\eta^n_{i,j_2} + a4^n_{ES,i}\left(\eta^n_{i,j_1}\right)^2 + a5^n_{ES,i}\left(\eta^n_{i,j_2}\right)^2 + a6^n_{ES,i}\left(\eta^n_{i,j_3}\right)^2 + a7^n_{ES,i}\eta^n_{i,j_1}\eta^n_{i,j_2}\right) \tag{4.19}$$

and this choice makes the results of the ES-BGK model with linearized $f^n_{ref,i,j}$ and $b=0$ identical to results of the BGK model with linearized $f^n_{ref,i,j}$.

For the new kinetic model I, the linearized dimensionless reference distribution from the first choice is

$$F^n_{NI,i,j} = \exp\left(-\left(\eta^n_{i,j}\right)^2\right)\cdot$$
$$\left(a1^n_{NI,i} + a2^n_{NI,i}\eta^n_{i,j_1} + a3^n_{NI,i}\eta^n_{i,j_2} + a4^n_{NI,i}\left(a4^n_{ES,i}\left(\eta^n_{i,j_1}\right)^2 + a5^n_{ES,i}\left(\eta^n_{i,j_2}\right)^2 + a6^n_{ES,i}\left(\eta^n_{i,j_3}\right)^2 + a7^n_{ES,i}\eta^n_{i,j_1}\eta^n_{i,j_2}\right)\right) \tag{4.20}$$

For the new kinetic model II, the linearized dimensionless reference distribution from the first choice is

$$F^n_{NII,i,j} = \exp\left(-\left(\eta^n_{i,j}\right)^2\right)\cdot$$
$$\left(a1^n_i + a2^n_i\eta^n_{i,j_1} + a3^n_i\eta^n_{i,j_2} + a4^n_i\left(\eta^n_{i,j_1}\right)^2 + a5^n_i\left(\eta^n_{i,j_2}\right)^2 + a6^n_i\left(\eta^n_{i,j_3}\right)^2 + a7^n_i\left(\eta^n_{i,j_2}\eta^n_{i,j_3}\right)\right) \tag{4.21}$$

For the ES-BGK model, the linearized dimensionless reference distribution from the second choice is

$$F^n_{ES,i,j} = \exp\left(-\varepsilon^n_{ES,xx,i}\left(\eta^n_{i,j_1}\right)^2 - \varepsilon^n_{ES,yy,i}\left(\eta^n_{i,j_2}\right)^2 - \varepsilon^n_{ES,zz,i}\left(\eta^n_{i,j_3}\right)^2 - \varepsilon^n_{ES,xy,i}\eta^n_{i,j_1}\eta^n_{i,j_2}\right)\cdot$$
$$\left(a1^n_{ES,i} + a2^n_{ES,i}\eta^n_{i,j_1} + a3^n_{ES,i}\eta^n_{i,j_2} + a4^n_{ES,i}\left(\eta^n_{i,j_1}\right)^2 + a5^n_{ES,i}\left(\eta^n_{i,j_2}\right)^2 + a6^n_{ES,i}\left(\eta^n_{i,j_3}\right)^2 + a7^n_{ES,i}\eta^n_{i,j_1}\eta^n_{i,j_2}\right), \tag{4.22}$$

where $\varepsilon^n_{ES,i}$ are the discrete values of the dimensionless coefficient $\varepsilon_{ij}RT$ in the ES-BGK model. After some manipulation, the expression for $\varepsilon^n_{ES,i}$ can be obtained as

$$\varepsilon^n_{ES,i} = \begin{bmatrix} \dfrac{\lambda^n_{yy,i}\lambda^n_{zz,i}}{\left|\lambda^n_i\right|} & -\dfrac{\lambda^n_{xy,i}\lambda^n_{zz,i}}{\left|\lambda^n_i\right|} & 0 \\ -\dfrac{\lambda^n_{xy,i}\lambda^n_{zz,i}}{\left|\lambda^n_i\right|} & \dfrac{\lambda^n_{zz,i}\lambda^n_{xx,i}}{\left|\lambda^n_i\right|} & 0 \\ 0 & 0 & \dfrac{\left(\lambda^n_{xx,i}\lambda^n_{yy,i} - \lambda^n_{xy,i}\lambda^n_{xy,i}\right)}{\left|\lambda^n_i\right|} \end{bmatrix}, \quad \lambda^n_{xx,i} = \frac{1}{p^n_i}\left(\frac{p^n_{BGK,xx,i}}{\mathrm{Pr}} + \left(1-\frac{1}{\mathrm{Pr}}\right)p^n_{xx,i}\right),$$

$$\lambda^n_{yy,i} = \frac{1}{p^n_i}\left(\frac{p^n_{BGK,yy,i}}{\mathrm{Pr}} + \left(1-\frac{1}{\mathrm{Pr}}\right)p^n_{yy,i}\right), \quad \lambda^n_{zz,i} = \frac{1}{p^n_i}\left(\frac{p^n_{BGK,zz,i}}{\mathrm{Pr}} + \left(1-\frac{1}{\mathrm{Pr}}\right)p^n_{zz,i}\right), \tag{4.23}$$

$$\lambda^n_{xy,i} = \frac{1}{p^n_i}\left(\frac{p^n_{BGK,xy,i}}{\mathrm{Pr}} + \left(1-\frac{1}{\mathrm{Pr}}\right)p^n_{xy,i}\right), \quad \left|\lambda^n_i\right| = \left(\lambda^n_{xx,i}\lambda^n_{yy,i} - \lambda^n_{xy,i}\lambda^n_{xy,i}\right)\lambda^n_{zz,i}.$$

For the new kinetic model I, the linearized dimensionless reference distribution from the second choice is

$$F^n_{NI,i,j} = \exp\left(-\varepsilon^n_{ES,xx,i}\left(\eta^n_{i,j_1}\right)^2 - \varepsilon^n_{ES,yy,i}\left(\eta^n_{i,j_2}\right)^2 - \varepsilon^n_{ES,zz,i}\left(\eta^n_{i,j_3}\right)^2 - \varepsilon^n_{ES,xy,i}\eta^n_{i,j_1}\eta^n_{i,j_2}\right)\cdot$$
$$\left(a1^n_{NI,i} + a2^n_{NI,i}\eta^n_{i,j_1} + a3^n_{NI,i}\eta^n_{i,j_2} + a4^n_{NI,i}\left(a4^n_{ES,i}\left(\eta^n_{i,j_1}\right)^2 + a5^n_{ES,i}\left(\eta^n_{i,j_2}\right)^2 + a6^n_{ES,i}\left(\eta^n_{i,j_3}\right)^2 + a7^n_{ES,i}\eta^n_{i,j_1}\eta^n_{i,j_2}\right)\right), \tag{4.24}$$

For the new kinetic model II, the linearized dimensionless reference distribution from the second choice is

$$F^n_{NII,i,j} = \exp\left(-\varepsilon^n_{ES,xx,i}\left(\eta^n_{i,j_1}\right)^2 - \varepsilon^n_{ES,yy,i}\left(\eta^n_{i,j_2}\right)^2 - \varepsilon^n_{ES,zz,i}\left(\eta^n_{i,j_3}\right)^2 - \varepsilon^n_{ES,xy,i}\eta^n_{i,j_1}\eta^n_{i,j_2}\right)\cdot$$
$$\left(a1^n_i + a2^n_i\eta^n_{i,j_1} + a3^n_i\eta^n_{i,j_2} + a4^n_i\left(\eta^n_{i,j_1}\right)^2 + a5^n_i\left(\eta^n_{i,j_2}\right)^2 + a6^n_i\left(\eta^n_{i,j_3}\right)^2 + a7^n_i\left(\eta^n_{i,j_2}\eta^n_{i,j_3}\right)\right). \tag{4.25}$$

4.2.4 Boundary conditions and initial guess

For 1DCF, the distribution at boundaries $f^n_{-1,j}(=f^n_{0,j})$, and $f^n_{I+1,j}$ $(=f^n_{I+2,j})$ changes with global iteration. Maxwell's boundary conditions [1, 70][15] and a classical ghost cell technique are used here. At the plate 1 (we can do a similar analysis for plate 2), the distribution is

$$f^n_{0,j}=\begin{cases} f^n_{1,j} & c_y^{j_2}<0 \\ (1-\alpha_{p1})\ddot{f}^n_{1,J}+\alpha_{p1}f^n_{p1,j} & c_y^{j_2}\geq 0 \end{cases}, \tag{4.26}$$

where

$$\ddot{f}^n_{1,j}\left(c_x^{j_1},c_y^{j_2},c_z^{j_3}\right)=f^n_{1,j}\left(c_x^{j_1},-c_y^{j_2},c_z^{j_3}\right). \tag{4.27}$$

α_{p1} is the accommodation coefficient, which ranges from 0 to 1, where $\alpha_{p1}=0$ means a "polished" boundary, and $\alpha_{p1}=1.0$ means thermalizing boundary. The accomodation coefficient and chosen as a constant in all iterations. $f^n_{p1,j}$ is a Maxwellian at plate temperature, where the density is chosen so as to have no accumulation of particles at the walls. How to determine $f^n_{p1,j}$ will be described below.

Define a dimensionless distribution

$$F^n_{p1,j}=a^n_{p1}\cdot\exp\left(-\Gamma^n_{p1}\left(\eta^n_{p1,j}\right)^2+\gamma^n_{p1}\eta^n_{p1,j_1}\right), \tag{4.28}$$

where $\eta^n_{p1,j_1}=\dfrac{c_x^{j_1}-u_{p1,x}}{\sqrt{2RT_{p1}}}=\dfrac{C^n_{p1,j_1}}{\sqrt{2RT_{p1}}}$, $\eta^n_{p1,j_2}=\dfrac{C^n_{p1,j_2}}{\sqrt{2RT_{p1}}}$, $\eta^n_{p1,j_3}=\dfrac{C^n_{p1,j_3}}{\sqrt{2RT_{p1}}}$, and $\left(\eta^n_{p1,j}\right)^2=\left(\eta^n_{p1,j_1}\right)^2+\left(\eta^n_{p1,j_2}\right)^2+\left(\eta^n_{p1,j_3}\right)^2=\dfrac{\left(C^n_{p1,j}\right)^2}{2RT_{p1}}$. T_{p1} is the temperature of plate 1, and $u_{p1,x}$ is the macroscopic velocity of plate 1, which both are constants in the whole iteration. Because these two values are constants, therefore, $F^n_{p1,j}=F_{p1,j}$, which means in the whole computation, their values only need be computed one time. The three conditions to determine the three coefficients in Eq. (4.28) are

$$\sum_{j=1}^{J}F_{p1,j}=1,\ \sum_{j=1}^{J}\eta_{p1,j_1}F_{p1,j}=0,\ \sum_{j=1}^{J}\frac{\left(\eta_{p1,j}\right)^2}{1.5}F_{p1,j}=1. \tag{4.29}$$

[15] There are some more advanced boundary conditions available [1]. Since our aim is to test kinetic models, we use this simple boundary condition.

After $F_{p1,j}$ are obtained,

$$f_{p1,j}^{n} = \frac{F_{p1,j}\rho_{p1}^{n}}{\Delta \mathbf{c}}, \tag{4.30}$$

where ρ_{p1}^{n}, the density of the thermalized particles, is not a constant during the process, therefore $f_{p1,j}^{n}$ is not a constant in the whole computation. The condition to determine ρ_{p1}^{n} and further $f_{0,j}^{n}$ as follows, which means no particle of fluid will go through the boundary.

$$\sum_{j,c_y^{j_2}>0}^{J} c_y^{j_2} f_{0,j}^{n} \Delta \mathbf{c} + \sum_{j,c_y^{j_2}<0}^{J} c_y^{j_2} f_{1,j}^{n} \Delta \mathbf{c} = 0. \tag{4.31}$$

If $\alpha_{W1} = 0.0$, then from Eq. (4.26), we get

$$f_{0,j}^{n} = \begin{cases} f_{1,j}^{n} & c_y^{j_2} < 0 \\ \ddot{f}_{1,j}^{n} & c_y^{j_2} \geq 0 \end{cases}, \tag{4.32}$$

which indeed satisfies the condition Eq. (4.31).

If $\alpha_{p1} \neq 0.0$, then from Eqs. (4.26, 4.30, 4.31), we get

$$\rho_{p1}^{n} = -\frac{\sum_{j,c_y^{j_2}<0}^{J} c_y^{j_2} f_{1,j}^{n} \Delta \mathbf{c} + (1-\alpha_{p1}) \sum_{j,c_y^{j_2}>0}^{J} c_y^{j_2} \ddot{f}_{1,j}^{n} \Delta \mathbf{c}}{\alpha_{p1} \sum_{j,c_y^{j_2}>0}^{J} c_y^{j_2} F_{p1,j}}, \tag{4.33}$$

where $\sum_{j,c_y^{j_2}>0}^{J} c_y^{j_2} F_{p1,j}$ is a constant during the computation. After ρ_{p1}^{n} is obtained, $f_{p1,BGK,j}^{n}$ and $f_{0,j}^{n}$ will be also obtained.

There are several choices for the initial guess of the distribution for 1DCF, such as, equilibrium distribution at one boundary, step function of the two distributions at boundaries, average value of the two distributions at boundaries, distribution corresponding to the average value of macroscopic parameters at boundaries, etc. We did

some tests, and realized that the choice of initial guess, which only changes results of the beginning several hundred iterations, does not change the final results of our computations. We prefer to choose the last choice, for it is the guess nearest to the final result for large Knudsen numbers and/or large plate velocity situations.

Since the total density should be conserved for 1DCF, $f_{i,j}^{n}$ are modified by a factor to guarantee this condition every certain iteration (such as, every 100 iteration in this work). What is done in this work is the same as in [34], which is that modified distributions equal to the original computed distributions times a factor, and this factor equals to the initial total mass divided by the current computed total mass.

4.3 Test examples

In the tests, several Knudsen numbers (Kn=0.025, 0.1, 0.5 and 1.0) have been chosen to represent the weak, medium and strong rarefaction effect, the two limiting situations for the molecular model, hard sphere molecules and Maxwell molecules, and three values of plate speed, 300.0m/s, 600.0m/s and 1000.0m/s, are considered. Altogether, there are twelve different test situations. Table 4.1 shows situations of numerical tests of kinetic models and DSMC, and Table 4.2 gives the parameters, with the same meaning as in Table 3.2, in the numerical tests of DSMC [71].

There are some common parameters in the numerical tests, which are, the material is argon, the temperatures of the two plates are both 273.0 K, the velocity of plate 1 is zero, the velociy of plate 2 is chosen as indicated in Table 4.1, the initial number density is 1.4E20 $1/m^3$, the viscosity at the reference temperature is 1.9552E-5 kg/m·s, the reference temperature is 273.0 K [71], Boltzmann's constant is 1.381E-23 J/K, Avogadro's Number is 6.022E23 1/mol, the molecular mass of argon is 39.95 g/mol [69]. Mean free path from Cercignani's definition, Eq. (3.38), is 8.833 mm.

Table 4.3 shows parameters used in the numerical tests of kinetic models. Direct output macroscopic parameters are density ρ, velocity u_1 and u_2, temperature T,

pressure p_{11}, p_{22} and p_{12}, and heat flux q_1 and q_2, which are the same as the DSMC results [69]. The test kinetic models are the BGK model, the ES-BGK model with $b=-0.5$, the $\nu(C)$-BGK model, the new kinetic model I with $b=-0.5$, the new kinetic model II with $\Pr=2/3$. For the reference distribution function f_{ref}, what are tested is not only the original expression (refer to Section 4.2.2), but also the two linearized expressions (refer to Section 4.2.3). In cases 4.1-4.12 of Table 4.3, which corresponds to the twelve basic situations in Table 4.1, all choices of kinetic model and reference distribution are tested. In cases 4.13-4.24 of Table 4.3, which aim is to test the influence of step of space grid (4.17-4.20), bounds of velocity grid (4.21-4.22) and step of velocity grid (4.13-4.16, 4.23-4.24) on the computational results, all kinetic models with the original reference distribution are tested.

Table 4.1: Situations of numerical tests of kinetic models and DSMC for 1DCF

Situation	Knudsen number	Molecular model	Velocity of plate(m/s)	Mach number	Reynolds number	Domain width (m)
Sa	0.025	Hard sphere	300.0	0.975	50.345	0.3533
Sb	0.025	Maxwell molecule	300.0	0.975	50.345	0.3533
Sc	0.1	Hard sphere	300.0	0.975	12.587	0.08833
Sd	0.1	Maxwell molecule	300.0	0.975	12.587	0.08833
Se	0.5	Hard sphere	300.0	0.975	2.518	0.01767
Sf	0.5	Maxwell molecule	300.0	0.975	2.518	0.01767
Sg	1.0	Hard sphere	300.0	0.975	1.259	0.008833
Sh	1.0	Maxwell molecule	300.0	0.975	1.259	0.008833
Si	0.5	Hard sphere	600.0	1.950	5.036	0.01767
Sj	0.5	Hard sphere	1000.0	3.251	8.393	0.01767
Sk	0.5	Maxwell molecule	600.0	1.950	5.036	0.01767
Sl	0.5	Maxwell molecule	1000.0	3.251	8.393	0.01767

Table 4.2: Some common parameters in the numerical tests of DSMC for 1DCF

Parameter	Value	Parameter	Value
FNUM	5.6E14	SP(1,1)	3.7758E-10 for hard sphere; 4.8057E-10 for Maxwell molecules
MNM	2.5E5	SP(3,1)	0.5 for hard sphere; 1.0 for Maxwell molecules
DTM	3.125E-7	SP(4,1)	1.0 for hard sphere; 0.4672 for Maxwell molecules
NIS	4	SP(5,1)	6.63E-26
NSP	1600	MNC	2000 for Kn=0.025; 500 for Kn=0.1; 100 for Kn=0.5; 50 for Kn=1.0
NPS	50	MNSC	20000 for Kn=0.025; 5000 for Kn=0.1; 1000 for Kn=0.5; 500 for Kn=1.0
NPT	1000		

Table 4.3: Parameters in the numerical test of kinetic models for 1DCF

Case	Situation	Number of cells	Ratio of cell width over mean free path	Iteration number	Number of velocities	Bound of velocities (m/s)	
						X1 direction	X2 (or X3)
4.1	Sa	100	2.5	40000	11*10*10	-1100, 1400	-1100, 1100
4.2	Sb	100	2.5	40000	11*10*10	-1100, 1400	-1100, 1100
4.3	Sc	50	5.0	40000	11*10*10	-1100, 1400	-1100, 1100
4.4	Sd	50	5.0	40000	11*10*10	-1100, 1400	-1100, 1100
4.5	Se	50	25.0	40000	11*10*10	-1100, 1400	-1100, 1100
4.6	Sf	50	25.0	40000	11*10*10	-1100, 1300	-1100, 1100
4.7	Sg	25	25.0	40000	11*10*10	-1100, 1300	-1100, 1100
4.8	Sh	25	25.0	40000	11*10*10	-1100, 1300	-1100, 1100
4.9	Si	50	25.0	40000	13*12*12	-1100, 1700	-1300, 1300
4.10	Sj	50	25.0	40000	16*14*14	-1200, 2200	-1500, 1500
4.11	Sk	50	25.0	40000	13*12*12	-1100, 1700	-1300, 1300
4.12	Sl	50	25.0	40000	15*14*14	-1200, 2200	-1600, 1600
4.13	Sa	100	2.5	60000	21*20*20	-1100, 1400	-1100, 1100
4.14	Sb	100	2.5	60000	21*20*20	-1100, 1400	-1100, 1100
4.15	Sj	50	25.0	60000 or 24000	26*24*24	-1200, 2200	-1500, 1500
4.16	Sl	50	25.0	60000 or 24000	25*24*24	-1200, 2200	-1600, 1600
4.17	Sh	50	50.0	40000	11*10*10	-1100, 1300	-1100, 1100
4.18	Sg	50	50.0	40000	11*10*10	-1100, 1300	-1100, 1100
4.19	Sc	100	10.0	60000 or 24000	11*10*10	-1100, 1400	-1100, 1100
4.20	Sd	100	10.0	60000 or 24000	11*10*10	-1100, 1400	-1100, 1100
4.21	Sc	100	10.0	60000 or 24000	15*14*14	-1500, 1800	-1600, 1600
4.22	Sd	100	10.0	60000 or 24000	15*14*14	-1500, 1800	-1600, 1600
4.23	Sa	100	2.5	24000	31*30*30	-1100, 1400	-1100, 1100
4.24	Sl	50	25.0	24000	35*34*34	-1200, 2200	-1600, 1600

4.4 Results and Discussion

4.4.1 Some important notes on dealing with results

In order to get converged results and do further analyses, similar steps as mentioned in Section 3.4.1 for shock waves have been done for Couette flow, such as, graphs, which show the output of one macroscopic parameter from different situations in one figure, and data (e.g. average relative error) are obtained for discussion of each kind of analysis. Here, only differences from Section 3.4.1 will be pointed out. No shifting need be done before discussing the results since the boundaries are fixed. Since the relative error becomes meaningless when a quantity approaches zero, average relative errors of velocity u_2, heat flux q_1 and q_2, for which it is hard to choose a domain in which relative error is meaningful, have not been computed in analyses. The direct output parameters for pressure tensor are p, p_{11}, p_{22} and p_{12} ($=\sigma_{12}$), not σ_{11} and σ_{22}, which are

computed from the output values of p, p_{11} and p_{22} with four digits accuracy[16]. Therefore, it is not surprising to see that average relative errors for σ_{11} and σ_{22} in the following analyses are a somewhat higher than average relative errors for ρ, u_1, T, p and σ_{12} at the same situation. One suggestion for future computation is to compute the values of σ_{11} and σ_{22} directly from the distribution function in the program.

Another thing that needs to be mentioned is that if the step of space grid is not the same for the two compared situations, some "smoothed" data will be derived from the original data with the smaller step of space grid and used in the comparison. The smoothing procedure means that the new value in one finite volume cell is the average of the original values in that finite volume cell size (one new cell covers several original cells). Of course, this smoothing procedure will introduce some numerical error, for profiles of macroscopic parameters are not exact linear in one new finite volume cell. Therefore, the computed average relative errors from this method cannot be used as a very precise criterion, but a little rough criterion, in the comparison. This type of situation, where curves on different step of space grid are compared, is met when the effect of cell width is considered, and when the results from kinetic models are compared to DSMC simulations.

4.4.2 Convergence of results

At the first stage of analysis (convergence of results), what we do is to compare results among the five certain iterations (which are 1/5, 2/5, 3/5, 4/5 and 5/5 of total iteration). Average relative errors of macroscopic parameters among these five certain iterations are computed. It is found that those average values are smaller than 0.01 for almost all cases. This shows that running so many iterations (at least 4800), values of macroscopic parameters change are very small; therefore the computational results are converged. As an example, Figure 4.1 shows profiles of some macroscopic parameters at five certain iterations for case 4.18 when the BGK model is used.

---

[16] When the numerical experiments were all done, it was not realized that a higher accuracy would be better. Since the computations take so long, there was no time to repeat them.

The simple estimate for time to reach converged results in Section 3.4.2 of Chapter 3 is $t = 9.2\tau$, where τ is the mean free time.

For the 1DCF, let us compute the mean free time using initial state, where the viscosity is computed from Eq. (2.32) (since $T = T_0 = 273.0$ K here, there is no difference of τ for hard sphere or Maxwell molecules),

$$\tau = \frac{\mu}{p} = \frac{\mu_0 \left(\frac{T}{T_0}\right)^{\omega}}{nkT} = \frac{1.9552 \times 10^{-5}}{1.4 \times 10^{20} \times 1.381 \times 10^{-23} \times 273.0} = 3.7 \times 10^{-5} (\mathrm{s}).$$

Therefore the magnitude of time to reach converged results for the 1DCF from the above simple estimation is 10^{-4} s. The magnitude of total time step in computation is $10^{-1} \sim 10^{-2}$ s (smallest value is about 4.78×10^{-3} s for cases 4.24), which is much larger than the above estimated time, for all our computational results. Table 4.4 shows the total time step (unit: seconds) for kinetic models in cases 4.1-4.12. Therefore, we can say that our computational results are the converged results from the above comparison. This is the reason why the iteration number for cases, computed a later time than others, is 24000, instead of 40000 or 60000 (see Table 4.3).

Similar tests have been done on the DSMC computation, and results are converged.

Table 4.4: Total time step (seconds) for kinetic models in cases 4.1-4.12

Kinetic models / Case and situation	BGK	ES-BGK	$\nu(C)$-BGK	New I	New II
4.1 Sa	0.117	0.120	0.0559	0.107	0.107
4.2 Sb	0.117	0.120	0.0560	0.120	0.120
4.3 Sc	0.0608	0.0617	0.0390	0.0583	0.0583
4.4 Sd	0.0609	0.0618	0.0396	0.0618	0.0618
4.5 Se	0.0126	0.0126	0.0114	0.0125	0.0125
4.6 Sf	0.0126	0.0126	0.0115	0.0126	0.0126
4.7 Sg	0.0126	0.0126	0.0114	0.0125	0.0125
4.8 Sh	0.0126	0.0126	0.0115	0.0126	0.0126
4.9 Si	0.0107	0.0107	0.00956	0.0106	0.0106
4.10 Sj	0.0092	0.0093	0.0082	0.0092	0.0092
4.11 Sk	0.0107	0.0107	0.0097	0.0107	0.0107
4.12 Sl	0.0088	0.0087	0.0080	0.0087	0.0087

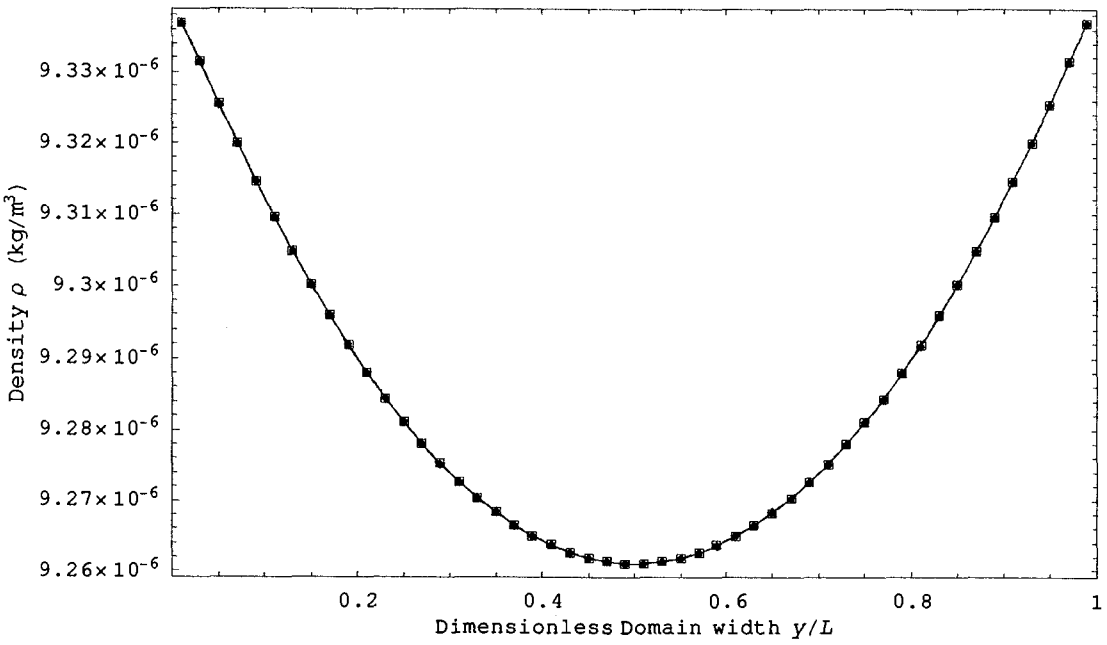

(a)

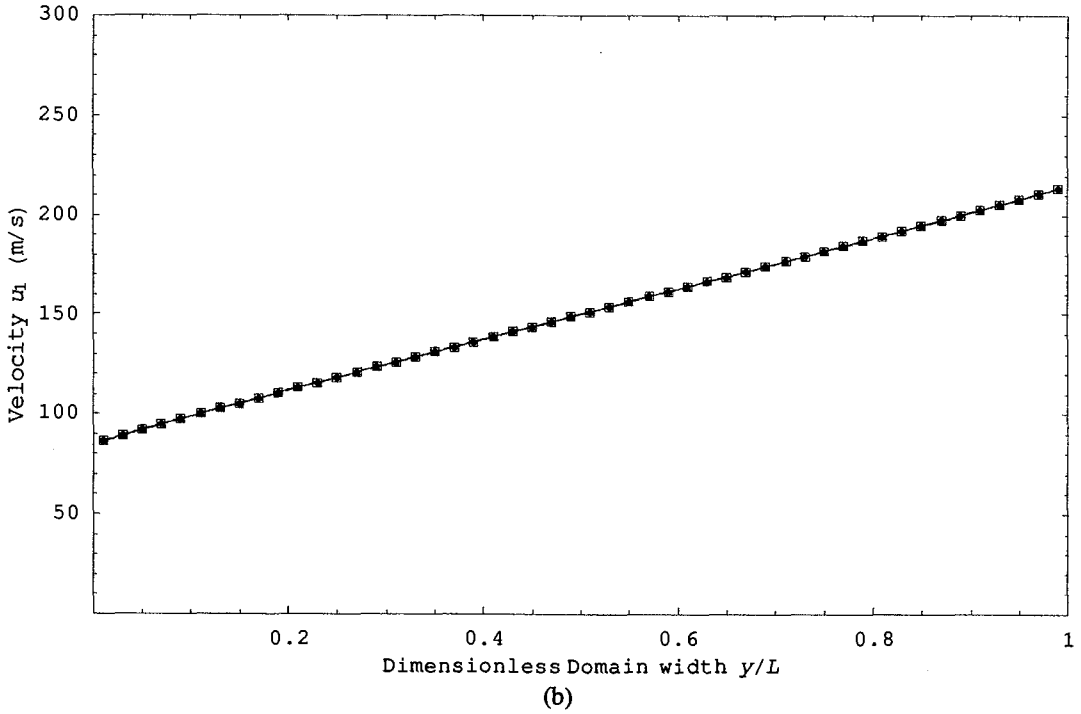

(b)

Figure 4.1: Profiles of some parameters at five certain iterations (BGK model, case 4.18: Kn=1.0, hard sphere molecules, 300.0 m/s plate velocity) (Triangle for iteration=8000, Star for iteration=16000, Diamond for iteration=24000, Box for iteration=32000, Triangle filled for iteration=40000)

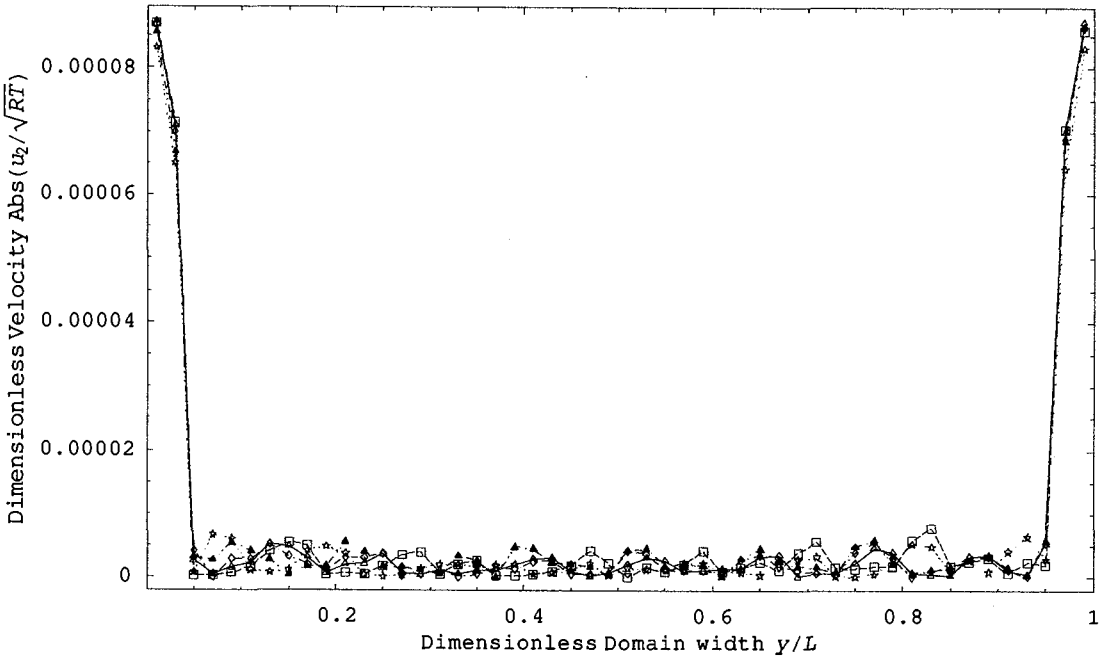

(c)

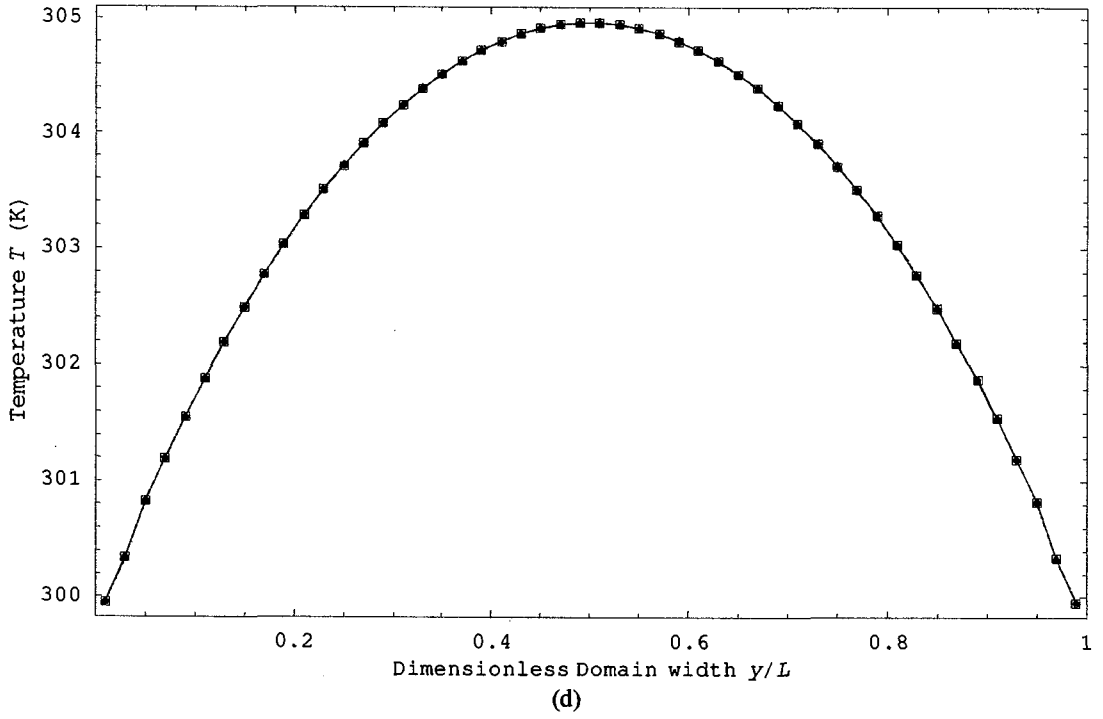

(d)

Figure 4.1: Profiles of some parameters at five certain iterations (BGK model, case 4.18: Kn=1.0, hard sphere molecules, 300.0 m/s plate velocity) (Triangle for iteration=8000, Star for iteration=16000, Diamond for iteration=24000, Box for iteration=32000, Triangle filled for iteration=40000)

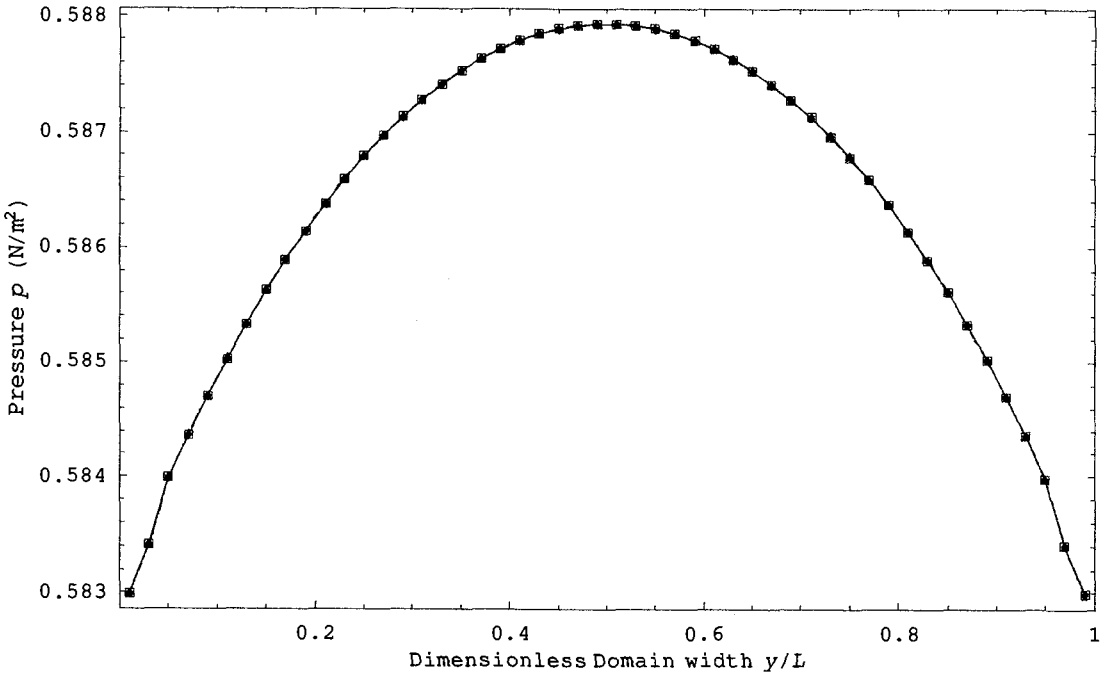

(e)

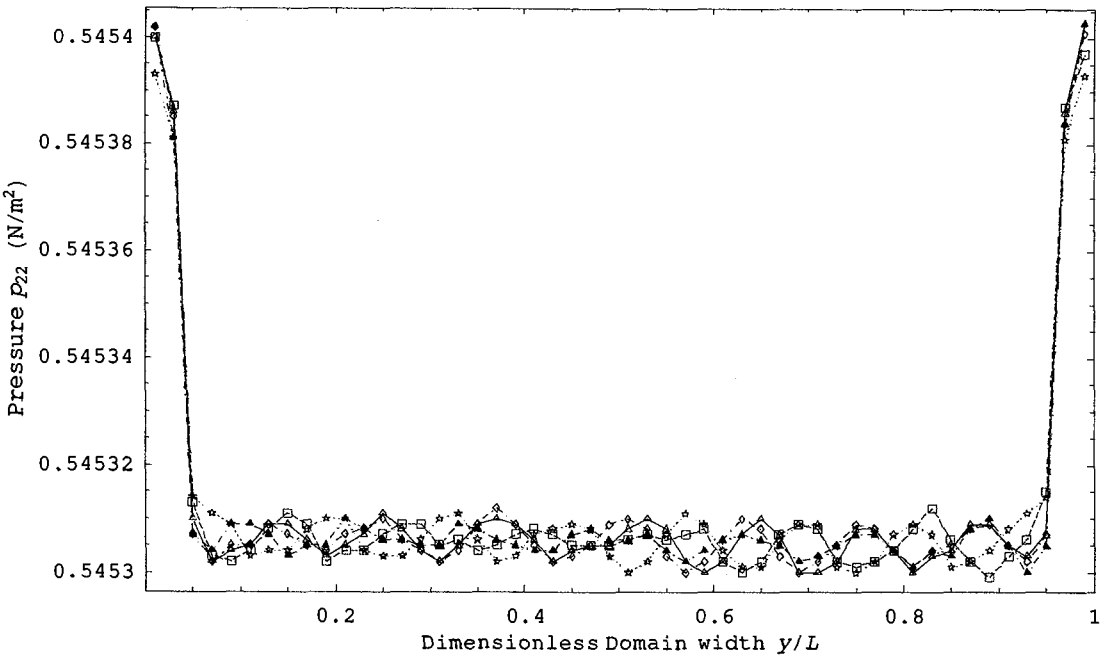

(f)

Figure 4.1: Profiles of some parameters at five certain iterations (BGK model, case 4.18: Kn=1.0, hard sphere molecules, 300.0 m/s plate velocity) (Triangle for iteration=8000, Star for iteration=16000, Diamond for iteration=24000, Box for iteration=32000, Triangle filled for iteration=40000)

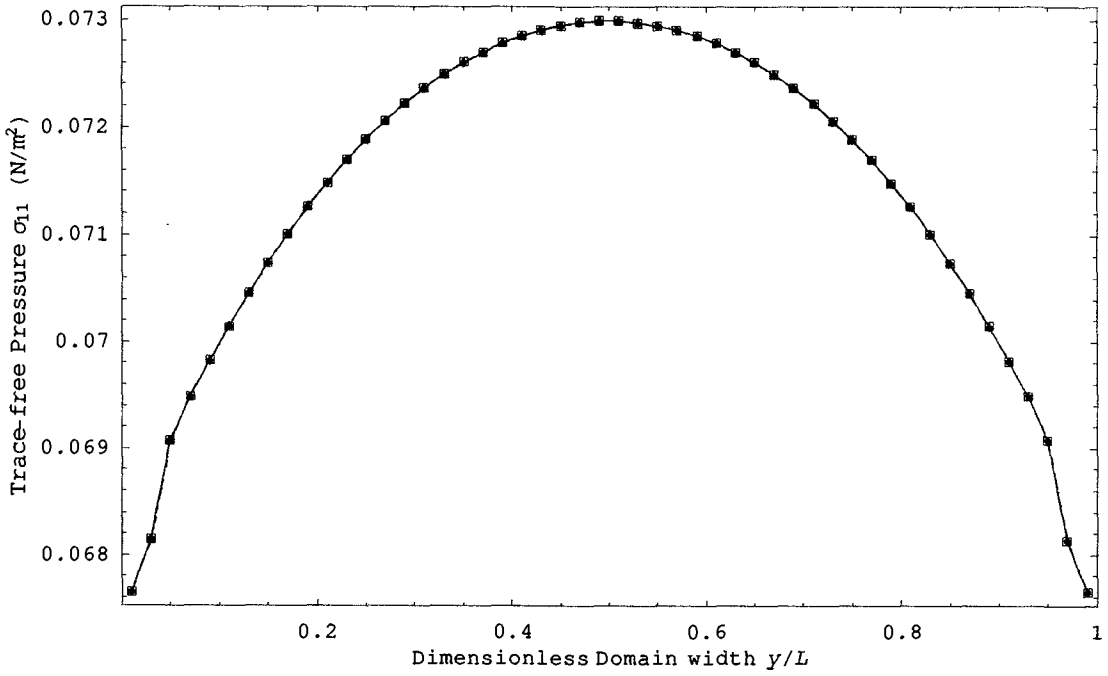

(g)

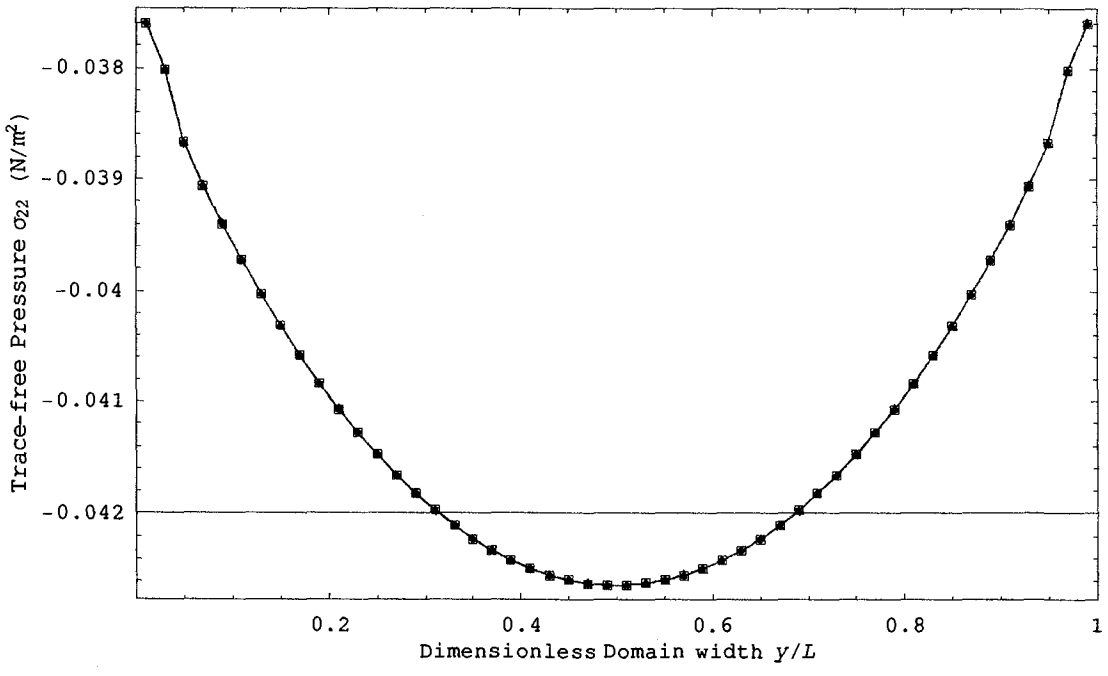

(h)

Figure 4.1: Profiles of some parameters at five certain iterations (BGK model, case 4.18: Kn=1.0, hard sphere molecules, 300.0 m/s plate velocity) (Triangle for iteration=8000, Star for iteration=16000, Diamond for iteration=24000, Box for iteration=32000, Triangle filled for iteration=40000)

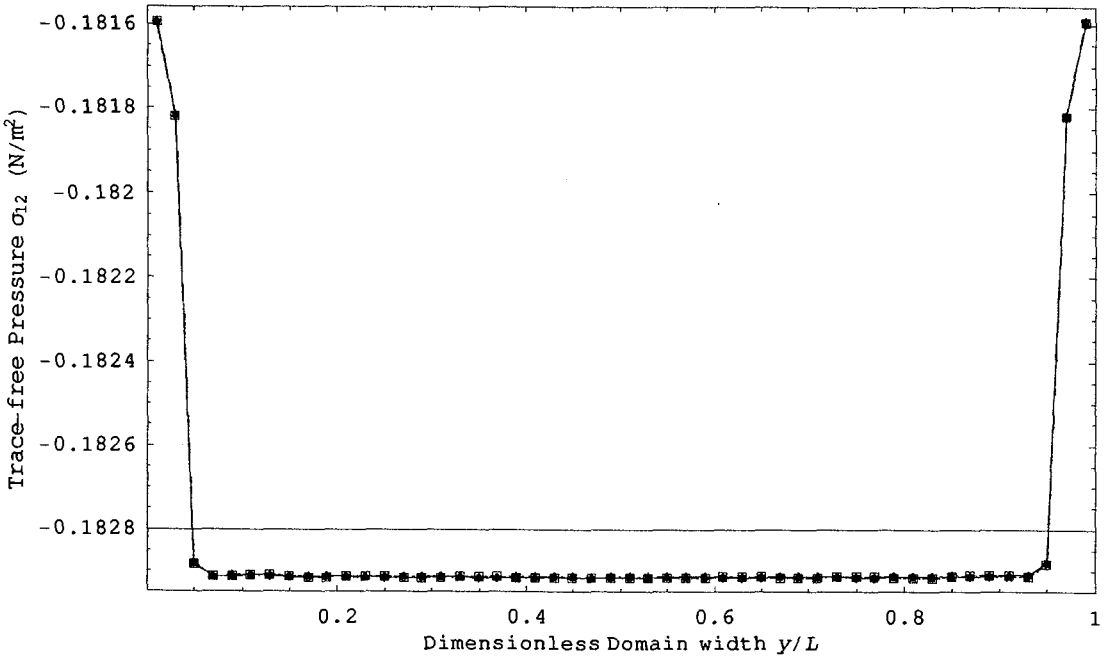

(i)

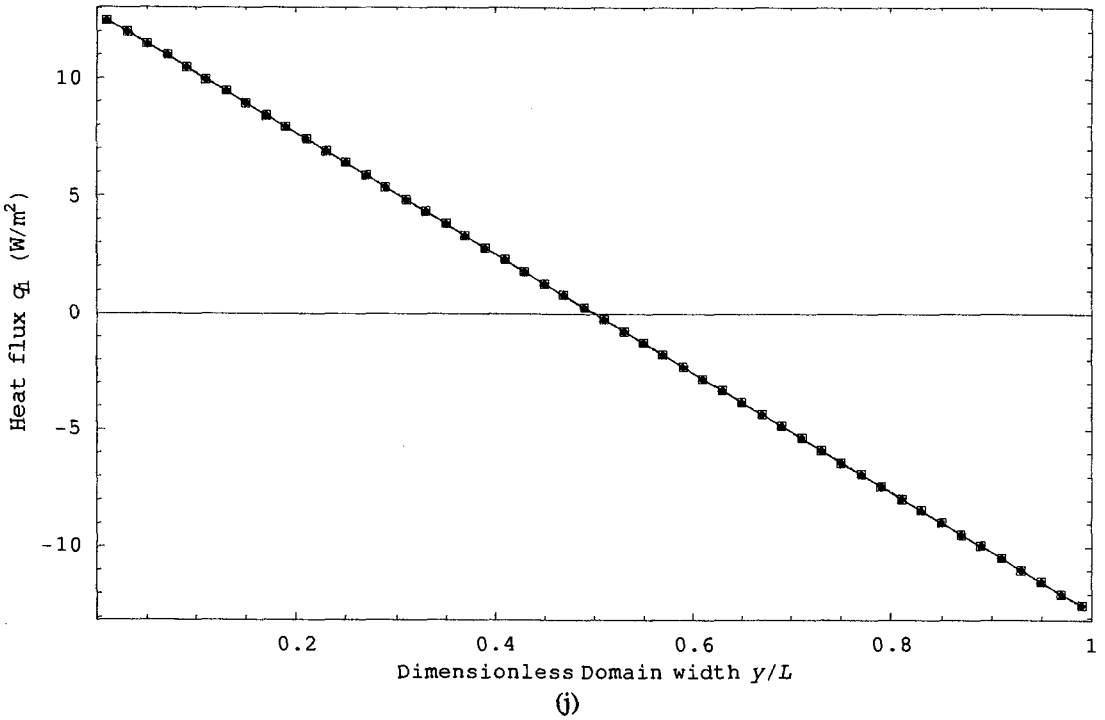

(j)

Figure 4.1: Profiles of some parameters at five certain iterations (BGK model, Case 4.18: Kn=1.0, hard sphere molecules, 300.0 m/s plate velocity) (Triangle for iteration=8000, Star for iteration=16000, Diamond for iteration=24000, Box for iteration=32000, Triangle filled for iteration=40000)

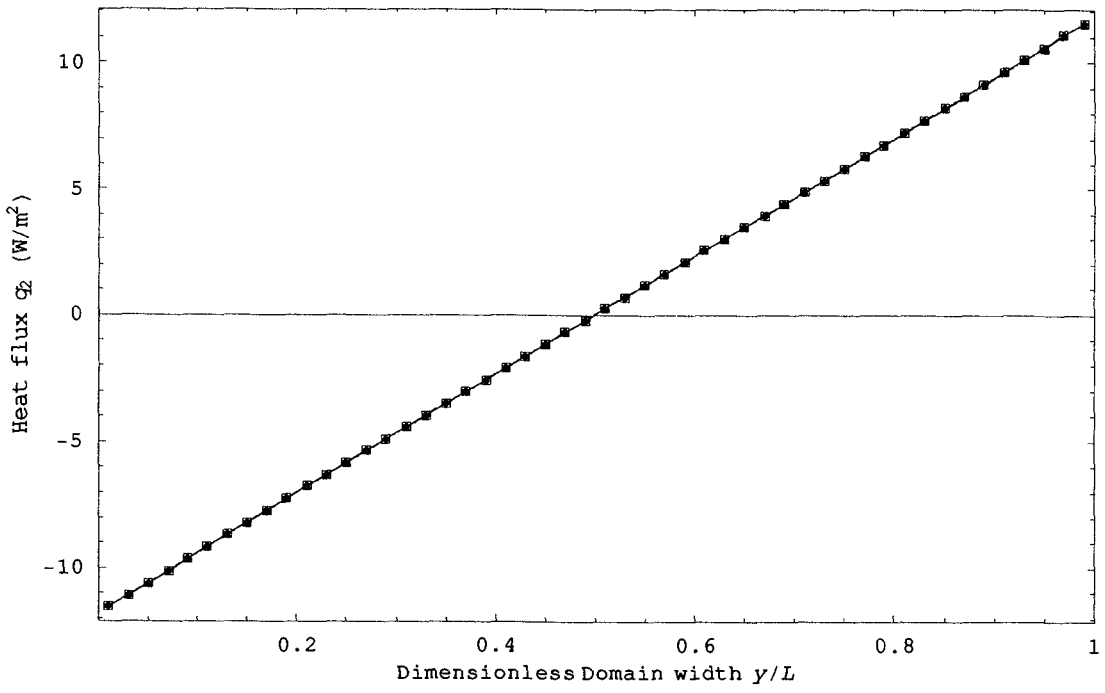

(k)

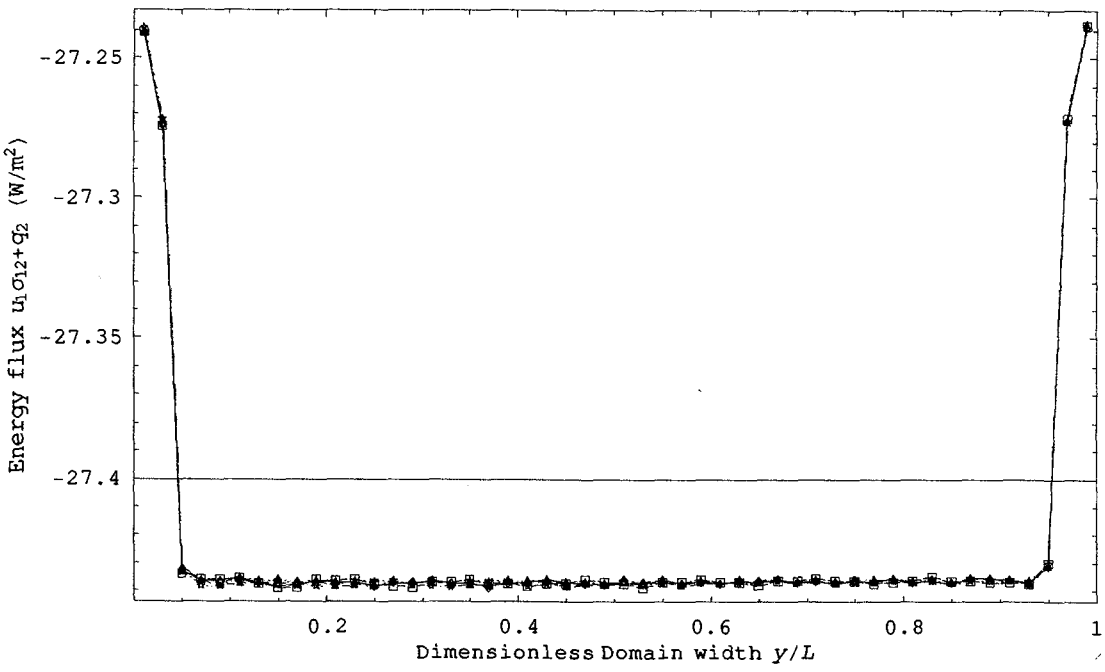

(l)

Figure 4.1: Profiles of some parameters at five certain iterations (BGK model, case 4.18: Kn=1.0, hard sphere molecules, 300.0 m/s plate velocity) (Triangle for iteration=8000, Star for iteration=16000, Diamond for iteration=24000, Box for iteration=32000, Triangle filled for iteration=40000)

4.4.3 Discussion

From Eq. (4.2), it is realized that four parameters (u_2, p_{22}, σ_{12}, $u_1\sigma_{12}+q_2$) should be constant (and $u_2 = 0.0$) in the whole domain at the steady state of 1DCF. Therefore, we can use these parameters to see whether the converged results are results at the steady state or not. At the steady state, the velocity perpendicular to the plates u_2 should be very small compared to the characteristic velocity $\sqrt{RT}$. Therefore the dimensionless velocity $u_2/\sqrt{RT}$ will be considered. After some analysis, it is found that the average values of $\left|u_2/\sqrt{RT}\right|$ for all positions is smaller than 10^{-4} in all test cases, and p_{22}, σ_{12} and $u_1\sigma_{12}+q_2$ are indeed almost constant in the whole domain, and vary near the boundaries (this jump, which is slight violation of the conservation laws due to numerical inaccuracy, can be reduced when the step of space grid becomes smaller, which example refer to graphs (g,j) in Figure 4.3)), which means the computational results are results at the steady state of Couette flow. Graphs (c, f, i, l) in Figure 4.1 can be used as examples here.

When the computational time for each iteration is considered, the observations are similar to 1DSW. The new kinetic model I needs the longest time, followed by the new kinetic model II, the $\nu(C)$-BGK model and the ES-BGK model, and the BGK model need the shortest time. The ratio of computational time for each iteration among the new kinetic model I, the ES-BGK model and the BGK model is about 3:2:1.

From the computational results Table 4.4, it is shown that the $\nu(C)$-BGK model has the smallest time step Δt_n (For situations Sa-Sd, it is only about 50% of Δt_n of other kinetic models) among tested kinetic models, and Δt_n for other kinetic models are similar.

Results from the new kinetic model I and the new kinetic model II are very similar (see Figures 4.4-4.7), and if the structure of program and computational time for one

iteration is considered, the new kinetic model II is better than the new kinetic model I. The computational time for one iteration of the new kinetic model II is something like 80% of the computational time need for one iteration of the new kinetic model I, the reason is that when the reference distribution is solved (which takes a large portion of computational time), the new kinetic model I needs results from the ES-BGK model, while the new kinetic model II need not, therefore the new kinetic model I needs to perform the N-R algorithm to find coefficients of reference distributions three times, while the new kinetic model II only needs to do the N-R algorithm two times.

Let us consider the use of the linearized reference distribution f_{ref} discussed in Section 4.2.3. From the data and graphs obtained from the two steps mentioned in Section 4.4.1, the following conclusions can be drawn.

- For the BGK model, the average relative errors for almost all macroscopic parameters and test situations (which are cases 4.1-4.12) are smaller than 0.001.

- For the $\nu(C)$-BGK model, the average relative errors for ρ, u_1, T, p and σ_{12} are smaller than 0.01 for almost all test situations, while the average relative errors for σ_{11} and σ_{22} are smaller than 0.02 for almost all test situations.

- For the ES-BGK model, and the new kinetic model II, there are two types of linearized f_{ref}, one is obtained based on an isotropic Gaussian distribution, another one is obtained based on an anisotropic Gaussian distribution. The average relative errors for ρ, u_1, T, p and σ_{12} are smaller than 0.005 (0.0005) for almost all test situations for the first (second) type of linearized f_{ref} of these two kinetic models, while the average relative errors for σ_{11} and σ_{22} are smaller than 0.02 (0.005) for almost all test situations for the first (second) type of linearized f_{ref} of these two kinetic models. Therefore, the second type of

linearized f_{ref} is better than the first type of linearized f_{ref} for these two kinetic models.

- For the first type linearized f_{ref} of the new kinetic model I with hard sphere molecules, diverged results (NaNQ appear in the output of the FORTRAN computation program) was obtained for all test situations; the reason for this is still being considered. The first type of linearized f_{ref} of the new kinetic model I with Maxwell molecules works well, such as, average relative errors for ρ, u_1, T, p and σ_{12} are smaller than 0.005 for almost all test situations, and average relative errors for σ_{11} and σ_{22} are smaller than 0.02 for almost all test situations.

- For the second type linearized f_{ref} of the new kinetic model I, no matter with hard sphere molecules or Maxwell molecules, it works well, such as, average relative errors of ρ, u_1, T, p and σ_{12} for almost all test situations are smaller than 0.005 for hard sphere molecules (0.0005 for Maxwell molecules), and average relative errors of σ_{11} and σ_{22} for almost all test situations are smaller than 0.02 for hard sphere molecules (0.003 for Maxwell molecules).

- When the computational time for each time step is considered, using the linearized f_{ref} can save 20-40% of computational time compared to using the original f_{ref}. This point is applicable for all kinetic models.

Let us consider the effect of step of space grid on computational results, based on the comparison of results of cases 4.17-4.20 with results of cases 4.7, 4.8, 4.3 and 4.4. From the data and graphs obtained from the two steps mentioned in Section 4.4.1, it is realized that the average relative errors for ρ, u_1, T and p are smaller than 0.001 for almost all test situations and all kinetic models, while the average relative errors for σ_{11}, σ_{22} and σ_{12} are smaller than 0.02 for almost all test situations and all kinetic models. Therefore, our choices of step of space grid in Table 4.3 are acceptable.

Let us consider the effect of bounds of velocity grid on computational results, based on the comparison of results of cases 4.21-4.22 with results of cases 4.19-4.20. From the data and graphs obtained from the two steps mentioned in Section 4.4.1, it is realized that the average relative errors for ρ, u_1, T, p and σ_{12} are smaller than 0.002 for almost all test situations, while the average relative errors for σ_{11} and σ_{22} are smaller than 0.015 for almost all test situations. Therefore, the effect of bounds of velocity grid on results can be neglected as long as the choice of bounds satisfied the standard given in Section 3.2.6.

Let us consider the effect of step of velocity grid on computational results, based on the comparison of results of cases 4.13-4.16 with results of cases 4.1, 4.2, 4.10 and 4.12, and also the comparison of results of cases 4.23-4.24 with results of cases 4.13 and 4.16.From the data and graphs of the above first series comparison obtained from the two steps mentioned in Section 4.4.1, it is realized that the average relative errors for ρ, u_1, T, p and σ_{12} are smaller than 0.02 for almost all test situations and all kinetic models, while the average relative errors for σ_{11} and σ_{22} sometimes are unacceptable large, such as 0.1, sometimes even higher for the $\nu(C)$-BGK model. While the average relative errors for all macroscopic parameters are smaller than 0.01 in the comparison of cases 4.23 and 4.24 with cases 4.13 and 4.16. Doubling the number of discrete velocities will increase the computational time of each iteration eight times, and a larger number of discrete velocities also imply smaller time steps by Eq. (4.4), which further means more iterations are needed to reach converged results. Therefore, tests with smaller step of velocity grid than the step of velocity grid shown in Table 4.3 is not suggested to be done, before some ways are applied to decrease the computational time, such as implicit numerical scheme, effective criterion to check whether the results are converged or not, parallel computing, etc.

As some example figures, Figure 4.2 shows the use of two types linearized f_{ref} and the effect of step of velocity grid in the new kinetic model II for situation Sa (Kn=0.025, hard sphere molecules, 300.0 m/s plate velocity) (cases 4.1 and 4.13); Figure 4.3 shows

the effect of bounds of velocity gird and the effect of step of space gird in situation Sc (Kn=0.1, hard sphere molecules, 300.0 m/s plate velocity) (cases 4.3, 4.19 and 4.21) from the ES-BGK model with original f_{ref}.

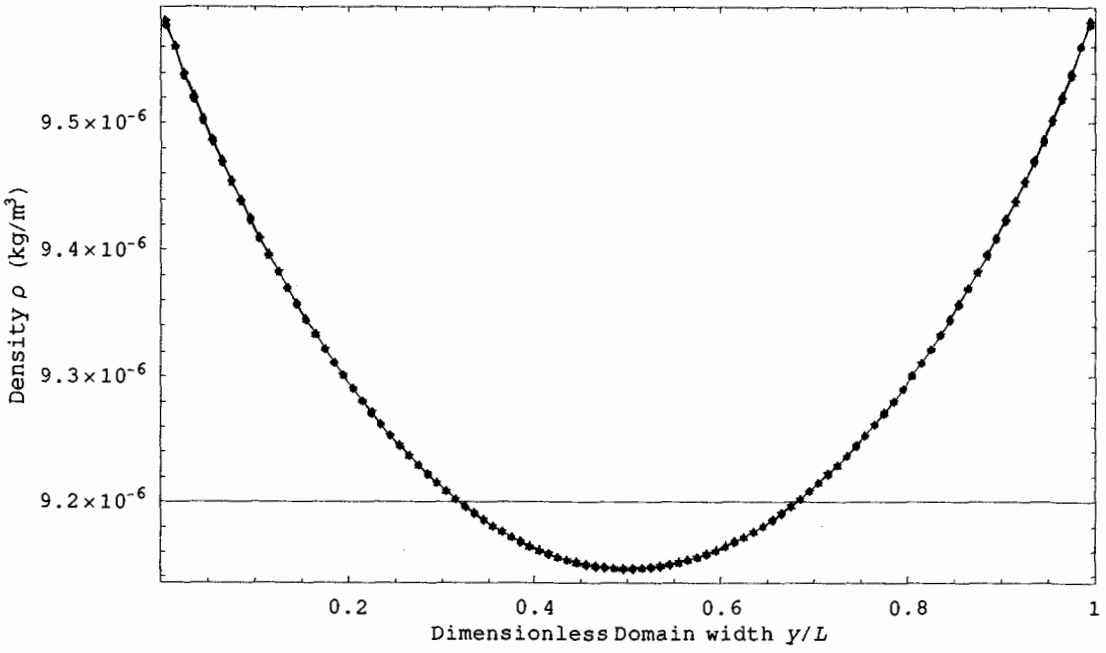

(a)

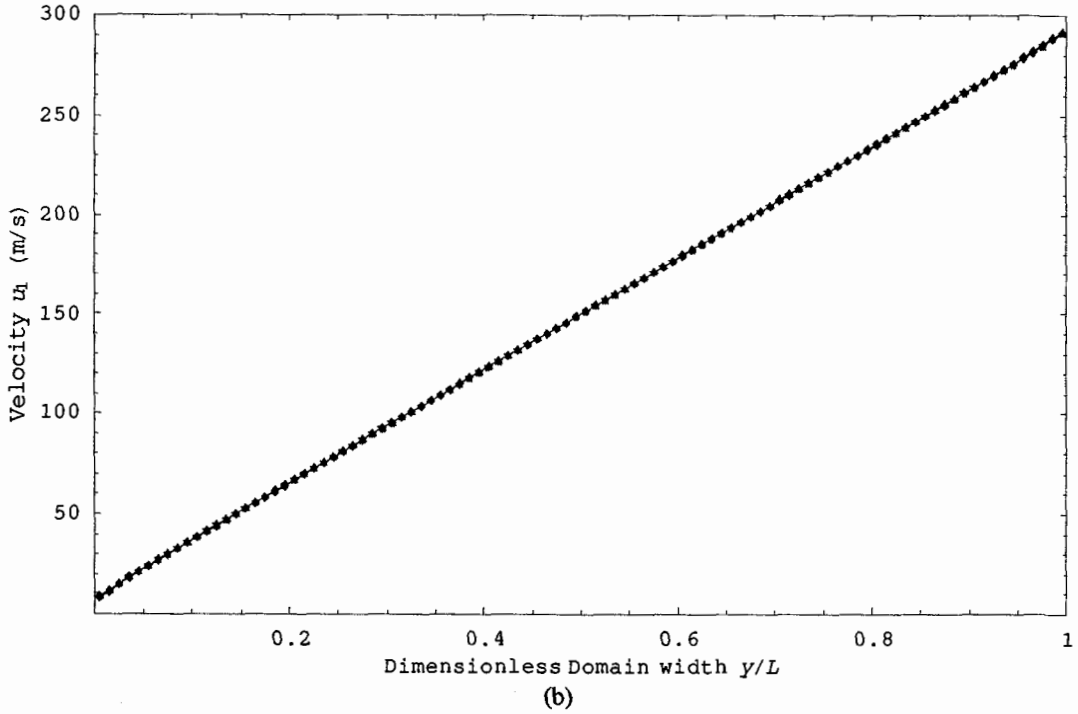

(b)

Figure 4.2: Results to show the use of linearized f_{ref} and the effect of step of velocity grid (new kinetic model II, situation Sa: Kn=0.025, hard sphere molecules, 300.0 m/s plate velocity) (Triangle for original f_{ref} in case 4.1, Triangle filled for first type linearized f_{ref} in case 4.1, Diamond for second type linearized f_{ref} in case 4.1, Diamond filled for original f_{ref} in case 4.13, Star for original f_{ref} in case 4.23)

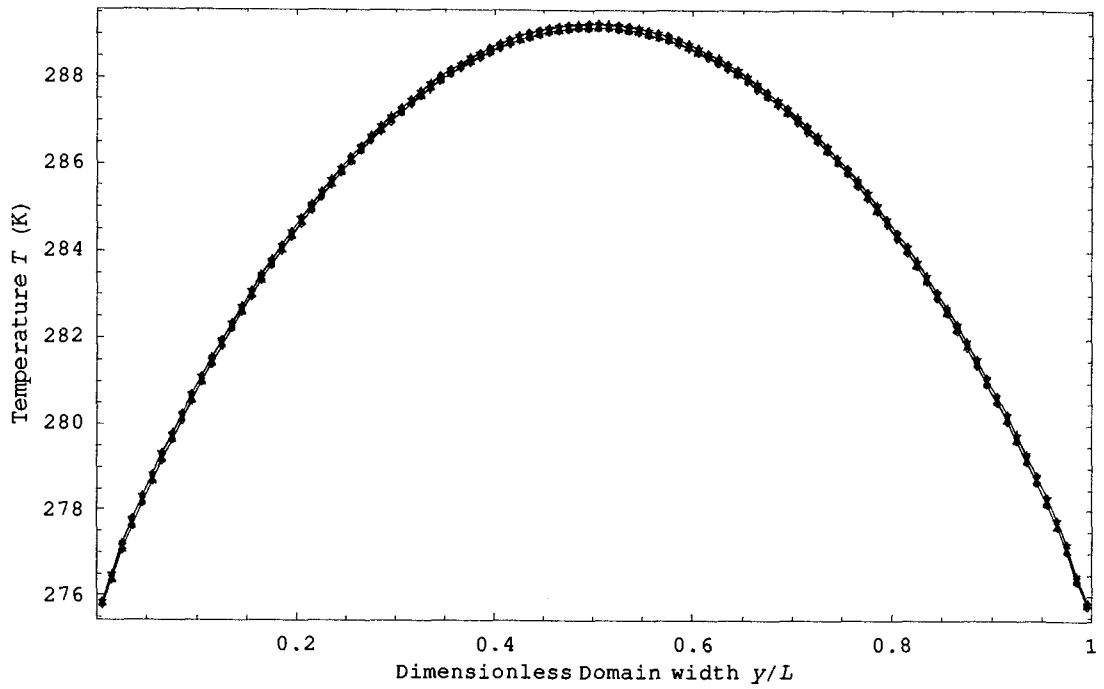

(c)

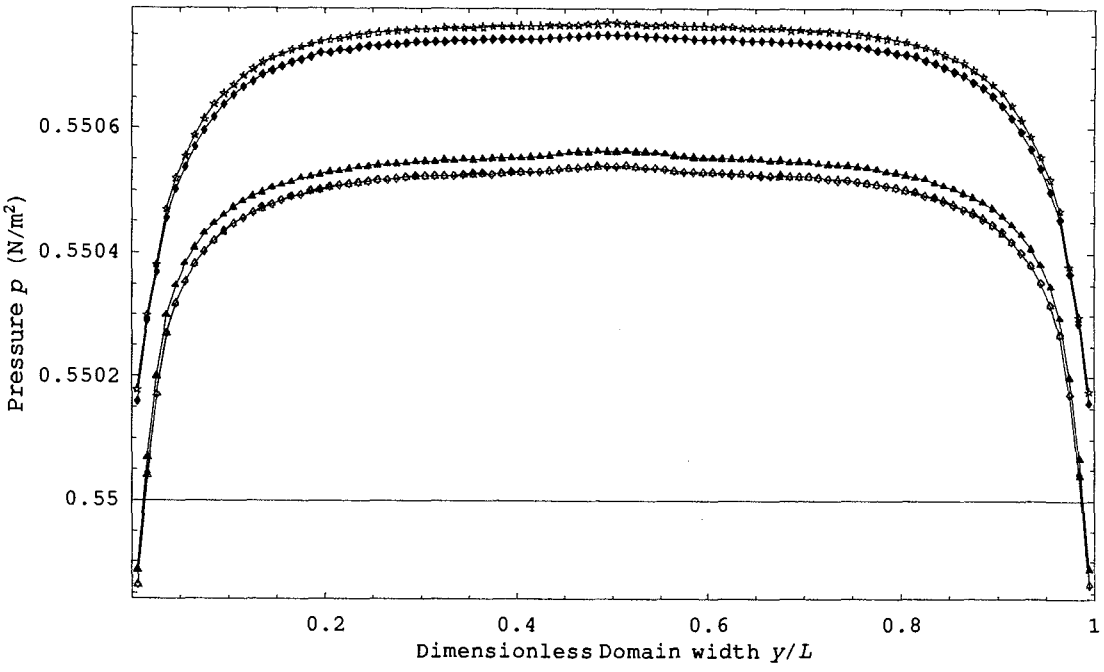

(d)

Figure 4.2: Results to show the use of linearized f_{ref} and the effect of step of velocity grid (new kinetic model II, situation Sa: Kn=0.025, hard sphere molecules, 300.0 m/s plate velocity) (Triangle for original f_{ref} in case 4.1, Triangle filled for first type linearized f_{ref} in case 4.1, Diamond for second type linearized f_{ref} in case 4.1, Diamond filled for original f_{ref} in case 4.13, Star for original f_{ref} in case 4.23)

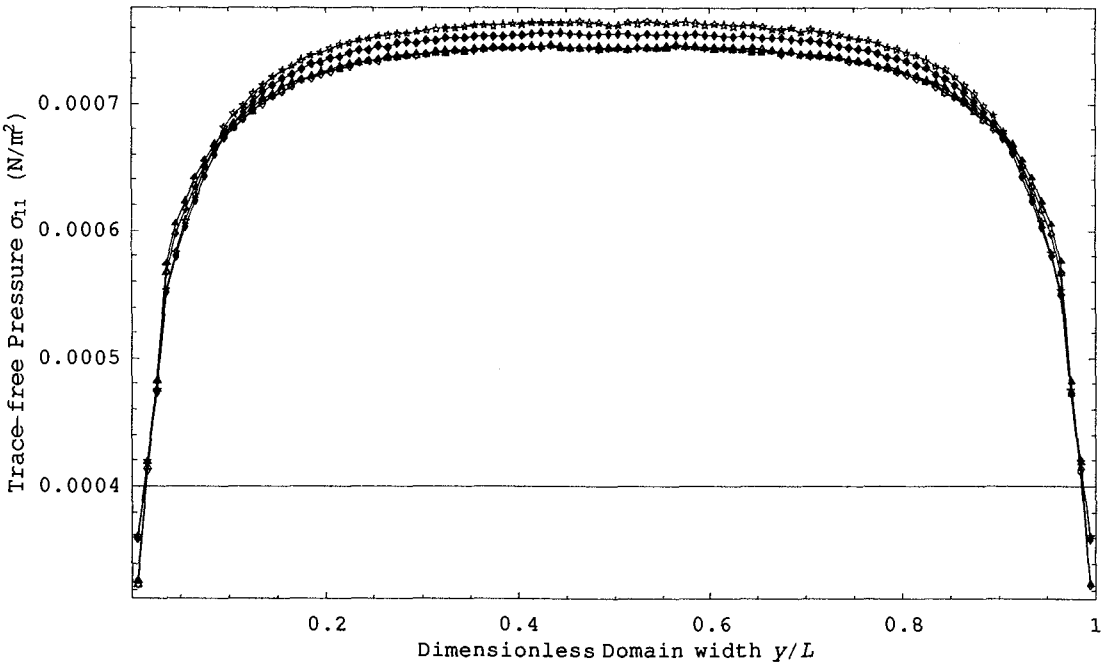

(e)

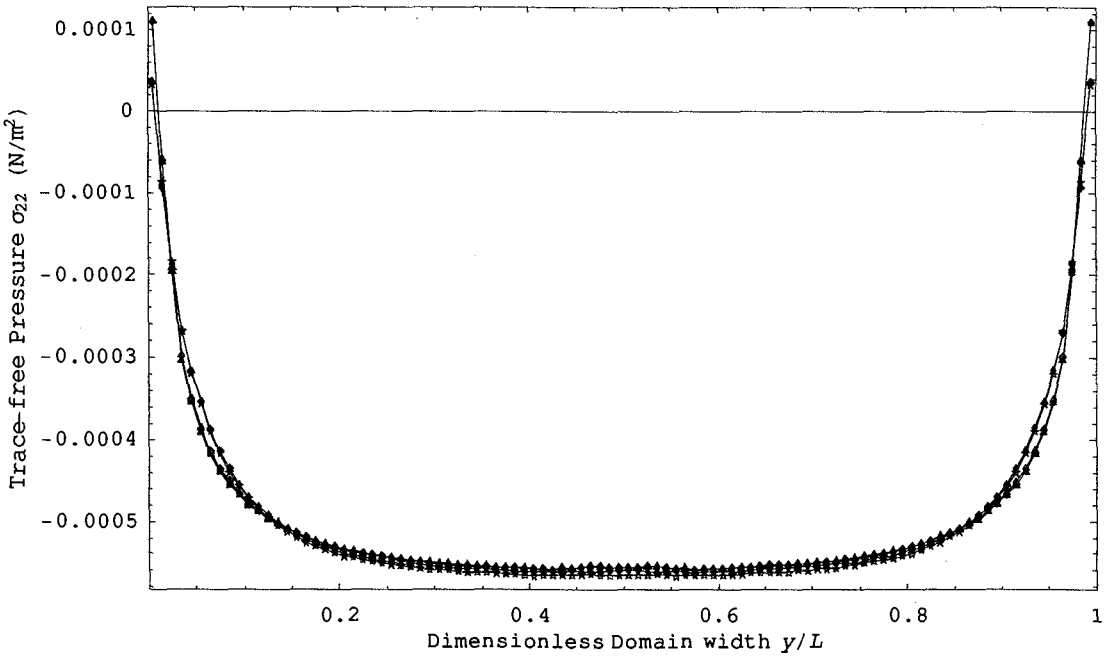

(f)

Figure 4.2: Results to show the use of linearized f_{ref} and the effect of step of velocity grid (new kinetic model II, situation Sa: Kn=0.025, hard sphere molecules, 300.0 m/s plate velocity) (Triangle for original f_{ref} in case 4.1, Triangle filled for first type linearized f_{ref} in case 4.1, Diamond for second type linearized f_{ref} in case 4.1, Diamond filled for original f_{ref} in case 4.13, Star for original f_{ref} in case 4.23)

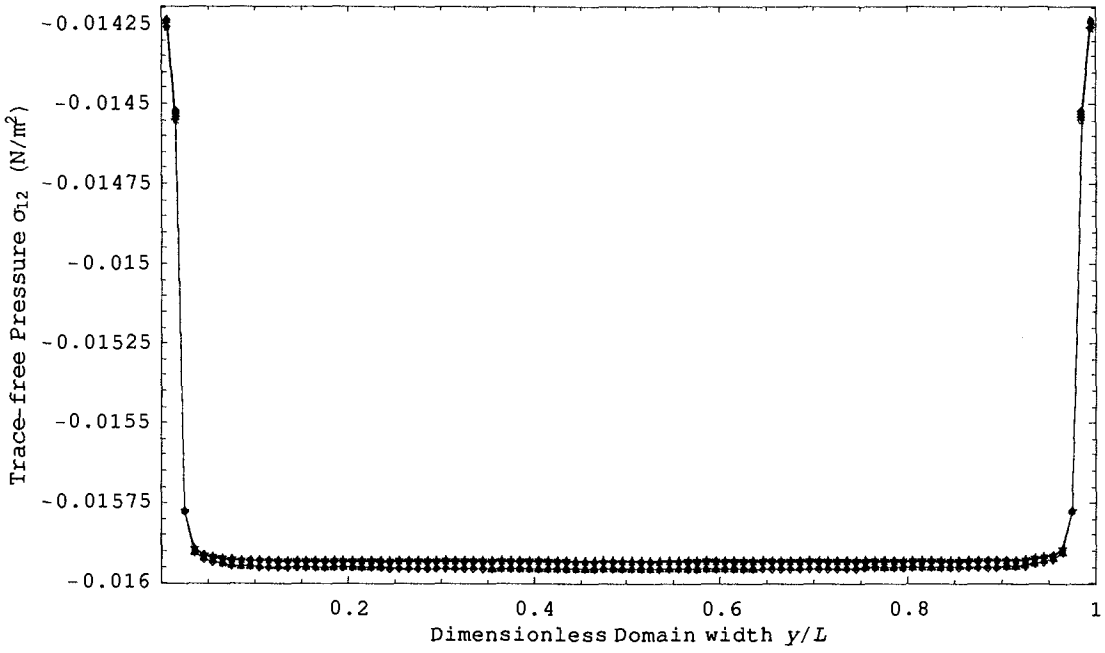

(g)

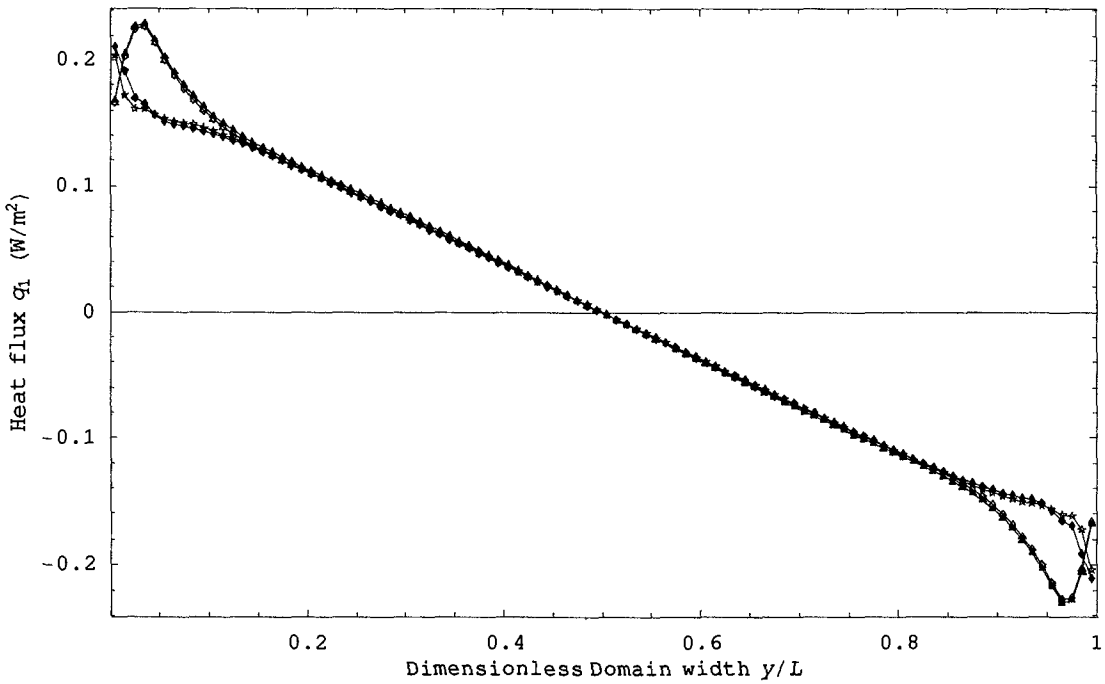

(h)

Figure 4.2: Results to show the use of linearized f_{ref} and the effect of step of velocity grid (new kinetic model II, situation Sa: Kn=0.025, hard sphere molecules, 300.0 m/s plate velocity) (Triangle for original f_{ref} in case 4.1, Triangle filled for first type linearized f_{ref} in case 4.1, Diamond for second type linearized f_{ref} in case 4.1, Diamond filled for original f_{ref} in case 4.13, Star for original f_{ref} in case 4.23)

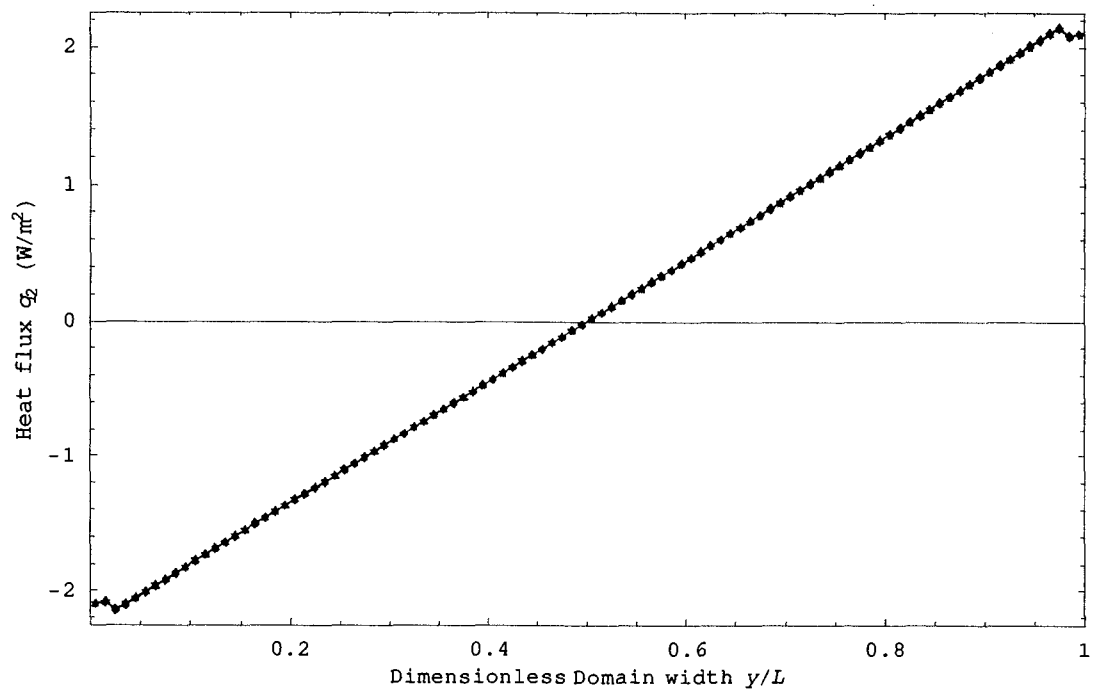

(i)

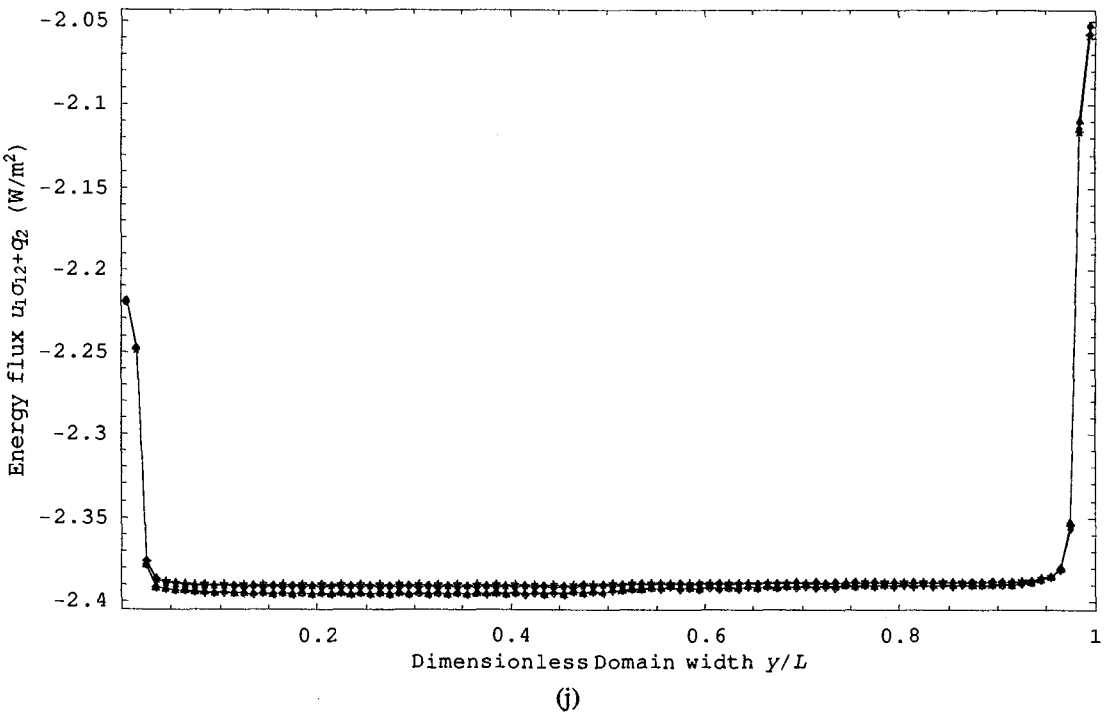

(j)

Figure 4.2: Results to show the use of linearized f_{ref} and the effect of step of velocity grid (new kinetic model II, situation Sa: Kn=0.025, hard sphere molecules, 300.0 m/s plate velocity) (Triangle for original f_{ref} in case 4.1, Triangle filled for first type linearized f_{ref} in case 4.1, Diamond for second type linearized f_{ref} in case 4.1, Diamond filled for original f_{ref} in case 4.13, Star for original f_{ref} in case 4.23)

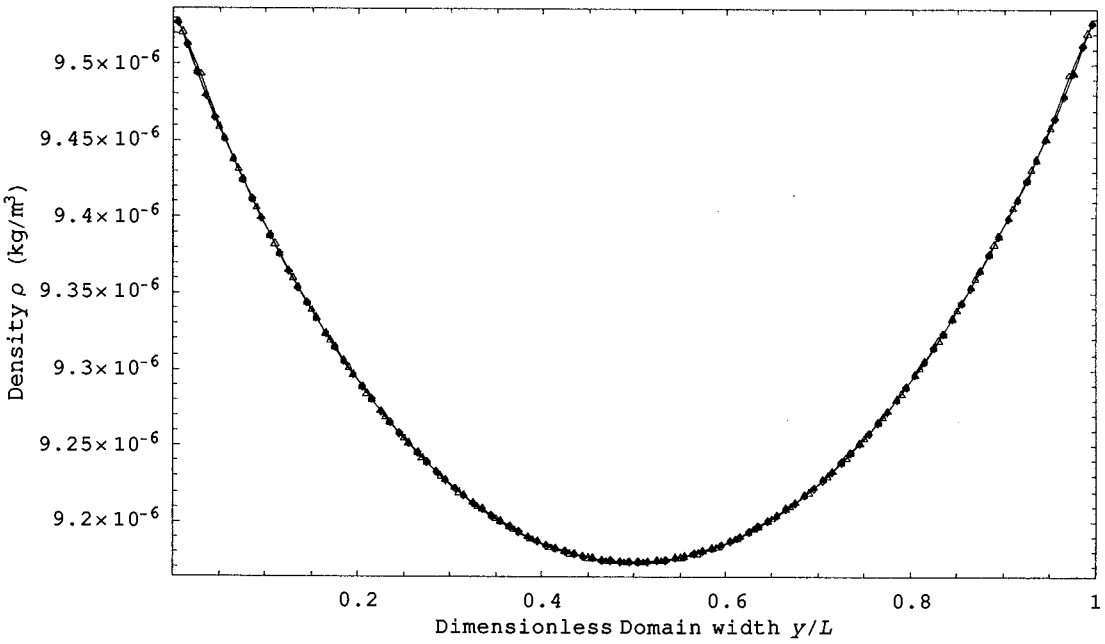

(a)

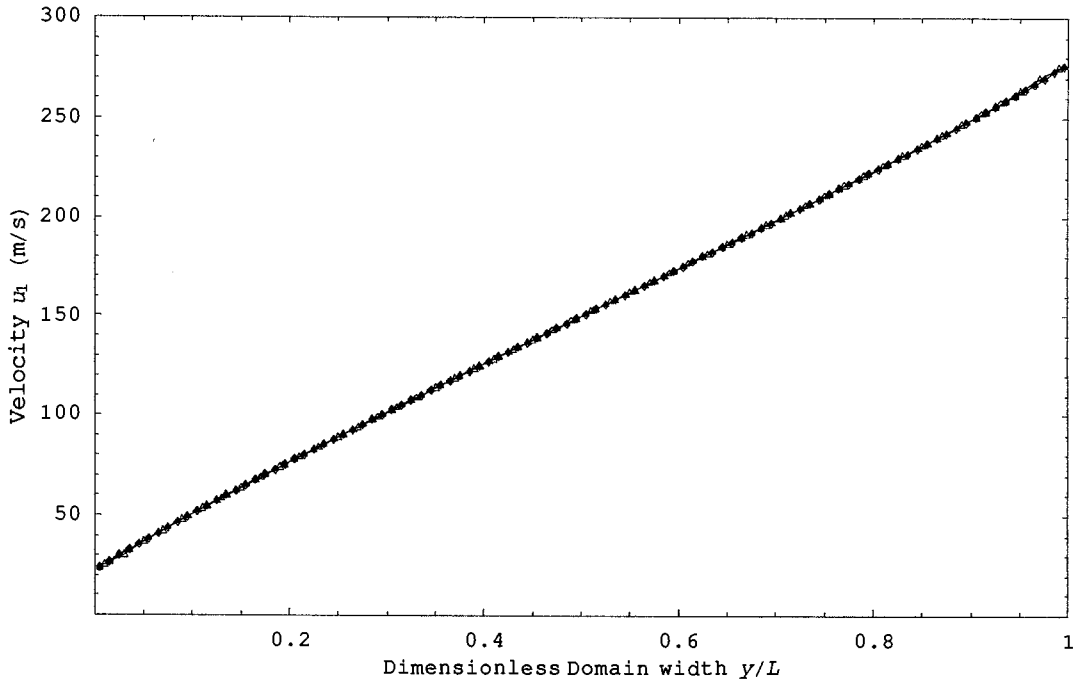

(b)

Figure 4.3: Results to show the effect of bounds of velocity grid and the effect of step of space grid (ES-BGK model, situation Sc: Kn=0.1, hard sphere molecules, 300.0 m/s plate velocity) (Triangle for case 4.3, Triangle filled for case 4.19, Diamond for case 4.21)

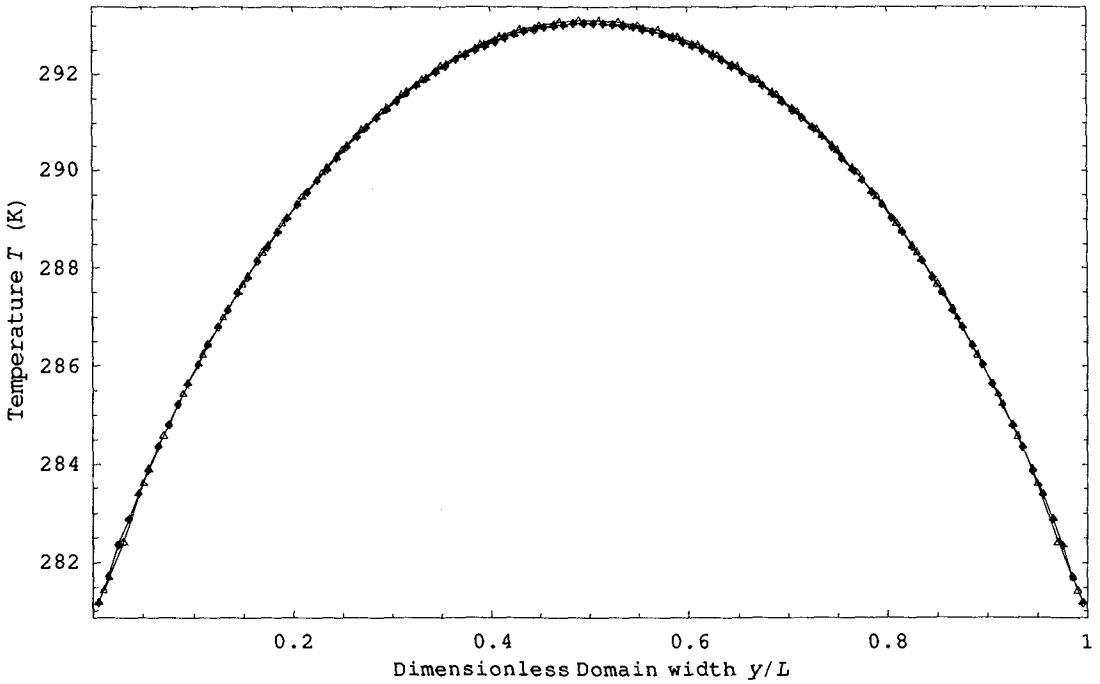

(c)

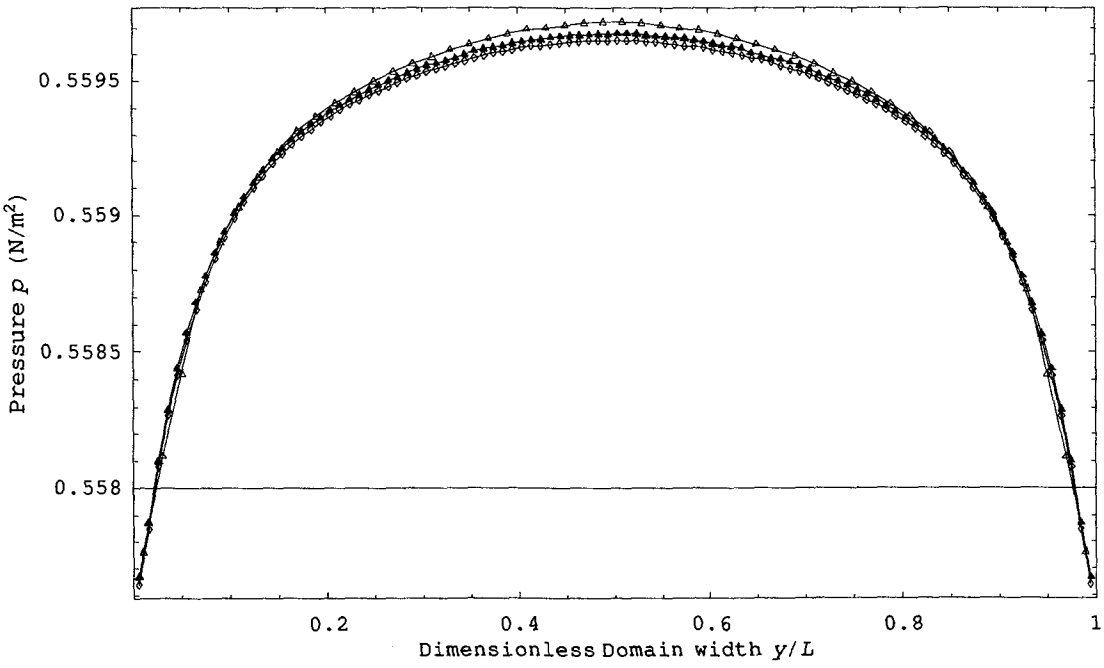

(d)

Figure 4.3: Results to show the effect of bounds of velocity grid and the effect of step of space grid (ES-BGK model, situation Sc: Kn=0.1, hard sphere molecules, 300.0 m/s plate velocity) (Triangle for case 4.3, Triangle filled for case 4.19, Diamond for case 4.21)

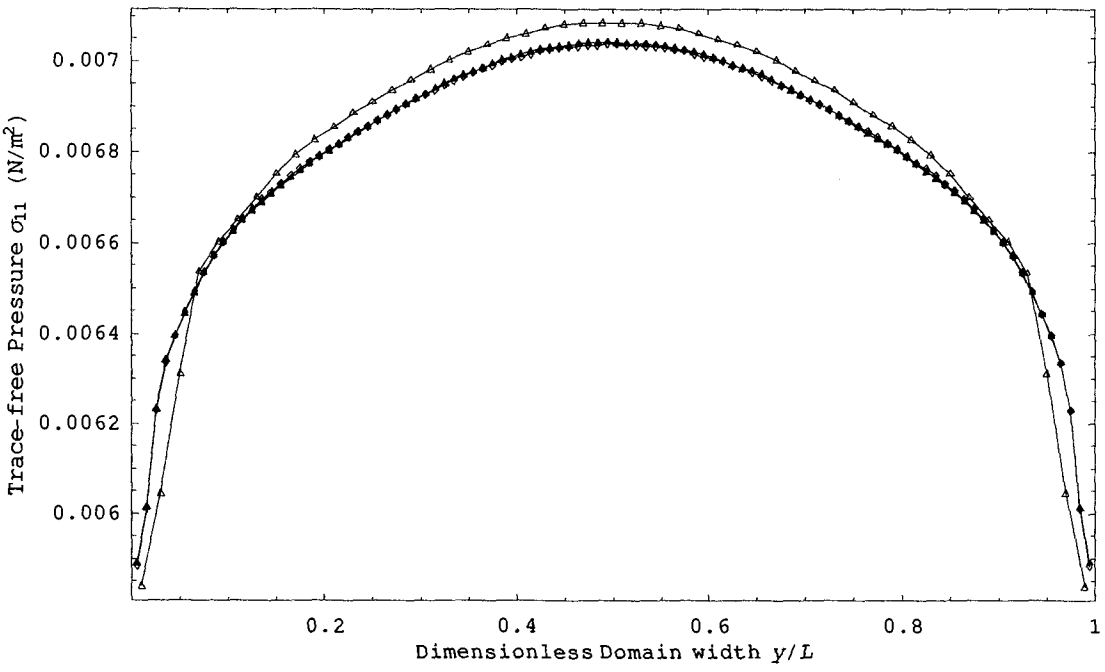

(e)

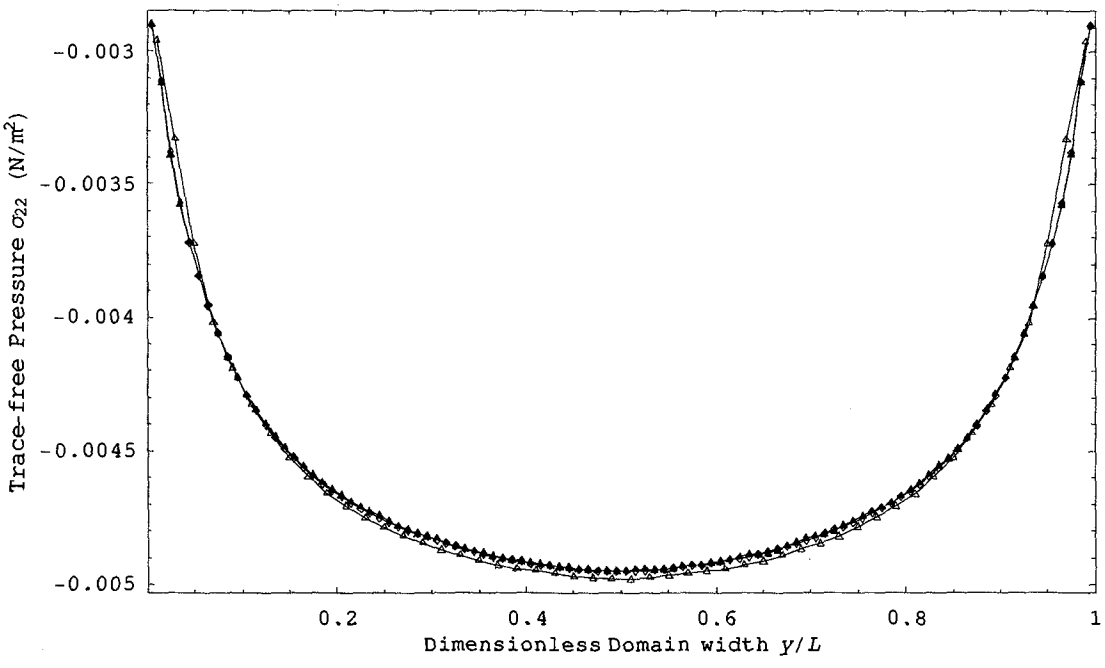

(f)

Figure 4.3: Results to show the effect of bounds of velocity grid and the effect of step of space grid (ES-BGK model, situation Sc: Kn=0.1, hard sphere molecules, 300.0 m/s plate velocity) (Triangle for case 4.3, Triangle filled for case 4.19, Diamond for case 4.21)

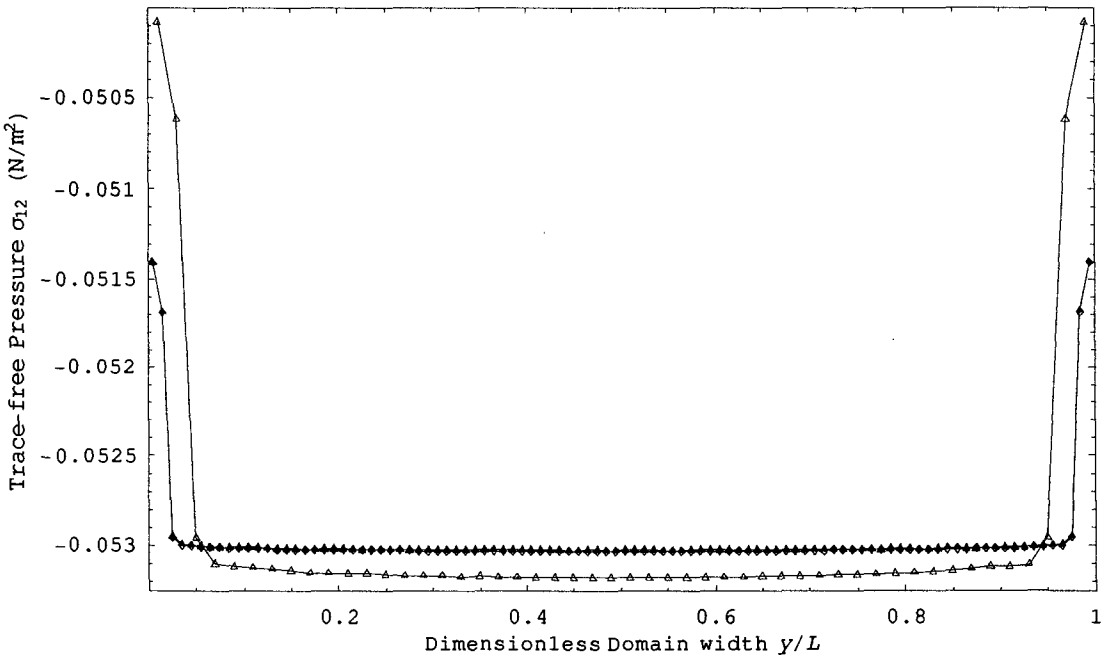

(g)

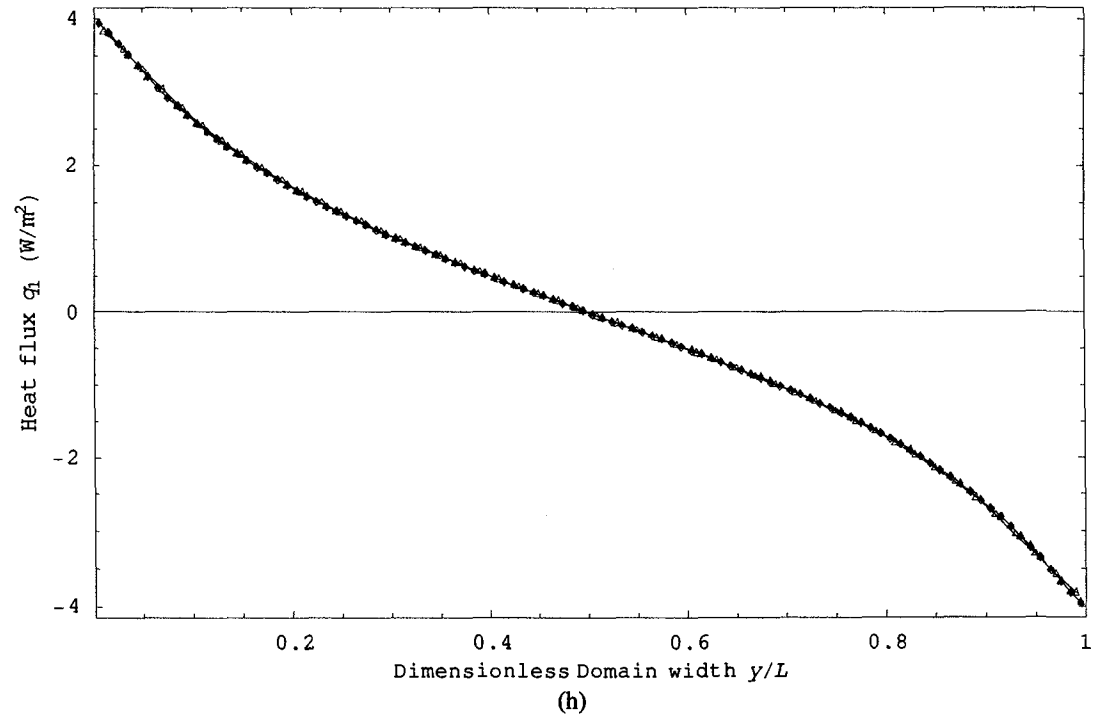

(h)

Figure 4.3: Results to show the effect of bounds of velocity grid and the effect of step of space grid (ES-BGK model, situation Sc: Kn=0.1, hard sphere molecules, 300.0 m/s plate velocity) (Triangle for case 4.3, Triangle filled for case 4.19, Diamond for case 4.21)

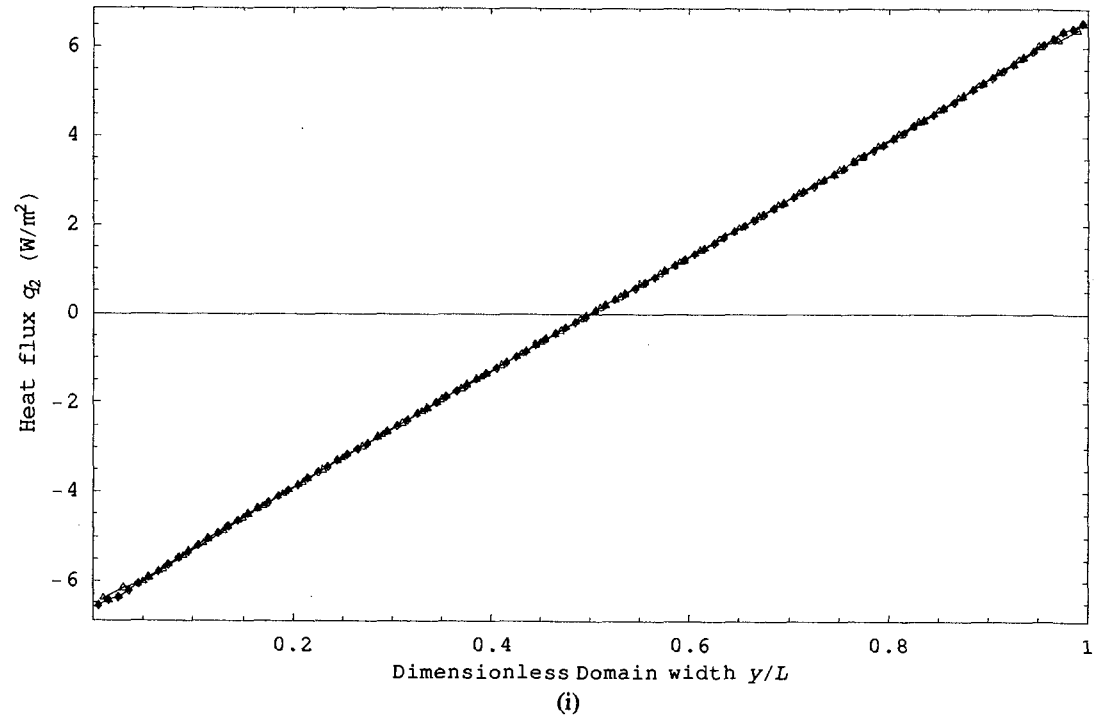

(i)

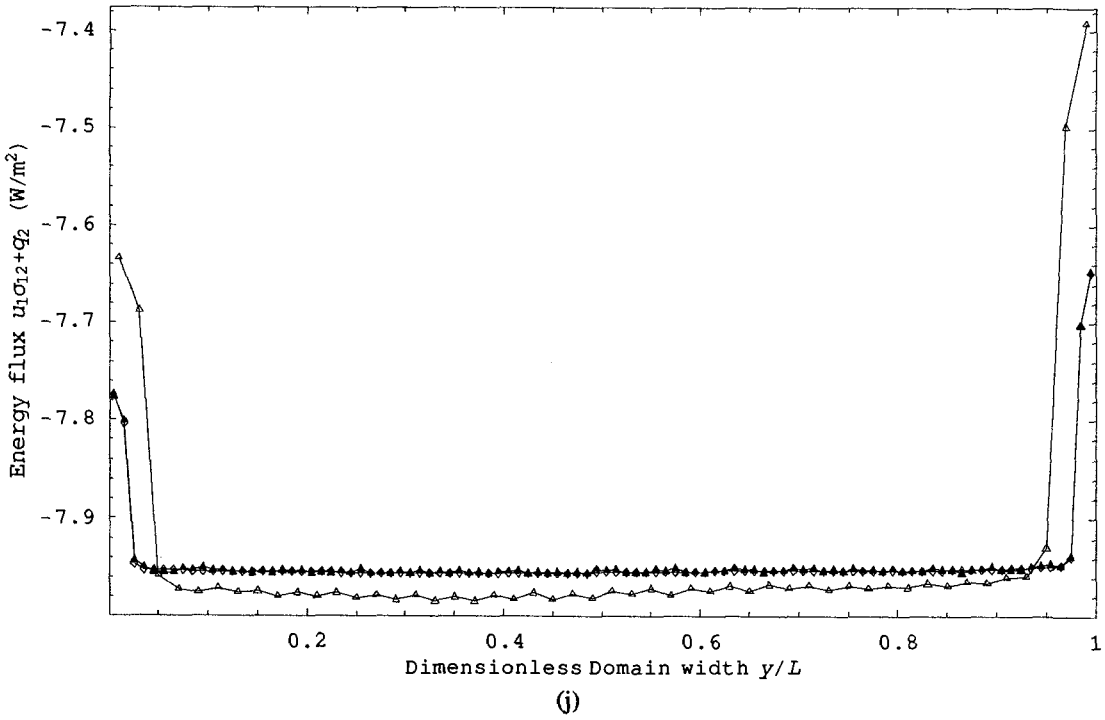

(j)

Figure 4.3: Results to show the effect of bounds of velocity grid and the effect of step of space grid (ES-BGK model, situation Sc: Kn=0.1, hard sphere molecules, 300.0 m/s plate velocity) (Triangle for case 4.3, Triangle filled for case 4.19, Diamond for case 4.21)

4.4.4 Comparison with DSMC

There are too many data and graphs obtained from the numerical tests mentioned in Section 4.4.1, so only some of them are shown in this thesis[17]. Tables D.2 to D.4 in Appendix D show average relative errors of macroscopic parameters from kinetic models we used compared to DSMC in cases 4.1-4.12. Figures 4.4 to 4.7 show the results of kinetic models and DSMC for cases 4.14, 4.6, 4.9 and 4.12.

First, let us consider the $\nu(C)$-BGK model. There are two main points against this model in Couette flow. One is that for larger Knudsen numbers (e.g. $\mathrm{Kn} \geq 0.5$), the shape of the density profile is too flat compared to the shape of the density profile from the DSMC (examples refer to graph (a) in Figures 4.5-4.7). This phenomenon was also pointed out in [34], and it is shown that this might be due to different possibilities for choosing the Knudsen number, but most likely it is a general failure of the $\nu(C)$-BGK model [34]. Moreover, the result of q_1 is the worst among all kinetic models. For small plate velocities (which corresponds to small Mach numbers), we even get the heat flux q_1 with opposite signs, compared to values from the DSMC (examples refer to graph (h) in Figures 4.4 and 4.7).

Then, let us consider the two new kinetic models. It is found that results from the new kinetic model I are very similar to results from the new kinetic model II for all test cases. Results from the new kinetic models locate in between results from the $\nu(C)$-BGK model and results from the ES-BGK model for hard sphere molecules, while the new kinetic models are identical to the ES-BGK model for Maxwellian molecules, for the collision frequency is a constant and independent of the microscopic velocity for Maxwellian molecules. Combining with the analysis about the $\nu(C)$-BGK model in the previous paragraph, the ES-BGK model is a little better for tested 1DCF than the new kinetic models from results and computational time.

---

[17] Graphs and data from these two steps are too many to be shown in this thesis. If interested in graphs and data which are not shown, contact the author (or his supervisor) for them.

At last, let us consider the BGK model and the ES-BGK model. For small Knudsen number situations ($\mathrm{Kn} \leq 0.1$), where the Prandtl number is meaningful, the ES-BGK model gives better results than the BGK model, and examples refer to Figure 4.4. This is meaningful, for $\mathrm{Pr} = 1$ in the BGK model, while $\mathrm{Pr} = 2/3$ in the ES-BGK model. While for large Knudsen number situations, it is realized that none of the kinetic models (BGK and ES-BGK) gives better results than another one for all tests. We suggest to using the ES-BGK model, instead of the BGK model for further consideration, especially for small Knudsen number situations.

Let us consider the effect of Knudsen number and Mach number on the accuracy of kinetic models, which means the difference between results from kinetic models and results from the DSMC. One parameter to show this difference is the average relative error, which values are shown in Table D.2-D.4 in Appendix D. When the Knudsen number changes with fixed plate velocity, it is found that there are no big changes in the accuracy of kinetic models. Accuracy of kinetic models at small Knudsen numbers seems to be lower than at large Knudsen numbers, since there are strong oscillations in the results of the DSMC. These are due to the strong stochastic noise of the DSMC method at smaller Knudsen numbers, which can not be considered as a good benchmark in these cases [47]. When the plate velocity is increased with fixed Knudsen number, it can be seen that the accuracy decreases for any parameter and any kinetic model. Therefore, the Mach number has a stronger effect on the accuracy of kinetic models than the Knudsen number.

When the degree of moments becomes higher, the accuracy of moment from kinetic models will be lower. As an example, differences of σ_{11}, σ_{22}, σ_{12} and q_1 between kinetic models and the DSMC are bigger than differences of ρ, u_1, T, and p for the same test situation.

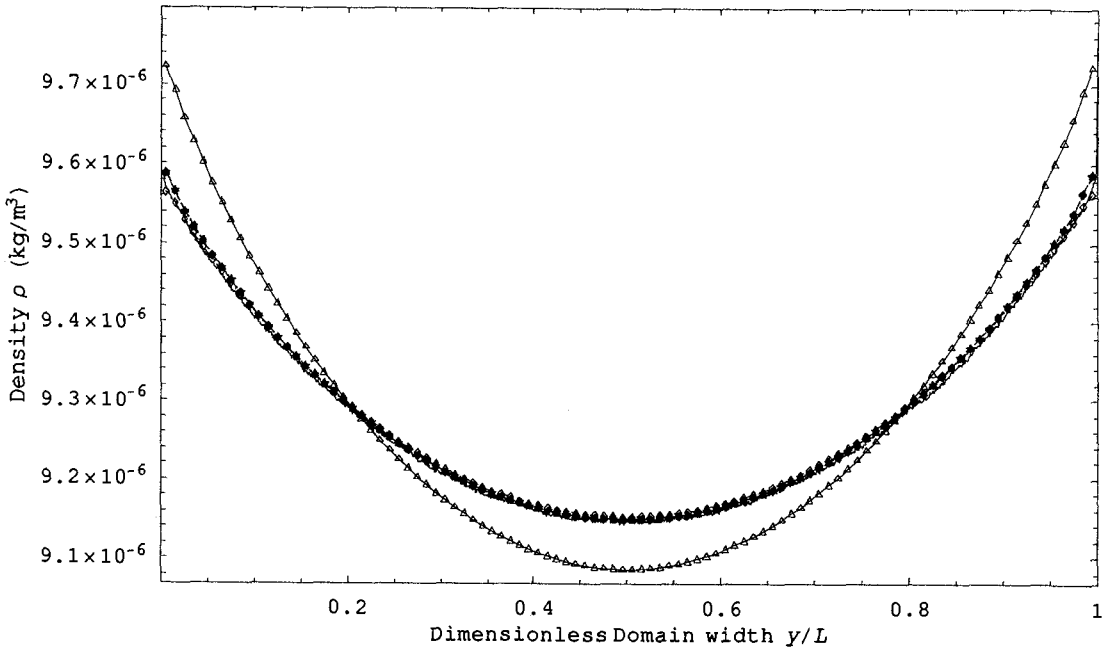

(a)

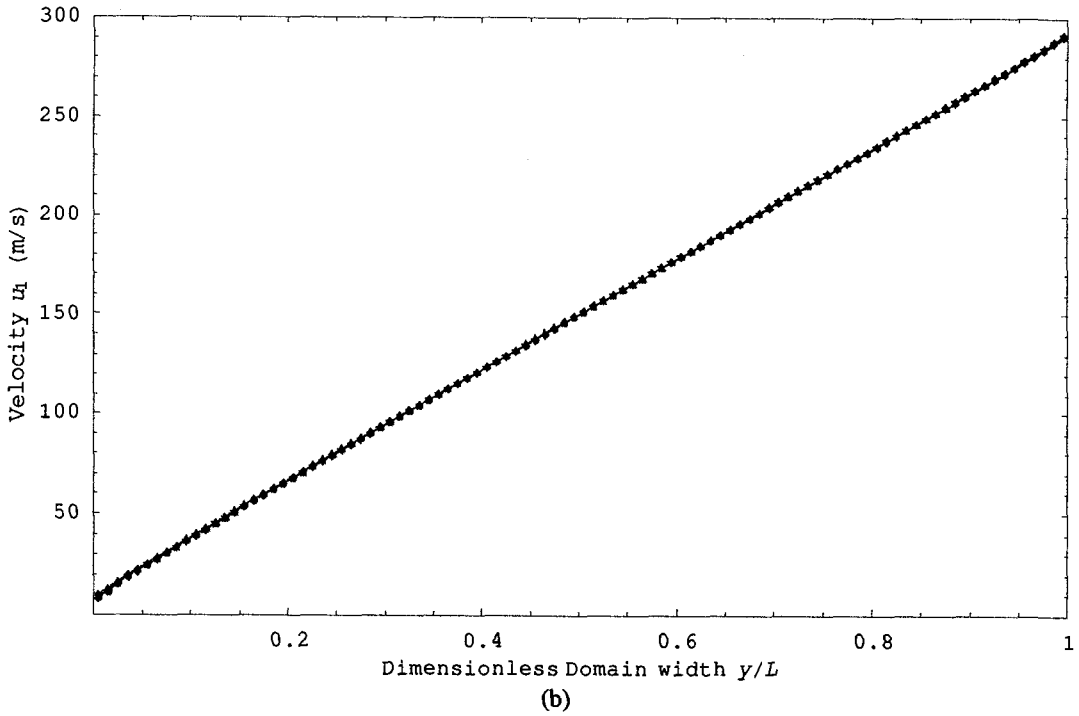

(b)

Figure 4.4: Comparison of kinetic models with DSMC (case 4.14: Kn=0.025, Maxwell molecules, 300.0 m/s plate velocity) (Line without symbols for DSMC, Triangle for BGK, Triangle filled for ES-BGK, Diamond for $\nu(C)$-BGK, Diamond filled for new kinetic model I, Star for new kinetic model II)

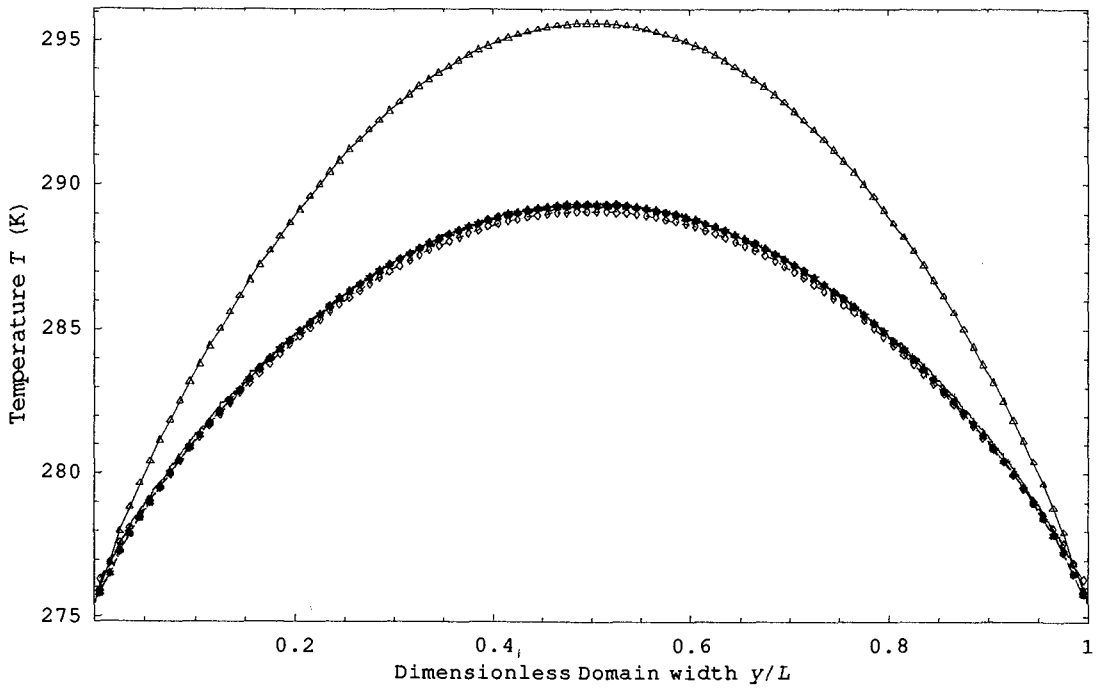

(c)

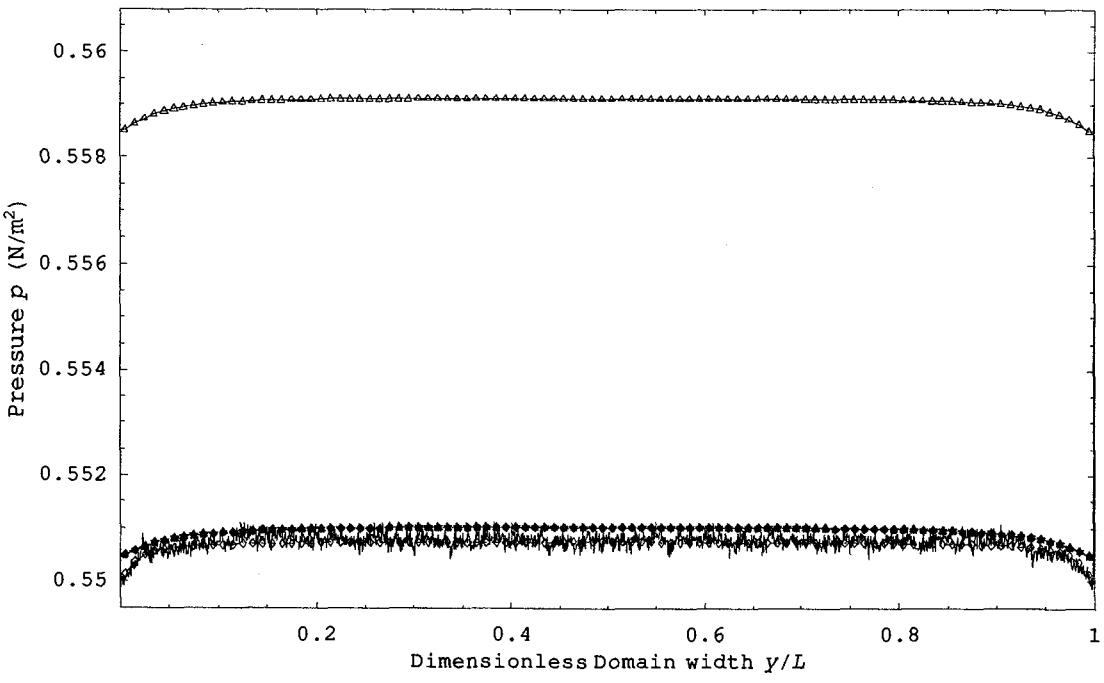

(d)

Figure 4.4: Comparison of kinetic models with DSMC (case 4.14: Kn=0.025, Maxwell molecules, 300.0 m/s plate velocity) (Line without symbols for DSMC, Triangle for BGK, Triangle filled for ES-BGK, Diamond for $\nu(C)$-BGK, Diamond filled for new kinetic model I, Star for new kinetic model II)

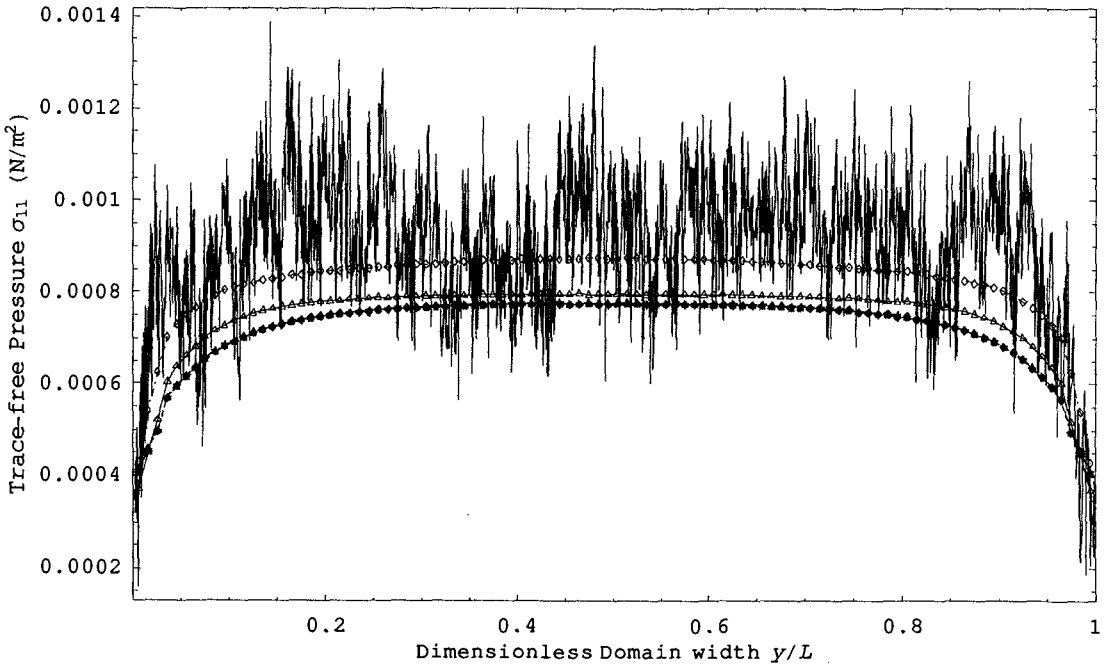

(e)

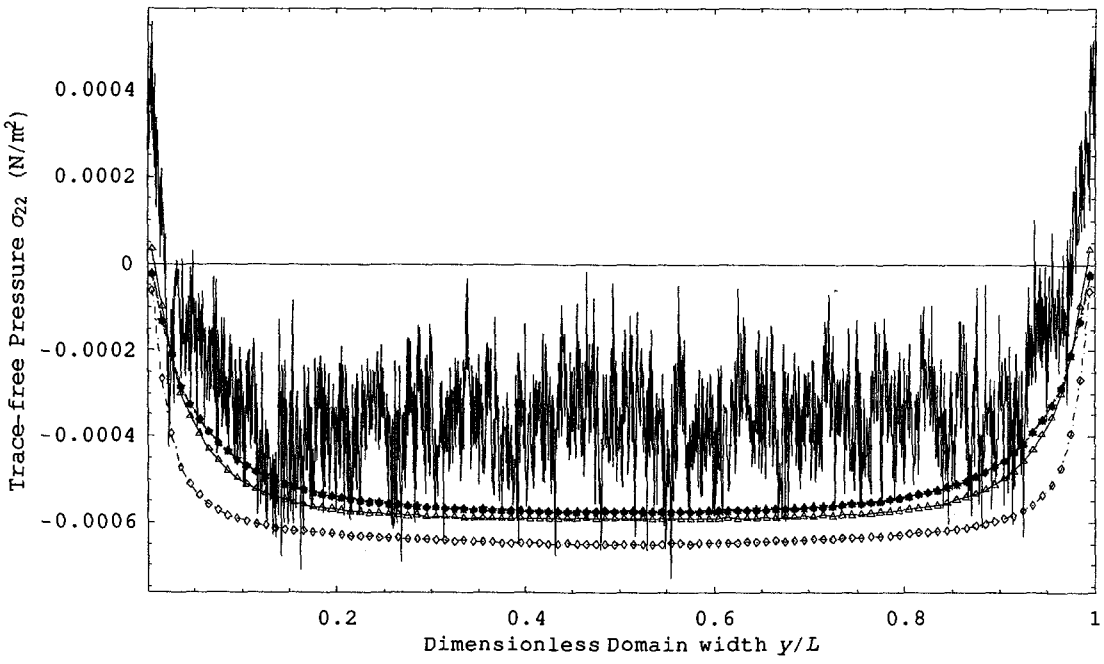

(f)

Figure 4.4: Comparison of kinetic models with DSMC (case 4.14: Kn=0.025, Maxwell molecules, 300.0 m/s plate velocity)) (Line without symbols for DSMC, Triangle for BGK, Triangle filled for ES-BGK, Diamond for $\nu(C)$-BGK, Diamond filled for new kinetic model I, Star for new kinetic model II)

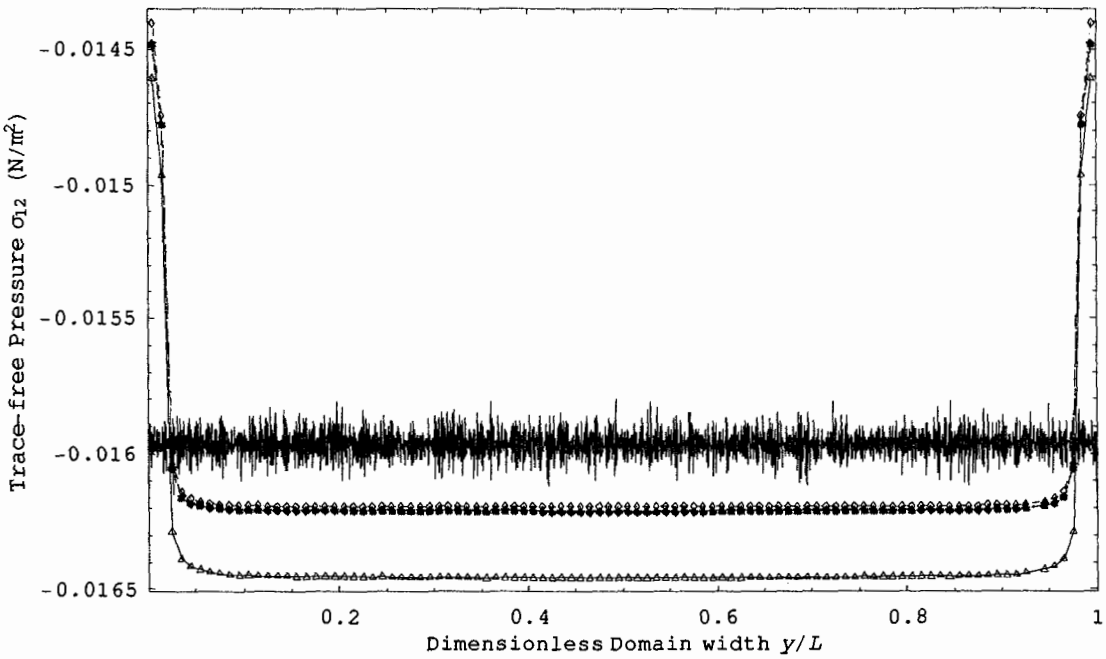

(g)

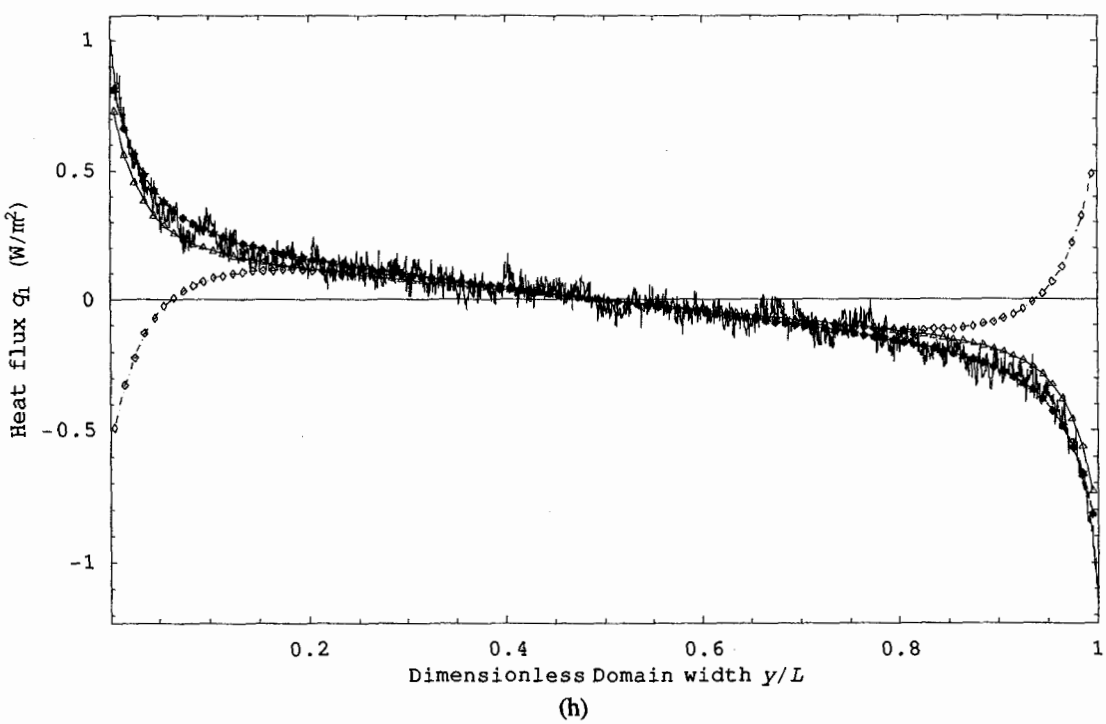

(h)

Figure 4.4: Comparison of kinetic models with DSMC (case 4.14: Kn=0.025, Maxwell molecules, 300.0 m/s plate velocity)) (Line without symbols for DSMC, Triangle for BGK, Triangle filled for ES-BGK, Diamond for $\nu(C)$-BGK, Diamond filled for new kinetic model I, Star for new kinetic model II)

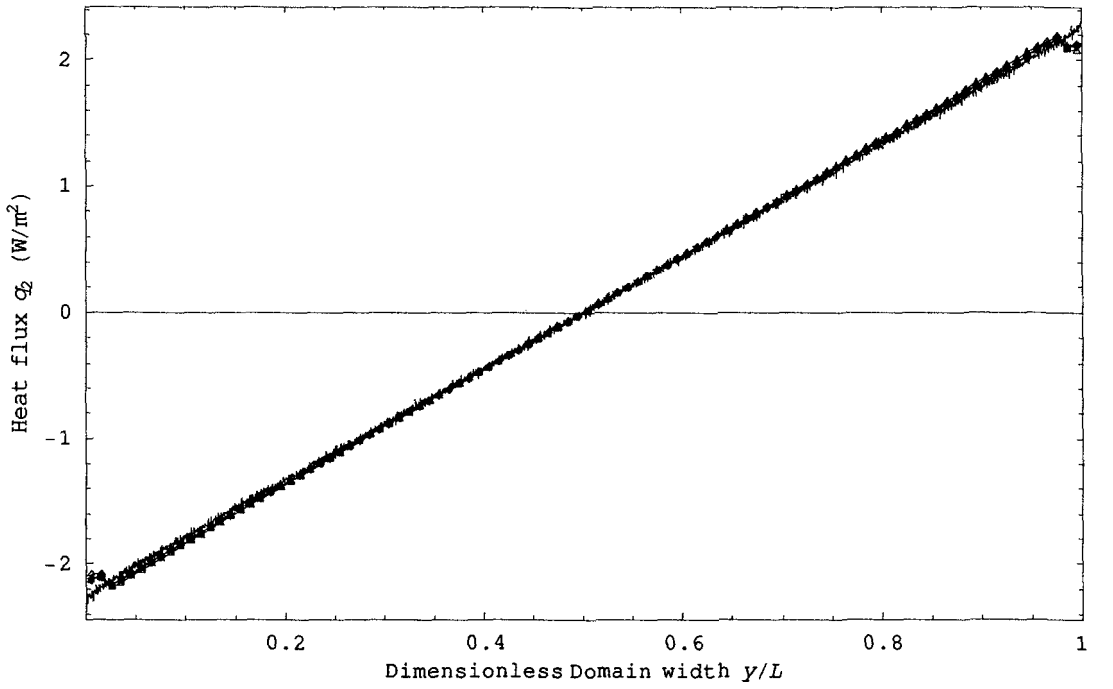

(i)

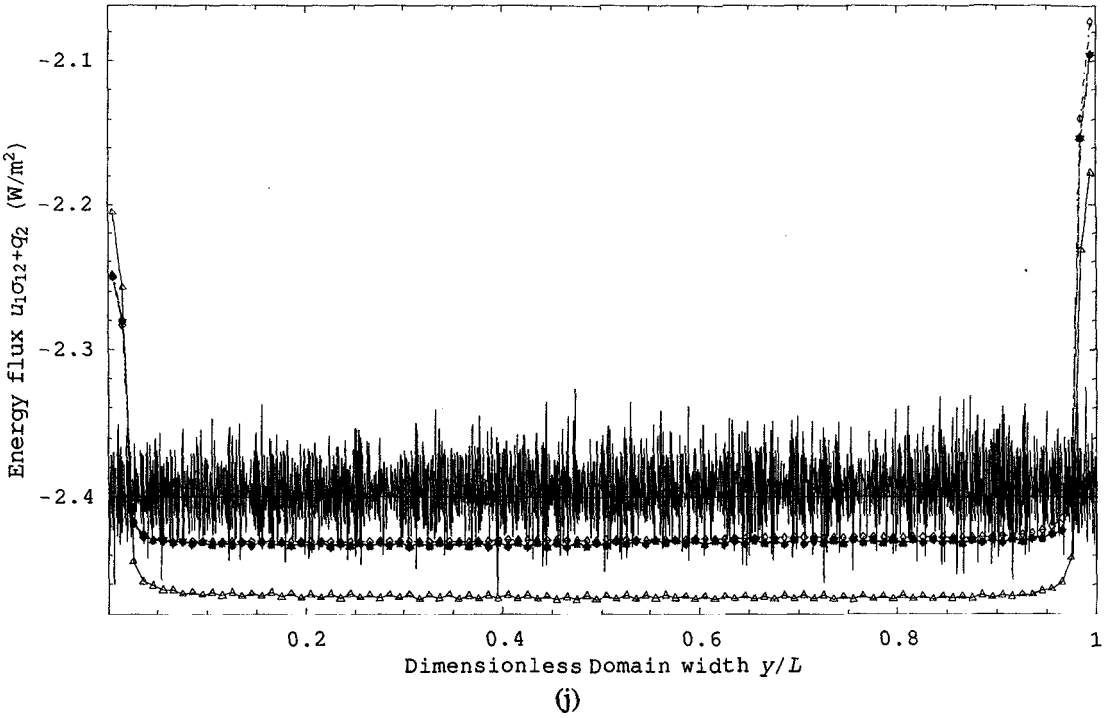

(j)

Figure 4.4: Comparison of kinetic models with DSMC (case 4.14: Kn=0.025, Maxwell molecules, 300.0 m/s plate velocity)) (Line without symbols for DSMC, Triangle for BGK, Triangle filled for ES-BGK, Diamond for $\nu(C)$-BGK, Diamond filled for new kinetic model I, Star for new kinetic model II)

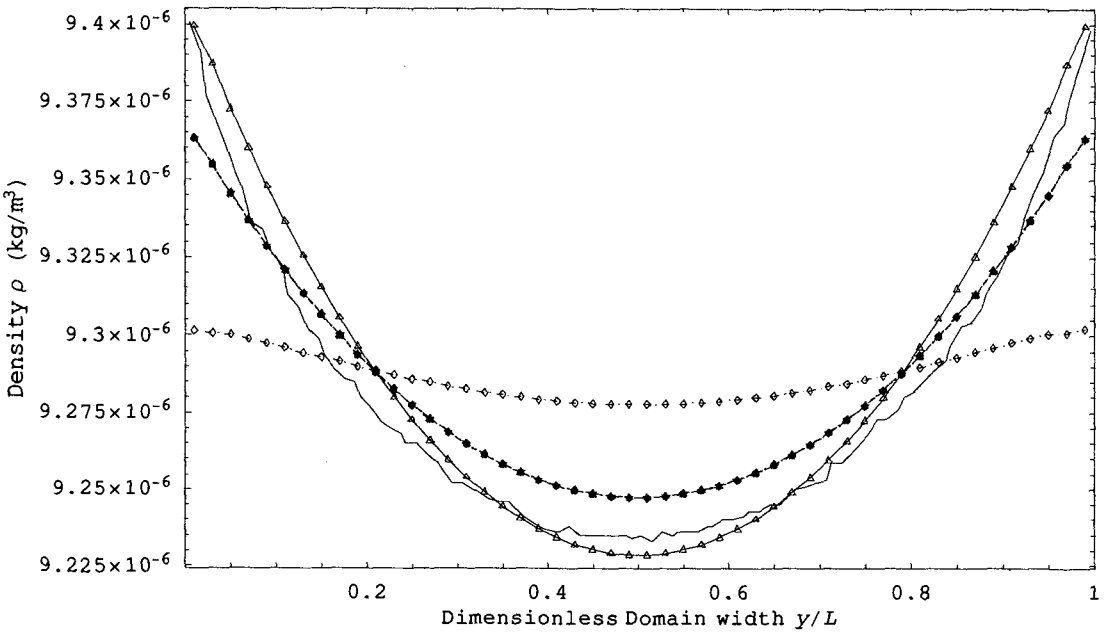

(a)

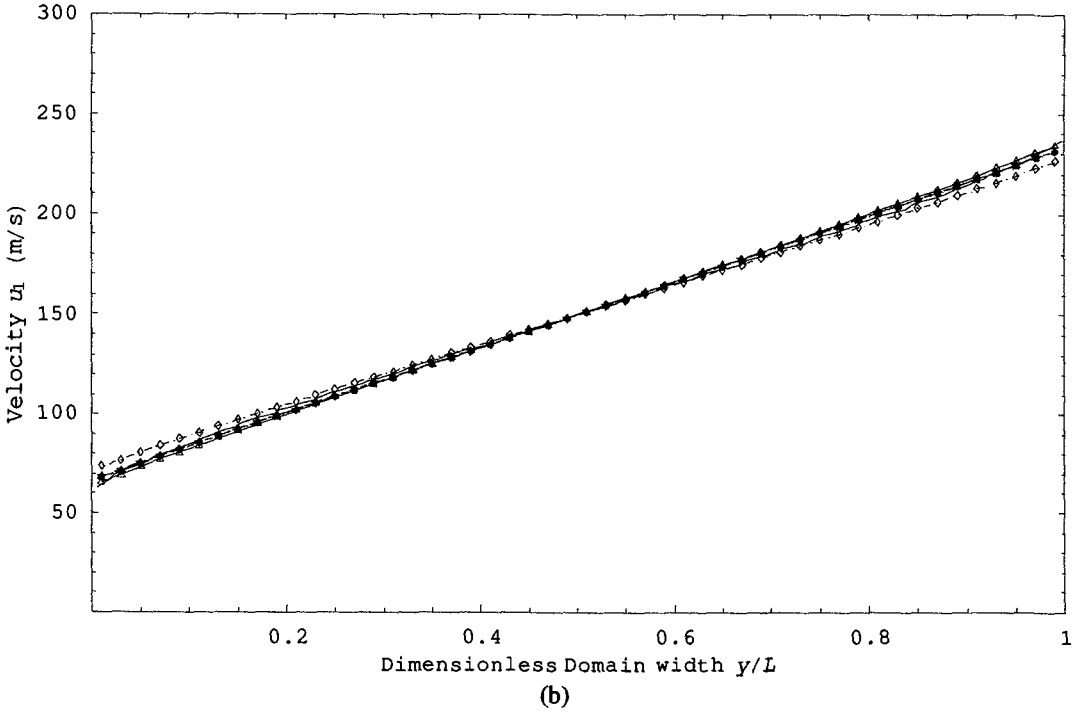

(b)

Figure 4.5: Comparison of kinetic models with DSMC (case 4.6: Kn=0.5, Maxwell molecules, 300.0 m/s plate velocity)) (Line without symbols for DSMC, Triangle for BGK, Triangle filled for ES-BGK, Diamond for $\nu(C)$-BGK, Diamond filled for new kinetic model I, Star for new kinetic model II)

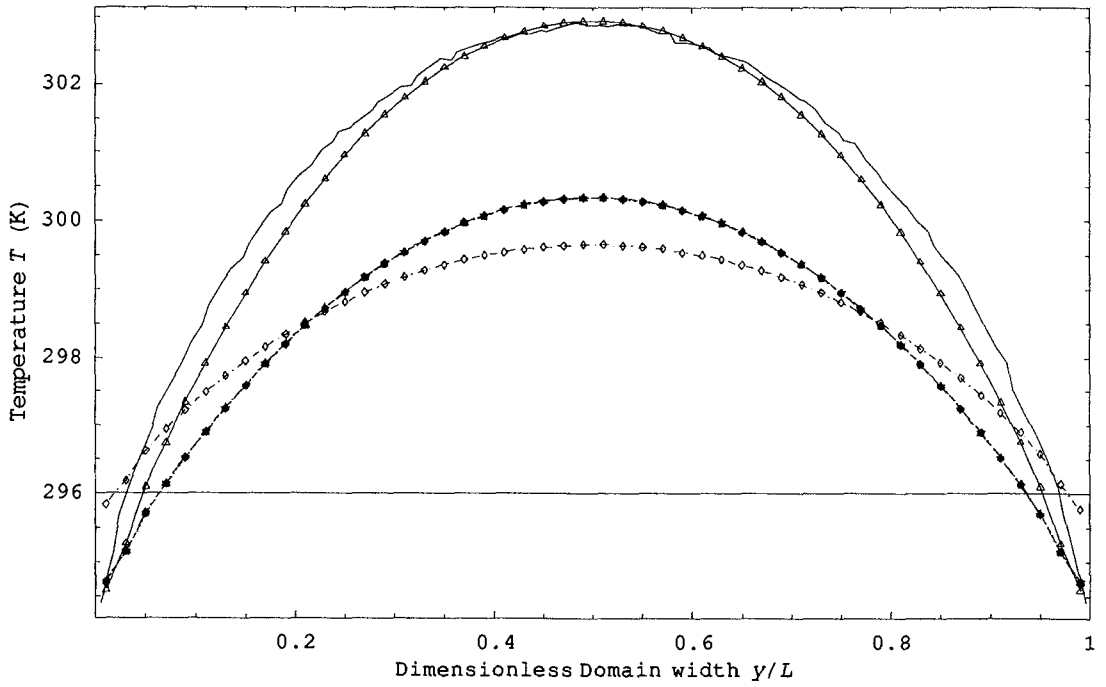

(c)

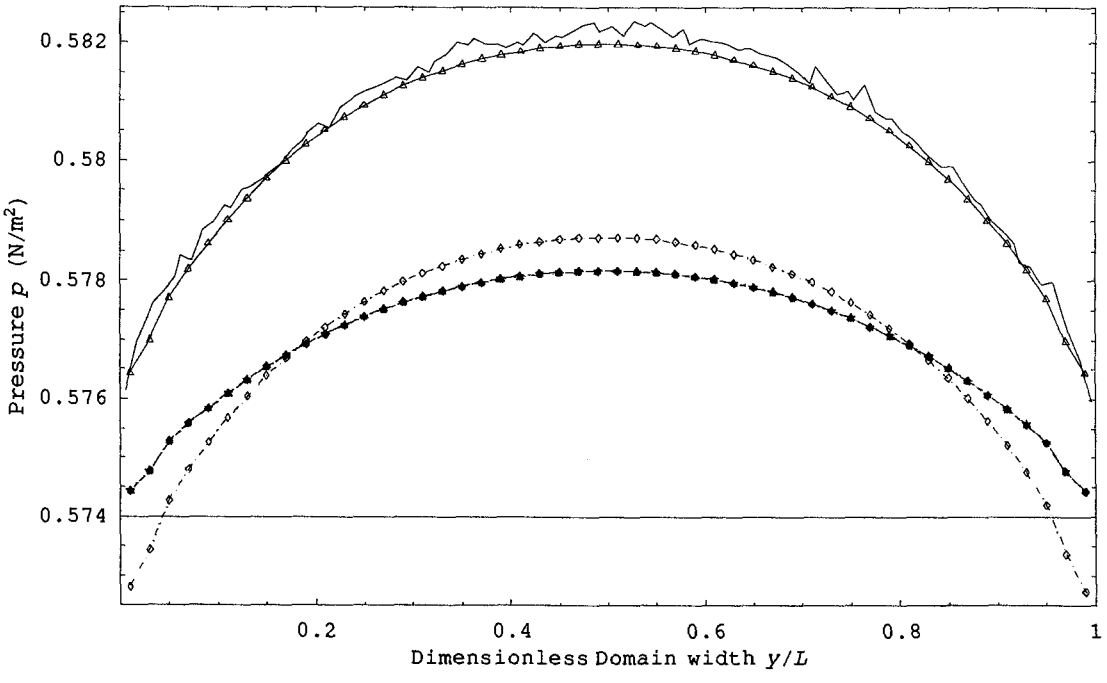

(d)

Figure 4.5: Comparison of kinetic models with DSMC (case 4.6: Kn=0.5, Maxwell molecules, 300.0 m/s plate velocity)) (Line without symbols for DSMC, Triangle for BGK, Triangle filled for ES-BGK, Diamond for $\nu(C)$-BGK, Diamond filled for new kinetic model I, Star for new kinetic model II)

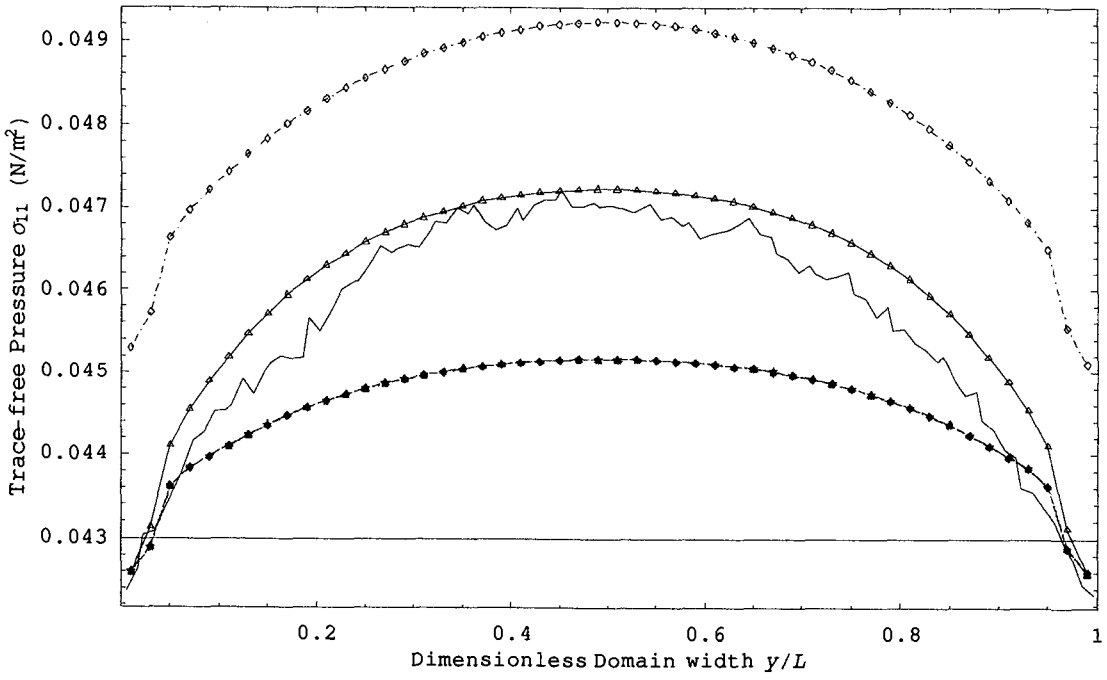

(e)

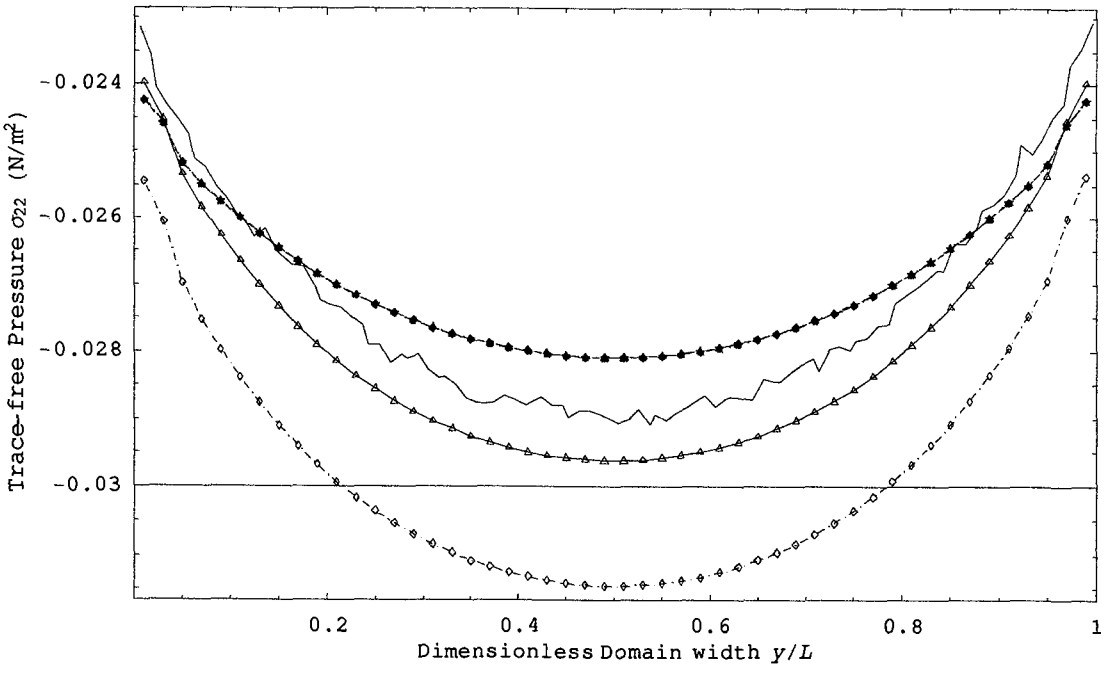

(f)

Figure 4.5: Comparison of kinetic models with DSMC (case 4.6: Kn=0.5, Maxwell molecules, 300.0 m/s plate velocity)) (Line without symbols for DSMC, Triangle for BGK, Triangle filled for ES-BGK, Diamond for $\nu(C)$-BGK, Diamond filled for new kinetic model I, Star for new kinetic model II)

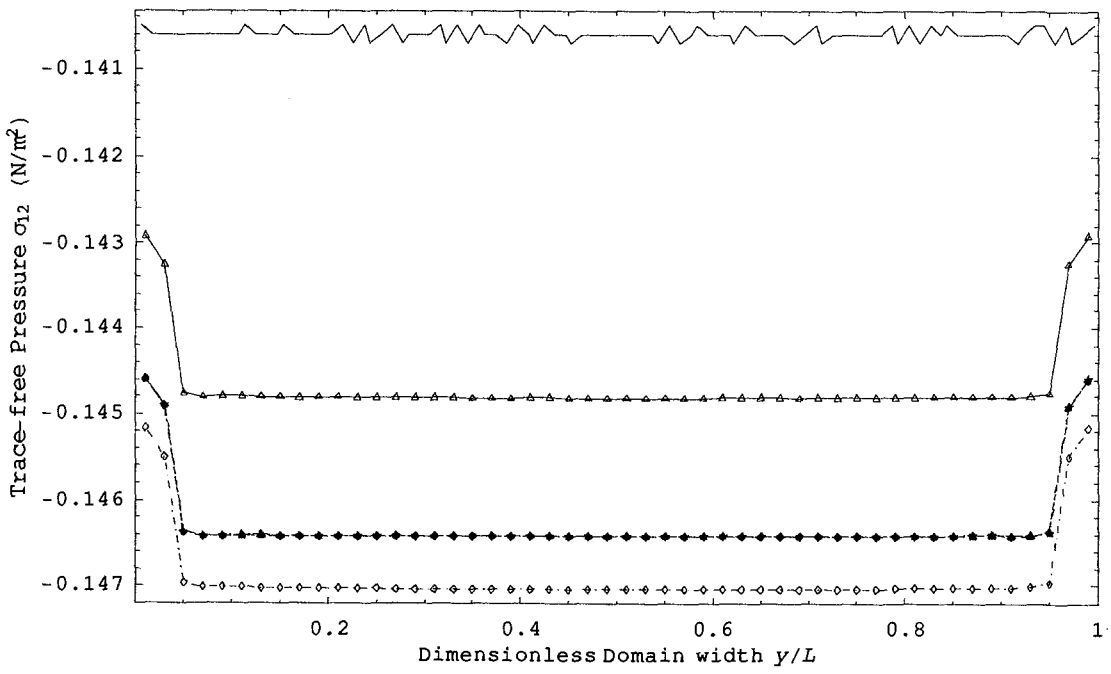

(g)

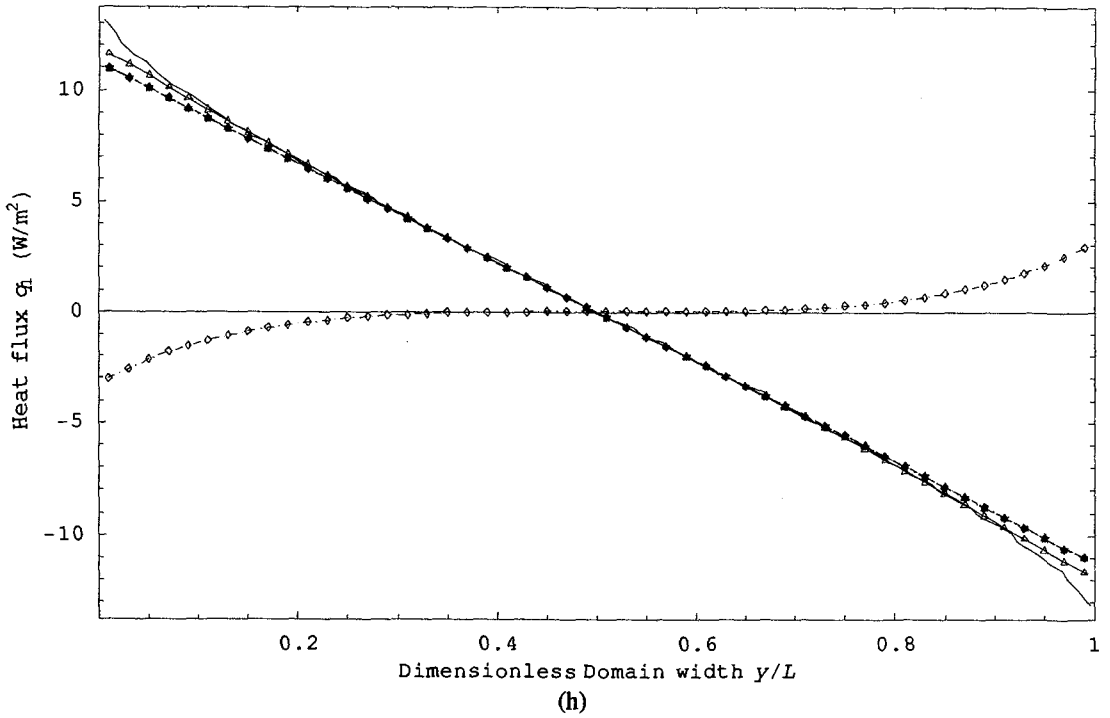

(h)

Figure 4.5: Comparison of kinetic models with DSMC (case 4.6: Kn=0.5, Maxwell molecules, 300.0 m/s plate velocity)) (Line without symbols for DSMC, Triangle for BGK, Triangle filled for ES-BGK, Diamond for $\nu(C)$-BGK, Diamond filled for new kinetic model I, Star for new kinetic model II)

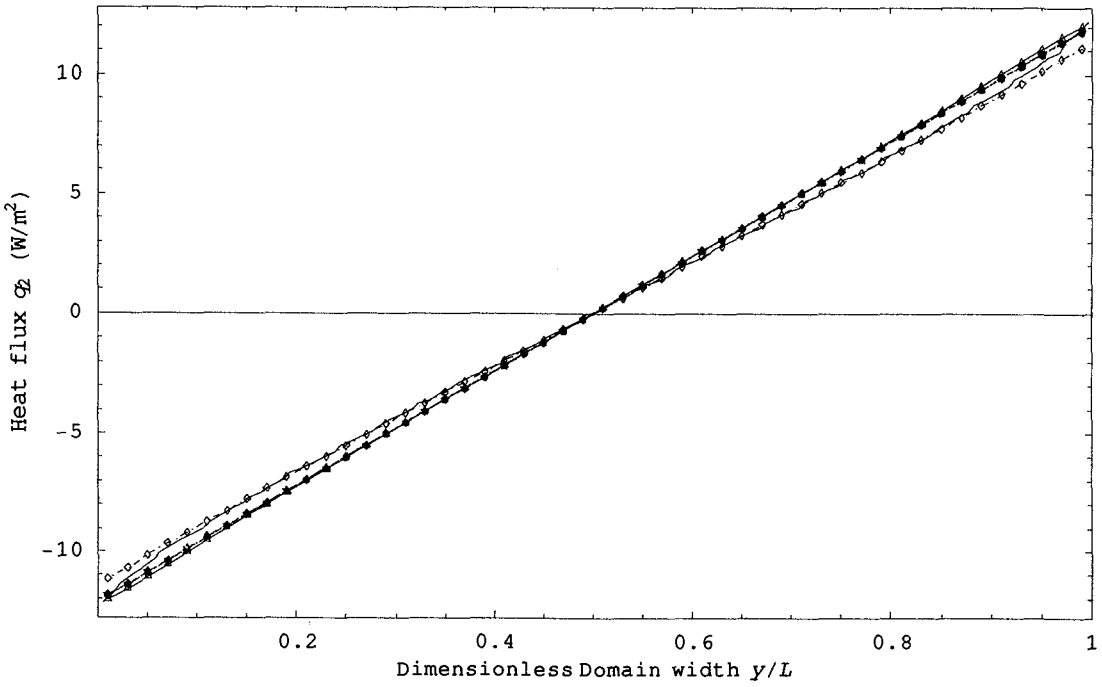

(i)

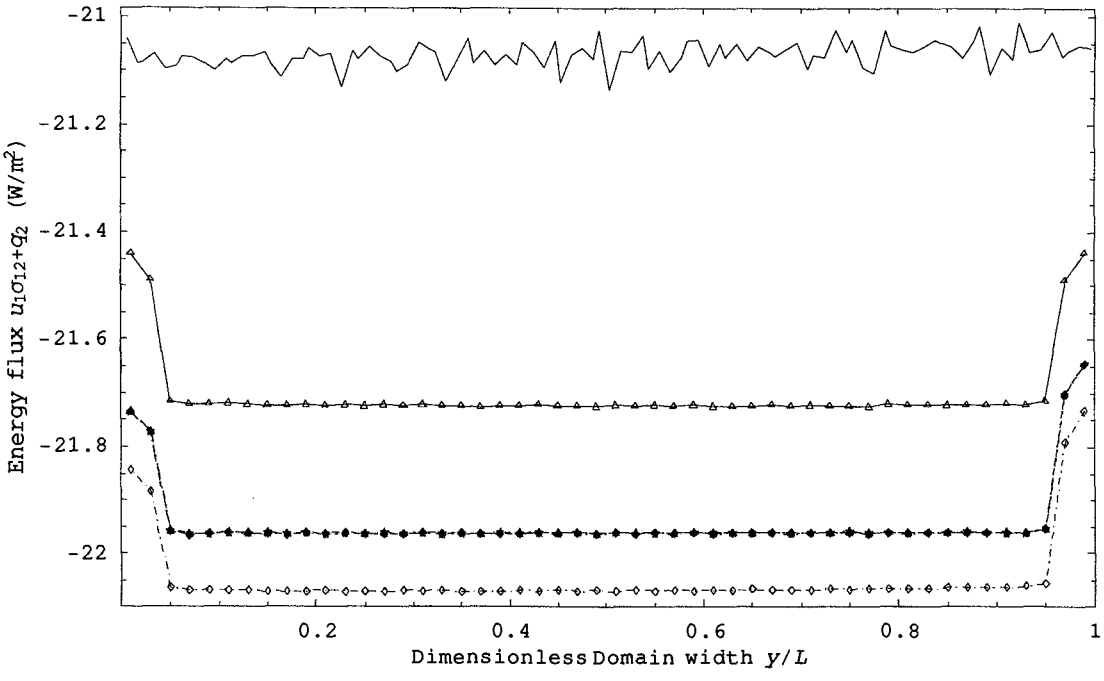

(j)

Figure 4.5: Comparison of kinetic models with DSMC (case 4.6: Kn=0.5, Maxwell molecules, 300.0 m/s plate velocity)) (Line without symbols for DSMC, Triangle for BGK, Triangle filled for ES-BGK, Diamond for $\nu(C)$-BGK, Diamond filled for new kinetic model I, Star for new kinetic model II)

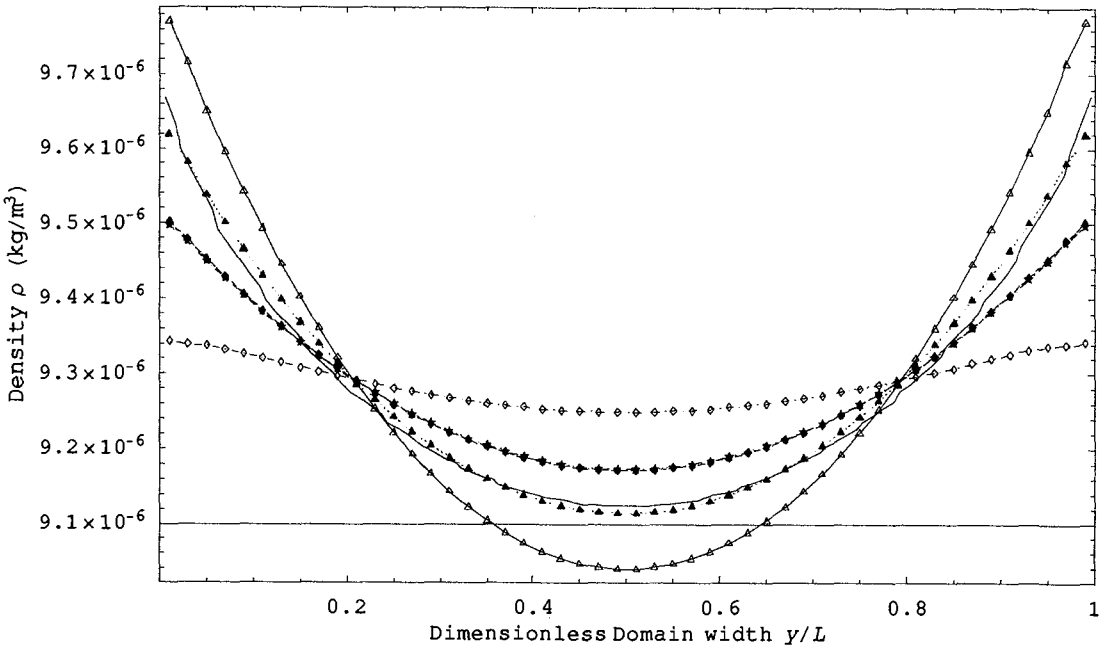

(a)

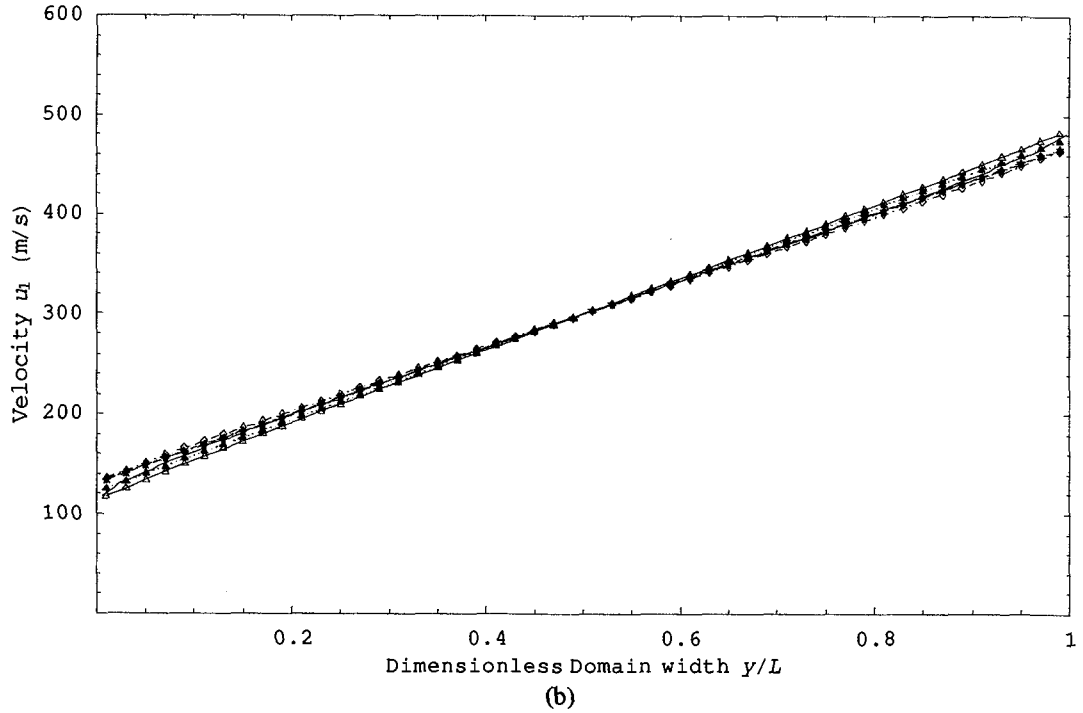

(b)

Figure 4.6: Comparison of kinetic models with DSMC (case 4.9: Kn=0.5, hard sphere molecules, 600.0 plate velocity)) (Line without symbols for DSMC, Triangle for BGK, Triangle filled for ES-BGK, Diamond for $\nu(C)$-BGK, Diamond filled for new kinetic model I, Star for new kinetic model II)

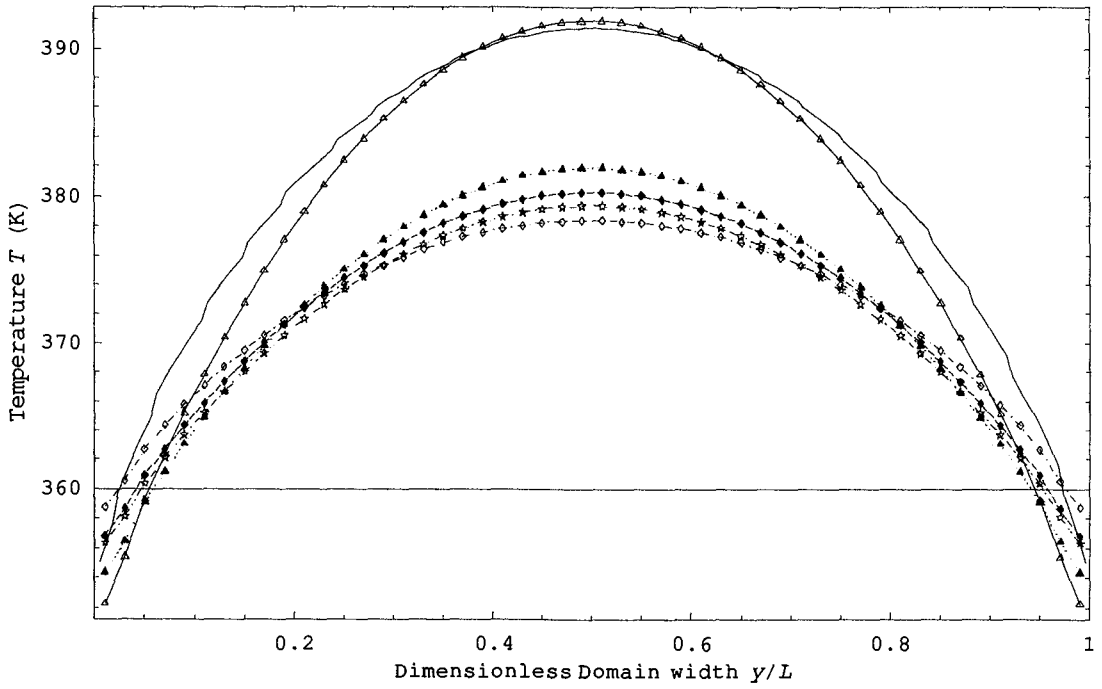

(c)

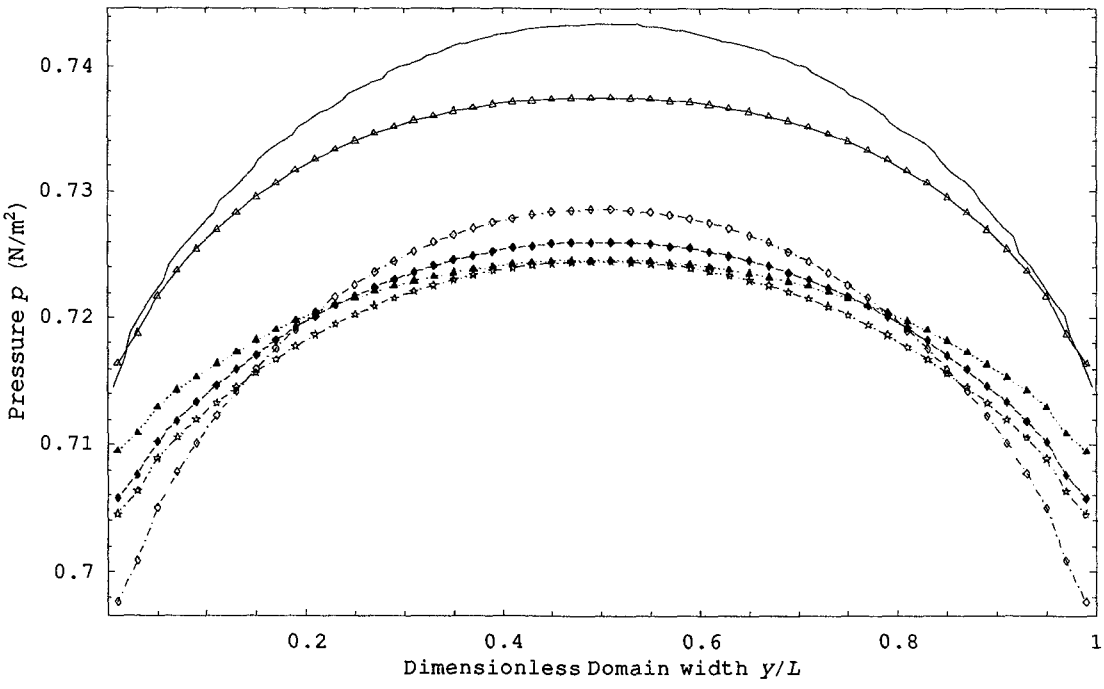

(d)

Figure 4.6: Comparison of kinetic models with DSMC (case 4.9: Kn=0.5, hard sphere molecules, 600.0 plate velocity)) (Line without symbols for DSMC, Triangle for BGK, Triangle filled for ES-BGK, Diamond for $\nu(C)$-BGK, Diamond filled for new kinetic model I, Star for new kinetic model II)

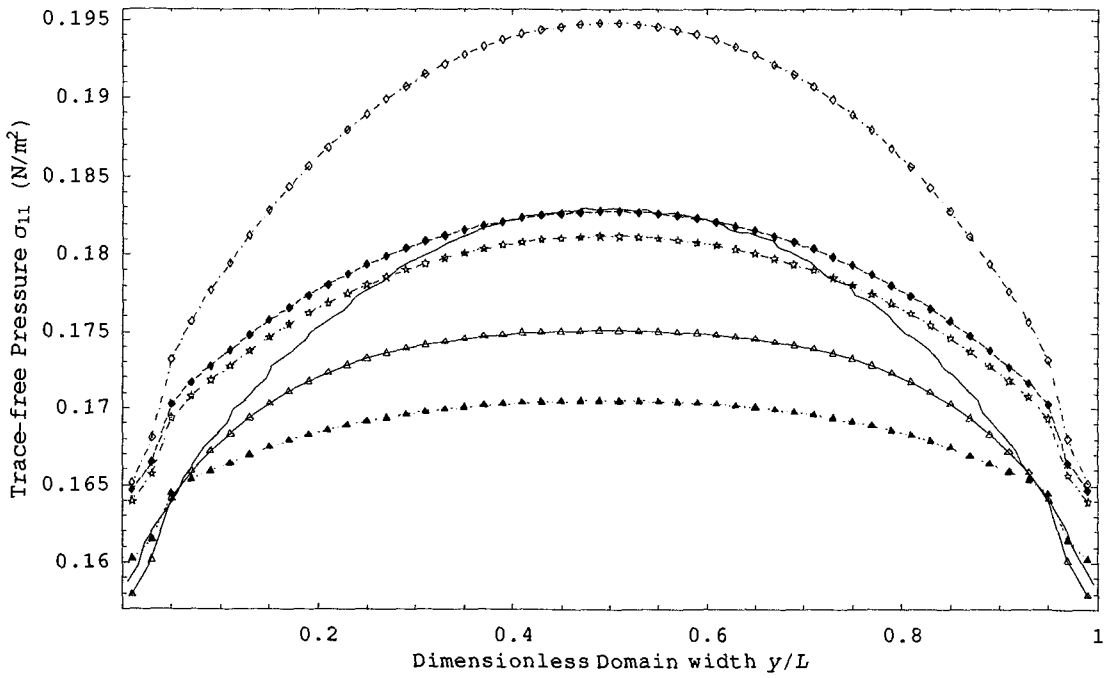

(e)

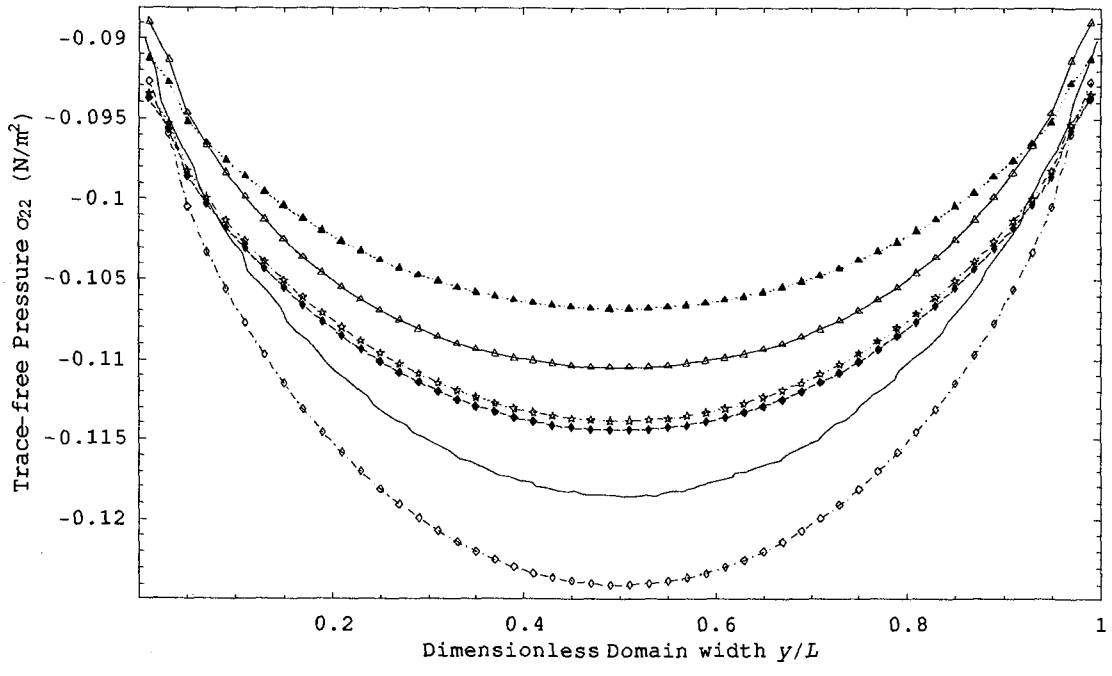

(f)

Figure 4.6: Comparison of kinetic models with DSMC (case 4.9: Kn=0.5, hard sphere molecules, 600.0 plate velocity)) (Line without symbols for DSMC, Triangle for BGK, Triangle filled for ES-BGK, Diamond for $\nu(C)$-BGK, Diamond filled for new kinetic model I, Star for new kinetic model II)

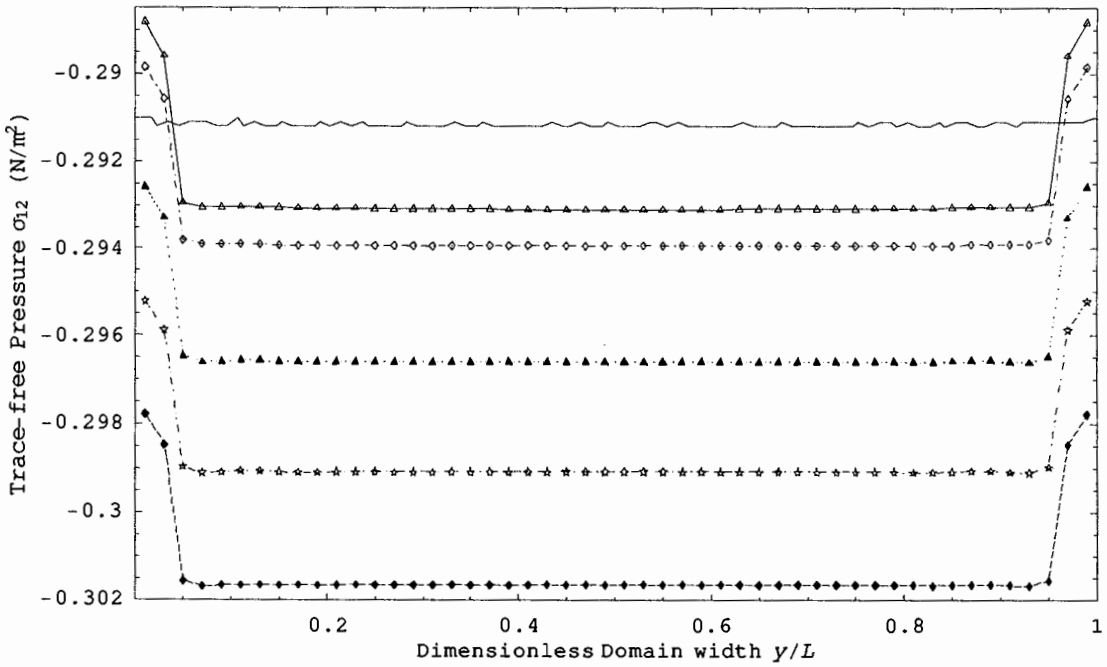

(g)

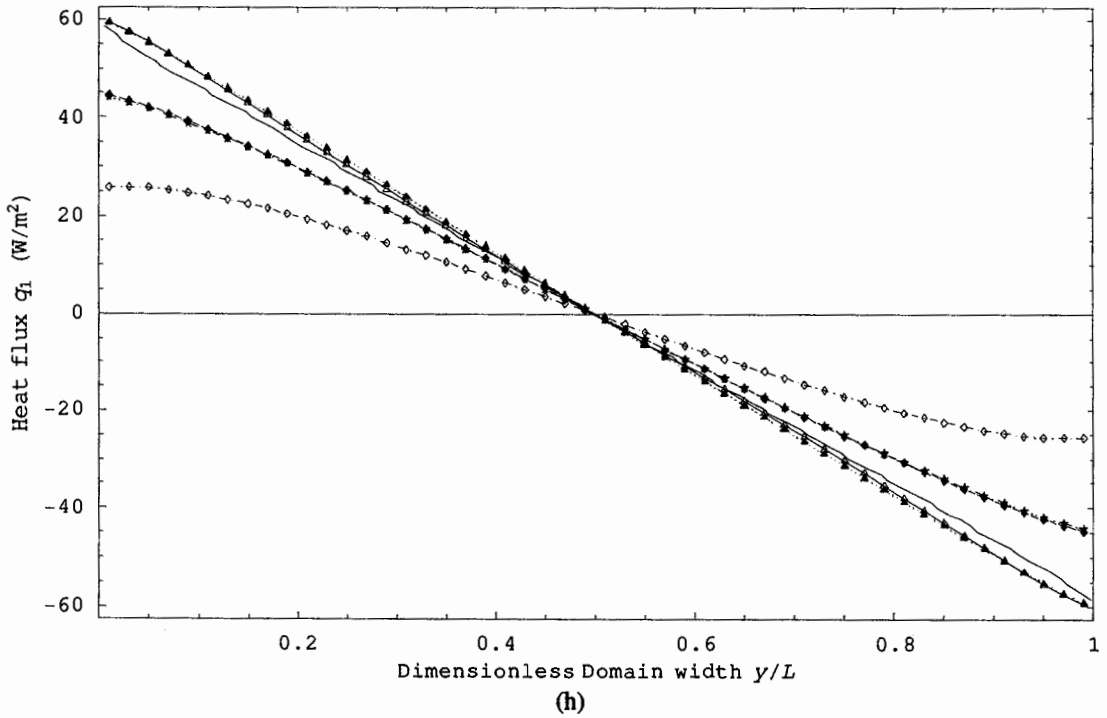

(h)

Figure 4.6: Comparison of kinetic models with DSMC (case 4.9: Kn=0.5, hard sphere molecules, 600.0 plate velocity)) (Line without symbols for DSMC, Triangle for BGK, Triangle filled for ES-BGK, Diamond for $\nu(C)$-BGK, Diamond filled for new kinetic model I, Star for new kinetic model II)

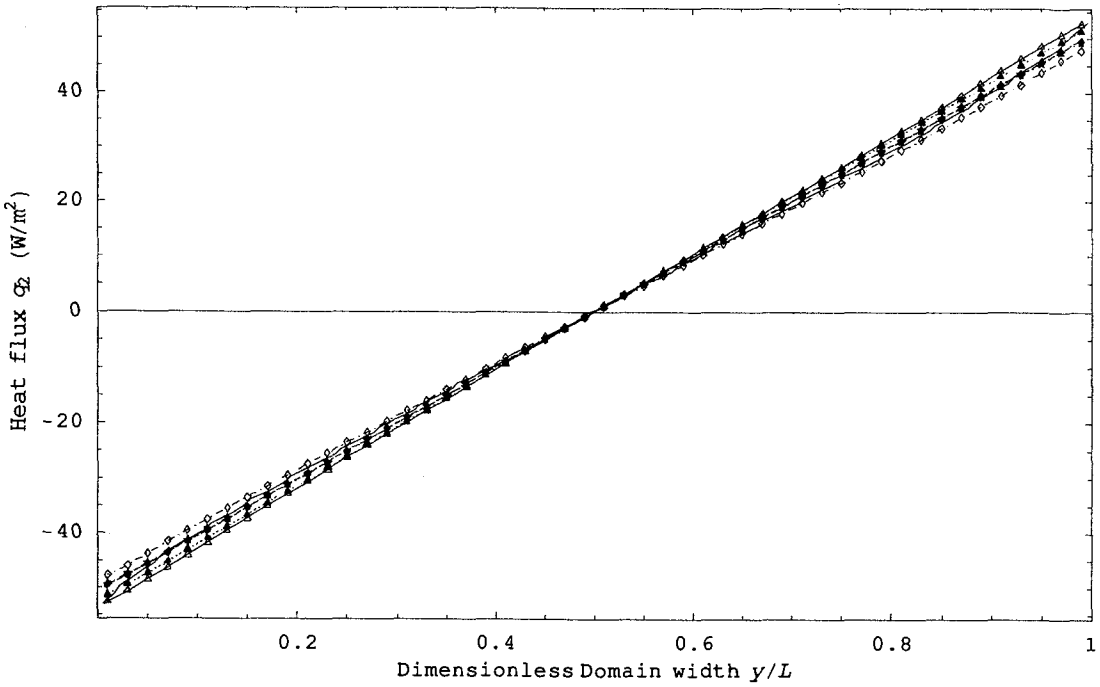

(i)

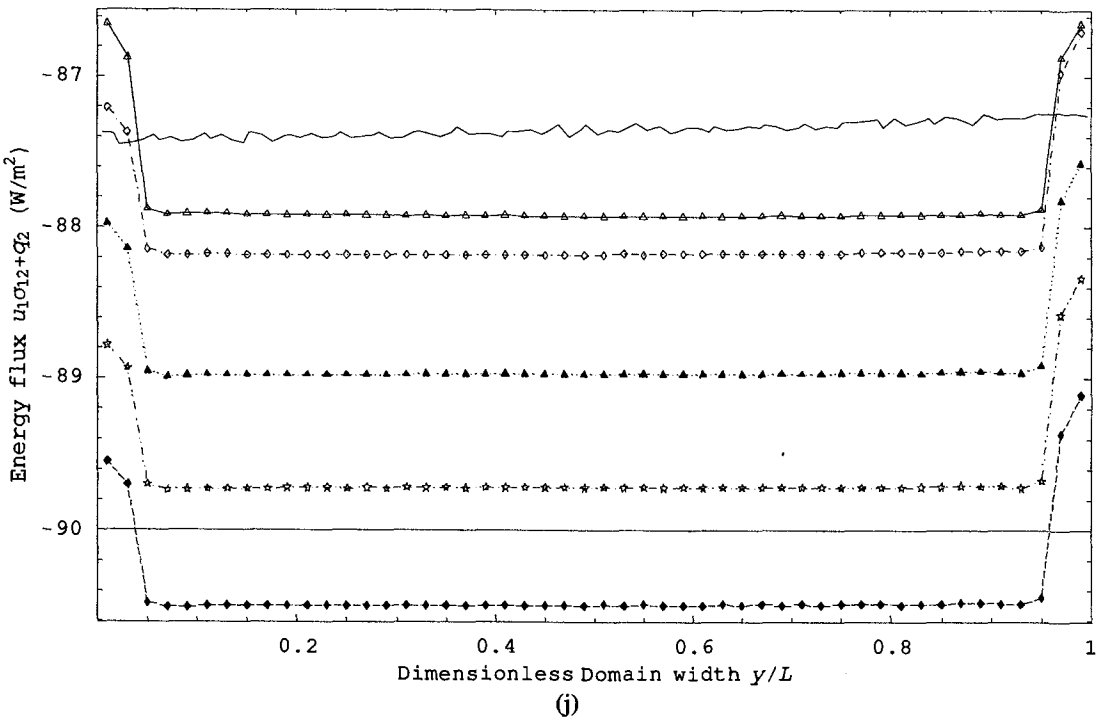

(j)

Figure 4.6: Comparison of kinetic models with DSMC (case 4.9: Kn=0.5, hard sphere molecules, 600.0 plate velocity)) (Line without symbols for DSMC, Triangle for BGK, Triangle filled for ES-BGK, Diamond for $\nu(C)$-BGK, Diamond filled for new kinetic model I, Star for new kinetic model II)

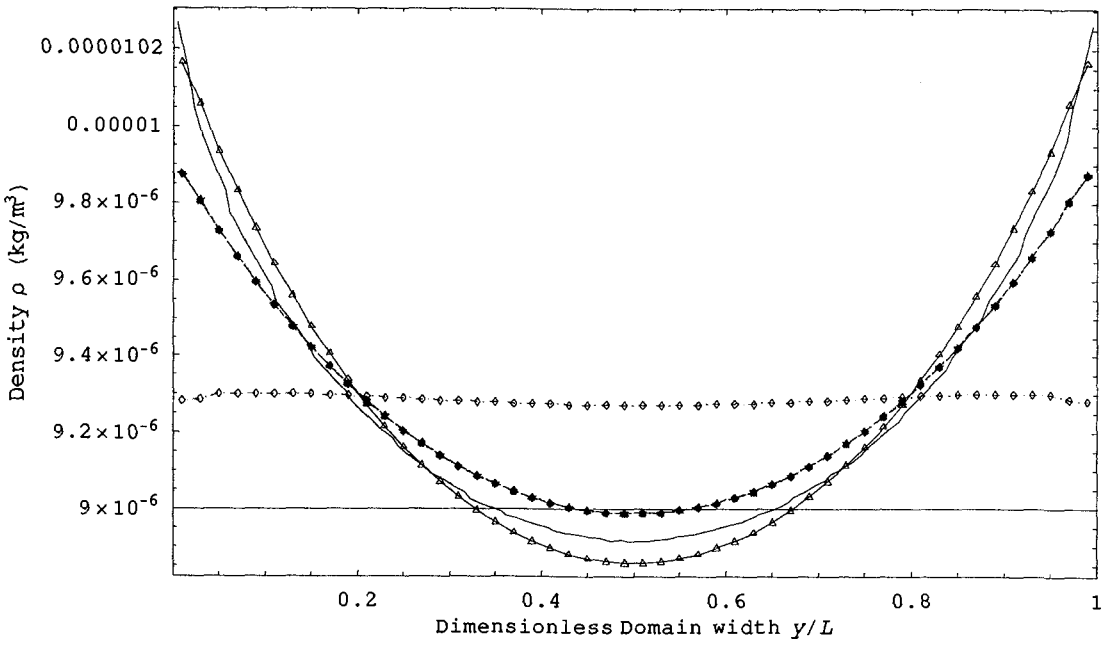

(a)

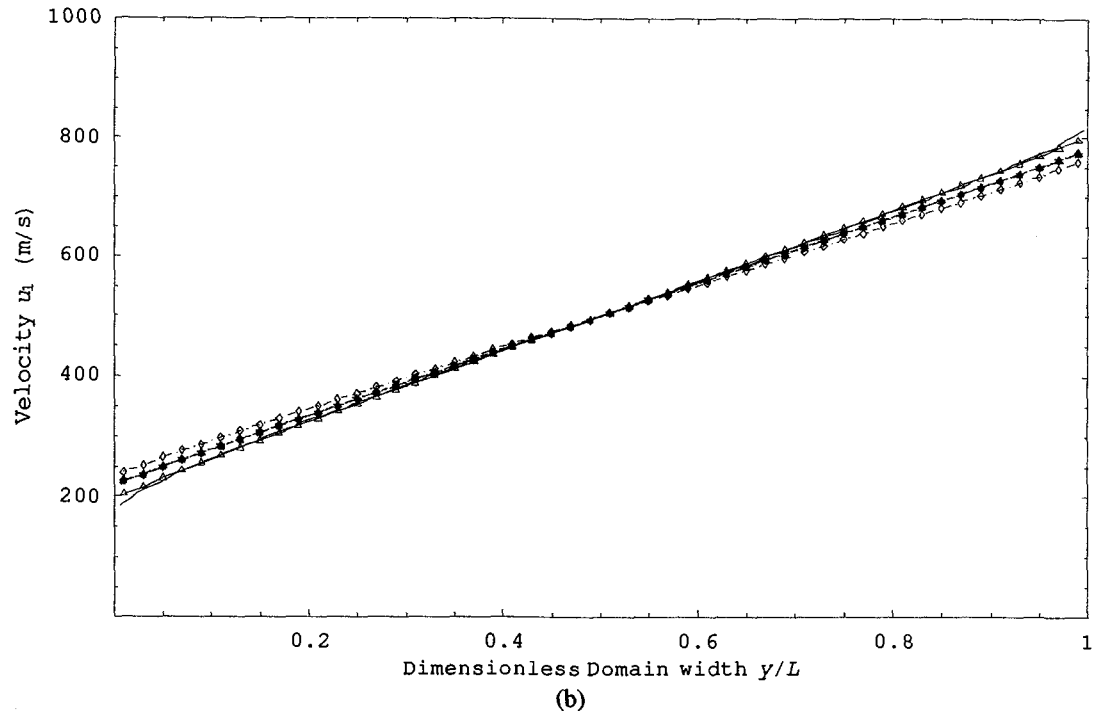

(b)

Figure 4.7: Comparison of kinetic models with DSMC (case 4.12: Kn=0.5, Maxwell molecules, 1000.0 m/s plate velocity)) (Line without symbols for DSMC, Triangle for BGK, Triangle filled for ES-BGK, Diamond for $\nu(C)$-BGK, Diamond filled for new kinetic model I, Star for new kinetic model II)

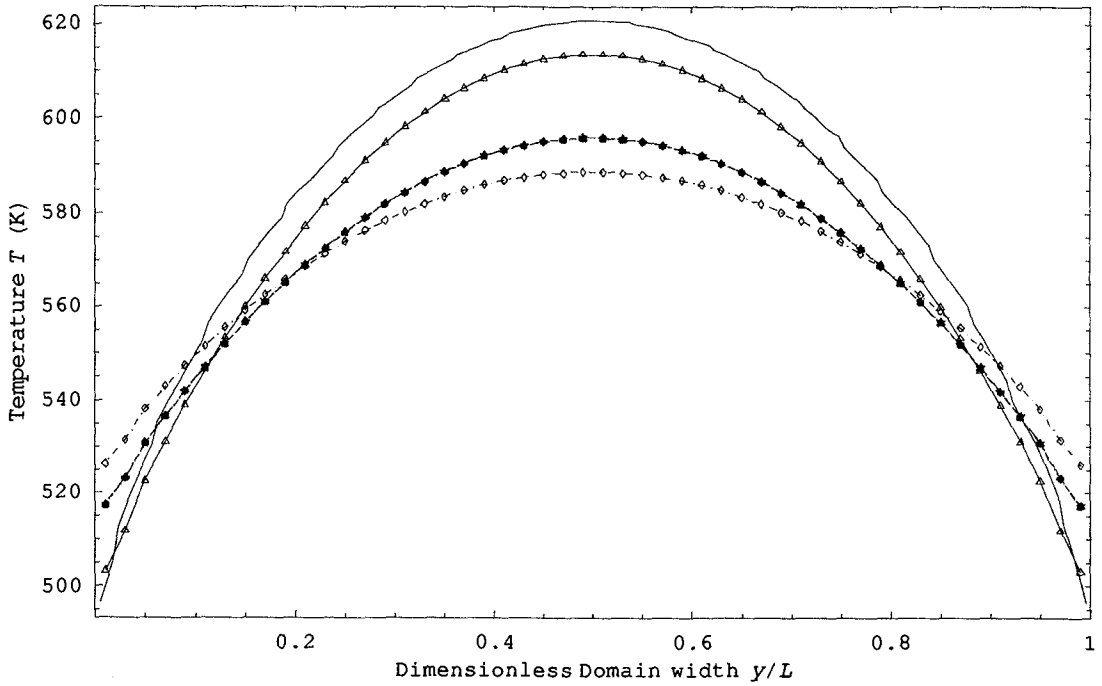

(c)

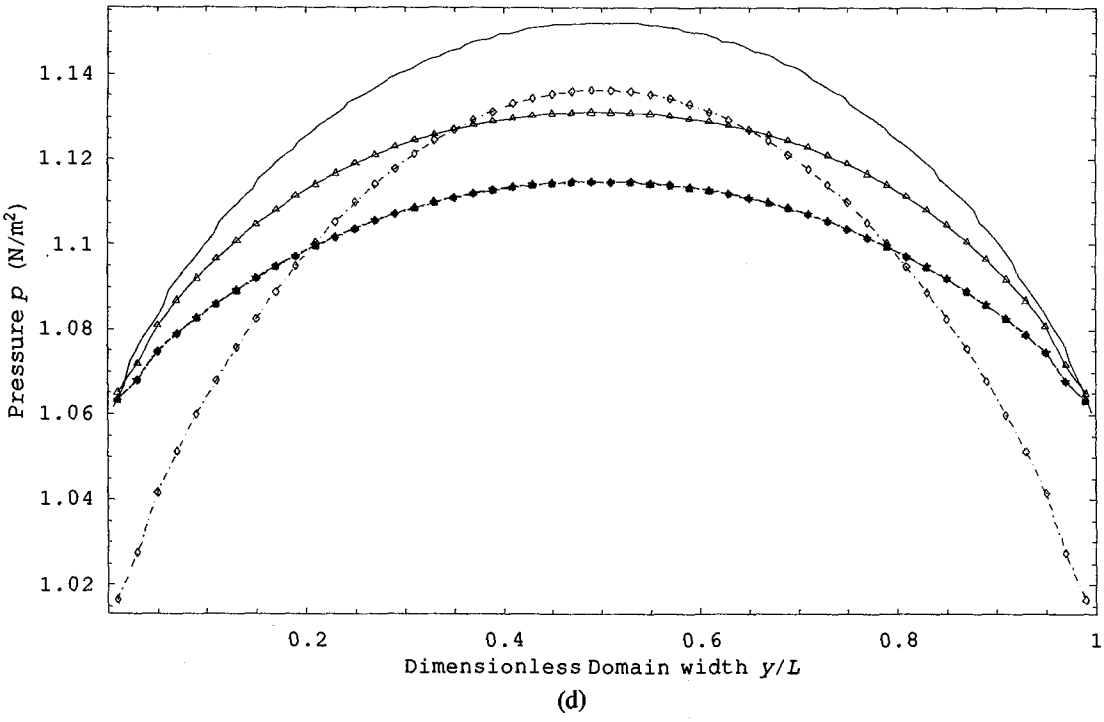

(d)

Figure 4.7: Comparison of kinetic models with DSMC (case 4.12: Kn=0.5, Maxwell molecules, 1000.0 m/s plate velocity)) (Line without symbols for DSMC, Triangle for BGK, Triangle filled for ES-BGK, Diamond for $\nu(C)$-BGK, Diamond filled for new kinetic model I, Star for new kinetic model II)

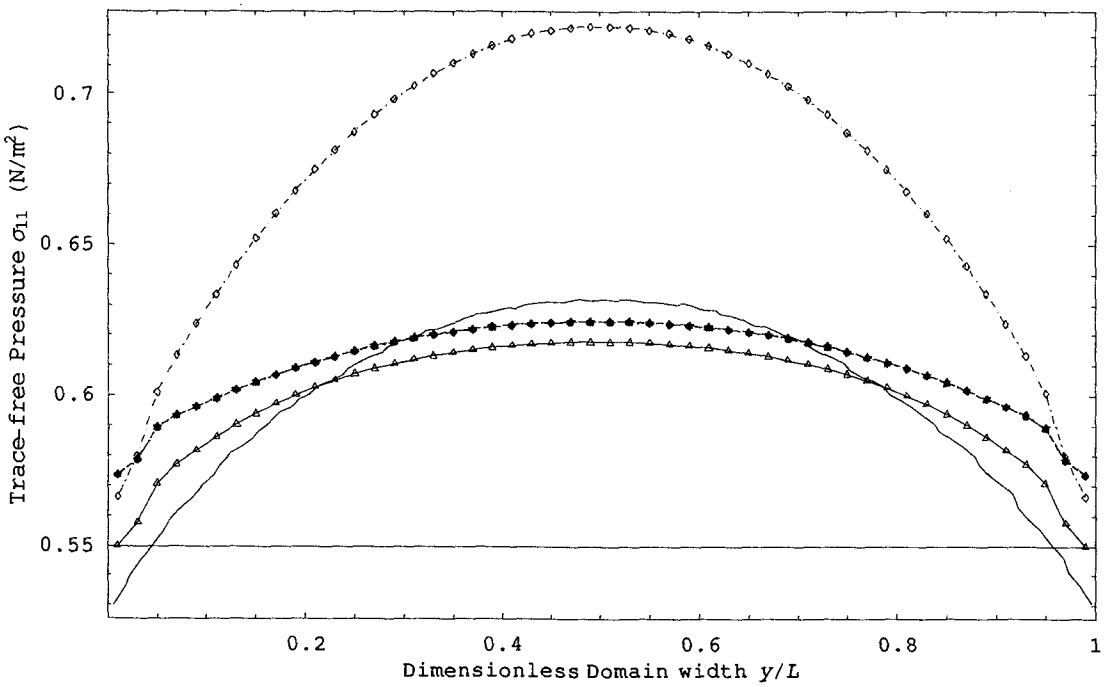

(e)

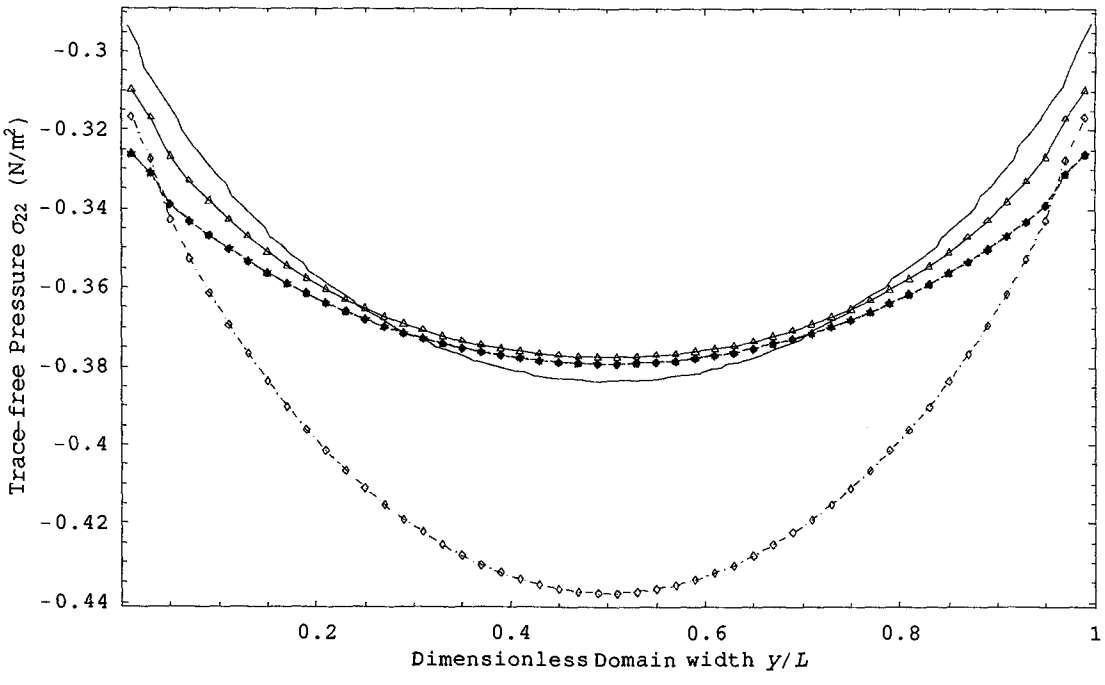

(f)

Figure 4.7: Comparison of kinetic models with DSMC (case 4.12: Kn=0.5, Maxwell molecules, 1000.0 m/s plate velocity)) (Line without symbols for DSMC, Triangle for BGK, Triangle filled for ES-BGK, Diamond for $\nu(C)$-BGK, Diamond filled for new kinetic model I, Star for new kinetic model II)

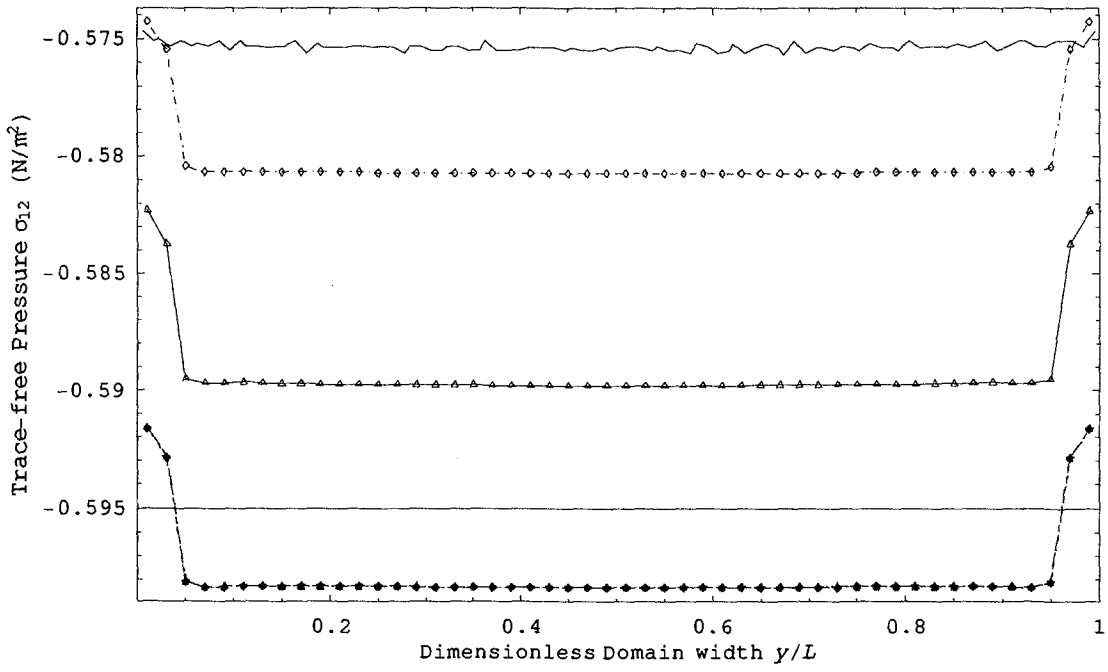

(g)

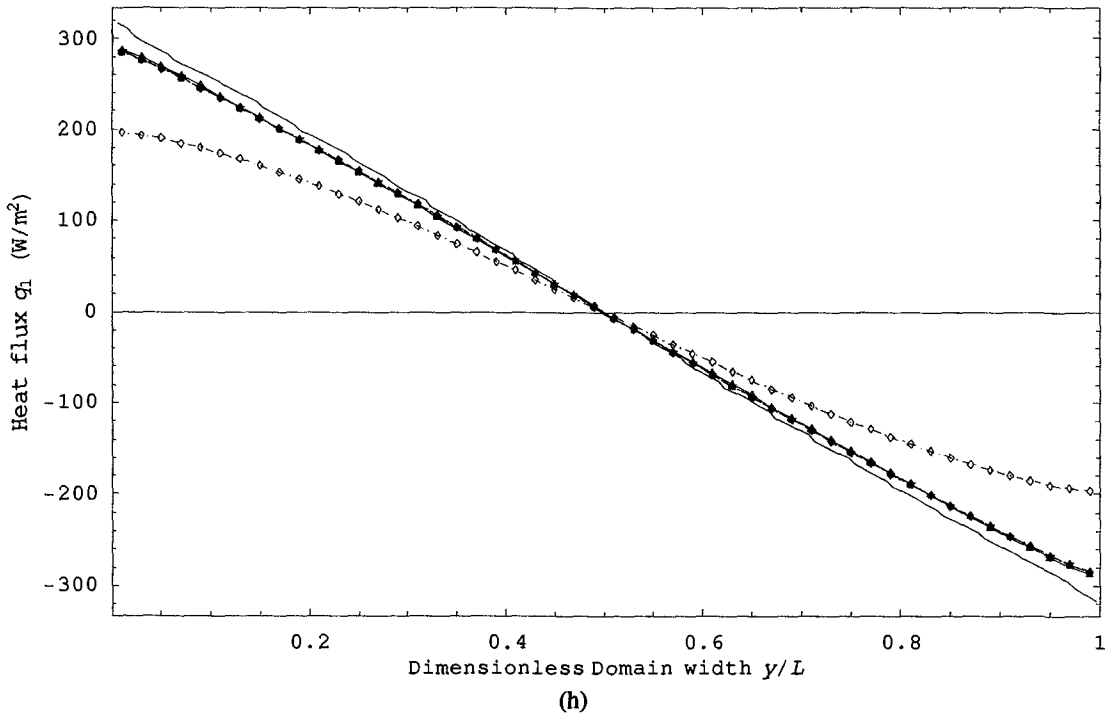

(h)

Figure 4.7: Comparison of kinetic models with DSMC (case 4.12: Kn=0.5, Maxwell molecules, 1000.0 m/s plate velocity)) (Line without symbols for DSMC, Triangle for BGK, Triangle filled for ES-BGK, Diamond for $\nu(C)$-BGK, Diamond filled for new kinetic model I, Star for new kinetic model II)

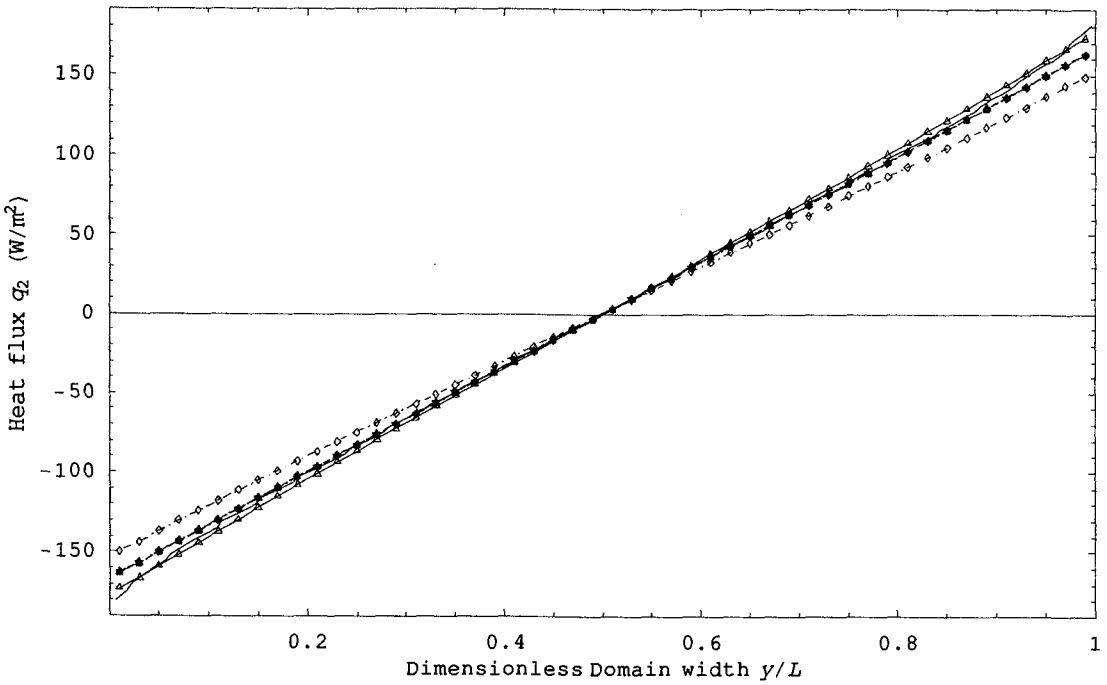

(i)

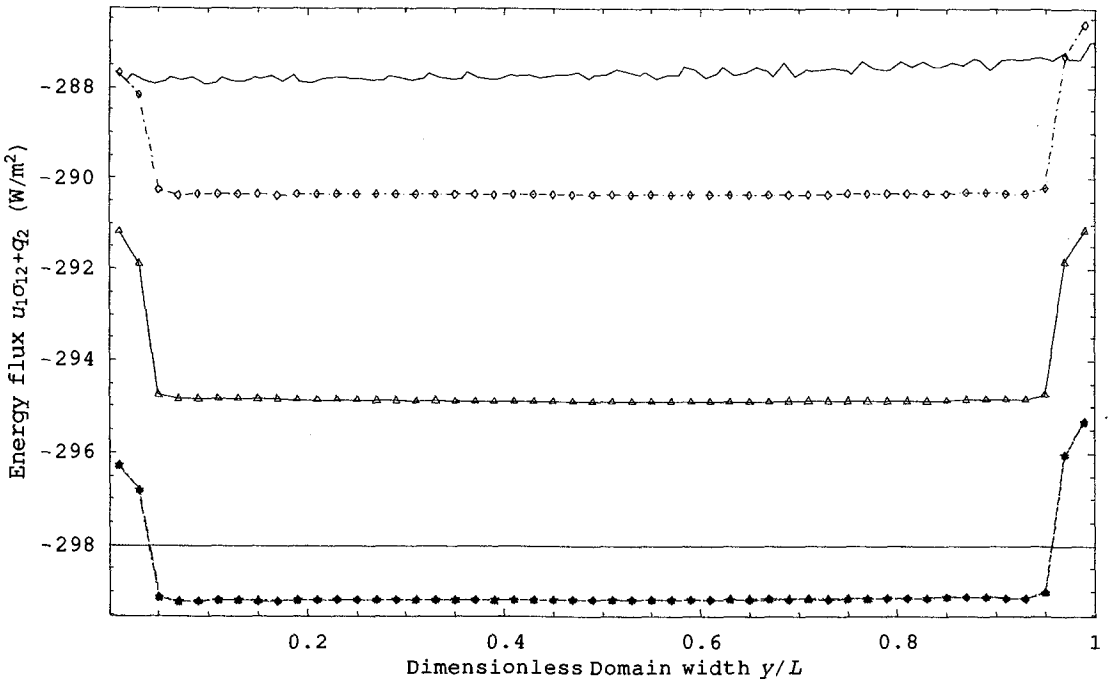

(j)

Figure 4.7: Comparison of kinetic models with DSMC (case 4.12: Kn=0.5, Maxwell molecules, 1000.0 m/s plate velocity)) (Line without symbols for DSMC, Triangle for BGK, Triangle filled for ES-BGK, Diamond for $\nu(C)$-BGK, Diamond filled for new kinetic model I, Star for new kinetic model II)

4.5 Conclusion

For the one-dimensional Couette flow problem, the following conclusion can be drawn from the above discussion.

When the computational time of each iteration is considered, the new kinetic model I needs the longest time, followed by the new kinetic model II, the $\nu(C)$-BGK model, the ES-BGK model and the BGK model. The time ratio of the new kinetic model I to the ES-BGK model to the BGK model is about 3:2:1.

When comparison with DSMC is considered, the $\nu(C)$-BGK is the worst, followed by the two new kinetic models. The ES-BGK model is better than the BGK model for small Knudsen number situations ($\mathrm{Kn} \leq 0.1$), while it is hard to say which one of the ES-BGK and the BGK is better for large Knudsen number situations.

Using linearized f_{ref} instead of original f_{ref} in program works well and gives almost identical results with shorter computational time (20-40% saved) for almost all test situations. The exception is the first type of linearized f_{ref} for the new kinetic model I with hard sphere molecules, which becomes unstable.

The second type of linearized f_{ref} is much better than the first type of linearized f_{ref} for the ES-BGK model, and the new kinetic models I and II.

As long as the size of finite volume cell is small enough (such as smaller than one half of the mean free path), making it smaller does not change the results too much, but makes the computational time for each iteration larger and requires more iterations (for smaller time step) to reach converged results. Therefore, one suggestion is to not use a very large number of cells.

Equation (3.37) determines the bounds of velocity grid with sufficient accuracy. Considering the computational time of each iteration and the value of time step, very large values of bounds of velocity grid are not suggested.

Based on Eq. (3.37) to determine of step of velocity grid is acceptable enough for consideration of density, velocity, temperature and pressure, while not enough when trace-free pressure and heat flux are considered. Some ways to decrease computational time, such as implicit numerical scheme, a proper criterion to check the convergence, parallel computing, and so on, are suggested to be applied before computation with high number of discrete velocities is done.

Chapter 5 Comparison of NSF, Burnett, Grad 13 and R13s equations to kinetic models

5.1 Introduction

From Chapters 3 and 4, one can see that when a kinetic model is used to compute a flow problem, the number of dimension of the variables (distribution function) in the program are at least five, three for velocity space, one for time step and one for position at one direction. There will be three indices for position nodes in a three-dimensional problem. Moreover, due to discretization, the actual number of is huge, e.g. $12\times11\times11\times2=2904$ variables for each position node in the case 3.1 in Table 3.1. This requires the memory of computer to be very large for the computation of kinetic models, and the computational time will be very long.

Compared with computation of kinetic models, in the program of computation of macroscopic continuum theory, the dimension of one variable will be at most four (max three for position nodes, and one for time step), and the number of variables for each position node, which is the number of moments considered, is not large, e.g. five variables are considered in the NSF and Burnett equations, and 13 variables are considered in the Grad 13 equations, and their regularization (R13).

Therefore, a macroscopic continuum theory is preferred to be applied to solve rarefied gas flow problems, instead of microscopic theory (such as DSMC, kinetic models), in order to save computational time and simplify the computational program. In the scope of macroscopic continuum theory of rarefied gas dynamics, there are the NSF equations, the Burnett equations from the C-E expansion method [11], while also there are the Grad13, the R13s (original and slightly linearized) from the moment method or related methods [15, 26]. It must be asked which set of macroscopic equations (NSF, Burnett, Grad13, or R13s) can give a good description of the flow, e.g. in relation to range of Knudsen number. To contribute to the answer on this question is the goal of this part of the work. In this chapter, the above sets of macroscopic equations from kinetic models will be compared with the kinetic models themselves. The kinetic models considered are the

BGK model and the ES-BGK model. Since the only difference between results for the BGK model and results for the ES-BGK model is that the Prandtl number $\Pr = \frac{1}{1-b}$, and $b=0$ for the BGK model, and $[-0.5,1.0]$ as the range of b for the ES-BGK model, therefore in the following description, we will focus on the ES-BGK model, and deal with the BGK model is a specific case for the ES-BGK model.

5.2 NSF and Burnett equations for BGK and ES-BGK models

5.2.1 NSF and Burnett equations in three dimensions[18]

The aim of the C-E method [3, 5, 9] is to obtain expressions for σ_{ij} and q_i from kinetic theory. The distribution function f in the form of an expansion in powers of the small parameter Kn (Eq. (1.6)) is looked for in the C-E method. In this method, a factor $1/\mathrm{Kn}$ is inserted in front of the collision term, that is to say, the ES-BGK model to be considered is

$$\frac{\partial f}{\partial t} + c_i \frac{\partial f}{\partial x_i} = \frac{1}{\mathrm{Kn}} \nu_{ES} (f_{ES} - f) \tag{5.1}$$

where the reference distribution f_{ES} is defined in Eq. (2.3). Substituting the expression of f in Eq. (1.6), rewrite as follows

$$f = \sum_{n=0}^{\infty} \mathrm{Kn}^n f^{(n)},$$

into Eq. (5.1), and equating the coefficients of the same power of Kn yields a set of equations for $f^{(n)}$. By solving this set of equations, an asymptotic solution of the distribution function f is obtained (note that Kn=1 is set in the ultimate expression).

According to the above ordering hypothesis, the trace-free pressure tensor σ_{ij} and heat flux q_i can also be written as a series

[18] This section and Section 5.2.2 are the main part of the paper "Burnett equations for the ellipsoidal statistical BGK model", by Zheng and Struchtrup [11]

$$\sigma_{ij} = \sum_{n=0}^{\infty} \mathrm{Kn}^n \sigma_{ij}^{(n)} = \sum_{n=0}^{\infty} \mathrm{Kn}^n \cdot \int C_{<i} C_{j>} f^{(n)} d\mathbf{c}, \tag{5.2}$$

$$q_i = \sum_{n=0}^{\infty} \mathrm{Kn}^n q_i^{(n)} = \sum_{n=0}^{\infty} \mathrm{Kn}^n \cdot \frac{1}{2} \int C^2 C_i f^{(n)} d\mathbf{c} \ .$$

The conserved quantities ρ, u_i, T, however, are not expanded. That is in the C-E expansion one assumes that each order of the expansion gives ρ, u_i, T, which is tantamount to

$$\{\rho, \ \rho u_i, \ 3p\} = \int \{1, \ c_i, \ C^2\} f d\mathbf{c} = \int \{1, \ c_i, \ C^2\} f^{(0)} d\mathbf{c} \ ,$$

and imples the so-called compatibility conditions

$$\int \{1, \ c_i, \ C^2\} f^{(n)} d\mathbf{c} = \{0, \ 0, \ 0\} \quad \text{for all } n \geq 1. \tag{5.3}$$

Note that, because of $p_{ij} = p\delta_{ij} + \sigma_{ij}$, it follows that $p_{ij}^{(n)} = \sigma_{ij}^{(n)}$ for all $n \geq 1$.

Since the reference distribution function f_{ES} is expressed in terms of the pressure tensor in the ES-BGK model, f_{ES} must also be expressed in the form of powers of Kn in the expansion

$$f_{ES} = \sum_{n=0}^{\infty} \mathrm{Kn}^n f_{ES}^{(n)} \ . \tag{5.4}$$

This expression for $f_{ES}^{(n)}$ will be derived later in this section.

Similar to the distribution function, time derivatives of density ρ, macroscopic flow velocity u_i and temperature T are likewise expressed as a series of operators,

$$\frac{\partial U_r}{\partial t} = \sum_{n=0}^{\infty} \mathrm{Kn}^n \frac{\partial_n U_r}{\partial t} \ , \tag{5.5}$$

where $U_r = \rho, u_i, T$, (r=1…5). Put Eqs. (5.2, 5.5) into the conservation law Eq. (1.5), and equating the coefficients of the same power of Kn yields the following expressions.

$$\frac{\partial_0 \rho}{\partial t} = -\frac{\partial \rho u_i}{\partial x_i}\ ,\quad \frac{\partial_m \rho}{\partial t} = 0\ ,$$

$$\frac{\partial_0 u_i}{\partial t} = -u_j \frac{\partial u_i}{\partial x_j} - \frac{1}{\rho}\frac{\partial p\delta_{ij} + \sigma_{ij}^{(0)}}{\partial x_j}\ ,\quad \frac{\partial_m u_i}{\partial t} = -\frac{1}{\rho}\frac{\partial \sigma_{ij}^{(m)}}{\partial x_j}\ , \tag{5.6}$$

$$\frac{\partial_0 T}{\partial t} = -u_i \frac{\partial T}{\partial x_i} - \frac{2}{3\rho R}\left(\frac{\partial q_i^{(0)}}{\partial x_i} + \left(p\delta_{ij} + \sigma_{ij}^{(0)}\right)\frac{\partial u_i}{\partial x_j}\right),\quad \frac{\partial_m T}{\partial t} = -\frac{2}{3\rho R}\left(\frac{\partial q_i^{(m)}}{\partial x_i} + \sigma_{ij}^{(m)}\frac{\partial u_i}{\partial x_j}\right),$$

where $m \geq 1$.

The next assumption of the C-E method is that the distribution function f depends on position x_i and time t only through the hydrodynamic variables U_r (= ρ, u_i, T, (r=1...5))and their space derivatives. That is to say, $f^{(n)} = f^{(n)}\left(U_r, \nabla U_r, ..., \nabla^n U_r; c_i\right)$, but $f^{(n)}$ is not a function of $\nabla^{n+k} U_r$ with $k \geq 1$.

At last, based on the above line of arguments, the sequence of equations for $f^{(n)}$ can be written as

$$\sum_{n=0}^{\infty} \mathrm{Kn}^n \left(\frac{\partial_n f}{\partial t} + c_i \frac{\partial f^{(n)}}{\partial x_i}\right) = \sum_{n=0}^{\infty} \nu_{\mathrm{ES}} \mathrm{Kn}^{n-1}\left(f_{ES}^{(n)} - f^{(n)}\right), \tag{5.7}$$

where

$$\frac{\partial_n f}{\partial t} = \sum_{\substack{m+k=n \\ m,k\geq 0}} \left(\frac{\partial f^{(m)}}{\partial U_r}\cdot\frac{\partial_k U_r}{\partial t} + \frac{\partial f^{(m)}}{\partial(\nabla U_r)}\cdot\frac{\partial_k(\nabla U_r)}{\partial t} + ... + \frac{\partial f^{(m)}}{\partial(\nabla^m U_r)}\cdot\frac{\partial_k(\nabla^m U_r)}{\partial t}\right),$$

$$\frac{\partial f^{(n)}}{\partial x_i} = \frac{\partial f^{(n)}}{\partial U_r}\cdot\frac{\partial U_r}{\partial x_i} + \frac{\partial f^{(n)}}{\partial(\nabla U_r)}\cdot\frac{\partial(\nabla U_r)}{\partial x_i} + ... + \frac{\partial f^{(n)}}{\partial(\nabla^n U_r)}\cdot\frac{\partial(\nabla^n U_r)}{\partial x_i}\ ,$$

with

$\frac{\partial_k\left(\nabla^m U_r\right)}{\partial t}=\nabla^m\left(\frac{\partial_k U_r}{\partial t}\right)$, since the position x_i and time t are independent to each other.

In order to obtain the expression for $f^{(2)}$ and the Burnett equations, we need to know $f_{ES}^{(n)}$ up to the second order of Kn. From the definition of the matrix λ_{ij} in Eq. (2.10) one obtains

$$\lambda_{ij}=RT\delta_{ij}+\frac{b}{\rho}\sigma_{ij}^{(1)}\mathrm{Kn}+\frac{b}{\rho}\sigma_{ij}^{(2)}\mathrm{Kn}^2+O\left(\mathrm{Kn}^3\right),$$

$$|\lambda|=(RT)^3\left(1-\left(\frac{b}{p}\right)^2\frac{\sigma_{kn}^{(1)}\sigma_{kn}^{(1)}}{2}\mathrm{Kn}^2\right)+O\left(\mathrm{Kn}^3\right), \tag{5.8}$$

$$\varepsilon_{ij}=\lambda_{ij}^{-1}=\frac{\delta_{ij}}{RT}-\frac{b}{pRT}\sigma_{ij}^{(1)}\mathrm{Kn}+\frac{b}{pRT}\left(\frac{b}{p}\sigma_{ik}^{(1)}\sigma_{kj}^{(1)}-\sigma_{ij}^{(2)}\right)\mathrm{Kn}^2+O\left(\mathrm{Kn}^3\right).$$

It follows for the expansion of the Gaussian

$$f_{ES}=f_{ES}^{(0)}+f_{ES}^{(1)}\mathrm{Kn}+f_{ES}^{(2)}\mathrm{Kn}^2+O\left(\mathrm{Kn}^3\right), \tag{5.9}$$

where

$$f_{ES}^{(0)}=f_M=\rho\left(\frac{1}{2\pi RT}\right)^{3/2}\exp\left(-\frac{C^2}{2RT}\right),$$

$$f_{ES}^{(1)}=f_M\left(\frac{b}{2pRT}\sigma_{ij}^{(1)}C_iC_j\right), \tag{5.10}$$

$$f_{ES}^{(2)}=f_M\left(\frac{b}{2p}\right)\left[\frac{b}{2p}\sigma_{kn}^{(1)}\sigma_{kn}^{(1)}-\frac{1}{RT}\left(\frac{b}{p}\sigma_{ik}^{(1)}\sigma_{kj}^{(2)}-\sigma_{ij}^{(2)}\right)C_iC_j+\frac{b}{4p(RT)^2}\sigma_{ij}^{(1)}\sigma_{kl}^{(1)}C_iC_jC_kC_l\right].$$

Here we have anticipated that $\sigma_{ij}^{(0)}=0$, as will be shown below. f_M is the local Maxwellian distribution.

First, let us consider the order of $O(1/\mathrm{Kn})$ in Eq. (5.7), which yields the constitutive relations for the Euler equations,

$$f^{(0)} = f_{ES}^{(0)} = f_M \ , \tag{5.11}$$

$$p_{ij}^{(0)} = p\delta_{ij} \ , \ \sigma_{ij}^{(0)} = 0 \ , \ q_i^{(0)} = 0 \ . \tag{5.12}$$

Next, we consider the order $O(\mathrm{Kn}^0)$ in Eq. (5.7), which yields

$$f^{(1)} = f_{ES}^{(1)} - \frac{1}{\nu_{ES}}\left(\frac{\partial_0 f}{\partial t} + c_i \frac{\partial f^{(0)}}{\partial x_i}\right) ,$$

where

$$\frac{\partial_0 f}{\partial t} = \frac{\partial f^{(0)}}{\partial U_r}\cdot\frac{\partial_0 U_r}{\partial t} = \frac{\partial f^{(0)}}{\partial \rho}\cdot\frac{\partial_0 \rho}{\partial t} + \frac{\partial f^{(0)}}{\partial u_i}\cdot\frac{\partial_0 u_i}{\partial t} + \frac{\partial f^{(0)}}{\partial T}\cdot\frac{\partial_0 T}{\partial t} \ ,$$

$$\frac{\partial f^{(0)}}{\partial x_i} = \frac{\partial f^{(0)}}{\partial U_r}\cdot\frac{\partial U_r}{\partial x_i} = \frac{\partial f^{(0)}}{\partial \rho}\cdot\frac{\partial \rho}{\partial x_i} + \frac{\partial f^{(0)}}{\partial u_j}\cdot\frac{\partial u_j}{\partial x_i} + \frac{\partial f^{(0)}}{\partial T}\cdot\frac{\partial T}{\partial x_i} \ .$$

After some manipulation, one obtains

$$f^{(1)} = f_M \frac{b}{2pRT}\sigma_{ij}^{(1)} C_i C_j - \frac{f_M}{\nu_{ES}}\left(\frac{C_i C_j}{RT}\cdot\frac{\partial u_{<i}}{\partial x_{j>}} + \frac{C_i}{T}\frac{\partial T}{\partial x_i}\left(\frac{C^2}{2RT} - \frac{5}{2}\right)\right) , \tag{5.13}$$

$$\sigma_{ij}^{(1)} = -2\mu\frac{\partial u_{<i}}{\partial x_{j>}} = -\frac{2}{1-b}\frac{p}{\nu_{ES}}\frac{\partial u_{<i}}{\partial x_{j>}} \quad , \quad q_i^{(1)} = -\kappa\frac{\partial T}{\partial x_i} = -\frac{5}{2}\frac{Rp}{\nu_{ES}}\frac{\partial T}{\partial x_i} \ . \tag{5.14}$$

The constitutive relations in Eq. (5.14) are the laws of Navier-Stokes and Fourier where $\mu = \frac{1}{1-b}\frac{p}{\nu_{ES}}$ is the viscosity, and $\kappa = \frac{5}{2}\frac{Rp}{\nu_{ES}}$ is the thermal conductivity. It follows that the Prandtl number is related to the coefficient b of the ES-BGK model by the relation

$$\mathrm{Pr} = \frac{5R\mu}{2\kappa} = \frac{1}{1-b} . \tag{5.15}$$

By means of the Navier-Stokes and Fourier laws Eq. (5.14), the distribution can be rewritten in a form that is familar from the Chapman-Enskog expansion of the Boltzmann equation of Maxwell molecules, viz.

$$f^{(1)} = -f_M \left(\frac{C_i C_j}{RT} \frac{\mu}{p} \frac{\partial u_{<i}}{\partial x_{j>}} + \left(\frac{C^2}{2RT} - \frac{5}{2} \right) C_i \frac{2}{5} \frac{\kappa}{pRT} \frac{\partial T}{\partial x_i} \right) . \tag{5.16}$$

It is straightforward to show that this expression indeed satisfies the compatibility relations (5.3). The relations between viscosities and collision frequency in Eq. (5.14) and Eq. (2.32) can be used to obtain an explicit relation between the latter and the variables ρ, T which reads

$$\nu_{ES} = \frac{1}{1-b} \frac{p}{\mu} = \nu_{ES0} \rho T^{1-\omega} , \tag{5.17}$$

where $\nu_{ES0} = \dfrac{RT_0^{\omega}}{(1-b)\mu_0}$ is a constant.

At last, let us consider the order $O(\mathrm{Kn})$ in Eq. (5.7), which yields

$$f^{(2)} = f_{ES}^{(2)} - \frac{1}{\nu_{ES}} \left(\frac{\partial_1 f}{\partial t} + c_i \frac{\partial f^{(1)}}{\partial x_i} \right) ,$$

where

$$\frac{\partial_1 f}{\partial t} = \frac{\partial f^{(0)}}{\partial U_r} \cdot \frac{\partial_1 U_r}{\partial t} + \frac{\partial f^{(1)}}{\partial U_r} \cdot \frac{\partial_0 U_r}{\partial t} + \frac{\partial f^{(1)}}{\partial (\nabla U_r)} \cdot \frac{\partial_0 (\nabla U_r)}{\partial t} ,$$

$$\frac{\partial f^{(1)}}{\partial x_i} = \frac{\partial f^{(1)}}{\partial U_r} \cdot \frac{\partial U_r}{\partial x_i} + \frac{\partial f^{(1)}}{\partial (\nabla U_r)} \cdot \frac{\partial (\nabla U_r)}{\partial x_i} .$$

After a tedious manipulation, the expression of $f^{(2)}$ is obtained as

$$f^{(2)} = f_{ES}^{(2)} + \frac{f_M}{\nu_{ES}^2} \Theta , \tag{5.18}$$

where

$$\Theta = -\frac{C_iC_j}{(1-b)\rho}\frac{\partial^2\rho}{\partial x_{\langle i}\partial x_{j\rangle}} + \frac{4-5b}{3(1-b)}C_i\frac{\partial^2 u_j}{\partial x_i\partial x_j} - \frac{C_i}{1-b}\frac{\partial^2 u_i}{\partial x_j\partial x_j} + \frac{C_iC_jC_k}{RT(1-b)}\frac{\partial^2 u_k}{\partial x_i\partial x_j}$$
$$-\frac{2-b}{3(1-b)}\frac{C_iC^2}{RT}\frac{\partial^2 u_j}{\partial x_i\partial x_j} + \frac{5R}{2}\frac{\partial^2 T}{\partial x_i\partial x_i} - \frac{7-5b}{2(1-b)}\frac{C_iC_j}{T}\frac{\partial^2 T}{\partial x_i\partial x_j} - \frac{3-5b}{6(1-b)}\frac{C^2}{T}\frac{\partial^2 T}{\partial x_i\partial x_i}$$
$$+\frac{C_iC_jC^2}{2RT^2}\frac{\partial^2 T}{\partial x_i\partial x_j} + \frac{C_{\langle i}C_{j\rangle}}{(1-b)\rho^2}\frac{\partial\rho}{\partial x_i}\frac{\partial\rho}{\partial x_j} + \frac{2C_j}{(1-b)\rho}\frac{\partial u_{\langle i}}{\partial x_{j\rangle}}\frac{\partial\rho}{\partial x_i} - \frac{C_iC_jC_k}{(1-b)\rho RT}\frac{\partial u_{\langle i}}{\partial x_{j\rangle}}\frac{\partial\rho}{\partial x_k}$$
$$-\frac{5R}{2\rho}\frac{\partial T}{\partial x_i}\frac{\partial\rho}{\partial x_i} + \frac{5-7b}{2(1-b)}\frac{C_iC_j}{\rho T}\frac{\partial T}{\partial x_i}\frac{\partial\rho}{\partial x_j} + \frac{5-3b}{6(1-b)}\frac{C^2}{\rho T}\frac{\partial T}{\partial x_i}\frac{\partial\rho}{\partial x_i} - \frac{C_iC_jC^2}{2\rho RT^2}\frac{\partial T}{\partial x_i}\frac{\partial\rho}{\partial x_j}$$
$$+\frac{2}{1-b}\frac{\partial u_{\langle i}}{\partial x_{j\rangle}}\frac{\partial u_i}{\partial x_j} + \frac{2(3.5-\omega)}{3(1-b)}\frac{C_kC_j}{RT}\frac{\partial u_{\langle k}}{\partial x_{j\rangle}}\frac{\partial u_i}{\partial x_i} - \frac{C_{\langle i}C_{j\rangle}}{(1-b)RT}\frac{\partial u_k}{\partial x_j}\frac{\partial u_i}{\partial x_k} - \frac{2C_iC_j}{(1-b)RT}\frac{\partial u_{\langle k}}{\partial x_{j\rangle}}\frac{\partial u_k}{\partial x_i}$$
$$-\frac{2}{3(1-b)}\frac{C^2}{RT}\frac{\partial u_{\langle i}}{\partial x_{j\rangle}}\frac{\partial u_i}{\partial x_j} + \frac{C_iC_jC_kC_l}{(1-b)R^2T^2}\frac{\partial u_{\langle k}}{\partial x_{l\rangle}}\frac{\partial u_{\langle i}}{\partial x_{j\rangle}} + \frac{1-\omega}{1-b}\frac{C_i}{T}\frac{\partial T}{\partial x_j}\frac{\partial u_i}{\partial x_j}$$
$$+\left(5+\frac{1-\omega}{1-b}\right)\frac{C_i}{T}\frac{\partial T}{\partial x_j}\frac{\partial u_j}{\partial x_i} - \frac{(15-15b)+(14-10b)(1-\omega)}{6(1-b)}\frac{C_i}{T}\frac{\partial T}{\partial x_i}\frac{\partial u_j}{\partial x_j}$$
$$-\frac{(14-7b)+2(1-\omega)}{2(1-b)}\frac{C_iC_jC_k}{RT^2}\frac{\partial T}{\partial x_i}\frac{\partial u_k}{\partial x_j} + \frac{(8.5-5b)+(2-b)(1-\omega)}{3(1-b)}\frac{C_iC^2}{RT^2}\frac{\partial T}{\partial x_i}\frac{\partial u_j}{\partial x_j}$$
$$-\frac{C_iC^2}{RT^2}\frac{\partial T}{\partial x_j}\frac{\partial u_j}{\partial x_i} + \frac{2-b}{2(1-b)}\frac{C_iC_jC_kC^2}{R^2T^3}\frac{\partial T}{\partial x_k}\frac{\partial u_{\langle i}}{\partial x_{j\rangle}} - \frac{5(1-\omega)}{2}\frac{R}{T}\frac{\partial T}{\partial x_i}\frac{\partial T}{\partial x_i}$$
$$+\left(\frac{39}{4}+\frac{5}{2}(1-\omega)\right)\frac{C_iC_j}{T^2}\frac{\partial T}{\partial x_i}\frac{\partial T}{\partial x_j} - \left(\frac{1}{3}-\frac{5}{6}(1-\omega)\right)\frac{C^2}{T^2}\frac{\partial T}{\partial x_i}\frac{\partial T}{\partial x_i} - \frac{8-\omega}{2}\frac{C_iC_jC^2}{RT^3}\frac{\partial T}{\partial x_i}\frac{\partial T}{\partial x_j}$$
$$+\frac{C_iC_jC^4}{4R^2T^4}\frac{\partial T}{\partial x_i}\frac{\partial T}{\partial x_j}\,.$$

It is straightforward, but cumbersome, to show that this expression indeed satisfies the compatibility conditions (5.3).

Pressure tensor and heat flux at the second order, the Burnett order, are computed as

$$p_{ij}^{(2)} = \sigma_{ij}^{(2)} = \frac{1}{(1-b)^2\nu_G^2}\cdot\Phi_{ij} \quad , \quad q_i^{(2)} = \frac{1}{(1-b)\nu_G^2}\cdot\Gamma_i \,, \tag{5.19}$$

where

$$\Phi_{ij} = -2R^2T^2\frac{\partial^2\rho}{\partial x_{\langle i}\partial x_{j\rangle}} - 2b\rho R^2T\frac{\partial^2 T}{\partial x_{\langle i}\partial x_{j\rangle}} + \frac{2R^2T^2}{\rho}\frac{\partial\rho}{\partial x_{\langle i}}\frac{\partial\rho}{\partial x_{j\rangle}} - 2R^2T\frac{\partial T}{\partial x_{\langle i}}\frac{\partial\rho}{\partial x_{j\rangle}}$$
$$+2p\frac{\partial u_{\langle i}}{\partial x_k}\frac{\partial u_{j\rangle}}{\partial x_k} + \frac{2-4\omega}{3}p\frac{\partial u_{\langle i}}{\partial x_{j\rangle}}\frac{\partial u_k}{\partial x_k} + 2\omega(1-b)\rho R^2\frac{\partial T}{\partial x_{\langle i}}\frac{\partial T}{\partial x_{j\rangle}} \,,$$

$$\Gamma_i = \frac{5b-4}{3} pRT \frac{\partial^2 u_j}{\partial x_i \partial x_j} + pRT \frac{\partial^2 u_i}{\partial x_j \partial x_j} - 2R^2T^2 \frac{\partial u_{<j}}{\partial x_{i>}} \frac{\partial \rho}{\partial x_j} + \left(6+\omega-\frac{7}{2}b\right) pR \frac{\partial u_i}{\partial x_j} \frac{\partial T}{\partial x_j}$$
$$+\left(1+\omega+\frac{3}{2}b\right) pR \frac{\partial u_j}{\partial x_i} \frac{\partial T}{\partial x_j} + \frac{(-13-b)+(14-10b)(1-\omega)}{6} pR \frac{\partial u_j}{\partial x_j} \frac{\partial T}{\partial x_i} \quad . \tag{5.20}$$

The above expressions for $\sigma_{ij}^{(2)}$ and $q_i^{(2)}$ are irreducible forms in terms of the gradients of density, velocity, and temperature.

For the special choice $b = 0$, the ES-BGK model reduces to the standard BGK model, and the corresponding Burnett expressions for $\sigma_{ij}^{(2)}$ and $q_i^{(2)}$ read

$$\sigma_{ij}^{(2)} = \frac{\mu^2}{p^2} \Phi_{BGK,ij} \quad , \quad q_i^{(2)} = \frac{\mu^2}{p^2} \cdot \Gamma_{BGK,i} \quad , \tag{5.21}$$

where

$$\Phi_{BGK,ij} = -2R^2T^2 \frac{\partial^2 \rho}{\partial x_{<i} \partial x_{j>}} + \frac{2R^2T^2}{\rho} \frac{\partial \rho}{\partial x_{<i}} \frac{\partial \rho}{\partial x_{j>}} - 2R^2T \frac{\partial T}{\partial x_{<i}} \frac{\partial \rho}{\partial x_{j>}} + 2p \frac{\partial u_{<i}}{\partial x_k} \frac{\partial u_{j>}}{\partial x_k}$$
$$+\frac{2-4\omega}{3} p \frac{\partial u_{<i}}{\partial x_{j>}} \frac{\partial u_k}{\partial x_k} + 2\omega\rho R^2 \frac{\partial T}{\partial x_{<i}} \frac{\partial T}{\partial x_{j>}} \quad ,$$

$$\Gamma_{BGK,i} = -\frac{4}{3} pRT \frac{\partial^2 u_j}{\partial x_i \partial x_j} + pRT \frac{\partial^2 u_i}{\partial x_j \partial x_j} - 2R^2T^2 \frac{\partial u_{<j}}{\partial x_{i>}} \frac{\partial \rho}{\partial x_j} + (6+\omega) pR \frac{\partial u_i}{\partial x_j} \frac{\partial T}{\partial x_j}$$
$$+(1+\omega) pR \frac{\partial u_j}{\partial x_i} \frac{\partial T}{\partial x_j} + \frac{1-14\omega}{6} pR \frac{\partial u_j}{\partial x_j} \frac{\partial T}{\partial x_i} \quad . \tag{5.22}$$

The Burnett equations for the BGK model are available in the literature, see [72-74]. In [72, 73], only hard sphere molecules ($\omega = 1/2$) were considered, and our results agree with those in [72, 73], when we set $\omega = 1/2$. The Burnett BGK equations reported in [74] are questionable: For example, since $\sigma_{ij}^{(2)}$ is a trace-free tensor, one finds that $\alpha_7/\alpha_8 = -2$ should hold in Eq. (11) of [74], but the authors report $\alpha_7/\alpha_8 = 3.5$ instead. Similar problems arise with other coefficients. Thus, it seems that the equations in [74] are not correct.

In order to compare the Burnett equations for the ES-BGK model with the Burnett equations for the Boltzmann equation, e.g. see [12, 13, 24], we rewrite Eqs. (5.19-5.20) as

$$\sigma_{ij}^{(2)} = \varpi_1 \frac{\mu^2}{p}\frac{\partial u_k}{\partial x_k}\frac{\partial u_{<i}}{\partial x_{j>}} + \varpi_2 \frac{\mu^2}{p}\left(-\frac{\partial}{\partial x_{<i}}\left(\frac{1}{\rho}\frac{\partial p}{\partial x_{j>}}\right) - \frac{\partial u_k}{\partial x_{<i}}\frac{\partial u_{j>}}{\partial x_k} - 2\frac{\partial u_k}{\partial x_{<j}}\frac{\partial u_{<i>}}{\partial x_{k>}}\right)$$
$$+ \varpi_3 \frac{\mu^2}{\rho T}\frac{\partial^2 T}{\partial x_{<i}\partial x_{j>}} + \varpi_4 \frac{\mu^2}{\rho p T}\frac{\partial T}{\partial x_{<i}}\frac{\partial p}{\partial x_{j>}} + \varpi_5 \frac{\mu^2}{\rho T^2}\frac{\partial T}{\partial x_{<i}}\frac{\partial T}{\partial x_{j>}} + \varpi_6 \frac{\mu^2}{p}\frac{\partial u_{<k}}{\partial x_{<i>}}\frac{\partial u_{<j>}}{\partial x_{k>}},$$

$$q_i^{(2)} = \theta_1 \frac{\mu^2}{\rho T}\frac{\partial u_j}{\partial x_j}\frac{\partial T}{\partial x_i} - \theta_2 \frac{\mu^2}{\rho T}\left(\frac{2T}{3}\frac{\partial^2 u_j}{\partial x_i \partial x_j} + \frac{2}{3}\frac{\partial u_j}{\partial x_j}\frac{\partial T}{\partial x_i} + 2\frac{\partial u_j}{\partial x_i}\frac{\partial T}{\partial x_j}\right),$$
$$- \theta_3 \frac{\mu^2}{\rho p}\frac{\partial u_{<i}}{\partial x_{j>}}\frac{\partial p}{\partial x_j} + \theta_4 \frac{\mu^2}{\rho}\frac{\partial^2 u_{<i}}{\partial x_j \partial x_{j>}} + \theta_5 \frac{3\mu^2}{\rho T}\frac{\partial u_{<i}}{\partial x_{j>}}\frac{\partial T}{\partial x_j} \qquad (5.23)$$

where the so-called Burnett coefficients ϖ_α and θ_α are given by

$$\varpi_1 = \frac{4}{3}\left(\frac{7}{2} - \omega\right),\ \varpi_2 = 2,\ \varpi_3 = 2(1-b),\ \varpi_4 = 0,\ \varpi_5 = 2\omega(1-b),\ \varpi_6 = 8, \qquad (5.24)$$

$$\theta_1 = \frac{5}{3}(1-b)^2\left(\frac{7}{2} - \omega\right), \qquad \theta_2 = \frac{5}{2}(1-b)^2, \qquad \theta_3 = 2(1-b), \qquad \theta_4 = 2(1-b),$$

$$\theta_5 = \frac{2}{3}(1-b)\left(7 + \omega - \frac{7}{2}b\right).$$

In particular we are interested in the case where the Prandtl number has its proper value $\mathrm{Pr} = 2/3$ which is the case for $b = -1/2$. Then, the coefficients ϖ_α and θ_α have the values

$$\varpi_1 = \frac{4}{3}\left(\frac{7}{2} - \omega\right),\ \varpi_2 = 2,\ \varpi_3 = 3,\ \varpi_4 = 0,\ \varpi_5 = 3\omega,\ \varpi_6 = 8,$$

$$\theta_1 = \frac{15}{4}\left(\frac{7}{2} - \omega\right),\ \theta_2 = \frac{45}{8},\ \theta_3 = 3,\ \theta_4 = 3,\ \theta_5 = \frac{35}{4} + \omega. \qquad (5.25)$$

For the special case of Maxwell molecules, where $\beta = 1$, the above expressions Eqs. (5.23, 5.25) are identical to the expressions given in [13]. For any molecule model with power interaction potentials, the above expressions are identical to the expressions given

in [12][19], which are the Burnett equations of the Boltzmann equation for a first order solution of the resulting integral equation in terms of Sonine polynomials.

Table 5.1 shows the values of the Burnett coefficients for different values of n (or ω) compared to values obtained by Reinecke and Kremer [24] from high accuracy computations for the full Boltzmann equation, i.e. a fifth-order expansion in Sonine polynomials. Note that the expansion in Sonine polynomials is necessary to solve the integral equations that appear in the Chapman-Enskog expansion of the full Boltzmann equation, so that in this case the Chapman-Enskog expansion of a given order can only be computed in an approximate manner. It must be noted here, that the fifth order expansion yields very accurate results, so that the results in [24] can be considered as almost exact.

For the ES-BGK model this additional difficulty does not arise due to the simpler collision term, and the Chapman-Enskog expansion of a given order can be computed exactly, without further approximations. However, we emphasize that the ES-BGK collision term itself is an approximation of the Boltzmann collision term and does not preserve the full physics of the Boltzmann equation.

Indeed, from the values in Table 5.1 it becomes apparent that the Burnett equations from the ES-BGK model agree with the Burnett equations from the Boltzmann equation only for Maxwell molecules ($\omega=1$). For other molecule models, the coefficients are close to those of the full Boltzmann equation, but different nevertheless. Thus we can state that the ES-BGK model agrees with the Boltzmann equation for Maxwell molecules up to second order in the Knudsen number, while for more realistic molecule models (e.g. $\omega=4/5$), some differences occur.

---

[19] Take into account that, by Eq. (2.27), $\frac{T}{\mu}\frac{d\mu}{dT}=\omega$.

Table 5.1: Burnett coefficients ϖ_1 to ϖ_6 and θ_1 to θ_5 for different power index n and $b=-1/2$

n	ω	ϖ_1	ϖ_2	ϖ_3	ϖ_4	ϖ_5	ϖ_6
5	1	10/3 (10/3)	2 (2)	3 (3)	0 (0)	3 (3)	8 (8)
23/3	4/5	3.60 (3.600370)	2 (2.004303)	3 (2.760746)	0 (0.253684)	2.40 (1.783502)	8 (7.748040)
∞	1/2	4.00 (4.057097)	2 (2.028549)	3 (2.415493)	0 (0.680112)	1.50 (0.232355)	8 (7.419524

n	ω	θ_1	θ_2	θ_3	θ_4	θ_5
5	1	75/8 (75/8)	45/8 (45/8)	3 (3)	3 (3)	39/4 (39/4)
23/3	4/5	10.13 (10.159655)	5.625 (5.655703)	3 (3.014430)	3 (2.760746)	9.55 (9.018759)
∞	1/2	11.25 (11.652480)	5.625 (5.826240)	3 (3.095605)	3 (2.415493)	9.25 (8.100700)

NOTES: The values in brackets are those from the full Boltzmann equation [24] where values for n=23/3 are interpolated.

As a conclusion of this section, the Burnett equations for the ES-BGK model with power interaction potentials have been computed by the Chapman-Enskog method to the second order. When the Prandtl number is adjusted to its proper value $\mathrm{Pr}=2/3$ ($b=-1/2$), the ES-BGK Burnett equations are found to be identical to the Burnett equations for the Boltzmann equation only in the case of Maxwell molecules, while the Burnett coefficients exhibit some differences for other interaction types (e.g. n = 23/3 or $n = \infty$ - hard spheres). This indicates that computations of processes with the ES-BGK equation will show some discrepancies to computations that are based on the Boltzmann equation. For processes at not too large Knudsen numbers these differences might be small. Since our analysis is based on an expansion in terms of the Knudsen number only

to second order, we can not make any prediction as of how close the ES-BGK model will be to the Boltzmann equation, when the Knudsen number is large.

5.2.2 Linear stability analysis of the Burnett equations for the ES-BGK model

The main point of critizism on the Burnett equations is the question of linear stability. It is well known [75] that the Burnett equations for the Boltzmann equation with Maxwell molecules are linearly unstable in transient processes. The ES-BGK model gives us some freedom to adjust the Prandtl number, and we reconsider the stability of the Burnett equations here, and will show that for some Prandtl numbers, the ES-BGK-Burnett equations are stable. Thus, in this section, we consider the linear stability of the Burnett equations for the ES-BGK model where we restrict ourselves to one-dimensional processes. We follow the procedure for stability analysis outlined in [75].

We are interested only in processes with small deviations from an equilibrium state ρ_0, T_0, and $u_{i,0} = 0$. Then, we can introduce dimensionless variables $\hat{\rho}$, $\hat{T}$, $\hat{u}_i$, $\hat{\sigma}_{ij}$ and $\hat{q}_i$ by

$$\rho = \rho_0(1+\hat{\rho}) \ , \ T = T_0\left(1+\hat{T}\right) , \ u_i = \sqrt{RT_0}\hat{u}_i \ , \ \sigma_{ij} = p_0\hat{\sigma}_{ij} \ , \ q_i = \rho_0(RT_0)^{3/2}\hat{q}_i \ .$$

The new variables measure the deviation from a global equilibrium state, and—in the linear case—are much smaller than unity.

Moreover, we use the mean free path l to introduce non-dimensional space and time variables $\hat{x}_i$ and $\hat{t}$ as

$$x_i = l\hat{x}_i \ , \ t = \frac{l}{\sqrt{RT_0}}\hat{t} = \frac{\mu}{p_0}\hat{t} \ , \ \text{where} \ \ l = \frac{\mu\sqrt{RT_0}}{p_0} \ .$$

Linearizing Eqs. (5.19, 5.20, 1.5) in the new variables yields the dimensionless linearized three dimensional Burnett equations as

$$\frac{\partial\hat{\rho}}{\partial\hat{t}} + \frac{\partial\hat{u}_i}{\partial\hat{x}_i} = 0 \ ,$$

$$\frac{\partial \hat{u}_i}{\partial \hat{t}}+\frac{\partial \hat{\rho}}{\partial \hat{x}_i}+\frac{\partial \hat{T}}{\partial \hat{x}_i}-\frac{\partial^2 \hat{u}_i}{\partial \hat{x}_j \partial \hat{x}_j}-\frac{1}{3}\frac{\partial^2 \hat{u}_j}{\partial \hat{x}_j \partial \hat{x}_i}-\frac{4}{3}\frac{\partial^3 \hat{\rho}}{\partial \hat{x}_j \partial \hat{x}_j \partial \hat{x}_i}-\frac{4b}{3}\frac{\partial^3 \hat{T}}{\partial \hat{x}_j \partial \hat{x}_j \partial \hat{x}_i}=0\ , \quad (5.26)$$

$$\frac{3}{2}\frac{\partial \hat{T}}{\partial \hat{t}}+\frac{\partial \hat{u}_i}{\partial \hat{x}_i}-\frac{5(1-b)}{2}\frac{\partial^2 \hat{T}}{\partial \hat{x}_i \partial \hat{x}_i}-\frac{(1-b)(1-5b)}{3}\frac{\partial^3 \hat{u}_j}{\partial \hat{x}_i \partial \hat{x}_i \partial \hat{x}_j}=0\ .$$

Note that the value of the viscosity exponent ω plays no role in the linear equations. The hats will be omitted in the sequel in order to simplify the notation.

For the case of one-dimensional processes where all variables depend only on $x_1 = x$, and where $u_i = \{u, 0, 0\}$, the above equations reduce further to

$$\begin{aligned}
&\frac{\partial \rho}{\partial t}+\frac{\partial u}{\partial x}=0\ ,\\
&\frac{\partial u}{\partial t}+\frac{\partial \rho}{\partial x}+\frac{\partial T}{\partial x}-\frac{4}{3}\frac{\partial^2 u}{\partial x^2}-\frac{4}{3}\frac{\partial^3 \rho}{\partial x^3}-\frac{4b}{3}\frac{\partial^3 T}{\partial x^3}=0\ , \qquad (5.27)\\
&\frac{3}{2}\frac{\partial T}{\partial t}+\frac{\partial u}{\partial x}-\frac{5(1-b)}{2}\frac{\partial^2 T}{\partial x^2}-\frac{(1-b)(1-5b)}{3}\frac{\partial^3 u}{\partial x^3}=0\ .
\end{aligned}$$

We now assume plane wave solutions of the form

$\rho = \tilde{\rho}\cdot\exp(\lambda t + ikx)$, $T = \tilde{T}\cdot\exp(\lambda t + ikx)$, $u = \tilde{u}\cdot\exp(\lambda t + ikx)$

where k is the positive real wave number, while λ is a complex number, whose real part can be interpreted as the negative of the damping of the wave, and whose imaginary part is the frequency of the wave. Stability of the system requires negative damping, so that $\mathrm{Re}\,\lambda \le 0$ must hold for all possible values of k.

Substitution of these solutions into Eqs. (5.27) yields a homogeneous algebraic system for the amplitudes $\tilde{\rho}$, $\tilde{u}$, and $\tilde{T}$ which reads

$$\begin{aligned}
&\lambda\cdot\tilde{\rho}+ik\cdot\tilde{u}=0\ ,\\
&\left(ik+\frac{4}{3}ik^3\right)\cdot\tilde{\rho}+\left(\lambda+\frac{4}{3}k^2\right)\cdot\tilde{u}+\left(ik+\frac{4b}{3}ik^3\right)\cdot\tilde{T}=0\ , \qquad (5.28)\\
&\left(ik+\frac{(1-b)(1-5b)}{3}ik^3\right)\cdot\tilde{u}+\left(\frac{3}{2}\lambda+\frac{5(1-b)}{2}k^2\right)\cdot\tilde{T}=0\ .
\end{aligned}$$

The condition for existence of a nontrivial solution of above system is that the determinant of the system equals to zero, that is

$$\lambda^3 + \frac{9-5b}{3}k^2\lambda^2 + k^2\lambda\cdot\left[\frac{5}{3} + k^2\frac{10b^2-24b+34}{9} + k^4\frac{8b(1-b)(1-5b)}{27}\right] + \frac{5(1-b)}{3}k^4\left(1+\frac{4}{3}k^2\right) = \Omega(\lambda,k) = 0\ . \tag{5.29}$$

Note that the ES-BGK model requires that $-1/2 \le b \le 1$. We will divide the whole range of b into three parts to discuss the roots of the above cubic equation for λ, and the linear stability of one-dimensional processes.

- **Part I** ($-1/2 \le b < 0$ **and** $1/5 < b < 1$)

We follow the line of arguments of [66]. For values of b in this range, it is easy to see that $\Omega(\lambda = 0, k) > 0$ and $\Omega(\lambda \to \infty, k) \to +\infty$ while for very large values of k

$$\Omega(\lambda = k^2, k) \approx \frac{8b(1-b)(1-5b)}{27}k^8 < 0$$

holds. Therefore, Eq. (5.29) has at least two positive real roots λ. It follows that the Burnett equations for the ES-BGK model are linearly unstable for values of b in the intervals $-1/2 \le b < 0$ and $1/5 < b < 1$.

- **Part II** ($b = 1$)

In this particular case, Eq. (5.29) simplifies to

$$\lambda^3 + \frac{4}{3}k^2\lambda^2 + k^2\lambda\cdot\left[\frac{5}{3} + k^2\frac{20}{9}\right] = 0\ .$$

The three roots for this cubic equation are

$$\lambda_1 = 0\ ,\quad \lambda_{2,3} = -\frac{2}{3}k^2 \pm i\sqrt{\frac{16}{9}k^4 + \frac{5}{3}k^2}\ .$$

Therefore, $\mathrm{Re}\,\lambda_{1,2,3} \le 0$, and the Burnett equations for the ES-BGK model are linearly stable for $b = 1$. Note that by this case corresponds to a gas with infinite viscosity and $\mathrm{Pr} = \infty$

- **Part III** ($0 \le b \le 1/5$)

A cubic equation has either three real roots, or one real root and two conjugate complex roots [76]. We shall analyze the roots of Eq. (5.29) for $0 \le b \le 1/5$ in the following.

Three real roots

Assume that the three roots of Eq. (5.29) are all real. Since the function $\Omega(\lambda, k)$ (the left hand side of Eq. (5.29)) increases when λ increases ($\lambda \ge 0$ assumed), and $\Omega(\lambda = 0, k) > 0$, it follows that Eq. (5.29) cannot have positive roots, and that all three real roots (so they exist) will be negative.

One real root and two conjugate complex roots

In this case, we assume that the three roots of Eq. (5.29) are one real value λ_1 and two conjugate complex values $\lambda_{2,3} = \lambda_R \pm i\lambda_i$, where λ_R and λ_i themselves are real numbers. Since for $\lambda \ge 0$ the function $\Omega(\lambda, k)$ increases when λ increases, and since $\Omega(\lambda = 0, k) > 0$, λ_1 must be negative. Furthermore, from Eq. (5.29), we obtain by inserting $\lambda = \lambda_R + i\lambda_i$

$$\lambda_R^3 - 3\lambda_R\lambda_i^2 + \frac{9-5b}{3}k^2\left(\lambda_R^2 - \lambda_i^2\right) + k^2\lambda_R \cdot \left[\frac{5}{3} + k^2\frac{10b^2 - 24b + 34}{9} + k^4\frac{8b(1-b)(1-5b)}{27}\right] +$$

$$+\frac{5(1-b)}{3}k^4\left(1 + \frac{4}{3}k^2\right) = 0$$

$$3\lambda_R^2 - \lambda_i^2 + \frac{9-5b}{3}k^2 2\lambda_R + k^2 \cdot \left[\frac{5}{3} + k^2\frac{10b^2 - 24b + 34}{9} + k^4\frac{8b(1-b)(1-5b)}{27}\right] = 0 \,. \qquad (5.30)$$

Eliminating λ_i between these two equations yields

$$\lambda_R^3 + \zeta_1\lambda_R^2 + \zeta_2\lambda_R + \zeta_3 = 0 \,, \qquad (5.31)$$

where the k-dependent coefficients are given by

$$\zeta_1 = \frac{9-5b}{3}k^2 \,,$$

$$\zeta_2 = \left(\frac{9-5b}{6}\right)^2 k^4 + \frac{k^2}{4}\cdot\left[\frac{5}{3} + k^2\frac{10b^2-24b+34}{9} + k^4\frac{8b(1-b)(1-5b)}{27}\right],$$

$$\zeta_3 = \frac{b(9-5b)(1-b)(1-5b)}{81}k^8 + \frac{123-163b+105b^2-25b^3}{108}k^6 + \frac{15-5b}{36}k^4 .$$

Since the coefficients ζ_1, ζ_2, and ζ_3 are positive for $0 \le b \le 1/5$, there are no positive roots of Eq. (5.31) and it follows that $\mathrm{Re}\,\lambda \le 0$.

Thus, $\mathrm{Re}\,\lambda \le 0$ holds for all values of b in the interval [0, 1/5] and we conclude that the Burnett equations for the ES-BGK model are linearly stable for $0 \le b \le 1/5$, that is for Prandtl numbers in $1 \le \mathrm{Pr} \le 5/4$. For all other values of b (or Pr) except $\mathrm{Pr} = \infty$, however, the Burnett equations for the ES-BGK model are linearly unstable – this includes the physically relevant case of Pr = 2/3.

The stability of the BGK-Burnett equations—where Pr=1—can be found in the literature [77]. Our anlysis shows that the stability can be obtained for a wider range of values for the Prandtl number.

As a conclusion of this section, our analysis of the linear stability of the ES-BGK Burnett equations revealed that the stability depends on the value of the Prandtl number. For $1 \le \mathrm{Pr} \le 5/4$ and for $\mathrm{Pr} = \infty$ the ES-BGK Burnett equations are linearly stable, while they are linearly unstable $2/3 < \mathrm{Pr} < 1$ and $5/4 < \mathrm{Pr} < \infty$. It follows that higher order Chapman-Enskog expansions do not necessarily lead to unstable equations.

5.2.3 NSF and Burnett equations for one-dimensional Couette flow at steady state

In the 1DCF at steady state we consider (one plate is stationary, while another plate is moving along X1 direction, and the direction perpendicular to the plates is the X2 direction), unknown variables in trace-free pressure and heat flux are σ_{11}, σ_{22}, σ_{12}, q_1,

and q_2, while $\sigma_{33} = -(\sigma_{11} + \sigma_{22})$, $\sigma_{21} = \sigma_{12}$, $\sigma_{31} = \sigma_{13} = 0$, $\sigma_{32} = \sigma_{23} = 0$, and $u_3 = 0$, $\frac{\partial}{\partial x_1} = \frac{\partial}{\partial x_3} = 0$.

From Eq. (5.14), after some manipulation, one obtains the following expressions for the NSF equations

$$\sigma_{11}^{NSF} = -2\mu \frac{\partial u_{<1}}{\partial x_{1>}} = -2\mu \left(\frac{2}{3} \frac{\partial u_1}{\partial x_1} - \frac{1}{3} \frac{\partial u_2}{\partial x_2} \right) = 0,$$

$$\sigma_{22}^{NSF} = -2\mu \frac{\partial u_{<2}}{\partial x_{2>}} = 0, \tag{5.32}$$

$$\sigma_{12}^{NSF} = -2\mu \frac{\partial u_{<1}}{\partial x_{2>}} = -\mu \frac{\partial u_1}{\partial x_2},$$

$$q_1^{NSF} = -\kappa \frac{\partial T}{\partial x_1} = 0.0, \; q_2^{NSF} = -\kappa \frac{\partial T}{\partial x_2}.$$

From Eq. (5.19), after some manipulation, one obtains the following expressions for the Burnett equations,

$$\sigma_{11}^{B} = \frac{\mu^2}{p^2} \cdot \Phi_{11}, \; \sigma_{22}^{B} = \frac{\mu^2}{p^2} \cdot \Phi_{22}, \; \sigma_{12}^{B} = -\mu \frac{\partial u_1}{\partial x_2} + \frac{\mu^2}{p^2} \cdot \Phi_{12},$$

$$q_1^{B} = \frac{\mu^2}{p^2 \, \mathrm{Pr}} \cdot \Gamma_1, \; q_2^{B} = -\kappa \frac{\partial T}{\partial x_2} + \frac{\mu^2}{p^2 \, \mathrm{Pr}} \cdot \Gamma_2. \tag{5.33}$$

where

$$\Phi_{11} = \frac{2}{3} R^2 T^2 \frac{\partial^2 \rho}{\partial x_2 \partial x_2} + \frac{2b}{3} \rho R^2 T \frac{\partial^2 T}{\partial x_2 \partial x_2} - \frac{2}{3} \frac{R^2 T^2}{\rho} \frac{\partial \rho}{\partial x_2} \frac{\partial \rho}{\partial x_2}$$
$$+ \frac{2}{3} R^2 T \frac{\partial T}{\partial x_2} \frac{\partial \rho}{\partial x_2} + \frac{4}{3} p \frac{\partial u_1}{\partial x_2} \frac{\partial u_1}{\partial x_2} - \frac{2\omega(1-b)}{3} \rho R^2 \frac{\partial T}{\partial x_2} \frac{\partial T}{\partial x_2},$$

$$\Phi_{22} = -\frac{4}{3} R^2 T^2 \frac{\partial^2 \rho}{\partial x_2 \partial x_2} - \frac{4b}{3} \rho R^2 T \frac{\partial^2 T}{\partial x_2 \partial x_2} + \frac{4}{3} \frac{R^2 T^2}{\rho} \frac{\partial \rho}{\partial x_2} \frac{\partial \rho}{\partial x_2}$$
$$- \frac{4}{3} R^2 T \frac{\partial T}{\partial x_2} \frac{\partial \rho}{\partial x_2} - \frac{2}{3} p \frac{\partial u_1}{\partial x_2} \frac{\partial u_1}{\partial x_2} + \frac{4\omega(1-b)}{3} \rho R^2 \frac{\partial T}{\partial x_2} \frac{\partial T}{\partial x_2},$$

$$\Phi_{12} = 0, \tag{5.34}$$

$$\Gamma_1 = pRT\frac{\partial^2 u_1}{\partial x_2 \partial x_2} - R^2T^2\frac{\partial u_1}{\partial x_2}\frac{\partial \rho}{\partial x_2} + \left(6+\omega-\frac{7}{2}b\right)pR\frac{\partial u_1}{\partial x_2}\frac{\partial T}{\partial x_2},$$

$$\Gamma_2 = 0.$$

From the above Eqs. (5.32-5.34), one can see that the expressions for σ_{12} and q_2 from the NSF equations and the Burnett equations are the same, while the expressions for σ_{11}, σ_{22} and q_1 from the NSF equations and the Burnett equations are different. Non-zero values of σ_{11}, σ_{22} and q_1 refer to rarefaction effects which are not described by the NSF equations, but by the Burnett equations, and the moment equations which will be discussed now.

5.3 Grad13 and R13s equations for BGK and ES-BGK models

5.3.1 Grad13 and R13s in three dimensions

There are 13 unknown variables, and 13 moment equations in the Grad 13 and the R13s for a three-dimensional problem. The unknown parameters are ρ, u_1, u_2, u_3, T, σ_{11}, σ_{22}, σ_{12}, σ_{13}, σ_{23}, q_1, q_2 and q_3, while other parameters can be derived from these parameters or equal to zero, such as, $p = \rho RT$, $\sigma_{33} = -(\sigma_{11}+\sigma_{22})$, $\sigma_{21} = \sigma_{12}$, $\sigma_{31} = \sigma_{13}$, $\sigma_{32} = \sigma_{23}$.

The Grad13 and the original R13 for the kinetic model (BGK or ES-BGK) are obtained from the same idea and procedure as for the Boltzmann equation with the Maxwellian molecular model, which are given in [26].

After multiplying the kinetic model equation Eq. (2.8) by polynomials of the peculiar velocity, viz. 1, C_i, C^2, $C_{<i}C_{j>}$ and $\frac{1}{2}C^2C_i$, and subsequent integration over velocity space, the basic 13 moment equations for the kinetic model are obtained as

$$\frac{\partial \rho}{\partial t} + \frac{\partial(\rho u_k)}{\partial x_k} = 0,$$

$$\rho\frac{\partial u_i}{\partial t}+\rho u_k\frac{\partial u_i}{\partial x_k}+\frac{\partial p}{\partial x_i}+\frac{\partial \sigma_{ik}}{\partial x_k}=0,$$

$$\frac{3}{2}\rho R\frac{\partial T}{\partial t}+\frac{3}{2}\rho R u_k\frac{\partial T}{\partial x_k}+\frac{\partial q_k}{\partial x_k}+p\frac{\partial u_k}{\partial x_k}+\sigma_{ik}\frac{\partial u_i}{\partial x_k}=0, \tag{5.35}$$

$$\frac{\partial \sigma_{ij}}{\partial t}+\frac{\partial(\sigma_{ij}u_k)}{\partial x_k}+\frac{4}{5}\frac{\partial q_{<i}}{\partial x_{j>}}+2p\frac{\partial u_{<i}}{\partial x_{j>}}+2\sigma_{k<i}\frac{\partial u_{j>}}{\partial x_k}+\frac{\partial \rho_{<ijk>}}{\partial x_k}=-\frac{p}{\mu}\sigma_{ij},$$

$$\frac{\partial q_i}{\partial t}+\frac{\partial(q_iu_k)}{\partial x_k}-\frac{5}{2}RT\frac{\partial p}{\partial x_i}-\frac{5}{2}RT\frac{\partial \sigma_{ik}}{\partial x_k}-\frac{\sigma_{ik}}{\rho}\frac{\partial p}{\partial x_k}-\frac{\sigma_{ij}}{\rho}\frac{\partial \sigma_{jk}}{\partial x_k}+\frac{7}{5}q_k\frac{\partial u_i}{\partial x_k}$$

$$+\frac{2}{5}q_k\frac{\partial u_k}{\partial x_i}+\frac{2}{5}q_i\frac{\partial u_k}{\partial x_k}+\frac{1}{2}\frac{\partial \rho_{rr<ik>}}{\partial x_k}+\frac{1}{6}\frac{\partial \rho_{rrss}}{\partial x_i}+\rho_{<ijk>}\frac{\partial u_j}{\partial x_k}=-\frac{\Pr p}{\mu}q_i$$

where the definition of moments refer to Eq. (1.3), and Eqs. (2.12, E.16) have been used to compute the right hand sides of the last two expressions in Eq. (5.35). Note that this set of 13 equations does not form a closed set of equations for the 13 variables, since it contains the higher degree moments $\rho_{<ijk>}$, $\rho_{rr<ik>}$ and ρ_{rrss}.

There are some rules about the computation of trace free part of a tensor [78].

$$A_{<ij>}=\frac{1}{2}A_{ij}+\frac{1}{2}A_{ji}-\frac{1}{3}A_{kk}\delta_{ij},$$

$$A_{<ijk>}=A_{(ijk)}-\frac{1}{5}\left(A_{(nni)}\delta_{jk}+A_{(nnj)}\delta_{ik}+A_{(nnk)}\delta_{ij}\right), \tag{5.36}$$

$$A_{(ijk)}=\frac{1}{6}\left(A_{ijk}+A_{ikj}+A_{jki}+A_{jik}+A_{kij}+A_{kji}\right).$$

Therefore, for three-degree and fourth-degree moments, we have

$$\rho_{ijk}=\rho_{<ijk>}+\frac{2}{5}\left(q_i\delta_{jk}+q_j\delta_{ik}+q_k\delta_{ij}\right), \qquad \rho_{rrik}=\rho_{rr<ik>}+\frac{1}{3}\rho_{rrss}\delta_{ik}. \tag{5.37}$$

In order to close the system for the 13 variables, a closure assumption is required that allows to relate the higher degree moments to the 13 variables, which requires to express the distribution function as a function of the 13 variables. As mentioned in Chapter 1, there are two ways to find the closure assumption, and here Grad's moment method is considered. In Grad's moment method, the distribution is related to the moments as an expansion in Hermite polynomials about the equilibrium distribution [5, 6, 26],

$$f_{|N} = f_M\left(1+\sum_{A=1}^{N}\Lambda_A\Psi_A\right) \tag{5.38}$$

where N is the number of moments considered in the system, Ψ_A $(A=1,...,N)$ means a set of N polynomials of the peculiar velocity, which corresponding macroscopic parameters are the N moments ρ_A considered, that is to say,

$$\rho_A = \int \Psi_A f_{|N} d\mathbf{c} \tag{5.39}$$

and the coefficients Λ_A are determined from the N moments considered. In particular, for the Grad's 13 moment equations, $N=13$, Ψ_A ={ 1, C_i, C^2, $C_{<i}C_{j>}$, $\frac{1}{2}C^2C_i$, and ρ_A are the 13 moments ρ, u_i, T, σ_{ij} and q_i, and one has

$$f_{|13} = f_M\left(1+\frac{1}{2pRT}\sigma_{ik}C_{<i}C_{k>}-\frac{1}{pRT}q_kC_k\left(1-\frac{C^2}{5RT}\right)\right) \tag{5.40}$$

From this expression for the distribution and Eqs. (1.3, 5.37), we have

$$\rho^{G13}_{<ijk>}=0.0, \quad \rho^{G13}_{<rr>ij}=7RT\sigma_{ij}, \qquad \rho^{G13}_{rrss}=15\frac{p^2}{\rho} \tag{5.41}$$

Grad's 13 moment equations form a hyperbolic system, which implies finite wave speeds and discontinuities in shocks that make the system difficult to handle [26]. In order to overcome these disadvantages of the Grad's moment system, Struchtrup and Torrilhon developed a method, named as regularization, in which some parabolic terms are added, which changes the character of the equations so that no discontinuities will occur [26, 27]. The additional terms are obtained from the Grad's moment equations for higher degree moments (than moments considered). In their work, the Boltzmann equation with Maxwell molecules is considered, while here the ES-BGK model (which includes the BGK model as a specific case) with Maxwell molecules will be considered with the same idea and procedure. Since we are interested in 13 moment equations, we will describe the idea and procedure based on this situation.

In order to perform the regularization, we define the derivations of $\rho_{<ijk>}$, $\rho_{<rr>ij}$ and ρ_{rrss} from their values obtained with the Grad 13 closure as

$$
\begin{aligned}
m_{ijk} &= \rho_{<ijk>} - \rho^{G13}_{<ijk>} = \rho_{<ijk>}, \\
R_{ij} &= \rho_{rr<ij>} - \rho^{G13}_{rr<ij>} = \rho_{rr<ij>} - 7RT\sigma_{ij}, \\
\Delta &= \rho_{rrss} - \rho^{G13}_{rrss} = \rho_{rrss} - 15\frac{p^2}{\rho}.
\end{aligned}
\tag{5.42}
$$

For the Grad 13 moment equations, we thus have

$$
m^{G13}_{ijk} = R^{G13}_{ij} = \Delta^{G13} = 0. \tag{5.43}
$$

The regularization of Grad's 13 moment equations is based on the Grad's moment equations for the three-degree and fourth-degree moments $\rho_{<ijk>}$, $\rho_{rr<ij>}$ and ρ_{rrss}, which have, for the ES-BGK model, the form

$$
\begin{aligned}
&\frac{\partial \rho_{<ijk>}}{\partial t} + \frac{\partial \rho_{<ijk>} u_l}{\partial x_l} + \frac{\partial \rho_{<ijkl>}}{\partial x_l} + \frac{3}{7}\frac{\partial \rho_{rr<ij}}{\partial x_{k>}} - \frac{3}{\rho}\sigma_{<ij}\frac{\partial p}{\partial x_{k>}} - \frac{3}{\rho}\sigma_{<ij}\frac{\partial \sigma_{k>l}}{\partial x_l} \\
&+ 3\rho_{<l<ij>}\frac{\partial u_{k>}}{\partial x_l} + \frac{12}{5}q_{<i}\frac{\partial u_j}{\partial x_{k>}} = -\frac{\Pr p}{\mu}\rho_{<ijk>} \\
&\frac{\partial \rho_{rr<ij>}}{\partial t} + \frac{\partial \rho_{rr<ij>} u_k}{\partial x_k} + \frac{\partial \rho_{rr<ijk>}}{\partial x_k} + \frac{2}{5}\frac{\partial \rho_{rrss<i}}{\partial x_{j>}} - \frac{2}{\rho}\rho_{<ijr>}\frac{\partial p_{rk}}{\partial x_k} - \frac{28}{5\rho}q_{<i}\frac{\partial p_{j>k}}{\partial x_k} \\
&+ 2\rho_{<ij>kl}\frac{\partial u_k}{\partial x_l} + 2\rho_{rrk<i}\frac{\partial u_{j>}}{\partial x_k} = -\frac{\Pr p}{\mu}\left(\rho_{rr<ij>} - 7bRT\sigma_{ij}\right) \\
&\frac{\partial \rho_{rrss}}{\partial t} + \frac{\partial \rho_{rrss} u_k}{\partial x_k} + \frac{\partial \rho_{rrssk}}{\partial x_k} - \frac{8}{\rho}q_i\frac{\partial p_{ik}}{\partial x_k} + 4\rho_{rrki}\frac{\partial u_i}{\partial x_k} = -\frac{\Pr p}{\mu}\left(\rho_{rrss} - 15\frac{p^2}{\rho}\right).
\end{aligned}
\tag{5.44}
$$

In the derivation of the above equation (5.45), the following expression for f_{ES} (Eqs. (E.16, E.24)) and Eq. (2.12) have been used,

$$
\begin{aligned}
&\int C_i C_j C_k f_{ES} d\mathbf{c} = 0, \\
&\int C_r C_r C_{<i} C_{j>} f_{ES} d\mathbf{c} = 7bRT\sigma_{ij}, \\
&\int C_r C_r C_s C_s f_{ES} d\mathbf{c} = 15\frac{p^2}{\rho},
\end{aligned}
\tag{5.45}
$$

After some manipulation, one obtains the equations for m_{ijk}, R_{ij} and Δ from Eqs. (5.35, 5.42, 5.44) as

$$\frac{\partial m_{ijk}}{\partial t}+\frac{\partial m_{ijk}u_l}{\partial x_l}+\frac{\partial \rho_{<ijkl>}}{\partial x_l}+\frac{3}{7}\frac{\partial \rho_{rr<ij}}{\partial x_{k>}}-\frac{3}{\rho}\sigma_{<ij}\frac{\partial p}{\partial x_{k>}}-\frac{3}{\rho}\sigma_{<ij}\frac{\partial \sigma_{k>l}}{\partial x_l}$$
$$+3\rho_{<l<ij>}\frac{\partial u_{k>}}{\partial x_l}+\frac{12}{5}q_{<i}\frac{\partial u_j}{\partial x_{k>}}=-\frac{\Pr p}{\mu}m_{ijk} \qquad (5.46)$$

$$\frac{\partial R_{ij}}{\partial t}+\frac{\partial \rho_{rr<ij>}u_k}{\partial x_k}+\frac{\partial \rho_{rr<ijk>}}{\partial x_k}+\frac{2}{5}\frac{\partial \rho_{rrss<i}}{\partial x_{j>}}-\frac{2}{\rho}\rho_{<ijr>}\frac{\partial p_{rk}}{\partial x_k}-\frac{28}{5\rho}q_{<i}\frac{\partial p_{j>k}}{\partial x_k}$$
$$+2\rho_{<ij>kl}\frac{\partial u_k}{\partial x_l}+2\rho_{rrk<i}\frac{\partial u_{j>}}{\partial x_k}-7RT\frac{\partial \sigma_{ij}u_k}{\partial x_k}-\frac{28}{5}RT\frac{\partial q_{<i}}{\partial x_{j>}}-7RT\frac{\partial \rho_{<ijk>}}{\partial x_k}$$
$$-14pRT\frac{\partial u_{<i}}{\partial x_{j>}}-7R\sigma_{ij}u_k\frac{\partial T}{\partial x_k}-\frac{14}{3}\frac{\sigma_{ij}}{\rho}\frac{\partial q_k}{\partial x_k}-\frac{14}{3}\frac{\sigma_{ij}}{\rho}p\frac{\partial u_k}{\partial x_k}-\frac{14}{3}\frac{\sigma_{ij}}{\rho}\sigma_{kl}\frac{\partial u_k}{\partial x_l}=-\frac{\Pr p}{\mu}R_{ij}$$

$$\frac{\partial \Delta}{\partial t}+\frac{\partial \rho_{rrss}u_k}{\partial x_k}+\frac{\partial \rho_{rrssk}}{\partial x_k}-\frac{8}{\rho}q_i\frac{\partial p_{ik}}{\partial x_k}+4\rho_{rrki}\frac{\partial u_i}{\partial x_k}-15pRT\frac{\partial u_k}{\partial x_k}-75R^2T^2u_k\frac{\partial \rho}{\partial x_k}$$
$$-30pRu_k\frac{\partial T}{\partial x_k}-20RT\frac{\partial q_k}{\partial x_k}-20pRT\frac{\partial u_k}{\partial x_k}-20RT\sigma_{ij}\frac{\partial u_i}{\partial x_j}=-\frac{\Pr p}{\mu}\left(\rho_{rrss}-15\frac{p^2}{\rho}\right)$$

Then at last, computing the left hand side terms in the above equation (5.46) with 13 moment distribution, one obtains the m_{ijk}, R_{ij} and Δ of the original R13 as

$$m_{ijk}^{R13I}=-3\frac{\Pr p}{\mu}\left(RT\frac{\partial \sigma_{<ij}}{\partial x_{k>}}-\frac{RT}{\rho}\sigma_{<ij}\frac{\partial \rho}{\partial x_{k>}}+\frac{4}{5}q_{<i}\frac{\partial u_j}{\partial x_{k>}}-\underline{\frac{\sigma_{<ij}}{\rho}\frac{\partial \sigma_{k>l}}{\partial x_l}}\right), \qquad (5.47)$$

$$R_{ij}^{R13I}=-\frac{28}{5}\frac{\Pr p}{\mu}\left(RT\frac{\partial q_{<i}}{\partial x_{j>}}+Rq_{<i}\frac{\partial T}{\partial x_{j>}}-\frac{RTq_{<i}}{\rho}\frac{\partial \rho}{\partial x_{j>}}-\underline{\frac{q_{<i}}{\rho}\frac{\partial \sigma_{j>k}}{\partial x_k}}\right)$$
$$-\frac{28}{5}\frac{\Pr p}{\mu}\left(\frac{5}{7}RT\left(\sigma_{k<i}\frac{\partial u_{j>}}{\partial x_k}+\sigma_{k<i}\frac{\partial u_k}{\partial x_{j>}}-\frac{2}{3}\sigma_{ij}\frac{\partial u_k}{\partial x_k}\right)-\underline{\frac{5}{6}\frac{\sigma_{ij}}{\rho}\frac{\partial q_k}{\partial x_k}-\frac{5}{6}\frac{\sigma_{ij}}{\rho}\sigma_{kl}\frac{\partial u_k}{\partial x_l}}\right),$$

$$\Delta^{R13I}=-8\frac{\Pr p}{\mu}\left(RT\frac{\partial q_k}{\partial x_k}+\frac{5}{2}Rq_k\frac{\partial T}{\partial x_k}-\frac{RTq_k}{\rho}\frac{\partial \rho}{\partial x_k}-\underline{\frac{q_i}{\rho}\frac{\partial \sigma_{ik}}{\partial x_k}}+RT\sigma_{ik}\frac{\partial u_i}{\partial x_k}\right).$$

The idea of last step is a Chapman-Enskog like procedure [26], which is adding $\frac{1}{\varepsilon}$ (which will be set equal to one at the end of the calculations) on the right hand side of Eq. (5.46) (not for Eq. (5.35)), and expanding moments (only for m_{ijk}, R_{ij} and Δ, not for the 13 variables) as

$$\rho_A = \sum_{n=0}^{\infty} \varepsilon^n \rho_A^{(n)}.$$

Then, it is straightforward to see that the zeroth-order approximation (balancing terms with the factor $\frac{1}{\varepsilon}$) just gives Grad's 13 moment case (Eq. (5.43)), and the first-order correction results (balancing terms with the factor ε^0) gives the Regularized 13 moment case (Eq. (5.47)).

The slightly linearized R13 equations is obtained from a new method [15], which is based on a different way to account orders in the Kn number, and provides a direct link between Grad type moment equations and the Kn number. The expression of m_{ijk}, R_{ij} and Δ of the slightly linearized R13 equations are found to be the original R13 equations (5.47) omitting the highest order terms, which are underlined in Eq. (5.47).

5.3.2 Grad13 and R13s in one-dimensional Couette flow at steady state

In the 1DCF we consider, there are nine unknown variables in the moment equations, which are ρ, u_1, u_2, T, σ_{11}, σ_{22}, σ_{12}, q_1, and q_2, and other parameters can be derived from these parameters or are zero value, $p = \rho RT$, $u_3 = 0$, $\sigma_{33} = -(\sigma_{11} + \sigma_{22})$, $\sigma_{21} = \sigma_{12}$, $\sigma_{31} = \sigma_{13} = 0$, $\sigma_{32} = \sigma_{23} = 0$, $q_3 = 0$, $\frac{\partial}{\partial x_1} = \frac{\partial}{\partial x_3} = 0$. Here only the equations for 1DCF are given, and their derivations from the general equations (refer to corresponding equations in the above Section 5.3.1) has been omitted.

The nine basic moment equations, which are the same for the Grad 13, the R13s, and kinetic models (BGK and ES-BGK), are

$$\frac{\partial \rho}{\partial t} + \frac{\partial (\rho u_2)}{\partial x_2} = 0,$$

$$\rho \frac{\partial u_1}{\partial t} + \rho u_2 \frac{\partial u_1}{\partial x_2} + \frac{\partial \sigma_{12}}{\partial x_2} = 0,$$

$$\rho\frac{\partial u_2}{\partial t}+\rho u_2\frac{\partial u_2}{\partial x_2}+\frac{\partial p}{\partial x_2}+\frac{\partial \sigma_{22}}{\partial x_2}=0,$$

$$\frac{3}{2}\rho R\frac{\partial T}{\partial t}+\frac{3}{2}\rho R u_2\frac{\partial T}{\partial x_2}+\frac{\partial q_2}{\partial x_2}+p\frac{\partial u_2}{\partial x_2}+\sigma_{12}\frac{\partial u_1}{\partial x_2}+\sigma_{22}\frac{\partial u_2}{\partial x_2}=0, \tag{5.48}$$

$$\frac{\partial \sigma_{11}}{\partial t}+\frac{\partial(\sigma_{11}u_2)}{\partial x_2}-\frac{4}{15}\frac{\partial q_2}{\partial x_2}-\frac{2}{3}p\frac{\partial u_2}{\partial x_2}+\frac{4}{3}\sigma_{21}\frac{\partial u_1}{\partial x_2}-\frac{2}{3}\sigma_{22}\frac{\partial u_2}{\partial x_2}+\frac{\partial \rho_{<112>}}{\partial x_2}=-\frac{p}{\mu}\sigma_{11},$$

$$\frac{\partial \sigma_{22}}{\partial t}+\frac{\partial(\sigma_{22}u_2)}{\partial x_2}+\frac{8}{15}\frac{\partial q_2}{\partial x_2}+\frac{4}{3}p\frac{\partial u_2}{\partial x_2}+\frac{4}{3}\sigma_{22}\frac{\partial u_2}{\partial x_2}-\frac{2}{3}\sigma_{21}\frac{\partial u_1}{\partial x_2}+\frac{\partial \rho_{<222>}}{\partial x_2}=-\frac{p}{\mu}\sigma_{22},$$

$$\frac{\partial \sigma_{12}}{\partial t}+\frac{\partial(\sigma_{12}u_2)}{\partial x_2}+\frac{2}{5}\frac{\partial q_1}{\partial x_2}+p\frac{\partial u_1}{\partial x_2}+\sigma_{21}\frac{\partial u_2}{\partial x_2}+\sigma_{22}\frac{\partial u_1}{\partial x_2}+\frac{\partial \rho_{<122>}}{\partial x_2}=-\frac{p}{\mu}\sigma_{12},$$

$$\begin{aligned}&\frac{\partial q_1}{\partial t}+\frac{\partial(q_1u_2)}{\partial x_2}-\frac{5}{2}RT\frac{\partial \sigma_{12}}{\partial x_2}-\frac{\sigma_{12}}{\rho}\frac{\partial p}{\partial x_2}-\frac{\sigma_{11}}{\rho}\frac{\partial \sigma_{12}}{\partial x_2}-\frac{\sigma_{12}}{\rho}\frac{\partial \sigma_{22}}{\partial x_2}\\&+\frac{7}{5}q_2\frac{\partial u_1}{\partial x_2}+\frac{2}{5}q_1\frac{\partial u_2}{\partial x_2}+\frac{1}{2}\frac{\partial \rho_{rr<12>}}{\partial x_2}+\rho_{<112>}\frac{\partial u_1}{\partial x_2}+\rho_{<122>}\frac{\partial u_2}{\partial x_2}=-\frac{\Pr p}{\mu}q_1\end{aligned},$$

$$\begin{aligned}&\frac{\partial q_2}{\partial t}+\frac{\partial(q_2u_2)}{\partial x_2}-\frac{5}{2}RT\frac{\partial p}{\partial x_2}-\frac{5}{2}RT\frac{\partial \sigma_{22}}{\partial x_2}-\frac{\sigma_{22}}{\rho}\frac{\partial p}{\partial x_2}-\frac{\sigma_{21}}{\rho}\frac{\partial \sigma_{12}}{\partial x_2}-\frac{\sigma_{22}}{\rho}\frac{\partial \sigma_{22}}{\partial x_2}\\&+\frac{11}{5}q_2\frac{\partial u_2}{\partial x_2}+\frac{2}{5}q_1\frac{\partial u_1}{\partial x_2}+\frac{1}{2}\frac{\partial \rho_{rr<22>}}{\partial x_2}+\frac{1}{6}\frac{\partial \rho_{rrss}}{\partial x_2}+\rho_{<212>}\frac{\partial u_1}{\partial x_2}+\rho_{<222>}\frac{\partial u_2}{\partial x_2}=-\frac{\Pr p}{\mu}q_2\end{aligned}.$$

Note that the above equations do not form a closed set of equations for the nine variables, since they contain the higher degree moments $\rho_{<112>}$, $\rho_{<122>}$, $\rho_{<222>}$, $\rho_{rr<12>}$, $\rho_{rr<22>}$ and ρ_{rrss}. The difference between the Grad13 equations, and their regularization comes in through the expressions for the higher degree moments, which can be decomposed according to Eq. (5.42),

$$\rho_{<112>}=m_{112},\ \rho_{<122>}=m_{122},\ \rho_{<222>}=m_{222}, \tag{5.49}$$

$$\rho_{rr<12>} = 7RT\sigma_{12} + R_{12},\ \rho_{rr<22>} = 7RT\sigma_{22} + R_{22},\ \rho_{rrs} = 15\frac{p^2}{\rho} + \Delta$$

For the Grad 13 moment equations, from Eq. (5.43), one gets

$$m_{112}^{G13} = m_{122}^{G13} = m_{222}^{G13} = R_{12}^{G13} = R_{22}^{G13} = \Delta^{G13} = 0. \tag{5.50}$$

For the original R13 moment equations, from Eq. (5.47)

$$\begin{aligned}
m_{112}^{R13I} &= -3\frac{\Pr p}{\mu}\left(\frac{1}{3}RT\frac{\partial\sigma_{11}}{\partial x_2} - \frac{2}{15}RT\frac{\partial\sigma_{22}}{\partial x_2} - \frac{1}{3}\frac{RT}{\rho}\sigma_{11}\frac{\partial\rho}{\partial x_2} + \frac{2}{15}\frac{RT}{\rho}\sigma_{22}\frac{\partial\rho}{\partial x_2}\right) \\
&\quad -3\frac{\Pr p}{\mu}\left(+\frac{16}{75}q_1\frac{\partial u_1}{\partial x_2} - \underline{\frac{1}{3}\frac{\sigma_{11}}{\rho}\frac{\partial\sigma_{22}}{\partial x_2} - \frac{8}{15}\frac{\sigma_{12}}{\rho}\frac{\partial\sigma_{12}}{\partial x_2} + \frac{2}{15}\frac{\sigma_{22}}{\rho}\frac{\partial\sigma_{22}}{\partial x_2}}\right), \\
m_{122}^{R13I} &= -3\frac{\Pr p}{\mu}\left(\frac{8}{15}RT\frac{\partial\sigma_{12}}{\partial x_2} - \frac{8}{15}\frac{RT}{\rho}\sigma_{12}\frac{\partial\rho}{\partial x_2} + \frac{16}{75}q_2\frac{\partial u_1}{\partial x_2}\right) \\
&\quad -3\frac{\Pr p}{\mu}\left(\underline{-\frac{1}{3}\frac{\sigma_{22}}{\rho}\frac{\partial\sigma_{12}}{\partial x_2} - \frac{8}{15}\frac{\sigma_{21}}{\rho}\frac{\partial\sigma_{22}}{\partial x_2} + \frac{2}{15}\frac{\sigma_{11}}{\rho}\frac{\partial\sigma_{12}}{\partial x_2}}\right), \\
m_{222}^{R13I} &= -3\frac{\Pr p}{\mu}\left(\frac{3}{5}RT\frac{\partial\sigma_{22}}{\partial x_2} - \frac{3}{5}\frac{RT}{\rho}\sigma_{22}\frac{\partial\rho}{\partial x_2} - \frac{4}{25}q_1\frac{\partial u_1}{\partial x_2} \underline{- \frac{3}{5}\frac{\sigma_{22}}{\rho}\frac{\partial\sigma_{22}}{\partial x_2} + \frac{2}{5}\frac{\sigma_{12}}{\rho}\frac{\partial\sigma_{12}}{\partial x_2}}\right), \\
R_{12}^{R13I} &= -\frac{28}{5}\frac{\Pr p}{\mu}\left(\frac{1}{2}RT\frac{\partial q_1}{\partial x_2} + \frac{1}{2}Rq_1\frac{\partial T}{\partial x_2} - \frac{1}{2}\frac{RTq_1}{\rho}\frac{\partial\rho}{\partial x_2} \underline{- \frac{1}{2}\frac{q_1}{\rho}\frac{\partial\sigma_{22}}{\partial x_2} - \frac{1}{2}\frac{q_2}{\rho}\frac{\partial\sigma_{12}}{\partial x_2}}\right), \\
&\quad -\frac{28}{5}\frac{\Pr p}{\mu}\left(\frac{5}{7}RT\left(+\frac{1}{2}\sigma_{11}\frac{\partial u_1}{\partial x_2} + \frac{1}{2}\sigma_{22}\frac{\partial u_1}{\partial x_2}\right) \underline{- \frac{5}{6}\frac{\sigma_{12}}{\rho}\frac{\partial q_2}{\partial x_2} - \frac{5}{6}\frac{\sigma_{12}}{\rho}\sigma_{12}\frac{\partial u_1}{\partial x_2}}\right), \\
R_{22}^{R13I} &= -\frac{28}{5}\frac{\Pr p}{\mu}\left(\frac{2}{3}RT\frac{\partial q_2}{\partial x_2} + \frac{2}{3}Rq_2\frac{\partial T}{\partial x_2} - \frac{2}{3}\frac{RTq_2}{\rho}\frac{\partial\rho}{\partial x_2} \underline{- \frac{2}{3}\frac{q_2}{\rho}\frac{\partial\sigma_{22}}{\partial x_2} + \frac{1}{3}\frac{q_1}{\rho}\frac{\partial\sigma_{12}}{\partial x_2}}\right), \\
&\quad -\frac{28}{5}\frac{\Pr p}{\mu}\left(\frac{5}{21}RT\sigma_{21}\frac{\partial u_1}{\partial x_2} \underline{- \frac{5}{6}\frac{\sigma_{22}}{\rho}\frac{\partial q_2}{\partial x_2} - \frac{5}{6}\frac{\sigma_{22}}{\rho}\sigma_{12}\frac{\partial u_1}{\partial x_2}}\right) \\
\Delta^{R13I} &= -8\frac{\Pr p}{\mu}\left(RT\frac{\partial q_2}{\partial x_2} + \frac{5}{2}Rq_2\frac{\partial T}{\partial x_2} - \frac{RTq_2}{\rho}\frac{\partial\rho}{\partial x_2} \underline{- \frac{q_1}{\rho}\frac{\partial\sigma_{12}}{\partial x_2} - \frac{q_2}{\rho}\frac{\partial\sigma_{22}}{\partial x_2}} + RT\sigma_{12}\frac{\partial u_1}{\partial x_2}\right).
\end{aligned} \tag{5.51}$$

Eq. (5.51) omitting the highest order terms (terms with underlined in equations) are the expressions for the slightly linearized R13 moment equations [15],

From Eq. (5.48), one obtains the following equations for the steady state of 1DCF,

$$u_2 = 0,$$

$$\frac{\partial \sigma_{12}}{\partial x_2} = 0,$$

$$\frac{\partial p}{\partial x_2} + \frac{\partial \sigma_{22}}{\partial x_2} = 0,$$

$$\frac{\partial q_2}{\partial x_2} + \sigma_{12}\frac{\partial u_1}{\partial x_2} = 0,$$

$$\begin{aligned}
&-\frac{4}{15}\frac{\partial q_2}{\partial x_2} + \frac{4}{3}\sigma_{21}\frac{\partial u_1}{\partial x_2} + \frac{\partial \rho_{<112>}}{\partial x_2} = -\frac{p}{\mu}\sigma_{11}, \\
&\frac{8}{15}\frac{\partial q_2}{\partial x_2} - \frac{2}{3}\sigma_{21}\frac{\partial u_1}{\partial x_2} + \frac{\partial \rho_{<222>}}{\partial x_2} = -\frac{p}{\mu}\sigma_{22}, \\
&\frac{2}{5}\frac{\partial q_1}{\partial x_2} + p\frac{\partial u_1}{\partial x_2} + \sigma_{22}\frac{\partial u_1}{\partial x_2} + \frac{\partial \rho_{<122>}}{\partial x_2} = -\frac{p}{\mu}\sigma_{12},
\end{aligned} \tag{5.52}$$

$$\begin{aligned}
&-\frac{5}{2}RT\frac{\partial \sigma_{12}}{\partial x_2} - \frac{\sigma_{12}}{\rho}\frac{\partial p}{\partial x_2} - \frac{\sigma_{11}}{\rho}\frac{\partial \sigma_{12}}{\partial x_2} - \frac{\sigma_{12}}{\rho}\frac{\partial \sigma_{22}}{\partial x_2} \\
&+\frac{7}{5}q_2\frac{\partial u_1}{\partial x_2} + \frac{1}{2}\frac{\partial \rho_{rr<12>}}{\partial x_2} + \rho_{<112>}\frac{\partial u_1}{\partial x_2} = -\frac{\Pr p}{\mu}q_1
\end{aligned},$$

$$\begin{aligned}
&-\frac{5}{2}RT\frac{\partial p}{\partial x_2} - \frac{5}{2}RT\frac{\partial \sigma_{22}}{\partial x_2} - \frac{\sigma_{22}}{\rho}\frac{\partial p}{\partial x_2} - \frac{\sigma_{21}}{\rho}\frac{\partial \sigma_{12}}{\partial x_2} - \frac{\sigma_{22}}{\rho}\frac{\partial \sigma_{22}}{\partial x_2} \\
&+\frac{2}{5}q_1\frac{\partial u_1}{\partial x_2} + \frac{1}{2}\frac{\partial \rho_{rr<22>}}{\partial x_2} + \frac{1}{6}\frac{\partial \rho_{rrss}}{\partial x_2} + \rho_{<212>}\frac{\partial u_1}{\partial x_2} = -\frac{\Pr p}{\mu}q_2
\end{aligned}.$$

If one uses the computational results from kinetic models for *all* moments, that is to say, without considering the closure relations (5.49-5.51), the above Eq. (5.52) should be satisfied. Indeed, the first four expressions in Eq. (5.52), that u_2, σ_{12}, p_{22}, and $q_2 + u_1\sigma_{12}$ are constant in the whole domain at steady state, have been applied in Chapter 4 already, are used also here to check whether the converged computational results are at

steady state. The verification of the last five expressions in Eq. (5.52) is difficult, since the computation is related to the calculation of derivatives. If a proper expression for the derivative is chosen, the last five expressions in Eq. (5.52) are found to be satisfied from the results of kinetic models as will be shown in Section 5.5.

Expressions to compute trace-free pressure tensor σ_{ij} and heat flux q_i, which are values at the right hand side of Eq (5.52), are rewritten from Eq. (5.52) for 1DCF at steady state as

$$\sigma_{11}^{M} = -\frac{\mu}{p}\left(-\frac{4}{15}\frac{\partial q_2}{\partial x_2}+\frac{4}{3}\sigma_{21}\frac{\partial u_1}{\partial x_2}+\frac{\partial \rho_{<112>}}{\partial x_2}\right),$$

$$\sigma_{22}^{M} = -\frac{\mu}{p}\left(+\frac{8}{15}\frac{\partial q_2}{\partial x_2}-\frac{2}{3}\sigma_{21}\frac{\partial u_1}{\partial x_2}+\frac{\partial \rho_{<222>}}{\partial x_2}\right),$$

$$\sigma_{12}^{M} = -\frac{\mu}{p}\left(+\frac{2}{5}\frac{\partial q_1}{\partial x_2}+p\frac{\partial u_1}{\partial x_2}+\sigma_{22}\frac{\partial u_1}{\partial x_2}+\frac{\partial \rho_{<122>}}{\partial x_2}\right), \tag{5.53}$$

$$q_1^{M} = -\frac{\mu}{\mathrm{Pr}\,p}\left(-\frac{5}{2}RT\frac{\partial \sigma_{12}}{\partial x_2}-\frac{\sigma_{12}}{\rho}\frac{\partial p}{\partial x_2}-\frac{\sigma_{11}}{\rho}\frac{\partial \sigma_{12}}{\partial x_2}-\frac{\sigma_{12}}{\rho}\frac{\partial \sigma_{22}}{\partial x_2}\right)$$
$$-\frac{\mu}{\mathrm{Pr}\,p}\left(+\frac{7}{5}q_2\frac{\partial u_1}{\partial x_2}+\frac{1}{2}\frac{\partial \rho_{rr<12>}}{\partial x_2}+\rho_{<112>}\frac{\partial u_1}{\partial x_2}\right),$$

$$q_2^{M} = -\frac{\mu}{\mathrm{Pr}\,p}\left(-\frac{5}{2}RT\frac{\partial p}{\partial x_2}-\frac{5}{2}RT\frac{\partial \sigma_{22}}{\partial x_2}-\frac{\sigma_{22}}{\rho}\frac{\partial p}{\partial x_2}-\frac{\sigma_{21}}{\rho}\frac{\partial \sigma_{12}}{\partial x_2}-\frac{\sigma_{22}}{\rho}\frac{\partial \sigma_{22}}{\partial x_2}\right)$$
$$-\frac{\mu}{\mathrm{Pr}\,p}\left(+\frac{2}{5}q_1\frac{\partial u_1}{\partial x_2}+\frac{1}{2}\frac{\partial \rho_{rr<22>}}{\partial x_2}+\frac{1}{6}\frac{\partial \rho_{rrss}}{\partial x_2}+\rho_{<212>}\frac{\partial u_1}{\partial x_2}\right).$$

The test of the different macroscopic equations will be done as follows: The closure relations from the Grad13 equations (5.49-5.50), or from the R13s equations (5.49, 5.51), are used to relate the third and fourth degree moments to the lower degree moments. Results from the kinetic models for first and second degree moments (such as density, heat flux, etc.) are then used in the right hand side of Eq. (5.53). This gives values for σ_{ij}^{M} and q_i^{M}, i.e. the left hand side of Eq. (5.53). The values computed this way will not necessarily be equal to those computed from the kinetic models. From the difference, one

can infer which set moment equations fits the kinetic model best. A similar method is used for the NSF equations and the Burnett equations that are presented in Section 5.2.

5.4 The Knudsen layer

At small Kn numbers, the behavior of a gas is conveniently expressed in the sum of two terms, which are the bulk part (or fluid-dynamic part, whose length scale of variation is of the order of geometry length, describes the overall behavior of the gas) and the boundary layer part, or Knudsen layer part, which is appreciable only in a thin layer with thickness of the order of the mean free path adjacent to the boundary, and represents a correction to the bulk part. Each term can be expanded in a power series of the Knudsen number [1, 5, 8, 9, 79].

The NSF equations are the equations at the first order of Kn, the Burnett equations are obtained at the second order of Kn, the Grad13 equations are equations between second and third order of Kn, the slightly linearized R13 equations are equations at the third order of Kn, and the original R13 are equations between third and fourth order of Kn [15]. Therefore, it will be expected that at small Knudsen numbers the R13s give the best results, followed by the Grad13, the Burnett equations, and that the NSF equations will give the worst results. This expectation will be seen to be true from the results in Section 5.7.2. In [10], Struchtrup gives detailed discussion about the Knudsen layer for the Burnett and super-Burnett equations and the original R13 equations, and shows that the boundary layer of the heat flux q_1 (parallel to the plates) from the original R13 equations has a different sign than that from the Burnett and super-Burnett equations (this issue is also shown in Section 5.7.2, such as graph (c) in Figure 5.2). Also in Ref. [10], the shape of the q_1 boundary layer of the R13 equations is found to be $A\sinh\left(\sqrt{\frac{5}{9}}\frac{x/L-0.5}{\mathrm{Kn}}\right)$, A denotes the amplitude, x is the position considered, and L is the domain width.

Since macroscopic continuum equations describe the bulk part better than the Knudsen layer part, it makes sense that the accuracy of macroscopic continuum equations in the middle part of the flow domain is higher than near the boundary. When the Knudsen number increases, the thickness of the boundary layer, which is about several mean free paths, also increases, and the bulk part becomes thinner and thinner. and the effect is lower accuracy of macroscopic continuum equations. Finally, the boundary layer extends over the full domain, and no bulk part in the domain.

5.5 Description about the test method

Since the boundary conditions for macroscopic continuum equations (except the NSF equations) are still developing and non-mature [15, 26, 49], a specific way will be used in the tests, in order to avoid the use of boundary conditions.

The test of the different macroscopic equations is done as follows: The closure relations from the Grad13 equations (5.49-5.50), or from the R13s equations (5.49, 5.51), are used to relate the third and fourth degree moments to the lower degree moments. Results from the kinetic models for 13 moments (i.e. ρ, u_i, T, σ_{ij} and q_i) are then used in the right hand side of Eq. (5.53). This gives values for σ_{ij}^M and q_i^M, i.e. the left hand side of Eq. (5.53). The values computed this way will not necessarily be equal to those computed from the kinetic models. From the difference, one can infer which set moment equations fits the kinetic model best. A similar method is used for the NSF equations and the Burnett equations in the Section 5.2, Eqs. (5.32-5.34). Some third-degree and fourth-degree moments will be treated similarly, in case of Grad13 and the R13s equations.

5.6 Test examples

The numerical test problem is one-dimensional Couette flow (1DCF) at steady state and kinetic models used are the BGK and the ES-BGK models with Maxwellian molecules, as described in Chapter 4. Table 5.2 shows the situations for the numerical tests used in this chapter, and Table 5.3 shows the parameters used in the numerical tests of kinetic models, while common parameters in the tests are the same as in Section 4.3. Some analyses, same as done in Chapter 4, has been done to show that the final computational results are converged and correspond to steady state. This time, the direct output macroscopic parameters are ρ, u_1, u_2, T, p, p_{11}, p_{22}, σ_{12}, q_1, q_2, and the third-degree and fourth-degree moments ρ_{112}, ρ_{122}, ρ_{222}, ρ_{rr12}, ρ_{rr22} and ρ_{rrss}. Other interesting parameters can be calculated from these.

Table 5.2: Situations of numerical tests of kinetic models for 1DCF in chapter 5

Situation	Knudsen number	Plate velocity (m/s)	Domain width (m)	Mach number	Reynolds number
Sb	0.025	300.0	0.3533	0.975	50.345
Sd	0.1	300.0	0.08833	0.975	12.587

Sf	0.5	300.0	0.01767	0.975	2.518
Sh	1.0	300.0	0.008833	0.975	1.259
Sk	0.5	600.0	0.01767	1.950	5.036
Sl	0.5	1000.0	0.01767	3.251	8.393
Sm	0.1	600.0	0.08833	1.950	25.174
Sn	0.1	1000.0	0.08833	3.251	41.970

Table 5.3: Parameters in the numerical tests of kinetic models for 1DCF in chapter 5

Case	Situation	Number of cells	Number of iteration	Ratio of cell width over mean free path	Number of velocities	Bound of velocities (m/s)	
						X1 direction	X2 (or X3)
5.1	Sb	200	60000	5.0	11*10*10	-1100.0, 1400.0	-1100.0, 1100.0
5.2	Sd	100	60000	10.0	11*10*10	-1100.0, 1400.0	-1100.0, 1100.0
5.3	Sf	100	60000	50.0	11*10*10	-1100.0, 1300.0	-1100.0, 1100.0
5.4	Sh	50	60000	50.0	11*10*10	-1100.0, 1300.0	-1100.0, 1100.0
5.5	Sk	100	60000	50.0	13*12*12	-1100.0, 1700.0	-1300.0, 1300.0
5.6	Sl	100	60000	50.0	15*14*14	-1200.0, 2200.0	-1600.0, 1600.0
5.7	Sm	100	60000	10.0	13*11*11	-1100.0, 1700.0	-1200.0, 1200.0
5.8	Sn	100	60000	10.0	15*13*13	-1100.0, 2100.0	-1400.0, 1400.0

5.7 Results and discussion

5.7.1 Some important notes on dealing with data

Four choices to compute the derivative have been used to compute trace-free pressure tensor σ_{ij} and heat flux q_i based on Eq. (5.53) and results of kinetic models (BGK or ES-BGK) for all moments at the right hand side of Eq. (5.53): three point formula (central difference) in [64], five point formula in [64], and the simplest and best expression mentioned in [80]

Let us consider the function $f = f(x)$, x is discretized as x_i, where $i = 1, 2, \ldots$, and the step is Δx, the first order derivative is denoted as $\frac{df}{dx} = f'$, and the second order derivative is denoted as $\frac{d^2 f}{dx^2} = f''$. Then the three-point formula in [64] is

$$\frac{df}{dx}\Big|_{x=x_i} = \frac{1}{2\Delta x}(f(x_{i+1}) - f(x_{i-1})). \tag{5.54}$$

The five-point formula in [64] gives

$$\frac{df}{dx}\Big|_{x=x_i} = \frac{1}{12\Delta x}(f(x_{i-2}) - 8f(x_{i-1}) + 8f(x_{x+1}) - f(x_{i+2})). \tag{5.55}$$

The simplest expression in [80] gives

$$\frac{df}{dx}\Big|_{x=x_i} = \frac{1}{\Delta x}\text{minmod}(f(x_{i+1}) - f(x_i), f(x_i) - f(x_{i-1})). \tag{5.56}$$

The best choice in [80] gives

$$\frac{df}{dx}\Big|_{x=x_i} = \frac{1}{\Delta x}\text{minmod}\left(f(x_{i+1}) - f(x_i) - \frac{1}{2}f''(x_{i+1})\Delta x, f(x_i) - f(x_{i-1}) + \frac{1}{2}f''(x_i)\Delta x\right),$$

$$f''(x_i) = \frac{1}{\Delta x}\text{minmod}(f(x_{i+1}) - 2f(x_i) + f(x_{i-1}), f(x_i) - 2f(x_{i-1}) + f(x_{i-2})), \tag{5.57}$$

where the definition of the minmod function refer to Section 3.2.1.

After some numerical tests, it is found that using the central difference formula (5.54) to compute the first order derivatives gives the computed values of σ_{ij}^K and q_i^K closest to the results of σ_{ij} and q_i from the same kinetic model directly.

Another thing that needs be mentioned is that if we do the above computation directly, the computed σ_{ij} and q_i have some small oscillations and a jump near the boundaries, see Figure 5.1. In order to reduce and eliminate that oscillation and jump phenomena, we smoothed the original results from kinetic models by half position points, so that values at new positions are the average values of two adjacent old position points, and then apply these smoothed data, instead of original results, in the computation. It is found that the oscillation phenomenon of the computed σ_{ij}^K and q_i^K based on the smoothed data decreases a lot, while at the same time, the profile from smoothed data is the same as the profile from those original results from kinetic models.

Therefore, two points, central differences for derivatives and smoothed original data, are applied in the following computations. Figure 5.1 shows an example (case 5.2:

Kn=0.1, 300.0 m/s plate velocity; BGK model) of the original and computed σ_{ij}^{K} and q_i^{K} without and with the smoothness procedure. Note that since the profile of σ_{11} is similar to the profile of $-\sigma_{22}$, and no new information can be obtained from graphs of σ_{22}, graphs of σ_{22} are omitted in the figures in this chapter. Tables D.5-D.6 in Appendix D show average relative errors of the computed σ_{ij} compared to (smoothed) original data, which are smaller than 0.01 for all test cases. For relative error is meaningless when a quantity approaches zero, and values of q_i are near to zero in the middle domain, thus it is hard to choose a domain to compute relative error for q_i. Therefore for the heat flux q_i, the average relative errors are not computed

Normally, performances shown by the ES-BGK model and its corresponding sets of macroscopic equations are also shown by the BGK model and its corresponding sets of macroscopic equations. Therefore, in the following discussion, we will mention kinetic model generally, and not specifically mention the BGK model or the ES-BGK model.

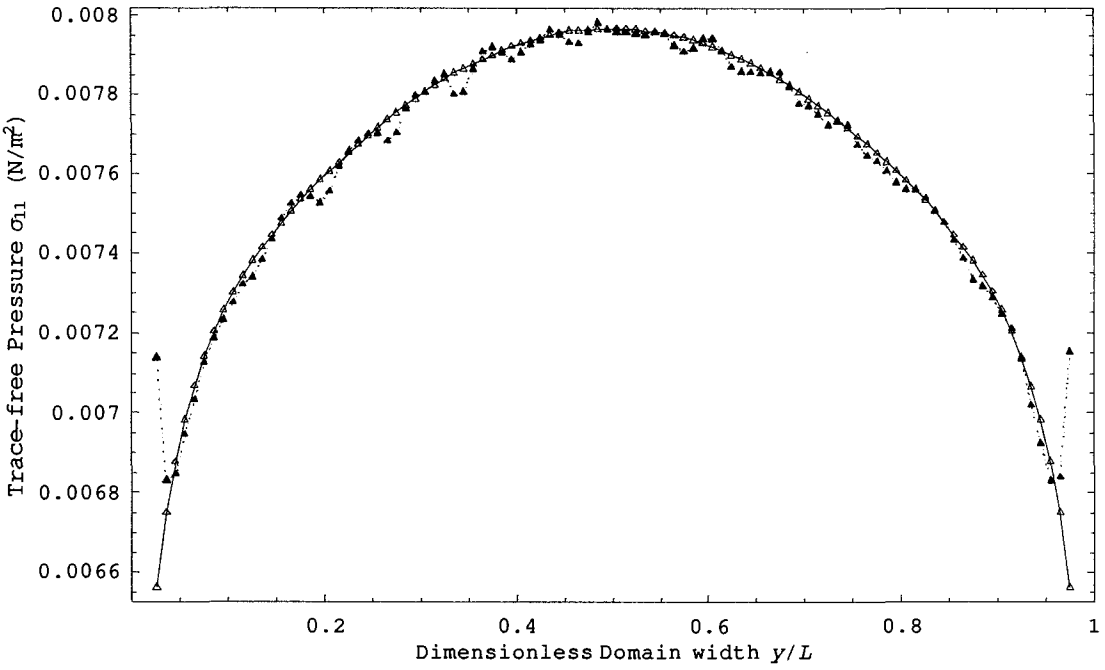

(a)

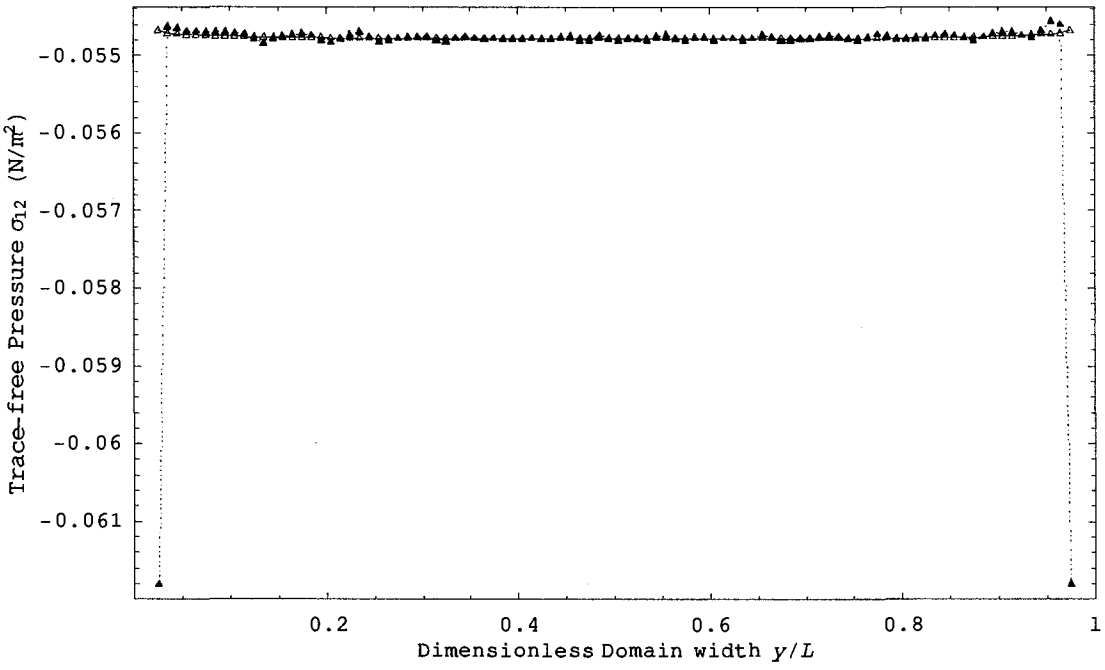

(b)

Figure 5.1: Comparison of original and computed trace-free pressure and heat flux (BGK model, case 5.2: Kn=0.1, 300.0 m/s plate velocity) (Triangle for original results, Triangle filled for computed results from Eq. (5.53), Diamond for original results smoothed by half number position points, Diamond filled for computed results from Eq. (5.53) with smoothed original data)

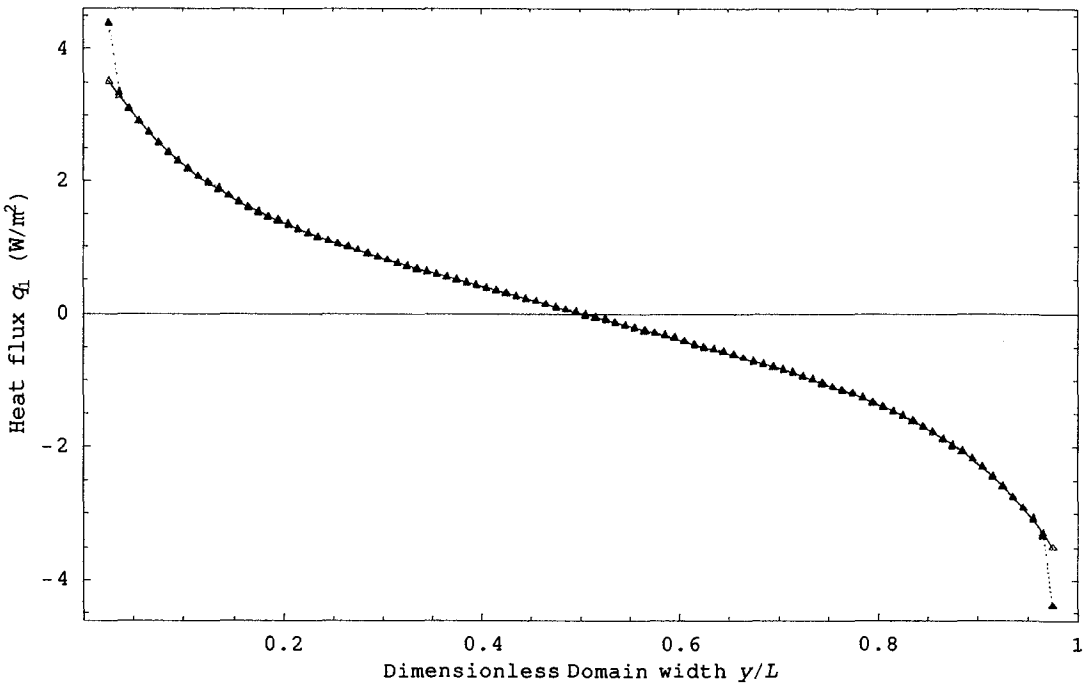

(c)

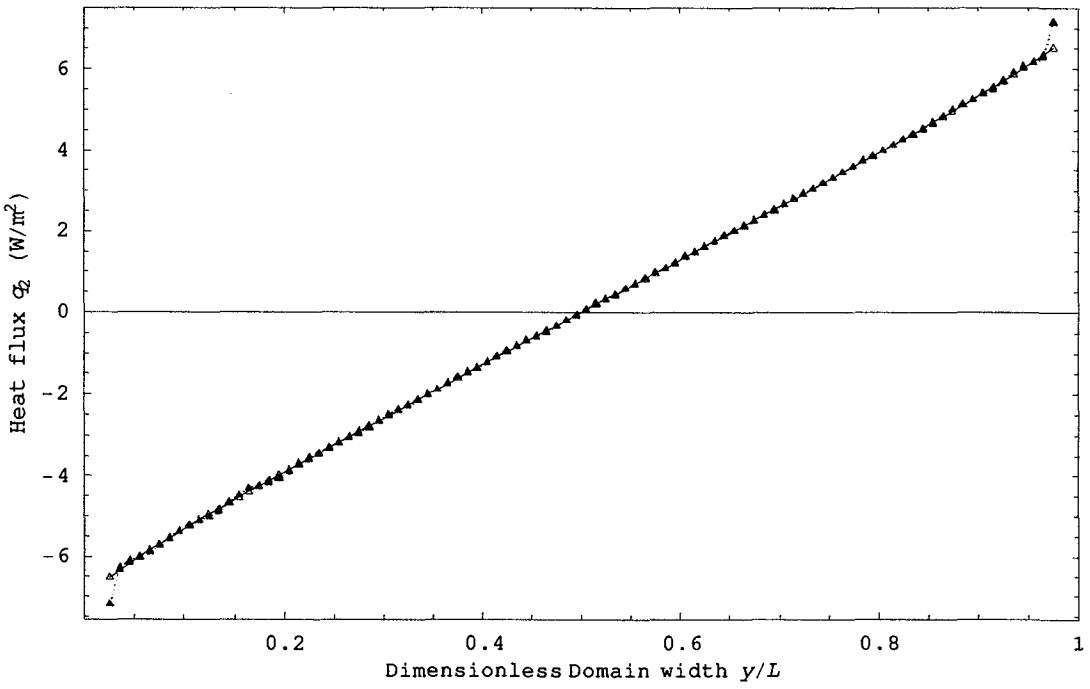

(d)

Figure 5.1: Comparison of original and computed trace-free pressure and heat flux (BGK model, case 5.2: Kn=0.1, 300.0 m/s plate velocity) (Triangle for original results, Triangle filled for computed results from Eq. (5.53), Diamond for original results smoothed by half number position points, Diamond filled for computed results from Eq. (5.53) with smoothed original data)

5.7.2 Results and discussion of σ_{ij} and q_i

Figures 5.2 to 5.5 show the (smoothed) original σ_{ij} and q_i, and the computed σ_{ij} and q_i based on the NSF equations (5.32), the Burnett equations (5.33-5.34), the Grad13 equations (5.49, 5.50, 5.53), the original and slightly linearized R13 equations (5.49, 5.51, 5.53), and the kinetic model itself, Eq. (5.53), with all (smoothed) original data at the right hand side. The test cases considered are case 5.1 (Kn=0.025, 300.0 m/s plate velocity) with the BGK model, case 5.7 (Kn=0.1, 600.0 m/s plate velocity) with the BGK model, case 5.6 (Kn=0.5, 1000.0 m/s plate velocity) with the ES-BGK model, and case 5.4 (Kn=1.0, 300.0 m/s plate velocity) with the ES-BGK model. Tables D.5-D.6 in Appendix D show the average relative errors of σ_{ij} between the above sets of macroscopic continuum equations and the kinetic model.

Generally, the computed values of σ_{ij} and q_i from all sets of macroscopic equations fit the original data well at small plate velocities (i.e. small Mach numbers) and small Knudsen numbers, and not so well at large plate velocities or/and large Knudsen numbers. In case 5.1 (Kn=0.025, 300.0 m/s plate velocity, Figure 5.2), the computed values of σ_{11}, σ_{22}, q_1 and q_2 give a very good agreement with the original data in the middle part for all models but the NSF equations. Recall that the NSF equations do not account for any rarefaction effects of σ_{11}, σ_{22} and q_1, and just gives their values as zero, while their values are not zero even in the middle domain. The R13s equations give the same shape as the kinetic model near the boundary, while the Burnett equations differ in shape (if the curve from the R13s is upward, then it from the Burnett is downward]. The computed values of σ_{12} are a good fit with the original data in the middle part, but not so good near the boundary. Therefore, at small Knudsen numbers, the R13 equations give the best results, followed by the Grad13, the Burnett equations, and the NSF equations, which give the worst result. When the plate velocity or/and the Knudsen number increase, the fitness becomes worse. As an example, in case 5.6 (Kn=0.5, 1000.0 m/s plate velocity, Figure 5.4), the computed σ_{ij} and q_i from the R13s even all have the

opposite sign as the original data. The above results are not surprising based on the description about the Knudsen layer in Section 5.4.

Let us consider the original and slightly linearized R13s. At small Knudsen numbers and plate velocities, results from both models are similar, while at large Knudsen number or large plate velocities, results from the slightly linearized R13 fit the original data from kinetic model better than results from the original R13. The original R13 equations only have some terms of the fourth order of Kn, but not all terms [15], so it might not be surprising that their results at some situations would be worse than results from the slightly linearized R13. Related to the complexity of equations, between these two R13models, the slightly linearized R13 is suggested, instead of the original R13, for their simpler form.

Next, let us compare the Grad13 and the R13s equations. At small Kn number and small plate velocities, results from the R13s fit the original data better than results from the Grad13, while at large Kn number and large plate velocities, it seems the conclusion is opposite, and it is hard to say which one is better for intermediate situations. Normally, the original values of σ_{ij} and q_i locate in between the values from the Grad13 and them from the R13s for large Kn numbers or large plate velocities, while for other situations, the original values of σ_{ij} and q_i locate beyond the values from the Grad13 and them from the R13s.

Then, let us consider the NSF equations and the Burnett equations. The expressions of σ_{12} and q_2 are the same from these two sets of equations. The NSF equations do not account for any rarefaction effect on σ_{11}, σ_{22} and q_1, while the Burnett equations do. At small Kn numbers, results from the Burnett equations fit the data from the kinetic model better than results from the NSF equations, while it is hard to say which one is better for other situations. Normally the original values of σ_{11}, σ_{22} and q_1 locate in between the values from the Burnett equations and them from the NSF equations (except q_1 for case 5.1-5.2)

Finally, let us consider the Grad13 and the Burnett equations. It is found that results from the Grad13 fit the original data from kinetic model better than results from the Burnett equations for almost all test cases.

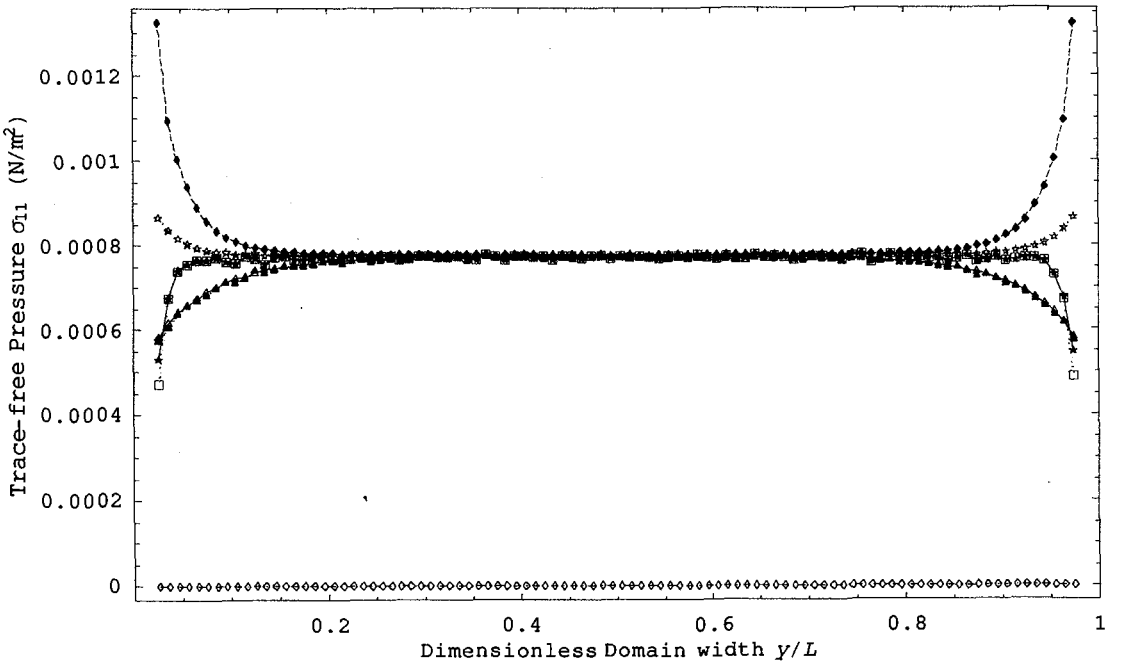

(a)

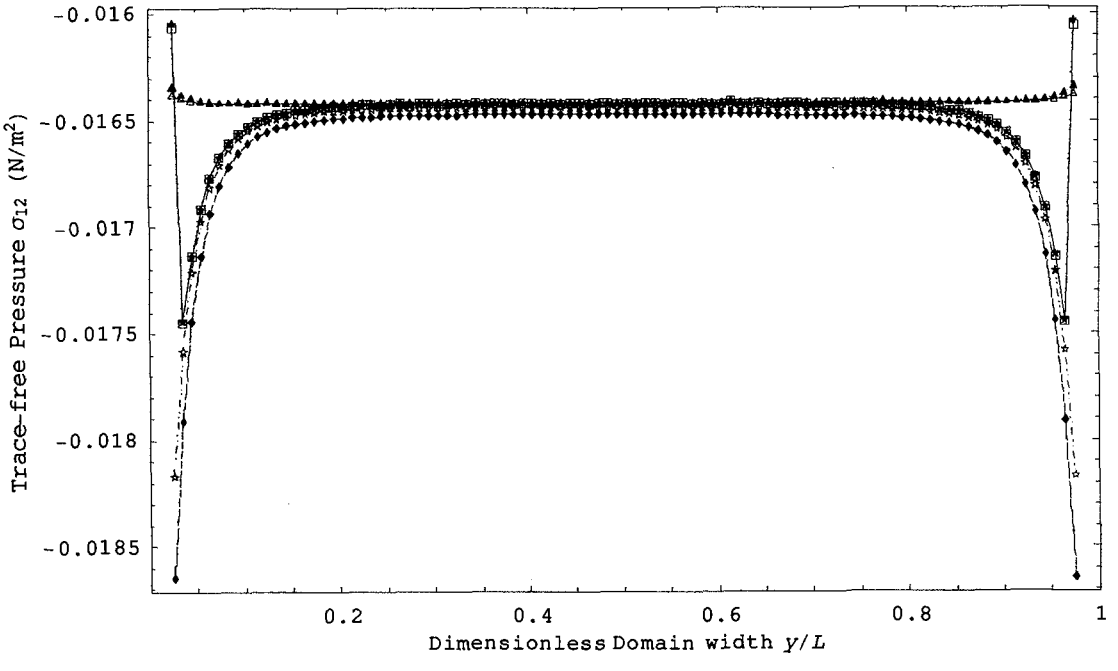

(b)

Figure 5.2: Results of trace-free pressure and heat flux from the BGK model and its corresponding sets of macroscopic equations (case 5.1: Kn=0.025, 300.0 plate velocity) (Triangle for original values from the BGK, Triangle filled for computed values from the BGK based on Eq. (5.53), Diamond for the NSF, Diamond filled for the Burnett, Star for the Grad13, Star filled for the original R13, Box for the slightly linearized R13)

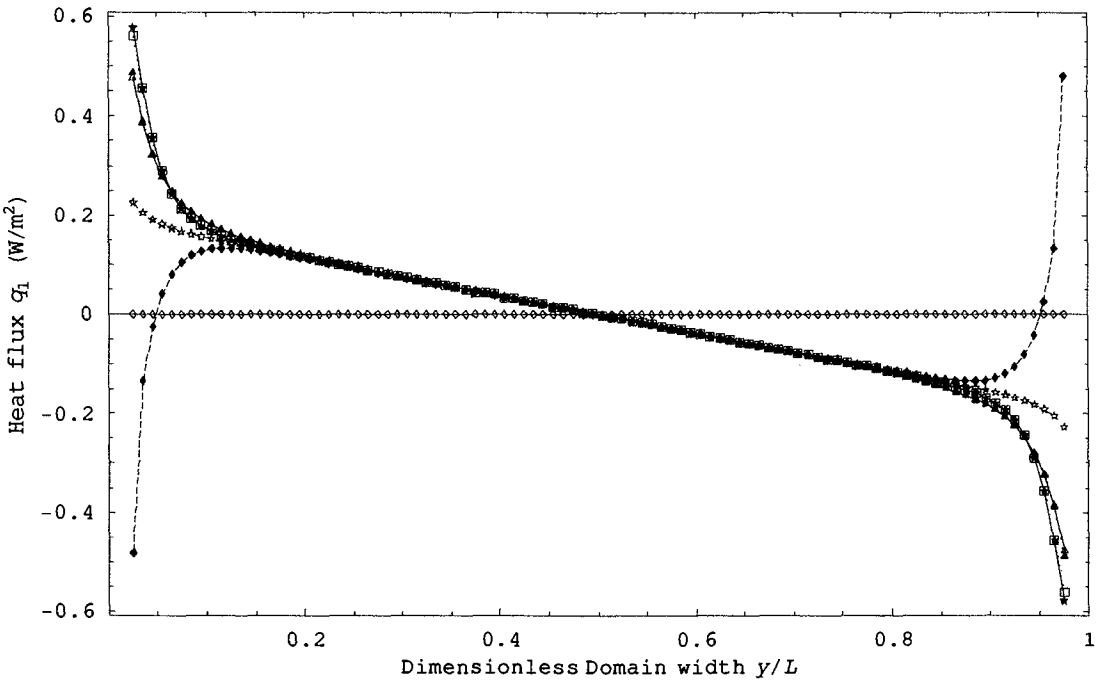

(c)

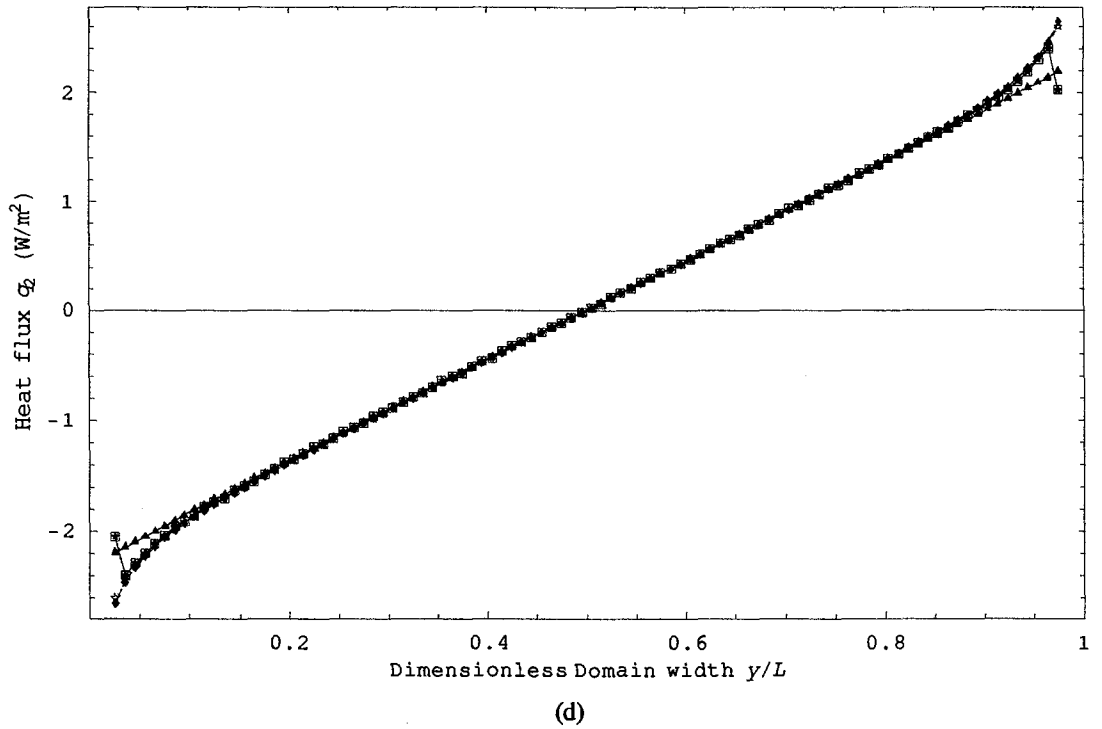

(d)

Figure 5.2: Results of trace-free pressure and heat flux from the BGK model and its corresponding sets of macroscopic equations (case 5.1: Kn=0.025, 300.0 plate velocity) (Triangle for original values from the BGK, Triangle filled for computed values from the BGK based on Eq. (5.53), Diamond for the NSF, Diamond filled for the Burnett, Star for the Grad13, Star filled for the original R13, Box for the slightly linearized R13)

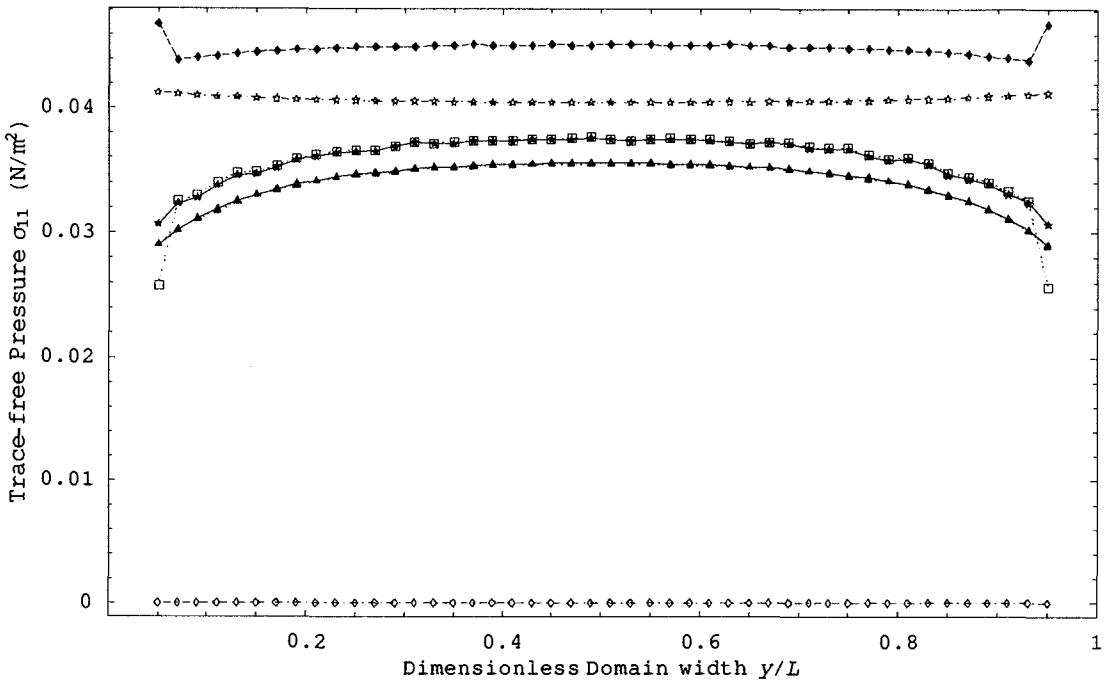

(a)

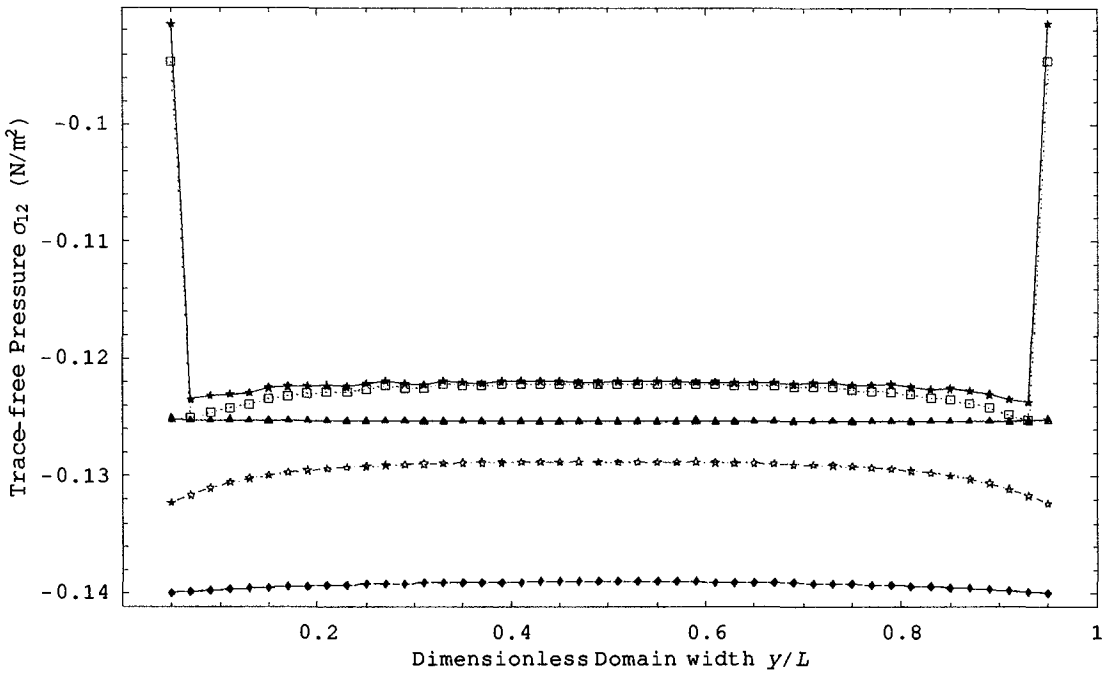

(b)

Figure 5.3: Results of trace-free pressure and heat flux from the BGK model and its corresponding sets of macroscopic equations (case 5.7: Kn=0.1, 600.0 plate velocity) (Triangle for original values from the BGK, Triangle filled for computed values from the BGK based on Eq. (5.53), Diamond for the NSF, Diamond filled for the Burnett, Star for the Grad13, Star filled for the original R13, Box for the slightly linearized R13)

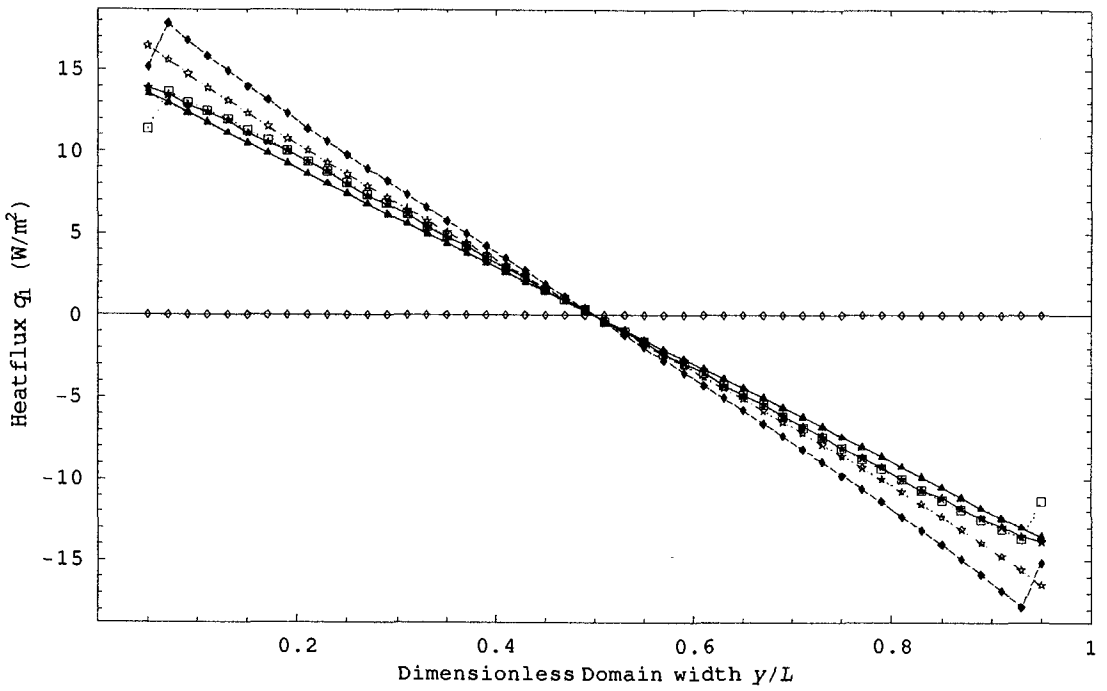

(c)

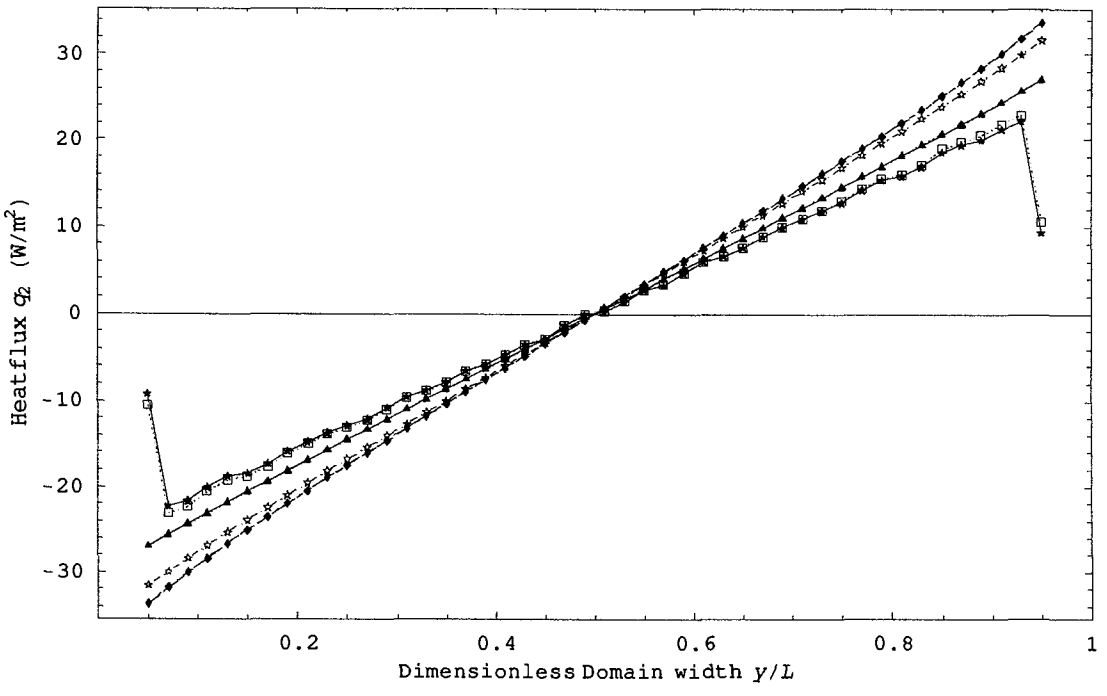

(d)

Figure 5.3: Results of trace-free pressure and heat flux from the BGK model and its corresponding sets of macroscopic equations (case 5.7: Kn=0.1, 600.0 plate velocity) (Triangle for original values from the BGK, Triangle filled for computed values from the BGK based on Eq. (5.53), Diamond for the NSF, Diamond filled for the Burnett, Star for the Grad13, Star filled for the original R13, Box for the slightly linearized R13)

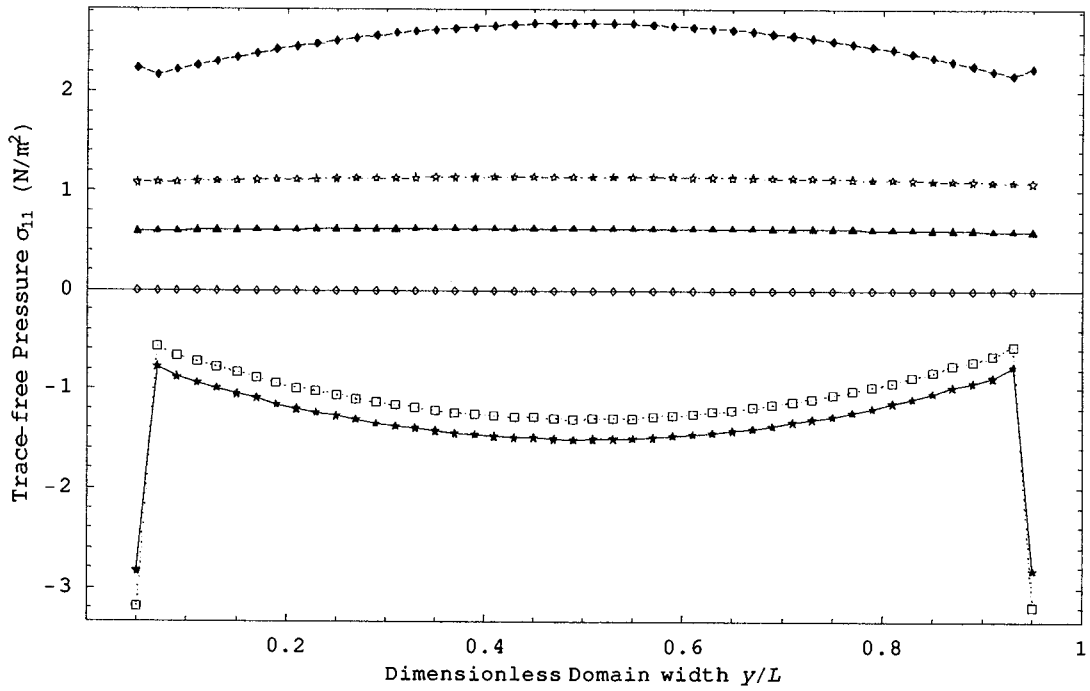

(a)

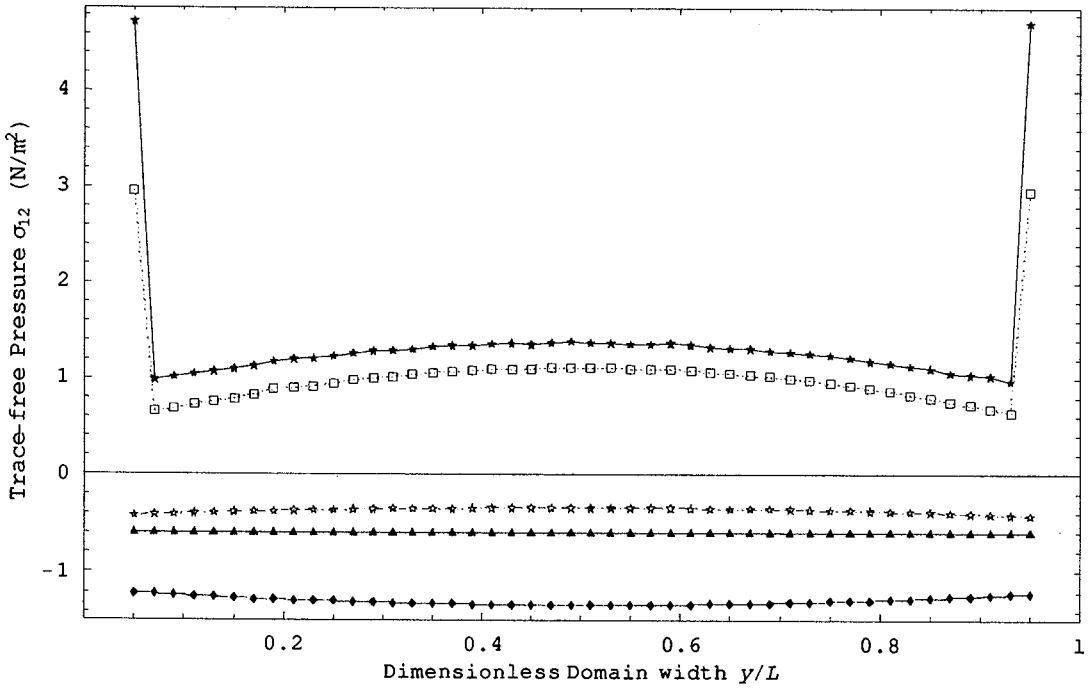

(b)

Figure 5.4: Results of trace-free pressure and heat flux from the ES-BGK model and its corresponding sets of macroscopic equations (case 5.6: Kn=0.5, 1000.0 plate velocity) (Triangle for original values from the ES-BGK, Triangle filled for computed values from the ES-BGK based on Eq. (5.53), Diamond for the NSF, Diamond filled for the Burnett, Star for the Grad13, Star filled for the original R13, Box for the slightly linearized R13)

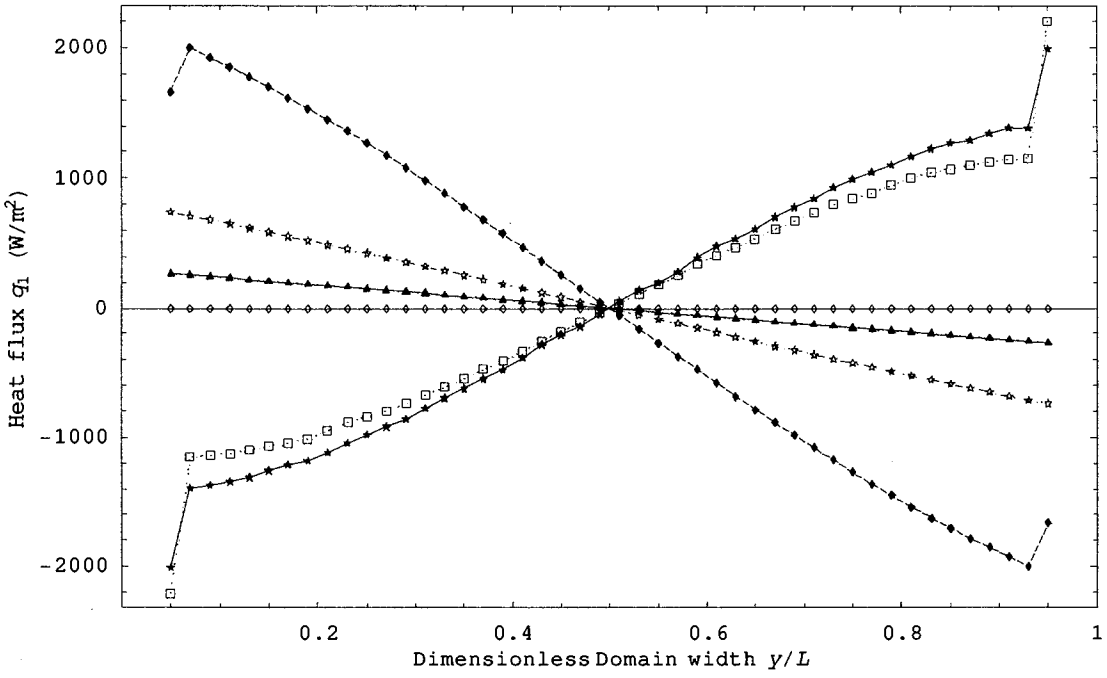

(c)

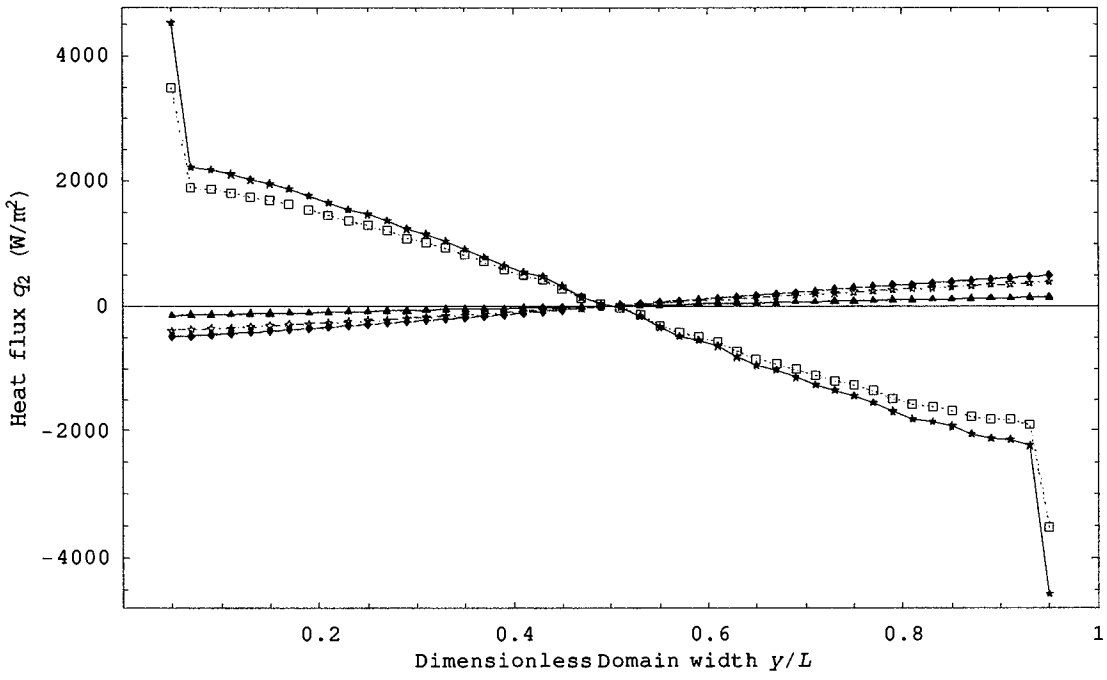

(d)

Figure 5.4: Results of trace-free pressure and heat flux from the ES-BGK model and its corresponding sets of macroscopic equations (case 5.6: Kn=0.5, 1000.0 plate velocity) (Triangle for original values from the ES-BGK, Triangle filled for computed values from the ES-BGK based on Eq. (5.53), Diamond for the NSF, Diamond filled for the Burnett, Star for the Grad13, Star filled for the original R13, Box for the slightly linearized R13)

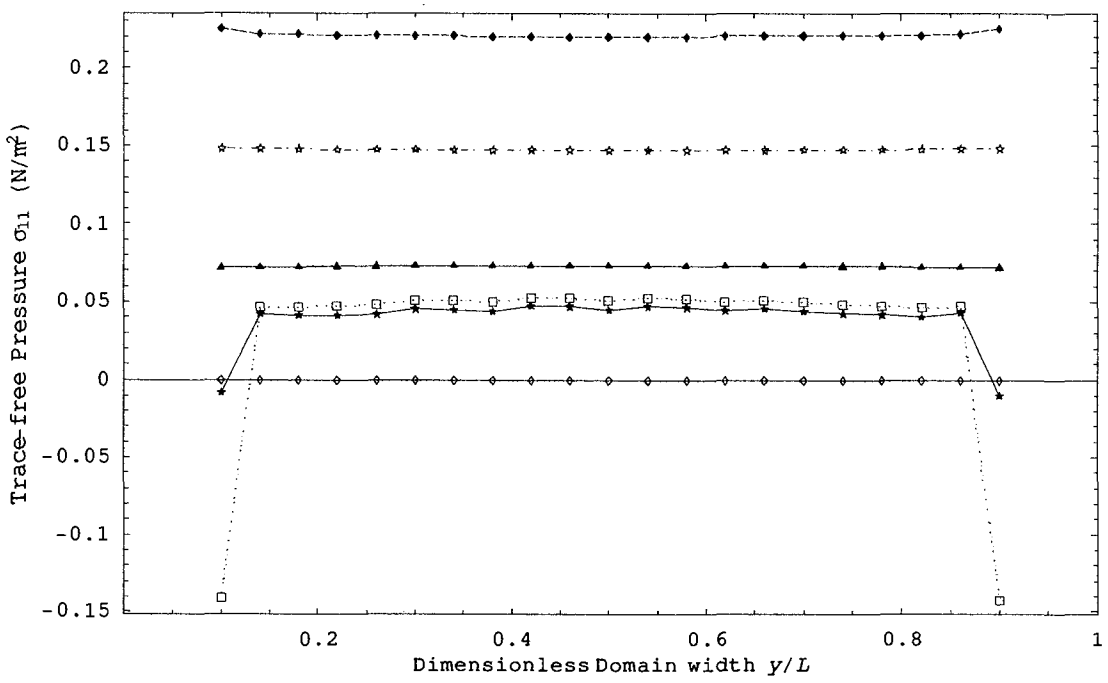

(a)

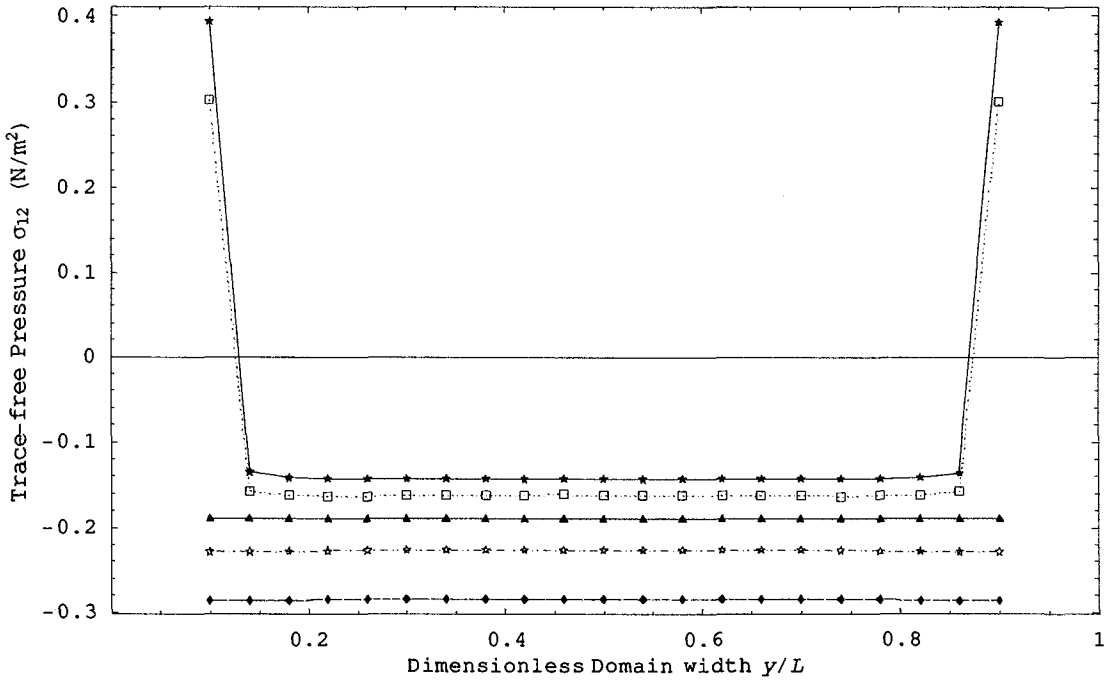

(b)

Figure 5.5: Results of trace-free pressure and heat flux from the ES-BGK model and its corresponding sets of macroscopic equations (case 5.4: Kn=1.0, 300.0 m/s plate velocity) (Triangle for original values from the ES-BGK, Triangle filled for computed values from the ES-BGK based on Eq. (5.53), Diamond for the NSF, Diamond filled for the Burnett, Star for the Grad13, Star filled for the original R13, Box for the slightly linearized R13)

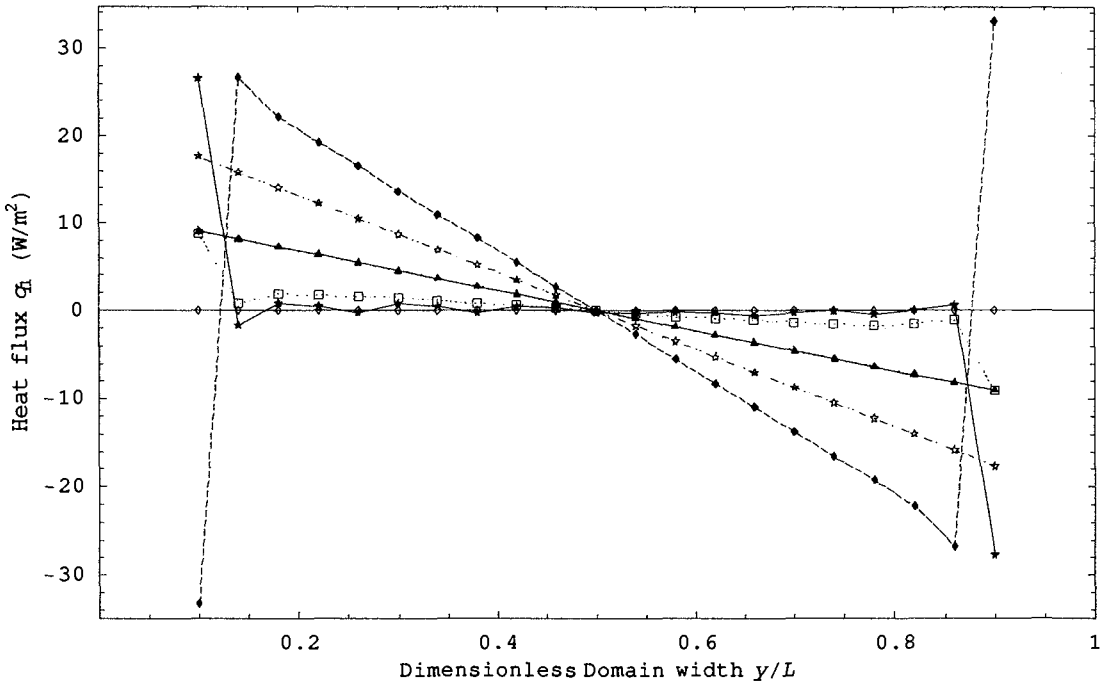

(c)

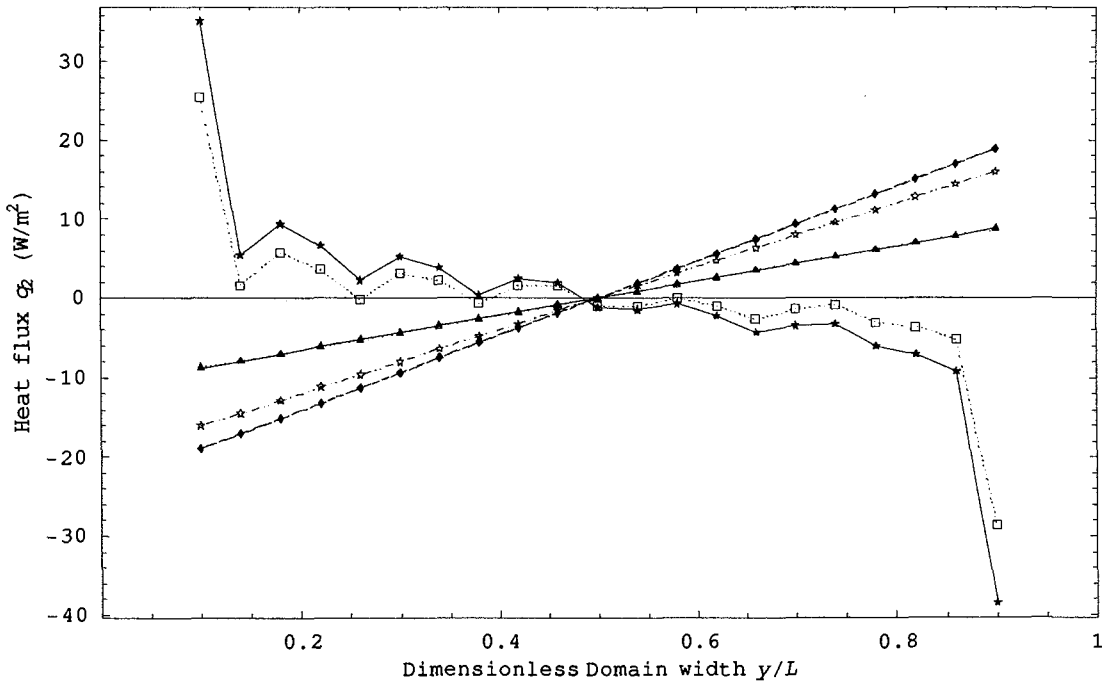

(d)

Figure 5.5: Results of trace-free pressure and heat flux from the ES-BGK model and its corresponding sets of macroscopic equations (case 5.4: Kn=1.0, 300.0 m/s plate velocity) (Triangle for original values from the ES-BGK, Triangle filled for computed values from the ES-BGK based on Eq. (5.53), Diamond for the NSF, Diamond filled for the Burnett, Star for the Grad13, Star filled for the original R13, Box for the slightly linearized R13)

5.7.3 Results and discussion about third-degree and fourth-degree moments

The only difference among the Grad13, the R13s (original and slightly linearized) and the kinetic model to compute σ_{ij} and q_i is how the third-degree and fourth-degree moments $\rho_{<ijk>}$, $\rho_{rr<ij>}$ and ρ_{rrss} used in Eq. (5.53) are computed. In this section, their values from the Grad13, the R13s and the kinetic model will be compared, and average relative errors among them are shown in Tables D.7-D.9 of Appendix D. As two examples, Figure 5.6 shows the comparison in case 5.1 (Kn=0.025, 300.0 m/s plate velocity) for the BGK model, while Figure 5.7 shows the comparison in case 5.6 (Kn=0.5, 1000.0m/s plate velocity) for the ES-BGK model.

After analysis, it is found that the computed values of the moments R_{22}, $\rho_{rr<22>}$ from the Grad13 fit the data from the kinetic model better than or at least similar to results from the R13s for all test cases, while for $\rho_{<ijk>}$, R_{12} and ρ_{rr12}, the conclusion is opposite, that is the R13s equations give better results. At small Knudsen numbers or small plate velocities, the computed values of ρ_{rrss} from the Grad13 and the R13s fit the original data very well, while not good for large Kn and large plate velocities. The computed Δ from the Grad13 and the R13s do not fit the original data.

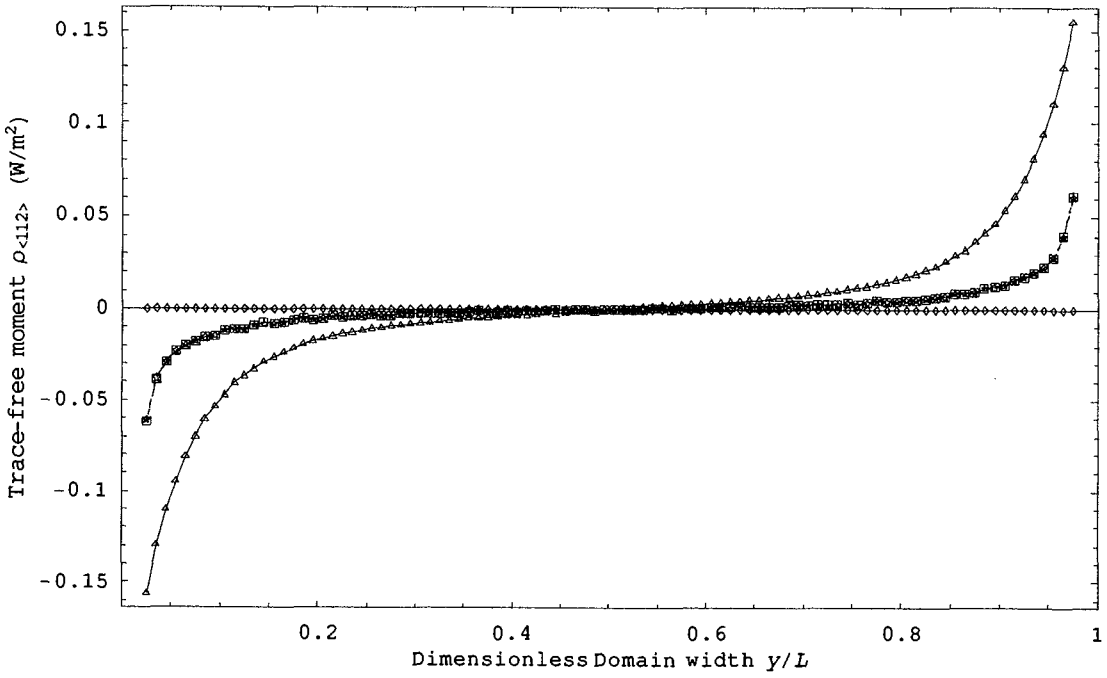

(a)

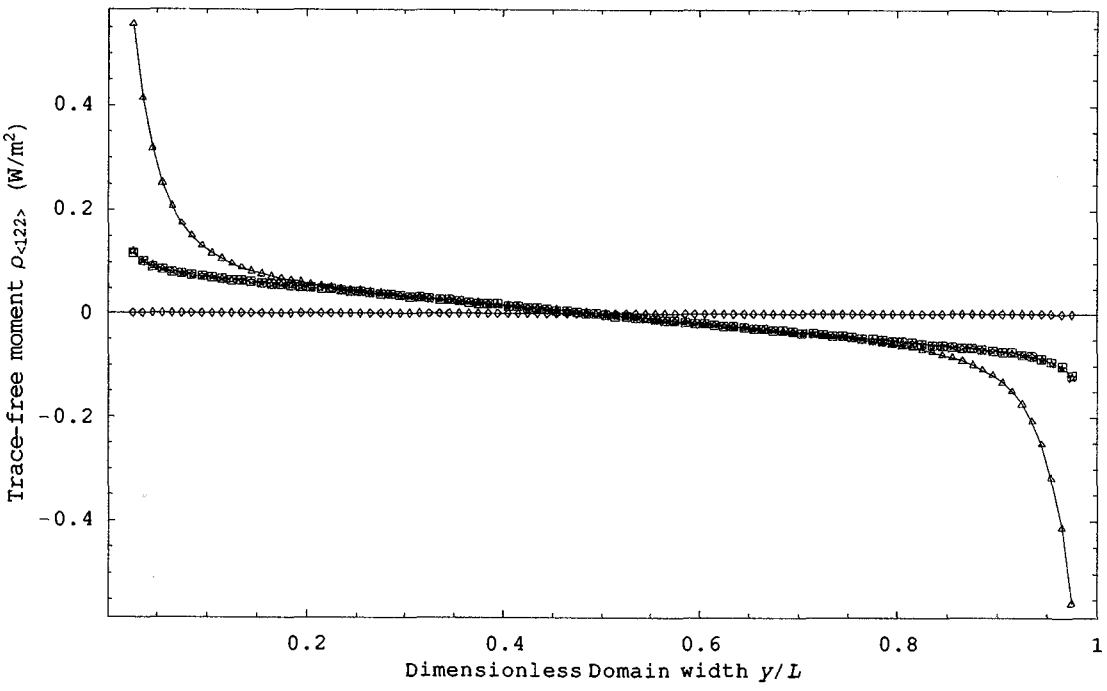

(b)

Figure 5.6: Results of third-degree and fourth-degree moments from the BGK model and its corresponding sets of moment equations (case 5.1: Kn=0.025, 300.0 m/s plate velocity) (Triangle for the BGK, Diamond for the Grad13, Star for the original R13, Box for the slightly linearized R13)

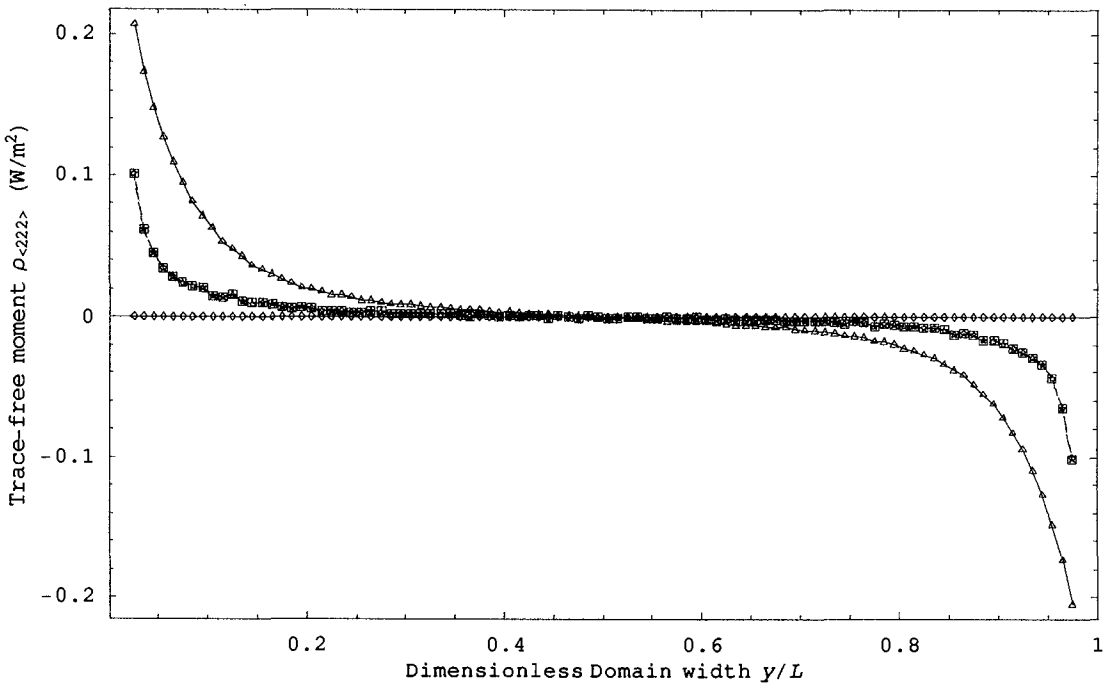

(c)

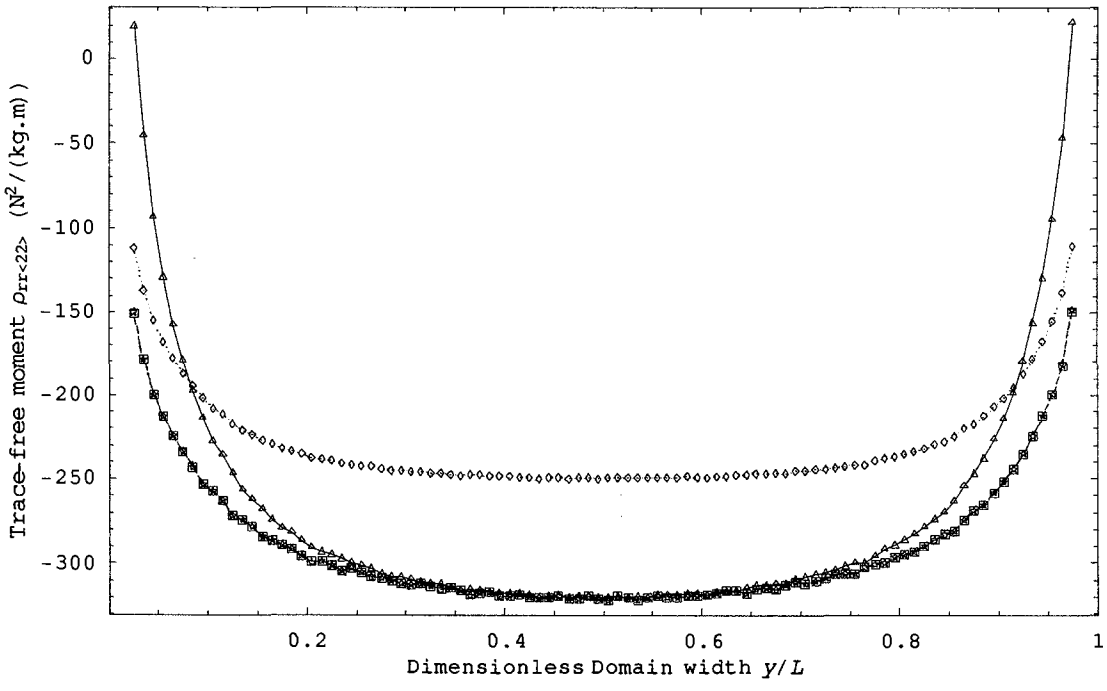

(d)

Figure 5.6: Results of third-degree and fourth-degree moments from the BGK model and its corresponding sets of moment equations (case 5.1: Kn=0.025, 300.0 m/s plate velocity) (Triangle for the BGK, Diamond for the Grad13, Star for the original R13, Box for the slightly linearized R13)

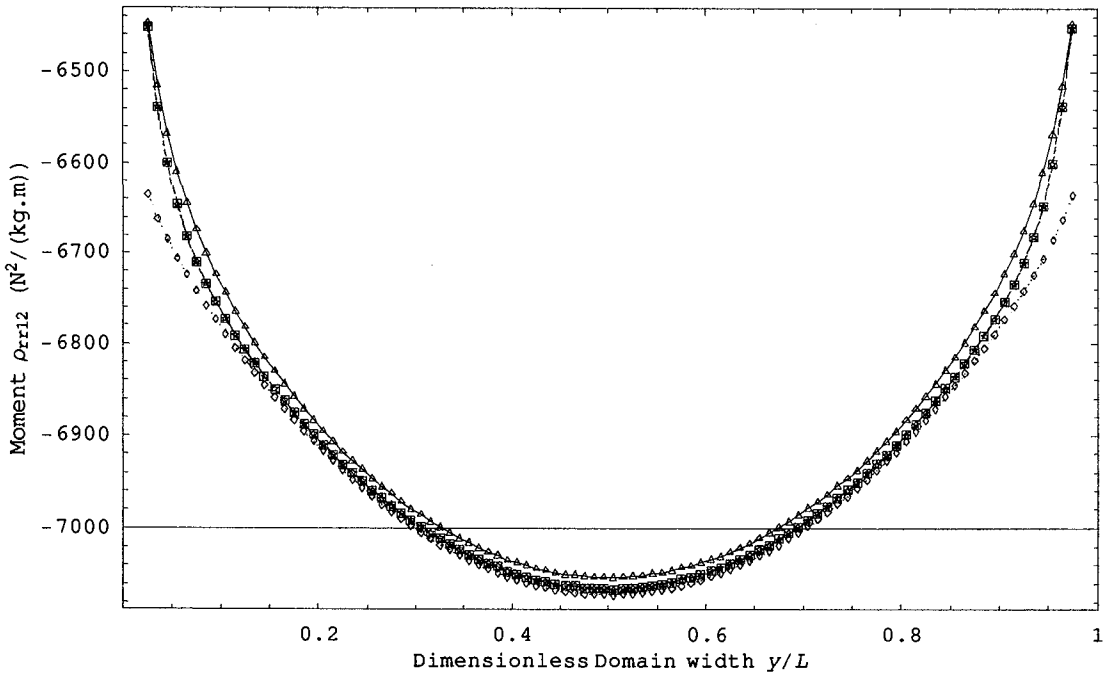

(e)

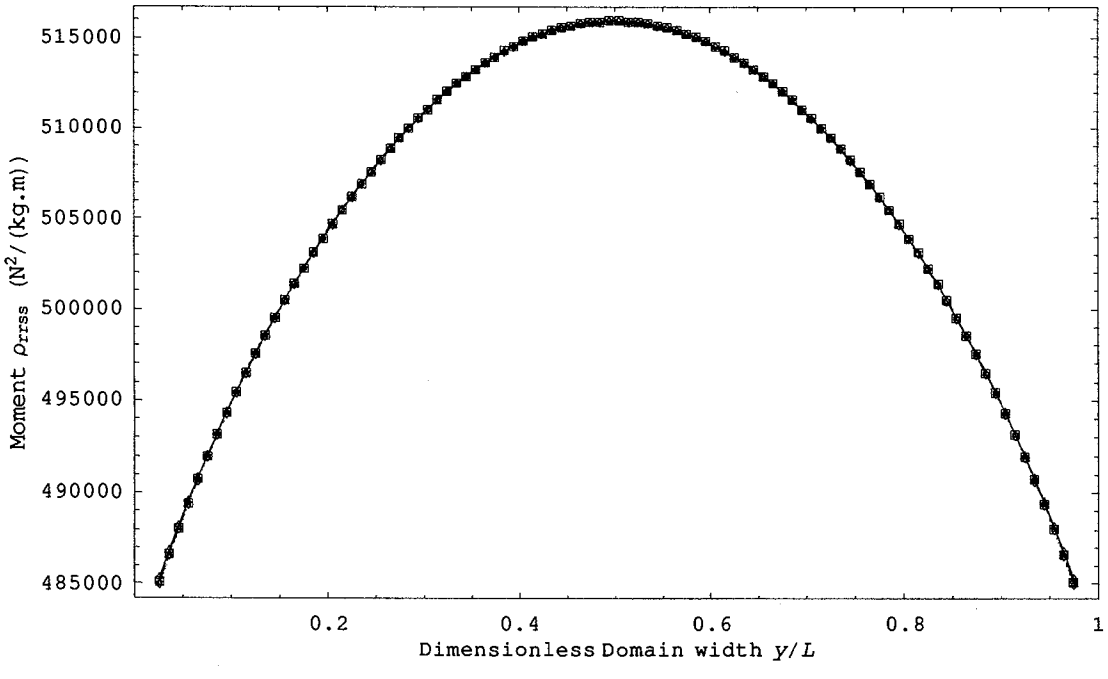

(f)

Figure 5.6: Results of third-degree and fourth-degree moments from the BGK model and its corresponding sets of moment equations (case 5.1: Kn=0.025, 300.0 m/s plate velocity) (Triangle for the BGK, Diamond for the Grad13, Star for the original R13, Box for the slightly linearized R13)

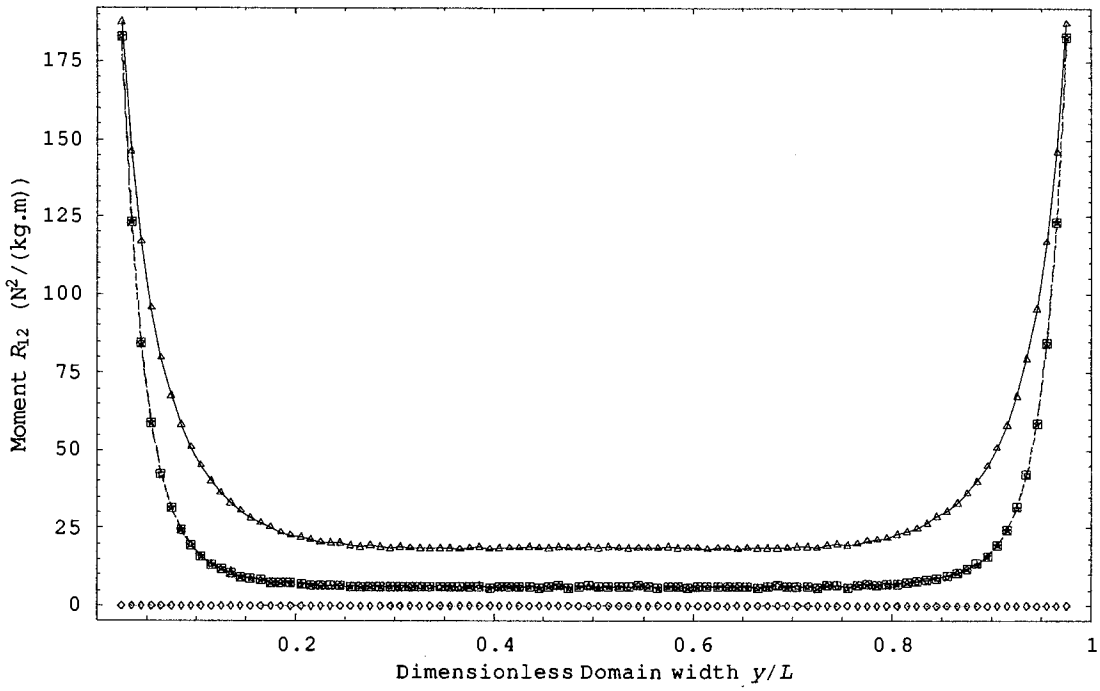

(g)

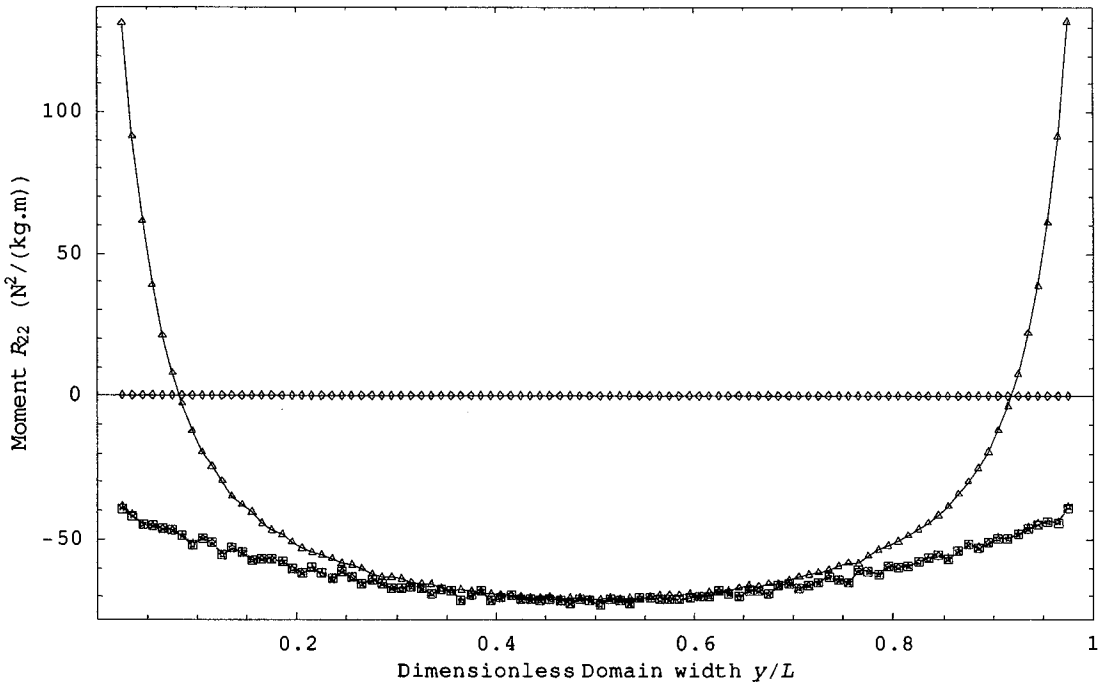

(h)

Figure 5.6: Results of third-degree and fourth-degree moments from the BGK model and its corresponding sets of moment equations (case 5.1: Kn=0.025, 300.0 m/s plate velocity) (Triangle for the BGK, Diamond for the Grad13, Star for the original R13, Box for the slightly linearized R13)

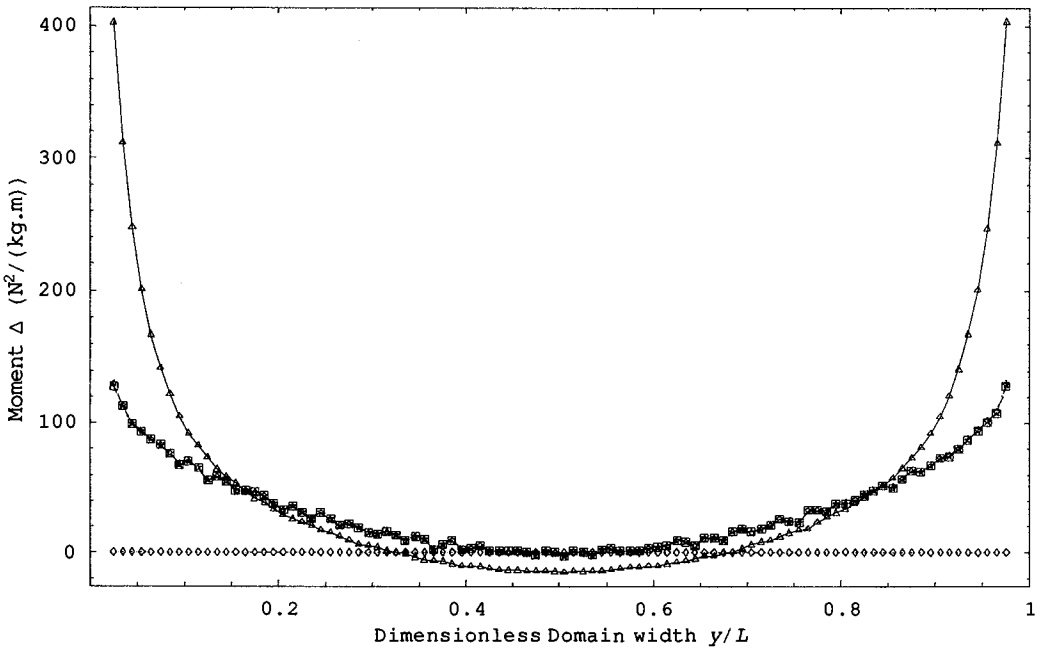

(i)

Figure 5.6: Results of third-degree and fourth-degree moments from the BGK model and its corresponding sets of moment equations (case 5.1: Kn=0.025, 300.0 m/s plate velocity) (Triangle for the BGK, Diamond for the Grad13, Star for the original R13, Box for the slightly linearized R13)

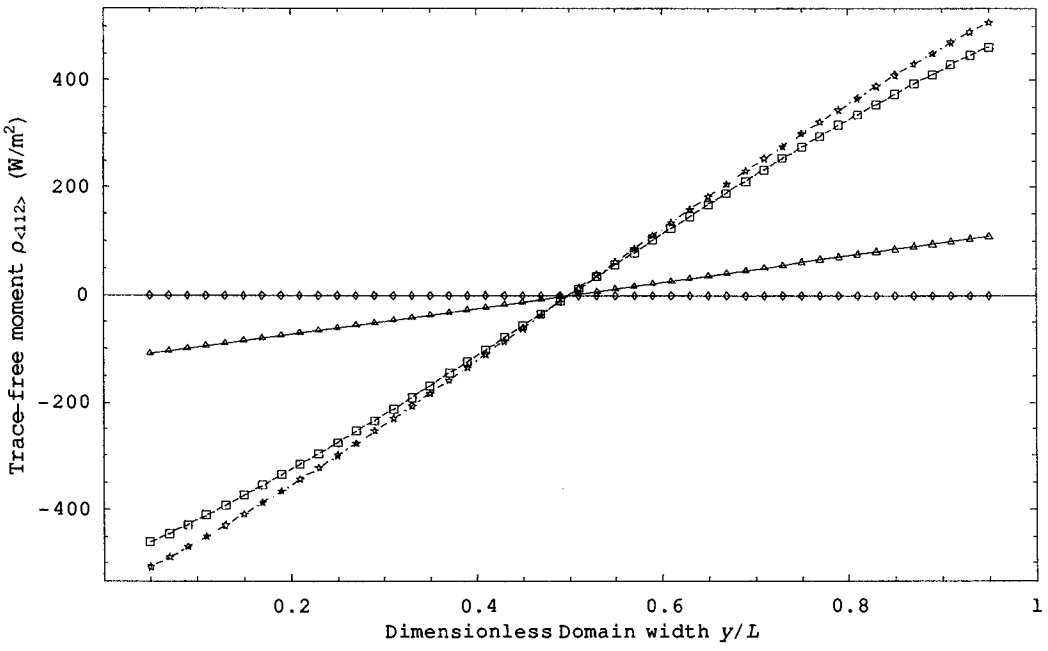

(a)

Figure 5.7: Results of third-degree and fourth-degree moments from the ES-BGK model and its corresponding sets of moment equations (case 5.6: Kn=0.5, 1000.0 m/s plate velocity) (Triangle for the ES-BGK, Diamond for the Grad13, Star for the original R13, Box for the slightly linearized R13)

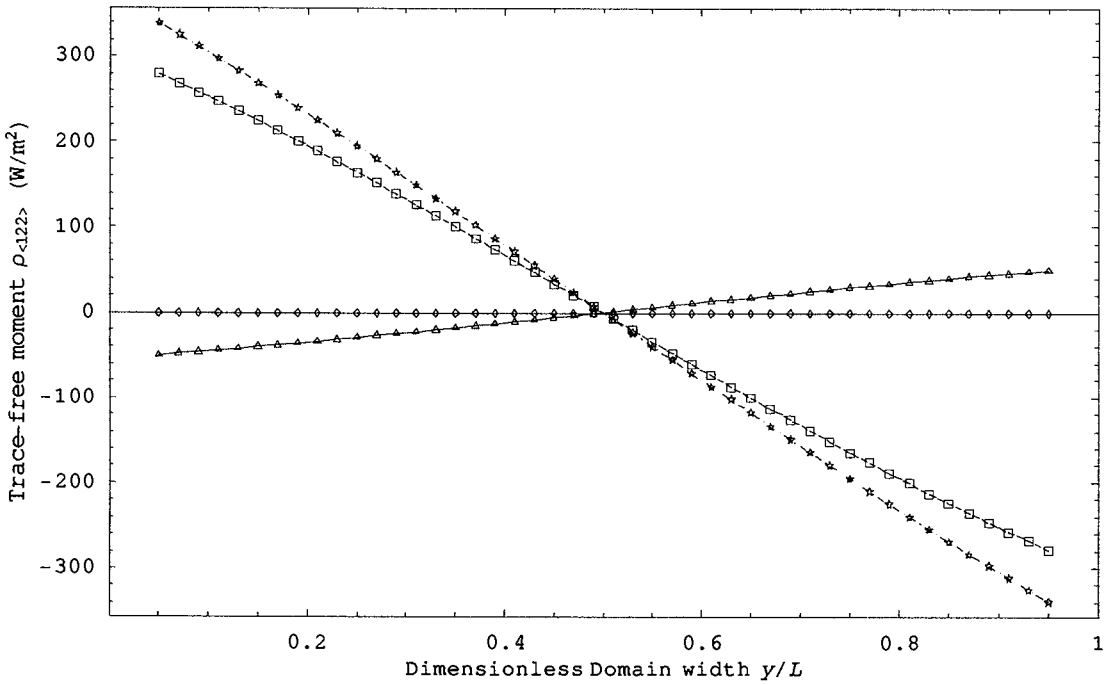

(b)

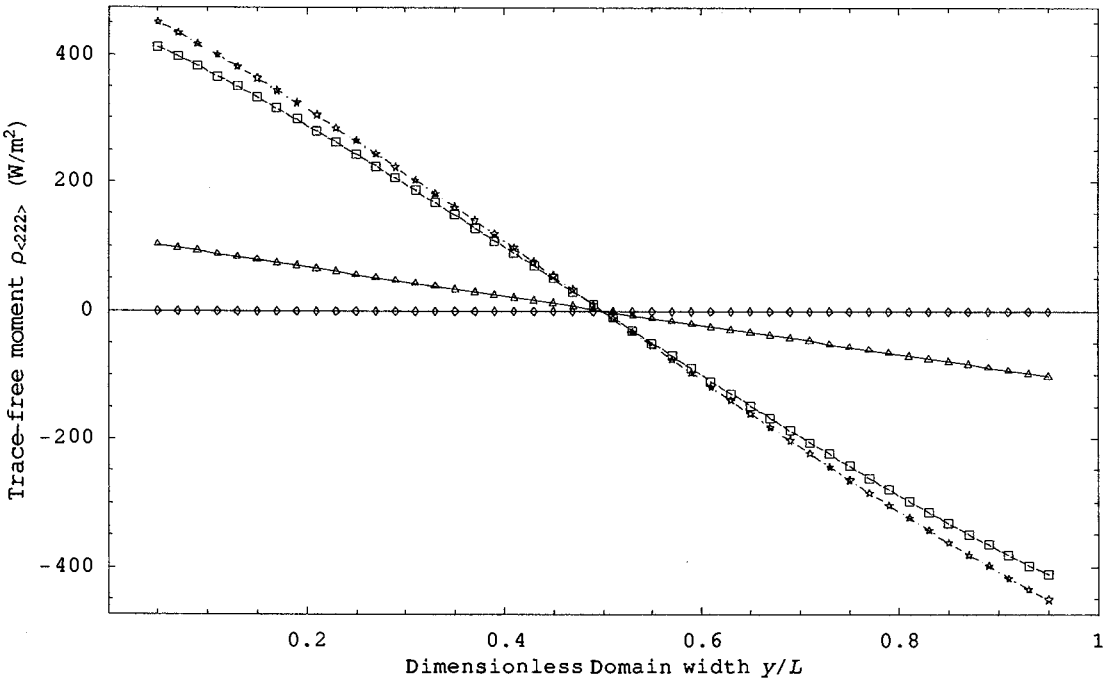

(c)

Figure 5.7: Results of third-degree and fourth-degree moments from the ES-BGK model and its corresponding sets of moment equations (case 5.6: Kn=0.5, 1000.0 m/s plate velocity) (Triangle for the ES-BGK, Diamond for the Grad13, Star for the original R13, Box for the slightly linearized R13)

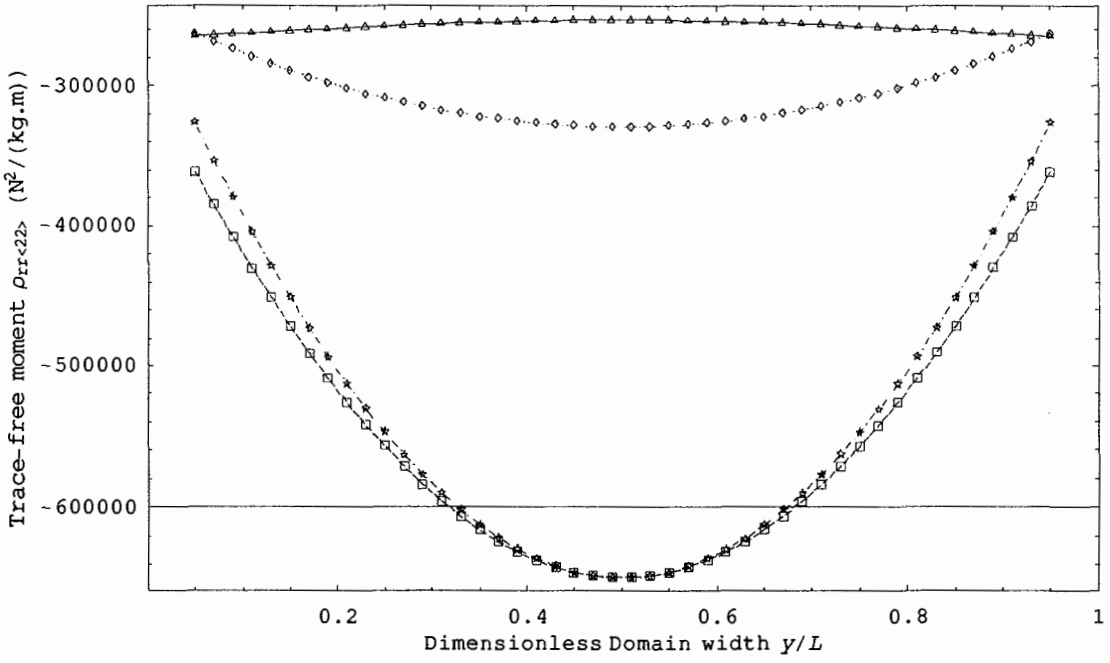

(d)

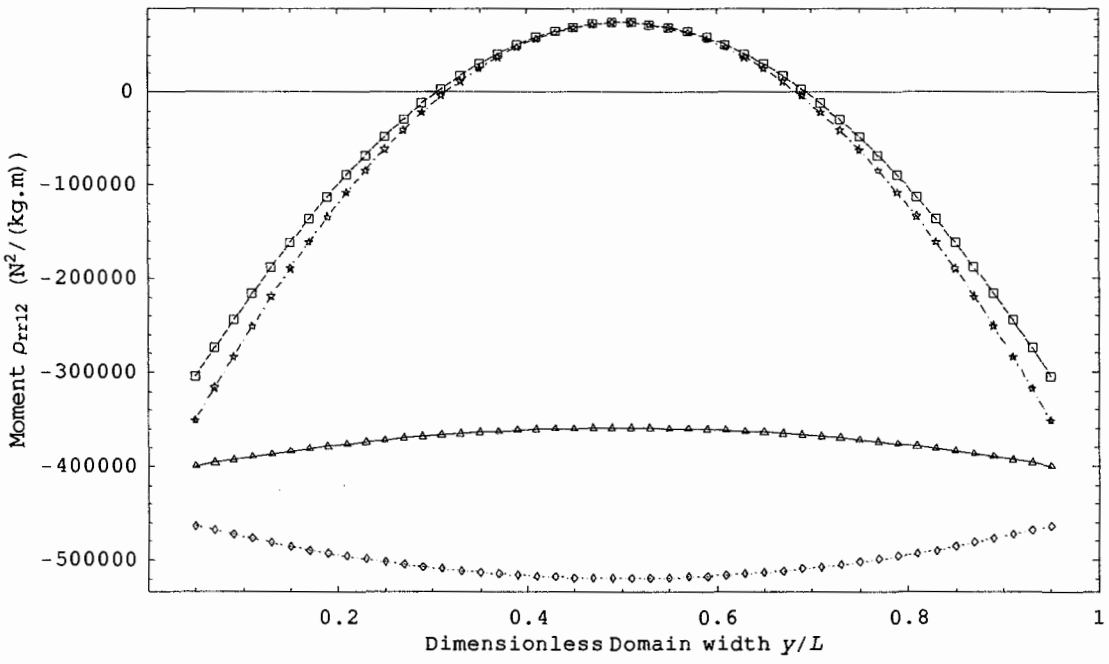

(e)

Figure 5.7: Results of third-degree and fourth-degree moments from the ES-BGK model and its corresponding sets of moment equations (case 5.6: Kn=0.5, 1000.0 m/s plate velocity) (Triangle for the ES-BGK, Diamond for the Grad13, Star for the original R13, Box for the slightly linearized R13)

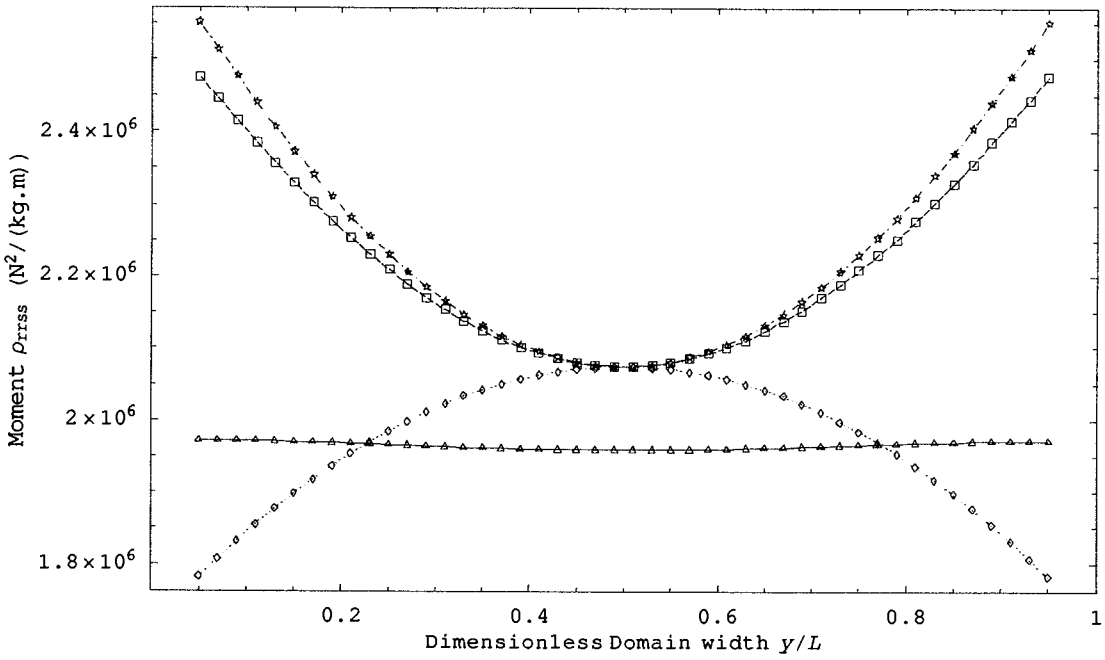

(f)

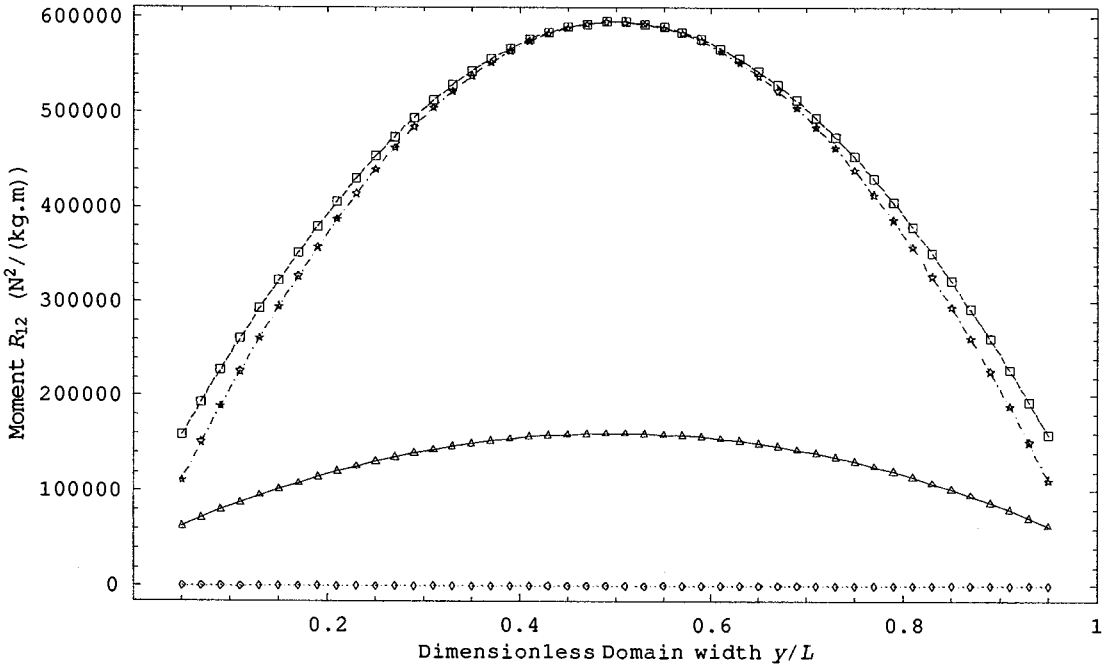

(g)

Figure 5.7: Results of third-degree and fourth-degree moments from the ES-BGK model and its corresponding sets of moment equations (case 5.6: Kn=0.5, 1000.0 m/s plate velocity) (Triangle for the ES-BGK, Diamond for the Grad13, Star for the original R13, Box for the slightly linearized R13)

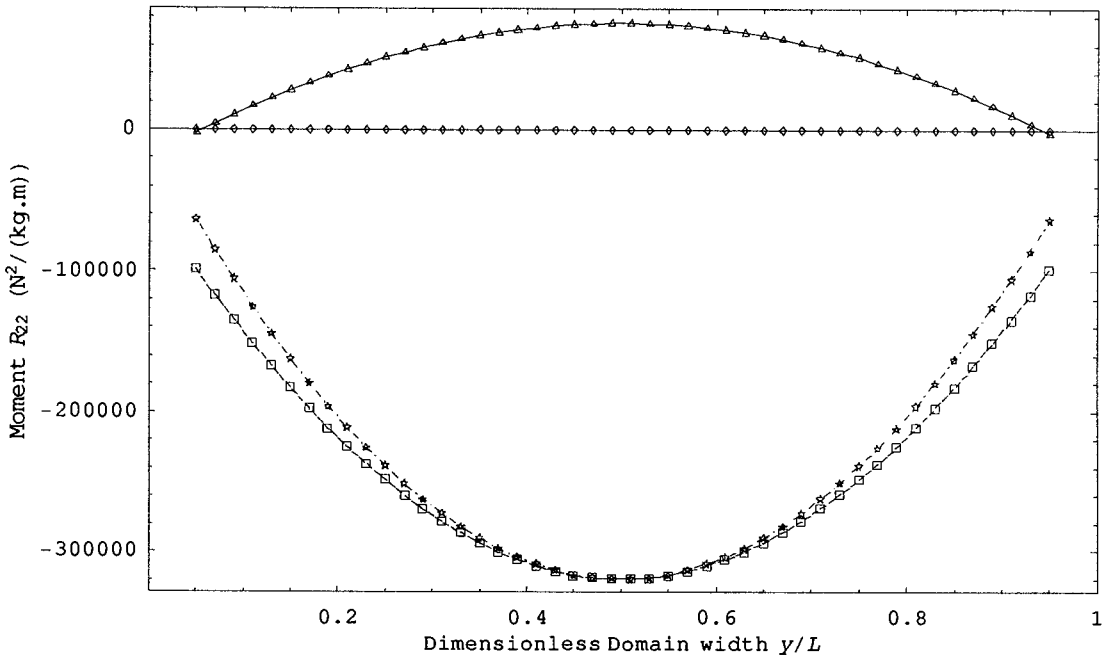

(h)

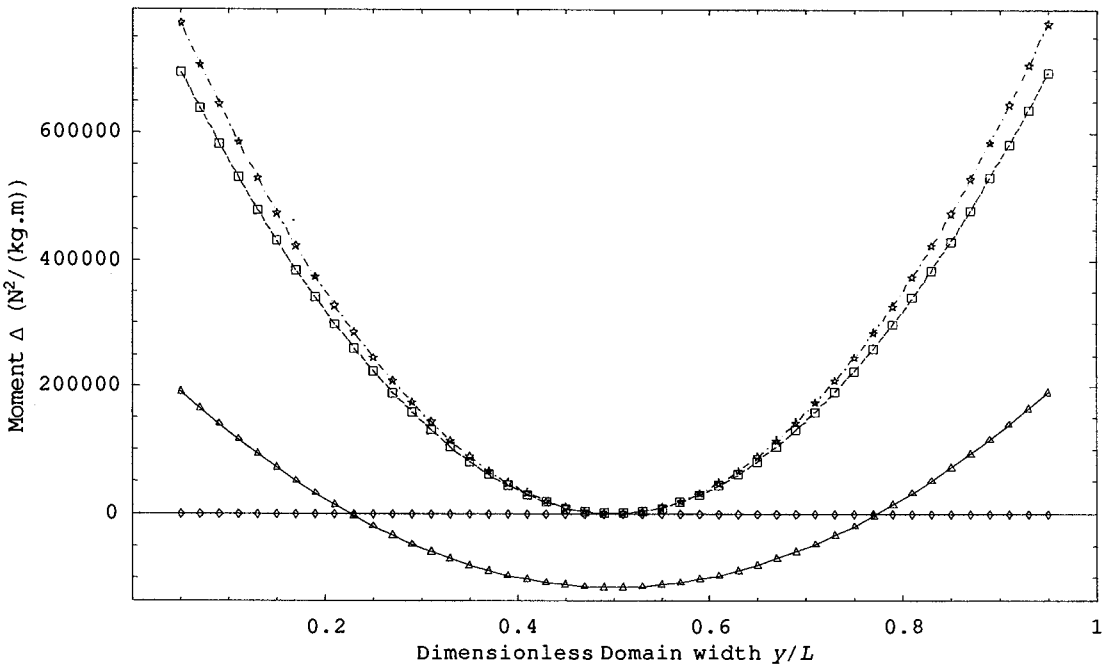

(i)

Figure 5.7: Results of third-degree and fourth-degree moments from the ES-BGK model and its corresponding sets of moment equations (case 5.6: Kn=0.5, 1000.0 m/s plate velocity) (Triangle for the ES-BGK, Diamond for the Grad13, Star for the original R13, Box for the slightly linearized R13)

5.8 Conclusion

In this chapter, the Grad13 equations, the original R13 equations, the slightly linearized R13 equations, the NSF equations and the Burnett equations for the BGK model and the ES-BGK model are compared with the kinetic models themself for steady state 1DCF.

At small Kn numbers and small plate velocities (Situations Sb and Sd, $\mathrm{Kn} \le 0.1$, plate velocity ≤ 300.0 m/s), all (except the NSF equations for σ_{11}, σ_{22} and q_1) work very well, especially at the middle part of the flow domain. As the Knudsen number or plate velocity increases, the accuracy of results from these sets of macroscopic equations becomes worse. Among these sets of equations, the slightly linearized R13 equations is better than the original R13 equations; the Grad13 equations is better than the Burnett equations and the NSF equations; while between the Grad13 equations and the R13s equations, between the Burnett equations and the NSF equations, it is hard to say which one is better (except at small Kn situations ($\mathrm{Kn} \le 0.1$), in which the R13s equations are better than the Grad13 equations, the Burnett equations is better than the NSF equations).

Therefore the slightly linearized R13 equations is suggested to be used as macroscopic continuum equations in the rarefied gas flow at $\mathrm{Kn} \le 0.1$, while for rarefied gas flow at $\mathrm{Kn} > 0.1$, none tested macroscopic continuum equations can be considered to be perfect. While the higher order models, in particular the R13s equations can describe rarefaction effects qualitatively, they certainly fail to give an accurate quantitative description. This can be attributed to their failure in describing boundary layer effects. For smaller Knudsen numbers, all higher order models give a good description of the bulk behavior, e.g. see Figure 5.2. When the Knudsen number grows, and boundary effects dominate, all models fail.

This matches with the observations in the computation of shock structures [26]: Burnett, Grad 13, and R13 equations yield shock structures in agreement with DSMC computations for Mach numbers below Ma=3.0, but not for higher Mach numbers, where rarefaction effects and deviations from equilibrium states become more important.

In conclusion we can state that the failure to describe Knudsen boundary layers, and strong shocks, puts strong limitations on the applicability of all macroscopic models considered.

Chapter 6 Conclusions and outlook

6.1 Conclusions

The Boltzmann equation is the basic equation to describe rarefied gas flows. Some kinetic models with simple collision term expressions have been proposed to reduce the mathematical complexity of the Boltzmann equation. The Boltzmann equation and kinetic models describe rarefied gases at the microscopic levewith great accuracy, but a cumbersome, and expensive, to solve.

Macroscopic models can be derived form the Boltzmann equation, or kinetic models, which reduce the number of variables drastically, but these can be applied only to flows with not too large Knudsen numbers. Important macroscopic models considered in this thesis are the Navier-Stokes-Fourier equations and the Burnett equations, which both follow from the Chapman-Enskog expansion, and extended sets of moment equations, in particular Grad's 13 moment equations, and their regularization (R13).

In the first part of this work, two new kinetic models (new kinetic model I and new kinetic model II) were proposed. Both models use a meaningful expression for the collision frequency, while retaining the important properties for a kinetic model at the same time. Both models can be reduced to the ES-BGK model and the $\nu(C)$-BGK model for suitable choices of parameters, and thus can be considered as more general kinetic models. The H-theorem of these two new kinetic models could be proven only for small Kn number situations.

In the second part of this work, several kinetic models (BGK, ES-BGK, $\nu(C)$-BGK, two new kinetic models) were tested numerically for the situations of one-dimensional shock waves at steady state and plane steady state Couette flow. Computational results from the kinetic models were compared to results obtained with the Direct Simulation Monte Carlo Method (DSMC), which serves as a benchmark in this work. The effects of space grid spacing, bounds and step size of the velocity grid on the computational results were discussed, and it was shown that shock wave problem at not small Mach numbers,

and Couette flow problem at small Knudsen numbers and large plate velocities, require very fine space and velocity grids to eliminate the numerical error due to discretization. This implies large computational times, which for the problems considered in the thesis are of the same order as those encountered in DSMC simulations. The benefit of discrete velocity models for kinetic schemes over DSMC simulations is that a deterministic solution is computed, and not a stochastic solution. Accordingly, the results do not suffer from stochastic noise, so that it will be no trouble to compute the derivative of macroscopic parameters and further transport coefficients (such as viscosity and thermal conductivity). Moreover, discrete velocity schemes allow to considering time dependent (means non steady state) problems, which are difficult to access for the DSMC method. The advantage of using kinetic models instead of the Boltzmann equation lies in the much easier numerical treatment of the collision term.

Results from the two new kinetic models are very similar, but the new kinetic model II is better for a simpler program structure, which further affects the computational time. For hard sphere molecules, results from the two new kinetic models locate in between results from the ES-BGK model and the $\nu(C)$-BGK model, while for the Maxwell molecules, the two new kinetic models are identical to the ES-BGK model.

For the shock wave problem, the new kinetic model II gives the best agreement to the DSMC simulation (See Table D.1, the average relative errors of density, velocity and temperature of the new kinetic model II comparing to the DSMC are smaller than 0.05 even for Ma=6.0); for Couette flow, however, the ES-BGK model gives best results (See Tables D.2-D.4, the average relative errors of density, velocity and temperature of the ES-BGK model comparing to the DSMC are smaller than 0.05 for all test situations ($\mathrm{Kn} \leq 1.0$)). The $\nu(C)$-BGK model gives results of insufficient accuracy in both cases, and requires the longest computational time (for it need more iterations to reach certain total time step than other kinetic models), and therefore should not be used to model flows

Also in the second part of this work, a modification of Mieussens's original numerical scheme was developed. The basic idea is to use linearized expressions for the reference distribution function f_{ref} (for the ES-BGK model and the two new kinetic models, there are two types linearized f_{ref}), instead of its exact expression, in the numerical program. Results from this modified scheme are almost identical to results from the original scheme for most test cases, while about 20-40 percent of computational time can be saved. For the ES-BGK model and the two new kinetic models, the second type linearized f_{ref}, which is based on an anisotropic Gaussian, is better than the first type linearized f_{ref}, which is based on an isotropic Gaussian. Some pity things about this modified numerical scheme are: the first type linearized f_{ref} of the new kinetic model I with hard sphere molecules is unstable for all test cases (NaNQ are output from the Fortran program), the second type linearized f_{ref} of the new kinetic model I with hard sphere molecules is unstable for high Mach (e.g. Ma=6.0) situations (NaNQ are output from the Fortran program), and the linearized f_{ref} of the $\nu(C)$-BGK model can not give results with accuracy enough for middle and high Mach situations.

In the third part of this work, several macroscopic continuum equations, the Navier-Stokes-Fourier equations, the Burnett equations, Grad 13 moment equations, and the regularized 13 moment equations (in original form and in slightly linearized form), were derived from the BGK and the ES-BGK models, and were then compared with the corresponding kinetic model for steady state Couette flow. At small Knudsen numbers and small plate velocities, all (except the NSF equations for σ_{11}, σ_{22} and q_1) work very well, especially at the middle part of the flow domain. As the Knudsen number or the plate velocity increases, results from these sets of macroscopic equations become increasingly different to results from kinetic models. Among these sets of equations, the slightly linearized R13 is better than the original R13, the Grad13 is better than the Burnett and the NSF, while it is hard to say which one of the Grad13 and the R13s, or the Burnett and the NSF, is better. For Knudsen numbers $\mathrm{Kn} \leq 0.1$, the R13 equations are better than the Grad13 equations, and the Burnett equations are better than the NSF equations. Therefore the slightly linearized R13 equations are suggested to be used as

macroscopic continuum equations in rarefied gas flows at $Kn \leq 0.1$, while for rarefied gas flows at larger Knudsen numbers none of the tested macroscopic continuum equations can be recommended without reservation.

6.2 Outlook

The results presented in this thesis show that numerical solutions of kinetic models can be used to model rarefied gas flows with sufficient accuracy (new kinetic models for shock wave, and ES-BGK model for Couette flow). In this thesis the standard test cases of shock waves and Couette flow were considered, and the natural next step is to simulate rarefied gas flows in more realistic applications, which will be two-dimensional or three-dimensional problems. However, the computational times involved are substantial, and in order to reduce these as much as possible, proper criteria for convergence should be developed which should allow to maximize time and space steps, in order to minimize computational time. Moreover, in order to reduce computational time, one also can consider to using parallel computing or/and implicit numerical schemes.

The examination of the macroscopic continuum models showed that these can describe rarefied gas flows outside the Knudsen layer in good agreement to solutions of microscopic models (i.e. kinetic models, and/or DSMC), but fail in the description of the Knudsen layer. Since the numerical effort for macroscopic models is substantially smaller than the effort to solve microscopic equations, the former should be considered wherever possible, that is outside of Knudsen layers and strong shocks. The Knudsen layer itself (and strong shocks) should be simulated with a microscopic model. This will lead to hybrid schemes, where microscopic and macroscopic models are solved in their respective domains. Hybrid models which connect the Boltzmann or kinetic model solutions to the Navier-Stokes-Fourier equations have been shown to be an effective way to save computational time and memory, e.g. [81-84]. The Navier-Stokes-Fourier equations cannot describe rarefaction effects, which are, however, described in the Burnett, the Grad 13, and the R13 equations. Since the Burnett equations suffer from instabilities, and the Grad 13 equations describe unphysical shocks, one should consider the (slightly linearized) R13 equations in flow areas where mild rarefaction plays a role,

and the Navier-Stokes-Fourier equations in regions were rarefaction effects are unimportant, together with a suitable kinetic model (e.g. the ES-BGK model) in areas of large rarefaction.

References

[1] C. Cercignani, *Rarefied gas dynamics: from basic concepts to actual calculations,* Cambridge University Press, 2000.

[2] M. S. Ghidaoui, J. Q. Deng, W. G. Gray, and K. Xu, *A Boltzmann based model for open channel flows*, International Journal for Numerical Methods in Fluids **35**, 449-494 (2001).

[3] C. Cercignani, *Theory and application of the Boltzmann equation*, Scottish Academic Press Ltd., 1975.

[4] C. Cercignani, *The Boltzmann equation and its applications*, Springer-Verlag New York Inc., 1988.

[5] S. Harris, *An introduction to the theory of the Boltzmann equation*, Holt, Rinehart and Winston, Inc., 1971

[6] I. Muller, *Thermodynamics*, Pitman Advanced Publishing Program, 1985.

[7] G. S. Springer, *Heat transfer in rarefied gases*, Advances in Heat Transfer **7**, 163-218 (1971).

[8] G. E. Karniadakis and A. Beskok, *Micro flows: fundamentals and simulation,* Springer-Verlag, New York, 2002.

[9] M. N. Kogan, *Rarefied gas dynamics,* Plenum Press, 1969.

[10] H. Struchtrup, *Failures of the Burnett and super-Burnett equations in steady state processes*, accepted for publication in Continuum Mechanics and Thermodynamics (2004).

[11] Y. Zheng and H. Struchtrup, *Burnett equations for the ellipsoidal statistical BGK model*, Continuum Mechanics and Thermodynamics **16** (1-2), 97-108 (2004).

[12] S. Chapman and T. G. Cowling, *The mathematical theory of non-uniform gases*, Third Edition, Cambridge Univerisity Press, 1970.

[13] J. H. Ferziger and H. G. Kaper, *Mathematical theory of transport processes in gases*, North-Holland Publishing Company, 1972.

[14] H. Struchtrup, *Some remarks on the equations of Burnett and Grad*, Transport in Transition Regimes, IMA Volume Series **135**, Springer New York (2003).

[15] H. Struchtrup, *Stable transport equations for rarefied gases at high orders in the Knudsen number*, Physics of Fluids **16** (11), 3921-3934 (2004).

[16] H. Grad, *Principles of the kinetic theory of gases*, Handbuch der Physik **XII**, 205-294 (1958)

[17] C. D. Levermore, *Entropy-based moment closures for kinetic equations*, Transport Theory and Statistical Physics **26**, 591-606 (1997)

[18] C. D. Levermore, *Moment closure hierarchies for kinetic theories*, Journal of Statistical Physics **83**, 1021-1065 (1996).

[19] C. D. Levermore, W. J. Morokoff, *The Gaussian moment closure for gas dynamics,* SIAM Journal of Applied Mathematics **59** (1), 72-96 (1998).

[20] W. Weiss, *Continuous shock structure in extended thermodynamics*, Physical Review E **52**, 5760 (1995).

[21] I. Muller and T. Ruggeri, *Rational extended thermodynamics*, Springer, New York, 1998.

[22] P. Charrier, B. Dubroca and J. L. Feugeas, *Levermore's moment closure of discrete Boltzmann equations for non-equilibrium kinetic flows*, 21st International Symposium on Rarefied Gas Dynamics **I**, Marseille France, 95-102 (1998).

[23] M. Junk, *Maximum entropy moment problems and extended Euler equations*, IMA workshop "Simulation of Transport in Transition Regimes", 2000, www.mathematik.uni-kl.de/~junk/publications/list.html

[24] S. Reinecke and G. M. Kremer, *Burnett's equations from a (13+9N) - field theory*, Continuum Mechanics and Thermodynamics **8**, 121-130 (1996).

[25] S. Reinecke and G. M. Kremer, *Method of moments of Grad*, Physical Review A **42** (2), 815-820 (1990).

[26] H. Struchtrup and M. Torrilhon, *Regularization of Grad's 13 moment equations: Derivation and linear analysis*, Physics of Fluids **15**, 2668-2680 (2003).

[27] M. Torrilhon and H. Struchtrup, *Regularized 13-Moment equations: shock structure calculations and comparison to Burnett models*, Journal of Fluid Mechanics **513**, 171-198 (2004).

[28] P.L. Bhatnagar, E.P. Gross and M. Krook, *A model for collision processes in gases. I: small amplitude processes in charged and neutral one-component systems*, Physical Review **94**, 511-525 (1954).

[29] J. Lowell H. Holway, *New statistical models for kinetic theory: methods of construction,* Physics of Fluids **9**, 1658-1673 (1966).

[30] J. Lowell H. Holway, *Kinetic theory of shock structure using an ellipsoidal distribution function,* Rarefied Gas Dynamics **I**, 193-215 (1965).

[31] F. Sharipov and V. Seleznev, *Data on internal rarefied gas flows*, Journal of Physical and Chemical Reference Data **27**, 657-706 (1998).

[32] P. Andries and B. Perthame, *The ES-BGK model equation with correct Prandtl number*, AIP Conference Proceedings **585** (1), 30-36 (2001).

[33] P. Andries, P. Le Tallec, J. Perlat and B. Perthame, *The Gaussian-BGK model of Boltzmann equation with small Prandtl numbers,* European Journal of Mechanics: B Fluids **19**(6), 813-830 (2000).

[34] L. Mieussens and H. Struchtrup, *Numerical comparison of BGK-models with proper Prandtl number,* Physics of Fluids **16**(8), 2797-2813 (2004).

[35] H. Struchtrup, *The BGK-model with velocity-dependent collision frequency*, Continuum Mechanics and Thermodynamics **9**, 23-31 (1997).

[36] E. M. Shakhov, *Generalization of the Krook kinetic relaxation equation*, Fluid Dynamics (English Translation of Izvestiya Akademii Nauk SSSR, Mekhanika Zhidkosti i Gaza) **3**, 95-96 (1968).

[37] E. M. Shakhov, *Kinetic model equations and numerical results*, the 14th International Symposium on Rarefied Gas Dynamics, Tsukuba Japan, 1984.

[38] G. Liu, *A method for constructing a model form for the Boltzmann equation*, Physics of Fluids A **2**, 277-280 (1990).

[39] V. Garzo, *Transport equations from the Liu model*, Physics of Fluids A **3**, 1980-1982 (1991).

[40] V. Garzo and M. L. d. Haro, *Kinetic model for heat and momentum transport*, Physics of Fluids **6**, 3787-3794 (1994).

[41] L. Mieussens, *Discrete-velocity models and numerical schemes for the Boltzmann-BGK equation in plane and axisymmetric geometries,* Journal of Computational Physics **162**(2), 429-466 (2000).

[42] L. Mieussens, *Convergence of a discrete-velocity model for the Boltzmann-BGK equation*, Computers and Mathematics with Applications **41**, 83-96 (2001).

[43] L. Mieussens, *Discrete velocity model and implicit scheme for the BGK equation of rarefied gas dynamics*, Mathematical Models and Methods in Applied Sciences **10**, 1121-1149 (2000).

[44] P. Charrier, B. Dubroca and L. Mieussens, *Discrete velocity BGK model and implicit scheme for computing rarefied gas flows*, 21st International Symposium on Rarefied Gas Dynamics **I**, Marseille France, 95-102 (1998).

[45] H. Babovsky and R. Illner, *A convergence proof for Nanbu's simulation method for the full Boltzmann equation*, SIAM Journal of Numerical Analysis **26**, 45-65 (1989).

[46] E. S. Oran, C. K. Oh and B. Z. Cybyk, *Direct simulation Monte Carlo: recent advances and applications*, Annual Review of Fluid Mechanics **30**, 403-441 (1998).

[47] G. A. Bird, *Molecular gas dynamics and the direct simulation of gas flows*, Oxford Science Publications, Oxford, 1994.

[48] http://www.gab.com.au

[49] Toby Thatcher's master thesis (in progress), Department of mechanical engineering, University of Victoria.

[50] P. Le Tallec, *A hierarchy of hyperbolic models linking Boltzmann to Navier Stokes equations for polyatomic gases*, ZAMM **80** (11-12), 779-789 (2000).

[51] J. O. Hirschfelder, C. F. Curtiss, and R. B. Bird, *Molecular theory of gases and liquids*: John Wiley & Sons, Inc., 1954.

[52] R. L. Liboff, *The theory of kinetic equations*, Wiley and Sons, New York, 1969.

[53] F. Bouchut and B. Perthame, *A BGK model for small Prandtl number in the Navier-Stokes approximation*, Journal of Statistical Physics **71**, 191-207 (1993).

[54] L. B. Barichello, A. C. R. Bartz, M. Camargo and C. E. Siewert, *The temperature-jump problem for a variable collision frequency model*, Physics of Fluids **14** (1), 382-391 (2002).

[55] S. K. Loyalka, *Velocity profile in the Knudsen layer for the Kramer's problem*, Physics of Fluids **18** (12), 1666-1669 (1975).

[56] S. K. Loyalka and K. A. Hickey, *Velocity slip and defect: Hard sphere gas*, Physics of Fluids A **1** (3), 612-614 (1989).

[57] http://documents.wolfram.com/v4/

[58] K. Xu, *A gas-kinetic BGK scheme for the Navier-Stokes equations and its connection with artificial dissipation and Godunov method*, Journal of Computational Physics **171**, 289-335(2001).

[59] http://physics.nad.ru/Physics/English/swa_txt.htm

[60] W. G. Vincenti and C. H. Kruger, Jr., *Introduction to physics gas dynamics*, John Wiley & Sons, Inc., 1965.

[61] H. C. Yee and J. L. Shinn, *Semi-implicit and fully implicit shock-capturing method for hyperbolic conservation laws with stiff source terms*, AIAA Paper, 87-1116 (1987).

[62] H. C. Yee, *Construction of explicit and implicit symmetric TVD schemes and their applications*, Journal of Computational Physics **68**, 151-179 (1987).

[63] W. H. Press, B. P. Flannery, S. A. Teukolsky and W. T. Vetterling, *Numerical Recipes*, Cambridge University Press, 1986.

[64] R. L. Burden and J. D. Faires, *Numerical Analysis*, Sixth Edition, Brooks/Cole Publishing Company, 1997.

[65] J. E. Dennis and R. B. Schnabel, *Numerical methods for unconstrained optimization and nonlinear equations*, Prentic Hall Inc., 1983.

[66] L. Mieussens (Toulouse France), private communicaton, 2003.

[67] A. Schuetze, *Direct simulation by Monte Carlo modeling one dimensional shock wave using dsmc1as.f: A user's manual*, Report, Department of mechanical engineering, University of Victoria, 2003.

[68] G. C. Pham-Van-Diep, D. A. Erwin and E. P. Muntz, *Testing continuum descriptions of low-Mach-number shock structures*, Journal of Fluid Mechanics **232**, 403-413 (1991).

[69] http://pearl1.lanl.gov/periodic/default.htm

[70] H. Struchtrup, *Kinetic schemes and boundary conditions for moment equations*, ZAMP **51**, 346-365 (2000).

[71] A. Schuetze, *Direct simulation by Monte Carlo modeling Couette flow using dsmc1as.f: A user's manual*, Report, Department of mechanical engineering, University of Victoria, 2003.

[72] V. Garzo, *On the derivation of the Burnett hydrodynamic equations from the Hilbert expansion*, Physica A **149**, 551-560 (1988).

[73] C. Y. Cha and B. J. McCoy, *Third-order constitutive equations for a monatomic gas*, Journal of Chemical Physics **34**, 4369-4372 (1971).

[74] R. K. Agarwal, K. Y. Yun, and R. Balakrishnan, *Beyond Navier-Stokes: Burnett equations for flows in the continuum-transition regime*, Physics of Fluids **13**, 3061-3085 (2001).

[75] A. V. Bobylev, *The Chapman-Enskog and Grad methods for solving the Boltzmann equation*, Soviet Physics. Dokl. **27**, 29-31 (1982).

[76] M. Kurtz, *Handbook of Applied Mathematics for Engineers and Scientists*, McGraw-Hill, Inc., 1991.

[77] R. Balakrishnan, *Entropy consistent formulation and numerical simulation of the BGK-Burnett equations for hypersonic flows in the continuum-transition regime*, Dissertation, Wichita State University 1999.

[78] H. Struchtrup, *Derivation of 13 moment equations for rarefied gas flow to second order accuracy for arbitrary interaction potentials*, Multiscale Modeling & Simulation, (2004) be in press.

[79] Y. Sone, *Flows induced by temperature fields in a rarefied gas and their ghost effect on the behavior of a gas in the continuum limit*, Annual Review of Fluid Mechanics **32**, 779-811 (2000).

[80] S. F. Liotta, V. Romano, and G. Russo, *Central schemes for balance laws of relaxation type*, SIAM Journal of Numerical Analysis **38**, 1337-1356 (2000).

[81] P. L. Tallec and J. P. Perlat, *Coupling kinetic models with Navier-Stokes equations*, in *Computational fluid dynamics review*, M. Hafez and K. Oshima, Eds. World Scientific, 833-855 (1998).

[82] J. Schneider, *Direct coupling of fluid and kinetic equations*, Transport Theory and Statistical Physics **25**, 681-698 (1996).

[83] S. P. Popov and F. G. Cheremisin, *Example of simultaneous numerical solution of the Boltzmann and Navier-Stokes equations*, Computational Mathematics and Mathematical Physics **41**, 457-468 (2001)

[84] J. F. Bourgat, P. L. Tallec, B. Perthame, and Y. Qiu, *Coupling Boltzmann and Euler equations without overlapping*, Contemporary Mathematics **157**, 377-398 (1994).

[85] J. M. Gere and W. Weaver, Jr., *Matrix algebra for engineers*, 2nd Edition, Wadsworth Inc., 1983.

[86] http://mathworld.wolfram.com/GammaFunction.html

Appendix A: Flow diagrams of N-R algorithm and computational programs

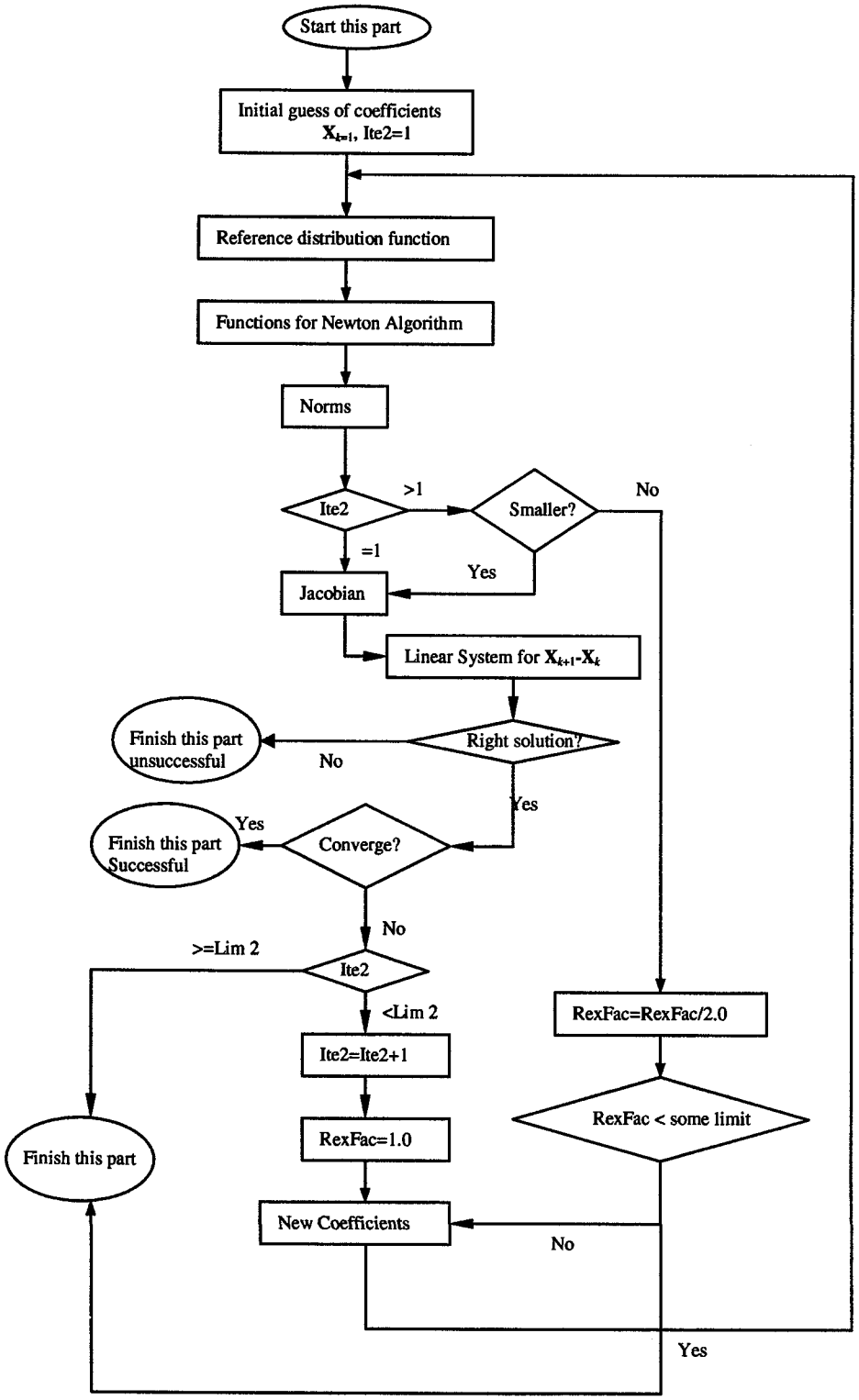

Figure A.1: Flow diagram of N-R algorithm used for reference distribution function

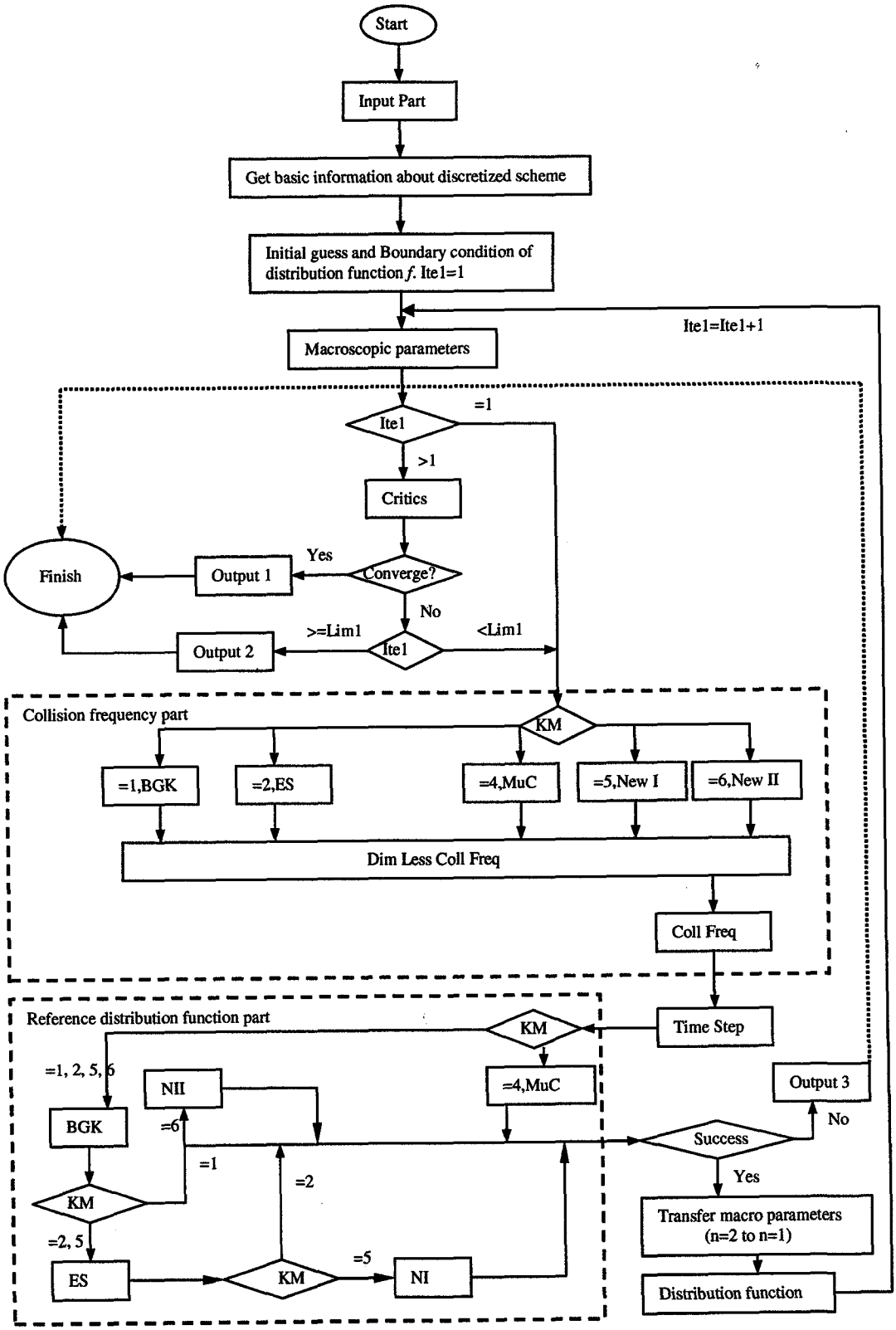

Figure A.2: Flow diagram of program for one-dimensional shock wave

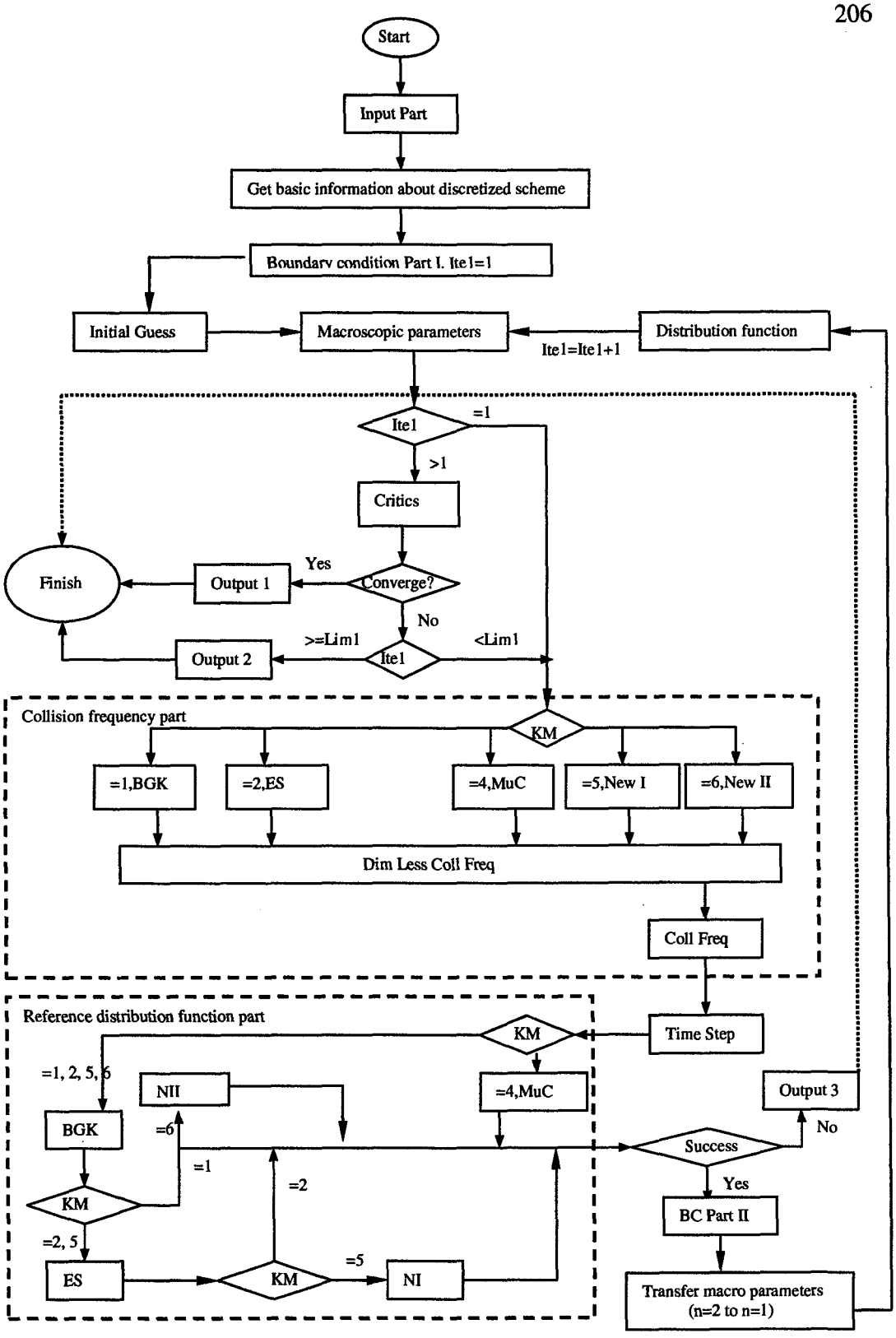

Figure A.3: Flow diagram of program for one-dimensional Couette flow

Appendix B Expression of functions and Jacobian in the N-R algorithm for all kinetic models

In this appendix, a subscript k is used to show the iteration number in the N-R algorithm, and the meaning and expression of dimensionless distributions and their coefficients, and so on, refer to corresponding part in Chapters 3 and 4. Figure A.1 shoe the flow diagram of the N-R algorithm used for reference distribution function.

B.1 BGK model

For the 1DSW, functions we compute in the N-R algorithm are

$$\tilde{F}1^n_{i,k} = \sum_{j=1}^{J} F^n_{BGK,i,j,k} - 1,\ \tilde{F}2^n_{i,k} = \sum_{j=1}^{J} \eta^n_{i,j_1} F^n_{BGK,i,j,k} - 0, \tag{B.1}$$

$$\tilde{F}3^n_{i,k} = \sum_{j=1}^{J} \frac{(\eta^n_{i,j})^2}{1.5} F^n_{BGK,i,j,k} - 1,$$

where the dimensionless distribution

$$F^n_{BGK,i,j,k} = \frac{f^n_{BGK,i,j,k}\Delta \mathbf{c}}{\rho^n_i} = a^n_{i,k} \cdot \exp\left(-\Gamma^n_{i,k}(\eta^n_{i,j})^2 + \gamma^n_{i,k}\eta^n_{i,j_1}\right).$$

The coefficients are obtained as follows

$$\mathbf{X}^n_{i,k+1} = \begin{bmatrix} a^n_{i,k+1} \\ \gamma^n_{i,k+1} \\ \Gamma^n_{i,k+1} \end{bmatrix} = \mathbf{X}^n_{i,k} + \mathbf{Y}^n_{i,k} = \begin{bmatrix} a^n_{i,k} \\ \gamma^n_{i,k} \\ \Gamma^n_{i,k} \end{bmatrix} + \begin{bmatrix} Y1^n_{i,k} \\ Y2^n_{i,k} \\ Y3^n_{i,k} \end{bmatrix},$$

$$\mathbf{J}^n_{i,k}\mathbf{Y}^n_{i,k} = \tilde{\mathbf{F}}^n_{i,k} = \begin{bmatrix} \tilde{F}1^n_{i,k} \\ \tilde{F}2^n_{i,k} \\ \tilde{F}3^n_{i,k} \end{bmatrix},$$

where the Jacobian $\mathbf{J}^n_{i,k}$ used in the computation is

$$\mathbf{J}^n_{i,k} = \begin{bmatrix} \frac{\partial \tilde{F}1^n_{i,k}}{\partial a^n_{i,k}} & \frac{\partial \tilde{F}1^n_{i,k}}{\partial \gamma^n_{i,k}} & \frac{\partial \tilde{F}1^n_{i,k}}{\partial \Gamma^n_{i,k}} \\ \frac{\partial \tilde{F}2^n_{i,k}}{\partial a^n_{i,k}} & \frac{\partial \tilde{F}2^n_{i,k}}{\partial \gamma^n_{i,k}} & \frac{\partial \tilde{F}2^n_{i,k}}{\partial \Gamma^n_{i,k}} \\ \frac{\partial \tilde{F}3^n_{i,k}}{\partial a^n_{i,k}} & \frac{\partial \tilde{F}3^n_{i,k}}{\partial \gamma^n_{i,k}} & \frac{\partial \tilde{F}3^n_{i,k}}{\partial \Gamma^n_{i,k}} \end{bmatrix}.$$

Since $\frac{\partial F^n_{BGK,i,j,k}}{\partial a^n_{i,k}} = \frac{F^n_{BGK,i,j,k}}{a^n_{i,k}}$, $\frac{\partial F^n_{BGK,i,j,k}}{\partial \gamma^n_{i,k}} = \eta^n_{i,j_1} F^n_{BGK,i,j,k}$, $\frac{\partial F^n_{BGK,i,j,k}}{\partial \Gamma^n_{i,k}} = -(\eta^n_{i,j})^2 F^n_{BGK,i,j,k}$,

$\frac{\partial \tilde{F}1^n_{i,k}}{\partial a^n_{i,k}} = \sum_{j=1}^{J} \frac{\partial \tilde{F}1^n_{i,k}}{\partial F^n_{BGK,i,j,k}} \frac{\partial F^n_{BGK,i,j,k}}{\partial a^n_{i,k}} = \frac{\sum_{j=1}^{J} F^n_{BGK,i,j,k}}{a^n_{i,k}}$, then

$$\mathbf{J}^n_{i,k} = \begin{bmatrix} \frac{\sum_{j=1}^{J} F^n_{BGK,i,j,k}}{a^n_{i,k}} & \sum_{j=1}^{J} \eta^n_{i,j_1} F^n_{BGK,i,j,k} & -\sum_{j=1}^{J} (\eta^n_{i,j})^2 F^n_{BGK,i,j,k} \\ \frac{\sum_{j=1}^{J} \eta^n_{i,j_1} F^n_{BGK,i,j,k}}{a^n_{i,k}} & \sum_{j=1}^{J} (\eta^n_{i,j_1})^2 F^n_{BGK,i,j,k} & -\sum_{j=1}^{J} (\eta^n_{i,j})^2 \eta^n_{i,j_1} F^n_{BGK,i,j,k} \\ \frac{\sum_{j=1}^{J} \frac{(\eta^n_{i,j})^2}{1.5} F^n_{BGK,i,j,k}}{a^n_{i,k}} & \sum_{j=1}^{J} \eta^n_{i,j_1} \frac{(\eta^n_{i,j})^2}{1.5} F^n_{BGK,i,j,k} & -\sum_{j=1}^{J} (\eta^n_{i,j})^2 \frac{(\eta^n_{i,j})^2}{1.5} F^n_{BGK,i,j,k} \end{bmatrix}. \quad \text{(B.2)}$$

For the 1DCF, functions we compute in the N-R algorithm are

$$\tilde{F}1^n_{i,k} = \sum_{j=1}^{J} F^n_{BGK,i,j,k} - 1, \quad \tilde{F}2^n_{i,k} = \sum_{j=1}^{J} \eta^n_{i,j_1} F^n_{BGK,i,j,k} - 0,$$

$$\tilde{F}3^n_{i,k} = \sum_{j=1}^{J} \eta^n_{i,j_2} F^n_{BGK,i,j,k} - 0, \qquad \tilde{F}4^n_{i,k} = \sum_{j=1}^{J} \frac{(\eta^n_{i,j})^2}{1.5} F^n_{BGK,i,j,k} - 1. \quad \text{(B.3)}$$

Jacobian used in the computation is

$$\mathbf{J}^n_{i,k} = \begin{bmatrix} \frac{\sum_{j=1}^{J} F^n_{BGK,i,j,k}}{a^n_{i,k}} & \sum_{j=1}^{J} \eta^n_{i,j_1} F^n_{BGK,i,j,k} & \sum_{j=1}^{J} \eta^n_{i,j_2} F^n_{BGK,i,j,k} & -\sum_{j=1}^{J} (\eta^n_{i,j})^2 F^n_{BGK,i,j,k} \\ \frac{\sum_{j=1}^{J} \eta^n_{i,j_1} F^n_{BGK,i,j,k}}{a^n_{i,k}} & \sum_{j=1}^{J} (\eta^n_{i,j_1})^2 F^n_{BGK,i,j,k} & \sum_{j=1}^{J} \eta^n_{i,j_2} \eta^n_{i,j_1} F^n_{BGK,i,j,k} & -\sum_{j=1}^{J} (\eta^n_{i,j})^2 \eta^n_{i,j_1} F^n_{BGK,i,j,k} \\ \frac{\sum_{j=1}^{J} \eta^n_{i,j_2} F^n_{BGK,i,j,k}}{a^n_{i,k}} & \sum_{j=1}^{J} \eta^n_{i,j_1} \eta^n_{i,j_2} F^n_{BGK,i,j,k} & \sum_{j=1}^{J} (\eta^n_{i,j_2})^2 F^n_{BGK,i,j,k} & -\sum_{j=1}^{J} (\eta^n_{i,j})^2 \eta^n_{i,j_2} F^n_{BGK,i,j,k} \\ \frac{\sum_{j=1}^{J} \frac{(\eta^n_{i,j})^2}{1.5} F^n_{BGK,i,j,k}}{a^n_{i,k}} & \sum_{j=1}^{J} \eta^n_{i,j_1} \frac{(\eta^n_{i,j})^2}{1.5} F^n_{BGK,i,j,k} & \sum_{j=1}^{J} \eta^n_{i,j_2} \frac{(\eta^n_{i,j})^2}{1.5} F^n_{BGK,i,j,k} & -\sum_{j=1}^{J} (\eta^n_{i,j})^2 \frac{(\eta^n_{i,j})^2}{1.5} F^n_{BGK,i,j,k} \end{bmatrix}. \quad \text{(B.4)}$$

B.2 ES-BGK model

For the 1DSW, functions we compute in the N-R algorithm are

$$\tilde{F}1^n_{i,k} = \sum_{j=1}^{J} F^n_{ES,i,j,k} - 1, \quad \tilde{F}2^n_{i,k} = \sum_{j=1}^{J} \eta^n_{i,j_1} F^n_{ES,i,j,k} - 0,$$

$$\tilde{F}3^n_{i,k} = \frac{\sum_{j=1}^{J} \left(\eta^n_{i,j_1}\right)^2 F^n_{ES,i,j,k}}{BB3^n_i} - 1, \quad \tilde{F}4^n_{i,k} = \frac{\sum_{j=1}^{J} \left(\eta^n_{i,j_2}\right)^2 F^n_{ES,i,j,k}}{BB4^n_i} - 1, \tag{B.5}$$

where $BB3^n_i = \frac{1}{2p^n_i}\left(\frac{p^n_{BGK,xx,i}}{\mathrm{Pr}} + \left(1 - \frac{1}{\mathrm{Pr}}\right)p^n_{xx,i}\right)$, $BB4^n_i = \frac{1}{2p^n_i}\left(\frac{p^n_{BGK,yy,i}}{\mathrm{Pr}} + \left(1 - \frac{1}{\mathrm{Pr}}\right)p^n_{yy,i}\right)$.

Jacobian used in the computation is

$$\mathbf{J}^n_{i,k} = \left[\mathbf{J}^n_{i,k,1} \quad \mathbf{J}^n_{i,k,2} \quad \mathbf{J}^n_{i,k,3} \quad \mathbf{J}^n_{i,k,4}\right], \tag{B.6}$$

$$\mathbf{J}^n_{i,k,1} = \begin{bmatrix} \dfrac{\sum_{j=1}^{J} F^n_{ES,i,j,k}}{a^n_{i,k}} \\ \dfrac{\sum_{j=1}^{J} \eta^n_{i,j_1} F^n_{ES,i,j,k}}{a^n_{i,k}} \\ \dfrac{\sum_{j=1}^{J} \left(\eta^n_{i,j_1}\right)^2 F^n_{ES,i,j,k}}{BB3^n_i a^n_{i,k}} \\ \dfrac{\sum_{j=1}^{J} \left(\eta^n_{i,j_2}\right)^2 F^n_{ES,i,j,k}}{BB4^n_i a^n_{i,k}} \end{bmatrix}, \quad \mathbf{J}^n_{i,k,2} = \begin{bmatrix} \sum_{j=1}^{J} \eta^n_{i,j_1} F^n_{ES,i,j,k} \\ \sum_{j=1}^{J} \left(\eta^n_{i,j_1}\right)^2 F^n_{ES,i,j,k} \\ \dfrac{\sum_{j=1}^{J} \left(\eta^n_{i,j_1}\right)^3 F^n_{ES,i,j,k}}{BB3^n_i} \\ \dfrac{\sum_{j=1}^{J} \eta^n_{i,j_1} \left(\eta^n_{i,j_2}\right)^2 F^n_{ES,i,j,k}}{BB4^n_i} \end{bmatrix},$$

$$\mathbf{J}^n_{i,k,3} = \begin{bmatrix} -\sum_{j=1}^{J} \left(\eta^n_{i,j_1}\right)^2 F^n_{ES,i,j,k} \\ -\sum_{j=1}^{J} \left(\eta^n_{i,j_1}\right)^3 F^n_{ES,i,j,k} \\ -\dfrac{\sum_{j=1}^{J} \left(\eta^n_{i,j_1}\right)^4 F^n_{ES,i,j,k}}{BB3^n_i} \\ -\dfrac{\sum_{j=1}^{J} \left(\eta^n_{i,j_1}\right)^2 \left(\eta^n_{i,j_2}\right)^2 F^n_{ES,i,j,k}}{BB4^n_i} \end{bmatrix}, \quad \mathbf{J}^n_{i,k,4} = \begin{bmatrix} -\sum_{j=1}^{J} \left(\left(\eta^n_{i,j_2}\right)^2 + \left(\eta^n_{i,j_3}\right)^2\right) F^n_{ES,i,j,k} \\ -\sum_{j=1}^{J} \left(\left(\eta^n_{i,j_2}\right)^2 + \left(\eta^n_{i,j_3}\right)^2\right) \eta^n_{i,j_1} F^n_{ES,i,j,k} \\ \dfrac{-\sum_{j=1}^{J} \left(\left(\eta^n_{i,j_2}\right)^2 + \left(\eta^n_{i,j_3}\right)^2\right) \left(\eta^n_{i,j_1}\right)^2 F^n_{ES,i,j,k}}{BB3^n_i} \\ \dfrac{-\sum_{j=1}^{J} \left(\left(\eta^n_{i,j_2}\right)^2 + \left(\eta^n_{i,j_3}\right)^2\right) \left(\eta^n_{i,j_2}\right)^2 F^n_{ES,i,j,k}}{BB4^n_i} \end{bmatrix}.$$

For the 1DCF, functions we compute in the N-R algorithm are

$$\tilde{F}1_{i,k}^{n}=\sum_{j=1}^{J}F_{ES,i,j,k}^{n}-1,\quad \tilde{F}2_{i,k}^{n}=\sum_{j=1}^{J}\eta_{i,j_1}^{n}F_{ES,i,j,k}^{n}-1,\qquad \tilde{F}3_{i,k}^{n}=\sum_{j=1}^{J}\eta_{i,j_2}^{n}F_{ES,i,j,k}^{n}-0,$$

$$\tilde{F}4_{i,k}^{n}=\frac{\sum_{j=1}^{J}\left(\eta_{i,j_1}^{n}\right)^2F_{ES,i,j,k}^{n}}{BB4_{i}^{n}}-1,\quad \tilde{F}5_{i,k}^{n}=\frac{\sum_{j=1}^{J}\left(\eta_{i,j_2}^{n}\right)^2F_{ES,i,j,k}^{n}}{BB5_{i}^{n}}-1, \tag{B.7}$$

$$\tilde{F}6_{i,k}^{n}=\frac{\sum_{j=1}^{J}\left(\eta_{i,j_3}^{n}\right)^2F_{ES,i,j,k}^{n}}{BB6_{i}^{n}}-1,\quad \tilde{F}7_{i,k}^{n}=\frac{\sum_{j=1}^{J}\eta_{i,j_1}^{n}\eta_{i,j_2}^{n}F_{ES,i,j,k}^{n}}{BB7_{i}^{n}}-1,$$

where

$$BB4_{i}^{n}=\frac{1}{2p_{i}^{n}}\left(\frac{p_{BGK,xx,i}^{n}}{\mathrm{Pr}}+\left(1-\frac{1}{\mathrm{Pr}}\right)p_{xx,i}^{n}\right),BB5_{i}^{n}=\frac{1}{2p_{i}^{n}}\left(\frac{p_{BGK,yy,i}^{n}}{\mathrm{Pr}}+\left(1-\frac{1}{\mathrm{Pr}}\right)p_{yy,i}^{n}\right),$$

$$BB6_{i}^{n}=\frac{1}{2p_{i}^{n}}\left(\frac{p_{BGK,zz,i}^{n}}{\mathrm{Pr}}+\left(1-\frac{1}{\mathrm{Pr}}\right)p_{zz,i}^{n}\right),\ BB7_{i}^{n}=\frac{1}{2p_{i}^{n}}\left(\frac{p_{BGK,xy,i}^{n}}{\mathrm{Pr}}+\left(1-\frac{1}{\mathrm{Pr}}\right)p_{xy,i}^{n}\right).$$

Note that $\tilde{F}7_{i,k}^{n}=\sum_{j=1}^{J}\eta_{i,j_1}^{n}\eta_{i,j_2}^{n}F_{ES,i,j,k}^{n}-BB7_{i}^{n}$ for situation $\mathrm{Abs}\left(BB7_{i}^{n}\right)<1.\mathrm{D}-5$. Jacobian used in the computation is

$$\mathbf{J}_{i,k}^{n}=\left[\mathbf{J}_{i,k,1}^{n}\quad\mathbf{J}_{i,k,2}^{n}\quad\mathbf{J}_{i,k,3}^{n}\quad\mathbf{J}_{i,k,4}^{n}\quad\mathbf{J}_{i,k,5}^{n}\quad\mathbf{J}_{i,k,6}^{n}\quad\mathbf{J}_{i,k,7}^{n}\right], \tag{B.8}$$

$$\mathbf{J}^n_{i,k,1}=\begin{bmatrix}\dfrac{\sum_{j=1}^{J}F^n_{ES,i,j,k}}{a^n_{i,k}}\\ \dfrac{\sum_{j=1}^{J}\eta^n_{i,j_1}F^n_{ES,i,j,k}}{a^n_{i,k}}\\ \dfrac{\sum_{j=1}^{J}\eta^n_{i,j_2}F^n_{ES,i,j,k}}{a^n_{i,k}}\\ \dfrac{\sum_{j=1}^{J}\left(\eta^n_{i,j_1}\right)^2F^n_{ES,i,j,k}}{BB4^n_i a^n_{i,k}}\\ \dfrac{\sum_{j=1}^{J}\left(\eta^n_{i,j_2}\right)^2F^n_{ES,i,j,k}}{BB5^n_i a^n_{i,k}}\\ \dfrac{\sum_{j=1}^{J}\left(\eta^n_{i,j_3}\right)^2F^n_{ES,i,j,k}}{BB6^n_i a^n_{i,k}}\\ \dfrac{\sum_{j=1}^{J}\eta^n_{i,j_1}\eta^n_{i,j_2}F^n_{ES,i,j,k}}{BB7^n_i a^n_{i,k}}\end{bmatrix},\quad \mathbf{J}^n_{i,k,2}=\begin{bmatrix}\sum_{j=1}^{J}\eta^n_{i,j_1}F^n_{ES,i,j,k}\\ \sum_{j=1}^{J}\eta^n_{i,j_1}\eta^n_{i,j_1}F^n_{ES,i,j,k}\\ \sum_{j=1}^{J}\eta^n_{i,j_1}\eta^n_{i,j_2}F^n_{ES,i,j,k}\\ \dfrac{\sum_{j=1}^{J}\eta^n_{i,j_1}\left(\eta^n_{i,j_1}\right)^2F^n_{ES,i,j,k}}{BB4^n_i}\\ \dfrac{\sum_{j=1}^{J}\eta^n_{i,j_1}\left(\eta^n_{i,j_2}\right)^2F^n_{ES,i,j,k}}{BB5^n_i}\\ \dfrac{\sum_{j=1}^{J}\eta^n_{i,j_1}\left(\eta^n_{i,j_3}\right)^2F^n_{ES,i,j,k}}{BB6^n_i}\\ \dfrac{\sum_{j=1}^{J}\eta^n_{i,j_1}\left(\eta^n_{i,j_1}\eta^n_{i,j_2}\right)F^n_{ES,i,j,k}}{BB7^n_i}\end{bmatrix},\quad \mathbf{J}^n_{i,k,3}=\begin{bmatrix}\sum_{j=1}^{J}\eta^n_{i,j_2}F^n_{ES,i,j,k}\\ \sum_{j=1}^{J}\eta^n_{i,j_2}\eta^n_{i,j_1}F^n_{ES,i,j,k}\\ \sum_{j=1}^{J}\eta^n_{i,j_2}\eta^n_{i,j_2}F^n_{ES,i,j,k}\\ \dfrac{\sum_{j=1}^{J}\eta^n_{i,j_2}\left(\eta^n_{i,j_1}\right)^2F^n_{ES,i,j,k}}{BB4^n_i}\\ \dfrac{\sum_{j=1}^{J}\eta^n_{i,j_2}\left(\eta^n_{i,j_2}\right)^2F^n_{ES,i,j,k}}{BB5^n_i}\\ \dfrac{\sum_{j=1}^{J}\eta^n_{i,j_2}\left(\eta^n_{i,j_3}\right)^2F^n_{ES,i,j,k}}{BB6^n_i}\\ \dfrac{\sum_{j=1}^{J}\eta^n_{i,j_2}\left(\eta^n_{i,j_1}\eta^n_{i,j_2}\right)F^n_{ES,i,j,k}}{BB7^n_i}\end{bmatrix},$$

$$\mathbf{J}^n_{i,k,4}=\begin{bmatrix}-\sum_{j=1}^{J}\left(\eta^n_{i,j_1}\right)^2F^n_{ES,i,j,k}\\ -\sum_{j=1}^{J}\left(\eta^n_{i,j_1}\right)^2\eta^n_{i,j_1}F^n_{ES,i,j,k}\\ -\sum_{j=1}^{J}\left(\eta^n_{i,j_1}\right)^2\eta^n_{i,j_2}F^n_{ES,i,j,k}\\ -\dfrac{\sum_{j=1}^{J}\left(\eta^n_{i,j_1}\right)^2\left(\eta^n_{i,j_1}\right)^2F^n_{ES,i,j,k}}{BB4^n_i}\\ -\dfrac{\sum_{j=1}^{J}\left(\eta^n_{i,j_1}\right)^2\left(\eta^n_{i,j_2}\right)^2F^n_{ES,i,j,k}}{BB5^n_i}\\ -\dfrac{\sum_{j=1}^{J}\left(\eta^n_{i,j_1}\right)^2\left(\eta^n_{i,j_3}\right)^2F^n_{ES,i,j,k}}{BB6^n_i}\\ -\dfrac{\sum_{j=1}^{J}\left(\eta^n_{i,j_1}\right)^2\left(\eta^n_{i,j_1}\eta^n_{i,j_2}\right)F^n_{ES,i,j,k}}{BB7^n_i}\end{bmatrix},\quad \mathbf{J}^n_{i,k,5}=\begin{bmatrix}-\sum_{j=1}^{J}\left(\eta^n_{i,j_2}\right)^2F^n_{ES,i,j,k}\\ -\sum_{j=1}^{J}\left(\eta^n_{i,j_2}\right)^2\eta^n_{i,j_1}F^n_{ES,i,j,k}\\ -\sum_{j=1}^{J}\left(\eta^n_{i,j_2}\right)^2\eta^n_{i,j_2}F^n_{ES,i,j,k}\\ -\dfrac{\sum_{j=1}^{J}\left(\eta^n_{i,j_2}\right)^2\left(\eta^n_{i,j_1}\right)^2F^n_{ES,i,j,k}}{BB4^n_i}\\ -\dfrac{\sum_{j=1}^{J}\left(\eta^n_{i,j_2}\right)^2\left(\eta^n_{i,j_2}\right)^2F^n_{ES,i,j,k}}{BB5^n_i}\\ -\dfrac{\sum_{j=1}^{J}\left(\eta^n_{i,j_2}\right)^2\left(\eta^n_{i,j_3}\right)^2F^n_{ES,i,j,k}}{BB6^n_i}\\ -\dfrac{\sum_{j=1}^{J}\left(\eta^n_{i,j_2}\right)^2\left(\eta^n_{i,j_1}\eta^n_{i,j_2}\right)F^n_{ES,i,j,k}}{BB7^n_i}\end{bmatrix},$$

$$\mathbf{J}^n_{i,k,6}=\begin{bmatrix} -\sum_{j=1}^{J}\left(\eta^n_{i,j_3}\right)^2 F^n_{ES,i,j,k} \\ -\sum_{j=1}^{J}\left(\eta^n_{i,j_3}\right)^2 \eta^n_{i,j_1} F^n_{ES,i,j,k} \\ -\sum_{j=1}^{J}\left(\eta^n_{i,j_3}\right)^2 \eta^n_{i,j_2} F^n_{ES,i,j,k} \\ -\dfrac{\sum_{j=1}^{J}\left(\eta^n_{i,j_3}\right)^2\left(\eta^n_{i,j_1}\right)^2 F^n_{ES,i,j,k}}{BB4^n_i} \\ -\dfrac{\sum_{j=1}^{J}\left(\eta^n_{i,j_3}\right)^2\left(\eta^n_{i,j_2}\right)^2 F^n_{ES,i,j,k}}{BB5^n_i} \\ -\dfrac{\sum_{j=1}^{J}\left(\eta^n_{i,j_3}\right)^2\left(\eta^n_{i,j_3}\right)^2 F^n_{ES,i,j,k}}{BB6^n_i} \\ -\dfrac{\sum_{j=1}^{J}\left(\eta^n_{i,j_3}\right)^2\left(\eta^n_{i,j_1}\eta^n_{i,j_2}\right) F^n_{ES,i,j,k}}{BB7^n_i} \end{bmatrix},\quad \mathbf{J}^n_{i,k,7}=\begin{bmatrix} -\sum_{j=1}^{J}\left(\eta^n_{i,j_1}\eta^n_{i,j_2}\right) F^n_{ES,i,j,k} \\ -\sum_{j=1}^{J}\left(\eta^n_{i,j_1}\eta^n_{i,j_2}\right)\eta^n_{i,j_1} F^n_{ES,i,j,k} \\ -\sum_{j=1}^{J}\left(\eta^n_{i,j_1}\eta^n_{i,j_2}\right)\eta^n_{i,j_2} F^n_{ES,i,j,k} \\ -\dfrac{\sum_{j=1}^{J}\left(\eta^n_{i,j_1}\eta^n_{i,j_2}\right)\left(\eta^n_{i,j_1}\right)^2 F^n_{ES,i,j,k}}{BB4^n_i} \\ -\dfrac{\sum_{j=1}^{J}\left(\eta^n_{i,j_1}\eta^n_{i,j_2}\right)\left(\eta^n_{i,j_2}\right)^2 F^n_{ES,i,j,k}}{BB5^n_i} \\ -\dfrac{\sum_{j=1}^{J}\left(\eta^n_{i,j_1}\eta^n_{i,j_2}\right)\left(\eta^n_{i,j_3}\right)^2 F^n_{ES,i,j,k}}{BB6^n_i} \\ -\dfrac{\sum_{j=1}^{J}\left(\eta^n_{i,j_1}\eta^n_{i,j_2}\right)\left(\eta^n_{i,j_1}\eta^n_{i,j_2}\right) F^n_{ES,i,j,k}}{BB7^n_i} \end{bmatrix}.$$

Note that for situation $\mathrm{Abs}\left(BB7^n_i\right)<1.\mathrm{D}-5$,

$$\mathbf{J}^n_{i,k,71}=\frac{\sum_{j=1}^{J}\eta^n_{i,j_1}\eta^n_{i,j_2}F^n_{ES,i,j,k}}{a^n_{i,k}},\ \mathbf{J}^n_{i,k,72}=\sum_{j=1}^{J}\eta^n_{i,j_1}\left(\eta^n_{i,j_1}\eta^n_{i,j_2}\right)F^n_{ES,i,j,k},\ \mathbf{J}^n_{i,k,73}=\sum_{j=1}^{J}\eta^n_{i,j_2}\left(\eta^n_{i,j_1}\eta^n_{i,j_2}\right)F^n_{ES,i,j,k},$$

$$\mathbf{J}^n_{i,k,74}=-\sum_{j=1}^{J}\left(\eta^n_{i,j_1}\right)^2\left(\eta^n_{i,j_1}\eta^n_{i,j_2}\right)F^n_{ES,i,j,k},\ \mathbf{J}^n_{i,k,75}=-\sum_{j=1}^{J}\left(\eta^n_{i,j_2}\right)^2\left(\eta^n_{i,j_1}\eta^n_{i,j_2}\right)F^n_{ES,i,j,k},$$

$$\mathbf{J}^n_{i,k,76}=-\sum_{j=1}^{J}\left(\eta^n_{i,j_3}\right)^2\left(\eta^n_{i,j_1}\eta^n_{i,j_2}\right)F^n_{ES,i,j,k},\ \mathbf{J}^n_{i,k,77}=-\sum_{j=1}^{J}\left(\eta^n_{i,j_1}\eta^n_{i,j_2}\right)\left(\eta^n_{i,j_1}\eta^n_{i,j_2}\right)F^n_{ES,i,j,k}.$$

B.3 $\nu(C)$-BGK model

For the 1DSW, functions we compute in the N-R algorithm are

$$\tilde{F}1^n_{i,k}=\frac{\sum_{j=1}^{J}\hat{v}^n_{i,j}F^n_{\gamma,i,j,k}}{\tilde{f}1^n_i}-1,\qquad \tilde{F}2^n_{i,k}=\frac{\sum_{j=1}^{J}\eta^n_{i,j_1}\hat{v}^n_{i,j}F^n_{\gamma,i,j,k}}{\tilde{f}2^n_i}-1, \tag{B.9}$$

$$\tilde{F}3_{i,k}^{n}=\frac{\sum_{j=1}^{J}\left(\eta_{i,j}^{n}\right)^{2}\hat{v}_{i,j}^{n}F_{\gamma,i,j,k}^{n}}{\tilde{f}3_{i}^{n}}-1,$$

where $\tilde{f}1_{i}^{n}=\sum_{j=1}^{J}\hat{v}_{i,j}^{n}\frac{f_{i,j}^{n}}{\rho_{i}^{n}}\Delta\mathbf{c}$, $\tilde{f}2_{i}^{n}=\sum_{j=1}^{J}\eta_{i,j_1}^{n}\hat{v}_{i,j}^{n}\frac{f_{i,j}^{n}}{\rho_{i}^{n}}\Delta\mathbf{c}$, $\tilde{f}3_{i}^{n}=\sum_{j=1}^{J}\left(\eta_{i,j}^{n}\right)^{2}\hat{v}_{i,j}^{n}\frac{f_{i,j}^{n}}{\rho_{i}^{n}}\Delta\mathbf{c}$. Note that $\tilde{F}2_{i,k}^{n}=\sum_{j=1}^{J}\eta_{i,j_1}^{n}\hat{v}_{i,j}^{n}F_{\gamma,i,j,k}^{n}-\tilde{f}2_{i}^{n}$ for situation $\mathrm{Abs}\left(\tilde{f}2_{i}^{n}\right)<1.\mathrm{D}-5$ (which may happen when $u_{x,i}^{n}\approx 0.0$. Jacobian used in the computation is

$$\mathbf{J}_{i,k}^{n}=\begin{bmatrix}\mathbf{J}_{i,k,1}^{n}\\ \mathbf{J}_{i,k,2}^{n}\\ \mathbf{J}_{i,k,3}^{n}\end{bmatrix}, \tag{B.10}$$

$$\mathbf{J}_{i,k,1}^{n}=\begin{bmatrix}\dfrac{\sum_{j=1}^{J}\hat{v}_{i,j}^{n}F_{\gamma,i,j,k}^{n}}{a_{i,k}^{n}\tilde{f}1_{i}^{n}} & \dfrac{\sum_{j=1}^{J}\eta_{i,j_1}^{n}\hat{v}_{i,j}^{n}F_{\gamma,i,j,k}^{n}}{\tilde{f}1_{i}^{n}} & -\dfrac{\sum_{j=1}^{J}\left(\eta_{i,j}^{n}\right)^{2}\hat{v}_{i,j}^{n}F_{\gamma,i,j,k}^{n}}{\tilde{f}1_{i}^{n}}\end{bmatrix},$$

$$\mathbf{J}_{i,k,2}^{n}=\begin{bmatrix}\dfrac{\sum_{j=1}^{J}\eta_{i,j_1}^{n}\hat{v}_{i,j}^{n}F_{\gamma,i,j,k}^{n}}{a_{i,k}^{n}\tilde{f}2_{i}^{n}} & \dfrac{\sum_{j=1}^{J}\left(\eta_{i,j_1}^{n}\right)^{2}\hat{v}_{i,j}^{n}F_{\gamma,i,j,k}^{n}}{\tilde{f}2_{i}^{n}} & -\dfrac{\sum_{j=1}^{J}\left(\eta_{i,j}^{n}\right)^{2}\eta_{i,j_1}^{n}\hat{v}_{i,j}^{n}F_{\gamma,i,j,k}^{n}}{\tilde{f}2_{i}^{n}}\end{bmatrix},$$

$$\mathbf{J}_{i,k,3}^{n}=\begin{bmatrix}\dfrac{\sum_{j=1}^{J}\left(\eta_{i,j}^{n}\right)^{2}\hat{v}_{i,j}^{n}F_{\gamma,i,j,k}^{n}}{a_{i,k}^{n}\tilde{f}3_{i}^{n}} & \dfrac{\sum_{j=1}^{J}\eta_{i,j_1}^{n}\left(\eta_{i,j}^{n}\right)^{2}\hat{v}_{i,j}^{n}F_{\gamma,i,j,k}^{n}}{\tilde{f}3_{i}^{n}} & -\dfrac{\sum_{j=1}^{J}\left(\eta_{i,j}^{n}\right)^{4}\hat{v}_{i,j}^{n}F_{\gamma,i,j,k}^{n}}{\tilde{f}3_{i}^{n}}\end{bmatrix},$$

Note that for situation $\mathrm{Abs}\left(\tilde{f}2_{i}^{n}\right)<1.\mathrm{D}-5$,

$$\mathbf{J}_{i,k,2}^{n}=\begin{bmatrix}\dfrac{\sum_{j=1}^{J}\eta_{i,j_1}^{n}\hat{v}_{i,j}^{n}F_{\gamma,i,j,k}^{n}}{a_{i,k}^{n}} & \sum_{j=1}^{J}\left(\eta_{i,j_1}^{n}\right)^{2}\hat{v}_{i,j}^{n}F_{\gamma,i,j,k}^{n} & -\sum_{j=1}^{J}\left(\eta_{i,j}^{n}\right)^{2}\eta_{i,j_1}^{n}\hat{v}_{i,j}^{n}F_{\gamma,i,j,k}^{n}\end{bmatrix}.$$

For the 1DCF, functions we compute in the N-R algorithm are

$$\tilde{F}1_{i,k}^n = \frac{\sum_{j=1}^{J} \hat{v}_{i,j}^n F_{\gamma,i,j,k}^n}{\tilde{f}1_i^n} - 1, \qquad \tilde{F}2_{i,k}^n = \frac{\sum_{j=1}^{J} \eta_{i,j_1}^n \hat{v}_{i,j}^n F_{\gamma,i,j,k}^n}{\tilde{f}2_i^n} - 1, \tag{B.11}$$

$$\tilde{F}3_{i,k}^n = \frac{\sum_{j=1}^{J} \eta_{i,j_2}^n \hat{v}_{i,j}^n F_{\gamma,i,j,k}^n}{\tilde{f}3_i^n} - 1, \quad \tilde{F}4_{i,k}^n = \frac{\sum_{j=1}^{J} \left(\eta_{i,j}^n\right)^2 \hat{v}_{i,j}^n F_{\gamma,i,j,k}^n}{\tilde{f}4_i^n} - 1,$$

where $\tilde{f}1_i^n = \sum_{j=1}^{J} \hat{v}_{i,j}^n \frac{f_{i,j}^n}{\rho_i^n} \Delta\mathbf{c}$, $\tilde{f}2_i^n = \sum_{j=1}^{J} \eta_{i,j_1}^n \hat{v}_{i,j}^n \frac{f_{i,j}^n}{\rho_i^n} \Delta\mathbf{c}$, $\tilde{f}3_i^n = \sum_{j=1}^{J} \eta_{i,j_2}^n \hat{v}_{i,j}^n \frac{f_{i,j}^n}{\rho_i^n} \Delta\mathbf{c}$,

$\tilde{f}4_i^n = \sum_{j=1}^{J} \left(\eta_{i,j}^n\right)^2 \hat{v}_{i,j}^n \frac{f_{i,j}^n}{\rho_i^n} \Delta\mathbf{c}$. Note that $\tilde{F}2_{i,k}^n = \sum_{j=1}^{J} \eta_{i,j_1}^n \hat{v}_{i,j}^n F_{\gamma,i,j,k}^n - \tilde{f}2_i^n$ for situation $\mathrm{Abs}\left(\tilde{f}2_i^n\right) < 1.\mathrm{D}-5$ (which may happen when $u_{x,i}^n \approx 0.0$), and $\tilde{F}3_{i,k}^n = \sum_{j=1}^{J} \eta_{i,j_2}^n \hat{v}_{i,j}^n F_{\gamma,i,j,k}^n - \tilde{f}3_i^n$ for situation $\mathrm{Abs}\left(\tilde{f}3_i^n\right) < 1.\mathrm{D}-5$ (which may happen when $u_{y,i}^n \approx 0.0$). Jacobian used in the computation is

$$\mathbf{J}_{i,k}^n = \begin{bmatrix} \mathbf{J}_{i,k,1}^n \\ \mathbf{J}_{i,k,2}^n \\ \mathbf{J}_{i,k,3}^n \\ \mathbf{J}_{i,k,4}^n \end{bmatrix}, \tag{B.12}$$

$$\mathbf{J}_{i,k,1}^n = \left[\frac{\sum_{j=1}^{J} \hat{v}_{i,j}^n F_{\gamma,i,j,k}^n}{a_{i,k}^n \tilde{f}1_i^n} \quad \frac{\sum_{j=1}^{J} \eta_{i,j_1}^n \hat{v}_{i,j}^n F_{\gamma,i,j,k}^n}{\tilde{f}1_i^n} \quad \frac{\sum_{j=1}^{J} \eta_{i,j_2}^n \hat{v}_{i,j}^n F_{\gamma,i,j,k}^n}{\tilde{f}1_i^n} \quad -\frac{\sum_{j=1}^{J} \left(\eta_{i,j}^n\right)^2 \hat{v}_{i,j}^n F_{\gamma,i,j,k}^n}{\tilde{f}1_i^n} \right],$$

$$\mathbf{J}_{i,k,2}^n = \left[\frac{\sum_{j=1}^{J} \eta_{i,j_1}^n \hat{v}_{i,j}^n F_{\gamma,i,j,k}^n}{a_{i,k}^n \tilde{f}2_i^n} \quad \frac{\sum_{j=1}^{J} \eta_{i,j_1}^n \eta_{i,j_1}^n \hat{v}_{i,j}^n F_{\gamma,i,j,k}^n}{\tilde{f}2_i^n} \quad \frac{\sum_{j=1}^{J} \eta_{i,j_2}^n \eta_{i,j_1}^n \hat{v}_{i,j}^n F_{\gamma,i,j,k}^n}{\tilde{f}2_i^n} \quad -\frac{\sum_{j=1}^{J} \left(\eta_{i,j}^n\right)^2 \eta_{i,j_1}^n \hat{v}_{i,j}^n F_{\gamma,i,j,k}^n}{\tilde{f}2_i^n} \right],$$

$$\mathbf{J}_{i,k,3}^n = \left[\frac{\sum_{j=1}^{J} \eta_{i,j_2}^n \hat{v}_{i,j}^n F_{\gamma,i,j,k}^n}{a_{i,k}^n \tilde{f}3_i^n} \quad \frac{\sum_{j=1}^{J} \eta_{i,j_1}^n \eta_{i,j_2}^n \hat{v}_{i,j}^n F_{\gamma,i,j,k}^n}{\tilde{f}3_i^n} \quad \frac{\sum_{j=1}^{J} \eta_{i,j_2}^n \eta_{i,j_2}^n \hat{v}_{i,j}^n F_{\gamma,i,j,k}^n}{\tilde{f}3_i^n} \quad -\frac{\sum_{j=1}^{J} \left(\eta_{i,j}^n\right)^2 \eta_{i,j_2}^n \hat{v}_{i,j}^n F_{\gamma,i,j,k}^n}{\tilde{f}3_i^n} \right],$$

$$\mathbf{J}_{i,k,4}^{n}=\left[\frac{\sum_{j=1}^{J}\left(\eta_{i,j}^{n}\right)^{2}\hat{v}_{i,j}^{n}F_{\gamma,i,j,k}^{n}}{a_{i,k}^{n}\tilde{f}4_{i}^{n}}\quad\frac{\sum_{j=1}^{J}\eta_{i,j_1}^{n}\left(\eta_{i,j}^{n}\right)^{2}\hat{v}_{i,j}^{n}F_{\gamma,i,j,k}^{n}}{\tilde{f}4_{i}^{n}}\quad\frac{\sum_{j=1}^{J}\eta_{i,j_2}^{n}\left(\eta_{i,j}^{n}\right)^{2}\hat{v}_{i,j}^{n}F_{\gamma,i,j,k}^{n}}{\tilde{f}4_{i}^{n}}\quad-\frac{\sum_{j=1}^{J}\left(\eta_{i,j}^{n}\right)^{2}\left(\eta_{i,j}^{n}\right)^{2}\hat{v}_{i,j}^{n}F_{\gamma,i,j,k}^{n}}{\tilde{f}4_{i}^{n}}\right].$$

Note that for situation $\mathrm{Abs}\left(\tilde{f}2_{i}^{n}\right)<1.\mathrm{D}-5$,

$$\mathbf{J}_{i,k,2}^{n}=\left[\frac{\sum_{j=1}^{J}\eta_{i,j_1}^{n}\hat{v}_{i,j}^{n}F_{\gamma,i,j,k}^{n}}{a_{i,k}^{n}}\quad\sum_{j=1}^{J}\eta_{i,j_1}^{n}\eta_{i,j_1}^{n}\hat{v}_{i,j}^{n}F_{\gamma,i,j,k}^{n}\quad\sum_{j=1}^{J}\eta_{i,j_2}^{n}\eta_{i,j_1}^{n}\hat{v}_{i,j}^{n}F_{\gamma,i,j,k}^{n}\quad-\sum_{j=1}^{J}\left(\eta_{i,j}^{n}\right)^{2}\eta_{i,j_1}^{n}\hat{v}_{i,j}^{n}F_{\gamma,i,j,k}^{n}\right],$$

and for situation $\mathrm{Abs}\left(\tilde{f}3_{i}^{n}\right)<1.\mathrm{D}-5$,

$$\mathbf{J}_{i,k,3}^{n}=\left[\frac{\sum_{j=1}^{J}\eta_{i,j_2}^{n}\hat{v}_{i,j}^{n}F_{\gamma,i,j,k}^{n}}{a_{i,k}^{n}}\quad\sum_{j=1}^{J}\eta_{i,j_1}^{n}\eta_{i,j_2}^{n}\hat{v}_{i,j}^{n}F_{\gamma,i,j,k}^{n}\quad\sum_{j=1}^{J}\eta_{i,j_2}^{n}\eta_{i,j_2}^{n}\hat{v}_{i,j}^{n}F_{\gamma,i,j,k}^{n}\quad-\sum_{j=1}^{J}\left(\eta_{i,j}^{n}\right)^{2}\eta_{i,j_2}^{n}\hat{v}_{i,j}^{n}F_{\gamma,i,j,k}^{n}\right]$$

B.4 New kinetic model I

For the 1DSW, functions we compute in the N-R algorithm are

$$\tilde{F}1_{i,k}^{n}=\frac{\sum_{j=1}^{J}\hat{v}_{i,j}^{n}F_{NI,i,j,k}^{n}}{\tilde{f}1_{i}^{n}}-1,\ \tilde{F}2_{i,k}^{n}=\frac{\sum_{j=1}^{J}\eta_{i,j_1}^{n}\hat{v}_{i,j}^{n}F_{NI,i,j,k}^{n}}{\tilde{f}2_{i}^{n}}-1,\ \tilde{F}3_{i,k}^{n}=\frac{\sum_{j=1}^{J}\left(\eta_{i,j}^{n}\right)^{2}\hat{v}_{i,j}^{n}F_{NI,i,j,k}^{n}}{\tilde{f}3_{i}^{n}}-1 \quad \text{(B.13)}$$

where $\tilde{f}1_{i}^{n}=\sum_{j=1}^{J}\hat{v}_{i,j}^{n}\frac{f_{i,j}^{n}}{\rho_{i}^{n}}\Delta\mathbf{c}$, $\tilde{f}2_{i}^{n}=\sum_{j=1}^{J}\eta_{i,j_1}^{n}\hat{v}_{i,j}^{n}\frac{f_{i,j}^{n}}{\rho_{i}^{n}}\Delta\mathbf{c}$, $\tilde{f}3_{i}^{n}=\sum_{j=1}^{J}\left(\eta_{i,j}^{n}\right)^{2}\hat{v}_{i,j}^{n}\frac{f_{i,j}^{n}}{\rho_{i}^{n}}\Delta\mathbf{c}$. Note that $\tilde{F}2_{i,k}^{n}=\sum_{j=1}^{J}\eta_{i,j_1}^{n}\hat{v}_{i,j}^{n}F_{NI,i,j,k}^{n}-\tilde{f}2_{i}^{n}$ for situation $\mathrm{Abs}(\tilde{f}2_{i}^{n})<1.\mathrm{D}-5$ (which may happen when $u_{x,i}^{n}\approx 0.0$). Jacobian used in the computation is

$$\mathbf{J}_{i,k}^{n}=\begin{bmatrix}\mathbf{J}_{i,k,1}^{n}\\ \mathbf{J}_{i,k,2}^{n}\\ \mathbf{J}_{i,k,3}^{n}\end{bmatrix}, \quad \text{(B.14)}$$

$$\mathbf{J}_{i,k,1}^{n}=\left[\frac{\sum_{j=1}^{J}\hat{v}_{i,j}^{n}F_{NI,i,j,k}^{n}}{a_{i,k}^{n}\tilde{f}1_{i}^{n}}\quad\frac{\sum_{j=1}^{J}\hat{v}_{i,j}^{n}\eta_{i,j_1}^{n}F_{NI,i,j,k}^{n}}{\tilde{f}1_{i}^{n}}\quad-\frac{\sum_{j=1}^{J}\hat{v}_{i,j}^{n}A_{i,j}^{n}F_{NI,i,j,k}^{n}}{\tilde{f}1_{i}^{n}}\right],$$

$$\mathbf{J}_{i,k,2}^{n}=\left[\frac{\sum_{j=1}^{J}\hat{v}_{i,j}^{n}\eta_{i,j_1}^{n}F_{NI,i,j,k}^{n}}{a_{i,k}^{n}\tilde{f}2_{i}^{n}}\quad\frac{\sum_{j=1}^{J}\hat{v}_{i,j}^{n}\left(\eta_{i,j_1}^{n}\right)^{2}F_{NI,i,j,k}^{n}}{\tilde{f}2_{i}^{n}}\quad-\frac{\sum_{j=1}^{J}\hat{v}_{i,j}^{n}A_{i,j}^{n}\eta_{i,j_1}^{n}F_{NI,i,j,k}^{n}}{\tilde{f}2_{i}^{n}}\right],$$

$$\mathbf{J}_{i,k,3}^{n}=\left[\frac{\sum_{j=1}^{J}\hat{v}_{i,j}^{n}\left(\eta_{i,j}^{n}\right)^{2}F_{NI,i,j,k}^{n}}{a_{i,k}^{n}\tilde{f}3_{i}^{n}}\quad\frac{\sum_{j=1}^{J}\hat{v}_{i,j}^{n}\eta_{i,j_1}^{n}\left(\eta_{i,j}^{n}\right)^{2}F_{NI,i,j,k}^{n}}{\tilde{f}3_{i}^{n}}\quad-\frac{\sum_{j=1}^{J}\hat{v}_{i,j}^{n}A_{i,j}^{n}\left(\eta_{i,j}^{n}\right)^{2}F_{NI,i,j,k}^{n}}{\tilde{f}3_{i}^{n}}\right].$$

Note that for situation $\text{Abs}(\tilde{f}2_{i}^{n})<1.\text{D}-5$,

$$\mathbf{J}_{i,k,2}^{n}=\left[\frac{\sum_{j=1}^{J}\hat{v}_{i,j}^{n}\eta_{i,j_1}^{n}F_{NI,i,j,k}^{n}}{a_{i,k}^{n}}\quad\sum_{j=1}^{J}\hat{v}_{i,j}^{n}\left(\eta_{i,j_1}^{n}\right)^{2}F_{NI,i,j,k}^{n}\quad-\sum_{j=1}^{J}\hat{v}_{i,j}^{n}A_{i,j}^{n}\eta_{i,j_1}^{n}F_{NI,i,j,k}^{n}\right].$$

For the 1DCF, functions we compute in the N-R algorithm are

$$\tilde{F}1_{i,k}^{n}=\frac{\sum_{j=1}^{J}\hat{v}_{i,j}^{n}F_{NI,i,j,k}^{n}}{\tilde{f}1_{i}^{n}}-1,\qquad\tilde{F}2_{i,k}^{n}=\frac{\sum_{j=1}^{J}\eta_{i,j_1}^{n}\hat{v}_{i,j}^{n}F_{NI,i,j,k}^{n}}{\tilde{f}2_{i}^{n}}-1,\qquad\text{(B.15)}$$

$$\tilde{F}3_{i,k}^{n}=\frac{\sum_{j=1}^{J}\eta_{i,j_2}^{n}\hat{v}_{i,j}^{n}F_{NI,i,j,k}^{n}}{\tilde{f}3_{i}^{n}}-1,\quad\tilde{F}4_{i,k}^{n}=\frac{\sum_{j=1}^{J}\left(\eta_{i,j}^{n}\right)^{2}\hat{v}_{i,j}^{n}F_{NI,i,j,k}^{n}}{\tilde{f}4_{i}^{n}}-1,$$

where $\tilde{f}1_{i}^{n}=\sum_{j=1}^{J}\hat{v}_{i,j}^{n}\frac{f_{i,j}^{n}}{\rho_{i}^{n}}\Delta\mathbf{c}$, $\tilde{f}2_{i}^{n}=\sum_{j=1}^{J}\eta_{i,j_1}^{n}\hat{v}_{i,j}^{n}\frac{f_{i,j}^{n}}{\rho_{i}^{n}}\Delta\mathbf{c}$, $\tilde{f}3_{i}^{n}=\sum_{j=1}^{J}\eta_{i,j_2}^{n}\hat{v}_{i,j}^{n}\frac{f_{i,j}^{n}}{\rho_{i}^{n}}\Delta\mathbf{c}$,

$\tilde{f}4_{i}^{n}=\sum_{j=1}^{J}\left(\eta_{i,j}^{n}\right)^{2}\hat{v}_{i,j}^{n}\frac{f_{i,j}^{n}}{\rho_{i}^{n}}\Delta\mathbf{c}$. Note that $\tilde{F}2_{i,k}^{n}=\sum_{j=1}^{J}\eta_{i,j_1}^{n}\hat{v}_{i,j}^{n}F_{NI,i,j,k}^{n}-\tilde{f}2_{i}^{n}$ for situation $\text{Abs}(\tilde{f}2_{i}^{n})<1.\text{D}-5$, and $\tilde{F}3_{i,k}^{n}=\sum_{j=1}^{J}\eta_{i,j_2}^{n}\hat{v}_{i,j}^{n}F_{NI,i,j,k}^{n}-\tilde{f}3_{i}^{n}$ for situation $\text{Abs}(\tilde{f}3_{i}^{n})<1.\text{D}-5$. Jacobian used in the computation is

$$\mathbf{J}_{i,k}^{n} = \begin{bmatrix} \mathbf{J}_{i,k,1}^{n} \\ \mathbf{J}_{i,k,2}^{n} \\ \mathbf{J}_{i,k,3}^{n} \\ \mathbf{J}_{i,k,4}^{n} \end{bmatrix}, \tag{B.16}$$

$$\mathbf{J}_{i,k,1}^{n} = \begin{bmatrix} \dfrac{\sum_{j=1}^{J} \hat{v}_{i,j}^{n} F_{NI,i,j,k}^{n}}{a_{i,k}^{n}} & \dfrac{\sum_{j=1}^{J} \hat{v}_{i,j}^{n} \eta_{i,j_1}^{n} F_{NI,i,j,k}^{n}}{\tilde{f}1_{i}^{n}} & \dfrac{\sum_{j=1}^{J} \hat{v}_{i,j}^{n} \eta_{i,j_2}^{n} F_{NI,i,j,k}^{n}}{\tilde{f}1_{i}^{n}} & -\dfrac{\sum_{j=1}^{J} \hat{v}_{i,j}^{n} A_{i,j}^{n} F_{NI,i,j,k}^{n}}{\tilde{f}1_{i}^{n}} \end{bmatrix},$$

$$\mathbf{J}_{i,k,2}^{n} = \begin{bmatrix} \dfrac{\sum_{j=1}^{J} \hat{v}_{i,j}^{n} \eta_{i,j_1}^{n} F_{NI,i,j,k}^{n}}{a_{i,k}^{n} \tilde{f}2_{i}^{n}} & \dfrac{\sum_{j=1}^{J} \hat{v}_{i,j}^{n} \eta_{i,j_1}^{n} \eta_{i,j_1}^{n} F_{NI,i,j,k}^{n}}{\tilde{f}2_{i}^{n}} & \dfrac{\sum_{j=1}^{J} \hat{v}_{i,j}^{n} \eta_{i,j_2}^{n} \eta_{i,j_1}^{n} F_{NI,i,j,k}^{n}}{\tilde{f}2_{i}^{n}} & -\dfrac{\sum_{j=1}^{J} \hat{v}_{i,j}^{n} A_{i,j}^{n} \eta_{i,j_1}^{n} F_{NI,i,j,k}^{n}}{\tilde{f}2_{i}^{n}} \end{bmatrix},$$

$$\mathbf{J}_{i,k,3}^{n} = \begin{bmatrix} \dfrac{\sum_{j=1}^{J} \hat{v}_{i,j}^{n} \eta_{i,j_2}^{n} F_{NI,i,j,k}^{n}}{a_{i,k}^{n} \tilde{f}3_{i}^{n}} & \dfrac{\sum_{j=1}^{J} \hat{v}_{i,j}^{n} \eta_{i,j_1}^{n} \eta_{i,j_2}^{n} F_{NI,i,j,k}^{n}}{\tilde{f}3_{i}^{n}} & \dfrac{\sum_{j=1}^{J} \hat{v}_{i,j}^{n} \eta_{i,j_2}^{n} \eta_{i,j_2}^{n} F_{NI,i,j,k}^{n}}{\tilde{f}3_{i}^{n}} & -\dfrac{\sum_{j=1}^{J} \hat{v}_{i,j}^{n} A_{i,j}^{n} \eta_{i,j_2}^{n} F_{NI,i,j,k}^{n}}{\tilde{f}3_{i}^{n}} \end{bmatrix},$$

$$\mathbf{J}_{i,k,4}^{n} = \begin{bmatrix} \dfrac{\sum_{j=1}^{J} \hat{v}_{i,j}^{n} (\eta_{i,j}^{n})^2 F_{NI,i,j,k}^{n}}{a_{i,k}^{n} \tilde{f}4_{i}^{n}} & \dfrac{\sum_{j=1}^{J} \hat{v}_{i,j}^{n} \eta_{i,j_1}^{n} (\eta_{i,j}^{n})^2 F_{NI,i,j,k}^{n}}{\tilde{f}4_{i}^{n}} & \dfrac{\sum_{j=1}^{J} \hat{v}_{i,j}^{n} \eta_{i,j_2}^{n} (\eta_{i,j}^{n})^2 F_{NI,i,j,k}^{n}}{\tilde{f}4_{i}^{n}} & -\dfrac{\sum_{j=1}^{J} \hat{v}_{i,j}^{n} A_{i,j}^{n} (\eta_{i,j}^{n})^2 F_{NI,i,j,k}^{n}}{\tilde{f}4_{i}^{n}} \end{bmatrix}.$$

Note that for situation $\mathrm{Abs}(\tilde{f}2_{i}^{n}) < 1.\mathrm{D}-5$,

$$\mathbf{J}_{i,k,2}^{n} = \begin{bmatrix} \dfrac{\sum_{j=1}^{J} \hat{v}_{i,j}^{n} \eta_{i,j_1}^{n} F_{NI,i,j,k}^{n}}{a_{I,k}^{n}} & \sum_{j=1}^{J} \hat{v}_{i,j}^{n} \eta_{i,j_1}^{n} \eta_{i,j_1}^{n} F_{NI,i,j,k}^{n} & \sum_{j=1}^{J} \hat{v}_{i,j}^{n} \eta_{i,j_2}^{n} \eta_{i,j_1}^{n} F_{NI,i,j,k}^{n} & -\sum_{j=1}^{J} \hat{v}_{i,j}^{n} A_{i,j}^{n} \eta_{i,j_1}^{n} F_{NI,i,j,k}^{n} \end{bmatrix},$$

and for situation $\mathrm{Abs}(\tilde{f}3_{i}^{n}) < 1.\mathrm{D}-5$,

$$\mathbf{J}_{i,k,3}^{n} = \begin{bmatrix} \dfrac{\sum_{j=1}^{J} \hat{v}_{i,j}^{n} \eta_{i,j_2}^{n} F_{NI,i,j,k}^{n}}{a_{i,k}^{n}} & \sum_{j=1}^{J} \hat{v}_{i,j}^{n} \eta_{i,j_1}^{n} \eta_{i,j_2}^{n} F_{NI,i,j,k}^{n} & \sum_{j=1}^{J} \hat{v}_{i,j}^{n} \eta_{i,j_2}^{n} \eta_{i,j_2}^{n} F_{NI,i,j,k}^{n} & -\sum_{j=1}^{J} \hat{v}_{i,j}^{n} A_{i,j}^{n} \eta_{i,j_2}^{n} F_{NI,i,j,k}^{n} \end{bmatrix}.$$

B.5 New kinetic model II

For the 1DSW, functions we compute in the N-R algorithm are

$$\tilde{F}1_{i,k}^n = \frac{\sum_{j=1}^{J} \hat{v}_{i,j}^n F_{NII,i,j,k}^n}{\tilde{f}1_i^n} - 1, \qquad \tilde{F}2_{i,k}^n = \frac{\sum_{j=1}^{J} \eta_{i,j_1}^n \hat{v}_{i,j}^n F_{NII,i,j,k}^n}{\tilde{f}2_i^n} - 1, \tag{B.17}$$

$$\tilde{F}3_{i,k}^n = \frac{\sum_{j=1}^{J} (\eta_{i,j_1}^n)^2 \hat{v}_{i,j}^n F_{NII,i,j,k}^n}{\tilde{f}3_i^n} - 1, \qquad \tilde{F}4_{i,k}^n = \frac{\sum_{j=1}^{J} (\eta_{i,j_2}^n)^2 \hat{v}_{i,j}^n F_{NII,i,j,k}^n}{\tilde{f}4_i^n} - 1,$$

where . $\tilde{f}1_i^n = \sum_{j=1}^{J} \hat{v}_{i,j}^n \frac{f_{i,j}^n}{\rho_i^n} \Delta \mathbf{c}$, $\tilde{f}2_i^n = \sum_{j=1}^{J} \eta_{i,j_1}^n \hat{v}_{i,j}^n \frac{f_{i,j}^n}{\rho_i^n} \Delta \mathbf{c}$,

$$\tilde{f}3_i^n = \sum_{j=1}^{J} (\eta_{i,j_1}^n)^2 \hat{v}_{i,j}^n \frac{f_{i,j}^n}{\rho_i^n} \Delta \mathbf{c} + \frac{(p_{BGK,xx,i}^n - p_{xx,i}^n)}{2p_i^n}, \tilde{f}4_i^n = \sum_{j=1}^{J} (\eta_{i,j_2}^n)^2 \hat{v}_{i,j}^n \frac{f_{i,j}^n}{\rho_i^n} \Delta \mathbf{c} + \frac{(p_{BGK,yy,i}^n - p_{yy,i}^n)}{2p_i^n}.$$

Note that $\tilde{F}2_{i,k}^n = \sum_{j=1}^{J} \eta_{i,j_1}^n \hat{v}_{i,j}^n F_{NII,i,j,k}^n - \tilde{f}2_i^n$ for situation $\text{Abs}(\tilde{f}2_i^n) < 1.\text{D}-5$ (which may happen when $u_{x,i}^n \approx 0.0$). Jacobian used in the computation is

$$\mathbf{J}_{i,k}^n = \begin{bmatrix} \mathbf{J}_{i,k,1}^n & \mathbf{J}_{i,k,2}^n & \mathbf{J}_{i,k,3}^n & \mathbf{J}_{i,k,4}^n \end{bmatrix}, \tag{B.18}$$

$$\mathbf{J}_{i,k,1}^n = \begin{bmatrix} \frac{\sum_{j=1}^{J} \hat{v}_{i,j}^n F_{NII,i,j,k}^n}{a_{i,k}^n \tilde{f}1_i^n} \\ \frac{\sum_{j=1}^{J} \hat{v}_{i,j}^n \eta_{i,j_1}^n F_{NII,i,j,k}^n}{a_{i,k}^n \tilde{f}2_i^n} \\ \frac{\sum_{j=1}^{J} \hat{v}_{i,j}^n (\eta_{i,j_1}^n)^2 F_{NII,i,j,k}^n}{a_{i,k}^n \tilde{f}3_i^n} \\ \frac{\sum_{j=1}^{J} \hat{v}_{i,j}^n (\eta_{i,j_2}^n)^2 F_{NII,i,j,k}^n}{a_{i,k}^n \tilde{f}4_i^n} \end{bmatrix}, \quad \mathbf{J}_{i,k,2}^n = \begin{bmatrix} \frac{\sum_{j=1}^{J} \hat{v}_{i,j}^n \eta_{i,j_1}^n F_{NII,i,j,k}^n}{\tilde{f}1_i^n} \\ \frac{\sum_{j=1}^{J} \hat{v}_{i,j}^n (\eta_{i,j_1}^n)^2 F_{NII,i,j,k}^n}{\tilde{f}2_i^n} \\ \frac{\sum_{j=1}^{J} \hat{v}_{i,j}^n (\eta_{i,j_1}^n)^3 F_{NII,i,j,k}^n}{\tilde{f}3_i^n} \\ \frac{\sum_{j=1}^{J} \hat{v}_{i,j}^n \eta_{i,j_1}^n (\eta_{i,j_2}^n)^2 F_{NII,i,j,k}^n}{\tilde{f}4_i^n} \end{bmatrix},$$

$$\mathbf{J}^n_{i,k,3}=\begin{bmatrix} -\dfrac{\sum_{j=1}^{J}\hat{v}^n_{i,j}\left(\eta^n_{i,j_1}\right)^2F^n_{NII,i,j,k}}{\tilde{f}1^n_i} \\ -\dfrac{\sum_{j=1}^{J}\hat{v}^n_{i,j}\left(\eta^n_{i,j_1}\right)^3F^n_{NII,i,j,k}}{\tilde{f}2^n_i} \\ -\dfrac{\sum_{j=1}^{J}\hat{v}^n_{i,j}\left(\eta^n_{i,j_1}\right)^4F^n_{NII,i,j,k}}{\tilde{f}3^n_i} \\ -\dfrac{\sum_{j=1}^{J}\hat{v}^n_{i,j}\left(\eta^n_{i,j_1}\right)^2\left(\eta^n_{i,j_2}\right)^2F^n_{NII,i,j,k}}{\tilde{f}4^n_i} \end{bmatrix},\quad \mathbf{J}^n_{i,k,4}=\begin{bmatrix} -\dfrac{\sum_{j=1}^{J}\hat{v}^n_{i,j}\left(\left(\eta^n_{i,j_2}\right)^2+\left(\eta^n_{i,j_3}\right)^2\right)F^n_{NII,i,j,k}}{\tilde{f}1^n_i} \\ -\dfrac{\sum_{j=1}^{J}\hat{v}^n_{i,j}\left(\left(\eta^n_{i,j_2}\right)^2+\left(\eta^n_{i,j_3}\right)^2\right)\eta^n_{i,j_1}F^n_{NII,i,j,k}}{\tilde{f}2^n_i} \\ -\dfrac{\sum_{j=1}^{J}\hat{v}^n_{i,j}\left(\left(\eta^n_{i,j_2}\right)^2+\left(\eta^n_{i,j_3}\right)^2\right)\left(\eta^n_{i,j_1}\right)^2F^n_{NII,i,j,k}}{\tilde{f}3^n_i} \\ -\dfrac{\sum_{j=1}^{J}\hat{v}^n_{i,j}\left(\left(\eta^n_{i,j_2}\right)^2+\left(\eta^n_{i,j_3}\right)^2\right)\left(\eta^n_{i,j_2}\right)^2F^n_{NII,i,j,k}}{\tilde{f}4^n_i} \end{bmatrix}.$$

Note that for situation $\mathrm{Abs}(\tilde{f}2^n_i)<1.\mathrm{D}-5$,

$$\mathbf{J}^n_{i,k,21}=\frac{\sum_{j=1}^{J}\hat{v}^n_{i,j}\eta^n_{i,j_1}F^n_{NII,i,j,k}}{a^n_{i,k}},\quad \mathbf{J}^n_{i,k,22}=\sum_{j=1}^{J}\hat{v}^n_{i,j}\left(\eta^n_{i,j_1}\right)^2F^n_{NII,i,j,k},$$

$$\mathbf{J}^n_{i,k,23}=-\sum_{j=1}^{J}\hat{v}^n_{i,j}\left(\eta^n_{i,j_1}\right)^3F^n_{NII,i,j,k},\quad \mathbf{J}^n_{i,k,24}=-\sum_{j=1}^{J}\hat{v}^n_{i,j}\left(\left(\eta^n_{i,j_2}\right)^2+\left(\eta^n_{i,j_3}\right)^2\right)\eta^n_{i,j_1}F^n_{NII,i,j,k}.$$

For the 1DCF, functions we compute in the N-R algorithm are

$$\tilde{F}1^n_{i,k}=\frac{\sum_{j=1}^{J}\hat{v}^n_{i,j}F^n_{NII,i,j,k}}{\tilde{f}1^n_i}-1,\ \tilde{F}2^n_{i,k}=\frac{\sum_{j=1}^{J}\eta^n_{i,j_1}\hat{v}^n_{i,j}F^n_{NII,i,j,k}}{\tilde{f}2^n_i}-1,\ \tilde{F}3^n_{i,k}=\frac{\sum_{j=1}^{J}\eta^n_{i,j_2}\hat{v}^n_{i,j}F^n_{NII,i,j,k}}{\tilde{f}3^n_i}-1,$$

$$\tilde{F}4^n_{i,k}=\frac{\sum_{j=1}^{J}\left(\eta^n_{i,j_1}\right)^2\hat{v}^n_{i,j}F^n_{NII,i,j,k}}{\tilde{f}4^n_i}-1,\qquad \tilde{F}5^n_{i,k}=\frac{\sum_{j=1}^{J}\left(\eta^n_{i,j_2}\right)^2\hat{v}^n_{i,j}F^n_{NII,i,j,k}}{\tilde{f}5^n_i}-1, \tag{B.19}$$

$$\tilde{F}6^n_{i,k}=\frac{\sum_{j=1}^{J}\left(\eta^n_{i,j_3}\right)^2\hat{v}^n_{i,j}F^n_{NII,i,j,k}}{\tilde{f}6^n_i}-1,\qquad \tilde{F}7^n_{i,k}=\frac{\sum_{j=1}^{J}\left(\eta^n_{i,j_1}\eta^n_{i,j_2}\right)\hat{v}^n_{i,j}F^n_{NII,i,j,k}}{\tilde{f}7^n_i}-1,$$

where $\tilde{f}1^n_i=\sum_{j=1}^{J}\hat{v}^n_{i,j}\frac{f^n_{i,j}}{\rho^n_i}\Delta\mathbf{c}$, $\tilde{f}2^n_i=\sum_{j=1}^{J}\eta^n_{i,j_1}\hat{v}^n_{i,j}\frac{f^n_{i,j}}{\rho^n_i}\Delta\mathbf{c}$, $\tilde{f}3^n_i=\sum_{j=1}^{J}\eta^n_{i,j_2}\hat{v}^n_{i,j}\frac{f^n_{i,j}}{\rho^n_i}\Delta\mathbf{c}$,

$$\tilde{f}4^n_i=\sum_{j=1}^{J}\left(\eta^n_{i,j_1}\right)^2\hat{v}^n_{i,j}\frac{f^n_{i,j}}{\rho^n_i}\Delta\mathbf{c}+\frac{\left(p^n_{BGK,xx,i}-p^n_{xx,i}\right)}{2p^n_i},\ \tilde{f}5^n_i=\sum_{j=1}^{J}\left(\eta^n_{i,j_2}\right)^2\hat{v}^n_{i,j}\frac{f^n_{i,j}}{\rho^n_i}\Delta\mathbf{c}+\frac{\left(p^n_{BGK,yy,i}-p^n_{yy,i}\right)}{2p^n_i},$$

$$\tilde{f}6^n_i=\sum_{j=1}^{J}\left(\eta^n_{i,j_3}\right)^2\hat{v}^n_{i,j}\frac{f^n_{i,j}}{\rho^n_i}\Delta\mathbf{c}+\frac{\left(p^n_{BGK,zz,i}-p^n_{zz,i}\right)}{2p^n_i},\ \tilde{f}7^n_i=\sum_{j=1}^{J}\left(\eta^n_{i,j_1}\eta^n_{i,j_2}\right)\hat{v}^n_{i,j}\frac{f^n_{i,j}}{\rho^n_i}\Delta\mathbf{c}+\frac{\left(p^n_{BGK,xy,i}-p^n_{xy,i}\right)}{2p^n_i}.$$

Note that $\tilde{F}2_{i,k}^{n} = \sum_{j=1}^{J} \eta_{i,j_1}^{n} \hat{v}_{i,j}^{n} F_{NII,i,j,k}^{n} - \tilde{f}2_{i}^{n}$ for situation $\text{Abs}(\tilde{f}2_{i}^{n}) < 1.\text{D}-5$, $\tilde{F}3_{i,k}^{n} = \sum_{j=1}^{J} \eta_{i,j_2}^{n} \hat{v}_{i,j}^{n} F_{NII,i,j,k}^{n} - \tilde{f}3_{i}^{n}$ for situation $\text{Abs}(\tilde{f}3_{i}^{n}) < 1.\text{D}-5$, and $\tilde{F}7_{i,k}^{n} = \sum_{j=1}^{J} (\eta_{i,j_1}^{n} \eta_{i,j_2}^{n}) \hat{v}_{i,j}^{n} F_{NII,i,j,k}^{n} - \tilde{f}7_{i}^{n}$ for situation $\text{Abs}(\tilde{f}7_{i}^{n}) < 1.\text{D}-5$. Jacobian used in the computation is

$$\mathbf{J}_{i,k}^{n} = \left[\mathbf{J}_{i,k,1}^{n} \quad \mathbf{J}_{i,k,2}^{n} \quad \mathbf{J}_{i,k,3}^{n} \quad \mathbf{J}_{i,k,4}^{n} \quad \mathbf{J}_{i,k,5}^{n} \quad \mathbf{J}_{i,k,6}^{n} \quad \mathbf{J}_{i,k,7}^{n}\right], \tag{B.20}$$

$$\mathbf{J}_{i,k,1}^{n} = \begin{bmatrix} \frac{\sum_{j=1}^{J} \hat{v}_{i,j}^{n} F_{NII,i,j,k}^{n}}{a_{i,k}^{n} \tilde{f}1_{i}^{n}} \\ \frac{\sum_{j=1}^{J} \hat{v}_{i,j}^{n} \eta_{i,j_1}^{n} F_{NII,i,j,k}^{n}}{a_{i,k}^{n} \tilde{f}2_{i}^{n}} \\ \frac{\sum_{j=1}^{J} \hat{v}_{i,j}^{n} \eta_{i,j_2}^{n} F_{NII,i,j,k}^{n}}{a_{i,k}^{n} \tilde{f}3_{i}^{n}} \\ \frac{\sum_{j=1}^{J} \hat{v}_{i,j}^{n} (\eta_{i,j_1}^{n})^2 F_{NII,i,j,k}^{n}}{a_{i,k}^{n} \tilde{f}4_{i}^{n}} \\ \frac{\sum_{j=1}^{J} \hat{v}_{i,j}^{n} (\eta_{i,j_2}^{n})^2 F_{NII,i,j,k}^{n}}{a_{i,k}^{n} \tilde{f}5_{i}^{n}} \\ \frac{\sum_{j=1}^{J} \hat{v}_{i,j}^{n} (\eta_{i,j_3}^{n})^2 F_{NII,i,j,k}^{n}}{a_{i,k}^{n} \tilde{f}6_{i}^{n}} \\ \frac{\sum_{j=1}^{J} \hat{v}_{i,j}^{n} (\eta_{i,j_1}^{n} \eta_{i,j_2}^{n}) F_{NII,i,j,k}^{n}}{a_{i,k}^{n} \tilde{f}7_{i}^{n}} \end{bmatrix}, \quad \mathbf{J}_{i,k,2}^{n} = \begin{bmatrix} \frac{\sum_{j=1}^{J} \hat{v}_{i,j}^{n} \eta_{i,j_1}^{n} F_{NII,i,j,k}^{n}}{\tilde{f}1_{i}^{n}} \\ \frac{\sum_{j=1}^{J} \hat{v}_{i,j}^{n} \eta_{i,j_1}^{n} \eta_{i,j_1}^{n} F_{NII,i,j,k}^{n}}{\tilde{f}2_{i}^{n}} \\ \frac{\sum_{j=1}^{J} \hat{v}_{i,j}^{n} \eta_{i,j_1}^{n} \eta_{i,j_2}^{n} F_{NII,i,j,k}^{n}}{\tilde{f}3_{i}^{n}} \\ \frac{\sum_{j=1}^{J} \hat{v}_{i,j}^{n} \eta_{i,j_1}^{n} (\eta_{i,j_1}^{n})^2 F_{NII,i,j,k}^{n}}{\tilde{f}4_{i}^{n}} \\ \frac{\sum_{j=1}^{J} \hat{v}_{i,j}^{n} \eta_{i,j_1}^{n} (\eta_{i,j_2}^{n})^2 F_{NII,i,j,k}^{n}}{\tilde{f}5_{i}^{n}} \\ \frac{\sum_{j=1}^{J} \hat{v}_{i,j}^{n} \eta_{i,j_1}^{n} (\eta_{i,j_3}^{n})^2 F_{NII,i,j,k}^{n}}{\tilde{f}6_{i}^{n}} \\ \frac{\sum_{j=1}^{J} \hat{v}_{i,j}^{n} \eta_{i,j_1}^{n} (\eta_{i,j_1}^{n} \eta_{i,j_2}^{n}) F_{NII,i,j,k}^{n}}{\tilde{f}7_{i}^{n}} \end{bmatrix}, \quad \mathbf{J}_{i,k,3}^{n} = \begin{bmatrix} \frac{\sum_{j=1}^{J} \hat{v}_{i,j}^{n} \eta_{i,j_2}^{n} F_{NII,i,j,k}^{n}}{\tilde{f}1_{i}^{n}} \\ \frac{\sum_{j=1}^{J} \hat{v}_{i,j}^{n} \eta_{i,j_2}^{n} \eta_{i,j_1}^{n} F_{NII,i,j,k}^{n}}{\tilde{f}2_{i}^{n}} \\ \frac{\sum_{j=1}^{J} \hat{v}_{i,j}^{n} \eta_{i,j_2}^{n} \eta_{i,j_2}^{n} F_{NII,i,j,k}^{n}}{\tilde{f}3_{i}^{n}} \\ \frac{\sum_{j=1}^{J} \hat{v}_{i,j}^{n} \eta_{i,j_2}^{n} (\eta_{i,j_1}^{n})^2 F_{NII,i,j,k}^{n}}{\tilde{f}4_{i}^{n}} \\ \frac{\sum_{j=1}^{J} \hat{v}_{i,j}^{n} \eta_{i,j_2}^{n} (\eta_{i,j_2}^{n})^2 F_{NII,i,j,k}^{n}}{\tilde{f}5_{i}^{n}} \\ \frac{\sum_{j=1}^{J} \hat{v}_{i,j}^{n} \eta_{i,j_2}^{n} (\eta_{i,j_3}^{n})^2 F_{NII,i,j,k}^{n}}{\tilde{f}6_{i}^{n}} \\ \frac{\sum_{j=1}^{J} \hat{v}_{i,j}^{n} \eta_{i,j_2}^{n} (\eta_{i,j_1}^{n} \eta_{i,j_2}^{n}) F_{NII,i,j,k}^{n}}{\tilde{f}7_{i}^{n}} \end{bmatrix},$$

$$\mathbf{J}^n_{i,k,4} = \begin{bmatrix} -\dfrac{\sum_{j=1}^{J} \hat{v}^n_{i,j} \left(\eta^n_{i,j_1}\right)^2 F^n_{NII,i,j,k}}{\tilde{f}1^n_i} \\ -\dfrac{\sum_{j=1}^{J} \hat{v}^n_{i,j} \left(\eta^n_{i,j_1}\right)^2 \eta^n_{i,j_1} F^n_{NII,i,j,k}}{\tilde{f}2^n_i} \\ -\dfrac{\sum_{j=1}^{J} \hat{v}^n_{i,j} \left(\eta^n_{i,j_1}\right)^2 \eta^n_{i,j_2} F^n_{NII,i,j,k}}{\tilde{f}3^n_i} \\ -\dfrac{\sum_{j=1}^{J} \hat{v}^n_{i,j} \left(\eta^n_{i,j_1}\right)^2 \left(\eta^n_{i,j_1}\right)^2 F^n_{NII,i,j,k}}{\tilde{f}4^n_i} \\ -\dfrac{\sum_{j=1}^{J} \hat{v}^n_{i,j} \left(\eta^n_{i,j_1}\right)^2 \left(\eta^n_{i,j_2}\right)^2 F^n_{NII,i,j,k}}{\tilde{f}5^n_i} \\ -\dfrac{\sum_{j=1}^{J} \hat{v}^n_{i,j} \left(\eta^n_{i,j_1}\right)^2 \left(\eta^n_{i,j_3}\right)^2 F^n_{NII,i,j,k}}{\tilde{f}6^n_i} \\ -\dfrac{\sum_{j=1}^{J} \hat{v}^n_{i,j} \left(\eta^n_{i,j_1}\right)^2 \left(\eta^n_{i,j_1} \eta^n_{i,j_2}\right) F^n_{NII,i,j,k}}{\tilde{f}7^n_i} \end{bmatrix}, \quad \mathbf{J}^n_{i,k,5} = \begin{bmatrix} -\dfrac{\sum_{j=1}^{J} \hat{v}^n_{i,j} \left(\eta^n_{i,j_2}\right)^2 F^n_{NII,i,j,k}}{\tilde{f}1^n_i} \\ -\dfrac{\sum_{j=1}^{J} \hat{v}^n_{i,j} \left(\eta^n_{i,j_2}\right)^2 \eta^n_{i,j_1} F^n_{NII,i,j,k}}{\tilde{f}2^n_i} \\ -\dfrac{\sum_{j=1}^{J} \hat{v}^n_{i,j} \left(\eta^n_{i,j_2}\right)^2 \eta^n_{i,j_2} F^n_{NII,i,j,k}}{\tilde{f}3^n_i} \\ -\dfrac{\sum_{j=1}^{J} \hat{v}^n_{i,j} \left(\eta^n_{i,j_2}\right)^2 \left(\eta^n_{i,j_1}\right)^2 F^n_{NII,i,j,k}}{\tilde{f}4^n_i} \\ -\dfrac{\sum_{j=1}^{J} \hat{v}^n_{i,j} \left(\eta^n_{i,j_2}\right)^2 \left(\eta^n_{i,j_2}\right)^2 F^n_{NII,i,j,k}}{\tilde{f}5^n_i} \\ -\dfrac{\sum_{j=1}^{J} \hat{v}^n_{i,j} \left(\eta^n_{i,j_2}\right)^2 \left(\eta^n_{i,j_3}\right)^2 F^n_{NII,i,j,k}}{\tilde{f}6^n_i} \\ -\dfrac{\sum_{j=1}^{J} \hat{v}^n_{i,j} \left(\eta^n_{i,j_2}\right)^2 \left(\eta^n_{i,j_1} \eta^n_{i,j_2}\right) F^n_{NII,i,j,k}}{\tilde{f}7^n_i} \end{bmatrix},$$

$$\mathbf{J}^n_{i,k,6} = \begin{bmatrix} -\dfrac{\sum_{j=1}^{J} \hat{v}^n_{i,j} \left(\eta^n_{i,j_3}\right)^2 F^n_{NII,i,j,k}}{\tilde{f}1^n_i} \\ -\dfrac{\sum_{j=1}^{J} \hat{v}^n_{i,j} \left(\eta^n_{i,j_3}\right)^2 \eta^n_{i,j_1} F^n_{NII,i,j,k}}{\tilde{f}2^n_i} \\ -\dfrac{\sum_{j=1}^{J} \hat{v}^n_{i,j} \left(\eta^n_{i,j_3}\right)^2 \eta^n_{i,j_2} F^n_{NII,i,j,k}}{\tilde{f}3^n_i} \\ -\dfrac{\sum_{j=1}^{J} \hat{v}^n_{i,j} \left(\eta^n_{i,j_3}\right)^2 \left(\eta^n_{i,j_1}\right)^2 F^n_{NII,i,j,k}}{\tilde{f}4^n_i} \\ -\dfrac{\sum_{j=1}^{J} \hat{v}^n_{i,j} \left(\eta^n_{i,j_3}\right)^2 \left(\eta^n_{i,j_2}\right)^2 F^n_{NII,i,j,k}}{\tilde{f}5^n_i} \\ -\dfrac{\sum_{j=1}^{J} \hat{v}^n_{i,j} \left(\eta^n_{i,j_3}\right)^2 \left(\eta^n_{i,j_3}\right)^2 F^n_{NII,i,j,k}}{\tilde{f}6^n_i} \\ -\dfrac{\sum_{j=1}^{J} \hat{v}^n_{i,j} \left(\eta^n_{i,j_3}\right)^2 \left(\eta^n_{i,j_1} \eta^n_{i,j_2}\right) F^n_{NII,i,j,k}}{\tilde{f}7^n_i} \end{bmatrix}, \quad \mathbf{J}^n_{i,k,7} = \begin{bmatrix} -\dfrac{\sum_{j=1}^{J} \hat{v}^n_{i,j} \left(\eta^n_{i,j_1} \eta^n_{i,j_2}\right) F^n_{NII,i,j,k}}{\tilde{f}1^n_i} \\ -\dfrac{\sum_{j=1}^{J} \hat{v}^n_{i,j} \left(\eta^n_{i,j_1} \eta^n_{i,j_2}\right) \eta^n_{i,j_1} F^n_{NII,i,j,k}}{\tilde{f}2^n_i} \\ -\dfrac{\sum_{j=1}^{J} \hat{v}^n_{i,j} \left(\eta^n_{i,j_1} \eta^n_{i,j_2}\right) \eta^n_{i,j_2} F^n_{NII,i,j,k}}{\tilde{f}3^n_i} \\ -\dfrac{\sum_{j=1}^{J} \hat{v}^n_{i,j} \left(\eta^n_{i,j_1} \eta^n_{i,j_2}\right) \left(\eta^n_{i,j_1}\right)^2 F^n_{NII,i,j,k}}{\tilde{f}4^n_i} \\ -\dfrac{\sum_{j=1}^{J} \hat{v}^n_{i,j} \left(\eta^n_{i,j_1} \eta^n_{i,j_2}\right) \left(\eta^n_{i,j_2}\right)^2 F^n_{NII,i,j,k}}{\tilde{f}5^n_i} \\ -\dfrac{\sum_{j=1}^{J} \hat{v}^n_{i,j} \left(\eta^n_{i,j_1} \eta^n_{i,j_2}\right) \left(\eta^n_{i,j_3}\right)^2 F^n_{NII,i,j,k}}{\tilde{f}6^n_i} \\ -\dfrac{\sum_{j=1}^{J} \hat{v}^n_{i,j} \left(\eta^n_{i,j_1} \eta^n_{i,j_2}\right) \left(\eta^n_{i,j_1} \eta^n_{i,j_2}\right) F^n_{NII,i,j,k}}{\tilde{f}7^n_i} \end{bmatrix}.$$

Note that for situation $\text{Abs}(\tilde{f}2_i^n) < 1.\text{D}-5$,

$$\mathbf{J}_{i,k,21}^n = \frac{\sum_{j=1}^{J} \hat{v}_{i,j}^n \eta_{i,j_1}^n F_{NII,i,j,k}^n}{a_{i,k}^n},\ \mathbf{J}_{i,k,22}^n = \sum_{j=1}^{J} \hat{v}_{i,j}^n \eta_{i,j_1}^n \eta_{i,j_1}^n F_{NII,i,j,k}^n,\ \mathbf{J}_{i,k,23}^n = \sum_{j=1}^{J} \hat{v}_{i,j}^n \eta_{i,j_2}^n \eta_{i,j_1}^n F_{NII,i,j,k}^n,$$

$$\mathbf{J}_{i,k,24}^n = -\sum_{j=1}^{J} \hat{v}_{i,j}^n (\eta_{i,j_1}^n)^2 \eta_{i,j_1}^n F_{NII,i,j,k}^n,\ \mathbf{J}_{i,k,25}^n = -\sum_{j=1}^{J} \hat{v}_{i,j}^n (\eta_{i,j_2}^n)^2 \eta_{i,j_1}^n F_{NII,i,j,k}^n,$$

$$\mathbf{J}_{i,k,26}^n = -\sum_{j=1}^{J} \hat{v}_{i,j}^n (\eta_{i,j_3}^n)^2 \eta_{i,j_1}^n F_{NII,i,j,k}^n,\ \mathbf{J}_{i,k,27}^n = -\sum_{j=1}^{J} \hat{v}_{i,j}^n (\eta_{i,j_1}^n \eta_{i,j_2}^n) \eta_{i,j_1}^n F_{NII,i,j,k}^n,$$

and for situation $\text{Abs}(\tilde{f}3_i^n) < 1.\text{D}-5$,

$$\mathbf{J}_{i,k,31}^n = \frac{\sum_{j=1}^{J} \hat{v}_{i,j}^n \eta_{i,j_2}^n F_{NII,i,j,k}^n}{a_{i,k}^n},\ \mathbf{J}_{i,k,32}^n = \sum_{j=1}^{J} \hat{v}_{i,j}^n \eta_{i,j_1}^n \eta_{i,j_2}^n F_{NII,i,j,k}^n,\ \mathbf{J}_{i,k,33}^n = \sum_{j=1}^{J} \hat{v}_{i,j}^n \eta_{i,j_2}^n \eta_{i,j_2}^n F_{NII,i,j,k}^n,$$

$$\mathbf{J}_{i,k,34}^n = -\sum_{j=1}^{J} \hat{v}_{i,j}^n (\eta_{i,j_1}^n)^2 \eta_{i,j_2}^n F_{NII,i,j,k}^n,\ \mathbf{J}_{i,k,35}^n = -\sum_{j=1}^{J} \hat{v}_{i,j}^n (\eta_{i,j_2}^n)^2 \eta_{i,j_2}^n F_{NII,i,j,k}^n,$$

$$\mathbf{J}_{i,k,36}^n = -\sum_{j=1}^{J} \hat{v}_{i,j}^n (\eta_{i,j_3}^n)^2 \eta_{i,j_2}^n F_{NII,i,j,k}^n,\ \mathbf{J}_{i,k,37}^n = -\sum_{j=1}^{J} \hat{v}_{i,j}^n (\eta_{i,j_1}^n \eta_{i,j_2}^n) \eta_{i,j_2}^n F_{NII,i,j,k}^n,$$

and for situation $\text{Abs}(\tilde{f}7_i^n) < 1.\text{D}-5$,

$$\mathbf{J}_{i,k,71}^n = \frac{\sum_{j=1}^{J} \hat{v}_{i,j}^n (\eta_{i,j_1}^n \eta_{i,j_2}^n) F_{NII,i,j,k}^n}{a_{i,k}^n},\ \mathbf{J}_{i,k,72}^n = \sum_{j=1}^{J} \hat{v}_{i,j}^n \eta_{i,j_1}^n (\eta_{i,j_1}^n \eta_{i,j_2}^n) F_{NII,i,j,k}^n,\ \mathbf{J}_{i,k,73}^n = \sum_{j=1}^{J} \hat{v}_{i,j}^n \eta_{i,j_2}^n (\eta_{i,j_1}^n \eta_{i,j_2}^n) F_{NII,i,j,k}^n,$$

$$\mathbf{J}_{i,k,74}^n = -\sum_{j=1}^{J} \hat{v}_{i,j}^n (\eta_{i,j_1}^n)^2 (\eta_{i,j_1}^n \eta_{i,j_2}^n) F_{NII,i,j,k}^n,\ \mathbf{J}_{i,k,75}^n = -\sum_{j=1}^{J} \hat{v}_{i,j}^n (\eta_{i,j_2}^n)^2 (\eta_{i,j_1}^n \eta_{i,j_2}^n) F_{NII,i,j,k}^n,$$

$$\mathbf{J}_{i,k,76}^n = -\sum_{j=1}^{J} \hat{v}_{i,j}^n (\eta_{i,j_3}^n)^2 (\eta_{i,j_1}^n \eta_{i,j_2}^n) F_{NII,i,j,k}^n,\ \mathbf{J}_{i,k,77}^n = -\sum_{j=1}^{J} \hat{v}_{i,j}^n (\eta_{i,j_1}^n \eta_{i,j_2}^n)(\eta_{i,j_1}^n \eta_{i,j_2}^n) F_{NII,i,j,k}^n.$$

Appendix C: Linearized dimensionless reference distribution $F^n_{ref,i,j}$

C.1 BGK model

For the 1DSW, linearized dimensionless reference distribution is

$$F^n_{BGK,i,j} = \exp\left(-\left(\eta^n_{i,j}\right)^2\right)\left(a1^n_i + a2^n_i \eta^n_{i,j_1} + a3^n_i \left(\eta^n_{i,j}\right)^2\right), \tag{C.1}$$

and three conditions to determine the three coefficients are

$$\begin{aligned}
&\sum_{j=1}^{J} F^n_{BGK,i,j} = a1^n_i J^n_{i,11} + a2^n_i J^n_{i,12} + a3^n_i J^n_{i,13} = 1,\\
&\sum_{j=1}^{J} \eta^n_{i,j_1} F^n_{BGK,i,j} = a1^n_i J^n_{i,21} + a2^n_i J^n_{i,22} + a3^n_i J^n_{i,23} = 0,\\
&\sum_{j=1}^{J} \left(\eta^n_{i,j}\right)^2 F^n_{BGK,i,j} = a1^n_i J^n_{i,31} + a2^n_i J^n_{i,32} + a3^n_i J^n_{i,33} = 1.5,
\end{aligned} \tag{C.2}$$

where

$$\mathbf{J}^n_i = \begin{bmatrix}
\sum_{j=1}^{J} \exp\left(-\left(\eta^n_{i,j}\right)^2\right) & \sum_{j=1}^{J} \eta^n_{i,j_1} \exp\left(-\left(\eta^n_{i,j}\right)^2\right) & \sum_{j=1}^{J} \left(\eta^n_{i,j}\right)^2 \exp\left(-\left(\eta^n_{i,j}\right)^2\right)\\
\sum_{j=1}^{J} \eta^n_{i,j_1} \exp\left(-\left(\eta^n_{i,j}\right)^2\right) & \sum_{j=1}^{J} \left(\eta^n_{i,j_1}\right)^2 \exp\left(-\left(\eta^n_{i,j}\right)^2\right) & \sum_{j=1}^{J} \left(\eta^n_{i,j}\right)^2 \eta^n_{i,j_1} \exp\left(-\left(\eta^n_{i,j}\right)^2\right)\\
\sum_{j=1}^{J} \left(\eta^n_{i,j}\right)^2 \exp\left(-\left(\eta^n_{i,j}\right)^2\right) & \sum_{j=1}^{J} \eta^n_{i,j_1} \left(\eta^n_{i,j}\right)^2 \exp\left(-\left(\eta^n_{i,j}\right)^2\right) & \sum_{j=1}^{J} \left(\eta^n_{i,j}\right)^2 \left(\eta^n_{i,j}\right)^2 \exp\left(-\left(\eta^n_{i,j}\right)^2\right)
\end{bmatrix}, \tag{C.3}$$

which is a symmetric matrix.

For the 1DCF, linearized dimensionless reference distribution is

$$F^n_{BGK,i,j} = \exp\left(-\left(\eta^n_{i,j}\right)^2\right)\left(a1^n_i + a2^n_i \eta^n_{i,j_1} + a3^n_i \eta^n_{i,j_2} + a4^n_i \left(\eta^n_{i,j}\right)^2\right), \tag{C.4}$$

and four conditions to determine the four coefficients are

$$\begin{aligned}
&\sum_{j=1}^{J} F^n_{BGK,i,j} = a1^n_i J^n_{i,11} + a2^n_i J^n_{i,12} + a3^n_i J^n_{i,13} + a4^n_i J^n_{i,14} = 1,\\
&\sum_{j=1}^{J} \eta^n_{i,j_1} F^n_{BGK,i,j} = a1^n_i J^n_{i,21} + a2^n_i J^n_{i,22} + a3^n_i J^n_{i,23} + a4^n_i J^n_{i,24} = 0,\\
&\sum_{j=1}^{J} \eta^n_{i,j_3} F^n_{BGK,i,j} = a1^n_i J^n_{i,31} + a2^n_i J^n_{i,32} + a3^n_i J^n_{i,33} + a4^n_i J^n_{i,34} = 0,
\end{aligned} \tag{C.5}$$

$$\sum_{j=1}^{J}\left(\eta_{i,j}^{n}\right)^{2} F_{BGK,i,j}^{n} = a1_{i}^{n} J_{i,41}^{n} + a2_{i}^{n} J_{i,42}^{n} + a3_{i}^{n} J_{i,43}^{n} + a4_{i}^{n} J_{i,44}^{n} = 1.5,$$

where

$$\mathbf{J}_{i}^{n} = \begin{bmatrix} \sum_{j=1}^{J}\exp\left(-\left(\eta_{i,j}^{n}\right)^{2}\right) & \sum_{j=1}^{J}\eta_{i,j_1}^{n}\exp\left(-\left(\eta_{i,j}^{n}\right)^{2}\right) & \sum_{j=1}^{J}\eta_{i,j_2}^{n}\exp\left(-\left(\eta_{i,j}^{n}\right)^{2}\right) & \sum_{j=1}^{J}\left(\eta_{i,j}^{n}\right)^{2}\exp\left(-\left(\eta_{i,j}^{n}\right)^{2}\right) \\ \sum_{j=1}^{J}\eta_{i,j_1}^{n}\exp\left(-\left(\eta_{i,j}^{n}\right)^{2}\right) & \sum_{j=1}^{J}\left(\eta_{i,j_1}^{n}\right)^{2}\exp\left(-\left(\eta_{i,j}^{n}\right)^{2}\right) & \sum_{j=1}^{J}\eta_{i,j_2}^{n}\eta_{i,j_1}^{n}\exp\left(-\left(\eta_{i,j}^{n}\right)^{2}\right) & \sum_{j=1}^{J}\left(\eta_{i,j}^{n}\right)^{2}\eta_{i,j_1}^{n}\exp\left(-\left(\eta_{i,j}^{n}\right)^{2}\right) \\ \sum_{j=1}^{J}\eta_{i,j_2}^{n}\exp\left(-\left(\eta_{i,j}^{n}\right)^{2}\right) & \sum_{j=1}^{J}\eta_{i,j_1}^{n}\eta_{i,j_2}^{n}\exp\left(-\left(\eta_{i,j}^{n}\right)^{2}\right) & \sum_{j=1}^{J}\left(\eta_{i,j_2}^{n}\right)^{2}\exp\left(-\left(\eta_{i,j}^{n}\right)^{2}\right) & \sum_{j=1}^{J}\left(\eta_{i,j}^{n}\right)^{2}\eta_{i,j_2}^{n}\exp\left(-\left(\eta_{i,j}^{n}\right)^{2}\right) \\ \sum_{j=1}^{J}\left(\eta_{i,j}^{n}\right)^{2}\exp\left(-\left(\eta_{i,j}^{n}\right)^{2}\right) & \sum_{j=1}^{J}\eta_{i,j_1}^{n}\left(\eta_{i,j}^{n}\right)^{2}\exp\left(-\left(\eta_{i,j}^{n}\right)^{2}\right) & \sum_{j=1}^{J}\eta_{i,j_2}^{n}\left(\eta_{i,j}^{n}\right)^{2}\exp\left(-\left(\eta_{i,j}^{n}\right)^{2}\right) & \sum_{j=1}^{J}\left(\eta_{i,j}^{n}\right)^{2}\left(\eta_{i,j}^{n}\right)^{2}\exp\left(-\left(\eta_{i,j}^{n}\right)^{2}\right) \end{bmatrix}, \tag{C.6}$$

which is a symmetric matrix.

C.2 ES-BGK model

From section 3.2.4 and section 4.2.4, there are two types linearized reference distribution $f_{ES,i,j}^{n}$ for the ES-BGK model. Here, only the discussion of first type linearized $f_{ES,i,j}^{n}$ is given, while the discussion of second type linearized $f_{ES,i,j}^{n}$ is omitted, which is similar to the discussion of first type.

For the 1DSW, linearized dimensionless reference distribution is

$$F_{ES,i,j}^{n} = \exp\left(-\left(\eta_{i,j}^{n}\right)^{2}\right)\cdot\left(a1_{i}^{n} + a2_{i}^{n}\eta_{i,j_1}^{n} + a3_{i}^{n}\left(\eta_{i,j_1}^{n}\right)^{2} + a4_{i}^{n}\left(\left(\eta_{i,j_2}^{n}\right)^{2} + \left(\eta_{i,j_3}^{n}\right)^{2}\right)\right), \tag{C.7}$$

and four conditions to determine the four coefficients are

$$\begin{aligned} &\sum_{j=1}^{J} F_{ES,i,j}^{n} = a1_{i}^{n} J_{i,11}^{n} + a2_{i}^{n} J_{i,12}^{n} + a3_{i}^{n} J_{i,13}^{n} + a4_{i}^{n} J_{i,14}^{n} = 1, \\ &\sum_{j=1}^{J} \eta_{i,j_1}^{n} F_{ES,i,j}^{n} = a1_{i}^{n} J_{i,21}^{n} + a2_{i}^{n} J_{i,22}^{n} + a3_{i}^{n} J_{i,23}^{n} + a4_{i}^{n} J_{i,24}^{n} = 0, \\ &\sum_{j=1}^{J} \left(\eta_{i,j_1}^{n}\right)^{2} F_{ES,i,j}^{n} = a1_{i}^{n} J_{i,31}^{n} + a2_{i}^{n} J_{i,32}^{n} + a3_{i}^{n} J_{i,33}^{n} + a4_{i}^{n} J_{i,34}^{n} = BB1_{i}^{n}, \\ &\sum_{j=1}^{J} \left(\eta_{i,j_2}^{n}\right)^{2} F_{ES,i,j}^{n} = a1_{i}^{n} J_{i,41}^{n} + a2_{i}^{n} J_{i,42}^{n} + a3_{i}^{n} J_{i,43}^{n} + a4_{i}^{n} J_{i,44}^{n} = BB2_{i}^{n}, \end{aligned} \tag{C.8}$$

where $BB1_i^n = \dfrac{\frac{p^n_{BGK,xx,i}}{\Pr} + \left(1-\frac{1}{\Pr}\right)p^n_{xx,i}}{2p_i^n}$, $BB2_i^n = \dfrac{\frac{p^n_{BGK,yy,i}}{\Pr} + \left(1-\frac{1}{\Pr}\right)p^n_{yy,i}}{2p_i^n}$,

$$\mathbf{J}_i^n = \left[\mathbf{J}_{i,1}^n \quad \mathbf{J}_{i,2}^n \quad \mathbf{J}_{i,3}^n \quad \mathbf{J}_{i,4}^n\right], \tag{C.9}$$

$$\mathbf{J}_{i,1}^n = \begin{bmatrix} \sum_{j=1}^{J} \exp\left(-(\eta_{i,j}^n)^2\right) \\ \sum_{j=1}^{J} \eta_{i,j_1}^n \exp\left(-(\eta_{i,j}^n)^2\right) \\ \sum_{j=1}^{J} (\eta_{i,j_1}^n)^2 \exp\left(-(\eta_{i,j}^n)^2\right) \\ \sum_{j=1}^{J} (\eta_{i,j_2}^n)^2 \exp\left(-(\eta_{i,j}^n)^2\right) \end{bmatrix}, \quad \mathbf{J}_{i,2}^n = \begin{bmatrix} \sum_{j=1}^{J} \eta_{i,j_1}^n \exp\left(-(\eta_{i,j}^n)^2\right) \\ \sum_{j=1}^{J} \eta_{i,j_1}^n \eta_{i,j_1}^n \exp\left(-(\eta_{i,j}^n)^2\right) \\ \sum_{j=1}^{J} \eta_{i,j_1}^n (\eta_{i,j_1}^n)^2 \exp\left(-(\eta_{i,j}^n)^2\right) \\ \sum_{j=1}^{J} \eta_{i,j_1}^n (\eta_{i,j_2}^n)^2 \exp\left(-(\eta_{i,j}^n)^2\right) \end{bmatrix},$$

$$\mathbf{J}_{i,3}^n = \begin{bmatrix} \sum_{j=1}^{J} (\eta_{i,j_1}^n)^2 \exp\left(-(\eta_{i,j}^n)^2\right) \\ \sum_{j=1}^{J} (\eta_{i,j_1}^n)^2 \eta_{i,j_1}^n \exp\left(-(\eta_{i,j}^n)^2\right) \\ \sum_{j=1}^{J} (\eta_{i,j_1}^n)^2 (\eta_{i,j_1}^n)^2 \exp\left(-(\eta_{i,j}^n)^2\right) \\ \sum_{j=1}^{J} (\eta_{i,j_1}^n)^2 (\eta_{i,j_2}^n)^2 \exp\left(-(\eta_{i,j}^n)^2\right) \end{bmatrix}, \quad \mathbf{J}_{i,4}^n = \begin{bmatrix} \sum_{j=1}^{J} \left((\eta_{i,j_2}^n)^2 + (\eta_{i,j_3}^n)^2\right) \exp\left(-(\eta_{i,j}^n)^2\right) \\ \sum_{j=1}^{J} \left((\eta_{i,j_2}^n)^2 + (\eta_{i,j_3}^n)^2\right) \eta_{i,j_1}^n \exp\left(-(\eta_{i,j}^n)^2\right) \\ \sum_{j=1}^{J} \left((\eta_{i,j_2}^n)^2 + (\eta_{i,j_3}^n)^2\right) (\eta_{i,j_1}^n)^2 \exp\left(-(\eta_{i,j}^n)^2\right) \\ \sum_{j=1}^{J} \left((\eta_{i,j_2}^n)^2 + (\eta_{i,j_3}^n)^2\right) (\eta_{i,j_2}^n)^2 \exp\left(-(\eta_{i,j}^n)^2\right) \end{bmatrix}.$$

For the 1DCF, linearized dimensionless reference distribution is

$$F_{ES,i,j}^n = \exp\left(-(\eta_{i,j}^n)^2\right)\cdot\left(a1_i^n + a2_i^n \eta_{i,j_1}^n + a3_i^n \eta_{i,j_2}^n + a4_i^n (\eta_{i,j_1}^n)^2 + a5_i^n (\eta_{i,j_2}^n)^2 + a6_i^n (\eta_{i,j_3}^n)^2 + a7_i^n \eta_{i,j_1}^n \eta_{i,j_2}^n\right), \tag{C.10}$$

and seven conditions to determine the seven coefficients are

$$\sum_{j=1}^{J} F_{ES,i,j}^n = a1_i^n J_{i,11}^n + a2_i^n J_{i,12}^n + a3_i^n J_{i,13}^n + a4_i^n J_{i,14}^n + a5_i^n J_{i,15}^n + a6_i^n J_{i,16}^n + a7_i^n J_{i,17}^n = 1, \tag{C.11}$$

$$\sum_{j=1}^{J} \eta_{i,j_1}^n F_{ES,i,j}^n = a1_i^n J_{i,21}^n + a2_i^n J_{i,22}^n + a3_i^n J_{i,23}^n + a4_i^n J_{i,24}^n + a5_i^n J_{i,25}^n + a6_i^n J_{i,26}^n + a7_i^n J_{i,27}^n = 0,$$

$$\sum_{j=1}^{J} \eta_{i,j_2}^n F_{ES,i,j}^n = a1_i^n J_{i,31}^n + a2_i^n J_{i,32}^n + a3_i^n J_{i,33}^n + a4_i^n J_{i,34}^n + a5_i^n J_{i,35}^n + a6_i^n J_{i,36}^n + a7_i^n J_{i,37}^n = 0,$$

$$\sum_{j=1}^{J} (\eta_{i,j_1}^n)^2 F_{ES,i,j}^n = a1_i^n J_{i,41}^n + a2_i^n J_{i,42}^n + a3_i^n J_{i,43}^n + a4_i^n J_{i,44}^n + a5_i^n J_{i,45}^n + a6_i^n J_{i,46}^n + a7_i^n J_{i,47}^n = BB1_i^n,$$

$$\sum_{j=1}^{J}\left(\eta_{i,j_2}^n\right)^2 F_{ES,i,j}^n = a1_i^n J_{i,51}^n + a2_i^n J_{i,52}^n + a3_i^n J_{i,53}^n + a4_i^n J_{i,54}^n + a5_i^n J_{i,55}^n + a6_i^n J_{i,56}^n + a7_i^n J_{i,57}^n = BB2_i^n,$$

$$\sum_{j=1}^{J}\left(\eta_{i,j_3}^n\right)^2 F_{ES,i,j}^n = a1_i^n J_{i,61}^n + a2_i^n J_{i,62}^n + a3_i^n J_{i,63}^n + a4_i^n J_{i,64}^n + a5_i^n J_{i,65}^n + a6_i^n J_{i,66}^n + a7_i^n J_{i,67}^n = BB3_i^n,$$

$$\sum_{j=1}^{J}\eta_{i,j_1}^n \eta_{i,j_2}^n F_{ES,i,j}^n = a1_i^n J_{i,71}^n + a2_i^n J_{i,72}^n + a3_i^n J_{i,73}^n + a4_i^n J_{i,74}^n + a5_i^n J_{i,75}^n + a6_i^n J_{i,76}^n + a7_i^n J_{i,77}^n = BB4_i^n$$

where

$$BB1_i^n = \frac{\frac{p_{BGK,xx,i}^n}{\mathrm{Pr}} + \left(1-\frac{1}{\mathrm{Pr}}\right)p_{xx,i}^n}{2p_i^n},\quad BB2_i^n = \frac{\frac{p_{BGK,yy,i}^n}{\mathrm{Pr}} + \left(1-\frac{1}{\mathrm{Pr}}\right)p_{yy,i}^n}{2p_i^n},$$

$$BB3_i^n = \frac{\frac{p_{BGK,zz,i}^n}{\mathrm{Pr}} + \left(1-\frac{1}{\mathrm{Pr}}\right)p_{zz,i}^n}{2p_i^n},\quad BB4_i^n = \frac{\frac{p_{BGK,xy,i}^n}{\mathrm{Pr}} + \left(1-\frac{1}{\mathrm{Pr}}\right)p_{xy,i}^n}{2p_i^n},$$

$$\mathbf{J}_i^n = \begin{bmatrix}\mathbf{J}_{i,1}^n & \mathbf{J}_{i,2}^n & \mathbf{J}_{i,3}^n & \mathbf{J}_{i,4}^n & \mathbf{J}_{i,5}^n & \mathbf{J}_{i,6}^n & \mathbf{J}_{i,7}^n\end{bmatrix}, \tag{C.12}$$

$$\mathbf{J}_{i,1}^n = \begin{bmatrix} \sum_{j=1}^{J}\exp\left(-\left(\eta_{i,j}^n\right)^2\right) \\ \sum_{j=1}^{J}\eta_{i,j_1}^n \exp\left(-\left(\eta_{i,j}^n\right)^2\right) \\ \sum_{j=1}^{J}\eta_{i,j_2}^n \exp\left(-\left(\eta_{i,j}^n\right)^2\right) \\ \sum_{j=1}^{J}\left(\eta_{i,j_1}^n\right)^2 \exp\left(-\left(\eta_{i,j}^n\right)^2\right) \\ \sum_{j=1}^{J}\left(\eta_{i,j_2}^n\right)^2 \exp\left(-\left(\eta_{i,j}^n\right)^2\right) \\ \sum_{j=1}^{J}\left(\eta_{i,j_3}^n\right)^2 \exp\left(-\left(\eta_{i,j}^n\right)^2\right) \\ \sum_{j=1}^{J}\eta_{i,j_1}^n \eta_{i,j_2}^n \exp\left(-\left(\eta_{i,j}^n\right)^2\right) \end{bmatrix},\quad \mathbf{J}_{i,2}^n = \begin{bmatrix} \sum_{j=1}^{J}\eta_{i,j_1}^n \exp\left(-\left(\eta_{i,j}^n\right)^2\right) \\ \sum_{j=1}^{J}\eta_{i,j_1}^n \eta_{i,j_1}^n \exp\left(-\left(\eta_{i,j}^n\right)^2\right) \\ \sum_{j=1}^{J}\eta_{i,j_1}^n \eta_{i,j_2}^n \exp\left(-\left(\eta_{i,j}^n\right)^2\right) \\ \sum_{j=1}^{J}\eta_{i,j_1}^n \left(\eta_{i,j_1}^n\right)^2 \exp\left(-\left(\eta_{i,j}^n\right)^2\right) \\ \sum_{j=1}^{J}\eta_{i,j_1}^n \left(\eta_{i,j_2}^n\right)^2 \exp\left(-\left(\eta_{i,j}^n\right)^2\right) \\ \sum_{j=1}^{J}\eta_{i,j_1}^n \left(\eta_{i,j_3}^n\right)^2 \exp\left(-\left(\eta_{i,j}^n\right)^2\right) \\ \sum_{j=1}^{J}\eta_{i,j_1}^n \left(\eta_{i,j_1}^n \eta_{i,j_2}^n\right) \exp\left(-\left(\eta_{i,j}^n\right)^2\right) \end{bmatrix},$$

$$\mathbf{J}_{i,3}^{n}=\begin{bmatrix}\sum_{j=1}^{J}\eta_{i,j_2}^{n}\exp\left(-(\eta_{i,j}^{n})^2\right)\\ \sum_{j=1}^{J}\eta_{i,j_2}^{n}\eta_{i,j_1}^{n}\exp\left(-(\eta_{i,j}^{n})^2\right)\\ \sum_{j=1}^{J}\eta_{i,j_2}^{n}\eta_{i,j_2}^{n}\exp\left(-(\eta_{i,j}^{n})^2\right)\\ \sum_{j=1}^{J}\eta_{i,j_2}^{n}(\eta_{i,j_1}^{n})^2\exp\left(-(\eta_{i,j}^{n})^2\right)\\ \sum_{j=1}^{J}\eta_{i,j_2}^{n}(\eta_{i,j_2}^{n})^2\exp\left(-(\eta_{i,j}^{n})^2\right)\\ \sum_{j=1}^{J}\eta_{i,j_2}^{n}(\eta_{i,j_3}^{n})^2\exp\left(-(\eta_{i,j}^{n})^2\right)\\ \sum_{j=1}^{J}\eta_{i,j_2}^{n}(\eta_{i,j_1}^{n}\eta_{i,j_2}^{n})\exp\left(-(\eta_{i,j}^{n})^2\right)\end{bmatrix},\ \mathbf{J}_{i,4}^{n}=\begin{bmatrix}\sum_{j=1}^{J}(\eta_{i,j_1}^{n})^2\exp\left(-(\eta_{i,j}^{n})^2\right)\\ \sum_{j=1}^{J}(\eta_{i,j_1}^{n})^2\eta_{i,j_1}^{n}\exp\left(-(\eta_{i,j}^{n})^2\right)\\ \sum_{j=1}^{J}(\eta_{i,j_1}^{n})^2\eta_{i,j_2}^{n}\exp\left(-(\eta_{i,j}^{n})^2\right)\\ \sum_{j=1}^{J}(\eta_{i,j_1}^{n})^2(\eta_{i,j_1}^{n})^2\exp\left(-(\eta_{i,j}^{n})^2\right)\\ \sum_{j=1}^{J}(\eta_{i,j_1}^{n})^2(\eta_{i,j_2}^{n})^2\exp\left(-(\eta_{i,j}^{n})^2\right)\\ \sum_{j=1}^{J}(\eta_{i,j_1}^{n})^2(\eta_{i,j_3}^{n})^2\exp\left(-(\eta_{i,j}^{n})^2\right)\\ \sum_{j=1}^{J}(\eta_{i,j_1}^{n})^2(\eta_{i,j_1}^{n}\eta_{i,j_2}^{n})\exp\left(-(\eta_{i,j}^{n})^2\right)\end{bmatrix},$$

$$\mathbf{J}_{i,5}^{n}=\begin{bmatrix}\sum_{j=1}^{J}(\eta_{i,j_2}^{n})^2\exp\left(-(\eta_{i,j}^{n})^2\right)\\ \sum_{j=1}^{J}(\eta_{i,j_2}^{n})^2\eta_{i,j_1}^{n}\exp\left(-(\eta_{i,j}^{n})^2\right)\\ \sum_{j=1}^{J}(\eta_{i,j_2}^{n})^2\eta_{i,j_2}^{n}\exp\left(-(\eta_{i,j}^{n})^2\right)\\ \sum_{j=1}^{J}(\eta_{i,j_2}^{n})^2(\eta_{i,j_1}^{n})^2\exp\left(-(\eta_{i,j}^{n})^2\right)\\ \sum_{j=1}^{J}(\eta_{i,j_2}^{n})^2(\eta_{i,j_2}^{n})^2\exp\left(-(\eta_{i,j}^{n})^2\right)\\ \sum_{j=1}^{J}(\eta_{i,j_2}^{n})^2(\eta_{i,j_3}^{n})^2\exp\left(-(\eta_{i,j}^{n})^2\right)\\ \sum_{j=1}^{J}(\eta_{i,j_2}^{n})^2(\eta_{i,j_1}^{n}\eta_{i,j_2}^{n})\exp\left(-(\eta_{i,j}^{n})^2\right)\end{bmatrix},\ \mathbf{J}_{i,6}^{n}=\begin{bmatrix}\sum_{j=1}^{J}(\eta_{i,j_3}^{n})^2\exp\left(-(\eta_{i,j}^{n})^2\right)\\ \sum_{j=1}^{J}(\eta_{i,j_3}^{n})^2\eta_{i,j_1}^{n}\exp\left(-(\eta_{i,j}^{n})^2\right)\\ \sum_{j=1}^{J}(\eta_{i,j_3}^{n})^2\eta_{i,j_2}^{n}\exp\left(-(\eta_{i,j}^{n})^2\right)\\ \sum_{j=1}^{J}(\eta_{i,j_3}^{n})^2(\eta_{i,j_1}^{n})^2\exp\left(-(\eta_{i,j}^{n})^2\right)\\ \sum_{j=1}^{J}(\eta_{i,j_3}^{n})^2(\eta_{i,j_2}^{n})^2\exp\left(-(\eta_{i,j}^{n})^2\right)\\ \sum_{j=1}^{J}(\eta_{i,j_3}^{n})^2(\eta_{i,j_3}^{n})^2\exp\left(-(\eta_{i,j}^{n})^2\right)\\ \sum_{j=1}^{J}(\eta_{i,j_3}^{n})^2(\eta_{i,j_1}^{n}\eta_{i,j_2}^{n})\exp\left(-(\eta_{i,j}^{n})^2\right)\end{bmatrix},$$

$$\mathbf{J}_{i,7}^{n}=\begin{bmatrix}\sum_{j=1}^{J}(\eta_{i,j_1}^{n}\eta_{i,j_2}^{n})\exp\left(-(\eta_{i,j}^{n})^2\right)\\ \sum_{j=1}^{J}(\eta_{i,j_1}^{n}\eta_{i,j_2}^{n})\eta_{i,j_1}^{n}\exp\left(-(\eta_{i,j}^{n})^2\right)\\ \sum_{j=1}^{J}(\eta_{i,j_1}^{n}\eta_{i,j_2}^{n})\eta_{i,j_2}^{n}\exp\left(-(\eta_{i,j}^{n})^2\right)\\ \sum_{j=1}^{J}(\eta_{i,j_1}^{n}\eta_{i,j_2}^{n})(\eta_{i,j_1}^{n})^2\exp\left(-(\eta_{i,j}^{n})^2\right)\\ \sum_{j=1}^{J}(\eta_{i,j_1}^{n}\eta_{i,j_2}^{n})(\eta_{i,j_2}^{n})^2\exp\left(-(\eta_{i,j}^{n})^2\right)\\ \sum_{j=1}^{J}(\eta_{i,j_1}^{n}\eta_{i,j_2}^{n})(\eta_{i,j_3}^{n})^2\exp\left(-(\eta_{i,j}^{n})^2\right)\\ \sum_{j=1}^{J}(\eta_{i,j_1}^{n}\eta_{i,j_2}^{n})(\eta_{i,j_1}^{n}\eta_{i,j_2}^{n})\exp\left(-(\eta_{i,j}^{n})^2\right)\end{bmatrix}, \text{ which is a symmetric matrix.}$$

C.3 $\nu(C)$-BGK model

For the 1DSW, linearized dimensionless reference distribution is

$$F_{\gamma,i,j}^{n}=\exp\left(-(\eta_{i,j}^{n})^2\right)\cdot\left(a1_i^n+a2_i^n\eta_{i,j_1}^{n}+a3_i^n(\eta_{i,j}^{n})^2\right), \tag{C.13}$$

and three conditions to determine the three coefficients are

$$\begin{aligned}
&\sum_{j=1}^{J}\hat{v}_{i,j}^{n}F_{\gamma,i,j}^{n}=a1_i^n J_{i,11}^{n}+a2_i^n J_{i,12}^{n}+a3_i^n J_{i,13}^{n}=\sum_{j=1}^{J}\hat{v}_{i,j}^{n}\frac{f_{i,j}^{n}}{\rho_i^n}\Delta\mathbf{c},\\
&\sum_{j=1}^{J}\hat{v}_{i,j}^{n}\eta_{i,j_1}^{n}F_{\gamma,i,j}^{n}=a1_i^n J_{i,21}^{n}+a2_i^n J_{i,22}^{n}+a3_i^n J_{i,23}^{n}=\sum_{j=1}^{J}\hat{v}_{i,j}^{n}\eta_{i,j_1}^{n}\frac{f_{i,j}^{n}}{\rho_i^n}\Delta\mathbf{c},\\
&\sum_{j=1}^{J}\hat{v}_{i,j}^{n}(\eta_{i,j}^{n})^2F_{\gamma,i,j}^{n}=a1_i^n J_{i,31}^{n}+a2_i^n J_{i,32}^{n}+a3_i^n J_{i,33}^{n}=\sum_{j=1}^{J}\hat{v}_{i,j}^{n}(\eta_{i,j}^{n})^2\frac{f_{i,j}^{n}}{\rho_i^n}\Delta\mathbf{c},
\end{aligned} \tag{C.14}$$

where

$$\mathbf{J}_i^n=\begin{bmatrix}\sum_{j=1}^{J}\hat{v}_{i,j}^{n}\exp\left(-(\eta_{i,j}^{n})^2\right) & \sum_{j=1}^{J}\hat{v}_{i,j}^{n}\eta_{i,j_1}^{n}\exp\left(-(\eta_{i,j}^{n})^2\right) & \sum_{j=1}^{J}\hat{v}_{i,j}^{n}(\eta_{i,j}^{n})^2\exp\left(-(\eta_{i,j}^{n})^2\right)\\ \sum_{j=1}^{J}\hat{v}_{i,j}^{n}\eta_{i,j_1}^{n}\exp\left(-(\eta_{i,j}^{n})^2\right) & \sum_{j=1}^{J}\hat{v}_{i,j}^{n}(\eta_{i,j_1}^{n})^2\exp\left(-(\eta_{i,j}^{n})^2\right) & \sum_{j=1}^{J}\hat{v}_{i,j}^{n}(\eta_{i,j}^{n})^2\eta_{i,j_1}^{n}\exp\left(-(\eta_{i,j}^{n})^2\right)\\ \sum_{j=1}^{J}\hat{v}_{i,j}^{n}(\eta_{i,j}^{n})^2\exp\left(-(\eta_{i,j}^{n})^2\right) & \sum_{j=1}^{J}\hat{v}_{i,j}^{n}\eta_{i,j_1}^{n}(\eta_{i,j}^{n})^2\exp\left(-(\eta_{i,j}^{n})^2\right) & \sum_{j=1}^{J}\hat{v}_{i,j}^{n}(\eta_{i,j}^{n})^2(\eta_{i,j}^{n})^2\exp\left(-(\eta_{i,j}^{n})^2\right)\end{bmatrix}, \tag{C.15}$$

which is a symmetric matrix.

For the 1DCF, linearized dimensionless reference distribution is

$$F^n_{\gamma,i,j} = \exp\left(-\left(\eta^n_{i,j}\right)^2\right)\left(a1^n_i + a2^n_i \eta^n_{i,j_1} + a3^n_i \eta^n_{i,j_2} + a4^n_i \left(\eta^n_{i,j}\right)^2\right), \tag{C.16}$$

and four conditions to determine the four coefficients are

$$\sum_{j=1}^{J} \hat{v}^n_{i,j} F^n_{\gamma,i,j} = a1^n_i J^n_{i,11} + a2^n_i J^n_{i,12} + a3^n_i J^n_{i,13} + a4^n_i J^n_{i,14} = \sum_{j=1}^{J} \hat{v}^n_{i,j} \frac{f^n_{i,j}}{\rho^n_i} \Delta \mathbf{c},$$

$$\sum_{j=1}^{J} \hat{v}^n_{i,j} \eta^n_{i,j_1} F^n_{\gamma,i,j} = a1^n_i J^n_{i,21} + a2^n_i J^n_{i,22} + a3^n_i J^n_{i,23} + a4^n_i J^n_{i,24} = \sum_{j=1}^{J} \hat{v}^n_{i,j} \eta^n_{i,j_1} \frac{f^n_{i,j}}{\rho^n_i} \Delta \mathbf{c}, \tag{C.17}$$

$$\sum_{j=1}^{J} \hat{v}^n_{i,j} \eta^n_{i,j_2} F^n_{\gamma,i,j} = a1^n_i J^n_{i,31} + a2^n_i J^n_{i,32} + a3^n_i J^n_{i,33} + a4^n_i J^n_{i,34} = \sum_{j=1}^{J} \hat{v}^n_{i,j} \eta^n_{i,j_2} \frac{f^n_{i,j}}{\rho^n_i} \Delta \mathbf{c},$$

$$\sum_{j=1}^{J} \hat{v}^n_{i,j} \left(\eta^n_{i,j}\right)^2 F^n_{\gamma,i,j} = a1^n_i J^n_{i,41} + a2^n_i J^n_{i,42} + a3^n_i J^n_{i,43} + a4^n_i J^n_{i,44} = \sum_{j=1}^{J} \hat{v}^n_{i,j} \left(\eta^n_{i,j}\right)^2 \frac{f^n_{i,j}}{\rho^n_i} \Delta \mathbf{c},$$

where $\mathbf{J}^n_i = \left[\mathbf{J}^n_{i,1} \quad \mathbf{J}^n_{i,2} \quad \mathbf{J}^n_{i,3} \quad \mathbf{J}^n_{i,4}\right]$, which is a symmetric matrix.

$$\mathbf{J}^n_{i,1} = \begin{bmatrix} \sum_{j=1}^{J} \hat{v}^n_{i,j} \exp\left(-\left(\eta^n_{i,j}\right)^2\right) \\ \sum_{j=1}^{J} \hat{v}^n_{i,j} \eta^n_{i,j_1} \exp\left(-\left(\eta^n_{i,j}\right)^2\right) \\ \sum_{j=1}^{J} \hat{v}^n_{i,j} \eta^n_{i,j_2} \exp\left(-\left(\eta^n_{i,j}\right)^2\right) \\ \sum_{j=1}^{J} \hat{v}^n_{i,j} \left(\eta^n_{i,j}\right)^2 \exp\left(-\left(\eta^n_{i,j}\right)^2\right) \end{bmatrix}, \quad \mathbf{J}^n_{i,2} = \begin{bmatrix} \sum_{j=1}^{J} \hat{v}^n_{i,j} \eta^n_{i,j_1} \exp\left(-\left(\eta^n_{i,j}\right)^2\right) \\ \sum_{j=1}^{J} \hat{v}^n_{i,j} \eta^n_{i,j_1} \eta^n_{i,j_1} \exp\left(-\left(\eta^n_{i,j}\right)^2\right) \\ \sum_{j=1}^{J} \hat{v}^n_{i,j} \eta^n_{i,j_1} \eta^n_{i,j_2} \exp\left(-\left(\eta^n_{i,j}\right)^2\right) \\ \sum_{j=1}^{J} \hat{v}^n_{i,j} \eta^n_{i,j_1} \left(\eta^n_{i,j}\right)^2 \exp\left(-\left(\eta^n_{i,j}\right)^2\right) \end{bmatrix}, \tag{C.18}$$

$$\mathbf{J}^n_{i,3} = \begin{bmatrix} \sum_{j=1}^{J} \hat{v}^n_{i,j} \eta^n_{i,j_2} \exp\left(-\left(\eta^n_{i,j}\right)^2\right) \\ \sum_{j=1}^{J} \hat{v}^n_{i,j} \eta^n_{i,j_2} \eta^n_{i,j_1} \exp\left(-\left(\eta^n_{i,j}\right)^2\right) \\ \sum_{j=1}^{J} \hat{v}^n_{i,j} \eta^n_{i,j_2} \eta^n_{i,j_2} \exp\left(-\left(\eta^n_{i,j}\right)^2\right) \\ \sum_{j=1}^{J} \hat{v}^n_{i,j} \eta^n_{i,j_2} \left(\eta^n_{i,j}\right)^2 \exp\left(-\left(\eta^n_{i,j}\right)^2\right) \end{bmatrix}, \quad \mathbf{J}^n_{i,4} = \begin{bmatrix} \sum_{j=1}^{J} \hat{v}^n_{i,j} \left(\eta^n_{i,j}\right)^2 \exp\left(-\left(\eta^n_{i,j}\right)^2\right) \\ \sum_{j=1}^{J} \hat{v}^n_{i,j} \left(\eta^n_{i,j}\right)^2 \eta^n_{i,j_1} \exp\left(-\left(\eta^n_{i,j}\right)^2\right) \\ \sum_{j=1}^{J} \hat{v}^n_{i,j} \left(\eta^n_{i,j}\right)^2 \eta^n_{i,j_2} \exp\left(-\left(\eta^n_{i,j}\right)^2\right) \\ \sum_{j=1}^{J} \hat{v}^n_{i,j} \left(\eta^n_{i,j}\right)^2 \left(\eta^n_{i,j}\right)^2 \exp\left(-\left(\eta^n_{i,j}\right)^2\right) \end{bmatrix}.$$

C.4 New kinetic model I

From section 3.2.4 and section 4.2.4, there are two types linearized reference distribution $f^n_{NI,i,j}$ for the new kinetic model I. Here, only the discussion of first type linearized $f^n_{NI,i,j}$ is given, while the discussion of second type linearized $f^n_{NI,i,j}$ is omitted, which is similar to the discussion of first type.

For the 1DSW, linearized dimensionless reference distribution is

$$F^n_{NI,i,j} = \exp\left(-\left(\eta^n_{i,j}\right)^2\right)\cdot\left(a1^n_i + a2^n_i \eta^n_{i,j_1} + a3^n_i A^n_{i,j}\right), \tag{C.19}$$

where $A^n_{i,j} = a3^n_{ES,i}\left(\eta^n_{i,j_1}\right)^2 + a4^n_{ES,i}\left(\left(\eta^n_{i,j_2}\right)^2 + \left(\eta^n_{i,j_3}\right)^2\right)$, and three conditions to determine the three coefficients are

$$\sum_{j=1}^{J} \hat{v}^n_{i,j} F^n_{NI,i,j} = a1^n_i J^n_{i,11} + a2^n_i J^n_{i,12} + a3^n_i J^n_{i,13} = \sum_{j=1}^{J} \hat{v}^n_{i,j} \frac{f^n_{i,j}}{\rho^n_i}\Delta\mathbf{c},$$

$$\sum_{j=1}^{J} \hat{v}^n_{i,j} \eta^n_{i,j_1} F^n_{NI,i,j} = a1^n_i J^n_{i,21} + a2^n_i J^n_{i,22} + a3^n_i J^n_{i,23} = \sum_{j=1}^{J} \hat{v}^n_{i,j} \eta^n_{i,j_1} \frac{f^n_{i,j}}{\rho^n_i}\Delta\mathbf{c}, \tag{C.20}$$

$$\sum_{j=1}^{J} \hat{v}^n_{i,j} \left(\eta^n_{i,j}\right)^2 F^n_{NI,i,j} = a1^n_i J^n_{i,31} + a2^n_i J^n_{i,32} + a3^n_i J^n_{i,33} = \sum_{j=1}^{J} \hat{v}^n_{i,j} \left(\eta^n_{i,j}\right)^2 \frac{f^n_{i,j}}{\rho^n_i}\Delta\mathbf{c},$$

where

$$\mathbf{J}^n_i = \begin{bmatrix} \sum_{j=1}^{J} \hat{v}^n_{i,j} \exp\left(-\left(\eta^n_{i,j}\right)^2\right) & \sum_{j=1}^{J} \hat{v}^n_{i,j} \eta^n_{i,j_1} \exp\left(-\left(\eta^n_{i,j}\right)^2\right) & \sum_{j=1}^{J} \hat{v}^n_{i,j} A^n_{i,j} \exp\left(-\left(\eta^n_{i,j}\right)^2\right) \\ \sum_{j=1}^{J} \hat{v}^n_{i,j} \eta^n_{i,j_1} \exp\left(-\left(\eta^n_{i,j}\right)^2\right) & \sum_{j=1}^{J} \hat{v}^n_{i,j} \left(\eta^n_{i,j_1}\right)^2 \exp\left(-\left(\eta^n_{i,j}\right)^2\right) & \sum_{j=1}^{J} \hat{v}^n_{i,j} A^n_{i,j} \eta^n_{i,j_1} \exp\left(-\left(\eta^n_{i,j}\right)^2\right) \\ \sum_{j=1}^{J} \hat{v}^n_{i,j} \left(\eta^n_{i,j}\right)^2 \exp\left(-\left(\eta^n_{i,j}\right)^2\right) & \sum_{j=1}^{J} \hat{v}^n_{i,j} \eta^n_{i,j_1} \left(\eta^n_{i,j}\right)^2 \exp\left(-\left(\eta^n_{i,j}\right)^2\right) & \sum_{j=1}^{J} \hat{v}^n_{i,j} A^n_{i,j} \left(\eta^n_{i,j}\right)^2 \exp\left(-\left(\eta^n_{i,j}\right)^2\right) \end{bmatrix}, \tag{C.21}$$

which is not a symmetric matrix.

For the 1DCF, linearized dimensionless reference distribution is

$$F^n_{NI,i,j} = \exp\left(-\left(\eta^n_{i,j}\right)^2\right)\cdot\left(a1^n_i + a2^n_i \eta^n_{i,j_1} + a3^n_i \eta^n_{i,j_2} + a4^n_i A^n_{i,j}\right), \tag{C.22}$$

where $A_{i,j}^n = a4_{ES,i}^n \left(\eta_{i,j_1}^n\right)^2 + a5_{ES,i}^n \left(\eta_{i,j_2}^n\right)^2 + a6_{ES,i}^n \left(\eta_{i,j_3}^n\right)^2 + a7_{ES,i}^n \eta_{i,j_1}^n \eta_{i,j_2}^n$, and four conditions to determine the four coefficients are

$$\sum_{j=1}^{J} \hat{v}_{i,j}^n F_{NI,i,j}^n = a1_i^n J_{i,11}^n + a2_i^n J_{i,12}^n + a3_i^n J_{i,13}^n + a4_i^n J_{i,14}^n = \sum_{j=1}^{J} \hat{v}_{i,j}^n \frac{f_{i,j}^n}{\rho_i^n} \Delta \mathbf{c}, \tag{C.23}$$

$$\sum_{j=1}^{J} \hat{v}_{i,j}^n \eta_{i,j_1}^n F_{NI,i,j}^n = a1_i^n J_{i,21}^n + a2_i^n J_{i,22}^n + a3_i^n J_{i,23}^n + a4_i^n J_{i,24}^n = \sum_{j=1}^{J} \hat{v}_{i,j}^n \eta_{i,j_1}^n \frac{f_{i,j}^n}{\rho_i^n} \Delta \mathbf{c},$$

$$\sum_{j=1}^{J} \hat{v}_{i,j}^n \eta_{i,j_2}^n F_{NI,i,j}^n = a1_i^n J_{i,31}^n + a2_i^n J_{i,32}^n + a3_i^n J_{i,33}^n + a4_i^n J_{i,34}^n = \sum_{j=1}^{J} \hat{v}_{i,j}^n \eta_{i,j_2}^n \frac{f_{i,j}^n}{\rho_i^n} \Delta \mathbf{c},$$

$$\sum_{j=1}^{J} \hat{v}_{i,j}^n \left(\eta_{i,j}^n\right)^2 F_{NI,i,j}^n = a1_i^n J_{i,41}^n + a2_i^n J_{i,42}^n + a3_i^n J_{i,43}^n + a4_i^n J_{i,44}^n = \sum_{j=1}^{J} \hat{v}_{i,j}^n \left(\eta_{i,j}^n\right)^2 \frac{f_{i,j}^n}{\rho_i^n} \Delta \mathbf{c},$$

where $\mathbf{J}_i^n = \left[\mathbf{J}_{i,1}^n \quad \mathbf{J}_{i,2}^n \quad \mathbf{J}_{i,3}^n \quad \mathbf{J}_{i,4}^n\right]$, which is not a symmetric matrix.

$$\mathbf{J}_{i,1}^n = \begin{bmatrix} \sum_{j=1}^{J} \hat{v}_{i,j}^n \exp\left(-\left(\eta_{i,j}^n\right)^2\right) \\ \sum_{j=1}^{J} \hat{v}_{i,j}^n \eta_{i,j_1}^n \exp\left(-\left(\eta_{i,j}^n\right)^2\right) \\ \sum_{j=1}^{J} \hat{v}_{i,j}^n \eta_{i,j_2}^n \exp\left(-\left(\eta_{i,j}^n\right)^2\right) \\ \sum_{j=1}^{J} \hat{v}_{i,j}^n \left(\eta_{i,j}^n\right)^2 \exp\left(-\left(\eta_{i,j}^n\right)^2\right) \end{bmatrix}, \mathbf{J}_{i,2}^n = \begin{bmatrix} \sum_{j=1}^{J} \hat{v}_{i,j}^n \eta_{i,j_1}^n \exp\left(-\left(\eta_{i,j}^n\right)^2\right) \\ \sum_{j=1}^{J} \hat{v}_{i,j}^n \eta_{i,j_1}^n \eta_{i,j_1}^n \exp\left(-\left(\eta_{i,j}^n\right)^2\right) \\ \sum_{j=1}^{J} \hat{v}_{i,j}^n \eta_{i,j_1}^n \eta_{i,j_2}^n \exp\left(-\left(\eta_{i,j}^n\right)^2\right) \\ \sum_{j=1}^{J} \hat{v}_{i,j}^n \eta_{i,j_1}^n \left(\eta_{i,j}^n\right)^2 \exp\left(-\left(\eta_{i,j}^n\right)^2\right) \end{bmatrix}, \tag{C.24}$$

$$\mathbf{J}_{i,3}^n = \begin{bmatrix} \sum_{j=1}^{J} \hat{v}_{i,j}^n \eta_{i,j_2}^n \exp\left(-\left(\eta_{i,j}^n\right)^2\right) \\ \sum_{j=1}^{J} \hat{v}_{i,j}^n \eta_{i,j_2}^n \eta_{i,j_1}^n \exp\left(-\left(\eta_{i,j}^n\right)^2\right) \\ \sum_{j=1}^{J} \hat{v}_{i,j}^n \eta_{i,j_2}^n \eta_{i,j_2}^n \exp\left(-\left(\eta_{i,j}^n\right)^2\right) \\ \sum_{j=1}^{J} \hat{v}_{i,j}^n \eta_{i,j_2}^n \left(\eta_{i,j}^n\right)^2 \exp\left(-\left(\eta_{i,j}^n\right)^2\right) \end{bmatrix}, \mathbf{J}_{i,4}^n = \begin{bmatrix} \sum_{j=1}^{J} \hat{v}_{i,j}^n A_{i,j}^n \exp\left(-\left(\eta_{i,j}^n\right)^2\right) \\ \sum_{j=1}^{J} \hat{v}_{i,j}^n A_{i,j}^n \eta_{i,j_1}^n \exp\left(-\left(\eta_{i,j}^n\right)^2\right) \\ \sum_{j=1}^{J} \hat{v}_{i,j}^n A_{i,j}^n \eta_{i,j_2}^n \exp\left(-\left(\eta_{i,j}^n\right)^2\right) \\ \sum_{j=1}^{J} \hat{v}_{i,j}^n A_{i,j}^n \left(\eta_{i,j}^n\right)^2 \exp\left(-\left(\eta_{i,j}^n\right)^2\right) \end{bmatrix}.$$

C.5 New kinetic model II

From section 3.2.4 and section 4.2.4, there are two types linearized reference distribution $f_{NII,i,j}^n$ for the new kinetic model II. Here, only the discussion of first type

linearized $f^n_{NII,i,j}$ is given, while the discussion of second type linearized $f^n_{NII,i,j}$ is omitted, which is similar to the discussion of first type.

For the 1DSW, linearized dimensionless reference distribution is

$$F^n_{NII,i,j} = \exp\left(-\left(\eta^n_{i,j}\right)^2\right)\cdot\left(a1^n_i + a2^n_i \eta^n_{i,j_1} + a3^n_i \left(\eta^n_{i,j_1}\right)^2 + a4^n_i \left(\left(\eta^n_{i,j_2}\right)^2 + \left(\eta^n_{i,j_3}\right)^2\right)\right), \qquad \text{(C.25)}$$

and four conditions to determine the four coefficients are

$$\sum_{j=1}^{J} \hat{v}^n_{i,j} F^n_{NII,i,j} = a1^n_i J^n_{i,11} + a2^n_i J^n_{i,12} + a3^n_i J^n_{i,13} + a4^n_i J^n_{i,14} = BB1^n_i,$$

$$\sum_{j=1}^{J} \hat{v}^n_{i,j} \eta^n_{i,j_1} F^n_{NII,i,j} = a1^n_i J^n_{i,21} + a2^n_i J^n_{i,22} + a3^n_i J^n_{i,23} + a4^n_i J^n_{i,24} = BB2^n_i,$$

$$\sum_{j=1}^{J} \hat{v}^n_{i,j} \left(\eta^n_{i,j_1}\right)^2 F^n_{NII,i,j} = a1^n_i J^n_{i,31} + a2^n_i J^n_{i,32} + a3^n_i J^n_{i,33} + a4^n_i J^n_{i,34} = BB3^n_i, \qquad \text{(C.26)}$$

$$\sum_{j=1}^{J} \hat{v}^n_{i,j} \left(\eta^n_{i,j_2}\right)^2 F^n_{NII,i,j} = a1^n_i J^n_{i,41} + a2^n_i J^n_{i,42} + a3^n_i J^n_{i,43} + a4^n_i J^n_{i,44} = BB4^n_i,$$

where

$$BB1^n_i = \sum_{j=1}^{J} \hat{v}^n_{i,j} \frac{f^n_{i,j}}{\rho^n_i} \Delta\mathbf{c},\ BB2^n_i = \sum_{j=1}^{J} \hat{v}^n_{i,j} \eta^n_{i,j_1} \frac{f^n_{i,j}}{\rho^n_i} \Delta\mathbf{c},$$

$$BB3^n_i = \frac{p^n_{BGK,xx,i} - p^n_{xx,i}}{2p^n_i} + \sum_{j=1}^{J} \hat{v}^n_{i,j} \left(\eta^n_{i,j_1}\right)^2 \frac{f^n_{i,j}}{\rho^n_i} \Delta\mathbf{c},\ BB4^n_i = \frac{p^n_{BGK,yy,i} - p^n_{yy,i}}{2p^n_i} + \sum_{j=1}^{J} \hat{v}^n_{i,j} \left(\eta^n_{i,j_2}\right)^2 \frac{f^n_{i,j}}{\rho^n_i} \Delta\mathbf{c},$$

$\mathbf{J}^n_i = \left[\mathbf{J}^n_{i,1} \quad \mathbf{J}^n_{i,2} \quad \mathbf{J}^n_{i,3} \quad \mathbf{J}^n_{i,4}\right]$, which is not a symmetric matrix.

$$\mathbf{J}^n_{i,1} = \begin{bmatrix} \sum_{j=1}^{J} \hat{v}^n_{i,j} \exp\left(-\left(\eta^n_{i,j}\right)^2\right) \\ \sum_{j=1}^{J} \hat{v}^n_{i,j} \eta^n_{i,j_1} \exp\left(-\left(\eta^n_{i,j}\right)^2\right) \\ \sum_{j=1}^{J} \hat{v}^n_{i,j} \left(\eta^n_{i,j_1}\right)^2 \exp\left(-\left(\eta^n_{i,j}\right)^2\right) \\ \sum_{j=1}^{J} \hat{v}^n_{i,j} \left(\eta^n_{i,j_2}\right)^2 \exp\left(-\left(\eta^n_{i,j}\right)^2\right) \end{bmatrix}, \mathbf{J}^n_{i,2} = \begin{bmatrix} \sum_{j=1}^{J} \hat{v}^n_{i,j} \eta^n_{i,j_1} \exp\left(-\left(\eta^n_{i,j}\right)^2\right) \\ \sum_{j=1}^{J} \hat{v}^n_{i,j} \eta^n_{i,j_1} \eta^n_{i,j_1} \exp\left(-\left(\eta^n_{i,j}\right)^2\right) \\ \sum_{j=1}^{J} \hat{v}^n_{i,j} \eta^n_{i,j_1} \left(\eta^n_{i,j_1}\right)^2 \exp\left(-\left(\eta^n_{i,j}\right)^2\right) \\ \sum_{j=1}^{J} \hat{v}^n_{i,j} \eta^n_{i,j_1} \left(\eta^n_{i,j_2}\right)^2 \exp\left(-\left(\eta^n_{i,j}\right)^2\right) \end{bmatrix}, \qquad \text{(C.27)}$$

$$\mathbf{J}_{i,3}^{n}=\begin{bmatrix}\sum_{j=1}^{J}\hat{v}_{i,j}^{n}\left(\eta_{i,j_1}^{n}\right)^2\exp\left(-\left(\eta_{i,j}^{n}\right)^2\right)\\ \sum_{j=1}^{J}\hat{v}_{i,j}^{n}\left(\eta_{i,j_1}^{n}\right)^2\eta_{i,j_1}^{n}\exp\left(-\left(\eta_{i,j}^{n}\right)^2\right)\\ \sum_{j=1}^{J}\hat{v}_{i,j}^{n}\left(\eta_{i,j_1}^{n}\right)^2\left(\eta_{i,j_2}^{n}\right)^2\exp\left(-\left(\eta_{i,j}^{n}\right)^2\right)\\ \sum_{j=1}^{J}\hat{v}_{i,j}^{n}\left(\eta_{i,j_1}^{n}\right)^2\left(\eta_{i,j_2}^{n}\right)^2\exp\left(-\left(\eta_{i,j}^{n}\right)^2\right)\end{bmatrix},\ \mathbf{J}_{i,4}^{n}=\begin{bmatrix}\sum_{j=1}^{J}\hat{v}_{i,j}^{n}\left(\left(\eta_{i,j_2}^{n}\right)^2+\left(\eta_{i,j_3}^{n}\right)^2\right)\exp\left(-\left(\eta_{i,j}^{n}\right)^2\right)\\ \sum_{j=1}^{J}\hat{v}_{i,j}^{n}\left(\left(\eta_{i,j_2}^{n}\right)^2+\left(\eta_{i,j_3}^{n}\right)^2\right)\eta_{i,j_1}^{n}\exp\left(-\left(\eta_{i,j}^{n}\right)^2\right)\\ \sum_{j=1}^{J}\hat{v}_{i,j}^{n}\left(\left(\eta_{i,j_2}^{n}\right)^2+\left(\eta_{i,j_3}^{n}\right)^2\right)\left(\eta_{i,j_1}^{n}\right)^2\exp\left(-\left(\eta_{i,j}^{n}\right)^2\right)\\ \sum_{j=1}^{J}\hat{v}_{i,j}^{n}\left(\left(\eta_{i,j_2}^{n}\right)^2+\left(\eta_{i,j_3}^{n}\right)^2\right)\left(\eta_{i,j_2}^{n}\right)^2\exp\left(-\left(\eta_{i,j}^{n}\right)^2\right)\end{bmatrix}.$$

For the 1DCF, linearized dimensionless reference distribution is

$$F_{NII,i,j}^{n}=\exp\left(-\left(\eta_{i,j}^{n}\right)^2\right)\cdot \left(a1_i^n+a2_i^n\eta_{i,j_1}^{n}+a3_i^n\eta_{i,j_2}^{n}+a4_i^n\left(\eta_{i,j_1}^{n}\right)^2+a5_i^n\left(\eta_{i,j_2}^{n}\right)^2+a6_i^n\left(\eta_{i,j_3}^{n}\right)^2+a7_i^n\left(\eta_{i,j_2}^{n}\eta_{i,j_3}^{n}\right)\right), \quad \text{(C.28)}$$

and seven conditions to determine the seven coefficients are

$$\sum_{j=1}^{J}\hat{v}_{i,j}^{n}F_{NII,i,j}^{n}=a1_i^nJ_{i,11}^{n}+a2_i^nJ_{i,12}^{n}+a3_i^nJ_{i,13}^{n}+a4_i^nJ_{i,14}^{n}+a5_i^nJ_{i,15}^{n}+a6_i^nJ_{i,16}^{n}+a7_i^nJ_{i,17}^{n}=BB1_i^n, \quad \text{(C.29)}$$

$$\sum_{j=1}^{J}\hat{v}_{i,j}^{n}\eta_{i,j_1}^{n}F_{NII,i,j}^{n}=a1_i^nJ_{i,21}^{n}+a2_i^nJ_{i,22}^{n}+a3_i^nJ_{i,23}^{n}+a4_i^nJ_{i,24}^{n}+a5_i^nJ_{i,25}^{n}+a6_i^nJ_{i,26}^{n}+a7_i^nJ_{i,27}^{n}=BB2_i^n,$$

$$\sum_{j=1}^{J}\hat{v}_{i,j}^{n}\eta_{i,j_2}^{n}F_{NII,i,j}^{n}=a1_i^nJ_{i,31}^{n}+a2_i^nJ_{i,32}^{n}+a3_i^nJ_{i,33}^{n}+a4_i^nJ_{i,34}^{n}+a5_i^nJ_{i,35}^{n}+a6_i^nJ_{i,36}^{n}+a7_i^nJ_{i,37}^{n}=BB3_i^n,$$

$$\sum_{j=1}^{J}\hat{v}_{i,j}^{n}\left(\eta_{i,j_1}^{n}\right)^2F_{NII,i,j}^{n}=a1_i^nJ_{i,41}^{n}+a2_i^nJ_{i,42}^{n}+a3_i^nJ_{i,43}^{n}+a4_i^nJ_{i,44}^{n}+a5_i^nJ_{i,45}^{n}+a6_i^nJ_{i,46}^{n}+a7_i^nJ_{i,47}^{n}=BB4_i^n,$$

$$\sum_{j=1}^{J}\hat{v}_{i,j}^{n}\left(\eta_{i,j_2}^{n}\right)^2F_{NII,i,j}^{n}=a1_i^nJ_{i,51}^{n}+a2_i^nJ_{i,52}^{n}+a3_i^nJ_{i,53}^{n}+a4_i^nJ_{i,54}^{n}+a5_i^nJ_{i,55}^{n}+a6_i^nJ_{i,56}^{n}+a7_i^nJ_{i,57}^{n}=BB5_i^n,$$

$$\sum_{j=1}^{J}\hat{v}_{i,j}^{n}\left(\eta_{i,j_3}^{n}\right)^2F_{NII,i,j}^{n}=a1_i^nJ_{i,61}^{n}+a2_i^nJ_{i,62}^{n}+a3_i^nJ_{i,63}^{n}+a4_i^nJ_{i,64}^{n}+a5_i^nJ_{i,65}^{n}+a6_i^nJ_{i,66}^{n}+a7_i^nJ_{i,67}^{n}=BB6_i^n,$$

$$\sum_{j=1}^{J}\hat{v}_{i,j}^{n}\left(\eta_{i,j_2}^{n}\eta_{i,j_3}^{n}\right)F_{NII,i,j}^{n}=a1_i^nJ_{i,71}^{n}+a2_i^nJ_{i,72}^{n}+a3_i^nJ_{i,73}^{n}+a4_i^nJ_{i,74}^{n}+a5_i^nJ_{i,75}^{n}+a6_i^nJ_{i,76}^{n}+a7_i^nJ_{i,77}^{n}=BB7_i^n,$$

where

$$BB1_i^n = \sum_{j=1}^{J} \hat{v}_{i,j}^n \frac{f_{i,j}^n}{\rho_i^n} \Delta \mathbf{c}, \qquad BB2_i^n = \sum_{j=1}^{J} \hat{v}_{i,j}^n \eta_{i,j_1}^n \frac{f_{i,j}^n}{\rho_i^n} \Delta \mathbf{c}, \qquad BB3_i^n = \sum_{j=1}^{J} \hat{v}_{i,j}^n \eta_{i,j_2}^n \frac{f_{i,j}^n}{\rho_i^n} \Delta \mathbf{c},$$

$$BB4_i^n = \frac{p_{BGK,xx,i}^n - p_{xx,i}^n}{2p_i^n} + \sum_{j=1}^{J} \hat{v}_{i,j}^n \left(\eta_{i,j_1}^n\right)^2 \frac{f_{i,j}^n}{\rho_i^n} \Delta \mathbf{c}, \quad BB5_i^n = \frac{p_{BGK,yy,i}^n - p_{yy,i}^n}{2p_i^n} + \sum_{j=1}^{J} \hat{v}_{i,j}^n \left(\eta_{i,j_2}^n\right)^2 \frac{f_{i,j}^n}{\rho_i^n} \Delta \mathbf{c},$$

$$BB6_i^n = \frac{p_{BGK,zz,i}^n - p_{zz,i}^n}{2p_i^n} + \sum_{j=1}^{J} \hat{v}_{i,j}^n \left(\eta_{i,j_3}^n\right)^2 \frac{f_{i,j}^n}{\rho_i^n} \Delta \mathbf{c}, \; BB7_i^n = \frac{p_{BGK,xy,i}^n - p_{xy,i}^n}{2p_i^n} + \sum_{j=1}^{J} \hat{v}_{i,j}^n \left(\eta_{i,j_2}^n \eta_{i,j_3}^n\right) \frac{f_{i,j}^n}{\rho_i^n} \Delta \mathbf{c}.$$

$\mathbf{J}_i^n = \left[\mathbf{J}_{i,1}^n \quad \mathbf{J}_{i,2}^n \quad \mathbf{J}_{i,3}^n \quad \mathbf{J}_{i,4}^n \quad \mathbf{J}_{i,5}^n \quad \mathbf{J}_{i,6}^n \quad \mathbf{J}_{i,7}^n\right]$, which is a symmetric matrix.

$$\mathbf{J}_{i,1}^n = \begin{bmatrix} \sum_{j=1}^{J} \hat{v}_{i,j}^n \exp\left(-\left(\eta_{i,j}^n\right)^2\right) \\ \sum_{j=1}^{J} \hat{v}_{i,j}^n \eta_{i,j_1}^n \exp\left(-\left(\eta_{i,j}^n\right)^2\right) \\ \sum_{j=1}^{J} \hat{v}_{i,j}^n \eta_{i,j_2}^n \exp\left(-\left(\eta_{i,j}^n\right)^2\right) \\ \sum_{j=1}^{J} \hat{v}_{i,j}^n \left(\eta_{i,j_1}^n\right)^2 \exp\left(-\left(\eta_{i,j}^n\right)^2\right) \\ \sum_{j=1}^{J} \hat{v}_{i,j}^n \left(\eta_{i,j_2}^n\right)^2 \exp\left(-\left(\eta_{i,j}^n\right)^2\right) \\ \sum_{j=1}^{J} \hat{v}_{i,j}^n \left(\eta_{i,j_3}^n\right)^2 \exp\left(-\left(\eta_{i,j}^n\right)^2\right) \\ \sum_{j=1}^{J} \hat{v}_{i,j}^n \eta_{i,j_1}^n \eta_{i,j_2}^n \exp\left(-\left(\eta_{i,j}^n\right)^2\right) \end{bmatrix}, \quad \mathbf{J}_{i,2}^n = \begin{bmatrix} \sum_{j=1}^{J} \hat{v}_{i,j}^n \eta_{i,j_1}^n \exp\left(-\left(\eta_{i,j}^n\right)^2\right) \\ \sum_{j=1}^{J} \hat{v}_{i,j}^n \eta_{i,j_1}^n \eta_{i,j_1}^n \exp\left(-\left(\eta_{i,j}^n\right)^2\right) \\ \sum_{j=1}^{J} \hat{v}_{i,j}^n \eta_{i,j_1}^n \eta_{i,j_2}^n \exp\left(-\left(\eta_{i,j}^n\right)^2\right) \\ \sum_{j=1}^{J} \hat{v}_{i,j}^n \eta_{i,j_1}^n \left(\eta_{i,j_1}^n\right)^2 \exp\left(-\left(\eta_{i,j}^n\right)^2\right) \\ \sum_{j=1}^{J} \hat{v}_{i,j}^n \eta_{i,j_1}^n \left(\eta_{i,j_2}^n\right)^2 \exp\left(-\left(\eta_{i,j}^n\right)^2\right) \\ \sum_{j=1}^{J} \hat{v}_{i,j}^n \eta_{i,j_1}^n \left(\eta_{i,j_3}^n\right)^2 \exp\left(-\left(\eta_{i,j}^n\right)^2\right) \\ \sum_{j=1}^{J} \hat{v}_{i,j}^n \eta_{i,j_1}^n \left(\eta_{i,j_1}^n \eta_{i,j_2}^n\right) \exp\left(-\left(\eta_{i,j}^n\right)^2\right) \end{bmatrix}, \tag{C.30}$$

$$\mathbf{J}_{i,3}^n = \begin{bmatrix} \sum_{j=1}^{J} \hat{v}_{i,j}^n \eta_{i,j_2}^n \exp\left(-\left(\eta_{i,j}^n\right)^2\right) \\ \sum_{j=1}^{J} \hat{v}_{i,j}^n \eta_{i,j_2}^n \eta_{i,j_1}^n \exp\left(-\left(\eta_{i,j}^n\right)^2\right) \\ \sum_{j=1}^{J} \hat{v}_{i,j}^n \eta_{i,j_2}^n \eta_{i,j_2}^n \exp\left(-\left(\eta_{i,j}^n\right)^2\right) \\ \sum_{j=1}^{J} \hat{v}_{i,j}^n \eta_{i,j_2}^n \left(\eta_{i,j_1}^n\right)^2 \exp\left(-\left(\eta_{i,j}^n\right)^2\right) \\ \sum_{j=1}^{J} \hat{v}_{i,j}^n \eta_{i,j_2}^n \left(\eta_{i,j_2}^n\right)^2 \exp\left(-\left(\eta_{i,j}^n\right)^2\right) \\ \sum_{j=1}^{J} \hat{v}_{i,j}^n \eta_{i,j_2}^n \left(\eta_{i,j_3}^n\right)^2 \exp\left(-\left(\eta_{i,j}^n\right)^2\right) \\ \sum_{j=1}^{J} \hat{v}_{i,j}^n \eta_{i,j_2}^n \left(\eta_{i,j_1}^n \eta_{i,j_2}^n\right) \exp\left(-\left(\eta_{i,j}^n\right)^2\right) \end{bmatrix}, \quad \mathbf{J}_{i,4}^n = \begin{bmatrix} \sum_{j=1}^{J} \hat{v}_{i,j}^n \left(\eta_{i,j_1}^n\right)^2 \exp\left(-\left(\eta_{i,j}^n\right)^2\right) \\ \sum_{j=1}^{J} \hat{v}_{i,j}^n \left(\eta_{i,j_1}^n\right)^2 \eta_{i,j_1}^n \exp\left(-\left(\eta_{i,j}^n\right)^2\right) \\ \sum_{j=1}^{J} \hat{v}_{i,j}^n \left(\eta_{i,j_1}^n\right)^2 \eta_{i,j_2}^n \exp\left(-\left(\eta_{i,j}^n\right)^2\right) \\ \sum_{j=1}^{J} \hat{v}_{i,j}^n \left(\eta_{i,j_1}^n\right)^2 \left(\eta_{i,j_1}^n\right)^2 \exp\left(-\left(\eta_{i,j}^n\right)^2\right) \\ \sum_{j=1}^{J} \hat{v}_{i,j}^n \left(\eta_{i,j_1}^n\right)^2 \left(\eta_{i,j_2}^n\right)^2 \exp\left(-\left(\eta_{i,j}^n\right)^2\right) \\ \sum_{j=1}^{J} \hat{v}_{i,j}^n \left(\eta_{i,j_1}^n\right)^2 \left(\eta_{i,j_3}^n\right)^2 \exp\left(-\left(\eta_{i,j}^n\right)^2\right) \\ \sum_{j=1}^{J} \hat{v}_{i,j}^n \left(\eta_{i,j_1}^n\right)^2 \left(\eta_{i,j_1}^n \eta_{i,j_2}^n\right) \exp\left(-\left(\eta_{i,j}^n\right)^2\right) \end{bmatrix},$$

$$\mathbf{J}_{i,5}^{n}=\begin{bmatrix}\sum_{j=1}^{J}\hat{v}_{i,j}^{n}\left(\eta_{i,j_2}^{n}\right)^2\exp\left(-\left(\eta_{i,j}^{n}\right)^2\right)\\ \sum_{j=1}^{J}\hat{v}_{i,j}^{n}\left(\eta_{i,j_2}^{n}\right)^2\eta_{i,j_1}^{n}\exp\left(-\left(\eta_{i,j}^{n}\right)^2\right)\\ \sum_{j=1}^{J}\hat{v}_{i,j}^{n}\left(\eta_{i,j_2}^{n}\right)^2\eta_{i,j_2}^{n}\exp\left(-\left(\eta_{i,j}^{n}\right)^2\right)\\ \sum_{j=1}^{J}\hat{v}_{i,j}^{n}\left(\eta_{i,j_2}^{n}\right)^2\left(\eta_{i,j_1}^{n}\right)^2\exp\left(-\left(\eta_{i,j}^{n}\right)^2\right)\\ \sum_{j=1}^{J}\hat{v}_{i,j}^{n}\left(\eta_{i,j_2}^{n}\right)^2\left(\eta_{i,j_2}^{n}\right)^2\exp\left(-\left(\eta_{i,j}^{n}\right)^2\right)\\ \sum_{j=1}^{J}\hat{v}_{i,j}^{n}\left(\eta_{i,j_2}^{n}\right)^2\left(\eta_{i,j_3}^{n}\right)^2\exp\left(-\left(\eta_{i,j}^{n}\right)^2\right)\\ \sum_{j=1}^{J}\hat{v}_{i,j}^{n}\left(\eta_{i,j_2}^{n}\right)^2\left(\eta_{i,j_1}^{n}\eta_{i,j_2}^{n}\right)\exp\left(-\left(\eta_{i,j}^{n}\right)^2\right)\end{bmatrix},\quad \mathbf{J}_{i,6}^{n}=\begin{bmatrix}\sum_{j=1}^{J}\hat{v}_{i,j}^{n}\left(\eta_{i,j_3}^{n}\right)^2\exp\left(-\left(\eta_{i,j}^{n}\right)^2\right)\\ \sum_{j=1}^{J}\hat{v}_{i,j}^{n}\left(\eta_{i,j_3}^{n}\right)^2\eta_{i,j_1}^{n}\exp\left(-\left(\eta_{i,j}^{n}\right)^2\right)\\ \sum_{j=1}^{J}\hat{v}_{i,j}^{n}\left(\eta_{i,j_3}^{n}\right)^2\eta_{i,j_2}^{n}\exp\left(-\left(\eta_{i,j}^{n}\right)^2\right)\\ \sum_{j=1}^{J}\hat{v}_{i,j}^{n}\left(\eta_{i,j_3}^{n}\right)^2\left(\eta_{i,j_1}^{n}\right)^2\exp\left(-\left(\eta_{i,j}^{n}\right)^2\right)\\ \sum_{j=1}^{J}\hat{v}_{i,j}^{n}\left(\eta_{i,j_3}^{n}\right)^2\left(\eta_{i,j_2}^{n}\right)^2\exp\left(-\left(\eta_{i,j}^{n}\right)^2\right)\\ \sum_{j=1}^{J}\hat{v}_{i,j}^{n}\left(\eta_{i,j_3}^{n}\right)^2\left(\eta_{i,j_3}^{n}\right)^2\exp\left(-\left(\eta_{i,j}^{n}\right)^2\right)\\ \sum_{j=1}^{J}\hat{v}_{i,j}^{n}\left(\eta_{i,j_3}^{n}\right)^2\left(\eta_{i,j_1}^{n}\eta_{i,j_2}^{n}\right)\exp\left(-\left(\eta_{i,j}^{n}\right)^2\right)\end{bmatrix},$$

$$\mathbf{J}_{i,7}^{n}=\begin{bmatrix}\sum_{j=1}^{J}\hat{v}_{i,j}^{n}\left(\eta_{i,j_1}^{n}\eta_{i,j_2}^{n}\right)\exp\left(-\left(\eta_{i,j}^{n}\right)^2\right)\\ \sum_{j=1}^{J}\hat{v}_{i,j}^{n}\left(\eta_{i,j_1}^{n}\eta_{i,j_2}^{n}\right)\eta_{i,j_1}^{n}\exp\left(-\left(\eta_{i,j}^{n}\right)^2\right)\\ \sum_{j=1}^{J}\hat{v}_{i,j}^{n}\left(\eta_{i,j_1}^{n}\eta_{i,j_2}^{n}\right)\eta_{i,j_2}^{n}\exp\left(-\left(\eta_{i,j}^{n}\right)^2\right)\\ \sum_{j=1}^{J}\hat{v}_{i,j}^{n}\left(\eta_{i,j_1}^{n}\eta_{i,j_2}^{n}\right)\left(\eta_{i,j_1}^{n}\right)^2\exp\left(-\left(\eta_{i,j}^{n}\right)^2\right)\\ \sum_{j=1}^{J}\hat{v}_{i,j}^{n}\left(\eta_{i,j_1}^{n}\eta_{i,j_2}^{n}\right)\left(\eta_{i,j_2}^{n}\right)^2\exp\left(-\left(\eta_{i,j}^{n}\right)^2\right)\\ \sum_{j=1}^{J}\hat{v}_{i,j}^{n}\left(\eta_{i,j_1}^{n}\eta_{i,j_2}^{n}\right)\left(\eta_{i,j_3}^{n}\right)^2\exp\left(-\left(\eta_{i,j}^{n}\right)^2\right)\\ \sum_{j=1}^{J}\hat{v}_{i,j}^{n}\left(\eta_{i,j_1}^{n}\eta_{i,j_2}^{n}\right)\left(\eta_{i,j_1}^{n}\eta_{i,j_2}^{n}\right)\exp\left(-\left(\eta_{i,j}^{n}\right)^2\right)\end{bmatrix}.$$

Appendix D: Average relative errors in comparisons

Table D.1: Average relative errors of kinetic models compared to DSMC in 1DSW

Parameters / Case and Kinetic model	Density ρ	Velocity u_1	Momentum ρu_1	Temperature T	Pressure p
3.4 BGK	.78E-02	.79E-02	.15E-03	.73E-02	.14E-01
3.4 ES-BGK	.34E-02	.34E-02	.14E-03	.34E-02	.68E-02
3.4 $\nu(C)$-BGK	.12E-01	.12E-01	.27E-03	.11E-01	.22E-01
3.4 New I	.28E-02	.29E-02	.14E-03	.29E-02	.57E-02
3.4 New II	.17E-02	.17E-02	.14E-03	.23E-02	.38E-02
3.5 BGK	.21E-01	.22E-01	.46E-03	.53E-01	.67E-01
3.5 ES-BGK	.20E-01	.21E-01	.14E-02	.84E-01	.10E+00
3.5 $\nu(C)$-BGK	.25E-01	.26E-01	.58E-03	.70E-01	.89E-01
3.5 New I	.12E-01	.12E-01	.25E-03	.25E-01	.36E-01
3.5 New II	.92E-02	.96E-02	.26E-03	.24E-01	.32E-01
3.6 BGK	.30E-01	.33E-01	.12E-02	.26E+00	.28E+00
3.6 ES-BGK	.31E-01	.34E-01	.28E-02	.49E+00	.53E+00
3.6 $\nu(C)$-BGK	.19E-01	.20E-01	.49E-03	.13E+00	.15E+00
3.6 New I	.18E-01	.19E-01	.46E-03	.54E-01	.70E-01
3.6 New II	.13E-01	.14E-01	.53E-03	.51E-01	.60E-01

Table D.2: Average relative errors of kinetic models compared to DSMC in 1DCF. Part I

Parameters / Case and Kinetic model	Density ρ	Velocity u_1	Temperature T	Pressure p	Pressure σ_{11}	Pressure σ_{22}	Pressure σ_{12}
4.1 BGK	.58E-2	.82E-2	.15E-1	.15E-1	.22E+0	.64E+0	.91E-2
4.1 ES-BGK	.64E-3	.10E-1	.58E-3	.68E-3	.24E+0	.60E+0	.72E-2
4.1 $\nu(C)$-BGK	.11E-2	.98E-2	.12E-2	.13E-2	.13E+0	.93E+0	.87E-2
4.1New I	.65E-3	.11E-1	.53E-3	.28E-3	.25E+0	.64E+0	.47E-2
4.1 New II	.65E-3	.11E-1	.54E-3	.29E-3	.23E+0	.59E+0	.45E-2
4.2 BGK	.56E-2	.65E-2	.14E-1	.15E-1	.17E+0	.13E+1	.33E-1
4.2 ES-BGK	.60E-3	.11E-1	.47E-3	.18E-3	.20E+0	.12E+1	.19E-1
4.2 $\nu(C)$-BGK	.95E-3	.10E-1	.93E-3	.77E-3	.12E+0	.16E+1	.27E-1
4.2 New I	.60E-3	.11E-1	.47E-3	.18E-3	.20E+0	.12E+1	.19E-1
4.2 New II	.60E-3	.11E-1	.47E-3	.18E-3	.20E+0	.12E+1	.19E-1
4.3 BGK	.48E-2	.15E-1	.95E-2	.96E-2	.36E-1	.25E-1	.70E-2
4.3 ES-BGK	.10E-2	.21E-1	.27E-2	.21E-2	.87E-1	.85E-1	.66E-2
4.3 $\nu(C)$-BGK	.20E-2	.72E-2	.38E-2	.31E-2	.10E+0	.15E+0	.59E-2
4.3 New I	.66E-3	.16E-1	.39E-2	.34E-2	.67E-1	.44E-1	.11E-1
4.3 New II	.67E-3	.17E-1	.39E-2	.33E-2	.43E-1	.30E-1	.98E-2
4.4 BGK	.43E-2	.11E-1	.89E-2	.92E-2	.17E-1	.39E-1	.28E-1
4.4 ES-BGK	.70E-3	.18E-1	.32E-2	.27E-2	.76E-1	.65E-1	.19E-1
4.4 $\nu(C)$-BGK	.24E-2	.57E-2	.45E-2	.37E-2	.11E+0	.20E+0	.23E-1
4.4 New I	.70E-3	.18E-1	.32E-2	.27E-2	.76E-1	.65E-1	.19E-1
4.4 New II	.70E-3	.18E-1	.32E-2	.27E-2	.76E-1	.65E-1	.19E-1

Table D.3: Average relative errors of kinetic models compared to DSMC in 1DCF. Part II

Parameters / Case and Kinetic model	Density ρ	Velocity u_1	Temperature T	Pressure p	Pressure σ_{11}	Pressure σ_{22}	Pressure σ_{12}
4.5 BGK	.17E-2	.23E-1	.17E-2	.77E-3	.50E-2	.25E-1	.57E-2
4.5 ES-BGK	.78E-3	.17E-1	.73E-2	.66E-2	.35E-1	.60E-1	.16E-1
4.5 $\nu(C)$-BGK	.29E-2	.99E-2	.74E-2	.66E-2	.49E-1	.43E-1	.20E-1
4.5 New I	.15E-2	.81E-2	.78E-2	.71E-2	.94E-2	.23E-1	.37E-1
4.5 New II	.15E-2	.85E-2	.79E-2	.72E-2	.12E-1	.18E-1	.33E-1
4.6 BGK	.99E-3	.15E-1	.11E-2	.35E-3	.97E-2	.26E-1	.29E-1
4.6 ES-BGK	.13E-2	.11E-1	.68E-2	.60E-2	.24E-1	.20E-1	.40E-1
4.6 $\nu(C)$-BGK	.36E-2	.19E-1	.71E-2	.61E-2	.56E-1	.90E-1	.45E-1
4.6 New I	.13E-2	.11E-1	.68E-2	.60E-2	.24E-1	.20E-1	.40E-1
4.6 New II	.13E-2	.11E-1	.68E-2	.60E-2	.24E-1	.20E-1	.40E-1
4.7 BGK	.73E-3	.11E-1	.22E-2	.15E-2	.44E-1	.29E-1	.13E-1
4.7 ES-BGK	.11E-2	.67E-2	.51E-2	.44E-2	.31E-1	.13E-1	.32E-1
4.7 $\nu(C)$-BGK	.24E-2	.20E-1	.59E-2	.52E-2	.52E-1	.47E-1	.33E-1
4.7 New I	.16E-2	.20E-1	.55E-2	.48E-2	.56E-1	.34E-1	.51E-1
4.7 New II	.16E-2	.19E-1	.56E-2	.49E-2	.59E-1	.39E-1	.47E-1
4.8 BGK	.10E-2	.65E-2	.14E-2	.71E-3	.61E-1	.77E-1	.36E-1
4.8 ES-BGK	.16E-2	.16E-1	.44E-2	.35E-2	.48E-1	.61E-1	.55E-1
4.8 $\nu(C)$-BGK	.28E-2	.31E-1	.53E-2	.43E-2	.66E-1	.93E-1	.55E-1
4.8 New I	.16E-2	.16E-1	.44E-2	.35E-2	.48E-1	.61E-1	.55E-1
4.8 New II	.16E-2	.16E-1	.44E-2	.35E-2	.48E-1	.61E-1	.55E-1

Table D.4: Average relative errors of kinetic models compared to DSMC in 1DCF. Part III

Parameters / Case and Kinetic model	Density ρ	Velocity u_1	Temperature T	Pressure p	Pressure σ_{11}	Pressure σ_{22}	Pressure σ_{12}
4.9 BGK	.70E-2	.22E-1	.57E-2	.50E-2	.24E-1	.52E-1	.65E-2
4.9 ES-BGK	.13E-2	.13E-1	.21E-1	.21E-1	.42E-1	.72E-1	.18E-1
4.9 $\nu(C)$-BGK	.11E-1	.16E-1	.23E-1	.21E-1	.60E-1	.41E-1	.89E-2
4.9 New I	.45E-2	.90E-2	.22E-1	.21E-1	.13E-1	.24E-1	.35E-1
4.9 New II	.46E-2	.85E-2	.23E-1	.23E-1	.12E-1	.26E-1	.25E-1
4.10 BGK	.19E-1	.15E-1	.94E-2	.13E-1	.46E-1	.66E-1	.23E-1
4.10 ES-BGK	.45E-2	.69E-2	.34E-1	.33E-1	.53E-1	.76E-1	.32E-1
4.10 $\nu(C)$-BGK	.27E-1	.23E-1	.38E-1	.34E-1	.88E-1	.56E-1	.88E-2
4.10 New I	.98E-2	.20E-1	.34E-1	.31E-1	.35E-1	.21E-1	.39E-1
4.10 New II	.96E-2	.16E-1	.38E-1	.35E-1	.21E-1	.27E-1	.24E-1
4.11 BGK	.31E-2	.11E-1	.48E-2	.42E-2	.10E-1	.12E-1	.27E-1
4.11 ES-BGK	.32E-2	.84E-2	.19E-1	.18E-1	.22E-1	.24E-1	.40E-1
4.11 $\nu(C)$-BGK	.13E-1	.30E-1	.22E-1	.19E-1	.78E-1	.94E-1	.32E-1
4.11 New I	.32E-2	.84E-2	.19E-1	.18E-1	.22E-1	.24E-1	.40E-1
4.11 New II	.32E-2	.84E-2	.19E-1	.18E-1	.22E-1	.24E-1	.40E-1
4.12 BGK	.50E-2	.56E-2	.13E-1	.12E-1	.17E-1	.16E-1	.24E-1
4.12 ES-BGK	.78E-2	.24E-1	.28E-1	.23E-1	.23E-1	.26E-1	.39E-1
4.12 $\nu(C)$-BGK	.31E-1	.46E-1	.34E-1	.24E-1	.12E+0	.12E+0	.86E-2
4.12 New I	.78E-2	.24E-1	.28E-1	.23E-1	.23E-1	.26E-1	.39E-1
4.12 New II	.78E-2	.24E-1	.28E-1	.23E-1	.23E-1	.26E-1	.39E-1

Table D.5: Average relative errors of macroscopic continuum equations compared to kinetic models. Part I

Case and kinetic model	set of equations / Parameters	NSF	Burnett	Grad13	R13I	R13II	Kinetic equations	R13II/R13I
5.1 BGK	Pressure σ_{11}	.10E+1	.10E+0	.50E-1	.28E-1	.30E-1	.55E-2	.25E-2
	Pressure σ_{22}	.10E+1	.26E+0	.11E+0	.66E-1	.69E-1	.10E-1	.30E-1
	Pressure σ_{12}	.12E-1	.12E-1	.85E-2	.53E-2	.53E-2	.18E-3	.51E-4
5.2 BGK	Pressure σ_{11}	.10E+1	.33E+0	.20E+0	.10E+0	.11E+0	.21E-2	.10E-1
	Pressure σ_{22}	.10E+1	.52E+0	.32E+0	.16E+0	.17E+0	.50E-2	.31E-1
	Pressure σ_{12}	.80E-1	.80E-1	.49E-1	.31E-1	.31E-1	.28E-3	.16E-2
5.3 BGK	Pressure σ_{11}	.10E+1	.15E+1	.79E+0	.19E+0	.24E+0	.12E-2	.17E+0
	Pressure σ_{22}	.10E+1	.19E+1	.12E+1	.32E+0	.37E+0	.31E-2	.73E+0
	Pressure σ_{12}	.43E+0	.43E+0	.23E+0	.10E+0	.13E+0	.57E-3	.50E-1
5.4 BGK	Pressure σ_{11}	.10E+1	.23E+1	.11E+1	.46E+0	.49E+0	.42E-3	.13E+2
	Pressure σ_{22}	.10E+1	.28E+1	.17E+1	.11E+1	.11E+1	.88E-3	.42E+1
	Pressure σ_{12}	.66E+0	.66E+0	.31E+0	.30E+0	.17E+0	.26E-3	.15E+0
5.5 BGK	Pressure σ_{11}	.10E+1	.21E+1	.87E+0	.66E+0	.59E+0	.41E-3	.72E+1
	Pressure σ_{22}	.10E+1	.27E+1	.13E+1	.12E+1	.11E+1	.99E-3	.11E+1
	Pressure σ_{12}	.73E+0	.73E+0	.10E+0	.82E+0	.63E+0	.19E-3	.55E+0
4.36 BGK	Pressure σ_{11}	.10E+1	.36E+1	.98E+0	.24E+1	.21E+1	.27E-3	.23E+0
	Pressure σ_{22}	.10E+1	.43E+1	.15E+1	.36E+1	.32E+1	.56E-3	.18E+0
	Pressure σ_{12}	.14E+1	.14E+1	.24E+0	.28E+1	.22E+1	.25E-3	.29E+0
5.7 BGK	Pressure σ_{11}	.10E+1	.33E+0	.20E+0	.56E-1	.61E-1	.14E-2	.95E-2
	Pressure σ_{22}	.10E+1	.45E+0	.33E+0	.80E-1	.88E-1	.26E-2	.12E-1
	Pressure σ_{12}	.11E+0	.11E+0	.34E-1	.34E-1	.29E-1	.31E-3	.56E-2
5.8 BGK	Pressure σ_{11}	.10E+1	.54E+0	.26E+0	.12E-1	.16E-1	.15E-2	.14E-1
	Pressure σ_{22}	.10E+1	.66E+0	.39E+0	.26E-1	.32E-1	.26E-2	.19E-1
	Pressure σ_{12}	.24E+0	.24E+0	.39E-1	.13E+0	.12E+0	.42E-3	.18E-1

Notes: 1. R13I means the original R13, R13II means the slightly linearized R13.

2. Values in column "Kinetic equations" mean the average relative errors between the computed values from the kinetic model based on Eq. (5.53) and the original values from the kinetic model.

3. Values in column "R13II/R13I" mean the average relative errors between the computed values from the R13II and the computed values from the R13I.

Table D.6: average relative errors of macroscopic continuum equations compared to kinetic models. Part II

Case and kinetic model	set of equations / Parameters	NSF	Burnett	Grad13	R13I	R13II	Kinetic equations	R13II/R 13I
5.1 ES-BGK	Pressure σ_{11}	.10E+1	.15E+0	.77E-1	.44E-1	.47E-1	.48E-2	.39E-2
	Pressure σ_{22}	.10E+1	.35E+0	.15E+0	.10E+0	.11E+0	.10E-1	.26E-1
	Pressure σ_{12}	.15E-1	.15E-1	.11E-1	.87E-2	.87E-2	.20E-3	.76E-4
5.2 ES-BGK	Pressure σ_{11}	.10E+1	.45E+0	.28E+0	.16E+0	.17E+0	.19E-2	.14E-1
	Pressure σ_{22}	.10E+1	.71E+0	.42E+0	.22E+0	.24E+0	.49E-2	.33E-1
	Pressure σ_{12}	.85E-1	.85E-1	.52E-1	.39E-1	.39E-1	.34E-3	.19E-2
5.3 Es-BGK	Pressure σ_{11}	.10E+1	.15E+1	.82E+0	.14E+0	.23E+0	.17E-2	.34E+0
	Pressure σ_{22}	.10E+1	.21E+1	.12E+1	.31E+0	.38E+0	.51E-2	.24E+0
	Pressure σ_{12}	.37E+0	.37E+0	.17E+0	.16E+0	.12E+0	.48E-3	.45E-1
5.4 ES-BGK	Pressure σ_{11}	.10E+1	.20E+1	.10E+1	.47E+0	.57E+0	.28E-3	.15E+1
	Pressure σ_{22}	.10E+1	.29E+1	.17E+1	.11E+1	.13E+1	.76E-3	.34E+1
	Pressure σ_{12}	.51E+0	.51E+0	.20E+0	.52E+0	.38E+0	.19E-3	.15E+0
5.5 ES-BGK	Pressure σ_{11}	.10E+1	.20E+1	.84E+0	.88E+0	.83E+0	.48E-3	.75E+0
	Pressure σ_{22}	.10E+1	.29E+1	.13E+1	.15E+1	.14E+1	.16E-2	.42E+0
	Pressure σ_{12}	.61E+0	.61E+0	.13E-1	.11E+1	.88E+0	.42E-3	.18E+1
BGK		.10E+1	.31E+1	.84E+0	.32E+1	.29E+1	.27E-3	.17E+0
	Pressure σ_{22}	.10E+1	.43E+1	.13E+1	.46E+1	.42E+1	.69E-3	.14E+0
	Pressure σ_{12}	.12E+1	.12E+1	.39E+0	.33E+1	.27E+1	.30E-3	.24E+0
5.7 ES-BGK	Pressure σ_{11}	.10E+1	.41E+0	.27E+0	.75E-1	.73E-1	.12E-2	.13E-1
	Pressure σ_{22}	.10E+1	.62E+0	.43E+0	.12E+0	.11E+0	.28E-2	.16E-1
	Pressure σ_{12}	.10E+0	.10E+0	.23E-1	.64E-1	.59E-1	.29E-3	.69E-2
BGK		.10E+1	.60E+0	.31E+0	.71E-1	.74E-1	.13E-2	.21E-1
	Pressure σ_{22}	.10E+1	.81E+0	.47E+0	.72E-1	.75E-1	.23E-2	.27E-1
	Pressure σ_{12}	.22E+0	.22E+0	.11E-1	.21E+0	.19E+0	.28E-3	.26E-1

Notes: 1. R13I means the original R13, R13II means the slightly linearized R13.

2. Values in column "Kinetic equations" mean the average relative errors between the computed values from the kinetic model based on Eq. (5.53) and the original values from the kinetic model.

3. Values in column "R13II/R13I" mean the average relative errors between the computed values from the R13II and the computed values from the R13I.

Table D.7: Average relative errors of third-degree and fourth-degree moments of moment equations compared to kinetic models. Part I

Case	Set of equations / Parameters	BGK				ES-BGK			
		Grad13	R13I	R13II	R13II/R13I	Grad13	R13I	R13II	R13II/R13I
5.1	ρ_{112}	.42E-1	.30E-1	.29E-1	.60E-4	.81E-1	.61E-1	.61E-1	.82E-4
	$\rho_{<112>}$	.10E+1	.69E+0	.69E+0	.53E-2	.10E+1	.75E+0	.75E+0	.48E-2
	ρ_{122}	.58E+0	.13E+0	.13E+0	.14E-2	.59E+0	.18E+0	.18E+0	.18E-2
	$\rho_{<122>}$	.10E+1	.20E+0	.20E+0	.31E-2	.10E+1	.28E+0	.28E+0	.40E-2
	ρ_{222}	.20E-1	.14E-1	.14E-1	.16E-4	.38E-1	.28E-1	.28E-1	.22E-4
	$\rho_{<222>}$	.10E+1	.71E+0	.71E+0	.26E-1	.10E+1	.76E+0	.76E+0	.40E-2
	ρ_{rr22}	.38E-3	.17E-3	.17E-3	.62E-6	.47E-3	.39E-3	.39E-3	.92E-6
	$\rho_{rr<22>}$	.36E+0	.31E+0	.31E+0	.31E-3	.49E+0	.59E+0	.59E+0	.39E-3
	ρ_{rr12}	.52E-2	.25E-2	.25E-2	.53E-5	.85E-2	.36E-2	.36E-2	.71E-5
	ρ_{rrss}	.11E-3	.59E-4	.59E-4	.25E-6	.20E-3	.13E-3	.13E-3	.37E-6
	R_{12}	.10E+1	.62E+0	.62E+0	.36E-2	.10E+1	.55E+0	.55E+0	.29E-2
	R_{22}	.10E+1	.88E+0	.89E+0	.14E-2	.10E+1	.17E+1	.17E+1	.11E-2
	Δ	.10E+1	.12E+2	.12E+2	.16E-2	.10E+1	.67E+0	.67E+0	.35E-2
5.2	ρ_{112}	.31E+0	.21E+0	.21E+0	.70E-3	.42E+0	.31E+0	.31E+0	.72E-3
	$\rho_{<112>}$	.10E+1	.67E+0	.67E+0	.53E-2	.10E+1	.72E+0	.72E+0	.41E-2
	ρ_{122}	.60E+0	.19E+0	.20E+0	.14E-1	.61E+0	.20E+0	.21E+0	.12E-1
	$\rho_{<122>}$	.10E+1	.31E+0	.32E+0	.29E-1	.10E+1	.33E+0	.34E+0	.24E-1
	ρ_{222}	.20E+0	.13E+0	.13E+0	.30E-3	.32E+0	.22E+0	.22E+0	.32E-3
	$\rho_{<222>}$	.10E+1	.64E+0	.64E+0	.47E-2	.10E+1	.68E+0	.69E+0	.36E-2
	ρ_{rr22}	.20E-2	.32E-2	.32E-2	.31E-4	.19E-2	.63E-2	.64E-2	.36E-4
	$\rho_{rr<22>}$	.12E+0	.21E+0	.21E+0	.12E-2	.13E+0	.39E+0	.39E+0	.12E-2
	ρ_{rr12}	.29E-1	.12E-1	.12E-1	.46E-4	.40E-1	.11E-1	.11E-1	.73E-4
	ρ_{rrss}	.10E-2	.43E-3	.44E-3	.12E-4	.18E-2	.11E-2	.11E-2	.15E-4
	R_{12}	.10E+1	.41E+0	.41E+0	.21E-2	.10E+1	.28E+0	.28E+0	.19E-2
	R_{22}	.10E+1	.33E+1	.33E+1	.44E-2	.10E+1	.65E+1	.65E+1	.32E-2
	Δ	.10E+1	.49E+0	.49E+0	.16E-1	.10E+1	.72E+0	.73E+0	.16E-1
5.3	ρ_{112}	.63E+0	.15E+0	.17E+0	.23E-1	.64E+0	.11E+0	.13E+0	.22E-1
	$\rho_{<112>}$	.10E+1	.23E+0	.26E+0	.41E-1	.10E+1	.18E+0	.21E+0	.37E-1
	ρ_{122}	.61E+0	.77E-1	.17E+0	.96E-1	.56E+0	.17E+0	.64E-1	.92E-1
	$\rho_{<122>}$	.10E+1	.13E+0	.27E+0	.17E+0	.10E+1	.31E+0	.11E+0	.15E+0
	ρ_{222}	.11E+1	.88E-1	.97E-1	.32E-1	.12E+1	.91E-1	.63E-1	.38E-1
	$\rho_{<222>}$	.10E+1	.81E-1	.90E-1	.31E-1	.10E+1	.76E-1	.53E-1	.27E-1
	ρ_{rr22}	.28E-2	.43E-1	.43E-1	.69E-3	.39E-2	.66E-1	.67E-1	.69E-3
	$\rho_{rr<22>}$	.13E-1	.58E+0	.58E+0	.34E-2	.32E-2	.93E+0	.93E+0	.29E-2
	ρ_{rr12}	.11E+0	.20E-1	.21E-1	.85E-3	.13E+0	.59E-1	.60E-1	.85E-3
	ρ_{rrss}	.27E-2	.86E-4	.29E-3	.26E-3	.38E-2	.11E-2	.14E-2	.25E-3
	R_{12}	.10E+1	.18E+0	.19E+0	.61E-2	.10E+1	.44E+0	.44E+0	.43E-2
	R_{22}	.10E+1	.92E+2	.94E+2	.91E-2	.10E+1	.95E+3	.96E+3	.60E-2
	Δ	.10E+1	.17E+0	.22E+0	.86E-1	.10E+1	.46E+0	.51E+0	.88E-1

Table D.8: Average relative errors of third-degree and fourth-degree moments of moment equations compared to kinetic models. Part II

Case	Set of equations / Parameters	BGK				ES-BGK			
		Grad13	R13I	R13II	R13II/R13I	Grad13	R13I	R13II	R13II/R13I
5.4	ρ_{112}	.67E+0	.22E+0	.16E+0	.44E-1	.67E+0	.25E+0	.20E+0	.41E-1
	$\rho_{<112>}$	.10E+1	.32E+0	.24E+0	.59E-1	.10E+1	.38E+0	.30E+0	.56E-1
	ρ_{122}	.56E+0	.20E+0	.15E-1	.18E+0	.49E+0	.63E+0	.37E+0	.16E+0
	$\rho_{<122>}$	.10E+1	.35E+0	.27E-1	.28E+0	.10E+1	.13E+1	.75E+0	.23E+0
	ρ_{222}	.17E+1	.90E+0	.78E+0	.46E+1	.16E+1	.10E+1	.91E+0	.41E+2
	$\rho_{<222>}$	.10E+1	.53E+0	.46E+0	.47E-1	.10E+1	.63E+0	.56E+0	.43E-1
	ρ_{rr22}	.29E-2	.87E-1	.88E-1	.97E-3	.47E-2	.13E+0	.13E+0	.87E-3
	$\rho_{rr<22>}$	.21E-1	.80E+0	.81E+0	.27E-2	.29E-1	.12E+1	.12E+1	.19E-2
	ρ_{rr12}	.16E+0	.71E-1	.72E-1	.11E-2	.18E+0	.13E+0	.13E+0	.93E-3
	ρ_{rrss}	.14E-2	.18E-2	.15E-2	.33E-3	.14E-2	.71E-3	.43E-3	.29E-3
	R_{12}	.10E+1	.44E+0	.44E+0	.45E-2	.10E+1	.71E+0	.71E+0	.27E-2
	R_{22}	.10E+1	.38E+2	.38E+2	.61E-2	.10E+1	.40E+2	.41E+2	.37E-2
	Δ	.10E+1	.37E+1	.32E+1	.14E+0	.10E+1	.81E+0	.58E+0	.37E+1
5.5	ρ_{112}	.64E+0	.35E+0	.29E+0	.50E-1	.64E+0	.61E+0	.53E+0	.48E-1
	$\rho_{<112>}$	.10E+1	.55E+0	.44E+0	.68E-1	.10E+1	.94E+0	.82E+0	.62E-1
	ρ_{122}	.19E+0	.16E+1	.13E+1	.10E+0	.11E-1	.26E+1	.22E+1	.10E+0
	$\rho_{<122>}$	.10E+1	.81E+1	.68E+1	.15E+0	.10E+1	.53E+3	.46E+3	.14E+0
	ρ_{222}	.12E+1	.82E+0	.70E+0	.20E+1	.12E+1	.13E+1	.12E+1	.45E+0
	$\rho_{<222>}$	.10E+1	.67E+0	.57E+0	.61E-1	.10E+1	.11E+1	.95E+0	.55E-1
	ρ_{rr22}	.22E-1	.14E+0	.15E+0	.89E-2	.26E-1	.23E+0	.24E+0	.10E-1
	$\rho_{rr<22>}$	.50E-1	.62E+0	.64E+0	.12E-1	.67E-1	.99E+0	.10E+1	.10E-1
	ρ_{rr12}	.18E+0	.13E+0	.14E+0	.75E-2	.21E+0	.27E+0	.28E+0	.93E-2
	ρ_{rrss}	.13E-1	.24E-1	.21E-1	.26E-2	.12E-1	.25E-1	.22E-1	.27E-2
	R_{12}	.10E+1	.73E+0	.78E+0	.28E-1	.10E+1	.13E+1	.13E+1	.18E-1
	R_{22}	.10E+1	.21E+2	.23E+2	.39E-1	.10E+1	.37E+2	.40E+2	.24E-1
	Δ	.10E+1	.72E+1	.66E+1	.13E+0	.10E+1	.56E+1	.51E+1	.81E-1
5.6	ρ_{112}	.66E+0	.16E+1	.14E+1	.72E-1	.65E+0	.25E+1	.23E+1	.74E-1
	$\rho_{<112>}$	.10E+1	.24E+1	.21E+1	.83E-1	.10E+1	.39E+1	.35E+1	.83E-1
	ρ_{122}	.41E+0	.42E+1	.36E+1	.11E+0	.90E+0	.69E+1	.60E+1	.12E+0
	$\rho_{<122>}$	.10E+1	.10E+2	.87E+1	.15E+0	.10E+1	.77E+1	.66E+1	.16E+0
	ρ_{222}	.14E+1	.34E+1	.30E+1	.16E+0	.13E+1	.47E+1	.43E+1	.13E+0
	$\rho_{<222>}$	.10E+1	.24E+1	.21E+1	.81E-1	.10E+1	.37E+1	.33E+1	.81E-1
	ρ_{rr22}	.11E+0	.38E+0	.37E+0	.44E-1	.12E+0	.53E+0	.54E+0	.72E-1
	$\rho_{rr<22>}$	.15E+0	.69E+0	.72E+0	.32E-1	.19E+0	.11E+1	.11E+1	.28E-1
	ρ_{rr12}	.27E+0	.42E+0	.44E+0	.44E-1	.34E+0	.81E+0	.85E+0	.23E+0
	ρ_{rrss}	.42E-1	.12E+0	.11E+0	.94E-2	.43E-1	.14E+0	.13E+0	.11E-1
	R_{12}	.10E+1	.14E+1	.15E+1	.42E+0	.10E+1	.22E+1	.24E+1	.71E-1
	R_{22}	.10E+1	.54E+1	.70E+1	.48E+0	.10E+1	.77E+1	.91E+1	.94E-1
	Δ	.10E+1	.55E+1	.51E+1	.76E-1	.10E+1	.85E+1	.78E+1	.87E-1

Table D.9: Average relative errors of third-degree and fourth-degree moments of moment equations compared to kinetic models. Part III

Case	Set of equations / Parameters	BGK				ES-BGK			
		Grad13	R13I	R13II	R13II/R13I	Grad13	R13I	R13II	R13II/R13I
5.7	ρ_{112}	.35E+0	.13E+0	.13E+0	.39E-2	.42E+0	.11E+0	.11E+0	.49E-2
	$\rho_{<112>}$	.10E+1	.36E+0	.37E+0	.15E-1	.10E+1	.26E+0	.27E+0	.14E-1
	ρ_{122}	.41E+0	.37E+0	.34E+0	.23E-1	.30E+0	.72E+0	.68E+0	.27E-1
	$\rho_{<122>}$	.10E+1	.89E+0	.82E+0	.39E-1	.10E+1	.24E+1	.23E+1	.46E-1
	ρ_{222}	.23E+0	.82E-1	.84E-1	.19E-2	.32E+0	.89E-1	.93E-1	.29E-2
	$\rho_{<222>}$	.10E+1	.36E+0	.37E+0	.14E-1	.10E+1	.28E+0	.29E+0	.14E-1
	ρ_{rr22}	.59E-2	.74E-2	.74E-2	.49E-3	.56E-2	.14E-1	.15E-1	.67E-3
	$\rho_{rr<22>}$	.90E-1	.14E+0	.15E+0	.61E-2	.13E+0	.27E+0	.28E+0	.73E-2
	ρ_{rr12}	.48E-1	.19E-1	.19E-1	.41E-3	.66E-1	.13E-1	.12E-1	.65E-3
	ρ_{rss}	.52E-2	.14E-2	.12E-2	.19E-3	.64E-2	.88E-3	.62E-3	.26E-3
	R_{12}	.10E+1	.40E+0	.38E+0	.49E-1	.10E+1	.19E+0	.17E+0	.33E-1
	R_{22}	.10E+1	.15E+1	.15E+1	.11E+0	.10E+1	.22E+1	.22E+1	.29E-1
	Δ	.10E+1	.15E+1	.14E+1	.20E-1	.10E+1	.20E+0	.17E+0	.29E-1
5.8	ρ_{112}	.43E+0	.92E-2	.15E-1	.78E-2	.47E+0	.14E+0	.13E+0	.10E-1
	$\rho_{<112>}$	.10E+1	.21E-1	.35E-1	.18E-1	.10E+1	.31E+0	.28E+0	.19E-1
	ρ_{122}	.27E+0	.85E+0	.81E+0	.22E-1	.88E-1	.15E+1	.14E+1	.29E-1
	$\rho_{<122>}$	.10E+1	.31E+1	.30E+1	.37E-1	.10E+1	.17E+2	.16E+2	.47E-1
	ρ_{222}	.33E+0	.21E-1	.27E-1	.58E-2	.40E+0	.80E-1	.70E-1	.10E-1
	$\rho_{<222>}$	.10E+1	.65E-1	.83E-1	.19E-1	.10E+1	.20E+0	.18E+0	.20E-1
	ρ_{rr22}	.21E-1	.37E-1	.35E-1	.24E-2	.19E-1	.50E-1	.48E-1	.37E-2
	$\rho_{rr<22>}$	.41E-1	.24E+0	.24E+0	.21E-1	.77E-1	.36E+0	.35E+0	.26E-1
	ρ_{rr12}	.81E-1	.16E-1	.14E-1	.19E-2	.11E+0	.13E-1	.12E-1	.34E-2
	ρ_{rss}	.21E-1	.13E-1	.13E-1	.92E-3	.24E-1	.18E-1	.16E-1	.14E-2
	R_{12}	.10E+1	.26E+0	.19E+0	.52E+1	.10E+1	.27E+0	.14E+0	.11E+0
	R_{22}	.10E+1	.65E+1	.64E+1	.12E+0	.10E+1	.10E+2	.10E+2	.16E+0
	Δ	.10E+1	.28E+1	.27E+1	.19E-1	.10E+1	.21E+1	.20E+1	.29E-1

Notes: Values in column "R13II/R13I" mean the average relative errors between the computed values from the R13II (the slightly linearized R13) and the computed values from the R13I (the original R13).

Appendix E: Moments computed from the reference distribution f_{ES} in the ES-BGK model

E.1 Some basic knowledge

The reference distribution f_{ES} in the ES-BGK model is Eq. (2.3), which is rewritten as

$$f_{ES} = \frac{\rho}{(2\pi)^{3/2}} \frac{1}{|\lambda|^{1/2}} \exp\left(-\frac{1}{2}\varepsilon_{ij} C_i C_j\right) = \frac{\rho}{(2\pi)^{3/2}} \frac{1}{|\lambda|^{1/2}} \exp\left(-\frac{1}{2}\mathbf{C}^T \boldsymbol{\varepsilon} \mathbf{C}\right), \tag{E.1}$$

where the vector of peculiar velocity $\mathbf{C} = \begin{bmatrix} C_1 \\ C_2 \\ C_3 \end{bmatrix}$, the superscript T on a vector or a matrix means the Transpose of the vector or the matrix, matrix

$$\boldsymbol{\lambda} = RT\mathbf{I} + \frac{b}{\rho}\boldsymbol{\sigma}, \tag{E.2}$$

where $\mathbf{I}$ is the unit matrix, $\boldsymbol{\sigma}$ is the trace-free pressure tensor, b a parameter that serves to adjust the Prandtl number, and $\boldsymbol{\varepsilon} = \boldsymbol{\lambda}^{-1}$, the superscript -1 on a matrix means the inverse matrix, $|\ |$ on a matrix means the determinate of the matrix.

In order to compute moments from f_{ES} at any conditions, we need to define some matrixes, which are $\mathbf{\Pi}$ (the modal matrix of matrix of $\boldsymbol{\varepsilon}$ (normalized eigenvectors), which is an orthogonal matrix), $\mathbf{M}$ (the inverse matrix of $\mathbf{\Pi}$), $\mathbf{E}$ (the spectral matrix of $\boldsymbol{\varepsilon}$ (eigenvalues along the principal diagonal), which is a diagonal matrix), vector $\mathbf{Y} = \mathbf{MC}$. The following relations among these matrixes and vectors can be obtained (basic knowledge about matrix refers to [76, 85])

$$\mathbf{\Pi}^{-1} = \mathbf{\Pi}^T, \quad |\mathbf{\Pi}| = 1, \tag{E.3}$$

$$\mathbf{M}^{-1} = \mathbf{\Pi} = \mathbf{M}^T \tag{E.4}$$

$$\mathbf{E} = \begin{bmatrix} \mathrm{E}_{11} & 0 & 0 \\ 0 & \mathrm{E}_{22} & 0 \\ 0 & 0 & \mathrm{E}_{33} \end{bmatrix}, \tag{E.5}$$

$$\mathbf{C} = \mathbf{M}^{-1}\mathbf{Y} = \mathbf{\Pi}\mathbf{Y}, \qquad d\mathbf{C} = |\mathbf{\Pi}| d\mathbf{Y} = d\mathbf{Y}, \tag{E.6}$$

$$\mathbf{\Pi}^{-1}\boldsymbol{\varepsilon}\mathbf{\Pi} = \mathbf{E}, \quad \boldsymbol{\varepsilon} = \mathbf{\Pi}\mathbf{E}\mathbf{\Pi}^{-1} = \mathbf{M}^T\mathbf{E}\mathbf{M}, \qquad |\boldsymbol{\varepsilon}| = |\mathbf{\Pi}| \cdot |\mathbf{E}| \cdot |\mathbf{\Pi}^{-1}| = |\mathbf{E}| = \mathrm{E}_{11}\mathrm{E}_{22}\mathrm{E}_{33}, \tag{E.7}$$

$$\boldsymbol{\varepsilon}^{-1} = \mathbf{M}^{-1}\mathbf{E}\mathbf{M} = \mathbf{\Pi}\mathbf{E}^{-1}\mathbf{\Pi}^T = \boldsymbol{\lambda}, |\boldsymbol{\lambda}| = \frac{1}{\mathrm{E}_{11}\mathrm{E}_{22}\mathrm{E}_{33}}, \ \lambda_{ij} = \Pi_{ik}\left(\mathrm{E}^{-1}\right)_{kl}\left(\Pi^T\right)_{lj} = \sum_{n=1}^{3}\frac{\Pi_{in}\Pi_{nj}}{\mathrm{E}_{nn}} \tag{E.8}$$

$$\mathbf{C}^T\boldsymbol{\varepsilon}\mathbf{C} = \mathbf{C}^T\mathbf{M}^T\mathbf{E}\mathbf{M}\mathbf{C} = \mathbf{Y}^T\mathbf{E}\mathbf{Y}, \qquad \varepsilon_{ij}C_iC_j = \mathrm{E}_{ii}\mathrm{Y}_i^2. \tag{E.9}$$

For the integration, we have

$$\int_{-\infty}^{+\infty} y^{2k} e^{-ay^2} dy = \frac{1}{a^{k+1/2}}\left(2\int_0^{\infty} e^{-t^2} t^{2(k+1/2)-1} dt\right) = \frac{\Gamma(k+1/2)}{a^{k+1/2}} = \frac{(2k-1)!!}{(2a)^k}\sqrt{\frac{\pi}{a}}, \tag{E.10}$$

where $a > 0$, $k = 0,1,2,\ldots, t = \sqrt{a}y$, and $\Gamma(\ )$ is the Γ function [86]. Some examples of Eq. (E.10): $\int e^{-ay^2} dy = \sqrt{\frac{\pi}{a}}$, $\int y^2 e^{-ay^2} dy = \frac{1}{2a}\sqrt{\frac{\pi}{a}}$.

E.2 Moments computed from f_{ES}

Let us consider the zeroth-degree moment, which is

$$\int f_{ES} d\mathbf{C} = \int \frac{\rho}{(2\pi)^{3/2}} \frac{1}{|\boldsymbol{\lambda}|^{1/2}} \exp\left(-\frac{1}{2}\mathbf{C}^T\boldsymbol{\varepsilon}\mathbf{C}\right) d\mathbf{C}. \tag{E.11}$$

From Eqs. (E.5, E.6, E.9), one get

$$\int f_{ES} d\mathbf{C} = \frac{\rho}{(2\pi)^{3/2}} \frac{1}{|\boldsymbol{\lambda}|^{1/2}} \iiint \exp\left(-\frac{1}{2}\mathrm{E}_{11}\mathrm{Y}_1^2 - \frac{1}{2}\mathrm{E}_{22}\mathrm{Y}_2^2 - \frac{1}{2}\mathrm{E}_{33}\mathrm{Y}_3^2\right) d\mathrm{Y}_1 d\mathrm{Y}_2 d\mathrm{Y}_3.$$

Since Y_1, Y_2 and Y_3 are independent, therefore

$$\int f_{ES} d\mathbf{C} = \frac{\rho}{(2\pi)^{3/2}} \sqrt{\mathrm{E}_{11}\mathrm{E}_{22}\mathrm{E}_{33}} \left(\int \exp\left(-\frac{1}{2}\mathrm{E}_{11}\mathrm{Y}_1^2\right) d\mathrm{Y}_1\right) \cdot \left(\int \exp\left(-\frac{1}{2}\mathrm{E}_{22}\mathrm{Y}_2^2\right) d\mathrm{Y}_2\right)\left(\int \exp\left(-\frac{1}{2}\mathrm{E}_{33}\mathrm{Y}_3^2\right) d\mathrm{Y}_3\right)$$

Then utilizing Eq. (E.10), we get

$$\int f_{ES} d\mathbf{C} = \frac{\rho}{(2\pi)^{3/2}} \sqrt{\mathrm{E}_{11}\mathrm{E}_{22}\mathrm{E}_{33}} \sqrt{\frac{2\pi}{\mathrm{E}_{11}}}\sqrt{\frac{2\pi}{\mathrm{E}_{22}}}\sqrt{\frac{2\pi}{\mathrm{E}_{33}}}.$$

At last, we get the zeroth-degree moment as

$$\int f_{ES} d\mathbf{C} = \rho , \tag{E.12}$$

which is the first expression in Eq. (2.12).

Let us consider the first-degree moment, which is

$$\int f_{ES} C_i d\mathbf{C} = \int C_i \frac{\rho}{(2\pi)^{3/2}} \frac{1}{|\lambda|^{1/2}} \exp\left(-\frac{1}{2}\mathbf{C}^T \boldsymbol{\varepsilon} \mathbf{C}\right) d\mathbf{C}. \tag{E.13}$$

From Eqs. (E.5, E.6, E.9), one can get

$$\int f_{ES} C_i d\mathbf{C} = \frac{\rho}{(2\pi)^{3/2}} \frac{1}{|\lambda|^{1/2}} \iiint (\Pi_{i1} Y_1 + \Pi_{i2} Y_2 + \Pi_{i3} Y_3) \exp\left(-\frac{1}{2} E_{11} Y_1^2 - \frac{1}{2} E_{22} Y_2^2 - \frac{1}{2} E_{33} Y_3^2\right) dY_1 dY_2 dY_3 .$$

Since $\Pi_{i1} Y_1 + \Pi_{i2} Y_2 + \Pi_{i3} Y_3$ is an odd function of Y_1, Y_2 and Y_3, while $\exp\left(-\frac{1}{2} E_{11} Y_1^2 - \frac{1}{2} E_{22} Y_2^2 - \frac{1}{2} E_{33} Y_3^2\right)$ is an even function of Y_1, Y_2 and Y_3, therefore, we have

$$\int f_{ES} C_i d\mathbf{C} = 0, \tag{E.14}$$

which is the second expression in Eq. (2.12).

Let us consider the N^{th}-degree moments (where N is an odd number), from the same idea as the first-degree moment, one get

$$\int C_{i_1} \ldots C_{i_N} f_{ES} dC = 0, \tag{E.15}$$

such as

$$\int C_i C^2 f_{ES} = 0,$$

$$\int C_i C_j C_k f_{ES} dC = 0, \tag{E.16}$$

which is the first expression in Eq. (5.45)

Let us consider the second-degree moments, which is

$$\int f_{ES} C_i C_j d\mathbf{C} = \int C_i C_j \frac{\rho}{(2\pi)^{3/2}} \frac{1}{|\lambda|^{1/2}} \exp\left(-\frac{1}{2}\mathbf{C}^T \boldsymbol{\varepsilon} \mathbf{C}\right) d\mathbf{C}. \tag{E.17}$$

From Eqs. (E.5, E.6, E.9), one get

$$\int C_i C_j f_{ES} d\mathbf{C} = \frac{\rho}{(2\pi)^{3/2}} \frac{1}{|\lambda|^{1/2}} \iiint \Pi_{ik} Y_k \Pi_{jl} Y_l \exp\left(-\frac{1}{2}E_{11}Y_1^2 - \frac{1}{2}E_{22}Y_2^2 - \frac{1}{2}E_{33}Y_3^2\right) dY_1 dY_2 dY_3$$

$$= \frac{\rho}{(2\pi)^{3/2}} \frac{1}{|\lambda|^{1/2}} \iiint \left(\Pi_{i1}\Pi_{j1}Y_1^2 + \Pi_{i2}\Pi_{j2}Y_2^2 + \Pi_{i3}\Pi_{j3}Y_3^2\right) \exp\left(-\frac{1}{2}E_{11}Y_1^2 - \frac{1}{2}E_{22}Y_2^2 - \frac{1}{2}E_{33}Y_3^2\right) dY_1 dY_2 dY_3$$

Since Y_1, Y_2 and Y_3 are independent, therefore

$$\int C_i C_j f_{ES} d\mathbf{C} = \frac{\rho}{(2\pi)^{3/2}} \frac{1}{|\lambda|^{1/2}} \left(\int \Pi_{i1}\Pi_{j1} Y_1^2 \exp\left(-\frac{1}{2}E_{11}Y_1^2\right) dY_1\right)\left(\int \exp\left(-\frac{1}{2}E_{22}Y_2^2\right) dY_2\right)\left(\int \exp\left(-\frac{1}{2}E_{33}Y_3^2\right) dY_3\right)$$
$$+ \frac{\rho}{(2\pi)^{3/2}} \frac{1}{|\lambda|^{1/2}} \left(\int \Pi_{i2}\Pi_{j2} Y_2^2 \exp\left(-\frac{1}{2}E_{22}Y_2^2\right) dY_2\right)\left(\int \exp\left(-\frac{1}{2}E_{33}Y_3^2\right) dY_3\right)\left(\int \exp\left(-\frac{1}{2}E_{11}Y_1^2\right) dY_1\right)$$
$$+ \frac{\rho}{(2\pi)^{3/2}} \frac{1}{|\lambda|^{1/2}} \left(\int \Pi_{i3}\Pi_{j3} Y_3^2 \exp\left(-\frac{1}{2}E_{33}Y_3^2\right) dY_3\right)\left(\int \exp\left(-\frac{1}{2}E_{11}Y_1^2\right) dY_1\right)\left(\int \exp\left(-\frac{1}{2}E_{22}Y_2^2\right) dY_2\right)$$

Then utilizing Eq. (E.10), one get

$$\int C_i C_j f_{ES} d\mathbf{C} = \frac{\rho}{(2\pi)^{3/2}} \sqrt{E_{11}E_{22}E_{33}} \left(\frac{\Pi_{i1}\Pi_{j1}}{E_{11}} + \frac{\Pi_{i2}\Pi_{j2}}{E_{22}} + \frac{\Pi_{i3}\Pi_{j3}}{E_{33}}\right) \sqrt{\frac{2\pi}{E_{11}}} \sqrt{\frac{2\pi}{E_{22}}} \sqrt{\frac{2\pi}{E_{33}}}$$
$$= \rho\left(\frac{\Pi_{i1}\Pi_{j1}}{E_{11}} + \frac{\Pi_{i2}\Pi_{j2}}{E_{22}} + \frac{\Pi_{i3}\Pi_{j3}}{E_{33}}\right)$$

At last, combining Eq. (E.2, E.8), we get

$$\int C_i C_j f_{ES} d\mathbf{C} = \rho\lambda_{ij},$$
$$\int C_{<i} C_{j>} f_{ES} d\mathbf{C} = b\sigma_{ij}, \qquad \text{(E.18)}$$
$$\int C^2 f_{ES} d\mathbf{C} = 3p,$$

which is the last expression in Eq. (2.12).

let us consider fourth-degree moments, which is

$$\int f_{ES} C_i C_j C_k C_l d\mathbf{C} = \int C_i C_j C_k C_l \frac{\rho}{(2\pi)^{3/2}} \frac{1}{|\lambda|^{1/2}} \exp\left(-\frac{1}{2}\mathbf{C}^T \boldsymbol{\varepsilon} \mathbf{C}\right) d\mathbf{C}. \qquad \text{(E.20)}$$

From Eq. (E.6), one can get

$$C_i C_j C_k C_l = \Pi_{ir} Y_r \Pi_{js} Y_s \Pi_{km} Y_m \Pi_{ln} Y_n$$
$$= (\Pi_{i1}Y_1 + \Pi_{i2}Y_2 + \Pi_{i3}Y_3)(\Pi_{j1}Y_1 + \Pi_{j2}Y_2 + \Pi_{j3}Y_3),$$
$$(\Pi_{k1}Y_1 + \Pi_{k2}Y_2 + \Pi_{k3}Y_3)(\Pi_{l1}Y_1 + \Pi_{l2}Y_2 + \Pi_{l3}Y_3) \qquad \text{(E.21)}$$

where altogether there are $3^4 = 81$ terms in the expansion, while only terms, which are even function of Y_1, Y_2 and Y_3, will have non-zero value when integration in Eq. (E.20) is done. Combining Eqs. (E.5, E.9, E.20, E.21), one get

$$\int C_i C_j C_k C_l f_{ES} d\mathbf{C} = \frac{\rho}{(2\pi)^{3/2}} \frac{1}{|\lambda|^{1/2}} \iiint \mathrm{X} \exp\left(-\frac{1}{2} E_{11} Y_1^2 - \frac{1}{2} E_{22} Y_2^2 - \frac{1}{2} E_{33} Y_3^2 \right) dY_1 dY_2 dY_3 ,$$

where

$$\begin{aligned} \mathrm{X} = {} & \Pi_{i1}\Pi_{j1}\Pi_{k1}\Pi_{l1} Y_1^4 + \Pi_{i2}\Pi_{j2}\Pi_{k2}\Pi_{l2} Y_2^4 + \Pi_{i3}\Pi_{j3}\Pi_{k3}\Pi_{l3} Y_3^4 \\ & + \left(\Pi_{i1}\Pi_{j1}\Pi_{k2}\Pi_{l2} + \Pi_{i2}\Pi_{j2}\Pi_{k1}\Pi_{l1} + \Pi_{i1}\Pi_{j2}\Pi_{k1}\Pi_{l2}\right) Y_1^2 Y_2^2 \\ & + \left(\Pi_{i2}\Pi_{j1}\Pi_{k2}\Pi_{l1} + \Pi_{i1}\Pi_{j2}\Pi_{k2}\Pi_{l1} + \Pi_{i2}\Pi_{j1}\Pi_{k1}\Pi_{l2}\right) Y_1^2 Y_2^2 \\ & + \left(\Pi_{i1}\Pi_{j1}\Pi_{k3}\Pi_{l3} + \Pi_{i3}\Pi_{j3}\Pi_{k1}\Pi_{l1} + \Pi_{i1}\Pi_{j3}\Pi_{k1}\Pi_{l3}\right) Y_1^2 Y_3^2 \\ & + \left(\Pi_{i3}\Pi_{j1}\Pi_{k3}\Pi_{l1} + \Pi_{i1}\Pi_{j3}\Pi_{k3}\Pi_{l1} + \Pi_{i3}\Pi_{j1}\Pi_{k1}\Pi_{l3}\right) Y_1^2 Y_3^2 \\ & + \left(\Pi_{i3}\Pi_{j3}\Pi_{k2}\Pi_{l2} + \Pi_{i2}\Pi_{j2}\Pi_{k3}\Pi_{l3} + \Pi_{i3}\Pi_{j2}\Pi_{k3}\Pi_{l2}\right) Y_2^2 Y_3^2 \\ & + \left(\Pi_{i2}\Pi_{j3}\Pi_{k2}\Pi_{l3} + \Pi_{i3}\Pi_{j2}\Pi_{k2}\Pi_{l3} + \Pi_{i2}\Pi_{j3}\Pi_{k3}\Pi_{l2}\right) Y_2^2 Y_3^2 \end{aligned} .$$

After some straightforward but tedious manipulation, we get

$$\begin{aligned} \int C_i C_j C_k C_l f_{ES} d\mathbf{C} = {} & \rho \left(\frac{\Pi_{i1}\Pi_{j1}}{E_{11}} + \frac{\Pi_{i2}\Pi_{j2}}{E_{22}} + \frac{\Pi_{i3}\Pi_{j3}}{E_{33}} \right) \left(\frac{\Pi_{k1}\Pi_{l1}}{E_{11}} + \frac{\Pi_{k2}\Pi_{l2}}{E_{22}} + \frac{\Pi_{k3}\Pi_{l3}}{E_{33}} \right) \\ & + \rho \left(\frac{\Pi_{i1}\Pi_{k1}}{E_{11}} + \frac{\Pi_{i2}\Pi_{k2}}{E_{22}} + \frac{\Pi_{i3}\Pi_{k3}}{E_{33}} \right) \left(\frac{\Pi_{j1}\Pi_{l1}}{E_{11}} + \frac{\Pi_{j2}\Pi_{l2}}{E_{22}} + \frac{\Pi_{j3}\Pi_{l3}}{E_{33}} \right) . \\ & + \rho \left(\frac{\Pi_{i1}\Pi_{l1}}{E_{11}} + \frac{\Pi_{i2}\Pi_{l2}}{E_{22}} + \frac{\Pi_{i3}\Pi_{l3}}{E_{33}} \right) \left(\frac{\Pi_{j1}\Pi_{k1}}{E_{11}} + \frac{\Pi_{j2}\Pi_{k2}}{E_{22}} + \frac{\Pi_{j3}\Pi_{k3}}{E_{33}} \right) \end{aligned}$$

At last, utilizing Eq. (E.8), we have

$$\int C_i C_j C_k C_l f_{ES} d\mathbf{C} = \rho \left(\lambda_{ij}\lambda_{kl} + \lambda_{ik}\lambda_{jl} + \lambda_{il}\lambda_{jk} \right). \tag{E.22}$$

Let us check the correction of the above equation through consider one specific situation $b = 0$. We know at this situation, $\lambda_{ij} = RT\delta_{ij}$, $f_{ES} = f_M$ from Eqs. (E.1, E.2), then from Eq. (E.22), we have

$$\int C_i C_j C_k C_l f_{ES} d\mathbf{C} = \rho \left(\lambda_{ij}\lambda_{kl} + \lambda_{ik}\lambda_{jl} + \lambda_{il}\lambda_{jk} \right) = pRT \left(\delta_{ij}\delta_{kl} + \delta_{ik}\delta_{jl} + \delta_{il}\delta_{jk} \right),$$

which is true, since we know [70]

$$\int C_i C_j C_k C_l f_M d\mathbf{C} = \int C^4 f_M d\mathbf{C} \left(\delta_{ij}\delta_{kl} + \delta_{ik}\delta_{jl} + \delta_{il}\delta_{jk} \right) = pRT \left(\delta_{ij}\delta_{kl} + \delta_{ik}\delta_{jl} + \delta_{il}\delta_{jk} \right).$$

Let us consider some specific fourth-degree moments, which are used in Chapter 5, from Eq. (E.22),

$$\int C_r C_r C_i C_j f_{ES} d\mathbf{C} = \rho\left(\lambda_{ij}\lambda_{rr} + \lambda_{ir}\lambda_{jr} + \lambda_{ir}\lambda_{jr}\right) = \rho\left(3RT\lambda_{ij} + 2\lambda_{ir}\lambda_{rj}\right),$$

$$\int C_r C_r C_{<i} C_{j>} f_{ES} d\mathbf{C} = \rho\left(3RT\frac{b}{\rho}\sigma_{ij} + 2\lambda_{r<i}\lambda_{j>r}\right), \tag{E.23}$$

$$\int C_r C_r C_s C_s f_{ES} d\mathbf{C} = \rho\left(\lambda_{ss}\lambda_{rr} + \lambda_{sr}\lambda_{sr} + \lambda_{sr}\lambda_{sr}\right) = \rho\left(9R^2T^2 + 2\lambda_{sr}\lambda_{rs}\right)$$

In the analysis, if we only consider the linear terms, and omit higher order terms, such as $\sigma_{ij}\sigma_{kl}$, then we have

$$\begin{aligned}\lambda_{rs}\lambda_{sr} &= \left(RT\delta_{rs} + \frac{b}{\rho}\sigma_{rs}\right)\left(RT\delta_{rs} + \frac{b}{\rho}\sigma_{rs}\right) \\ &= 3R^2T^2 + 2RT\frac{b}{\rho}\sigma_{rr} + \left(\frac{b}{\rho}\right)^2\sigma_{rs}\sigma_{sr} \approx 3R^2T^2\end{aligned},$$

$$\begin{aligned}\lambda_{ri}\lambda_{rj} &= \left(RT\delta_{ri} + \frac{b}{\rho}\sigma_{ri}\right)\left(RT\delta_{rj} + \frac{b}{\rho}\sigma_{rj}\right) \\ &= R^2T^2\delta_{ij} + 2RT\frac{b}{\rho}\sigma_{ij} + \left(\frac{b}{\rho}\right)^2\sigma_{ri}\sigma_{jr} \approx R^2T^2\delta_{ij} + 2RT\frac{b}{\rho}\sigma_{ij}\end{aligned},$$

$$\lambda_{r<i}\lambda_{j>r} \approx R^2T^2\delta_{<ij>} + 2RT\frac{b}{\rho}\sigma_{<ij>} = 2RT\frac{b}{\rho}\sigma_{ij}.$$

At last, we get

$$\int C_r C_r C_s C_s f_{ES} d\mathbf{C} = \rho\left(9R^2T^2 + 2\lambda_{sr}\lambda_{rs}\right) \approx 15\frac{p^2}{\rho}, \tag{E.24}$$

$$\int C_r C_r C_{<i} C_{j>} f_{ES} d\mathbf{C} = \rho\left(3RT\frac{b}{\rho}\sigma_{ij} + 4RT\frac{b}{\rho}\sigma_{ij}\right) = 7bRT\sigma_{ij},$$

which are the second and third expressions in Eq. (5.45).